

Investigation and Application of 3-Oxabicyclo[4.1.0]heptane as  
a Mechanistic Target of Rapamycin (mTOR) Kinase Hinge  
Binding Fragment.

Thesis submitted to the University of Strathclyde as part of the  
assessment towards a degree of Doctor of Philosophy

Declan M Summers

2019



## **Abstract**

The modulation of kinase activity for treatment of diseases has gained increased attention over the last 20 years and drugs targeting kinases have been developed for a range of diseases including cancers,<sup>1-3</sup> inflammatory diseases,<sup>4,5</sup> central nervous system disorders,<sup>6</sup> cardiovascular diseases and complications related to diabetes.<sup>7</sup> Recently, this attractive class of targets have been investigated for treatment of Idiopathic Pulmonary Fibrosis (IPF), a progressive and fatal lung disease which causes 40,000 deaths per year in the USA<sup>8</sup> and is an increasingly prominent problem within our ageing society. This thesis presents scientific research towards the identification of small molecule therapies for Idiopathic Pulmonary Fibrosis through targeting a lipid kinase pathway.

Chapter 1 concerns a theoretical and experimental investigation into 3-oxabicyclo[4.1.0]heptane (cyclopropylpyran) which has recently been identified as a novel hinge binding fragment for mechanistic target of rapamycin (mTOR) and related lipid kinases, whilst chapter 2 concerns the application of this 3-oxabicyclo[4.1.0]heptane hinge binding fragment to a series of pyrazolopyrimidine based mTOR inhibitor compounds.

The research aims were firstly to investigate the scope of 3-oxabicyclo[4.1.0]heptane as a kinase hinge binding fragment. To do this a range of computational, crystallographic and spectroscopic experiments have been used to investigate the conformational preferences of a range of 3-oxabicyclo[4.1.0]heptane containing tool compounds.

Subsequently, knowledge gained in chapter 1 was applied to the development of a series of mTOR inhibitor compounds based on a pyrazolopyrimidine core. This work focused on identifying highly active compounds with appropriate physicochemical profiles which have the potential to progress further into pharmacokinetic studies.

The results presented in this thesis demonstrate significant advancements towards these goals, and offer encouragement that an improved standard of care for IPF is possible.

## **Acknowledgements**

Firstly, I would like to thank my academic supervisor, Dr. Craig Jamieson. Thank you for all of the help and support you have given me during my PhD. studies. Your enthusiasm, energy and effort has helped my scientific and personal development a great deal. Thank you for including me as a member of your research group during my secondment at Strathclyde and for kindly agreeing to let me bombard you with samples for X-ray crystallography.

I would also like to thank my industrial supervisor, Dr. Simon Peace. Thank you for giving me the opportunity to pursue such an interesting project within your group and for your patience and guidance in my development. Thank you for entrusting me with the development of the pyrazolopyrimidine series and for allowing me to shape my own research. Finally thank you for reviewing my reports and for your encouragement to “talk it up”.

I would like to thank Dr. Heather Hobbs. Thank you for your role in my scientific and professional development and for providing guidance and expertise on the medicinal chemistry of the pyrazolopyrimidine series. Thank you also to the mTOR project team, who have made smartLAB bay 17 such an exciting and motivating place to work for the past 3 and a half years.

Thank you to all of the scientists who have helped me with aspects of this work. Thank you to Dr. Sandeep Pal and Dr. Peter Pogany for their computational expertise. Thank you to Dr. Alan Kennedy for your extensive work on the X-ray crystallography, Dr. Maire Convery for your work on the PI3K $\delta$  protein co-crystal structures and Richard Upton for your work on the ROESY NMR studies.

I would like to thank Prof. John Murphy for your rigorous scientific examination of my 9- and 21- month report submissions.

A big thank-you to Prof. Harry Kelly and Prof. William Kerr for giving me the opportunity to conduct this PhD. and for conceiving and running this innovative scheme, which I feel incredibly lucky to have been a part of. Thank you also to Andrea Malley for all of your work in ensuring the scheme runs smoothly and sorting out all of my conference bookings.

Finally, A huge thank you to all of my family and friends, who have been a constant source of motivation and encouragement during the difficult patches. I would especially like to thank my partner, Charli. Your support, belief, understanding and encouragement has made this possible, Thank you.

**Contents**

<b>Abstract</b> .....	2
<b>Acknowledgements</b> .....	3
<b>Abbreviations</b> .....	8
<b>Chapter I: A theoretical and experimental investigation into the conformational bias of aryl cyclopropylpyrans, novel bioisosteres for <i>N</i>-aryl morpholine</b> .....	13
<b>1. Introduction</b> .....	14
<b>1.1 Idiopathic Pulmonary Fibrosis</b> .....	14
<b>1.1.1 IPF Pathogenesis</b> .....	15
<b>1.1.2 Current Treatments for IPF</b> .....	16
<b>1.1.3 IPF Treatments in Development</b> .....	18
<b>1.2 Kinases</b> .....	20
<b>1.2.1 Introduction to Kinases</b> .....	20
<b>1.1.2 Kinase Structure</b> .....	21
<b>1.2.3 Kinase Inhibitor Classification</b> .....	23
<b>1.2.4 Phosphatidylinositol 3-kinase (PI3K)-Related Protein Kinases (PIKKs)</b> .....	26
<b>1.3 Mechanistic Target of Rapamycin (mTOR)</b> .....	27
<b>1.3.1 PI3K-AKT-mTOR Pathway</b> .....	27
<b>1.3.2 mTOR and Fibrosis</b> .....	29
<b>1.3.3 Small Molecule mTOR Inhibitors</b> .....	32
<b>1.4.1 Importance of Morpholine Hinge Binding Fragment in PIKK Inhibitors</b> .....	36
<b>1.4.2 Discovery of Cyclopropylpyran</b> .....	37
<b>1.4.3 Dihedral Angle Scanning Study of Cyclopropylpyran</b> .....	39
<b>2. Results and Discussion</b> .....	42
<b>2.1 Project Aims</b> .....	42
<b>2.2 Tool Compounds</b> .....	43
<b>2.2.1 Tool Compound Selection</b> .....	43
<b>2.2.2 Tool Compound Synthesis</b> .....	45
<b>2.3 X-ray Crystal Structures</b> .....	60
<b>2.4 Natural Bond Orbital Analysis</b> .....	65
<b>2.4 ROESY NMR Study</b> .....	67
<b>2.5 Biological Screening and PI3K<math>\delta</math> Co-Crystallography of Tool Compounds</b> .....	70
<b>2.6 Conclusion</b> .....	74



<b>Chapter II: Development of pyrazolopyrimidine based mTOR inhibitor compounds with a cyclopropylpyran hinge binding motif.</b> .....	77
<b>1. Introduction</b> .....	78
<b>1.1 Bicyclic mTOR Inhibitors</b> .....	78
<b>2.1 Compound Profiling</b> .....	79
<b>2.1.1 mTOR Kinobead Chemoproteomic Binding Assay</b> .....	79
<b>2.1.2 phospho-Akt Cellular Assay</b> .....	81
<b>2.1.3 “Scar-in-a-jar” Phenotypic Assay</b> .....	82
<b>2.1.4 PI3K TR-FRET Assay</b> .....	83
<b>2.1.5 Physicochemical Assays</b> .....	85
<b>2.1.6 Ames Mutagenicity Test</b> .....	87
<b>2.1.7 Compound Testing</b> .....	89
<b>2.2 Dihedral Angle Scanning for Cyclopropylpyran Bicyclic Compounds</b> .....	90
<b>2.3 Bicyclic Core Compounds</b> .....	93
<b>2.3.1 AZD8055 Matched Molecular Pair</b> .....	93
<b>2.3.2 5,6-Bicyclic Core Scan</b> .....	95
<b>2.3.1 Synthesis of Cyclopropylpyran 5,6 Bicyclic Core Compounds</b> .....	96
<b>2.3.2 Cyclopropylpyran 5,6-Bicyclic Core Compound Analysis</b> .....	99
<b>2.4 Literature Review of Pyrazolopyrimidine Based mTOR Inhibitor Compounds</b> .....	103
<b>2.4.1 Literature Backpocket Group Optimisation</b> .....	104
<b>2.4.2 Literature Ribose Group Optimisation</b> .....	111
<b>2.4.3 Literature Hinge Group Optimisation</b> .....	114
<b>2.5 Inhaled Administration of Drugs</b> .....	119
<b>2.6 CZ415 and Vistusertib – Benchmark Compounds</b> .....	121
<b>2.7 Project Aims</b> .....	124
<b>2.8 Literature Matched-Molecular Pair Compounds</b> .....	125
<b>2.8.1 Synthesis of Literature MMP Compounds</b> .....	126
<b>2.8.2 Literature Compounds</b> .....	136
<b>2.8.3 Cyclopropylpyran Matched Molecular Pair Compounds</b> .....	140
<b>2.8 Optimisation of <i>N</i>-1 Substituent</b> .....	143
<b>2.8.1 Synthesis of Cyclohexyl-<i>N</i>1-Substituted Pyrazolopyrimidine Compounds</b> .....	144
<b>2.8.2 Cyclohexyl-<i>N</i>1-Substituted Compounds</b> .....	148
<b>2.9 Optimisation of Position-6 Substituent (Backpocket Group)</b> .....	152
<b>2.9.1 Synthesis of Pyrazolopyrimidine 150 Analogues</b> .....	154

2.9.2 Synthesis of 199 Analogues .....	157
2.9.3 Evaluation of Backpacket Optimisation .....	164
2.10 Further Analysis of 203a .....	170
2.10.1 Ames Mutagenicity Test of 203a .....	170
2.10.2 Kinobead Lipid Kinase Selectivity Profiling .....	173
2.10.3 Comparison of Compound 203a to CZ415 .....	175
2.11 Attempts to Further Optimise N1-Substituent of 203a .....	177
2.11.1 Synthesis of Compounds with Varied N1-Substituent .....	178
2.11.2 Biological Profiling of Compound 199a Analogues .....	188
2.12 Conclusions and Future Work .....	190
Experimental Section .....	194
3.1 General Information .....	195
3.2 Tool Compound Synthesis .....	198
3.3 Pyrazolopyrimidine Compounds .....	221
3.3.1 Literature Matched Pair Compounds .....	221
3.3.2 Cyclohexyl-N1-Substituted compounds .....	242
3.3.3 Backpacket Optimisation Compounds .....	248
3.3.4 N1-Substituent Optimisation Compounds .....	271
Appendix .....	301
X-Ray Crystal Structure Data .....	301
PI3K $\delta$ Protein Co-Crystal Structure Data .....	303
ROESY NMR Experimental and Spectra .....	305
Molecular Mechanical Modelling Details .....	305
3-(6-(3-oxabicyclo[4.1.0]heptan-6-yl)pyridin-2-yl)phenol (34) .....	306
3-(5-(3-oxabicyclo[4.1.0]heptan-6-yl)pyridin-3-yl)phenol (40) .....	307
3-(4-(3-oxabicyclo[4.1.0]heptan-6-yl)pyridin-2-yl)phenol (41) .....	308
1-(3'-(3-oxabicyclo[4.1.0]heptan-6-yl)[1,1'biphenyl]-4-yl)-3-ethylurea (42) .....	309
Cyclopropylpyran Stereochemical Assignment .....	310
Assay Experimental Procedures .....	311
PI3K-Isoform HTRF Assay .....	311
Phospho-Akt Cellular Assay .....	312
mTOR Kinobead Proteomic Binding Assay .....	312
“Scar-in-a-Jar” Phenotypic Assay .....	313
Charged Aerosol Detection (CAD) solubility .....	313

<b>ChromLogD</b> .....	313
<b>Artificial Membrane Permeability</b> .....	313
<b>References</b> .....	314

**Abbreviations**

4EBP1	Eukaryotic Translation Initiation Factor 4E Binding Protein 1
ADMET	Absorption, Distribution, Metabolism, Excretion, Toxicity
Akt	Protein Kinase B
AMP	Artificial Membrane Permeability
AO	Atomic Orbital
Asp	Aspartic Acid
ATM	Ataxia-Telangiectasia Mutated Kinase
ATP	Adenosine Triphosphate
ATR	Ataxia Telangiectasia and Rad3-Related Protein
B3LYP	Becke 3-Parameter (Exchange), Lee, Yang and Parr
BCR-Abl	Breakpoint Cluster Region – Abelson Murine Leukaemia Viral Oncogene Homolog 1
BEI	Binding Efficiency Index
BRCA1	Breast Cancer Type 1 Susceptibility Protein
BTK	Bruton's Tyrosine Kinase
CataCXium A	Di(1-adamantyl)- <i>n</i> -butylphosphine
CHI	Chromatographic hydrophobicity index
CHK 1/2	Checkpoint Kinase 1/2
CPP	Cyclopropylpyran (3-oxabicyclo[4.1.0]heptane)
CRO	Contract Research Organisation
CYP450	Cytochrome P450
Cys	Cysteine
DCE	Dichloroethane
DCM	Dichloromethane
DELFI	Dissociation-enhanced Lanthanide Fluorescence Immunoassay
DEPTOR	DEP domain-containing mTOR-interacting protein

DFT	Density Functional Theory
DHP	Dihydropyran
DIPEA	Diisopropylamine
DMAP	4-Dimethylaminopyridine
DMF	<i>N,N</i> -Dimethylformamide
DMP	Dess–Martin Periodinane
DMSO	Dimethyl sulfoxide
DNA	Deoxyribonucleic Acid
DNA-PK	DNA-dependent Protein Kinase
ECM	Extra Cellular Matrix
EDTA	Ethylenediaminetetraacetic Acid
eHOMO	Energy of the Highest Occupied Molecular Orbital
FaSSIF	Fasted-state Simulated Intestinal Fluid
FDA	Food and Drug Administration
FKBP12	FK506 Binding Protein 12
FRAP1	FK506-binding protein 12-rapamycin-associated protein 1
FTIH	First Time in Human
FTIR	Fourier-transform Infrared Spectroscopy
FVC	Forced Vital Capacity
Gln	Glutamine
GLP	Good Laboratory Practice
GSK	GlaxoSmithKline
HATU	1-[Bis(dimethylamino)methylene]-1 <i>H</i> -1,2,3-triazolo[4,5- <i>b</i> ]pyridinium 3-oxide Hexafluorophosphate
HBC	Human Blood Donor Count
HeLa	Henrietta Lacks Human Uterine Cervical Carcinoma Cell Line
hERG	Human <i>Ether-a-go-go</i> -related Gene
HFIP	Hexafluoro-2-propanol

His	Histidine
HMBC	Heteronuclear Multiple Bond Correlation
HPLC	High Performance Liquid Chromatography
HRMS	High Resolution Mass Spectroscopy
HTS	High Throughput Screen
HuT-78	Human T Cell Lymphoma Cell Line
IPF	Idiopathic Pulmonary Fibrosis
IRK	Insulin Receptor Kinase
IVC	<i>In Vitro</i> Clearance
LCMS	Liquid Chromatography Mass Spectroscopy
Leu	Leucine
LipE/LLE	Lipophilic (Ligand) Efficiency
LNCap	Lymph Node Carcinoma of the Prostate Cells
Lys	Lysine
<i>m</i> -CPBA	<i>meta</i> -Chloroperoxybenzoic Acid
MDAP	Mass Directed Auto Purification System
MDCK	Madin-Darby Canine Kidney Cells
MDM2	Mouse Double Minute 2 Homolog
MEK	Mitogen-activated Protein Kinase
MLST8	Mammalian Lethal with SEC13 Protein 8
MMFF94x	Merck Molecular Force Field 94x
MO	Molecular Orbital
MOE	Molecular Operating Environment
mTOR	Mechanistic Target of Rapamycin
mTORC 1/2	Mechanistic Target of Rapamycin Complex 1/2
NBO	Natural Bond Orbital
NBS1	Nibrin

NF- $\kappa$ B	Nuclear Factor kappa-light-chain-enhancer of Activated B Cells
NHS	National Health Service
NMD	Nonsense-mediated mRNA Decay
NMR	Nuclear Magnetic Resonance
NOE	Nuclear Overhauser Effect
p53	Tumour Suppressor 53
PDB	Protein Data Bank
Phe	Phenylalanine
PI3K	Phosphatidylinositol-4,5-bisphosphate 3-kinase
PIKK	Phosphatidylinositol 3-Kinase-Related Kinases
PIP <sub>2</sub>	Phosphatidylinositol 4,5-bisphosphate
PIP <sub>3</sub>	Phosphatidylinositol (3,4,5)-trisphosphate
PK/PD	Pharmacokinetic/ Pharmacodynamic
PMA	Phosphomolybdic Acid
PRAS40	Proline-rich Akt substrate of 40 kDa
PTEN	Phosphatase and Tensin Homolog
RAPTOR	Regulatory-associated protein of mTOR
RBF	Round Bottom Flask
RHEB	Ras homolog enriched in brain
RICTOR	Rapamycin-insensitive companion of mTOR
RIPF	Radiation Induced Pulmonary Fibrosis
ROESY	Rotating Frame Overhauser Effect Spectroscopy
S6K1	Ribosomal Protein S6 Kinase beta-1
SAR	Structure-activity Relationship
SASP	Senescence-associated Secretory Phenotype
Ser	Serine
SLF	Simulated Lung Fluid

STAB	Sodium Triacetoxyborohydride
TBAF	Tetra Butyl Ammonium Fluoride
TBS	<i>tert</i> -Butyldimethylsilyl Ether
TCDI	1,1'-Thiocarbonyldiimidazole
TEA	Triethylamine
TGF- $\beta$	Transforming Growth Factor Beta
THF	Tetrahydrofuran
THP	Tetrahydropyran
TLC	Thin Layer Chromatography
TNF $\alpha$	Tumour Necrosis Factor Alpha
TR-FRET	Time-Resolved Fluorescence Resonance Energy Transfer
Trp	Tryptophan
TSC 1/2	Tuberous Sclerosis Protein 1/2
UV	Ultraviolet
Val	Valine
WSG	Water-Solubilising Group



**Chapter I:** A theoretical and  
experimental investigation into the  
conformational bias of aryl  
cyclopropylpyrans, novel bioisosteres for  
*N*-aryl morpholine

# **1. Introduction**

## **1.1 Idiopathic Pulmonary Fibrosis**

Idiopathic pulmonary fibrosis (IPF) is a fatal age-associated disease that is characterised by progressive and irreversible scarring of the tissue and space around the alveoli (interstitium). IPF has an unknown aetiology and a complex interplay of genetic and environmental risk factors, ageing-associated processes and epigenetic reprogramming have been implicated.<sup>9</sup> Most commonly patients are current or past smokers and have a median age of 60 years.<sup>10</sup>

Current studies suggest that IPF is a result of abnormal epithelial wound healing process. It was previously thought that IPF was inflammation driven, however clinical trials involving anti-inflammatory drugs failed to improve patient outcomes and caused increased mortality.<sup>11</sup>

In IPF patients, a gradual loss of lung architecture leads to a reduced capacity for gaseous exchange.<sup>12</sup> This degradation of lung structure can be seen in cross sections of lungs taken from IPF patient autopsies and is referred to as ‘honeycombing’ (**Figure 1**).



**Figure 1:** Cross section of a IPF patient lung, showing characteristic honeycomb structure.<sup>13</sup>

Patients with IPF usually display symptoms that include; shortness of breath (dyspnea); a dry, unproductive cough and clubbing of the hands and feet. The classic clinical finding in IPF patients is considered to be the presence of a “Velcro-crackle” sound when the lower lungs are examined by stethoscope.<sup>12</sup> These symptoms are not unique to IPF and to comprehensively diagnose IPF over other lung diseases, histological lesions must be observed by viewing lung biopsies under a microscope.<sup>14</sup>

A 2006 study showed that there were 50,000 new cases of IPF and 40,000 deaths from IPF per year in the USA.<sup>8</sup> IPF is estimated to occur with similar frequency to cancers of the stomach,

brain and testicles.<sup>15,16</sup> This highlights the great patient need and potential market for a safe and effective treatment for IPF. Currently, the median survival rate for IPF patients is just 2-3 years following diagnosis.<sup>17</sup>

The main methods by which physicians measure disease progression is through lung function, expressed as forced vital capacity (FVC). This is the maximum amount of air that can be expelled from the lungs following a maximal inhalation. Rather than a smooth decline in lung function, it has been discovered that there are multiple classes of disease progression including, rapid, slow and stable. The progression of some patients conditions is also exacerbated by rapid disease progression, often due to other complications, such as emphysema.<sup>18</sup>

### **1.1.1 IPF Pathogenesis**

Although the precise mechanisms that underlie the development of IPF are not understood, it has been demonstrated in a number of studies that IPF is initiated by endogenous or exogenous lung epithelial injury. There are two types of lung epithelial cells, type I and type II. Type II pneumocytes account for just a small (around 5%) proportion of the cell population however they have an important role in the repair of damaged lung epithelium.<sup>19</sup> Lung injury can occur by several mechanisms as the lungs are exposed to many insults. In normal healthy individuals, a coordinated sequence of events is triggered by various growth factors and cytokines which are produced during the repair process to recruit immune cells. During this process, fibroblasts become activated to myofibroblasts and produce a type 1 collagen rich extra-cellular matrix (ECM) to repair the damaged epithelium. Following repair, myofibroblasts then undergo apoptosis to maintain homeostasis.

In IPF patients however, this repair process is disrupted, resulting in aberrant repair which eventually leads to chronic lung fibrosis. Transforming growth factor beta (TGF- $\beta$ ) is a pro-fibrotic growth factor which is produced in response to a lung injury. It has been shown that TGF- $\beta$  activates the transformation of fibroblasts to myofibroblasts which leads to the production of type 1 collagen ECM.<sup>20,21</sup> It is currently thought that IPF results following aberrant wound healing from an unknown, chronic lung insult which increases the production of TGF- $\beta$ . This encourages uncontrolled production of excessive type-1 collagen ECM *via* myofibroblast activation. Eventually, the collagen-rich ECM distorts the structure of the lung, which severely hinders its ability to perform gaseous exchange.

IPF-fibroblasts differ from normal fibroblasts in their response to type-1 collagen. Normal fibroblast proliferation and survival is inhibited in response to type 1 collagen by PTEN inhibition of the PI3K/Akt/mTOR pathway.<sup>22,23</sup> In IPF-fibroblasts however, there is enhanced PI3K/Akt/mTOR activity due to PTEN suppression. This causes IPF-fibroblasts to have a viable and proliferative phenotype within a collagen rich ECM, which leads to further progression of the disease in a positive feedback mechanism.<sup>23,24</sup> A pathway for the development of IPF is shown in **Figure 2**.

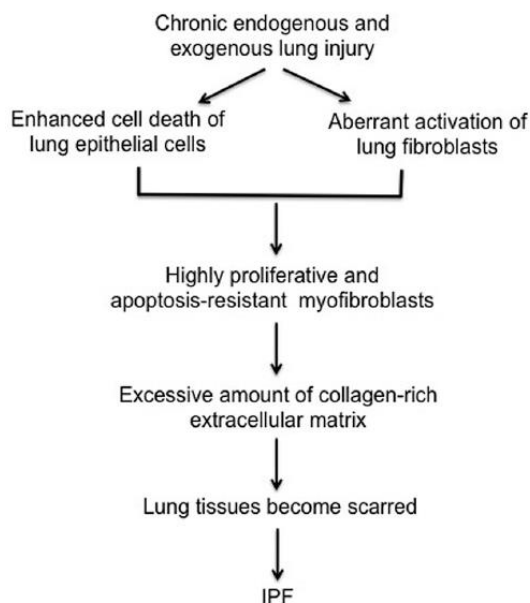


**Figure 2:** Proposed pathway for IPF.<sup>19</sup>

### **1.1.2 Current Treatments for IPF**

Historically, there were no drugs designed specifically for IPF and the management of IPF involved immune suppression, however this was found to be ineffective and associated with increased mortality.<sup>11</sup> The only effective treatment option was surgical intervention in the form of lung transplantation.<sup>25</sup> In 2014 this changed when two novel therapies were approved for the treatment of IPF.

The first of these therapies is pirfenidone (**1**), a low molecular weight molecule with a poorly understood mechanism of action (**Figure 3**). Pirfenidone exhibits anti-fibrotic properties in animal models. It is thought that pirfenidone suppresses fibroblast proliferation, inhibits pro-fibrotic/ pro-inflammatory cytokines and reduces collagen production, although the mechanisms by which these effects are mediated are not understood.<sup>26,27</sup> Pirfenidone was

approved for use based on a meta-analysis of pooled clinical trial data, which showed it conveyed improved rates of survival in comparison with a placebo.<sup>28</sup> It was also shown that there was significant reduction in the decline of forced vital capacity (FVC) for patients taking the medication. Pirfenidone however, does not alleviate the other symptoms associated with IPF, such as dyspnoea and cough,<sup>29</sup> and only slows lung function decline. Pirfenidone, therefore, does not stop or reverse the lung damage caused by IPF.

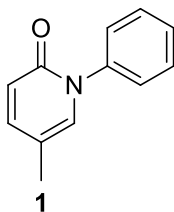


**Figure 3:** Structure of pirfenidone.

A daily dose of pirfenidone comprises of three 267 mg tablets taken three times a day, totalling a 2.4 g daily dose. This is a large dose and requires patients to take medication on a frequent basis. The cost of treatment is ~£26K per year, although a confidential patient access scheme has provided some level of discount to the NHS in the UK.<sup>30</sup> The large dose, frequent dosing regime and high-cost are all areas which could be improved upon by a novel therapeutic.

The large dose of pirfenidone is likely a contributing factor to its undesirable side-effect profile. Pirfenidone has reported side-effects including photosensitivity, which prevents the patient from being exposed to sunlight, fatigue, dizziness, weight loss, gastroesophageal reflux disease, and hepatic dysfunction.<sup>31</sup> These side-effects can prevent patient adherence to the medication and may lead to termination of treatment.

The second therapy currently approved for the treatment of IPF is Nintedanib (**2**). Nintedanib is a receptor tyrosine kinase (RTK) inhibitor which is believed to be active at a number of RTK's including; Platelet-derived growth factor receptor (PDGF), Vascular endothelial growth factor receptor (VEGF) and Fibroblast growth factor receptor (FGFR) which leads to suppression of fibrosis.<sup>32</sup> In clinical trials it was shown that Nintedanib demonstrated a significant reduction in the decline of FVC, although the translation of this effect into reduced mortality was not significant.<sup>33</sup>

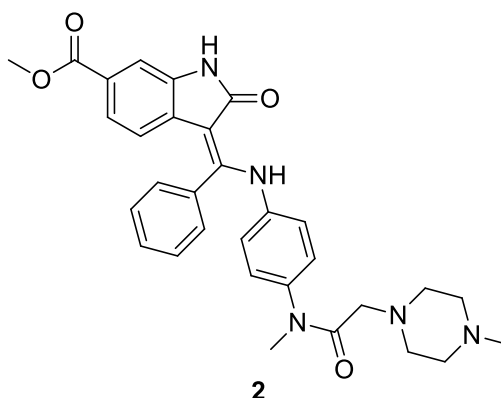


**Figure 4:** Structure of Nintedanib.

Patients taking Nintedanib must take a 150 mg tablet twice a day, although this represents a substantial reduction over pirfenidone, this is still a reasonably large dose and does not conform to the accepted “gold-standard” of once-a-day treatment, meaning there is an opportunity for a novel therapeutic to offer improvement.

The side-effect profile of Nintedanib is quite severe which might be expected from a systemic kinase inhibitor. Diarrhoea and nausea are the most common side effects, and in clinical trials it was noted that an elevation of liver enzymes and increase in bleeding events occurred. The clinical trial also observed a significantly greater proportion of patients in the Nintedanib patient group suffering myocardial infarction.<sup>33</sup>

The cost of treatment for Nintedanib is very similar to pirfenidone (~£26K per year) and a similar patient access scheme has been agreed with the NHS.<sup>34</sup> Cost-effectiveness analysis of Pirfenidone and Nintedanib has led the NHS to limit treatment to patients who have a forced vital capacity (FVC) between 50% and 80% of predicted.<sup>30,34</sup> This severely limits treatment options for patients who fall outside of this category and highlights the unmet need for novel therapeutics.

### **1.1.3 IPF Treatments in Development**

Given the severity of IPF and the lack of effective treatment options, many pharmaceutical companies have potential treatments for IPF in various stages of development. A review published in 2017 has summarised the various clinical candidates for treatment of IPF (**Table 1**).

Drug	Company	Phase	Mechanism	Observations
Pamrevlumab	Fibrogen	II	Anti-CTGF monoclonal AB	Overall safety and marginally favourable outcomes demonstrated
IW001	ImmuneWorks	I	Oral collagen V. Aims to induce immune tolerance	Safe and well tolerated
Lorsartan	University of South Florida	II	Angiotensin II antagonist	Stabilised lung function. No control group in study
PRM-151	Promedior	II	Recombinant pentaraxin II	Overall safety and marginally favourable outcomes demonstrated
Carlumab	Centocor	II	Anti-CCL2 antibody	No evidence of treatment benefit compared with placebo. Project now terminated
Tanzisertib	Celgene	II	JNK antagonist	Clinically effective but 46% of patients discontinued study due to adverse events
Octreotide	Inserm	II	Long-lasting somatostatin analogue	Well tolerated
Simtuzumab	Gilead	II	Monoclonal AB to bind LOXL2	Terminated due to lack of efficacy
Lebrikizumab	Genentech/ Tanox	II	Anti-IL-13 antibody	Ongoing
Tralokinumab	AZ/ MedImmune	II	Anti-IL-13 antibody	Terminated due to lack of efficacy
SAR156597	Sanofi	II	Monoclonal AB targeting IL-13 and IL-14	Ongoing
KD015	Kadmon Corp.	II	ROCK2 antagonist	Ongoing
Tipelukast	MediciNova	II	Leukotriene antagonist; PDE4 and thromboxane A2 inhibitor	Safe and well tolerated
GLPG1690	Galapagos	II	Autotaxin inhibitor	FVC stabilised over 12 weeks compared with placebo. PIII trial planned
GLP1205	Galapagos	I	GPR84 inhibitor	Safe and well tolerated. PII trial planned
BMS-986020	Bristol-Myers Squibb	II	LPA1 antagonist	Trial stopped for unknown reason
Everolimus	University of Virginia	n.a.	mTORC1 inhibitor	Worsening of FVC and disease progression
GSK2126458	GlaxoSmithKline	I	PI3K/mTOR inhibitor	Completed. No results reported
GSK3008348	GlaxoSmithKline	I	$\alpha_v\beta_6$ antagonist	Ongoing
PBI-4050	Prometric Biosciences	II	Reduces production of TGF- $\beta$ , CTGF, IL-23, p19 and IL-6	Completed. No results reported

Drug	Company	Phase	Mechanism	Observations
Rituximab	University of Alabama	II	Chimeric anti-CD20 monoclonal antibody	Completed. No results reported
Inhaled TD139	Galecto Biotech	II	Galectin-3-inhibitor	Safe and well tolerated
Nandrolone decanoate	University of Sao Paulo	II	Synthetic androgen to decrease telomere attrition.	Ongoing
Vismodegib + Pirfenidone	Hoffman-La Roche	I	Hedgehog pathway inhibitor	Completed. No results reported

**Table 1:** Summary of selected novel clinical drug candidates for IPF. Key: green= generally positive results, red= negative results, yellow= ongoing or no published results.

There are a range of clinical trials ongoing for IPF indications with biologicals. Whilst these therapies have the advantage of being very specific, as they are genetically engineered to specifically bind to a single target cell or protein,<sup>35</sup> immunotherapies are expensive to produce<sup>36</sup> and rely on intravenous or subcutaneous administration.<sup>37</sup>

## 1.2 Kinases

### 1.2.1 Introduction to Kinases

A kinase is an intracellular signalling enzyme which functions by transfer of a phosphate group from adenosine triphosphate (ATP) onto a target; this target can be protein, lipid or nucleic acid with most kinases functioning on protein substrates.<sup>38</sup> Kinases are ubiquitous in human cells and they make up 1.7% of the Human genome. There are 518 protein kinases and 20 lipid kinases in the human kinome.<sup>39</sup> Kinases are known to have active roles in key cellular activities including; proliferation, survival, apoptosis, metabolism and differentiation.<sup>39</sup> The phosphorylation of a target substrate modifies the activity of the substrate and kinases often operate in phosphorylation cascades (**Figure 5**) which result in a given cellular response.



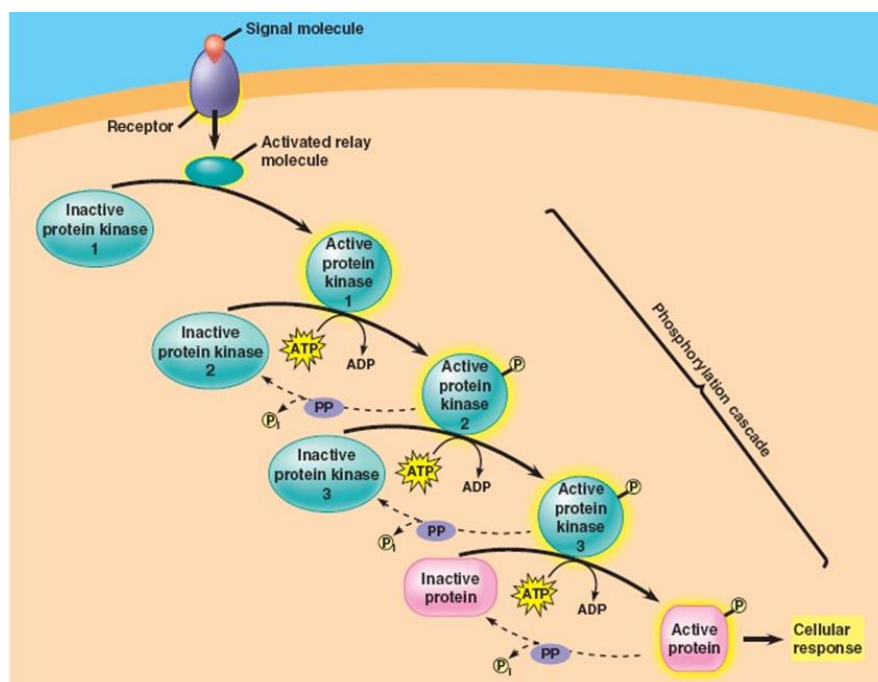


**Figure 5:** Illustration of a general kinase-mediated intracellular message transfer. An extracellular signalling molecule triggers a cell surface receptor which activates protein kinase 1. This in turn activates protein kinase 2 by transferring a phosphate group to it from ATP. This will activate other kinases in a domino effect until a final protein is activated, which invokes a cellular response.<sup>40</sup>

Due to their role in cellular activities, Kinases have been extensively pursued by the pharmaceutical industry as drug targets. Over the past 30 years there have been 38 kinase inhibitor molecules approved by the FDA<sup>41</sup> for a range of indications including; cancers,<sup>1-3</sup> inflammatory diseases,<sup>4,5</sup> central nervous system disorders<sup>6</sup>, cardiovascular diseases and complications related to diabetes.<sup>7</sup>

### **1.1.2 Kinase Structure**

The general structure of kinases enzymes is well defined due to the existence of multiple published X-ray crystal structures.<sup>42</sup> Generally, a protein kinase consists of a smaller  $\beta$ -structured N-lobe connected by a short hinge fragment to a larger  $\alpha$ -helical C-lobe. The ATP binding pocket is located in the hinge region between these terminal lobes where ATP is sandwiched between hydrophobic residues and forms hydrogen bonding interactions with the kinase hinge.<sup>43</sup> The general structure of a protein kinase is shown in **Figure 6**.

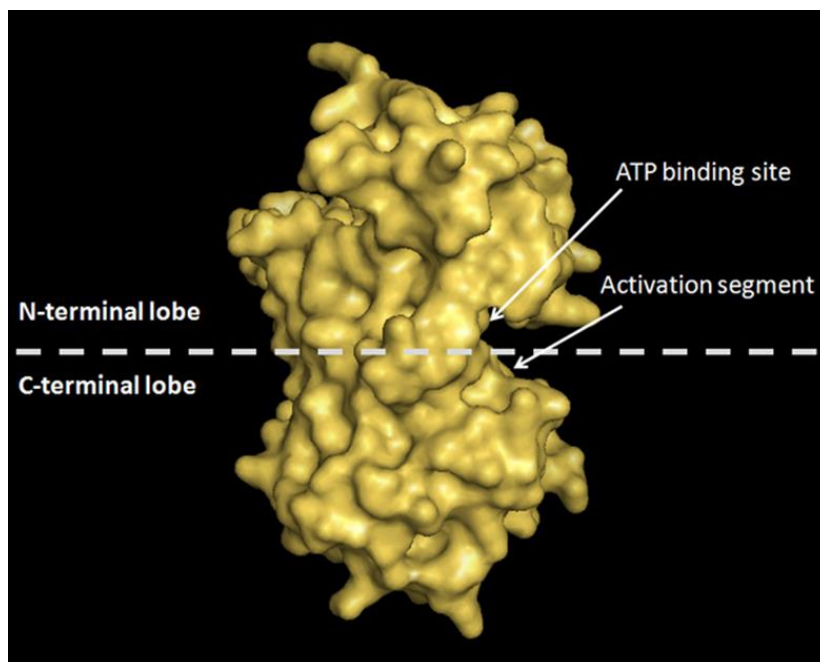


**Figure 6:** A solved X-ray structure of Aurora A kinase.<sup>44</sup>

The hinge region is lined with a number of domains involved in catalytic activity. These include; the A-loop which can adopt an open conformation (when ATP is bound) or a variety of closed conformations (inactive states). The A-loop is able to be stabilised in the active open conformation by phosphorylation. The DFG motif (made up of the amino acid residues, aspartic acid (D), phenylalanine (F) and glycine (G)), is a section of the A-loop where an Asp residue binds the  $Mg^{2+}$  ions that coordinate the  $\beta$ - and  $\gamma$ -phosphates of ATP. The other end of the A-loop contains a short EF-helix which contains a conserved Glu residue which binds the kinase substrate. Helix-C contains a Glu residue that forms a salt-bridge with the active site Lys (the Ala-X-Lys motif in the  $\beta$ 3-strand), thereby anchoring and orienting the ATP molecule. The P-loop is also involved in ATP coordination, as well as containing the catalytic loop which is responsible for phosphate group transfer to the substrate.<sup>45-47</sup> an example of the ATP-cleft arrangement for IRK can be seen in **Figure 7**. The active sites of all kinases bind ATP and therefore have structural homology, particularly whilst in the DFG-in conformation. For this reason, identification of highly selective small molecule inhibitors remains a challenge.

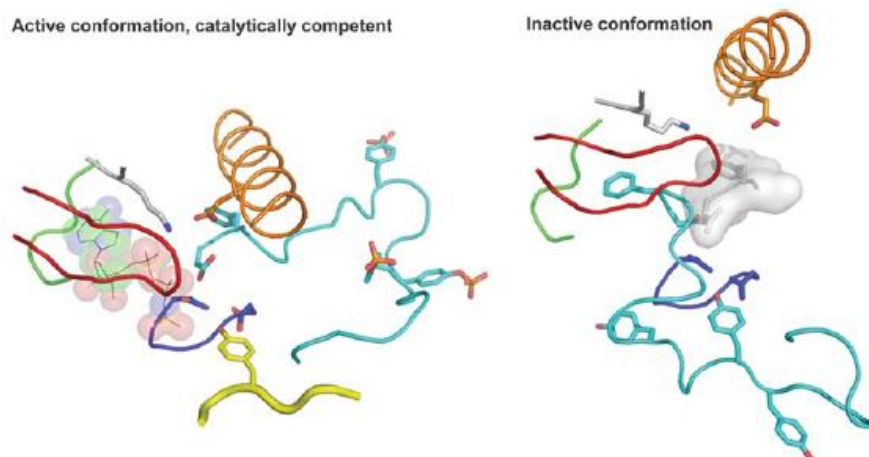


**Figure 7:** Helix-C (orange), P-loop (red), hinge region (green), catalytic loop (blue), A-loop (cyan), conserved lysine (grey), and substrate peptide (yellow) in active IRK and the location of the same features in inactive IRK showing structural elements and residues important for the mechanism of action. In the left-hand panel, the bound ATP molecule is shown as a transparent structure. In the right-hand panel, the location of the DFG motif in the corresponding active conformation is shown by a transparent surface (grey).<sup>45</sup>

### **1.2.3 Kinase Inhibitor Classification**

Kinase inhibitors are broadly divided into two main classes; covalent inhibitors and non-covalent inhibitors. Covalent inhibitors (sometimes referred to as type VI inhibitors) are often Michael acceptors and form a bond with various poorly conserved reactive cysteine residues within the ATP cleft.<sup>48</sup> Ibrutinib<sup>49</sup> and Afatinib<sup>50</sup> are FDA approved chemotherapies and are covalent inhibitors for Brn-3 tyrosine kinase (BTK) and epidermal growth factor receptor (ErbB-1), respectively. More recently a kinase-conserved lysine has also been targeted for inhibition of phosphoinositide 3-kinase delta (PI3K $\delta$ ).<sup>51</sup> Non-covalent inhibitors are further divided into sub-classes based on the position in which they bind to the kinase. This leads to the classification of reversible kinase inhibitors.<sup>43</sup>

Type I inhibitors bind to the hinge of kinases in their active conformation (DFG-in conformation) meaning when the inhibitor is bound the structural elements of the ATP cleft adopt an arrangement similar to that of when ATP is bound.<sup>47</sup> As stated above, the hinge region of an active enzyme has good structural homology across the kinome, therefore type I kinase inhibitors gain selectivity by exploiting differences in other regions of the ATP cleft which are less conserved, such as the back-pocket region.<sup>43</sup>

Type I  $\frac{1}{2}$  inhibitors are a further subtype of type I inhibitors where the kinase is bound in an inactive conformation; however, the kinase is in a DFG-in conformation (typical for an active kinase). An example of this is Lapatinib in ErbB-1 which displaces the helix-C and produces an inactive conformation.<sup>52</sup>

Type II reversible inhibitors bind to the hinge region whilst the kinase is in the DFG-out, inactive conformation. The displacement of the DFT motif exposes a hydrophobic pocket adjacent to the ATP binding site which can be exploited by type II inhibitors.<sup>53</sup> Imatinib<sup>54</sup> and Sorafenib<sup>55</sup> are examples of FDA approved type II kinase inhibitors which each target multiple tyrosine kinases. Type II inhibition has benefits over type I inhibitors including improved selectivity and slower off-rates.<sup>56</sup> However the identification of novel type II kinase inhibitors represents a considerable challenge as they are often overlooked in traditional enzymatic assays and high-throughput screening (HTS), because of low affinity to active, phosphorylated kinases.<sup>57</sup>

Property	Type I	Type I $\frac{1}{2}$	Type II	Type III	Type IV	Type VI
<b>Binding Location</b>	ATP Pocket of active conformation	ATP Pocket of inactive conformation, DFG-Asp in	ATP Pocket of inactive conformation, DFG-Asp out	Allosteric inhibitor bound in site adjacent to ATP pocket	Allosteric inhibitor bound in site away from ATP pocket	Covalent inhibitor
<b>Extends into back cleft?</b>	No	Type A: Yes Type B: No	Type A: Yes Type B: No	Yes	No	Variable
<b>DFG-Asp</b>	In	In	Out	Variable	Variable	Variable
<b>Activation loop</b>	Out	Variable	Variable	Variable	Variable	Variable
<b><math>\alpha</math>Helix-C</b>	In	Variable	Variable	Out	Variable	Variable
<b>Spine</b>	In	Distorted	Usually distorted	Distorted	Variable	Variable
<b>ATP-Competitive</b>	Yes	Yes	Yes	No	No	No
<b>Reversible</b>	Yes	Yes	Yes	Yes	Yes	Usually not

**Table 2:** Classification of small molecule protein kinase inhibitors.<sup>58</sup>

Type III reversible inhibitors differ in the fact that they are non-competitive to ATP and instead bind to allosteric sites adjacent to the ATP binding site. These allosteric sites are normally kinase specific and therefore type 3 kinase inhibitors are more selective than competitive inhibitors.<sup>47</sup> TEK-733 is a allosteric Mitogen-activated protein kinase (MEK) 1/2 inhibitor which is currently in phase 1 clinical trials for treatment of patients with advanced solid tumors.<sup>59</sup>

Type IV inhibitors are also allosteric inhibitors; however, they bind to sites which are distant to the ATP cleft. An example of a type IV inhibitor is GNF-2, an antagonist of BCR–Abl, which binds to the myristoyl binding site and stabilizes the inactive enzyme form.<sup>60</sup> A summary of the various kinase inhibitor classifications is shown in **Table 2**

The vast majority of approved kinase inhibitors are in class I and in the current study, we have focused on this class of inhibitor.

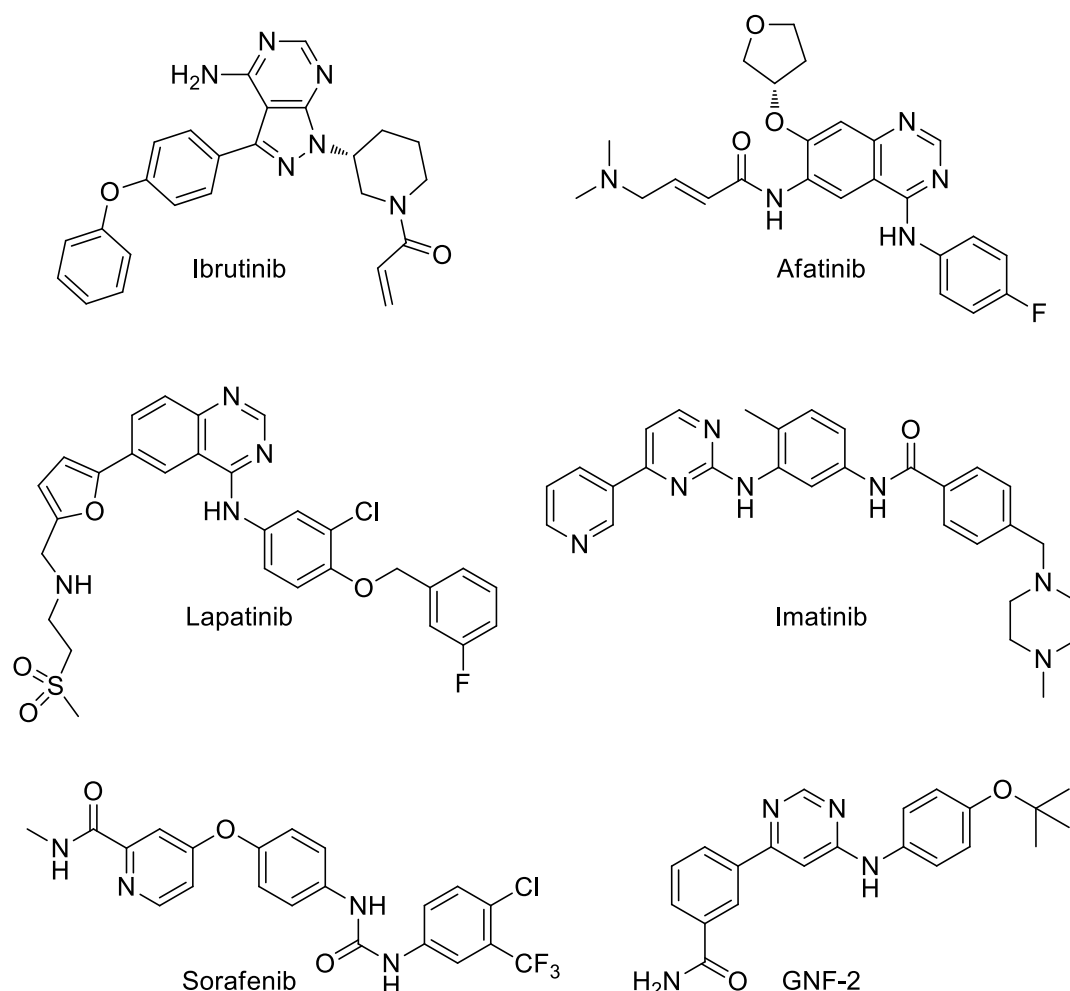


**Figure 8:** Kinase inhibitor compounds.

### **1.2.4 Phosphatidylinositol 3-kinase (PI3K)-Related Protein Kinases (PIKKs)**

During the 1990s a class of kinases known as the phosphatidylinositol 3-kinase (PI3K)-related protein kinase (PIKK) family of proteins were discovered.<sup>61</sup> There are two main defining features of this kinase family;

- All known members are very large, ranging from 280 to 470 kDa in size.
- The kinase domain of PIKK family members is more closely related to the PI3K family of phospholipid kinases (20-25% identity) than other protein serine/threonine or tyrosine kinases.

Although they share structural homology with the PI3K family in their active site, the available evidence suggests that the PIKKs do not target lipids. The primary specificities of the PIKK and PI3K families are different, but due to their similarities in the ATP cleft they likely bring about catalysis by very similar mechanisms.<sup>62</sup> Due to this structural homology it can be challenging to obtain compounds that are selective for one PIKK family member over other PIKKs or the PI3K family of kinases. For example, there are many examples in the literature of dual mTOR/PI3K inhibitors.<sup>63-65</sup> In **Table 3** the PIKK family members are listed along with their established cellular roles.

<b>PIKK</b>	<b>Functions</b>
<b>mTOR</b>	Key regulator of cell growth; believed to modulate cap-dependent translation and through phosphorylation and regulation of 4E-BP1 and S6 kinase. mTOR has also been shown to be involved in transcription, actin organisation, membrane traffic and protein degradation. <sup>66,67</sup>
<b>DNA-PK</b>	Involved in a heterotrimeric holoenzyme complex (DNA-PK). This complex functions to recruit and/or phosphorylate additional NHEJ factors to repair lesions in double stranded DNA.
<b>ATM &amp; ATR</b>	Signallers of genome damage. ATM phosphorylates, and therefore appears to modulate the activities of, the key cell-cycle control proteins p53, BRCA1, NBS1, MDM2, RAD17, and CHK2. ATR acts to delay cell-cycle progression in response to other types of DNA damage, such as those induced by ultraviolet light. ATR is known to target p53, RAD17, BRCA1, and CHK1.
<b>SGM-1</b>	A regulator of nonsense-mediated mRNA decay (NMD). NMD serves to recognise and eliminate mRNA species that contain premature translation termination codons and thus code for non-functional or potentially harmful polypeptides.

**Table 3:** Known cellular functions of PIKKs

## **1.3 Mechanistic Target of Rapamycin (mTOR)**

### **1.3.1 PI3K-AKT-mTOR Pathway**

In normal cells, the PI3K/Akt/mTOR axis is an intracellular signalling pathway which is an important regulator of cell metabolism, proliferation, differentiation and survival.<sup>68</sup> The pathway is deregulated in a number of diseases including: solid tumors,<sup>69</sup> immune mediated diseases<sup>70</sup> and idiopathic pulmonary fibrosis<sup>71</sup> and is therefore an attractive therapeutic target.

The pathway is activated by extracellular growth factors and cytokines, which act as substrates for cell surface tyrosine kinase receptors. The activation of these cell surface receptors activates the p110 catalytic subunit of PI3K. This activation then catalyses the phosphorylation of PIP<sub>2</sub> into PIP<sub>3</sub> which locates Akt at the intracellular membrane where it is phosphorylated by mTORC2.<sup>72</sup> Phosphorylated Akt then has a number of downstream targets including mTORC1, Fox proteins and Bcl-2 anti-apoptotic protein. mTORC1 is arguably the most important downstream target of pAkt, it is an important regulator of protein and lipid biosynthesis, cell cycle progression, proliferation, survival and senescence.<sup>73-76</sup>

The importance of mTOR within this pathway was first established when it was shown that rapamycin had antiproliferative properties caused by its ability to inhibit signalling pathways required for cell growth and proliferation.<sup>77</sup> Recognising this key role, researchers have found that mTOR is involved in many other cellular processes and its central role in regulating diseases such as fibrosis and cancer have established it as a valuable drug target.<sup>78,79</sup> A simplified schematic of the PI3K/Akt/mTOR pathway is shown in **Figure 9**

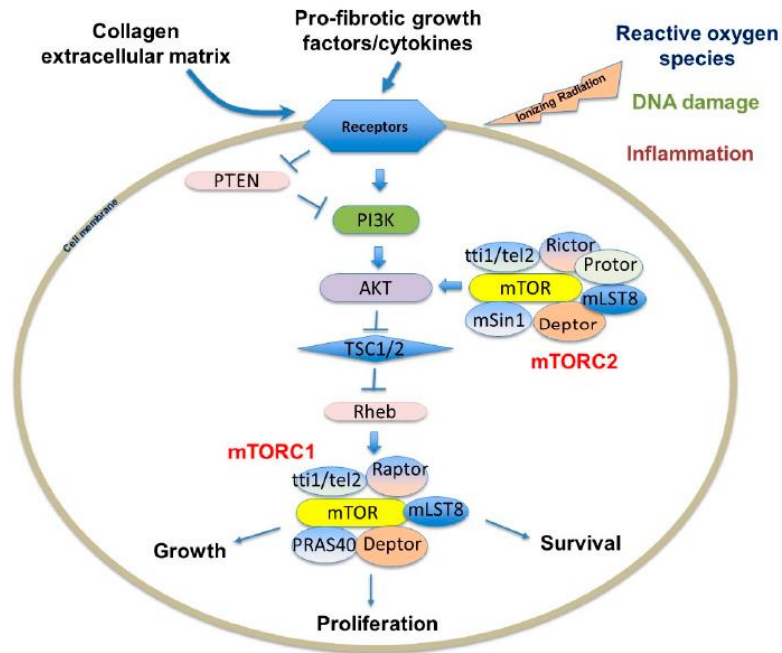


**Figure 9:** Schematic diagram showing the PI3K/Akt/mTOR pathway.<sup>19</sup> The mTORC1 and mTORC2 complexes are shown with their individual sub-units. **mTORC1** is associated with; RAPTOR, mLST8, PRAS40, DEPTOR and the scaffold protein TTI1/TEL2 complex. **mTORC2** is associated with RICTOR, mLST8, mSIN1, protor 1/2, DEPTOR and the scaffold protein TTI1/TEL2 complex.

The mTOR complexes have overlapping and unique sub-units which contribute to signalling activity, the individual roles of these subunits are summarised in **Table 4**



Subunit	Functions
<b>mTORC1 specific</b>	
<b>RAPTOR</b> (Regulatory-associated protein of mTOR)	Facilitates substrate recruitment of 4EBP1 and S6K1 to mTORC1 and is required for the correct subcellular localisation of mTORC1. <sup>80,81</sup>
<b>PRAS40</b> (Proline-rich Akt substrate of 40 kDa)	Inhibitory subunit that interacts with RAPTOR and binds to mTORC1 in insulin deprived cells resulting in inhibition of cell growth. <sup>82</sup>
<b>mTORC2 specific</b>	
<b>RICTOR</b> (Rapamycin-insensitive companion of mTOR)	Responsible for the phosphorylation of Akt at Ser473. This phosphorylation activates Akt and is vital for the PI3K/Akt/mTOR pathway. <sup>72</sup>
<b>Protor 1/2</b>	mTORC2 can function in absence of subunit. Protor-1 has a role in SGK1 activation (a protein kinase that is responsible for ion channel activation). Protor-2 has a role in mRNA stability regulation in stressful environments. <sup>83,84</sup>
<b>mSIN1</b> (mammalian stress-activated protein kinase interacting protein 1)	Responsible for SGK1 phosphorylation. SGK1 is a downstream protein kinase target of mTORC2 responsible for epithelial ion channel activation. <sup>85</sup> mSIN1 is also responsible for mTORC2 inactivation in response to mTORC1 activation, its phosphorylation causes dissociation of mTORC2.
<b>Common to Both mTORC1 and mTORC2</b>	
<b>DEPTOR</b> (DEP domain-containing mTOR-interacting protein)	DEPTOR is an inhibitory subunit which downregulates activity of mTORC1 and mTORC2, however when overexpressed (in some cancers) it can inhibit mTORC1, leading to activation of mTORC2. <sup>86</sup>
<b>TTI1/TEL2</b>	Positive regulator. TTI1/TEL2 is a complex of two proteins that regulate stability of PIKKs. depletion of TTI1/TEL2 causes disassembly of mTOR complexes leading to loss of activity. <sup>87</sup>
<b>mLST8</b> (mammalian lethal with SEC13 protein 8)	Associates with mTOR catalytic domain and stabilises activation loop (A-loop). <sup>88</sup>

**Table 4:** Summary of the sub-units which combine with mTOR to form the complexes mTORC1 and mTORC2.

### **1.3.2 mTOR and Fibrosis**

mTOR signalling is thought to play a central role in the proliferation of various types of fibroblasts in fibrotic conditions. For example, mTOR has been proven to promote keloid fibroblast proliferation.<sup>89</sup> The authors of this study also demonstrated that Palomid 529, a known dual mTORC1/ mTORC2 inhibitor exerted an anti-keloid effects in keloid fibroblasts.<sup>89</sup>

mTOR signalling is also important for cell survival. mTORC2 phosphorylates Akt, which is a key effector of PI3K survival signalling.<sup>72</sup> mTORC1 is also thought to modulate cell survival. Inhibition of mTORC1 can lead to increased autophagy and macropinocytosis, therefore permitting survival in low nutrient conditions.<sup>90</sup> When normal lung fibroblasts are treated with autophagy inhibitors, they become sensitised to collagen matrix driven death. IPF fibroblasts in contrast, maintained a viable phenotype under the same conditions. This study showed that

increased mTOR activity desensitises IPF-fibroblasts to collagen-matrix driven stress by suppressing autophagy, so IPF-fibroblasts remain viable on collagen.

Since mTORC1 activation is known to indirectly inhibit mTORC2 *via* a negative feedback loop the exclusive inhibition of mTORC1 may paradoxically promote cell survival via activation of the PI3K/Akt pathway (**Figure 10**).

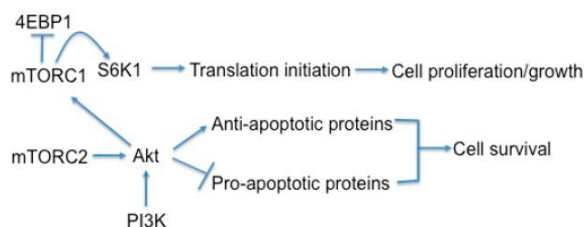


**Figure 10:** The role of mTORC1 and mTORC2 in regulation of cell-growth, proliferation and survival. (arrows indicate positive regulation and T symbols indicate inhibition).<sup>19</sup>

There are a number of other factors which through mTOR signalling lead to fibroblast proliferation and survival, which in turn leads to excessive collagen production. IPF is considered a disease which results from micro-injuries to pneumocytes. This results in insufficient healing and myofibroblast production.<sup>91</sup> Lung injuries lead to inflammation and the release of pro-inflammatory cytokines, in particular TGF- $\beta$  which is considered a primary-player in IPF progression. TGF- $\beta$  can stimulate fibroblast proliferation and collagen deposition through a number of pathways, importantly it is capable of activating the PI3K/Akt/mTOR pathway.<sup>92</sup>

Dysregulated autophagy has already been mentioned as a key factor in cell survival of IPF-fibroblasts. It is thought that when IPF-fibroblasts are cultured on a collagen-rich medium, autophagy is low as a result of high levels of mTOR activation.<sup>93</sup> mTOR inhibition reactivated autophagy in these cells leading to collagen-induced cell death. This provides evidence that normal lung fibroblasts view collagen as an apoptosis-triggering environment whilst IPF-fibroblasts are insensitive to collagen, meaning they continue to be viable and produce further collagen, leading to a progression of IPF symptoms. This tolerance to collagen is thought to be mediated through elevated levels of mTOR activity which alters autophagic activity.<sup>19</sup>

Cellular senescence is a process where cells cease to divide, and is potentially linked to IPF. Senescent cells propagate the senescence-associated secretory phenotype (SASP) which is a complex mixture of cytokines that have been implicated in radiation-induced fibrosis and are associated with mTOR pathways.<sup>73,74,94</sup> It is thought that accelerated senescence plays a role in IPF as it is responsible for depleting epithelial cells and encouraging myofibroblast

differentiation.<sup>95</sup> Importantly, it has been shown that mTORC1 inhibition resulted in decreases SASP cytokines and pneumocyte senescence, resulting in a decrease of fibrosis.<sup>73</sup>

This evidence, taken together provides a solid rationale for inhibition of mTOR as a potential treatment for IPF. In addition to this, histologic analysis of IPF patient lung tissue demonstrated increased mTOR expression. This level of mTOR expression correlated with the degree of fibrosis observed.<sup>96</sup>

Pre-clinical studies have investigated mTOR inhibitors in fibrosis. In one study the mTOR/PI3K inhibitor **GSK2126458 (3)**, which has completed phase 1 oncology trials, was shown to be capable of inhibiting PI3K signalling and functional response in IPF-fibroblasts.<sup>97</sup>

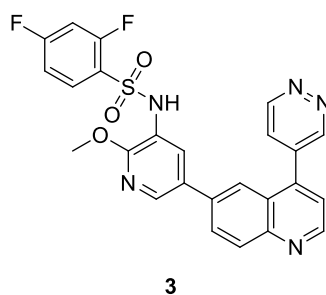


**Figure 11:** Structure of dual PI3K/mTOR inhibitor **GSK2126458**.

A summary of the roles which mTORC1 and mTORC2 have in the development of pulmonary fibrosis is shown in **Figure 12**. mTOR complexes are intricately involved in promoting mechanisms that favour activated lung fibroblast survival and uncontrolled collagen deposition. This provides a very good rationale for targeting mTOR inhibition as a treatment for IPF. It is this aim which is pursued as part of this thesis.

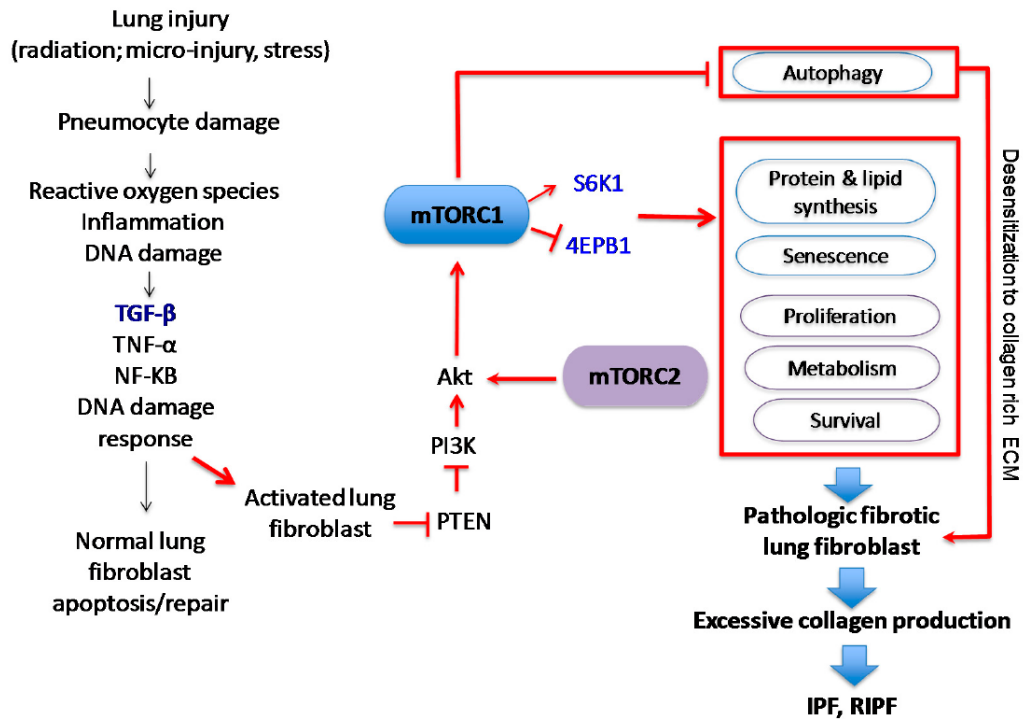
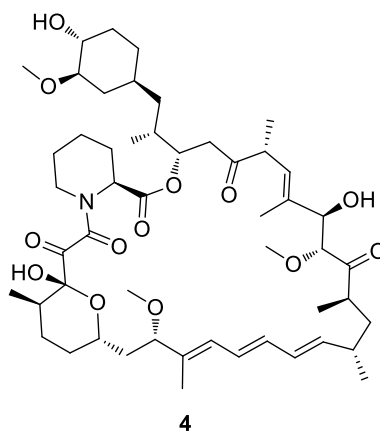


Figure 12: Schematic diagram showing the role of mTOR in the development and progression of IPF.<sup>19</sup>

### 1.3.3 Small Molecule mTOR Inhibitors

The first generation of mTOR inhibitors were based on the natural product rapamycin, which was isolated from *Streptomyces hygroscopicus* in soil samples collected from Easter Island.<sup>98</sup> Rapamycin (Figure 13) is a macrocyclic lactone that contains two binding moieties both required for activity. One moiety binds to FKBP12, which is a protein present in the cytosol with peptidylprolyl isomerase activity. Binding to FKBP12 causes no change to the activity of the enzyme, but allows for formation of a ternary complex with mTOR.<sup>99</sup> The rapamycin-FKBP12 dimer binds mTOR away from the catalytic site and therefore does not directly inhibit kinase activity, it is thought to bind to the FRB domain and displace RAPTOR. As RAPTOR is responsible for recruitment of 4EBP1 and S6K1, rapamycin-FKBP1 binding interferes with the association of mTORC1 with its substrates.<sup>100</sup> Despite the presence of mTOR in both mTORC1 and mTORC2, rapamycin is only active at mTORC1 and it is thought that the unique subunits of mTORC2 (*vide-supra*) prevent rapamycin binding. Rapamycin itself was approved as an immunotherapy treatment in 1997 for use in transplant patients and in 2003 for use in coronary-artery stents.<sup>101</sup>



**Figure 13:** Structure of rapamycin.

Rapamycin has poor solubility, which translates into low oral bioavailability (~14%). To overcome this several analogues of rapamycin, termed rapalogs have been developed. However, this was challenging as both sides of the molecule are responsible for binding. All modifications were by substituting the alcohol at C-40-O with water-solubilising groups (**Figure 14**). In 2007 Temsirolimus became the first rapalog approved by the FDA as a cancer treatment (renal cell carcinoma).<sup>102</sup>

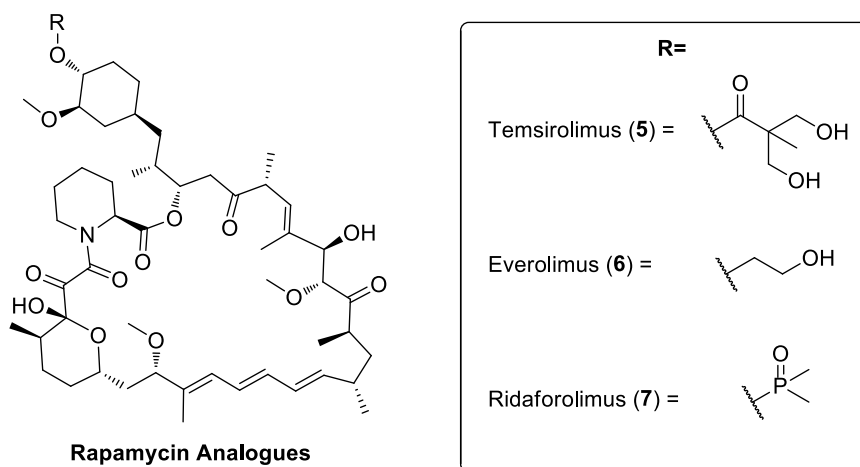


**Figure 14:** Structure of rapalogs.

Rapalogs however, have been met with limited clinical success in a cancer setting and have failed to be effective in the majority of solid tumours.<sup>103</sup> One of the reasons behind this is that mTORC1 inhibition causes upregulation of the PI3K/Akt pathway *via* mTORC2 which promotes cellular survival.<sup>104</sup> One strategy around this is to target the catalytic site of mTOR, as this is present in both mTORC1 and mTORC2 and consequently, inhibitors can block

activity of both complexes, leading to a reduction in the mTORC2 dependent activations of Akt.

The development of ATP-competitive mTOR inhibitors began with PI3K inhibitors, as the structure of the PI3K isoforms has a high degree of homology with mTOR and therefore compounds such as the morpholine-pyrimidine derivative **PI-103**, which was developed as a pan-PI3K compound, was found to also inhibit mTOR.

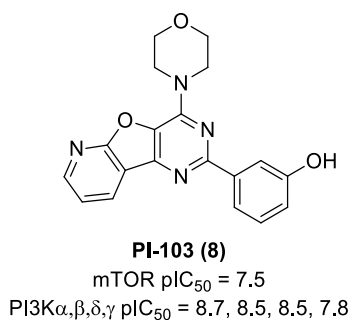


**Figure 15:** Structure of dual PI3K/mTOR inhibitor **PI-103**.

There have been several other inhibitors based on the structure of PI-103 which have dual mTOR/PI3K activity such as GDC-0980 (**9**), GNE-493 (**10**) and GNE-477 (**11**) (**Figure 16**). There is a potential concern around the toxicity of dual PI3K/mTOR inhibitors owing to the diverse functions of the different PI3K isoforms. Because of this, more selective mTOR inhibitors were targeted.

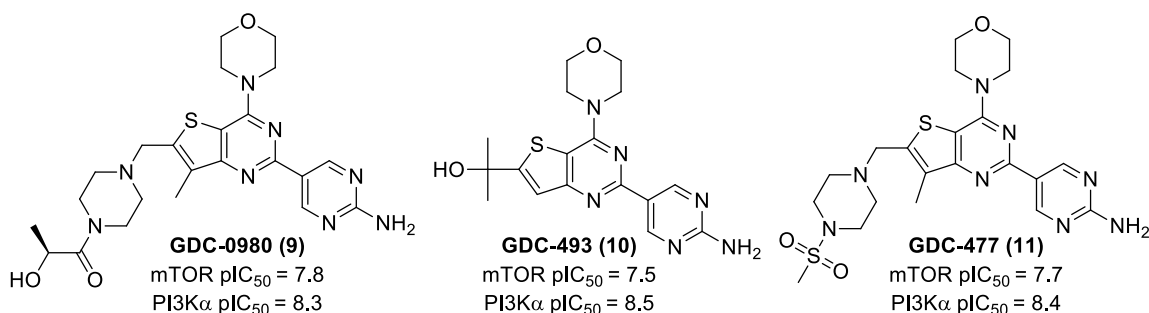


**Figure 16:** Structure of PI3K/mTOR dual inhibitors.

The morpholine-pyrimidine scaffold also proved to be effective in producing inhibitors with selectivity for mTOR. These selective inhibitors include WAY-600 (**12**), WYE-687 (**13**), WYE354 (**14**),<sup>105</sup> KU0063794 (**15**)<sup>106</sup> and AZD8055 (**16**)<sup>107</sup> (**Figure 16**).

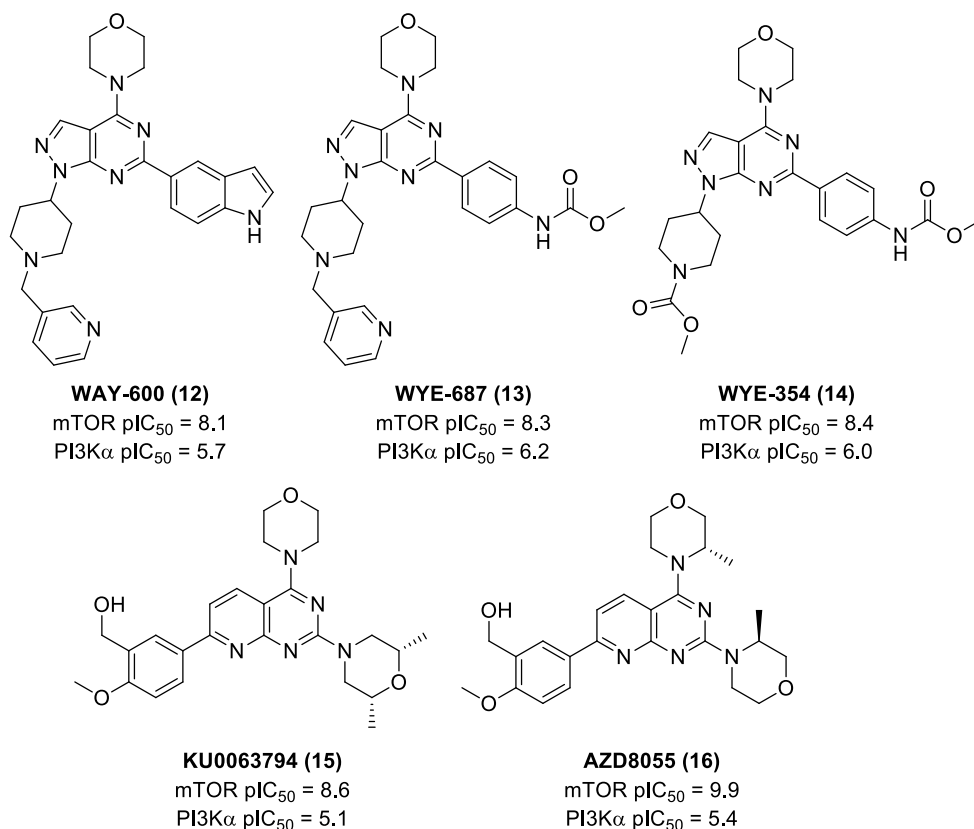


**Figure 17:** mTOR inhibitors with selectivity over PI3K.

In comparison with rapalogs, ATP-competitive mTOR inhibitors are more effective at blocking cell proliferation and inducing apoptosis in tumour models.<sup>108,109</sup> Several ATP-competitive mTOR inhibitors have progressed to clinical trials, including the morpholine-pyrimidine based compound vistusertib (**17**)<sup>110</sup> (**Figure 18**) which is highly selective for mTOR and progressed into phase II clinical trials for numerous cancer indications before being terminated in late 2018.

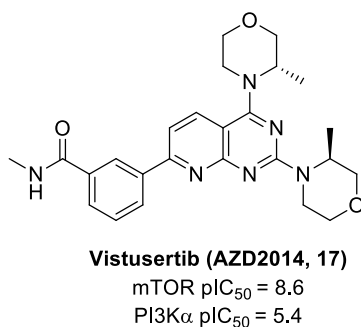


**Figure 18:** Structure of Vistusertib (AZD2014).

The morpholine-pyrimidine core-hinge fragment has proven to be very privileged in mTOR inhibitors. A Scifinder search of this structure in the mTOR kinase space alone produced in excess of 4800 hits. The extensive use of this morpholine-pyrimidine fragment in ATP

competitive mTOR inhibitors means that finding novel alternatives would be advantageous, preferably motifs conferring a potency, selectivity or physicochemical advantage.

## 1.4 Cyclopropylpyran as a novel hinge-binding fragment

### 1.4.1 Importance of Morpholine Hinge Binding Fragment in PIKK Inhibitors

A number of independent lead optimisation programmes have identified 4-(Pyrimidin-4-yl)morpholine as a privileged pharmacophore for lipid kinase and PIKK inhibitors.<sup>107,108,111,112</sup> It has been shown through X-ray co-crystal structures of compounds bound to mTOR (**Figure 19**) that the morpholine oxygen facilitates hydrogen bonding with the backbone of the kinase hinge region. In order for this hydrogen bond to be formed, the morpholine must adopt a co-planar conformation with respect to the core ring of the molecule.<sup>88</sup>

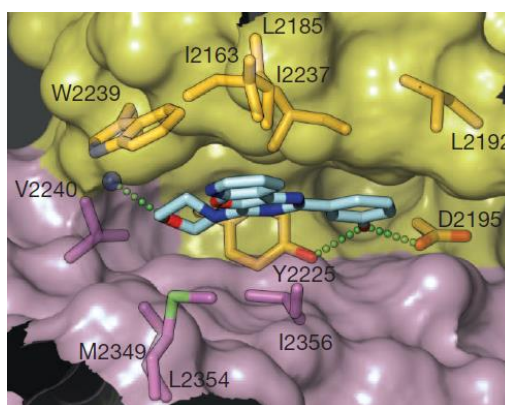


**Figure 19:** X-ray co-crystal structure of **PI-103 (8)** bound to the active site of mTOR.<sup>88</sup> The mTOR cleft is shown in transparent surface representation, with the *N*-lobe in yellow and the *C*-lobe in pink. Green dotted lines indicate atoms within hydrogen-bonding distance.

The co-planar conformation required for efficient hydrogen bonding to the mTOR ATP cleft is favoured for morpholine substituted pyrimidine systems. This has been confirmed by molecular mechanical and quantum mechanical modelling of morpholine-pyrimidine containing compounds (*vide infra*). The conformational preference exhibited by these compounds is thought to be due to a lone pair donation from the morpholine nitrogen into the electron deficient pyrimidine heterocycle forming a stabilising interaction.

Substitution of the morpholine ring has been reported within the literature and is associated with an increase in potency and selectivity for mTOR. 3-(*S*)-Methyl morpholine is frequently utilised and offers a potency and selectivity enhancement over the corresponding unsubstituted



morpholine. Molecular modelling has shown that in mTOR, a small, rigid pocket formed primarily by Trp3339 is correctly positioned to be exploited by the methyl group (**Figure 20**).<sup>113</sup> This pocket is not present in PI3K isoforms and thus confers a selectivity advantage. Similarly, bridged bicyclomorpholines offer a selectivity advantage due to the presence of a larger cavity in this region of mTOR because of a leucine to phenylalanine difference between mTOR and PI3K (*vide infra*).<sup>114</sup>

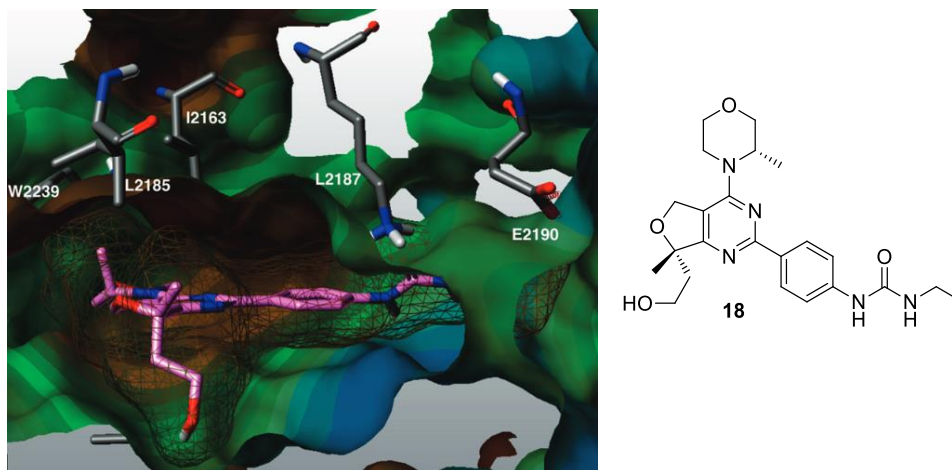


**Figure 20:** Docking study depicting **18** (pink) in the active site of the mTOR homology model with a VdW surface color-coded by lipophilic potential (tan-brown= lipophilic, cyan-blue = polar, green = between lipophilic and polar) added to the protein and with a mesh surface also color-coded by lipophilic potential added to the ligand to show shape and lipophilic complementarity.<sup>113</sup>

### 1.4.2 Discovery of Cyclopropylpyran

Replacements for these morpholine based fragments are desirable due to their widely reported use in ATP competitive mTOR inhibitors. Previous attempts to replace the morpholine hinge binding fragment have been limited to heteroaromatic rings or one report of a dihydropyran (DHP) fragment (*vide infra*). Despite maintaining good cross-kinome selectivity, the DHP has not been widely utilised in the literature, presumably due to its reduced Fsp<sup>3</sup> character, poor solubility profile and potential chemical or metabolic reactivity.

With these previous results, the efforts in our laboratory aimed to discover an alternative hinge binding fragment that fulfilled the following criteria:

- Maintained an mTOR potency comparable to morpholine through adoption of, or at least access to, a favourable co-planar conformation.

- Maintained a similar level of selectivity for mTOR over the PI3K isoforms as 3-methyl morpholine.
- Offered an improved or differentiated physicochemical profile.
- Unreported within the literature in order to impart additional novelty to emerging compounds.

With these criteria in mind, a number of potential hinge binding fragments were considered based on structure **19** (Figure 21). The most synthetically tractable of these was cyclopropylpyran **20** and therefore synthetic efforts were undertaken within our laboratories to furnish this hinge binding fragment.<sup>115</sup>

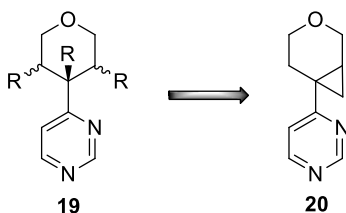


**Figure 21:** Cyclopropylpyran hinge binding fragment.

It was initially proposed that the cyclopropylpyran hinge binding fragment would have little conformational preference and therefore there would be a negligible energy penalty associated with adopting the desired, co-planar active conformation. It was thought that this would lead to comparable potency of cyclopropylpyran-containing compounds to their morpholine-containing matched pairs. In addition to this the CH<sub>2</sub> moiety of the cyclopropyl ring has the potential to occupy a similar region of the mTOR active site to the methyl group of 3-(*S*)-methyl morpholine suggesting comparable levels of selectivity were also feasible.

Additionally, it was thought that the inclusion of cyclopropylpyran would improve physicochemical properties such as solubility due to an increase in fraction sp<sup>3</sup> (Fsp<sup>3</sup>). Fsp<sup>3</sup> is a measure of saturation and is defined as the number of sp<sup>3</sup> hybridized carbons divided by the total carbon count. This metric has been shown to be associated with improved solubility, selectivity and developability of drug-like molecules.<sup>116,117</sup>

Cyclopropylpyran, to the best of our knowledge has never been included within a drug and therefore the cyclopropylpyran hinge binding fragment increases the novelty of compounds in which it is contained. This is advantageous given the crowded patent space surrounding mTOR/PI3K inhibitors meaning that, even if an effective compound is developed it may not be possible to patent the compound.

Whilst cyclopropylpyran has not previously been included in a drug compound, the aza-analogue, 3-azabicyclo[4.1.0]heptane, is a structural motif that is included in a number of triple reuptake inhibitors for treatment of depression. For example, the GSK developed compound GSK1360707 (**21**) is a potent and selective triple reuptake inhibitor.<sup>118</sup> The compound was halted in phase I clinical trials for strategic reasons.<sup>119</sup> It is interesting to note the orthogonal conformation observed between the two rings in the X-ray crystal structure of this compound (**Figure 22**).<sup>120</sup>

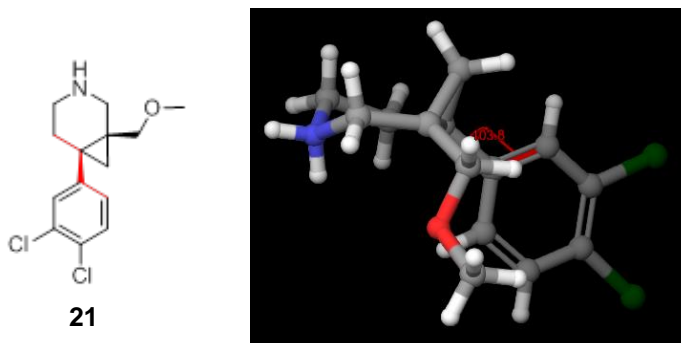


**Figure 22:** Structure of triple reuptake inhibitor GSK1360707 (**21**) and X-ray crystal structure<sup>120</sup> of GSK1360707 (**21**) L-tartrate (counter anion omitted for clarity). The dihedral angle highlighted in red on the structure was measured at 103.8 °.

### 1.4.3 Dihedral Angle Scanning Study of Cyclopropylpyran

In order to further understand the cyclopropylpyran fragment and its likely conformational preferences, a series of dihedral angle scans were carried out using DFT calculations. Firstly, dihedral angle scans of morpholine, DHP and THP were compared to CPP (**Figure 23**).<sup>121</sup>

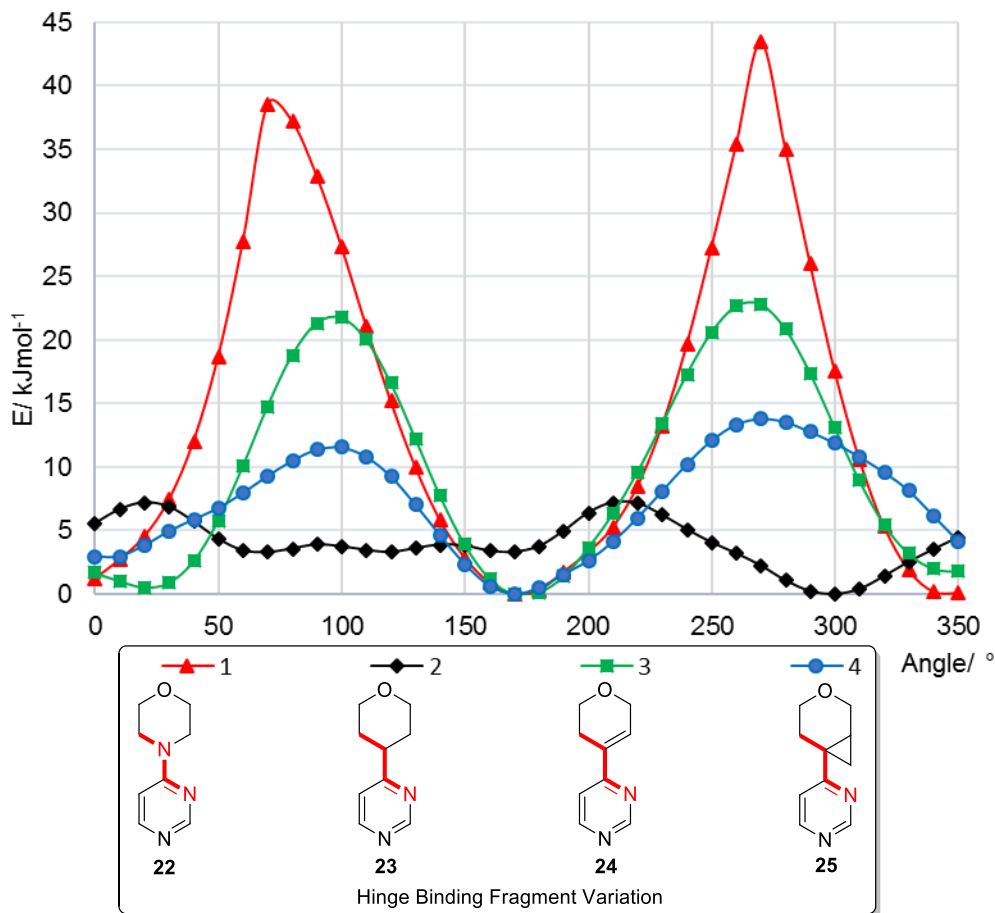


**Figure 23:** Dihedral angle scanning plot for hinge binding fragment variation.<sup>121</sup>

Dihedral angle scanning was performed using Density Functional Theory (DFT/6-31G\*\*/B3LYP). The DFT calculations are carried out using Jaguar.<sup>122</sup> Prior to the scan the molecules were drawn using the Molecule Editor in MOE<sup>123</sup> and all of the compounds were minimized using the MMFX94 force-field. The dihedral angles, highlighted in bold red on structures **22-25**, were rotated incrementally by an angle of 10° and for each increment, energy minimization of the conformation was performed. The procedure was performed until a complete rotation of 360° was achieved. This provided the relative energy profiles shown in **Figure 23**.

The dihedral angle scan suggests a co-planar conformation with a large rotational energy barrier (40 kJmol<sup>-1</sup>) is predicted for morpholine **22** which is attributed to interaction of the nitrogen non-bonded electron pair with the pyrimidine  $\pi$ -system. Conjugation between the C=C bond in DHP **24** also results a co-planar conformation whereas the tetrahydropyran **23** is predicted to exhibit a limited preference for an orthogonal conformation.

Cyclopropyl C-C bonds are known to display similarities to alkene bonds.<sup>124</sup> The Walsh cyclopropane molecular orbitals (MOs)<sup>125,126</sup> describe 3 occupied orbitals;  $\sigma$  and quasi- $\pi$  ( $e_s/e_a$ ) and these orbitals are reminiscent of the  $\sigma$  and  $\pi$  orbitals which make up an alkene C=C bond (**Figure 24**).<sup>127</sup> Due to this similarity, cyclopropyl rings may interact with adjacent  $\pi$ -systems when in the appropriate conformation.

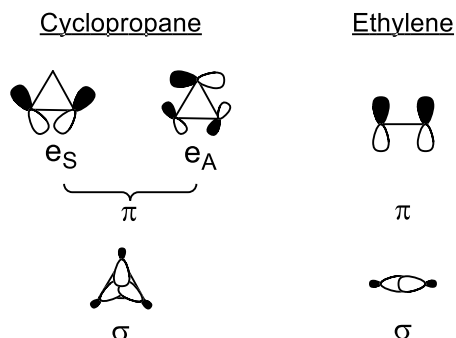


**Figure 24:** Bonding molecular orbital (MO) description of bonding in cyclopropane and ethylene.<sup>127</sup>

This highlights the similarities between the bonding of cyclopropane and ethylene. The bonding MO's in cyclopropane are made up of linear combination of three  $sp^2$ -hybridised atomic orbitals (AOs), while the other two ( $e_s$  and  $e_a$ ) are degenerate linear combinations of three p-AOs differing only in their symmetry properties. This picture is strongly reminiscent of the most common description of a C=C double-bond by two occupied MOs, one linear combination each of two  $sp^2$  AOs ( $\sigma$ -MO) and two p AOs ( $\pi$ -MO).

Accordingly, DFT calculations predict a co-planar conformation for CPP **25**, and it is reasonable that electronic overlap may contribute towards stabilisation of a co-planar conformation (**Figure 25**). This interaction is less stabilising in nature than the corresponding alkene which may account for the difference in rotational barrier height between **24** and **25**.

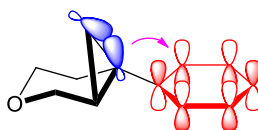


**Figure 25:** Pictorial representation of stabilising overlap between cyclopropane and aryl ring systems.

Cyclopropyl rings are efficient  $\pi$ -donors and poor  $\pi$ -acceptors, therefore interaction with an adjacent  $\pi$ -system is likely to be highly dependent on the electronic nature of the aryl ring. The dihedral angle scan of compounds **25-30** (**Figure 26**) shows how the most electron-deficient pyrimidine cores (**25** and **26**) have low energy co-planar conformations, suggesting donation from the cyclopropyl ring into the pyrimidine  $\pi$ -system. This effect is also predicted for 2-

pyridine **27**. In this case, the barrier height is lower which suggests stabilization from  $\pi$ -donation is less profound. Conversely, 4-pyridine **29**, which is electronically analogous to 2-pyridine **27**, has low-energy orthogonal conformations. It is proposed that in this case stabilizing  $\pi$ -donation is countered by steric destabilization arising from two adjacent aryl hydrogen atoms. A similar result is obtained for the 3-pyridine **28** and phenyl **30** analogues; however, it is notable that the co-planar conformation is significantly less favorable than for 4-pyridine **29** which may be due to weaker  $\pi$ -donation into these ring systems.

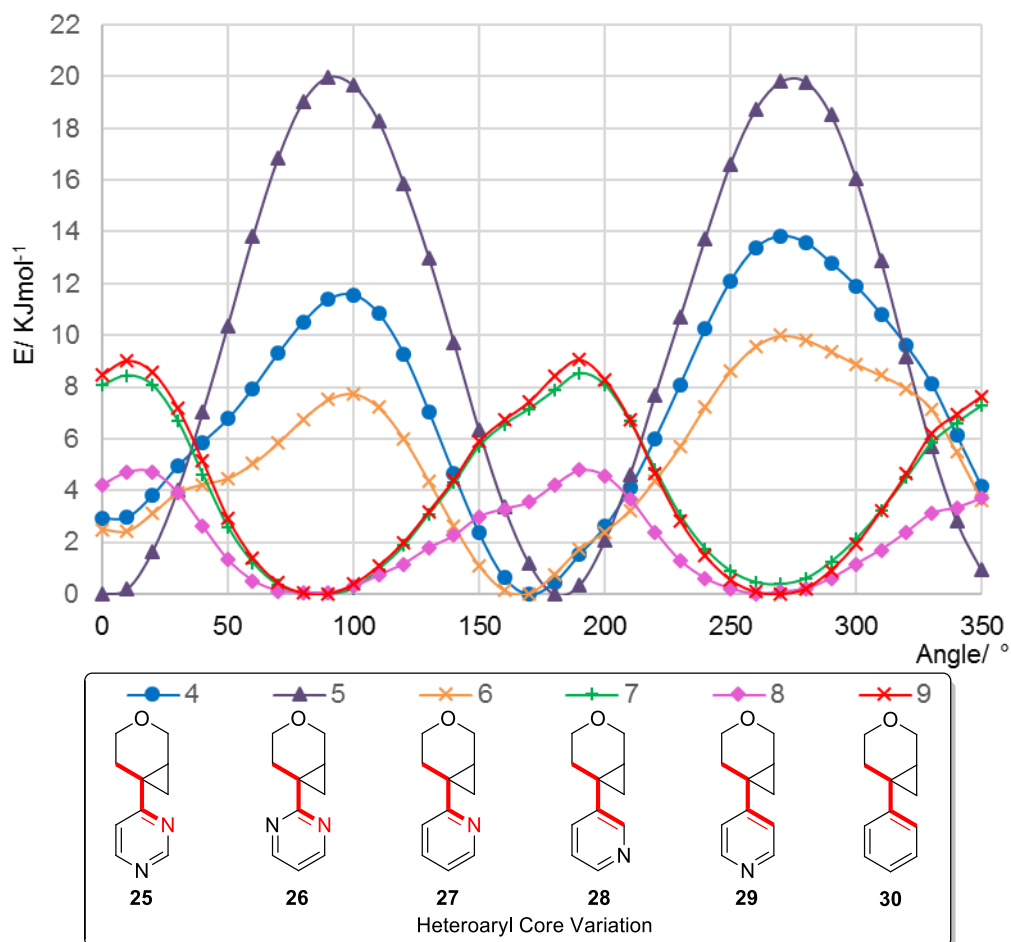


Figure 26: Dihedral angle scanning plot for heteroaryl ring variation 25-30.<sup>121</sup>

## 2. Results and Discussion

### 2.1 Project Aims

In order to further our understanding of the properties of cyclopropylpyran in the context of its use as a PIKK hinge binding fragment, synthesis of a selection of tool compounds was required. The purpose of these tool compounds is to enable the properties of cyclopropylpyran

to be studied in greater detail. Compounds which have been investigated by DFT studies will have their conformational preferences investigated utilising;

- Small molecule X-ray crystallography to probe solid-state conformation. This will be supported by NOE NMR studies to probe conformation in solution.
- Biological and physicochemical assays in order to further understand how conformational preference effects target activity and physicochemical properties.
- Protein co-crystal studies to confirm cyclopropylpyran compound binding conformation in lipid kinases.
- Further computational studies to further elucidate the factors which contribute to conformational bias of the cyclopropylpyran hinge binding fragment.

The overarching aim is to use the results obtained within this chapter to increase our understanding of the cyclopropylpyran hinge binding fragment, in order to enable effective utilisation of this compound within a series of mTOR inhibitors. Further to this, it is anticipated that this work will inform the medicinal chemist on situations in which cyclopropylpyran may be an appropriate alternative to an *N*-aryl amine, both in the context of PIKK inhibition and more widely in drug discovery.

## **2.2 Tool Compounds**

### **2.2.1 Tool Compound Selection**

In order to further investigate the cyclopropylpyran hinge binding fragment, a series of tool compounds were considered. Firstly, a suite of matched pair compounds were targeted in which the hinge binding ring was varied (**Figure 26**). These compounds were based on a 2-pyridine core ring, which despite not being widely reported within the literature, was predicted to occupy a co-planar conformation with cyclopropylpyran (**Figure 23**, Compound **27**). This 2-pyridyl fragment has also been applied successfully elsewhere within our laboratory.<sup>128</sup> As this pyridine ring is less electron-deficient than pyrimidine, the behaviour of CPP with this core heterocycle is a more robust challenge of its propensity to occupy a low energy co-planar conformation therefore conformational analysis was performed on this matched suite of compounds (**31-34**). Morpholine **31** and DHP **32** are included to compare biological and physicochemical properties whilst the THP **33**, which is expected to be a poor hinge binding fragment, was included in order to compare the low energy conformation to that of CPP **34**. The compounds have a 3-phenol ring in the 6-position of the pyridine ring. This is a known

pan-lipid kinase back-pocket,<sup>129</sup> and therefore was included to give the tool compounds measurable potency within *in vitro* biological assays.

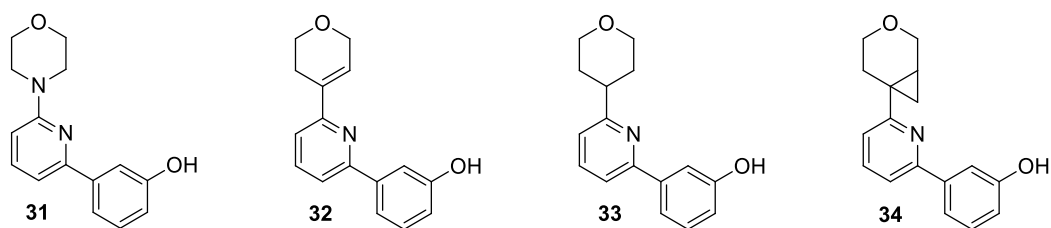


**Figure 27:** 2-pyridyl hinge binding fragment variation tool compounds **31-34**.

A matched set of 4-pyrimidine compounds was also synthesised (**Figure 28**). As this pyrimidine-morpholine fragment is extensively reported upon within the literature (*vide infra*) it was suspected that this set of compounds would show the highest levels of target engagement and therefore offer the most pertinent biological comparison of the hinge binding fragments.

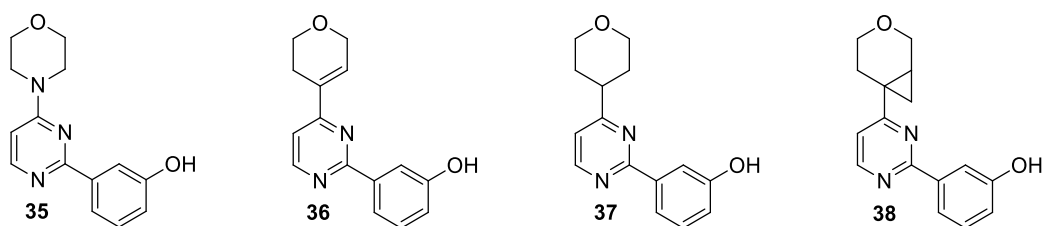


**Figure 28:** 4-pyrimidyl hinge binding fragment variation tool compounds **35-38**.

In addition to this, a selection of 6-membered heterocyclic core rings coupled with the CPP hinge binding motif were also synthesised to enable investigation into the properties of CPP whilst coupled to heterocycles with a range of electronic and steric profiles. The compounds selected for synthesis are outlined in **Figure 29**. All of the compounds **39-41** were combined with the 3-phenol backpocket group. CPP-benzene was combined with a 4-ethyl urea backpocket group, which is a commonly reported mTOR inhibitor backpocket, to give compound **42**. This was in order to give a less lipophilic compound which could ultimately be crystallised.



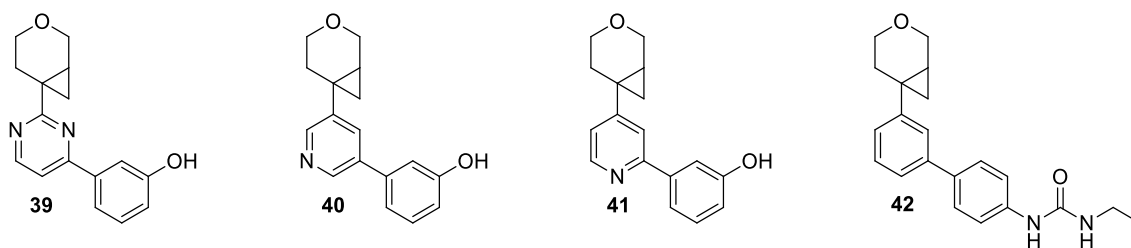
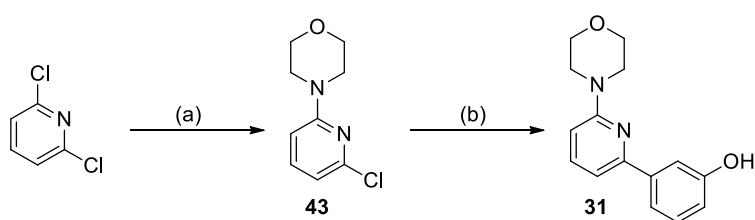


**Figure 29:** 6-membered heterocyclic variation tool compounds **39-42**.

### 2.2.2 Tool Compound Synthesis

Morpholine containing compounds **31** and **35** were synthesised *via* a two-step process which involves a nucleophilic displacement of a halogen on a core aromatic ring with morpholine, followed by addition of the 3-phenol backpocket by Suzuki-Miyaura cross-coupling. For the 2-pyridyl compound **31** a nucleophilic substitution was performed on 2,6 dichloropyridine in neat morpholine, and this furnished morpholine intermediate **43** in good yield (77%) following chromatographic purification to remove a minor *bis*-morpholine side product (8% of reaction mixture by LCMS analysis). Despite the large excess of the morpholine nucleophile the *bis*-product was expected to be formed only in small quantities as addition of the initial morpholine increases the electron density of the aromatic system, therefore making it less susceptible to further  $S_NAr$  reactivity.<sup>130</sup> Intermediate **43** underwent Suzuki Miyaura cross-coupling with 3-(4,4,5,5-tetramethyl-1,3-dioxolan-2-yl)phenol installed the 3-phenol backpocket in good yield to give tool compound **31** (**Scheme 1**).

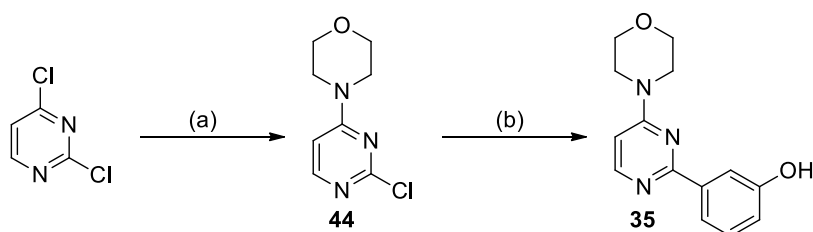


(a) Morpholine (neat), 100 °C, 3 h. 77% yield (b) ) 3-(4,4,5,5-tetramethyl-1,3,2-dioxaborolan-2-yl)phenol, Pd(dppf)Cl<sub>2</sub>.CH<sub>2</sub>Cl<sub>2</sub>, K<sub>2</sub>CO<sub>3</sub>, 2-propanol/H<sub>2</sub>O (5:1) 100 °C, 16 h. 65% yield

**Scheme 1:** Synthesis of Compound **31**.

The 4-pyrimidyl tool compound **35** was synthesised in an analogous fashion. 2,4-Dichloropyrimidine was treated with morpholine and DIPEA in DMF and stirred at room temperature for 1 h. The desired 4-(2-chloropyrimidin-4-yl)morpholine **44** is expected to be

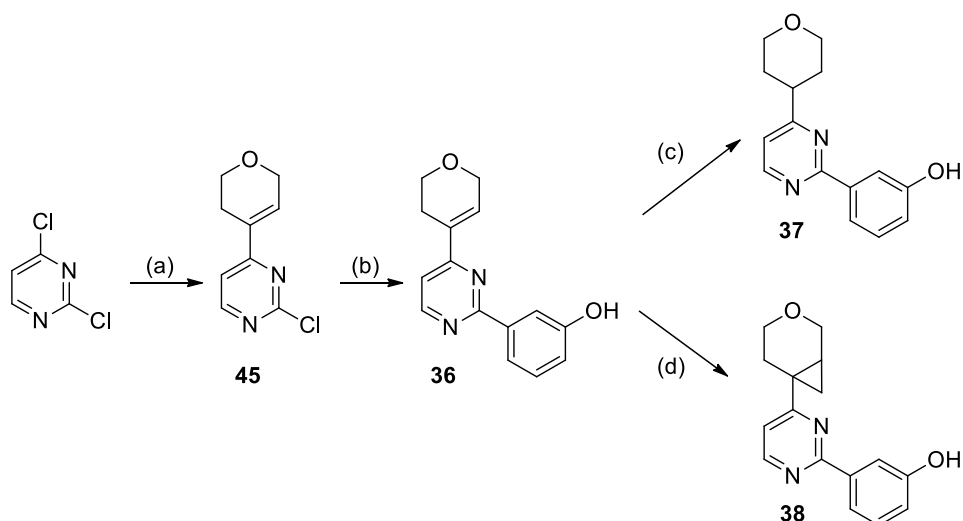
the major product.<sup>131,132</sup> This is because in general, chloride is more easily displaced at C-4 than C-2. In our hands the reaction proceeded with 4:1 selectivity (determined by LCMS) for the desired regioisomer and the desired product **44** was isolated in 75% yield following column chromatography. The 3-phenol backpacket moiety was added by a Suzuki-Miyaura cross-coupling to give **35** in 42% yield (**Scheme 2**). As the focus of this project was to analyse the final products, attempts to improve the yield of this reaction were not undertaken as sufficient quantities of the target compound could be obtained.



(a) Morpholine, DIPEA, DMF, 1 h. r.t. 70% yield (b) -(4,4,5,5-tetramethyl-1,3,2-dioxaborolan-2-yl)phenol, Pd(dppf)Cl<sub>2</sub>.CH<sub>2</sub>Cl<sub>2</sub>, K<sub>2</sub>CO<sub>3</sub>, 2-propanol/H<sub>2</sub>O (5:1) 100 °C, 16 h. 42% yield

**Scheme 2:** Synthesis of Compound **35**.

For CPP, DHP and THP containing compounds, it was initially envisaged that all compounds could be furnished from a common intermediate *via* a divergent synthesis. For 4-pyrimidine compounds **36-38** this proved possible (**Scheme 3**). In this case, the use of the DHP compound **38** as a common intermediate enabled synthesis of THP **37** and CPP **38** in a more efficient manner than linear synthesis would allow.



(a) 2-(3,6-dihydro-2*H*-pyran-4-yl)-4,4,5,5-tetramethyl-1,3,2-dioxaborolane, Pd(PPh<sub>3</sub>)<sub>4</sub>, K<sub>2</sub>CO<sub>3</sub>, toluene/DMF (9:1), 120 °C,  $\mu$ Wave, 4 h, 38% yield (b) 3-(4,4,5,5-tetramethyl-1,3,2-dioxaborolan-2-yl)phenol, Pd(dppf)Cl<sub>2</sub>.CH<sub>2</sub>Cl<sub>2</sub>, K<sub>2</sub>CO<sub>3</sub>, 2-propanol/H<sub>2</sub>O (5:1) 100 °C,  $\mu$ Wave, 1 h. 70% yield; (c) COware apparatus, Pd (5% on carbon), AcOH, Zn-Powder, 4M HCl, r.t.- 50 °C, 20 h. 46% yield (d) NaH, Me<sub>3</sub>SOCl, DMSO, 65 °C, 4 h., 18% yield.

**Scheme 3:** Divergent chemical synthesis of compound **36-38**.

For the formation of THP compound **37**, CO-ware apparatus<sup>133</sup> was used (**Figure 30**). In this procedure, hydrogen gas is generated from hydrochloric acid and zinc, this increases safety as no external hydrogen gas source is needed. The reaction to form compound **37** proceeded well although the isolated yield was significantly lower than expected (46%). This was not further investigated on this fragment as sufficient product was isolated.

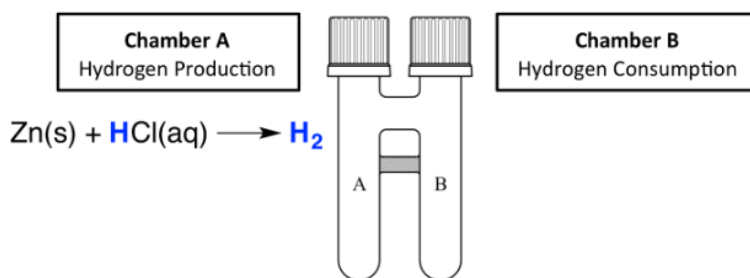
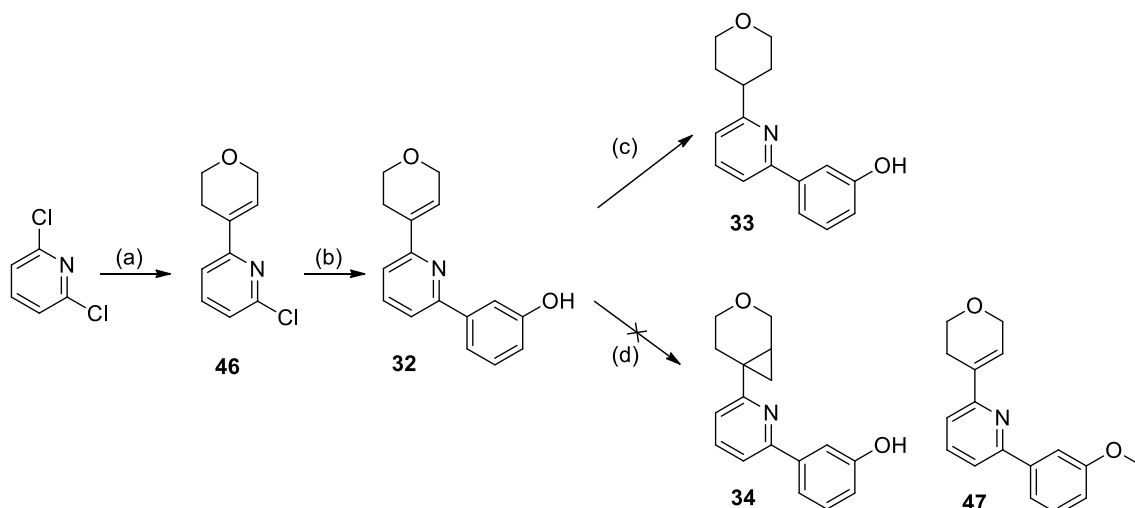


**Figure 30:** Two-chamber system (COware), in which hydrogen gas is generated in chamber A by reacting aqueous HCl with granular metallic zinc. The produced gaseous hydrogen was utilized directly in a hydrogenation reaction in Chamber B.<sup>133</sup>

CPP-pyrimidine **38** was formed *via* a nucleophilic cyclopropanation utilising Corey-Chaykovsky derived chemistry<sup>134</sup> which was identified as an alternative route by other members of our laboratory<sup>128</sup> after failure of Simmons-Smith cyclopropanation chemistry suggested that the alkene was electron-deficient in nature. LCMS analysis indicated that this reaction contained a complex mixture of components and purification was problematic due to close running impurities in both normal and reverse phase chromatography. Despite this, an adequate yield (18%) of desired product was obtained to enable conformational studies.

An analogous, divergent synthesis was initially pursued in order to furnish 2-pyridyl compounds **32-34**. Whilst DHP **32** and THP **33** were both synthesised following this methodology in similar or improved yield compared with the corresponding 4-pyrimidyl compounds, subjecting DHP **32** to Corey-Chaykovsky cyclopropanation conditions however, afforded no desired product and instead the undesired methylated phenolic ether side product **47** was formed; this is most likely due to the increased electron density of pyridine compared to pyrimidine.

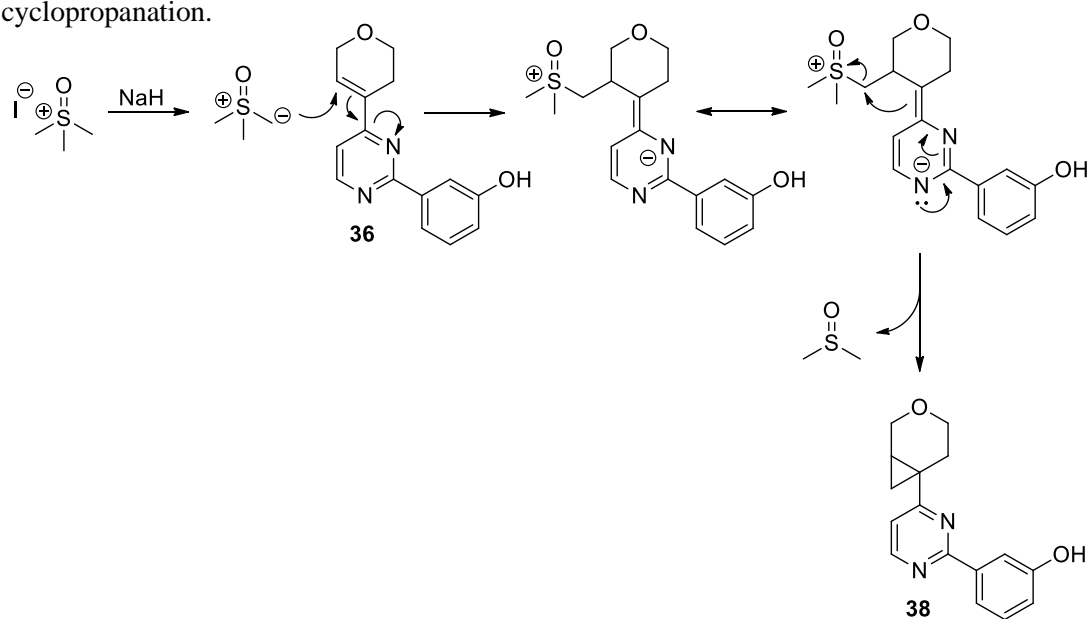


2-(3,6-dihydro-2*H*-pyran-4-yl)-4,4,5,5-tetramethyl-1,3,2-dioxaborolane, Pd(dppf)Cl<sub>2</sub>.CH<sub>2</sub>Cl<sub>2</sub>, K<sub>2</sub>CO<sub>3</sub>, 2-propanol/H<sub>2</sub>O (5:1), r.t., 16 h. 60 % yield; (b) 3-(4,4,5,5-tetramethyl-1,3,2-dioxaborolan-2-yl)phenol, Pd(dppf)Cl<sub>2</sub>.CH<sub>2</sub>Cl<sub>2</sub>, K<sub>2</sub>CO<sub>3</sub>, 2-propanol/H<sub>2</sub>O (5:1) 100 °C,  $\mu$ Wave, 1 h, 51% yield; (c) COware apparatus, Pd (5% on carbon), AcOH, Zn-Powder, 4M HCl., r.t.- 50 °C, 4 h. 70% yield; (d) NaH, Me<sub>3</sub>SOCl, DMSO, 65 °C, 4 h, 0% yield, 38% yield of undesired **47**.

**Scheme 4:** Attempted divergent chemical synthesis of compound **32-34**.

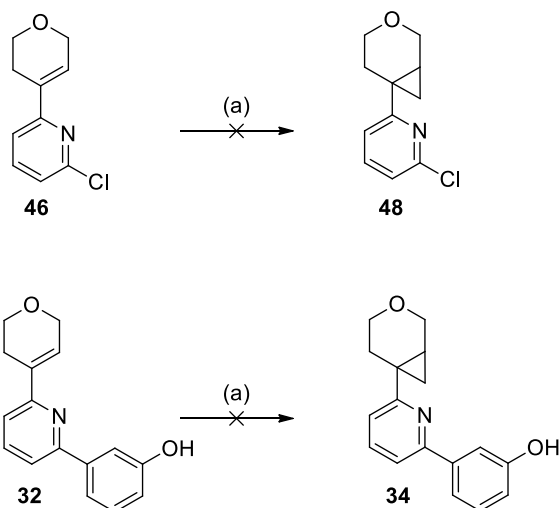
The mechanism for Corey-Chaykovsky cyclopropanation is shown in **Scheme 5**. The classical substrate for this type of reaction is an  $\alpha$ ,  $\beta$ -unsaturated carbonyl, however in the current study we postulate that the reaction proceeds *via* an anion intermediate. This intermediate anion can be resonance-stabilised in the pyrimidine ring and therefore the reaction is able to proceed

more readily than with pyridine. This is not the case with pyridine and we postulated that the alkene in DHP **32** has an insufficient level of electron deficiency to undergo nucleophilic cyclopropanation.



**Scheme 5:** Proposed mechanism for Corey-Chaykovsky cyclopropanation of DHP **36** to form CPP **38**. Note the intermediate anion resonance stabilisation. It is postulated that this stabilisation enables the reaction to proceed and lack of stabilisation is behind failure of DHP **32** to undergo analogous chemistry.

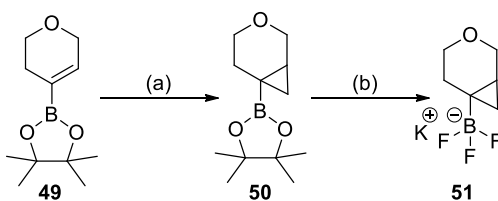
The failure of the Corey-Chaykovsky cyclopropanation chemistry on pyridine **32** raised some questions on the nature of the alkene double-bond in this pyridine-DHP system. It had been assumed that the double bond in **32** would be too electron-deficient to engage in electrophilic Simmons-Smith chemistry.<sup>135,136</sup> However the disparity between reactivity of 4-pyrimidine **36** and 2-pyridine **32** with respect to nucleophilic cyclopropanation suggested that the alkene in 2-pyridine **32** had increased electron density. A Simmons-Smith reaction was therefore attempted on DHP **32** and the precursor **46** (**Scheme 6**). Unfortunately, no product was observed in either reaction, and work-up returned starting material.



(a)  $\text{Et}_2\text{Zn}$  (15% wt. in toluene) (1.5 eq.),  $\text{CH}_2\text{I}_2$  (1.5 eq.), toluene, r.t-  $50^\circ\text{C}$  up to 30 h, no desired product.

**Scheme 6:** Failed attempts at Simmons-Smith cyclopropanation chemistry on compounds **46** and **34**.

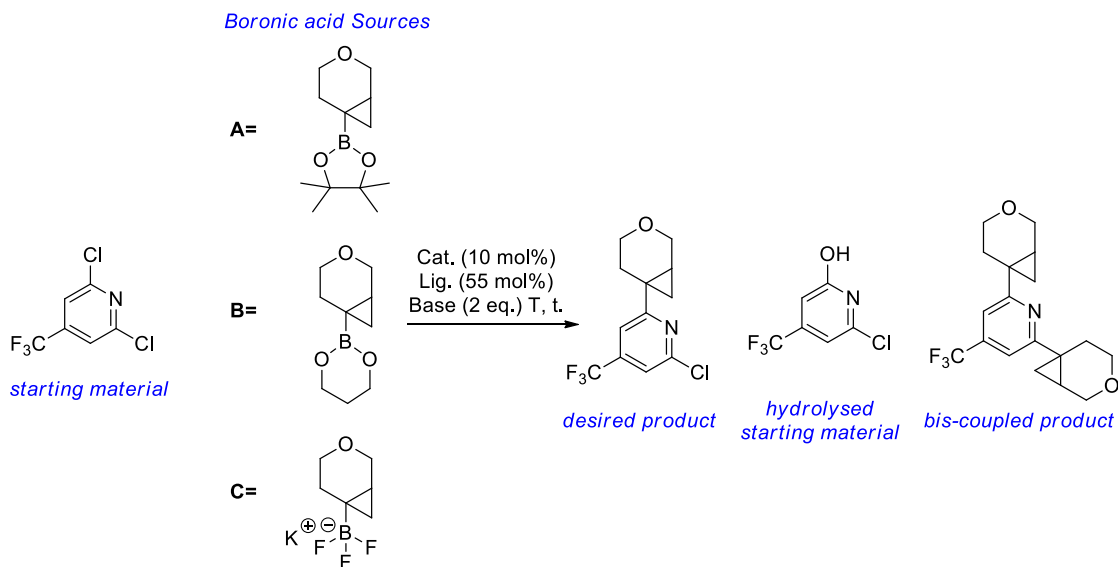
Due to the failure of attempts to cyclopropanate DHP **32** an alternative synthesis was required for CPP **34** and related CPP compounds **39-42**. The cyclopropylpyran building block **51** was synthesized by Simmons-Smith cyclopropanation of commercially available DHP pinacol boronate **49** to obtain cyclopropylpyran pinacol boronate **50**. This was followed by conversion to the corresponding trifluoroborate salt **51** utilizing modified non-etching conditions (**Scheme 7**).<sup>137</sup> Trifluoroborate salt **51** is a coupling partner suitable for  $\text{sp}^2\text{-sp}^3$  Suzuki-Miyaura cross coupling and conditions have been reported in the literature for Pd-mediated coupling of similar compounds.<sup>138</sup>



(a)  $\text{Et}_2\text{Zn}$ ,  $\text{ICl}_2\text{Cl}$ ,  $\text{C}_6\text{H}_5\text{F}$ ,  $-5^\circ\text{C}$ , 5 h, 78% yield; (b)  $\text{KF}_{(\text{aq})}$ , *L*-(+)-tartaric acid, MeCN/MeOH (1:1) r.t. 0.5 h, 100%

**Scheme 7:** Synthesis of trifluoroborate **51**.

A screen of conditions for this reaction carried out by another member of our laboratory for a related substrate (**Table 5**)<sup>139</sup> identified a procedure very similar to previous reports in the literature. In this screen, it was established that the PdCl<sub>2</sub>(dppf).CH<sub>2</sub>Cl<sub>2</sub> adduct was a good catalyst for this coupling reaction (**entry 1-5**). Potassium trifluoroborate **51** is the most efficient coupling partner (**entry 5 vs. entry 3 and 4**). As in the literature, The Pd(OAc)<sub>2</sub>/CataCXium<sup>®</sup> system is the most efficient catalyst for this transformation. This catalytic system is so efficient that complete conversion to the *bis*-coupled product is observed within 4 hours (**entry 6**). This over-reactivity can be controlled by reducing the stoichiometry of potassium trifluoroborate **51**, and we have carried out analogous coupling reactions using ~1.2 eq. of potassium trifluoroborate in which acceptable yields of the desired product are achieved.



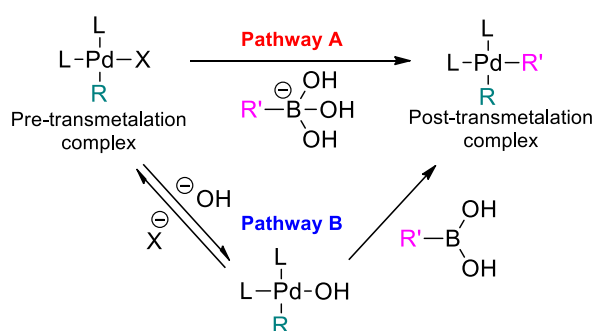
Entry	Boron	Cat./Ligand	Base	Temp (°C)	Solvent System	T (h)	Desired Product	SM	Hydrol SM	Bis-Prod.
1	A	PdCl <sub>2</sub> (dppf) CH <sub>2</sub> Cl <sub>2</sub> adduct	CsOH	120	THF/H <sub>2</sub> O (10:1)	3.5	39%	3%	9%	7%
						18.5	42%	2%	11%	8%
2	B	PdCl <sub>2</sub> (dppf) CH <sub>2</sub> Cl <sub>2</sub> adduct	CsOH	120	THF/H <sub>2</sub> O (10:1)	2	20%	45%	16%	3%
						6	17%	33%	12%	3%
						19.5	50%	14%	7%	7%
3	A	PdCl <sub>2</sub> (dppf) CH <sub>2</sub> Cl <sub>2</sub> adduct	CsOH	80	THF/H <sub>2</sub> O (10:1)	4.5	50%	12%	8%	7%
						19.5	53%	8%	7%	8%
						2	41%	11%	17%	4%
4	B	PdCl <sub>2</sub> (dppf) CH <sub>2</sub> Cl <sub>2</sub> adduct	CsOH	80	THF/H <sub>2</sub> O (10:1)	4.5	42%	9%	17%	7%
						19.5	40%	5%	20%	9%
						6	66%	1%	0%	11%
6	C	Pd(OAc) <sub>2</sub> , cataCXium <sup>®</sup> A	Cs <sub>2</sub> CO <sub>3</sub>	80	Tol./H <sub>2</sub> O (10:1)	1.5	9%	0%	0%	73%
						2.5	7%	0%	0%	93%
						4	0%	0%	0%	100%
						6	0%	0%	0%	94%

**Table 5:** LCMS analysis of trial Suzuki-Miyaura cross coupling reactions with CPP boronates. Carried out by another member of our laboratory.<sup>139</sup>

Formation of the trifluoroborate salt **51** added an additional step to the synthesis, however, this is associated with a ~3-fold increase in the yield of the Suzuki-Miyaura cross-coupling. It has been reported previously that when using pinacol boronates similar to compound **50** the major product was protodeboronation of the starting material.<sup>138</sup> Trifluoroborate salts can mitigate formation of protodeboronation by-products.<sup>140</sup> To understand the importance of variables including; the choice of boronate, choice of base, solvent-system and stoichiometry, it is important to understand the mechanism of the Suzuki-Miyaura catalytic cycle.

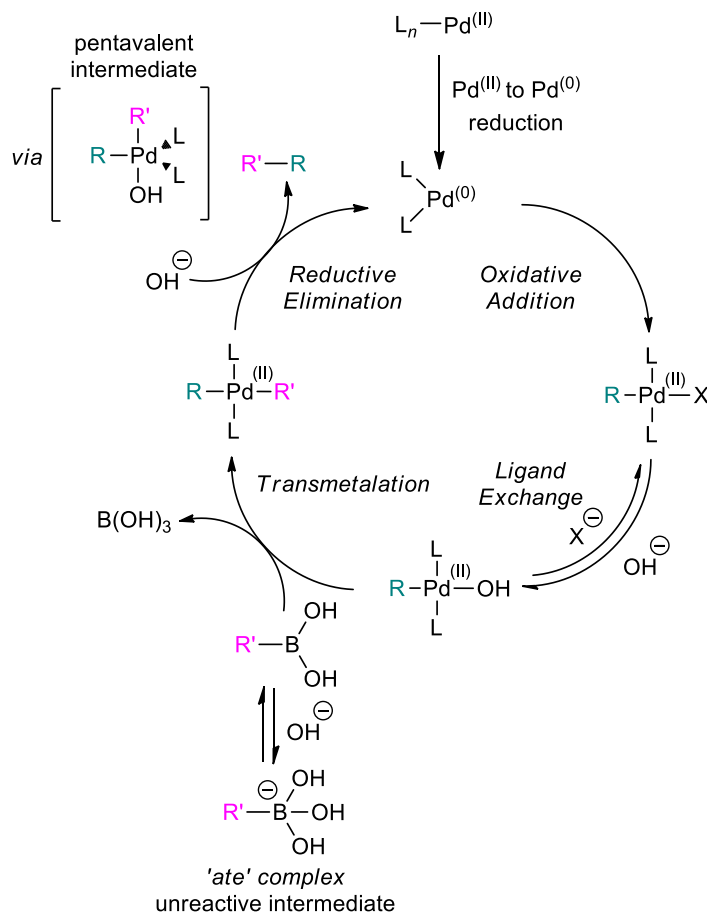


The Suzuki-Miyaura cross-coupling reaction was first reported in 1981<sup>141,142</sup> and over the past 40 years has become vitally important for C-C bond formation, a review in 2014 found that ~20% of all new pharmaceutical syntheses contain at least one Suzuki-Miyaura cross-coupling step.<sup>143</sup> As recognition of the significance of this reaction, Suzuki received a share of the 2010 Nobel prize for chemistry.<sup>144</sup> Despite the great importance of this reaction, its mechanism has been under debate until recently. This debate centred around the rate-determining transmetalation step and the identity of the active pre-transmetalation intermediates. There are two proposed routes by which this transmetalation step may feasibly occur (**Scheme 8**) Pathway A: in which a palladium halide complex reacts with trihydroxyborate and pathway B: in which a palladium hydroxo- complex reacts with a boronic acid.



**Scheme 8:** Two competing pathways for the transmetalation step of the Suzuki-Miyaura cross coupling reaction.

Kinetic studies have established that pathway B is the dominant pathway and is favoured over pathway A by more than four orders of magnitude.<sup>145-148</sup> In addition to this, the use of rapid injection NMR has shown the formation of the suspected pre-transmetalation intermediates occurs much more readily *via* pathway B.<sup>149</sup> With this evidence in hand, the catalytic cycle of the Suzuki-Miyaura cross-coupling reaction can be best represented as shown in **Scheme 9**.

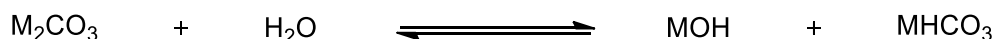


**Scheme 9:** General Suzuki-Miyaura cross-coupling reaction catalytic cycle.

$sp^3$  Alkyl boronates are known to be susceptible to protodeboronation and the transmetalation step with these substrates is comparatively slow.<sup>140</sup> This effect is likely to be accentuated even further with bulky tertiary  $sp^3$  boronate esters such as **50**. Organotrifluoroborates have emerged as alternative nucleophilic partners in Suzuki-Miyaura cross-coupling. Their tetracoordinate nature masks the inherent reactivity of the C-B bond. This makes organotrifluoroborates essentially protected forms of boronic acids, and their reactivity can be unveiled under analogous conditions to those required for cross-coupling. Under Suzuki-Miyaura reaction conditions, the organotrifluoroborates are slowly hydrolysed to the corresponding boronic acids, which are the reactive species.<sup>150</sup> This slow hydrolysis maintains a low concentration of the boronic acid species which undergoes reaction quickly after formation, thereby preventing large quantities of protodeboronation by-product.

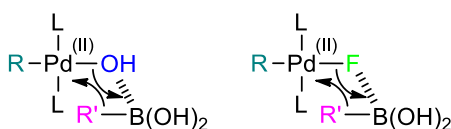
There have been three roles of the base determined within the Suzuki-Miyaura cross coupling, and thus selection of the optimal base and its stoichiometry can have a large impact on the

outcome of the reaction. The first role of hydroxide is formation of a Pd(L)<sub>2</sub>ArOH complex, which has been shown to be the active pre-transmetallation catalytic species. Displacement of a halide (X) with a hydroxide facilitates transmetallation *via* coordination of the highly oxophilic boronate species.<sup>145</sup> The reductive elimination step of the catalytic cycle is also facilitated by hydroxide. The hydroxide coordinates to the post- transmetallation species Pd(L)<sub>2</sub>ArAr' to form a pentavalent intermediate in which the two R-groups are *cis*-, therefore favouring elimination.<sup>145</sup> As well as its role in promoting the reaction, hydroxide also has a role in hindering reactivity. Hydroxide ions enable formation of the inactive 'ate' complex, which undergoes transmetallation at a very slow rate.<sup>145</sup> Due to these opposing roles, the rate of the transmetallation step (*k*<sub>obs</sub>) follows a bell-shaped curve with respect to increasing concentration of hydroxide ions. It is clear that hydroxide ions are the active basic species in the reaction. This has been demonstrated by the greatly decreased rate observed when the reaction is carried out with "dry" Cs<sub>2</sub>CO<sub>3</sub> with "dry" reaction solvent, as under these conditions there will not be a significant amount of hydroxide formed.<sup>146</sup> Carbonate bases can be used, however they are converted to the active hydroxide ion *via* reaction with water (**Scheme 10**). Reactions in which carbonate-based bases are often carried out in a solvent mixture containing around ~10% water.



**Scheme 10:** Reaction of carbonate base with water.

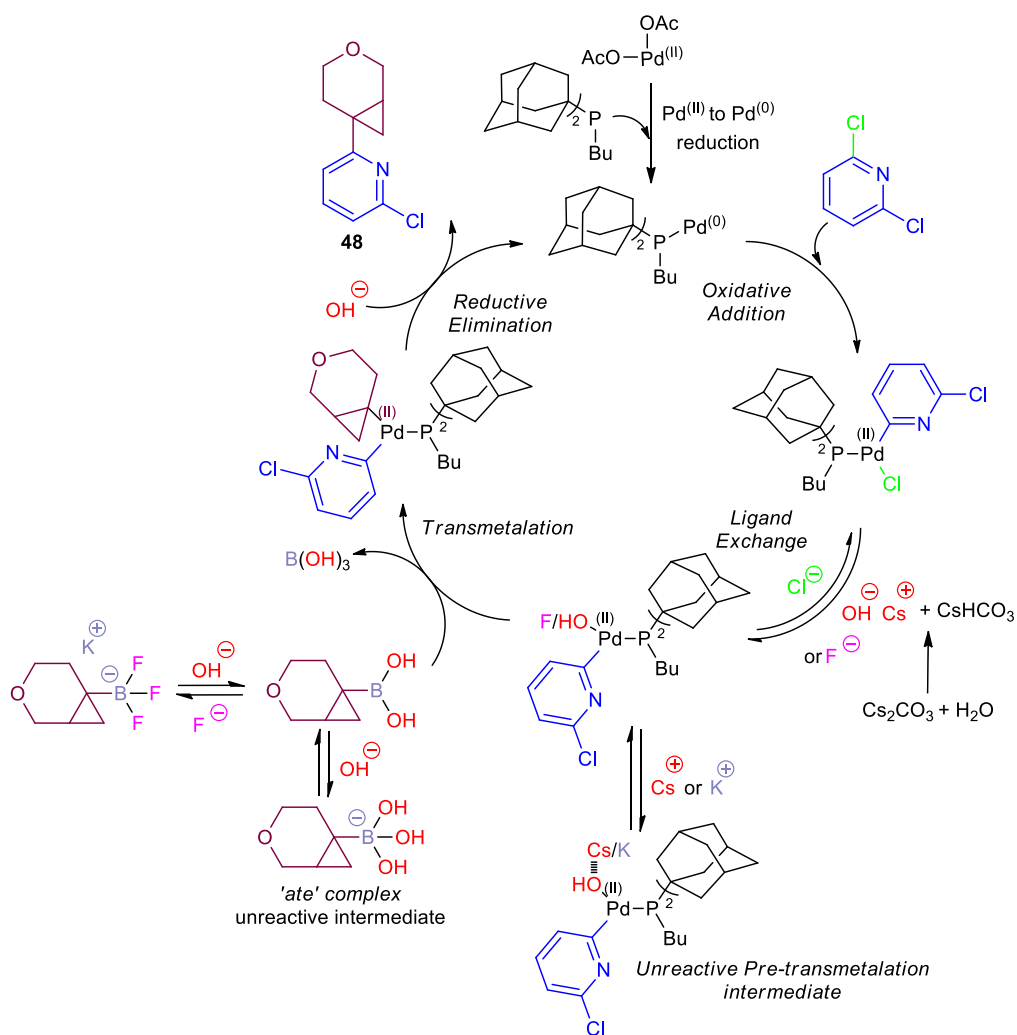
It has also been demonstrated that fluoride ions (F<sup>-</sup>) are capable of performing the same roles as hydroxide ions within the Suzuki-Miyaura cross coupling. Importantly, it has been shown that PdR(L)<sub>2</sub>F is able to undergo transmetallation with a boronic acid in an analogous fashion to PdR(L)<sub>2</sub>OH, as a consequence of the fluorophilicity of the boron centre (**Scheme 11**).<sup>151</sup> The reactivity of fluoride in the Suzuki reaction is important to consider when using organotrifluoroboronate coupling partners, as the fluoride released on hydrolysis to the corresponding boronic acid is able to take part in the catalytic cycle.



**Scheme 11:** Transmetalation step from  $\text{PdR(L)}_2\text{OH}$  and the analogous step from the corresponding fluoride containing complex  $\text{PdR(L)}_2\text{F}$ .

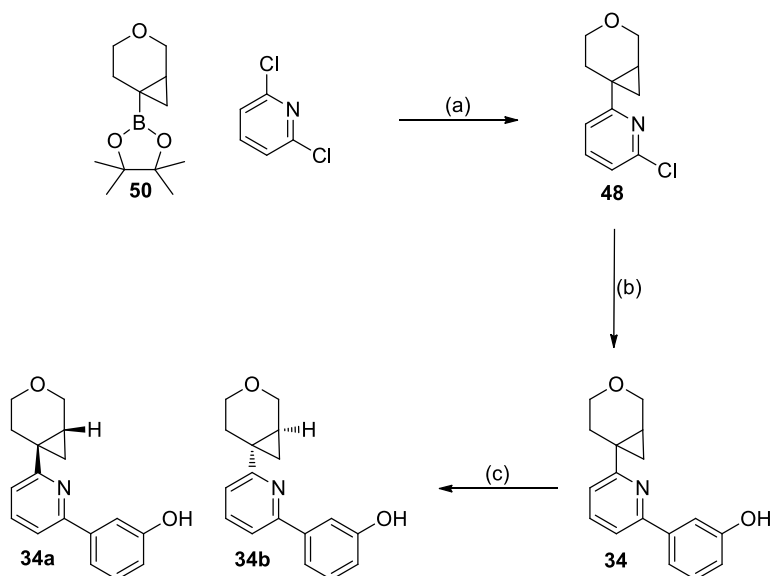
Inclusion of an anionic base inevitably comes associated with a counter cation. The identity of this cation can also have an impact on the reaction. In particular, the counter carbocation has a decelerating effect on the transmetalation step. This is due to complexation of the hydroxoligand of  $\text{PdR(L)}_2\text{OH}$  by the counter cation. The level to which this decreases the rate of transmetalation is correlated to the oxophilicity of the cation ( $\text{Na}^+ > \text{Cs}^+ > \text{K}^+$ ).<sup>152</sup> The cation however has another role, which can promote transmetalation. The ligand exchange step is reversible and by complexing with halide that has been displaced by hydroxide, equilibrium can be driven to form more of the active pre-transmetalation species  $\text{PdR(L)}_2\text{OH}$ . This is the reason that  $\text{Ag}^+$  or  $\text{Tl}^+$  have been shown to enhance the rate of reaction for Suzuki-Miyaura cross couplings,<sup>153</sup> the  $\text{AgX/TlX}$  compound which is formed is insoluble and therefore the halide is removed from the equilibria, driving formation of increased concentration of  $\text{PdR(L)}_2\text{OH}$ .

In standard  $\text{sp}^2\text{-sp}^2$  for Suzuki-Miyaura cross couplings reactions, the oxidative addition step is usually rate determining when using aryl chloride coupling partners. However, it is unclear whether this is the case with Suzuki-Miyaura cross couplings involving CPP **51**, due to the comparatively slow rate of the transmetalation step with tertiary alkyl boronates. It is therefore difficult to state the rate determining step of the catalytic cycle without kinetic studies. CataCXium® A was reported within the literature to be a particularly active ligand for Suzuki-Miyaura cross coupling reactions with aryl chlorides. This is because CataCXium® A is a bulky, electron rich mono-phosphine and stabilises a  $\text{Pd(PR}_3)$  species, which is thought to undergo facile oxidative addition with aryl chlorides.<sup>154-156</sup> We have reasoned that this accounts for the superiority of CataCXium® A over other ligands in literature screening on similar compounds to **33**. A proposed catalytic cycle for Suzuki-Miyaura cross coupling reactions involving CPP **51** and using the  $\text{Pd(OAc)}_2/\text{CataCXium® A}$  catalytic system is shown in **Scheme 12**.



**Scheme 12:** Proposed Suzuki-Miyaura catalytic cycle for formation of cross-coupled product **48**.

Using the conditions reported within the literature, and identified by another member of our laboratory,<sup>139</sup> Suzuki-Miyaura cross-coupling gave cyclopropylpyran containing compound **48**. Compound **48** was subjected to an additional Suzuki-Miyaura cross-coupling to introduce the 3-phenol backpacket group and furnish the final product **34** as a racemic mixture. The racemic final product was separated into single enantiomers **34a** and **34b** using chiral column chromatography elsewhere within our laboratory. This synthesis is shown in **Scheme 13**.



(a) Pd(dppf)Cl<sub>2</sub>.CH<sub>2</sub>Cl<sub>2</sub>, CsOH.H<sub>2</sub>O, THF: H<sub>2</sub>O (10:1), 100 °C, 3 h, 27% (b) 3-(4,4,5,5-tetramethyl-1,3,2-dioxaborolan-2-yl)phenol, Pd(dppf)Cl<sub>2</sub>.CH<sub>2</sub>Cl<sub>2</sub>, K<sub>2</sub>CO<sub>3</sub>, 2-propanol/H<sub>2</sub>O (5:1) 100 °C,  $\mu$ Wave, 1.5 h, 48% yield; (c) Chiral HPLC purification.

**Scheme 13:** Synthesis of **34a** and **34b**. NB: absolute stereochemistry was assigned from X-ray crystal structure of **34a** (*vide infra*).

This methodology was further utilised to furnish CPP containing final products **40-42** (**Scheme 14**). The yield for CPP Suzuki-Miyaura cross-coupling is reasonably consistent for each example (yield ranges between 31% and 41%) The major side-products which contributed to a low yield in these reactions include *bis*-coupled product and hydrolysed starting material (**Figure 31**), however despite this, an acceptable yield of product was obtained in all cases. The CPP-containing intermediates **52-54** had the appropriate back-pocket group installed *via* a Suzuki-Miyaura cross-coupling reaction to give racemic final products **40-42**. Racemic compounds **40-42** were again separated into their respective single enantiomers by chiral HPLC.

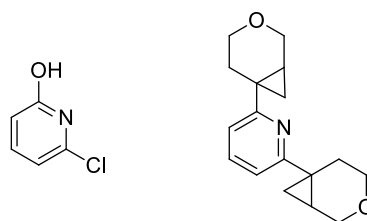
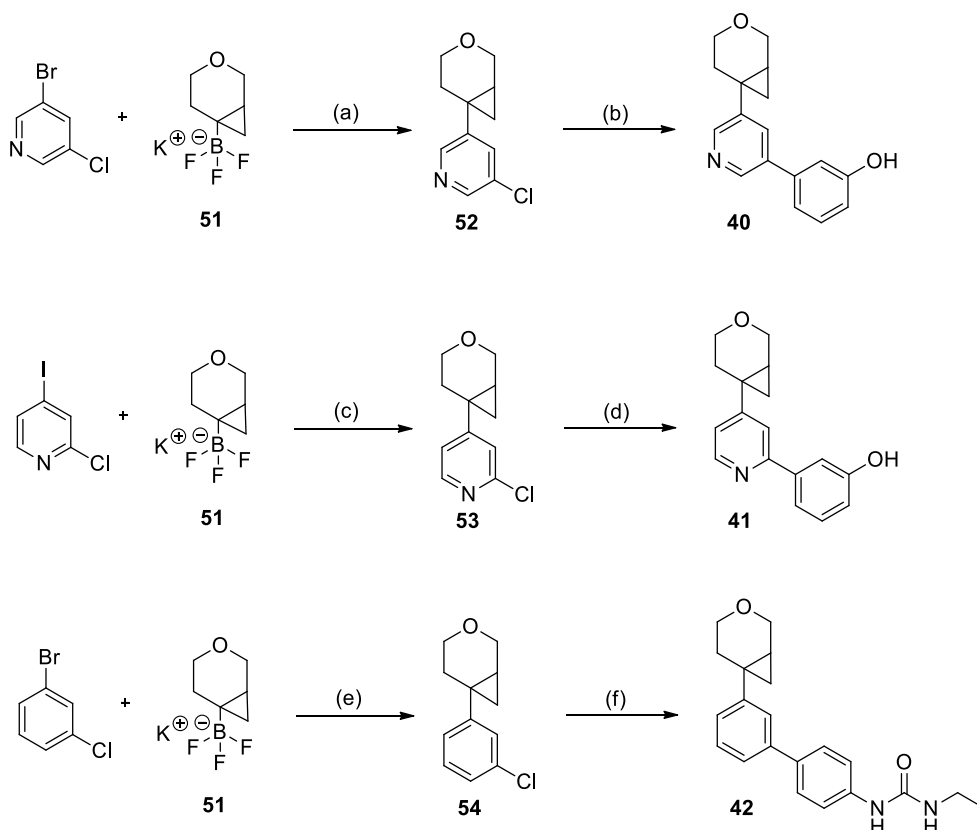


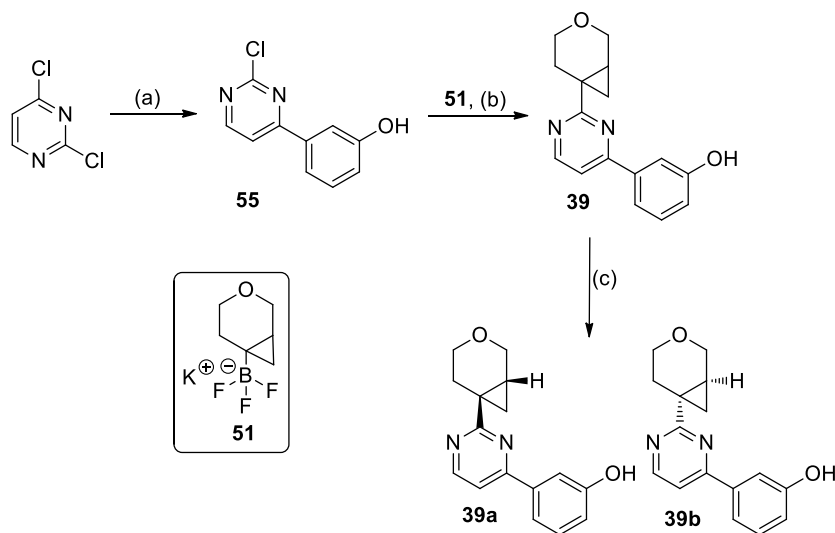
**Figure 31:** Side-products (not isolated, corresponding mass observed in LCMS) for formation of **48**.



(a) Pd(OAc)<sub>2</sub>, CataCXium® A, Cs<sub>2</sub>CO<sub>3</sub>, toluene/H<sub>2</sub>O (10:1), 90 °C, 16 h, 41% yield; (b) 3-(4,4,5,5-tetramethyl-1,3,2-dioxaborolan-2-yl)phenol, Pd(II)(dppf)Cl<sub>2</sub>.CH<sub>2</sub>Cl<sub>2</sub>, K<sub>2</sub>CO<sub>3</sub>, 2-propanol/H<sub>2</sub>O (5:1) 100 °C, 3 h, 21% yield; (c) Pd(OAc)<sub>2</sub>, CataCXium® A, Cs<sub>2</sub>CO<sub>3</sub>, toluene/H<sub>2</sub>O (10:1), 90 °C, 16 h, 37% yield; (d) 3-(4,4,5,5-tetramethyl-1,3,2-dioxaborolan-2-yl)phenol, Pd(II)(dppf)Cl<sub>2</sub>.CH<sub>2</sub>Cl<sub>2</sub>, K<sub>2</sub>CO<sub>3</sub>, 2-propanol/H<sub>2</sub>O (5:1) 100 °C, 3 h, 55% yield; (e) Pd(OAc)<sub>2</sub>, CataCXium® A, Cs<sub>2</sub>CO<sub>3</sub>, toluene/H<sub>2</sub>O (10:1), 90 °C, 16 h, 37% yield; (f) 1-ethyl-3-(4-(4,4,5,5-tetramethyl-1,3,2-dioxaborolan-2-yl)phenyl)urea, Pd(II)(dppf)Cl<sub>2</sub>.CH<sub>2</sub>Cl<sub>2</sub>, K<sub>2</sub>CO<sub>3</sub>, 2-propanol/H<sub>2</sub>O (5:1) 100 °C, 3 h, 37% yield.

**Scheme 14:** Synthesis of Compounds **40-42**. Final products were subjected to chiral HPLC to obtain single enantiomer products **40a/40b**, **41a/41b** and **42a/42b**.

2-Pyrimidine **39** was also synthesised using analogous chemistry, however, the order of steps is reversed to account for the inherent reactivity of the pyrimidine heterocycle. The 3-phenol back-pocket group is installed first into the more reactive 4-position to give 2-chloropyrimidine **55**, followed by installation of the CPP group at the less reactive 2-position between the two ring nitrogens (**Scheme 15**). This gives racemic compound **39** which was separated into single enantiomers by chiral HPLC.



(a) 3-(4,4,5,5-tetramethyl-1,3,2-dioxaborolan-2-yl)phenol,  $K_2CO_3$ ,  $Pd(dppf)Cl_2 \cdot CH_2Cl_2$ , 2-propanol:  $H_2O$  (5:1), 100 °C, 3 h, 20% yield; (b)  $Pd(OAc)_2$ , cataCXium® A,  $Cs_2CO_3$ , toluene/ $H_2O$  (10:1) 100 °C, 3 h, 21% yield; (c) Chiral HPLC.

**Scheme 15:** Synthesis of 2-pyrimidine compounds **39a** and **39b**.

### 2.3 X-ray Crystal Structures

The tool compounds were recrystallised using toluene or acetonitrile in order to facilitate X-ray crystallography. Firstly, X-ray crystal structures of the 2-pyridine matched set of compounds **31-34** were obtained. Gratifyingly the X-ray crystal structures of 2-pyridine morpholine **31**, DHP **32**, THP **33** and CPP **34a** (**Table 6**) align closely to the conformation of these compounds predicted by DFT (**Figure 23**). As predicted, morpholine **31** and DHP **32** have co-planar conformations, likely due to the stabilising effects of *N*-lone pair donation and  $\pi$ -bond conjugation respectively. For these compounds the predicted minimum energy dihedral angle closely agrees with the measured dihedral angle. It is important to note that the predicted minimum energy dihedral angle is only accurate to the nearest multiple of ten, as in the dihedral angle scanning experiment, the test molecule is measured at 10° increments of rotation around the dihedral angle of interest.



Another measurement which was found to be useful in assessing the co-planarity of these molecules is the angle between the average plane of each ring, as measured in the crystallographic software package Mercury (**Figure 32**).<sup>157</sup> This gives an impression of how “flat” the profile of the molecule is. This parameter is useful as it is reported that only molecules which are able to adopt a co-planar conformation and sterically mimic the ATP natural ligands are effective hinge binding fragments.<sup>158</sup>

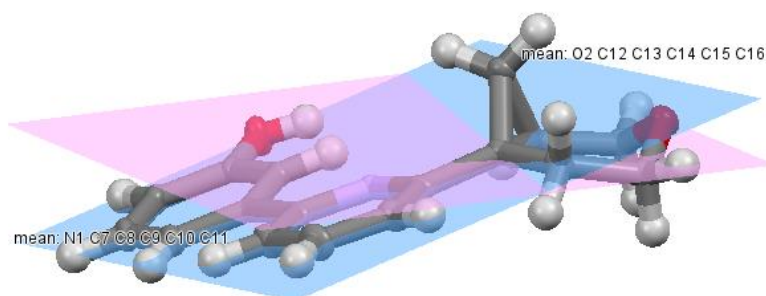
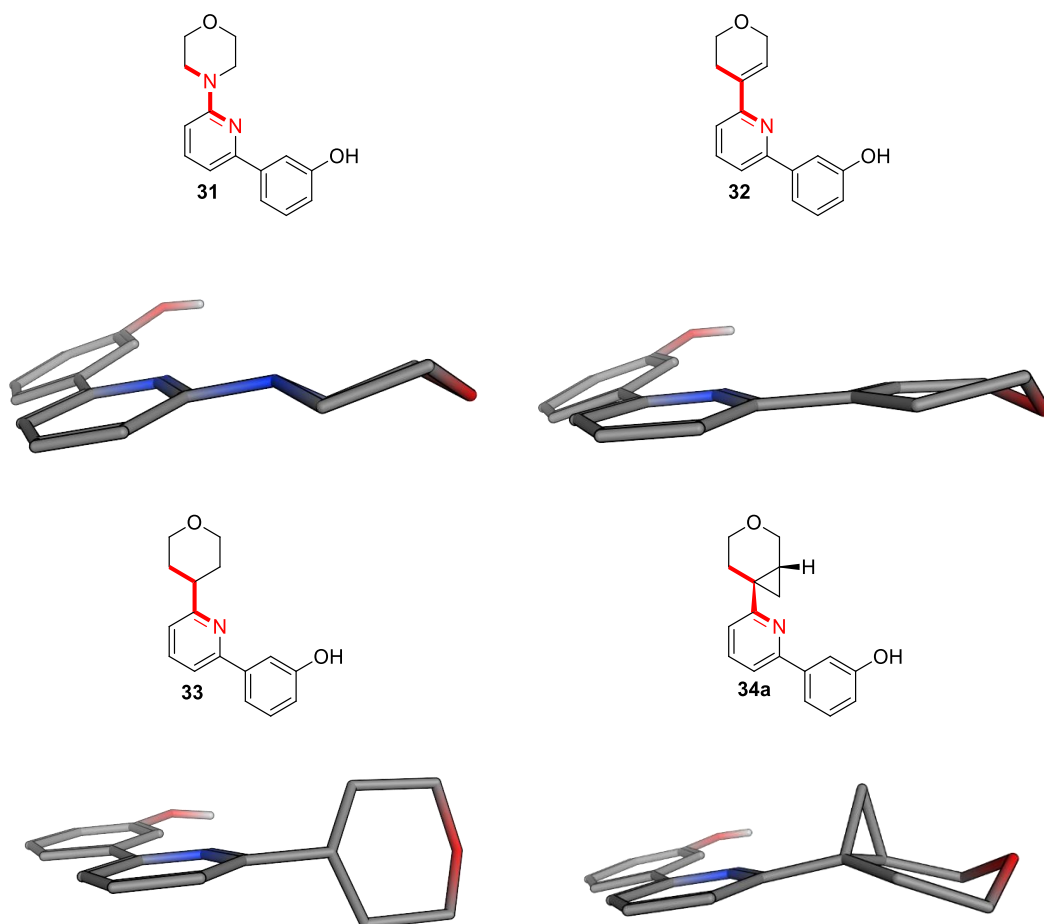


**Figure 32:** Example of average ring planes in CPP **34a**. Planes were generated, and angles were measured using Mercury v3.7.

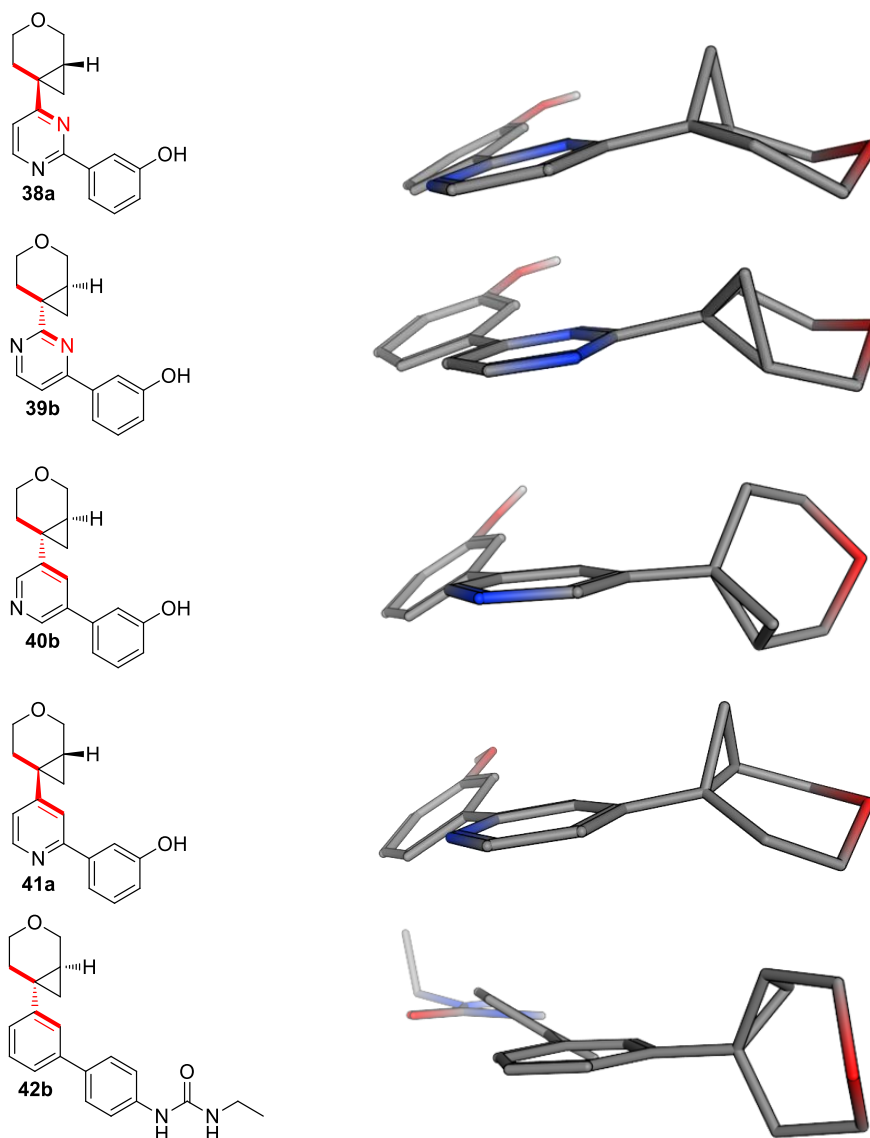
The fully saturated tetrahydropyran ring has no orbitals available for overlap, and therefore as predicted the THP containing compound **33** preferentially occupies the sterically favourable orthogonal conformation. Addition of a cyclopropane ring to form CPP **34a** is associated with a switch in conformational preference. CPP **34a** occupies a co-planar conformation and it was postulated that this was due to a stabilising interaction, akin to conjugation, between the cyclopropyl and aryl ring systems (*vide supra*).



Entry	Compound Number	Predicted dihedral angle	Measured dihedral angle	Angle between average ring planes
1	<b>31</b>	170 °	-173.4 °	16.9 °
2	<b>32</b>	170 °	178.2 °	9.3 °
3	<b>33</b>	300 °	-75.9 °	70.7 °
4	<b>34a</b>	170 °	-169.2 ° 162.3 °	15.0 ° 44.1 °

**Table 6:** X-ray crystal structures for 2-pyridyl compounds **31-34a**. Measured angles shown for comparison to those predicted from dihedral angle scans. The angle between the average plane of each ring is also shown as an additional measure of co-planarity. If more than 1 conformer is present in the unit cell of the crystal, data for all conformers is shown in the table.

With the result for 2-pyridyl CPP **34a** in hand, attention was turned to compounds **38-42** in which the core 6-membered aryl ring is varied. The X-ray crystal structures for these compounds are shown in **Table 7**.



Entry	Compound Number	Predicted dihedral angle	Measured dihedral angle	Angle between average ring planes
1	<b>38a</b>	170 °	-167.7 °	26.3
			-175.7°	36.8
			15.0 °	34.6
			-179.5°	35.2
2	<b>39b</b>	0 ° and 170 °	172.2 °	26.1
			5.6 °	27.6
3	<b>40b</b>	90 °	121.1 °	51.7
			66.1 °	81.4
4	<b>41a</b>	260 °	-149.2 °	28.6
			-0.3 °	26.4
5	<b>42b</b>	270 °	-106.1 °	83.8

**Table 7:** X-ray crystal structures for CPP compounds **38-42**. Measured angles shown for comparison to those predicted from dihedral angle scans. The angle between the average plane of each ring is also shown as an additional measure of co-planarity. If more than 1 conformer is present in the unit cell of the crystal, data for all conformers is shown in the table. Enantiomers shown selected on quality of crystal.

Generally, the CPP containing compounds displayed a good agreement between the predicted low energy conformation and measured solid-state conformation. Pyrimidine isomers **38** and **39** both have multiple molecules within their unit cell however, all of these molecules can be described as having a co-planar conformation. The unit cell of 4-pyrimidine **38** (**Figure 32**) is complex with four individual molecules. Three of the molecules within the unit cell have a measured dihedral angle that is within  $10^\circ$  of the predicted  $170^\circ$  dihedral angle. The final molecule however, has a measured dihedral angle of  $15^\circ$ . This is due to this molecule occupying opposite co-planar conformation, which is a local energy minimum (**Figure 26**). Similarly, for 2-pyrimidine **39** (**Figure 34**) there is a molecule occupying each of the energetically equivalent minimum energy conformations.

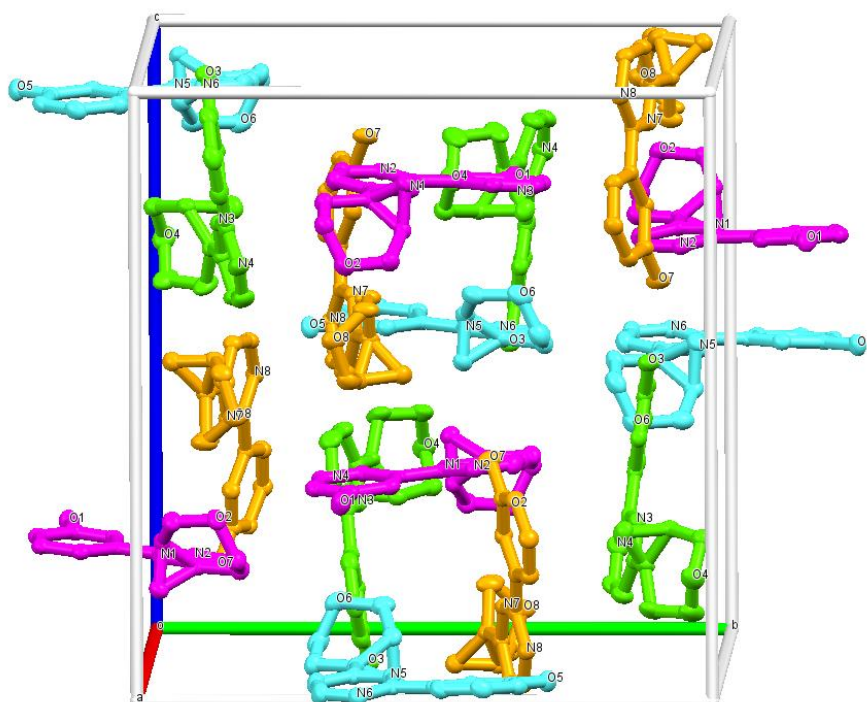


**Figure 33:** Crystal packing for 4-pyrimidine **38a**. Molecules are coloured by symmetry equivalence so that the four individual molecules that make up an asymmetric unit can be seen.

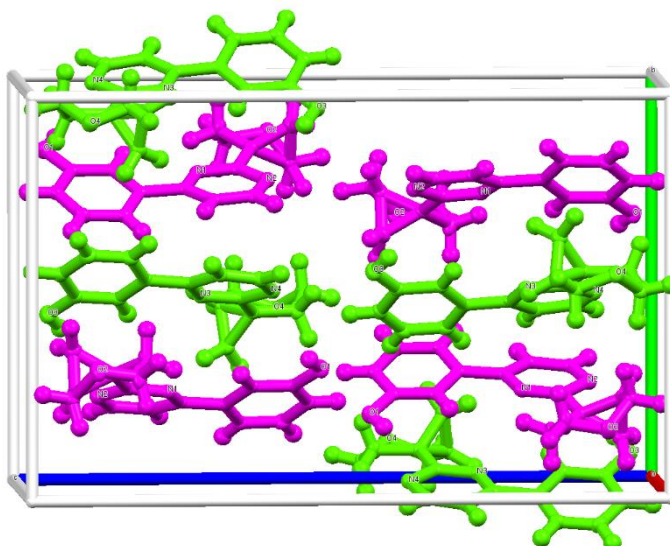


**Figure 34:** Crystal packing for 2-pyrimidine **39b**. Molecules are coloured by symmetry equivalence so that the two individual molecules that make up an asymmetric unit can be seen.

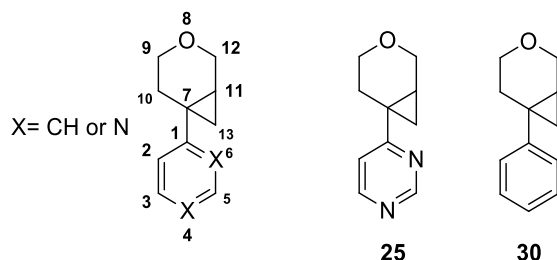
3-Pyridine **40b** and phenyl **42b** are predicted to occupy orthogonal conformations and the X-ray crystal structures of these compounds agree with these predictions. The CPP ring is twisted out of plane and therefore the value of the measured dihedral angle ranges from  $66^\circ$  to  $121^\circ$ . The presence of an orthogonal conformation which is unsuitable for target engagement, likely makes these hinge-core fragments unsuitable for mTOR inhibitors (*vide supra*)

4-Pyridine **41a** is particularly interesting. This compound was computationally predicted to occupy an orthogonal conformation; at the time, it was postulated that this was a steric effect due to the observation that 4-pyridine is electronically analogous to 2-pyridine. It was therefore thought that the increased steric bulk of an adjacent methine system accounted for the disparity in predicted conformation between 2-pyridine **34a** and 4-pyridine **41a**. However, the X-ray crystal structure of 4-pyridine **34a** has molecules with a co-planar conformation. It was postulated that, in this case, the magnitude of stabilisation inferred by electronic overlap is underestimated in the predicted conformation. However, it is also plausible that this is an artefact of crystal packing in the solid state.

## **2.4 Natural Bond Orbital Analysis**

In order to further understand the steric and electronic factors which contribute to conformation, a natural bond orbital analysis was carried out by another member of our laboratories.<sup>159</sup>

Natural bond orbital (NBO) analysis is an energy and wavefunction decomposition method whereby localised electron pair orbitals are generated for bonding pairs and lone pairs. Using second order perturbation analysis the interaction of these bonding NBO's with anti-bonding NBO's can be measured.<sup>160</sup> This technique was used to compare the cyclopropyl to aryl interactions in tool compounds **25** and **30**.



Orbital Contribution					
System	B(7-13) → B*(1-6)	B(Ar) → B*(CPP)	B(CPP) → B*(Ar)	orbital	Δ orbital
<b>25</b> (170 °)	24.3	60.5	106.1	166.6	
<b>Min Energy</b>					<b>9.0</b>
<b>25</b> (270 °)	2.5	60.6	97.0	157.6	
<b>Max Energy</b>					
<b>30</b> (190 °)	8.3	72.5	83.4	155.9	
<b>Max Energy</b>					
<b>30</b> (270 °)	0.00	73.0	81.1	154.1	
<b>Min Energy</b>					<b>1.8</b>
Steric Contribution					
System	Steric (6-H)	Steric (Ar)	Steric (CPP)	steric	Δ steric
<b>25</b> (170 °)	n. a	-168.1	-201.5	-369.6	
<b>Min Energy</b>					<b>5.5</b>
<b>25</b> (270 °)	n. a	-179.8	-195.3	-375.1	
<b>Max Energy</b>					
<b>30</b> (190 °)	-19.7	-173.3	-222.6	-395.8	
<b>Max Energy</b>					
<b>30</b> (270 °)	-4.5	-178.5	-205.5	-383.9	
<b>Min Energy</b>					<b>-11.9</b>

**Table 8:** NBO second order perturbation analysis. Orbital stabilisation and steric analysis. Values in kJ mol<sup>-1</sup>. Positive values denote stabilisation, negative values denote destabilisation. B= bonding orbital, B\*= anti-bonding orbital. Atom numbering relates to generalised structure shown above.

The NBO analysis provides an insight into the minimum energy conformation of CPP-containing compounds. Orbital contribution is stabilisation arising from electron transfer from the cyclopropyl bonding orbitals into the aryl  $\pi$ -system and *vice versa*. The donation from cyclopropane bonding orbital into the aryl antibonding orbital is greater than in the other direction, which is expected given the  $\pi$ -donation properties of cyclopropane.<sup>127</sup> Orbital

interactions stabilise co-planar conformations in both cases, although this effect is  $7.2 \text{ kJ mol}^{-1}$  greater for 4-pyrimidine **25**. It was postulated that the increased stabilisation of the co-planar conformation of 4-pyrimidine **25** is a consequence of the increased electron deficiency of this aryl ring compared to benzene.

Steric considerations also favour the co-planar conformation for 4-pyrimidine **25** contributing  $5.5 \text{ kJ mol}^{-1}$ , whereas the co-planar conformation for phenyl **30** is strongly destabilised by  $-11.9 \text{ kJ mol}^{-1}$  ostensibly due to the steric impact of the additional adjacent methine system.

This interesting steric result can go some way to accounting for the incorrect conformational prediction of 4-pyridine **41a**. This system is predicted to have a reasonable orbital stabilisation, and as it is sterically analogous to phenyl **30**, steric destabilisation can be estimated to be  $\sim 12 \text{ kJ mol}^{-1}$ . In this situation it is possible that the energy barrier to rotation for 4-pyridine **41a** is very small, and therefore it has been suggested that crystal packing forces may stabilise a co-planar conformation in the solid state.

## **2.4 ROESY NMR Study**

With the X-ray crystal structures in hand, attention was turned towards the conformational preferences in solution, as drug-target interactions occur in the solution phase, this is arguably the most important parameter for assessing the likelihood of biological activity. To probe the conformation in solution, ROESY NMR experiments were conducted on CPP compounds **34** and **40-42**.

ROESY (rotating-frame Overhauser spectroscopy experiment) is an experimental method to easily obtain NOE (nuclear Overhauser effect) information for a molecule in a single experiment without prior knowledge of the special assignment or molecular structure. NOE NMR is able to provide information on dipolar coupling between protons which are in close spatial proximity, and hence provide information on molecular conformation. Before discussing the NOE data in detail, it is important to understand the theoretical background of the technique and how NOE data is generated, as this will provide an insight into the limitations of this technique within systems such as those of interest to the current study.

Nuclear Overhauser effect (NOE) is defined as alteration of the normal spin populations of a nucleus (**X**) which causes the populations and therefore signal intensities of other non-irradiated nuclei (**A**), which are referred to as “interesting protons” to change, providing **X** is causing  $T_1$  relaxation of **A** by the dipole-dipole mechanism.<sup>161</sup> When two protons are close in space their magnetic dipoles interact. The dipole-dipole interactions are normally averaged out

by tumbling of molecules in solution; they do however dominate the  $^1\text{H}$   $T_1$  relaxation processes in most molecules that contain more than one proton.

To gain an understanding of the nuclear Overhauser effect, consider the pair of protons labelled **AX**, which are close in space but not  $J$  coupled. When the **X** proton (known as the source proton) is irradiated at its Larmor frequency, the populations of the  $\alpha\alpha$  and  $\alpha\beta$  states become equalized, as do the  $\beta\alpha$  and  $\beta\beta$  states (**Figure 35**). This reduces the population difference towards zero (called saturation). Once the radio frequency pulse is switched off, the population difference of the source proton (**X**) will return to its equilibrium state ( $\beta$  to  $\alpha$ ), the excited state **X** proton can return to the ground state by two mechanisms;  $\omega_2$  and  $\omega_0$ . For small molecules  $\omega_2$  is the most important transition. This is a double quantum transition meaning both **A** and **X** are in the excited state ( $\beta$ ) and simultaneously flip back into the ground state. As this happens the source proton **X** returns to equilibrium, however this causes more “interesting” protons (**A**) to inhabit the ground state that at equilibrium. This increases the population difference of proton **A** which results in an increase in the intensity of the proton NMR peak for **A**, this is NOE. As the dipole-dipole interactions are only active over a range of  $>4 \text{ \AA}$  the NOE spectrum can provide valuable information about the proximity of different protons in space and therefore conformational preferences of the molecule.<sup>161,162</sup>

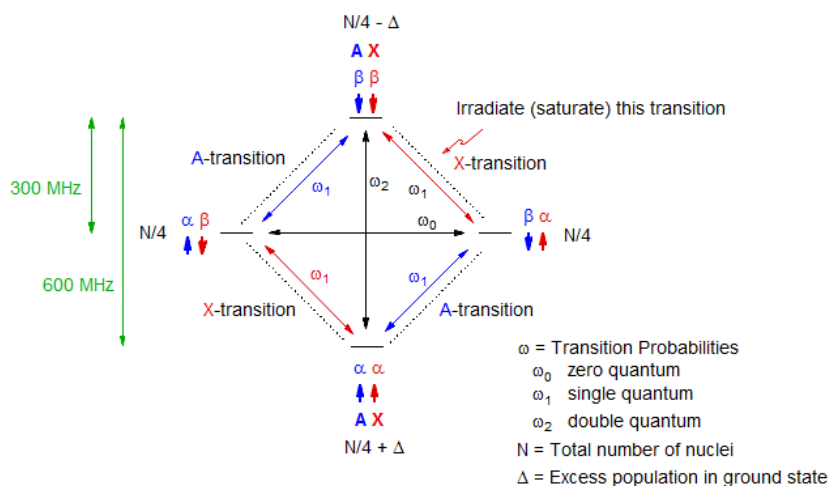


**Figure 35:** Energy level diagram for a two-proton system (XA) which can undergo NOE.

There are various difficulties when interpreting NOE data to obtain information about molecular conformation. The main issue is that the NOE enhancement attenuates to  $1/r^6$  of the internuclear separation<sup>163</sup> - which means that NOE enhancement rapidly decreases with distance.



This  $1/r^6$  relationship between the relevant NOE crosspeak and internuclear distance, (**Figure 36**) makes it challenging to extract reliable data from systems such as those of interest to the current study in which there is rotation around the CPP - pyridine bond. This is because the experiment is biased towards molecules in which there are shorter internuclear distances, and will display larger NOE peaks, even if only a small proportion of the sample occupies this conformation at any one time. NOE studies are, however, a useful tool as they allow us to determine if the system is capable of adopting certain conformations in solution, even if the relative populations of molecules in each conformation cannot be accurately quantified.

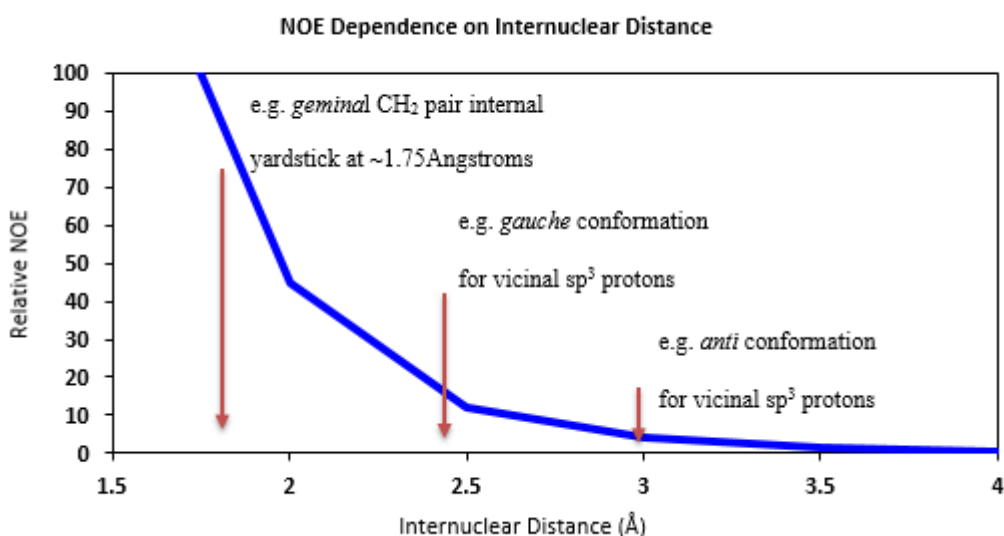
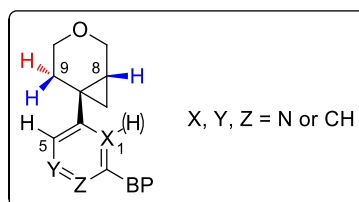
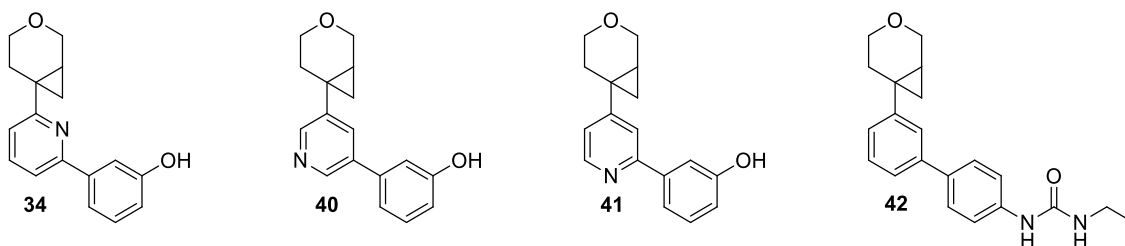


**Figure 36:** Graph showing the  $1/r^6$  relationship between relative NOE and internuclear distance.

To probe the conformations of the tool compounds by ROESY NMR, firstly, molecular mechanical models were generated by the author in MOE<sup>164</sup> in order to obtain internuclear distances for the predicted orthogonal conformations. For all low energy conformers generated by molecular mechanics studies the 9-CH<sub>2</sub> to 5-CH distances, and where applicable, the 9-CH<sub>2</sub> to 1-CH were all greater than 3.1 Å (see **Table 9** for numbering convention). Furthermore, the 5-CH to 8-CH, and where applicable, the 1-CH to 8-CH distances were all >2.8 Å. Hence, this group of relatively long distances are characteristic of the orthogonal conformers calculated by molecular mechanics.

The significantly shorter distances indicated by NMR imply that 2-pyridine **34** clearly has more co-planar conformations in solution. The distance of 2.37 Å is close to the co-planar crystal structure distance (2.05 Å), especially when the presence of higher energy orthogonal

conformations in solution is considered. To a much lesser extent, 4-pyridine **41** also appears to show the presence of co-planar conformations in solution (**Table 9**).

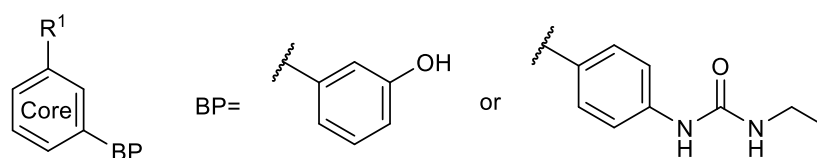


Entry	Compound No.	Inter-nuclear distance	X	Molecular Mechanical Prediction (Å)	NOE Distance (Å)	Crystal Structure distance (Å)
1	<b>34</b>	9CH'-5CH	N	3.39	2.37	2.05
2	<b>40</b>	9CH''-1CH	CH	3.40	2.90	2.71
3	<b>41</b>	9CH'-5CH	CH	3.48	2.80	2.25
4	<b>42</b>	9CH'-5CH	CH	3.49	3.28	2.68

**Table 9:** Comparison of internuclear distances predicted from model structures to those measured from X-ray crystal structures and ROESY NMR for compounds **34** and **40-42**.

## 2.5 Biological Screening and PI3K $\delta$ Co-Crystallography of Tool Compounds

Tool compounds were tested in a range of biochemical and physicochemical assays in order to determine if, as expected, the propensity of certain CPP- core combinations to preferentially occupy low energy co-planar conformations translates into improved biological activity in lipid kinases and PIKKs. Results from the PI3K isoform TR-FRET screening is shown in **Table 10**.



Entry	Compound No.	Core	Hinge (R <sup>1</sup> )	Isomer	PI3K $\alpha$ pIC <sub>50</sub>	PI3K $\beta$ pIC <sub>50</sub>	PI3K $\delta$ pIC <sub>50</sub>	PI3K $\gamma$ pIC <sub>50</sub>
1	<b>31</b>	2-Py.	Morph.	-	5.4	5.1	5.4 ( $\pm$ 0.4)	5.1 ( $\pm$ 0.4)
2	<b>32</b>		DHP	-	4.9	4.9	5.4	5.1 ( $\pm$ 0.5)
3	<b>34a</b>		CPP	1R, 6S	4.7	< 4.5	4.5	< 4.5
4	<b>34b</b>			1S, 6R	4.7	< 4.5	5.2	< 4.5
5	<b>33</b>		THP	-	4.6	< 4.1	4.8	4.5
6	<b>35</b>	4-Pyrim.	Morph.	-	6.3	6.2 ( $\pm$ 0.4)	6.6	6.1
7	<b>36</b>		DHP	-	5.5 ( $\pm$ 0.6)	5.6 ( $\pm$ 0.4)	5.9	5.5 ( $\pm$ 0.7)
8	<b>38a</b>		CPP	1R, 6S	5.2	4.9	5.5 ( $\pm$ 0.4)	5.0
9	<b>38b</b>			1S, 6R	5.6	5.0	5.9	5.3 ( $\pm$ 0.5)
10	<b>37</b>		THP	-	4.8	4.6	5.1	4.7
11	<b>39a</b>	2-Pyrim.	CPP	1R, 6S	5.5	4.9	5.7	5.5
12	<b>39b</b>			1S, 6R	4.9	< 4.5	5.1	5.0 ( $\pm$ 0.4)
13	<b>40a</b>	3-Py.	CPP	1R, 6S	< 4.3	< 4.3	4.7	4.6
14	<b>40b</b>			1S, 6R	< 4.3	< 4.3	4.7	4.6
15	<b>41a</b>	4-Py.	CPP	1R, 6S	4.6	< 4.3	5.0 ( $\pm$ 0.5)	4.7
16	<b>41b</b>			1S, 6R	< 4.3	< 4.3	4.5	4.5
17	<b>42a</b>	Phenyl.	CPP	1R, 6S	5.1	4.6	4.9 ( $\pm$ 0.6)	4.8 ( $\pm$ 0.4)
18	<b>42b</b>			1S, 6R	< 4.3	4.4	4.8	4.7

**Table 10:** Results of PI3K isoform TR-FRET assays. N=3 or greater in all cases. Potency ranges are shown for values which fall outside the error of the assay (0.3) otherwise potency range is not shown. NB: A description of this assay procedure can be found in chapter II of this thesis.

The results show that CPP is most active at PI3K $\delta$  over the other PI3K isoforms. The matched set of 4-pyrimidine compounds shows how in these small tool compounds the CPP **38b** is not as active as morpholine **35** (5-fold lower activity). It is thought that this is due to the greater selectivity which CPP containing compounds display for mTOR over closely related lipid kinase/ PIKKs (*vide-infra*). It is encouraging that the most active CPP enantiomer **38b** is equipotent with DHP **36**, which is reported in the literature as a morpholine replacement.<sup>158</sup> CPP **38b** is also significantly more active than the corresponding THP analogue **37** (~ 6 fold increase in potency).

Similarly, in the 2-pyridyl matched set, the morpholine **31** and DHP **32** containing compounds have similar potency to the most active CPP containing compound **34b** (~1.6-fold difference in activity, which is within the limits of error within this assay) and the corresponding THP **33**

has a lower activity. It is worth noting, in general the 2-pyridyl core is less favourable, this is thought to be due to other factors which the core ring influences, such as position of the back-pocket.

The 2-pyrimidine **39** is also active, although the opposite enantiomer (1*R*, 6*S*) **39a** is more active in this case, and the reasons behind this are currently unclear. Although predicted to occupy co-planar conformations, neither enantiomer of 4-pyridine **41** is significantly more biologically active than 3-pyridine **40** or phenyl **42**.

To confirm that compounds were binding in the proposed mode, another member of our laboratory produced protein co-crystal structures of CPP **34b**, Morpholine **31** and THP **33** in murine PI3K $\delta$  (**Figure 37**). CPP compound **34b** and morpholine compound **31** bind to the protein in analogous modes, both participating in hydrogen bonding interactions with Val828 in the hinge region and the phenol forming a H-bond to Tyr813 in the backpocket. The crystal structure demonstrates the importance of the co-planar conformation for favourable alignment in the active site. THP **33** also occupies a co-planar conformation when bound to murine PI3K $\delta$ , forming hydrogen bonding interactions with Val828 and Asp787. The unfavourable conformation adopted for binding may explain the lower activity observed for THPs (**33**, **37**) relative to the morpholine (**31**, **35**) and CPP analogues (**34b**, **38b**)

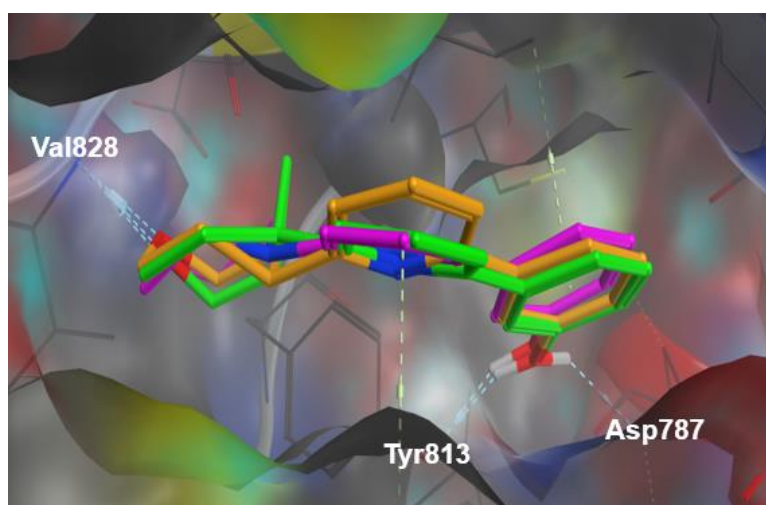
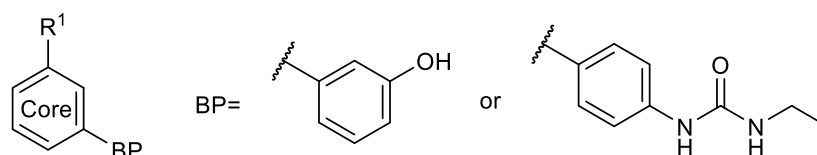


**Figure 37:** Morpholine **31** (fuchsia), CPP **34b** (green) and THP **33** (orange) bound to the active site of mouse PI3K $\delta$ .

The tool compounds were also tested within the mTOR kinobead assay (**Table 11**) (*vide-infra*). Although CPP is envisaged as a mTOR hinge binding moiety, the potencies observed within this assay were very low. It is thought that this is likely to be because of the low-

molecular weight of the tool compounds. It was also noted that the 3-phenol backpacket, which was employed in the majority of tool these tool compounds, is known to be a less efficient motif in this context when applied to mTOR. Therefore, in this study the PI3K biological data was used to inform on the level of activity which more highly elaborated project compounds may be expected to have at mTOR.



Entry	Compound No.	Core	Hinge (R <sup>1</sup> )	Isomer	mTOR pIC <sub>50</sub>
1	<b>31</b>	2-Py.	Morph.	-	3.9
2	<b>32</b>		DHP	-	4.2
3	<b>34a</b>		CPP	1 <i>R</i> , 6 <i>S</i>	3.0
4	<b>34b</b>			1 <i>S</i> , 6 <i>R</i>	3.5
5	<b>33</b>		THP	-	3.0
6	<b>35</b>	4-Pyrim.	Morph.	-	5.9
7	<b>36</b>		DHP	-	5.7
8	<b>38a</b>		CPP	1 <i>R</i> , 6 <i>S</i>	3.0
9	<b>38b</b>			1 <i>S</i> , 6 <i>R</i>	5.1
10	<b>37</b>		THP	-	4.5
11	<b>39a</b>	2-Pyrim.	CPP	1 <i>R</i> , 6 <i>S</i>	4.5
12	<b>39b</b>			1 <i>S</i> , 6 <i>R</i>	4.5
13	<b>40a</b>	3-Py.	CPP	1 <i>R</i> , 6 <i>S</i>	5.3
14	<b>40b</b>			1 <i>S</i> , 6 <i>R</i>	5.3
15	<b>41a</b>	4-Py.	CPP	1 <i>R</i> , 6 <i>S</i>	4.4
16	<b>41b</b>			1 <i>S</i> , 6 <i>R</i>	4.3
17	<b>42a</b>	Phenyl.	CPP	1 <i>R</i> , 6 <i>S</i>	5.3
18	<b>42b</b>			1 <i>S</i> , 6 <i>R</i>	3.0

**Table 11:** Results of the mTOR Kinobead assay. N= 3 or greater in all cases. All potency ranges fall within the error of the assay (0.3) and therefore are not shown. NB: A description of this assay procedure can be found in chapter II of this thesis.

As well as biological activity, it is important to understand how the replacement of morpholine with CPP may affect the physicochemical properties of potential drug molecules. The tool compounds were tested in physicochemical assays in order to determine lipophilicity, solubility and permeability (

**Table 12)** CPP-containing compounds are more lipophilic than their morpholine containing analogues, however, somewhat counter-intuitively, solubility is improved, and permeability

remains at an encouraging level, therefore the addition of the CPP group has the potential to tune physicochemical properties in interesting ways depending on

Entry	Compound No.	Core	Hinge (R <sup>1</sup> )	Isomer	Solubility $\mu\text{g/mL}$	AMP nM/sec	Chrom LogD pH 7.4	Chrom LogP
1	<b>31</b>	2-Py.	Morph.	-	304	680	4.2	4.21
2	<b>32</b>		DHP	-	391	577	4.45	4.46
3	<b>34a</b>		CPP	1 <i>R</i> , 6 <i>S</i>	355	546	5.02	5.00
4	<b>34b</b>		1 <i>S</i> , 6 <i>R</i>	353	553	4.98	4.98	
5	<b>33</b>		THP	-	385	530	4.25	4.25
6	<b>35</b>	4-Pyrim.	Morph.	-	414	500	2.72	2.73
7	<b>36</b>		DHP	-	443	573	3.57	3.56
8	<b>38a</b>		CPP	1 <i>R</i> , 6 <i>S</i>	460	605	4.02	4.02
9	<b>38b</b>		1 <i>S</i> , 6 <i>R</i>	525	570	4.01	4.02	
10	<b>37</b>		THP	-	390	490	3.34	3.33
11	<b>39a</b>	2-Pyrim.	CPP	1 <i>R</i> , 6 <i>S</i>	358	435	4.09	4.10
12	<b>39b</b>			1 <i>S</i> , 6 <i>R</i>	429	475	4.11	4.12
13	<b>40a</b>	3-Py.	CPP	1 <i>R</i> , 6 <i>S</i>	355	330	3.39	3.40
14	<b>40b</b>			1 <i>S</i> , 6 <i>R</i>	451	305	3.39	3.40
15	<b>41a</b>	4-Py.	CPP	1 <i>R</i> , 6 <i>S</i>	519	525	3.72	3.72
16	<b>41b</b>			1 <i>S</i> , 6 <i>R</i>	463	495	3.71	3.71
17	<b>42a</b>	Phenyl.	CPP	1 <i>R</i> , 6 <i>S</i>	68	425	5.23	5.49
18	<b>42b</b>			1 <i>S</i> , 6 <i>R</i>	65	400	5.24	5.49

the requirements of a project.

**Table 12:** Physicochemical properties for tool compounds **31-42**. Description of the Solubility, permeability and chromLogD/P assays are available in chapter II of this thesis.

## **2.6 Conclusion**

Within this chapter, a range of techniques including DFT studies, X-ray crystallography, NMR and biological/ physicochemical assays have been utilised in an attempt to fully delineate the properties of the cyclopropylpyran hinge binding fragment.

Analysis of the cyclopropylpyran hinge binding fragment has illuminated several areas in which significant improvements over the commonly used cyclic *N*-aryl based hinge binding fragments has been achieved. The first of these is novelty, morpholine based hinge binding fragments are ubiquitous in the literature, and therefore a previously unreported alternative which has demonstrated comparable potency in model compounds when tested against lipid kinase targets offers a significant advantage in the discovery of novel compounds.

As well as the proprietary advantage offered by cyclopropylpyran, the fragment also offers a number of advantages which improve the quality of inhibitor compounds. The first of these is an increase in fraction  $sp^3$ , this is a measure of the 3-D character of a molecule and an increase in this parameter has been previously associated with a higher chance of developability and an increase in selectivity.<sup>116,117</sup> Cyclopropylpyran also has a number of perceived toxicity improvements over corresponding *N*-aryl amine compounds, for instance removal of an embedded aniline which removes the risk of genotoxic metabolites forming *in vivo*.<sup>165</sup> It was also postulated at this stage that the lower propensity for electron donation into aromatic systems observed for cyclopropylpyran compared with corresponding *N*-aryl amine compounds may offer a toxicity advantage for compounds which contain aniline-based backpocket groups. This particular factor is investigated in detail within chapter II of this thesis.

It is also important to consider the limitations of cyclopropylpyran. The synthesis of compounds containing cyclopropylpyran is significantly more complex than the corresponding *N*-aryl amine containing compounds and currently involves synthesis of a bespoke boronate which then undergoes a challenging  $sp^2$ - $sp^3$  Suzuki-Miyaura cross-coupling. This reaction is often low yielding and could prove challenging and expensive in the later stages of lead optimisation, where multi-gram quantities of final product would be required. In addition to this, the resulting cyclopropylpyran-containing compound is racemic and therefore currently requires chiral separation, as an enantioselective synthesis has yet to be developed. The process of chiral separation is required as the regulatory agencies require that drug compounds are marketed as single enantiomers, unless the racemic mixture is a more effective drug.<sup>166</sup> On a small scale, as is the case with the current study, chiral HPLC is an appropriate technique for separation of racemic mixtures. However, on a larger scale this is extremely costly, and the large quantities of solvent required are environmentally unfriendly. With these limitations in mind, progression of cyclopropylpyran containing compounds to the later stages of drug development would be challenging with current synthetic strategy. Within our group work is ongoing on a chiral synthesis of cyclopropylpyran building blocks to overcome this challenge.

As well as the chemical tractability of cyclopropylpyran-containing compounds, this investigation has demonstrated that substitution of *N*-aryl amines for cyclopropylpyran is associated with an increase in lipophilicity. An increase in lipophilicity generally contributes to decreasing solubility, selectivity and absorption, as well as increased permeability and metabolic turnover.<sup>167</sup> For the cyclopropylpyran/ morpholine matched molecular pair

compounds contained in this chapter however, there is a general concurrent increase in both lipophilicity and solubility. Further studies in the following chapter will aim to elucidate how an increase in lipophilicity affects other parameters such as selectivity.

The work carried out in this chapter has also aimed to determine the aryl rings with which cyclopropylpyran is compatible, assuming as in this study, that co-planarity is a requirement for biological activity. It has been found that electron deficient rings such as pyrimidine are compatible, as are pyridine rings in which there is a nitrogen adjacent to the cyclopropylpyran fragment. These compounds were predicted by DFT studies to preferentially occupy co-planar conformations and this was confirmed experimentally utilising a range of techniques such as X-ray crystallography, NOE NMR and evaluation of biological activity. Logically these results can be extrapolated to other electron-deficient systems such as triazines although these have not been considered in the current study.

The incompatibility of 3-pyridine and phenyl rings was also predicted by DFT before being confirmed experimentally. 4-Pyridine was predicted incorrectly by DFT to strongly prefer an orthogonal conformation. This compound crystallises in a co-planar conformation however NMR studies offer a less clear result. This result highlights a level of uncertainty around DFT predictions. However, generally these predictions have allowed identification of suitable cyclopropylpyran - core combinations and offers an advantage prior to compound synthesis.

It is anticipated that the results of this study provide a solid foundation to inform the medicinal chemist situations where incorporation of the cyclopropylpyran fragment or related structure may be effective both for PIKK inhibition space and more widely in drug discovery. With the results from this study in hand, chapter II of this thesis details the application of cyclopropylpyran to a series of mTOR inhibitor compounds.



**Chapter II: Development of  
pyrazolopyrimidine based mTOR  
inhibitor compounds with a  
cyclopropylpyran hinge binding motif.**

## 1. Introduction

### 1.1 Bicyclic mTOR Inhibitors

With the positive results reported for the application of the CPP hinge binding fragment to monocyclic systems in the previous chapter of this thesis, our investigation was focused on whether this could be replicated in bicyclic systems, which have proved to be highly potent and selective molecules in the literature.

In a series of publications which were disclosed between 2009 and 2010, medicinal chemistry groups at Wyeth Research reported the discovery of a series of 5,6-bicyclic mTOR inhibitors. A number of fused bicyclic cores were investigated including: pyrrolopyrimidines,<sup>168</sup> thienopyrimidines,<sup>169,170</sup> triazolopyrimidines<sup>171</sup> and purines.<sup>172</sup> Example lead compounds from these series are shown in **Figure 38**.

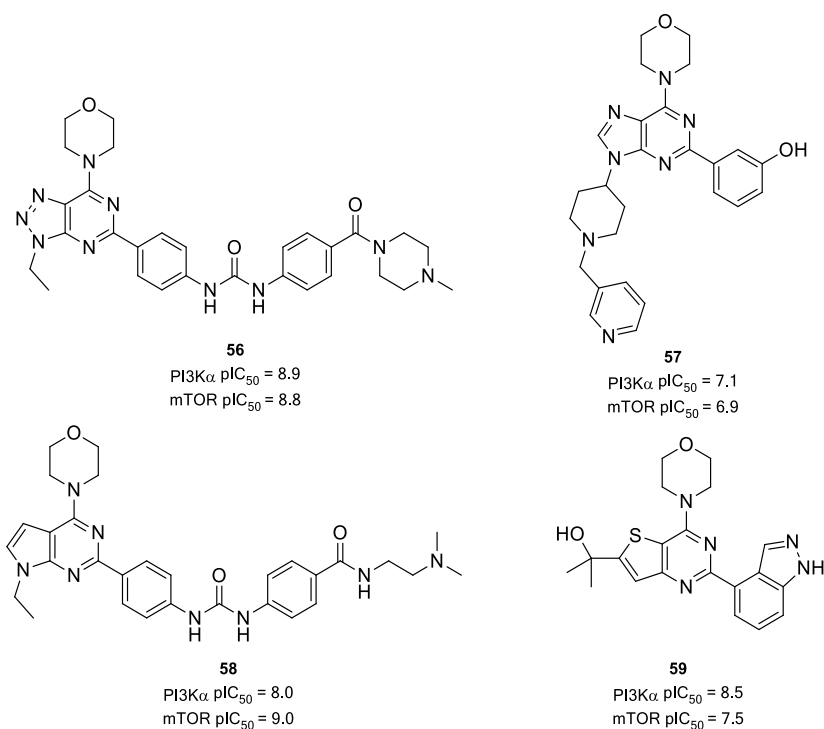


**Figure 38:** Example 5,6-bicyclic compounds from the literature.

In addition to these commonly employed 5,6 bicyclic systems, a number of 6,6 bicyclic systems have also been reported by AstraZeneca. The most notable examples of these compounds are Vistusertib (AZD2014) **17** which reached phase II clinical trials for a broad range of cancers, before being discontinued in November 2018 for safety/efficacy reasons,<sup>173</sup> and AZD8055 **16** which progressed to phase I clinical trials before being discontinued due to

risks around accurately predicting clinical exposure.<sup>174</sup> The structures and related biological data for these compounds are shown in **Figure 39**. Both compounds are based on a pyridopyrimidine structure, although examples based on a pteridine core **60** were also investigated and found to also have reasonable activity.<sup>110</sup>

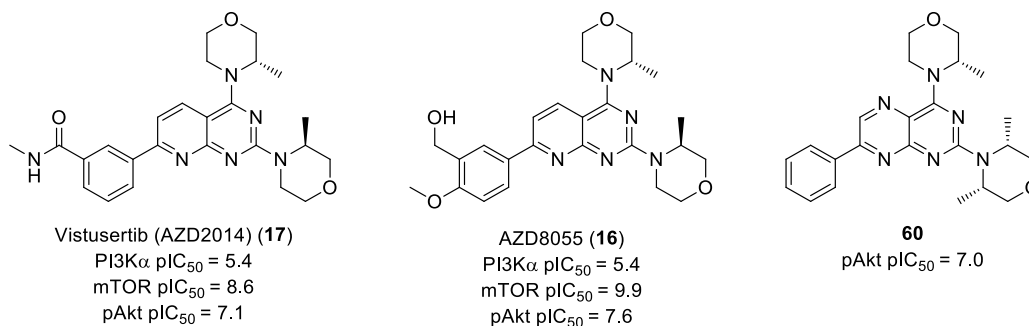


**Figure 39:** 6,6-bicyclic compounds reported by AstraZeneca.<sup>110</sup>

## 2.1 Compound Profiling

Before synthesis and analysis of any compounds, it is important to establish how they will be assessed. This section outlines the biological and physicochemical assays to which the compounds will be subject. This section also provides information on the procedure and underlying scientific concepts behind the assays which are used to evaluate potential inhibitor compounds. Assays were performed elsewhere within our laboratories.

### 2.1.1 mTOR Kinobead Chemoproteomic Binding Assay

When compounds are synthesised, they will be tested in a variety of *in vitro* assays to assess which compounds are suitable for progression into *in vivo* animal models. Compounds are first tested in the primary mTOR Kinobead assay, which provides the mTOR potency for the compound. This is a chemoproteomic binding assay which assesses potency against native full-length proteins directly from cells, providing a more accurate representation of the activity of a compound than biochemical assays which use recombinant protein.<sup>175</sup> A schematic showing the assay procedure is shown in **Figure 40**.

The mTOR chemoproteomic binding assay is a competition binding assay based on affinity enrichment of endogenous mTOR from whole cell lysate (HuT-78) with a Kinobead binding matrix in the presence of a test inhibitor compound. A kinobead is a polymer bead which contains, on its surface, immobilised broad-spectrum kinase inhibitors. After a period of incubation, the plates are washed which removes any enzyme which remains unbound. Remaining bound enzyme is then eluted from the Kinobeads. The eluted enzyme is then

incubated on a nitrocellulose membrane with a primary rabbit anti-mTOR antibody and a secondary anti-rabbit antibody coupled to an infra-red dye. The membrane is then scanned, and signal intensities are quantified. Reduced binding of mTOR to the Kinobeads in the presence of an inhibitor will lead to a lower/absent signal, and therefore the potency of the test compound can be quantified.

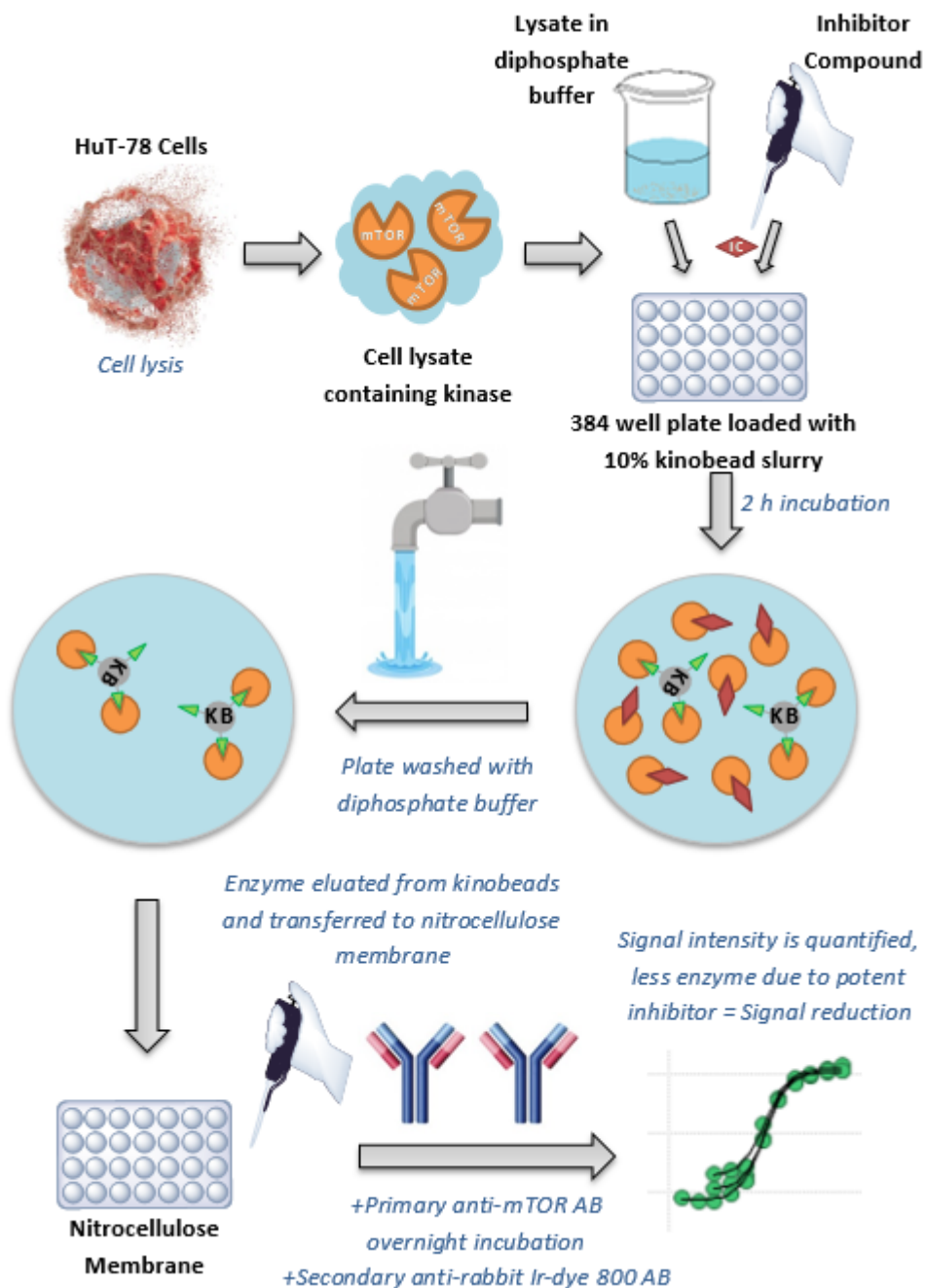
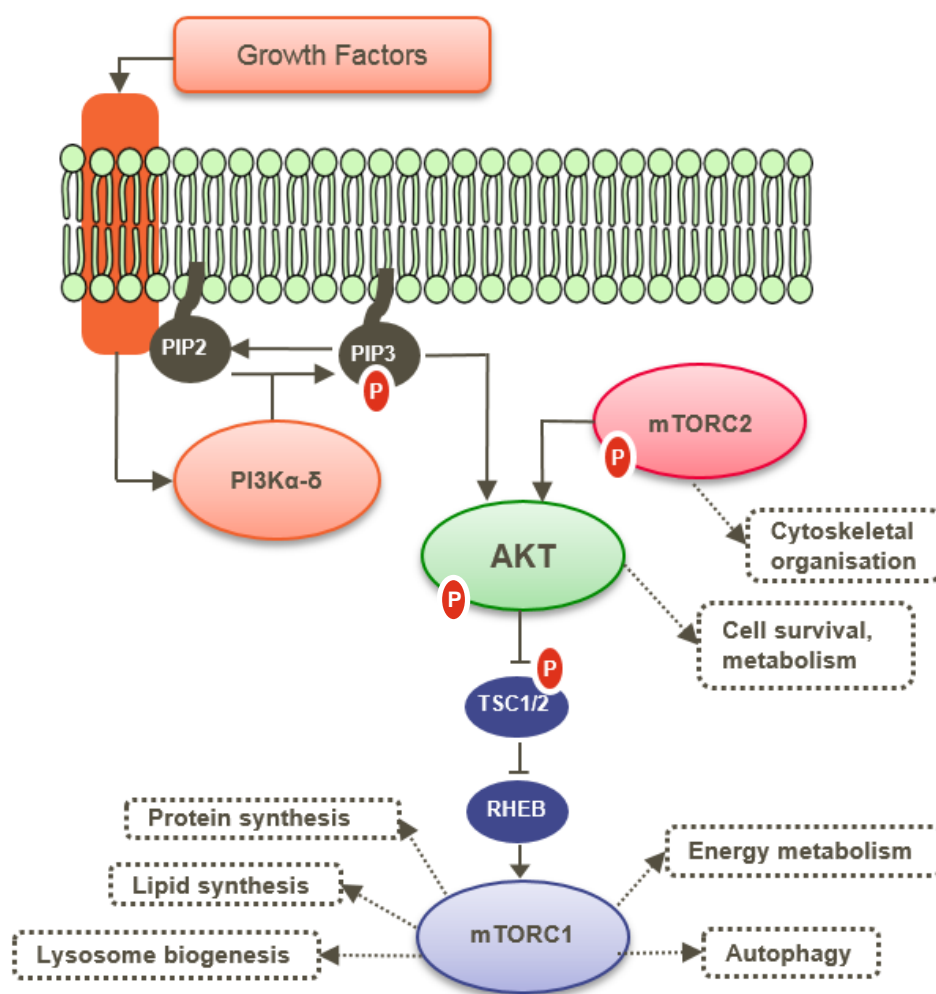


Figure 40: Schematic diagram showing the mTOR kinobead binding assay procedure.<sup>175</sup>

## 2.1.2 phospho-Akt Cellular Assay

As well as an indication of compound potency at the target enzyme, a cellular assay is able to provide information on the ability of a compound to cross the cellular phospholipid bilayer. This is important for an intracellular target such as mTOR, and therefore cellular assays are a vital component of the compound screening process.

Akt (protein kinase B) is a kinase which is a downstream target of mTORC2 (**Figure 41**) Akt is positioned at the membrane *via* binding to PIP<sub>3</sub> where it is phosphorylated by mTOR. Phosphorylated Akt then has a number of downstream cellular effects.<sup>72</sup> The level of phosphorylated Akt in a cell is therefore an indication of mTOR activity in a cellular context. This is the principle underlying the pAkt cellular assay.



**Figure 41:** Simplified view of the PI3K/mTOR/Akt pathway.<sup>78</sup>

The procedure for the cellular pAkt assay is shown in **Figure 42**. Human lung fibroblasts are dispensed onto 384 well plates, which are then treated with test inhibitor compound and

incubated. Cell signalling lysis buffer is added which prevents any further phosphorylation of Akt. This cell lysate is then transferred onto a GAR plate and shaken overnight. Antibodies are added to detect both total and phosphorylated Akt. These antibodies are attached to electrochemiluminescent labels (SULFO-TAG) which emit light when an electric current is applied. This light emission is used to quantify the amount of phosphorylated Akt. A highly potent mTOR inhibitor will prevent phosphorylation of Akt, and therefore a weaker signal is observed in this case.

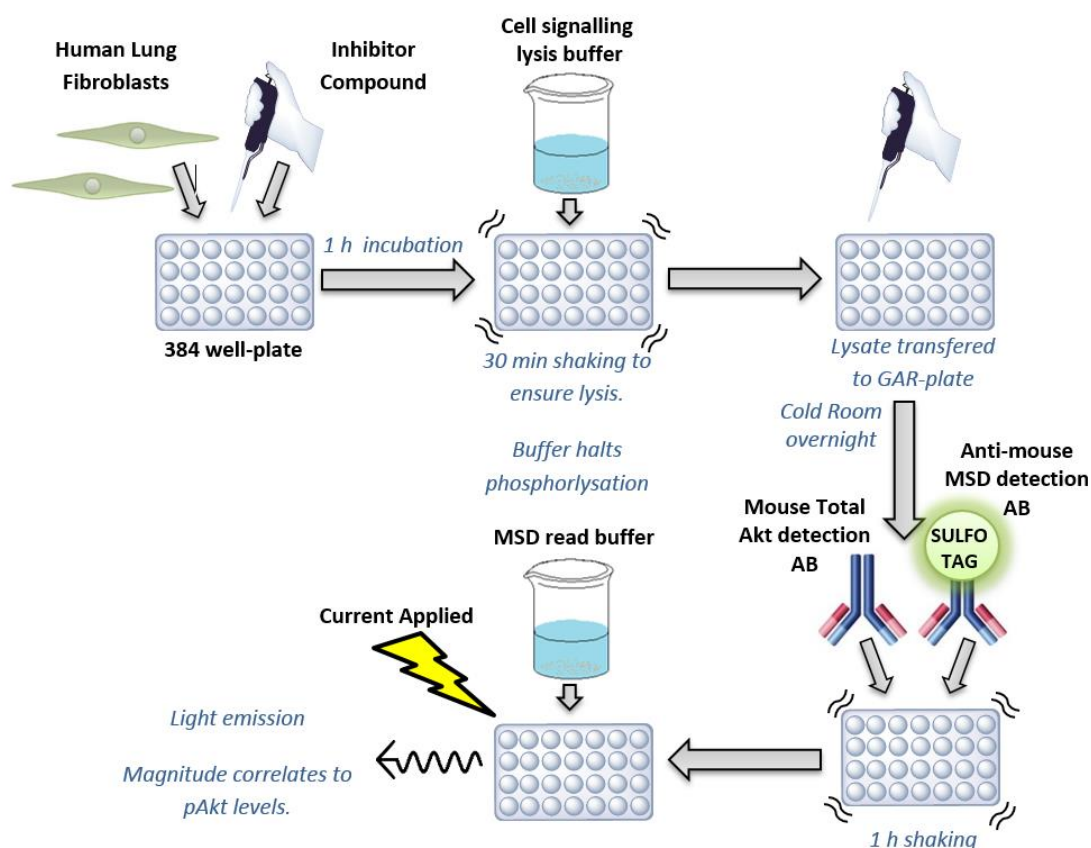


**Figure 42:** Schematic diagram showing the electrochemiluminescence pAkt assay.<sup>176</sup>

### **2.1.3 “Scar-in-a-jar” Phenotypic Assay**

Fibrotic conditions such as IPF are characterised by excessive production and deposition of collagen, which converts normal tissue into scar tissue and is associated with loss of function. Therefore, to validate the effectiveness of any promising lead compounds which are synthesised, their ability to prevent collagen production must be assessed. The scar-in-a-jar assay is an *in vitro* phenotypic assay which examines collagen 1 deposition and pro-collagen 1 c-terminal peptide generation. This is an effective representation of clinical disease and reduces the need for animal models within the early drug discovery stage.

The assay measures collagen deposits produced directly by cells in a macromolecular environment. A macromolecule, FiColl mix, is added to mimic molecular crowding and this accelerates the deposition of collagen in the time-frame of the assay. TGF- $\beta$  is used to induce collagen deposition in fibroblast cultures. This causes fibroblasts to lay down mature collagen 1 which is detected by immunocytochemistry and quantified by image algorithms using an INCell 2000 analyser. The presence of a highly potent mTOR inhibitor reduces the level of collagen and therefore an IC<sub>50</sub> value can be obtained from the relative levels of collagen that can be visualised. There are two versions of the assay; one in which healthy lung tissue is used, and another where tissue from diseased donors is used. The general procedure for the assay is shown in **Figure 43**.

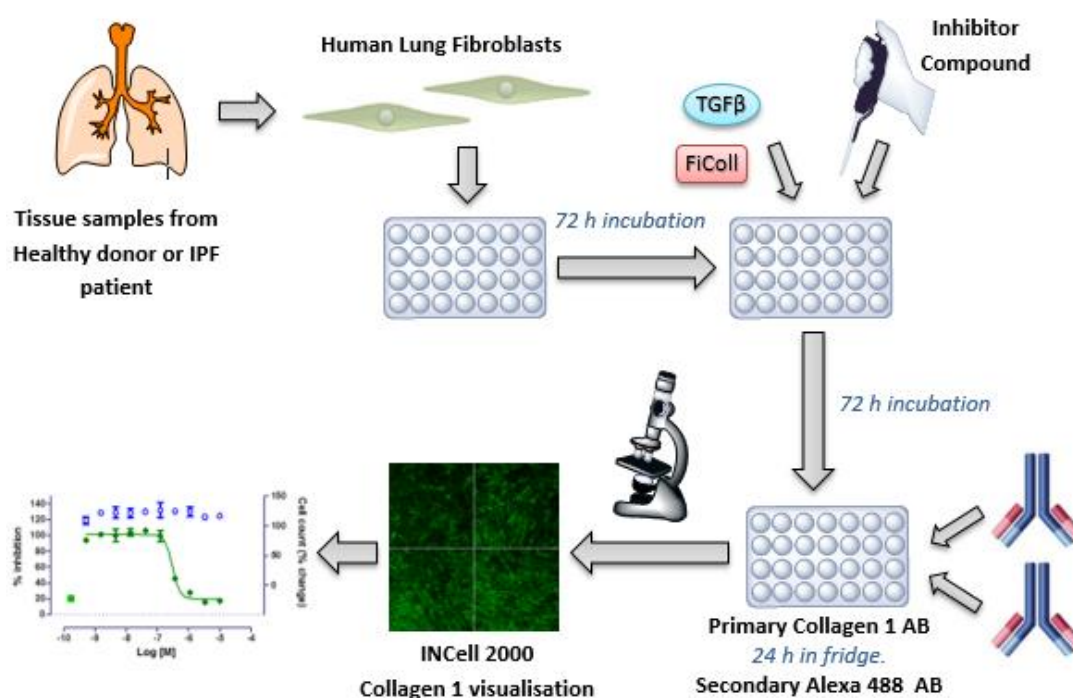


**Figure 43:** Schematic diagram of the scar-in-a-jar assay.<sup>97,177</sup>

### **2.1.4 PI3K TR-FRET Assay**

Obtaining high selectivity for mTOR over the closely related PI3K family of lipid kinases is challenging, it is however desirable for compounds to be highly specific for mTOR as this may cause fewer side effects meaning that the compound will be better tolerated. To assess selectivity over the PI3K family, compounds were tested against the PI3Ks in a TR-FRET assay. The principles of this assay are outlined in **Figure 44**.



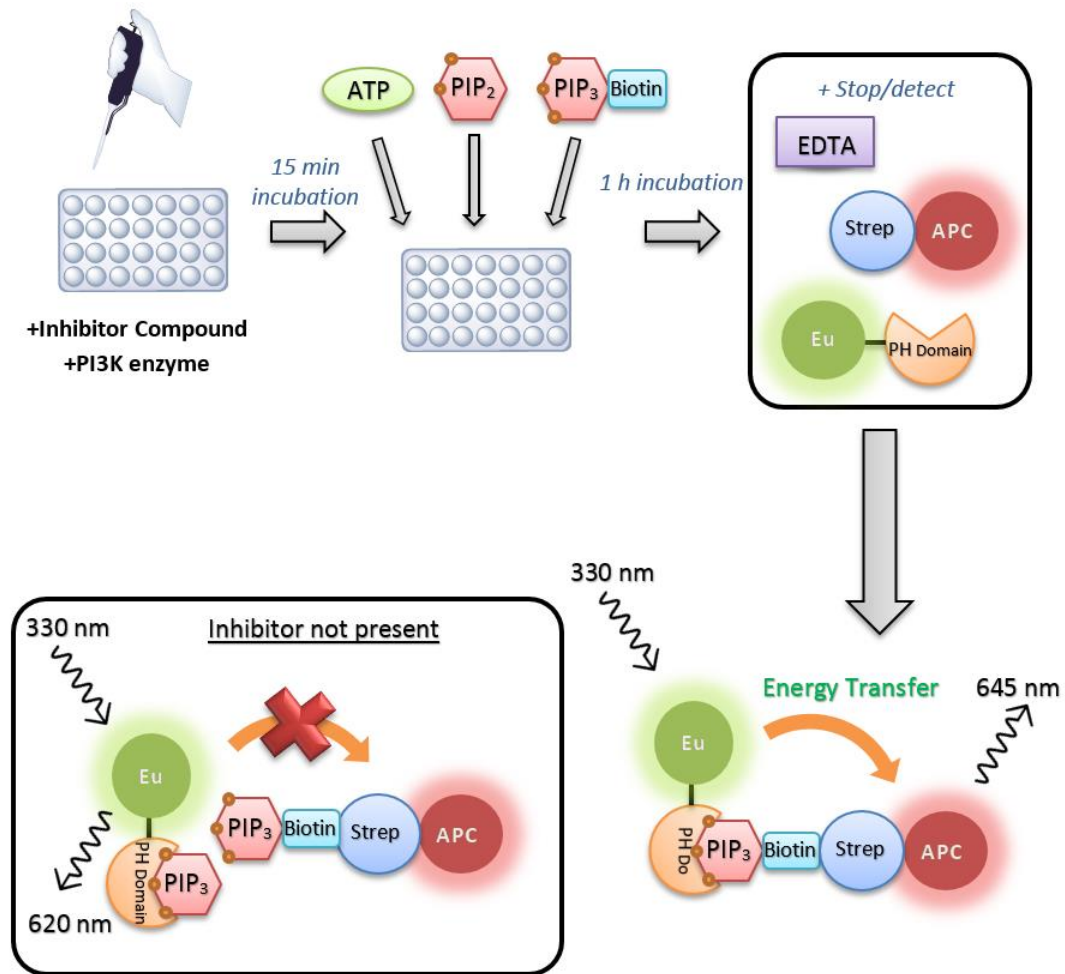


**Figure 44:** Schematic diagram showing the TR-FRET assay for PI3K.<sup>178</sup>

This assay is based on the principle that the PI3K family of kinases phosphorylate phosphatidylinositol 4,5-bisphosphate (PIP<sub>2</sub>) to form PIP<sub>3</sub>. PIP<sub>3</sub> binds to the PH domain of GPR-1 with high affinity. In this assay there is a PIP<sub>3</sub>-biotin complex which is able to bind to the PH domain of (Eu)-labelled anti-GST, GST tagged GRP1 through PIP<sub>3</sub>, whilst simultaneously binding to streptavidin tagged allophycocyanin (strep-APC) through biotin. APC is a fluorescent protein and Eu excitation of the complex with 330 nm light causes an energy transfer to APC which then emits light at 665 nm.

When PI3K enzymes are able to convert PIP<sub>2</sub> into PIP<sub>3</sub>, the free PIP<sub>3</sub> is able to compete for binding to GRP-1 and therefore a reduction in signal occurs. The more effective a PI3K inhibitor is, the less PIP<sub>3</sub> is produced which results in greater PIP<sub>3</sub>-biotin binding to GRP-1, resulting in an increased signal. This signal can be quantified to give a IC<sub>50</sub> value for the test compound.<sup>178</sup> This was carried out with each PI3K isoform of interest ( $\alpha$ ,  $\beta$ ,  $\delta$ ,  $\gamma$ ).



### 2.1.5 Physicochemical Assays

In addition to high potency against the desired target and selectivity over closely related targets, a potential drug compound must have favourable physicochemical properties, so that it can reach the intended site of action and possess appropriate pharmacokinetics. To assess their properties, lead compounds are tested in various physicochemical assays.

Solubility is assessed with a kinetic solubility measurement using a HPLC charged aerosol detection (CAD) technique.<sup>179</sup> In this assay the kinetic aqueous solubility at neutral pH is determined by measuring the concentration of solute in solution after precipitation from a DMSO stock solution. This method is useful as it is high-throughput, and therefore compound data can be obtained for a large number of compounds in a short space of time. This assay however, has the drawback that it is not particularly representative of a biological system, and in addition to this, the CAD solubility assay is precipitative from DMSO. This technique removes and factors due to slow dissolution. Promising compounds can therefore be further tested in a dissolution assay using simulated lung fluid (SLF).<sup>180</sup> SLF is a buffer with an ionic composition similar to human lung fluid, and therefore the solubility of compounds in this medium is likely to be more representative of their *in vivo* solubility.

Permeability is a measure of the ability of a compound to cross the cellular phospholipid bilayer, which is important when a compound is required to cross a cellular wall in order to reach the site or action. To measure their permeability, compounds were tested using a HPLC artificial membrane permeability assay in a high-throughput manner. Another assay that can be used to investigate compound permeability is the Madin-Darby Canine Kidney (MDCK) assay.<sup>181</sup> This assay requires solid material and therefore was only used for more promising lead compounds.

The lipophilicity of a compound is important to know when optimising lead compounds as it has an effect on a number of ADMET (absorption, distribution, metabolism, excretion, toxicity) parameters such as: volume of distribution,<sup>182</sup> protein binding<sup>183</sup> and hERG activity.<sup>184</sup> Lipophilicity is measured in terms of LogP, which is the partition coefficient between octanol and water.<sup>185</sup> In our laboratories a chromatographic hydrophobicity index (CHI) is utilised.<sup>186</sup> A test compound is eluted on a reverse-phase column with water/acetonitrile, and the retention time is used in combination with the hydrogen bond donor count (HBC) to calculate the relative lipophilicity value in octanol (LogP) using **equation 1** in **Figure 45**.<sup>187</sup> An early study, performed in 1977, reported that LogP values are not an accurate representation of the lipophilicity of compounds with ionisable groups.<sup>188</sup> The degree

of ionisation is dependent on the pH of the solution in which it is dissolved. The study asserted that a more accurate representation would, therefore, involve undertaking the partition experiment in a solvent buffered to physiological pH (pH 7.4). The authors termed this the distribution coefficient, expressed as LogD. In our laboratories, we are able to generate LogD values using a similar CHI experiment conducted at a specific pH. This will give a LogD value using **equation 2** in **Figure 45**.<sup>186</sup> Subsequent research showed that CHI logD values did not correlate well to logD values generated from shake-flask experiments. Based on this a new equation was subsequently derived to convert CHI logD into chromLogD values, which more closely represent the values obtained from shake-flask experiments. (**equation 3** in **Figure 45**).<sup>189</sup>

$$\text{LogP} = 0.05\text{CHI} + 0.41\text{HBC} - 1.41 \quad \text{(Equation 1)}$$

$$\text{LogD}_{\text{pH}} = \text{CHI}_{\text{pH}} - 1.46 \quad \text{(Equation 2)}$$

$$\text{Chrom LogD}_{\text{pH}} = 0.08\text{CHI}_{\text{pH}} - 2 \quad \text{(Equation 3)}$$

**Figure 45:** The equations used for calculating LogP and LogD values from CHI chromatographic retention times.

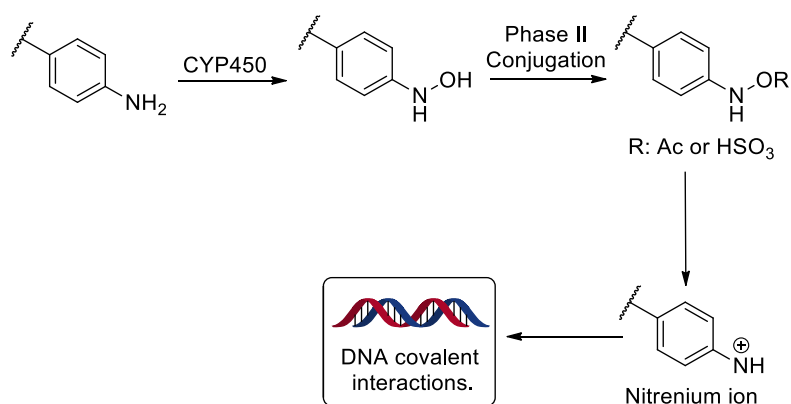
It is also important to understand the metabolism of potential drug compounds, as this can provide information on the likely half-life of a drug once it reaches the systemic circulation. For an oral compound, a low clearance is desirable as this means that the active drug is available to exert its effect for a longer period of time. In an inhaled project however, this can be reversed, and a moderate-to-high clearance is often preferred. The reason for this is that the drug interacts directly with the site of action (the lungs) and once it passes into the systemic circulation, rapid metabolism can help to minimise unwanted systemic exposure of the drug, therefore addressing issues related to target-mediated side effects provided the metabolites are inactive and non-toxic.

Clearance can be measured *in vitro* using liver microsomes. These are sub-cellular fractions which contain membrane bound enzymes that metabolise drugs.<sup>190</sup> The liver is the most important site of drug metabolism in the body and approximately 60% of marketed compounds are cleared by hepatic CYP-mediated metabolism.<sup>191</sup> The experiment was run with microsomes from both humans and mice, as their CYP profiles differ. Given that early *in vivo* experiments would be carried out in mice, it is useful to understand the behaviour of compounds in this species. Some of the more promising lead compounds in the current study had microsomal stability tested.

## 2.1.6 Ames Mutagenicity Test

Aromatic amines are a class of compounds in which many members are carcinogenic. However, they are a privileged structure and appear in ~13% of currently marketed drugs.<sup>192</sup> It is therefore vital to understand what causes this mutagenicity and be able to establish if a novel aniline containing compound is likely to be carcinogenic.

The toxicity of aromatic amines is thought to be caused by their oxidation within the liver by CYP450 enzymes. This forms *N*-hydroxyl amines (primary metabolism). Secondary sulfination or acetylation enables formation of a nitrenium ion, which is an electrophile capable of binding to DNA (Scheme 16). This is thought to be one of the major routes through which DNA binding and subsequent mutations can occur.<sup>193,194</sup>



**Scheme 16:** Metabolism of aniline based compounds leading to genotoxic metabolites.

The Ames test is an assay that measures bacterial revertant colony formation. It was named after Bruce Ames, who first reported this assay in 1974.<sup>195</sup> The Ames test uses bacteria which are unable to biosynthesise their own histidine (*Salmonella typhimurium* His<sup>-</sup>). These strains are autotoxic as they require histidine for growth and therefore are unable to grow on histidine free media. In the presence of a possible mutagen, the bacterial DNA may undergo point-mutations which allows the mutant bacteria to start producing histidine, meaning they are able to grow. If significantly more bacterial colonies grow on the plate treated with test compound, then this compound is deemed mutagenic. Rat liver extract (S9-Mix) is included to metabolise the compound of interest, as this enables the test to also establish if any metabolites are genotoxic (Figure 46).<sup>196</sup>

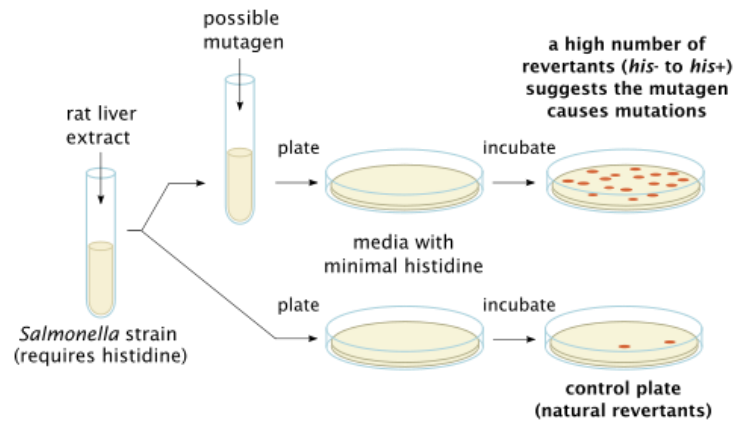


**Figure 46:** Schematic diagram showing the Ames mutagenicity test.

## 2.1.7 Compound Testing

**Figure 47** summarises the screening cascade in which compounds will be tested. This centres around the project aims (*vide-infra*) of achieving a novel series of mTOR inhibitor compounds which offer a range of differentiated physicochemical properties.

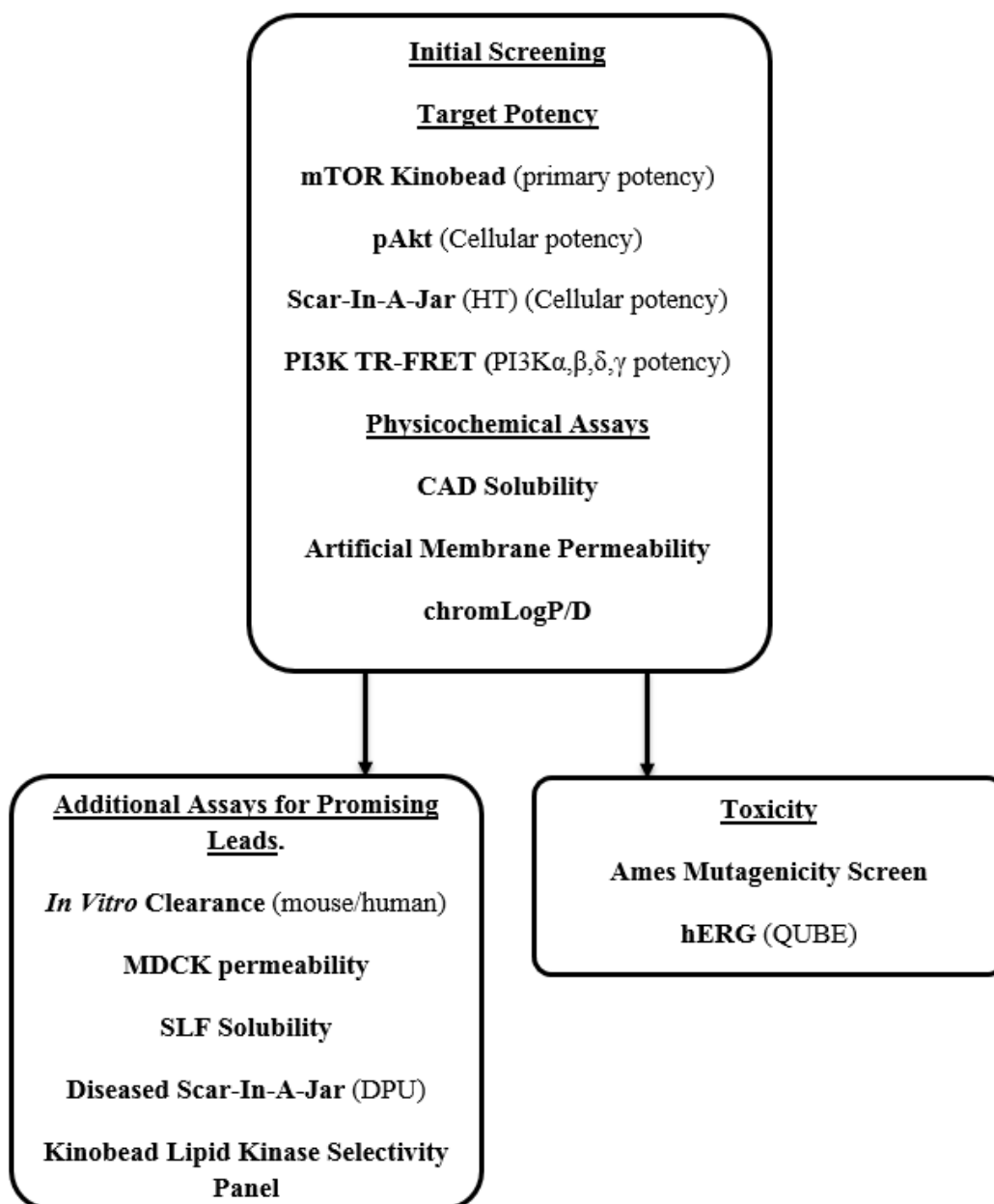


**Figure 47:** Screening cascade for target compounds.

## 2.2 Dihedral Angle Scanning for Cyclopropylpyran Bicyclic Compounds

Before synthesis of any compounds, examples of potential 5,6- and 6,6- bicyclic cyclopropylpyran containing compounds were modelled in a dihedral angle scanning study (**Figure 47 & 48**) in order to predict if compounds were likely to be able to occupy the coplanar conformation required for interaction with the mTOR binding pocket. This same methodology was used to assess tool compounds **22-30** in the previous chapter and generally provided good predictions of the favoured CPP conformation observed within X-ray crystal structures (*vide supra*).

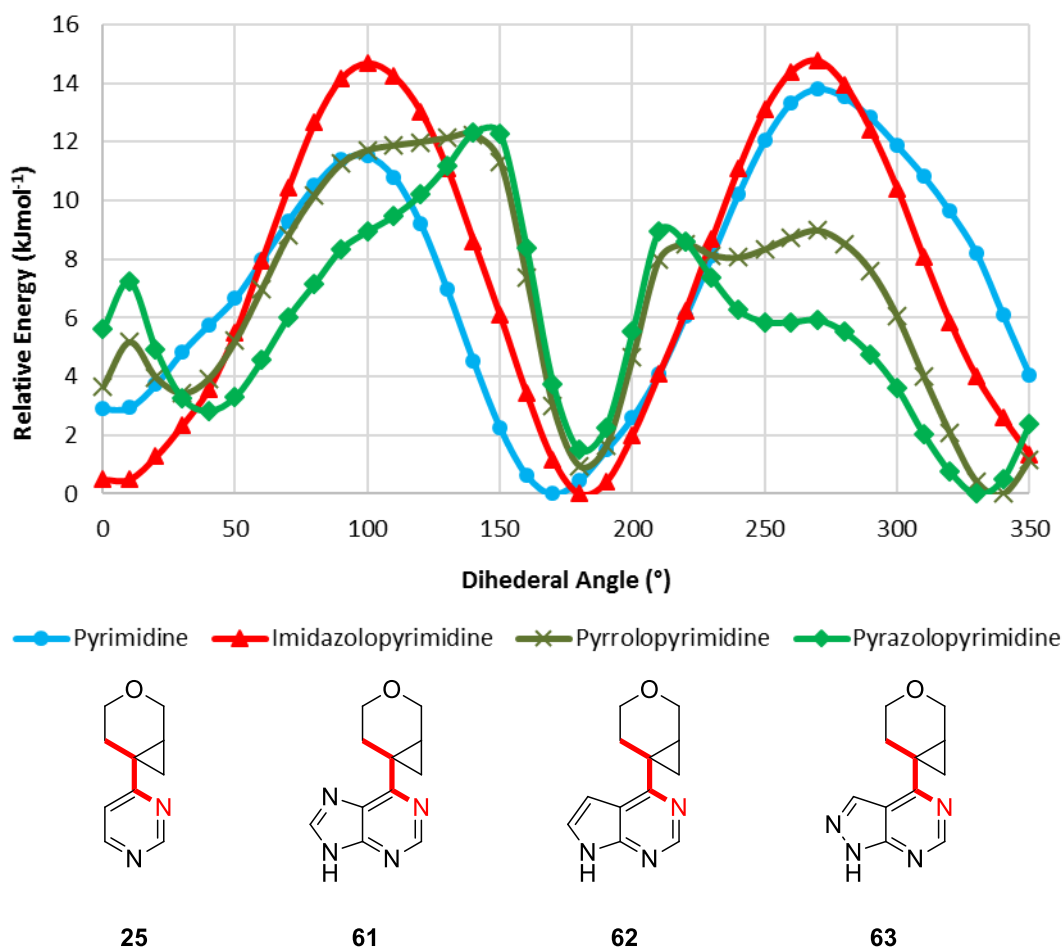


**Figure 48:** Dihedral scan showing minimum energy conformations for CPP 5,6 bicyclic systems (**61-63**). Parent pyrimidine (**25**) is included for comparison.<sup>121</sup>

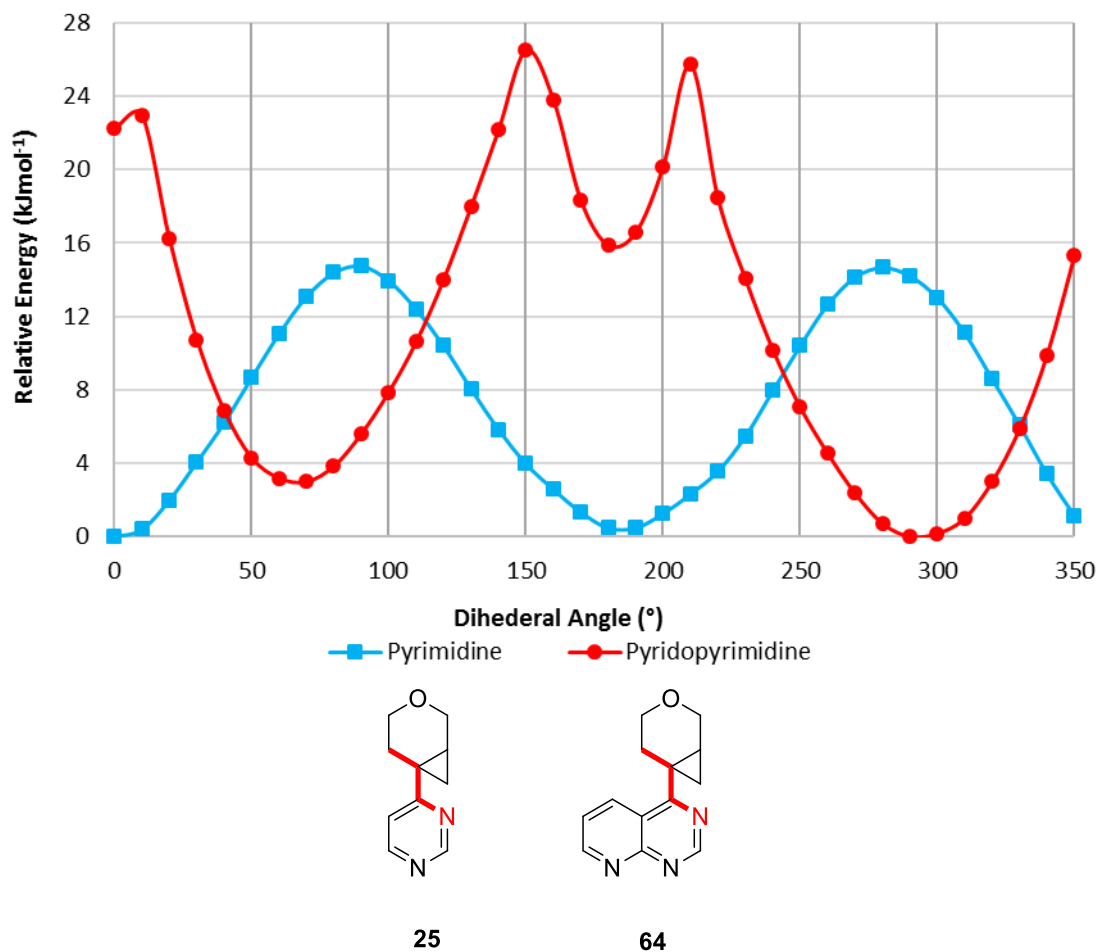


**Figure 49:** Dihedral scan showing minimum energy conformations for CPP pyridopyrimidine **64**. Parent pyrimidine **25** is included for comparison.<sup>121</sup>

5,6-Bicyclic systems (**61-63**) appeared from the dihedral angle scanning study to be compatible with cyclopropylpyran in terms of the favourable co-planar conformation being adopted. Imidazolopyrimidine **61** in particular has an energy profile which is very similar to pyrimidine **7**. For pyrazolopyrimidine **63** and pyrrolopyrimidine **62** the system is complicated by the steric impact of the proton at position-3 of the 5-membered ring. For 5,6 Bicyclic systems this proton is at a sufficient distance that co-planar conformations are favoured. **Figure 50** shows the two low energy conformations of pyrazolopyrimidine. We have postulated that the lowest energy conformation for this compound (**Figure 50, pane A**) represents a compromise between steric clash and stabilising electronic overlap. Interestingly, the local minimum at 180° (**Figure 50, pane B**) appears to be caused by the favourable placement of the position-3 proton between the two geminal cyclopropylpyran protons, this co-planar conformation may also be stabilised by electronic overlap.

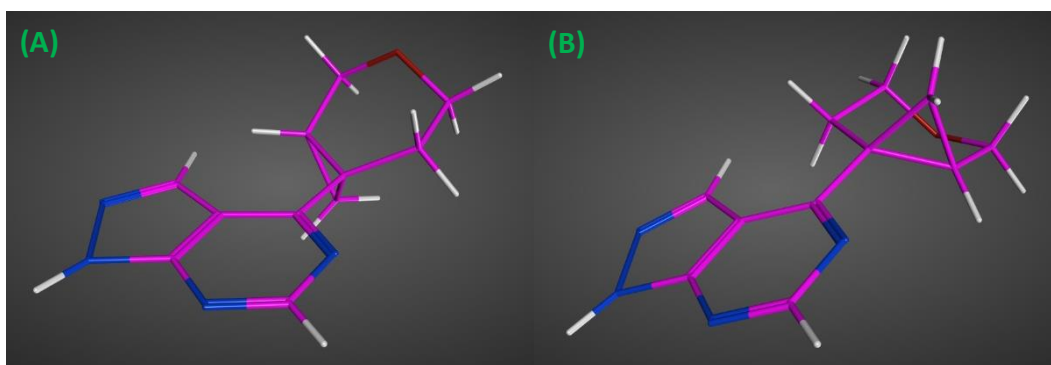
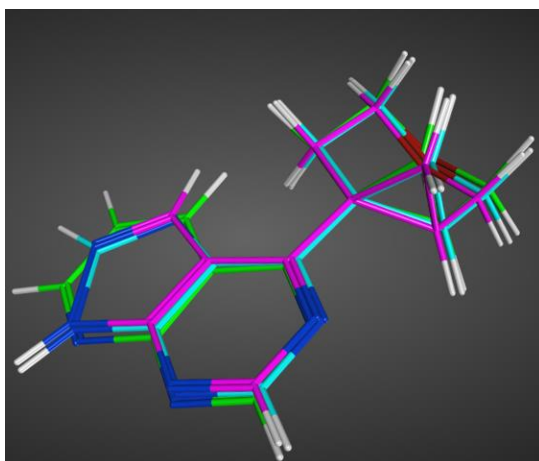


**Figure 50:** Structures of pyrazolopyrimidine **63** generated in MOE. The dihedral angle was manually set to show minimum energy conformation as predicted in dihedral angle scanning study. **(A)** 330 ° global minimum. **(B)** 180 ° local minimum

Pyridopyrimidine **64** is not predicted from the dihedral angle scanning study to occupy a coplanar conformation (**Figure 49**). This is thought to be due to the closer proximity of the proton in position-5 of the pyridopyrimidine ring compared with the corresponding proton within a 5,6-bicyclic system (**Table 13**)



Entry	Compound	Syn-H	Anti-H
1	<b>64</b>	1.68	1.32
2	<b>63</b>	2.00	1.68

**Table 13:** Distances between geminal CH<sub>2</sub> protons and proton in adjacent ring of the bicyclic system for pyrazolopyrimidine **63** and pyridopyrimidine **64**. NB: *Syn*- represents proton on the same side of the pyran ring as the cyclopropane ring.

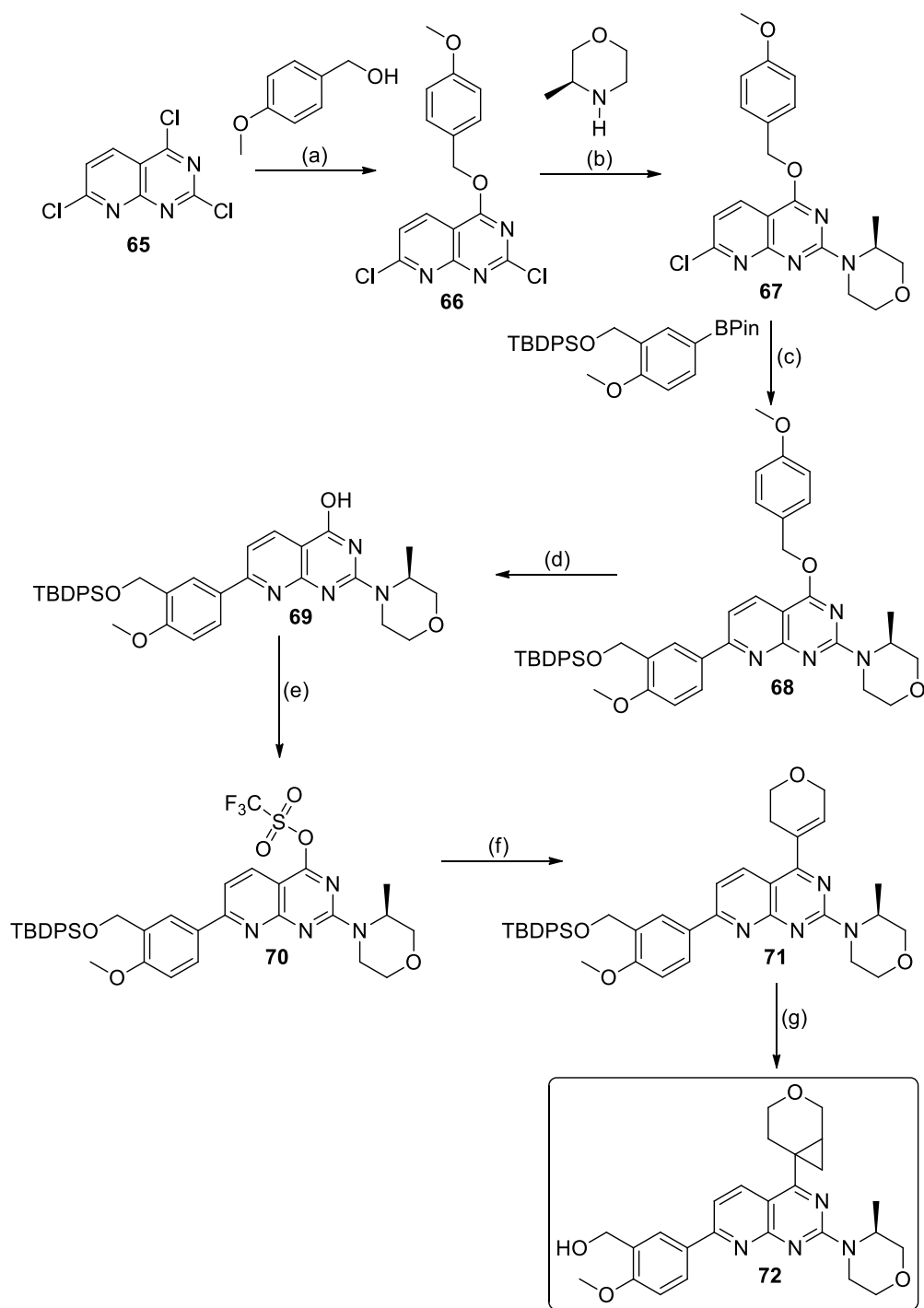
The predictions made by these dihedral scanning experiments suggest that 5,6-bicyclic systems may tolerate cyclopropylpyran as a replacement hinge binding fragment, whereas 6,6-bicyclic systems are unlikely to do so.



## **2.3 Bicyclic Core Compounds**

### **2.3.1 AZD8055 Matched Molecular Pair**

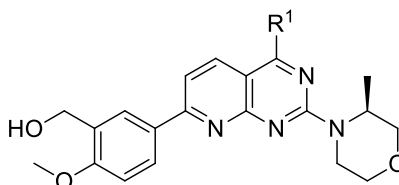
Cyclopropylpyran containing pyridopyrimidine compounds were synthesised by another member of our laboratory<sup>139</sup> and these compounds allow us to further build confidence in the validity of predictions based on dihedral scanning experiments. AZD8055 (**16**) was a highly potent and selective compound which progressed into phase I clinical trials. Its clinical development was terminated due to high hepatic turnover, and for this reason the core fragment may offer advantages as an inhaled molecule. At the time of synthesis, the validity of predictions from the dihedral scanning experiments was not well established and so the cyclopropylpyran AZD8055 analogue **72** was synthesised despite predictions that it may not occupy the required conformation for binding. The synthesis of this compound is shown in **Scheme 17** and was performed by another member of our laboratories.<sup>139</sup>



(a) LiHMDS, THF, DCM, r.t., 30 min, 68% yield (b) DIPEA, 2-MeTHF, r.t., 30 h, 94% yield (c) Pd(dppf)Cl<sub>2</sub>, K<sub>2</sub>CO<sub>3</sub>, 2-propanol: H<sub>2</sub>O,  $\mu$ Wave, 110 °C, 40 min, 47% yield (d) H<sub>2</sub>, Pd/C, EtOH, EtOAc, r.t., 24 h, 34% yield (e) Tf<sub>2</sub>O, TEA, CHCl<sub>3</sub>, r.t., 5 h, quant. (f) 2-(3,6-dihydro-2H-pyran-4-yl)-4,4,5,5-tetramethyl-1,3,2-dioxaborolane, Pd(dppf)Cl<sub>2</sub>, 1,4-dioxane, H<sub>2</sub>O,  $\mu$ Wave, 110 °C, 30 min, 110 °C, 44% yield (g) (I) Me<sub>3</sub>SOCl, NaH, DMSO, r.t., 21 °C, 20h (II) TFA, r.t., 16 h, 27% yield over 2 steps.

**Scheme 17:** Synthesis of cyclopropylpyran AZD8055 analogue.<sup>139</sup>

Comparison of the cyclopropylpyran analogue **72** with AZD8055 (**16**) confirmed that the cyclopropylpyran hinge binding fragment is poorly tolerated. The compound is ~100 fold lower in potency at mTOR. Compound **72** is also >100 fold less active in the cellular Akt assay. Compound **72** has increased lipophilicity compared with AZD8055 and as a result of this its permeability is slightly improved whilst solubility is decreased. Due to the significantly lower activity of compound **72**, cyclopropylpyran was not further considered in pyridopyrimidine based compounds. The poor performance of CPP **72** further validates the use of dihedral angle scanning studies to predict the suitability of CPP containing compounds.



Entry	Compound	R <sup>1</sup>	mTOR pIC <sub>50</sub>	pAkt pIC <sub>50</sub>	Solubility (µg/mL)	AMP (nm/sec)	LogD/ LogP
1	<b>16</b>		8.5	7.5	356	459	4.6/4.7
2	<b>72</b>		6.5 (n=2)	5.4 (n=1)	206	500	4.9/4.9

**Table 14:** In-house Biological and physicochemical data for AZD8055 (**16**) and the cyclopropylpyran containing analogue **72**. N=3 or greater unless shown. All potency ranges fall within the error of the assay (mTOR= 0.3, Akt= 0.5) and therefore are not shown.

### 2.3.2 5,6-Bicyclic Core Scan

With DFT predictions indicating the potential suitability of 5,6 bicyclic compounds for combination with the cyclopropylpyran hinge, work was carried out elsewhere within our laboratory to establish the most efficient 5,6 bicyclic core – cyclopropylpyran combination.<sup>197</sup> A range of 5,6 bicyclic cores were considered and these are shown in **Figure 51**.

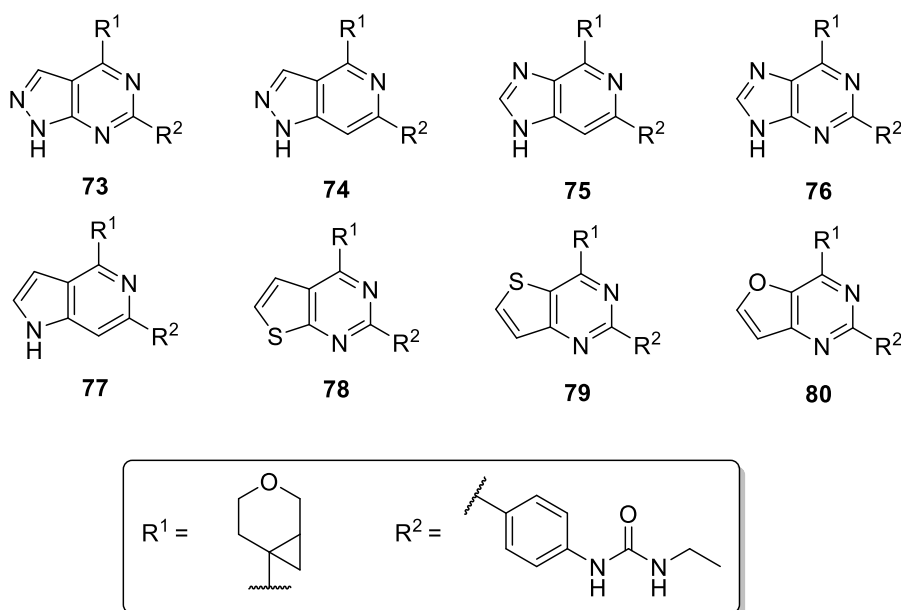
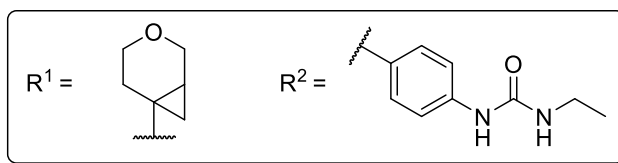
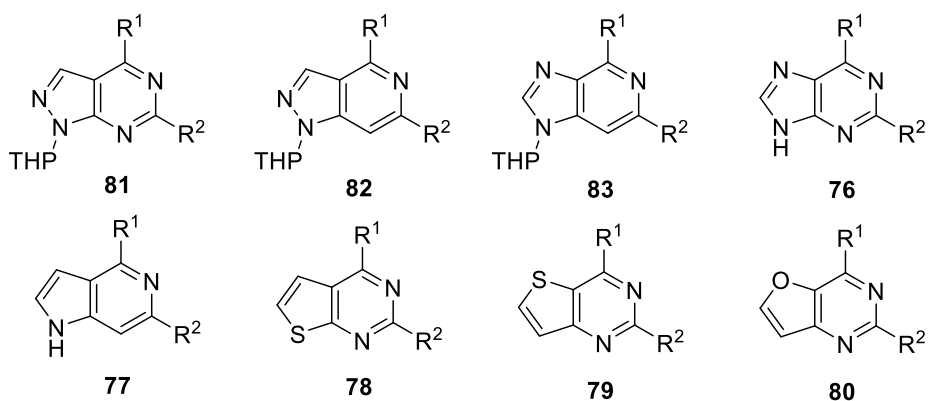
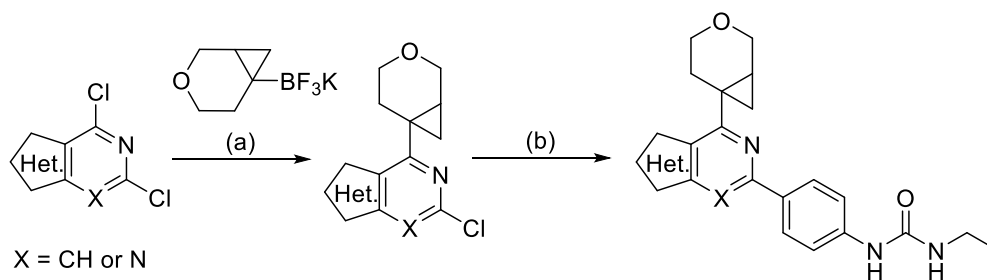


**Figure 51:** Cyclopropylpyran 5,6 bicyclic compounds proposed for synthesis.

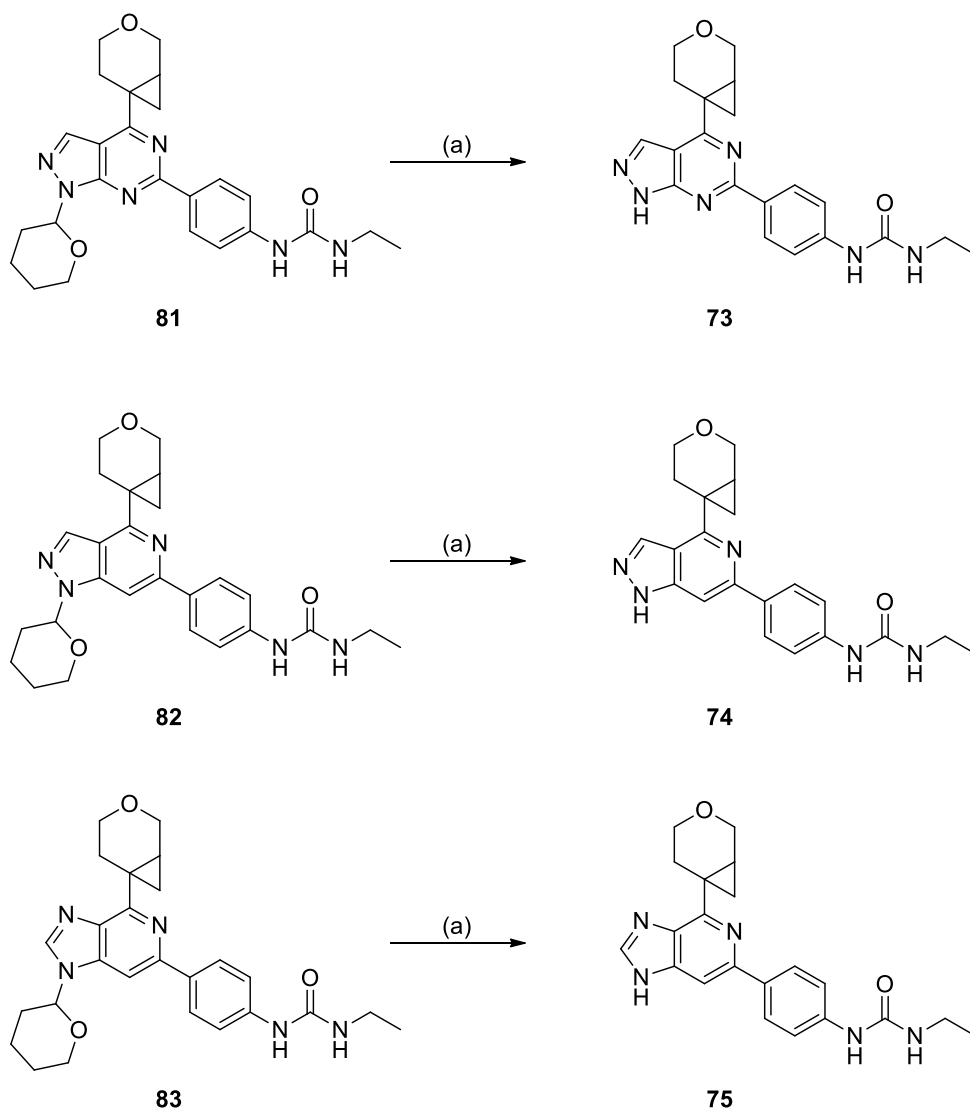
### **2.3.1 Synthesis of Cyclopropylpyran 5,6 Bicyclic Core Compounds**

5,6 Bicyclic compounds **73-80** were synthesised by another member of our laboratories.<sup>197</sup> Commercially available 5,6 bicyclic starting materials were utilised. The cyclopropylpyran hinge binding fragment was installed *via* a Suzuki-Miyaura cross coupling reaction. This challenging  $sp^2 - sp^3$  disconnection is discussed in greater detail in the previous chapter of this thesis. The yield of this reaction was generally poor, which is likely attributable to coupling at the 2-position of the dichloropyrimidine, leading to formation of unwanted bis- coupled by-product. In the synthesis of compounds **76-83** the yield of step (a) varied between 20-40% yield. The CPP containing intermediates then underwent an additional Suzuki-Miyaura cross coupling reaction (b) to install the 4-ethyl urea back pocket group. The reaction yields for this reaction remained unoptimized and products were purified by mass-directed auto purification (MDAP) to give final products of high purity in sufficient quantities for biological testing (**Scheme 18**). Pyrazolopyrimidine **81**, pyrazolopyridine **82** and imidazopyridine **83** were deprotected without purification and the deprotected final products were purified by MDAP (**Scheme 19**).



(a) Pd(OAc)<sub>2</sub>, CataCXium® A, Cs<sub>2</sub>CO<sub>3</sub>, toluene/H<sub>2</sub>O (10:1),  $\mu$ Wave, 120 °C, 2 h. (b) 1-ethyl-3-(4-(4,4,5,5-tetramethyl-1,3,2-dioxaborolan-2-yl)phenyl)urea, Pd(dppf)Cl<sub>2</sub>, Cs<sub>2</sub>CO<sub>3</sub>, dioxane:H<sub>2</sub>O (10:1), 80 °C, 5 h.

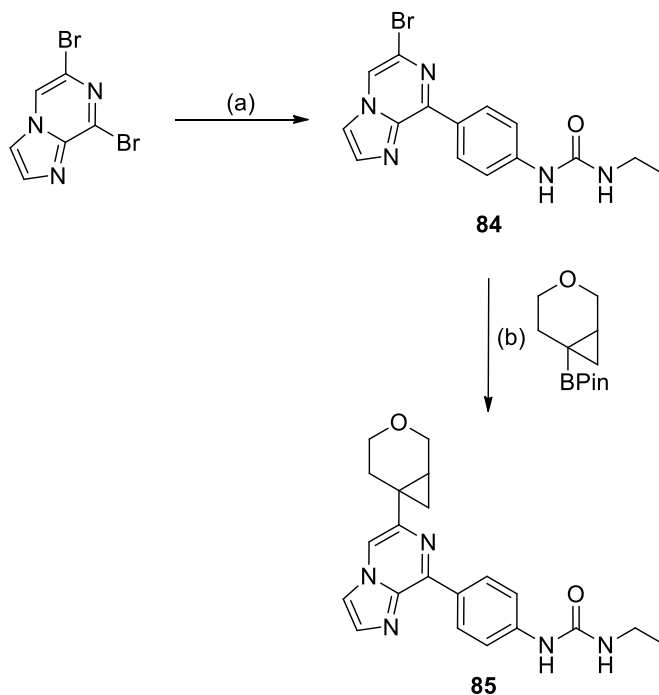
**Scheme 18:** Synthesis of 5,6 bicyclic compounds **76-80**.<sup>197</sup>



(a) HCl (4 M in dioxane), r.t., 16 h.

**Scheme 19:** THP deprotection of compounds **116**, **117** and **118**.

Imidazo[1,2-a]pyrazine **85** was synthesised by first installing the 4-ethyl urea back pocket group *via* Suzuki-Miyaura cross coupling reaction with commercially available 6,8-dibromoimidazo[1,2-a]pyrazine. This gives the desired substitution pattern within the product, as the bromide at position-8 is more reactive and forms intermediate **84** as the major product in a 4.5:1 ratio. Bromide **84** then underwent a subsequent Suzuki-Miyaura cross coupling reaction to install the cyclopropylpyran motif at position-6 and furnish compound **85** (**Scheme 20**).



(a) 1-ethyl-3-(4-(4,4,5,5-tetramethyl-1,3,2-dioxaborolan-2-yl)phenyl)urea, Pd(dppf)Cl<sub>2</sub>, Cs<sub>2</sub>CO<sub>3</sub>, dioxane:H<sub>2</sub>O (10:1), 100 °C, 15 h, 17% yield. (b) Pd(dppf)Cl<sub>2</sub>, dioxane/H<sub>2</sub>O (10:1), 100 °C, 14 h, 7% yield.

**Scheme 20:** Synthesis of **85**.

### **2.3.2 Cyclopropylpyran 5,6-Bicyclic Core Compound Analysis**

When selecting a starting point for a drug discovery project, it is important to carefully select the most promising fragment, as this is more likely to lead to high quality target compounds. Clearly the potency of a compound against the desired target is of paramount importance, however potency is known to positively correlate with both molecular weight<sup>198</sup> and lipophilicity.<sup>199</sup> Therefore optimising for potency alone will likely lead to larger more lipophilic lead compounds, which has been attributed to a number of issues such as: poor metabolic stability,<sup>200</sup> increased promiscuity<sup>201</sup> and decreased absorption (due to poor solubility<sup>202</sup> and/or permeability).<sup>203</sup>

To enable potency measurements to be normalised for molecular weight and lipophilicity, leading to a fairer comparison, efficiency measurements such as binding efficiency index (BEI)<sup>204</sup> and lipophilic ligand efficiency (LipE)<sup>199</sup> are used. BEI can be defined as the potency per unit of mass whereas LipE subtracts the lipophilicity (chromLogD) from the potency

(pIC<sub>50</sub>). For oral candidate compounds, a LipE of between 5-6 is considered optimal. The equations used to derive the two-efficiency metrics are shown in **Figure 52**.

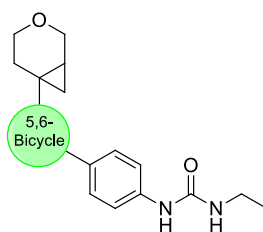
$$\text{BEI} = \text{Target Potency (pIC}_{50}) \times 1000 / \text{Molecular Weight (kDa)} \quad \text{(Equation 1)}$$

$$\text{LipE} = \text{Target Potency (pIC}_{50}) - \text{chromLogD} \quad \text{(Equation 2)}$$

**Figure 52:** Equations to calculate binding efficiency index (BEI) and lipophilic ligand efficiency (LipE).

The potency, efficiency and selected physicochemical data for cyclopropylpyran 5,6 bicyclic compounds **73-80** is shown in **Table 15**.





Entry	Compound No.	Structure	mTOR pIC <sub>50</sub>	pAkt pIC <sub>50</sub>	BEI	LipE	Chrom LogD/P	cLND sol. (µg/mL)
1	<b>76</b>		6.1	NT	16.1	3.2	2.87 2.88	125
2	<b>75</b>		5.4	4.8	14.3	2.9	2.51 2.52	469
3	<b>77</b>		4.3	4.7*	11.4	0.8	3.45 3.50	328
4	<b>78</b>		6.4	6.5	16.2	1.0	5.39 5.50	43
5	<b>79</b>		6.6	6.5	16.7	1.5	5.06 5.10	47
6	<b>80</b>		6.4	6.6*	16.9	1.8	4.65 4.69	114
7	<b>73</b>		7.0	6.7*	18.5	3.5	3.49 3.50	3
8	<b>74</b>		5.8	5.7	15.9	2.7	3.27 3.27	22
9	<b>85</b>		6.2	5.8	16.4	2.4	3.79 3.79	422

**Table 15:** Biological and physicochemical measured data for compounds **73-80** and **85**. NB: pIC<sub>50</sub> values marked with \* are n= 2, all other pIC<sub>50</sub> values are n= 3 or greater. All potency ranges fall within the error of the assay (mTOR= 0.3, Akt= 0.5) and therefore are not shown.

Pyrazolopyrimidine **73** was the most potent compound from this initial screen and it was also the most efficient compound (in terms of BEI and LLE). The solubility of **73** is very low, however this compound was still considered a promising lead given its other properties,

particularly given the level of potency in the pAkt cellular assay. The compound has two vectors through which groups can be incorporated in order to further improve both potency and physicochemical properties. As we were targeting an inhaled drug compound (*vide supra*), low solubility was considered less problematic, and we were interested in exploring a wide range of physicochemical space. For these reasons, further work was focused on developing a pyrazolopyrimidine series of mTOR inhibitors. The vectors which were the focus of our optimisation as well as their expected position within the ATP-binding site of mTOR are highlighted in **Figure 53**.

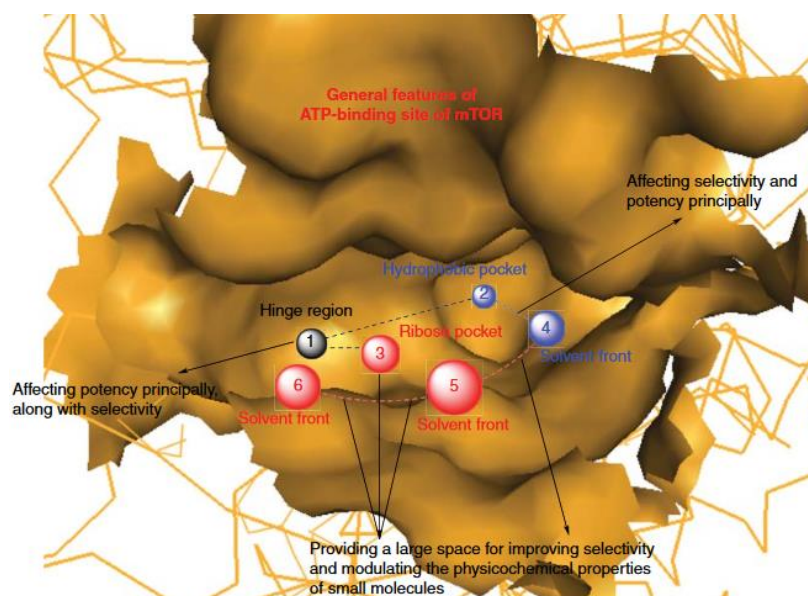
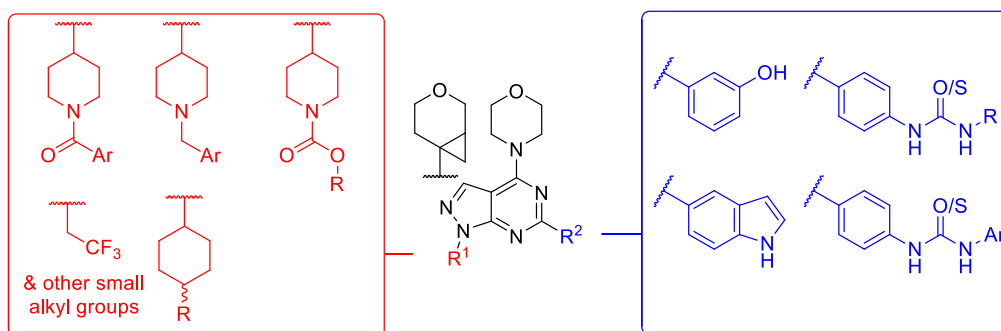


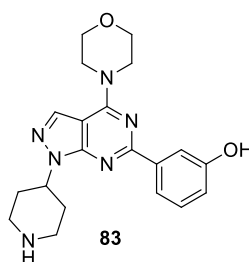
**Figure 53:** Vectors for optimisation in pyrazolopyrimidine compounds.  $R^1$  = Ribose region.  $R^2$  = Backpacket Region (hydrophobic pocket). General examples of groups exemplified within the literature are shown. The diagram shows the positioning of the inhibitors within mTOR ATP-binding site including the hinge region (black-1), hydrophobic pocket (blue-2), ribose pocket (red-3) and solvent front (red-5, -6 and blue-4). Note the colouring of  $R^1$  and  $R^2$  correspond to their different binding regions.<sup>205</sup>

Other 5,6 bicyclic cores were not as efficient as pyrazolopyrimidine **73**. Removal of 1 nitrogen from the pyrimidine ring to give pyrazolopyridine **74** causes a 10-fold decrease in potency. Similarly, a 5-fold decrease in potency is observed between imidazolopyrimidine **76** and the corresponding imidazopyridine **75**. Imidazopyridine **75** is 8-fold less potent than imidazolopyrimidine **73**. However, due to the lower lipophilicity of **75** the LipE of these two compounds is similar, the BEI of pyrazolopyrimidine **73** however, is significantly better. Thienopyrimidine compounds **78** and **79** have reasonably good target affinity, however due to their high lipophilicity the LipE value for these compounds is very low.

## 2.4 Literature Review of Pyrazolopyrimidine Based mTOR Inhibitor Compounds

Pyrazolopyrimidine **73** proved to be the most efficient core at mTOR when combined with cyclopropylpyran and this is also the most highly exemplified class of 5,6-bicyclic compounds. There have been extensive publications from Wyeth on this class of compounds and the highly potent and selective compounds reported within these publications, coupled with our own initial data, prompted further investigation into this class of compounds.

Compound **83** (Table 16) was first discovered through a high throughput screen for mTOR inhibitors<sup>206</sup> and was chosen as a promising lead-like starting point due to its low molecular weight, low lipophilicity, reasonable ligand efficiency<sup>207</sup> and reasonable mTOR potency. This compound, however, was 6-fold more potent at PI3K $\alpha$ , highlighting the considerable challenge associated with achieving highly potent and selective inhibitors for mTOR.



mTOR PIC <sub>50</sub>	6.7
PI3K $\alpha$ PIC <sub>50</sub>	7.4
MW	297
cLogP	1.86
Ligand efficiency	0.34

**Table 16:** Literature biological and physicochemical data for compound **83**.

As highlighted in **Figure 54(a)** there are 3 plausible vectors which can be optimised for potency and selectivity. This includes: the aryl substituent at the 6-position of pyrazolopyrimidine, the 1-position and the 4-position of the pyrazolopyrimidine ring. Docking studies<sup>206</sup> with compound **83** have been performed in an mTOR homology model, derived from the X-ray crystal structure of PI3K $\gamma$ . This shows that the morpholine in the 4-position potentially forms a hydrogen bonding interaction with the hinge region of the kinase active site (Val2240). The 3-phenol in the 6-position forms an additional hydrogen bonding interaction with the backpocket region of the kinase active site (Asp2195). The piperidine ring in the 1-position occupies the region of the active site which is occupied by the ribose ring of the natural substrate (ATP). This is commonly referred to as the ribose region.

The docking study shown in **Figure 54(b)** also suggests why selectivity for mTOR over PI3K $\alpha$  is a challenge. The active site only differs at two locations within 3 Å of compound **83**, Trp2239 to Val850 and Leu2354 to Phe930. In the figure these residues are shown in orange. These amino acid residues are close to the hinge binding morpholine but do not form hydrogen bonding interactions with the ligand.

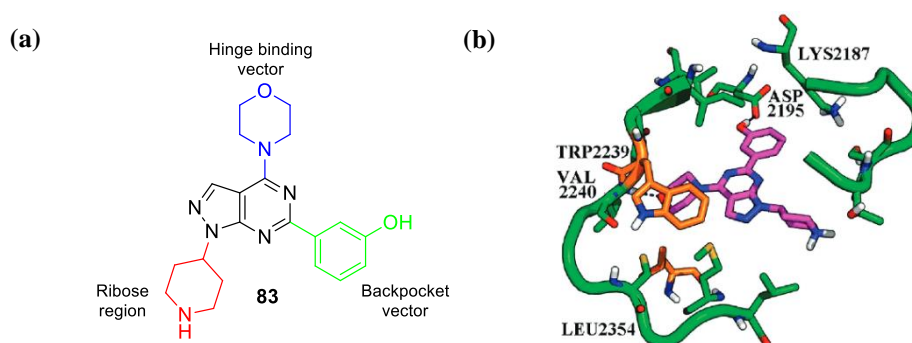
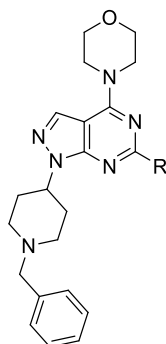


**Figure 54:** (a) Compound **83** highlighting the positions of each substituent when bound to mTOR active site (b) Putative binding mode of compound **83** with the mTOR homology model.

### 2.4.1 Literature Backpocket Group Optimisation

The most extensively explored vector within the literature is the aryl substituent in the 6-position, which occupies the backpocket region of the kinase active site. A variety of aryl substituents were examined in this position and the results are summarised in **Table 17**. Movement of the phenolic hydroxyl group to either the 2- or 4- position of the aryl ring led to a reduction in activity, presumably due to loss of the hydrogen bonding interaction to Asp2195. A variety of indole substituents were also tested in this position, of which, the 5-indolyl

analogue **89** was the most potent. Alkylation of the indole nitrogen to form compound **90** further emphasizes the importance of a hydrogen bond donor in the backpocket, as this compound is ~6.5-fold less potent than indole **89**.

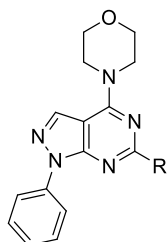


Entry	Compound No.	R	mTOR pIC <sub>50</sub>	PI3K $\alpha$ pIC <sub>50</sub>
1	<b>84</b>		7.1	7.4
2	<b>85</b>		5.9	5.4
3	<b>86</b>		6.8	6.1
4	<b>87</b>		6.9	6.0
5	<b>88</b>		6.8	6.6
6	<b>89</b>		7.1	6.0
7	<b>90</b>		6.2	5.3

**Table 17:** Phenol and indole backpocket groups.<sup>108</sup>

In a further study to identify potential alternative backpocket groups, 3- or 4- anilino substitution led to a decrease in mTOR activity. However it was discovered that introducing a nitrogen into the ring to give the 2-aminopyridin-5-yl derivative gave an increase in mTOR potency (**Table 18**).<sup>108</sup> This increase in potency was attributed to the formation of an additional hydrogen bonding interaction between the ring nitrogen and an amino acid residue (Lys2187).

Regioisomers of aminopyridine **93** (compounds **94** and **95**) did not provide this same increase in potency. Interestingly, the mTOR potency was maintained when the hydrogen bond donor was moved to an exocyclic position, such as in compound **96**. Modelling has shown that the carbonyl oxygen in acetamide **96** is likely to maintain the same H-bonding interaction with Lys2187.<sup>108</sup> The data in **Table 18** indicates the importance of combining a hydrogen bond donor and acceptor in the backpocket group. Compound **97** is not able to form a hydrogen bonding interaction due to *N*-methylation, this results in a 30-fold decrease in mTOR activity for this compound in comparison with compound **96**.



Entry	Compound No.	R	mTOR pIC <sub>50</sub>	PI3K $\alpha$ pIC <sub>50</sub>
1	<b>91</b>		7.0	6.4
2	<b>92</b>		7.1	6.5
3	<b>93</b>		8.0	7.2
4	<b>94</b>		6.9	6.0
5	<b>95</b>		6.8	6.0
6	<b>96</b>		7.8	6.9
7	<b>97</b>		6.3	6.1

**Table 18:** Anilino and aminopyridine based backpockets.<sup>108</sup> note phenyl ring in position 1. This was used for backpocket exploration due to synthetic tractability of this core.

Building on the high potency of acetamide **96**, the authors explored varying the carbonyl group attached to the aniline in order to further improve potency and increase selectivity. Methyl



hydrogen bonding interaction in the backpocket region. The urea carbonyl oxygen interacts with Lys2187 and both urea NH groups form a hydrogen bond with Asp2195. Again, the presence of a third interaction in the backpocket region provides an increase in mTOR potency for this compound. These compounds also show reasonable selectivity over PI3K $\alpha$

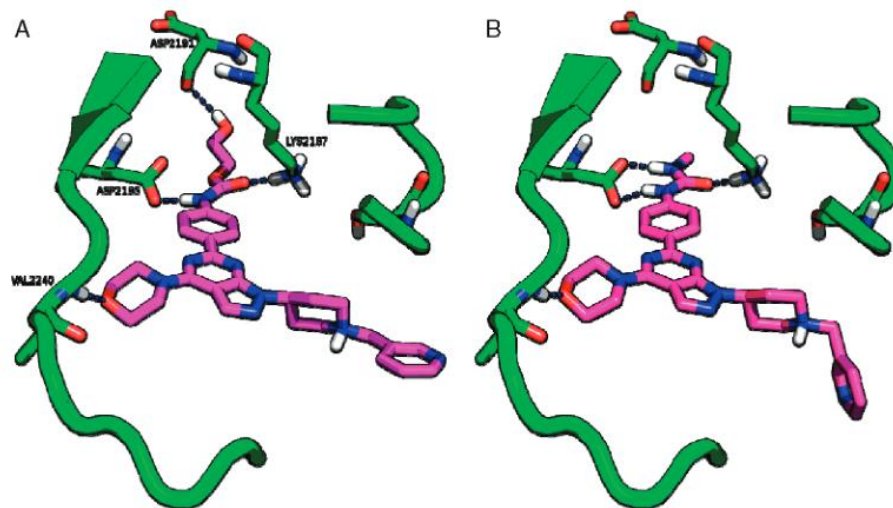
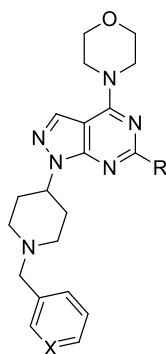


**Figure 55:** (a) Docking study of Compound **100** in mTOR homology model. (b) Docking study of Compound **102** in mTOR homology model.<sup>108</sup>

Further examples of urea based backpocket groups were then explored by the authors, the most highly potent of which was the hydroxyethyl urea **105**. Considering compounds **100** and **102** it is plausible that this compound forms 4 hydrogen bonding interactions in the backpocket region, which can account for its superior mTOR potency. Urea isosteres were also briefly investigated by the authors however it was found that these were all inferior to the parent urea compound (**Table 20**).





Entry	Compound No.	X	R	mTOR PIC <sub>50</sub>	PI3K $\alpha$ PIC <sub>50</sub>	Selectivity	LNCaP PIC <sub>50</sub>
1	<b>105</b>	CH		9.5	7.1	282	7.6
2	<b>106</b>	N		8.3	6.6	56	5.9
3	<b>107</b>	N		6.7	5.4	23	5.4
4	<b>108</b>	CH		8.7	6.9	69	7.2

**Table 20:** Urea optimisation and exploration of potential urea isosteres.<sup>108</sup>

Since these initial reports, additional publications have further expanded the backpocket groups and incorporated diaryl urea groups in this position. An X-ray crystal structure of the 4-pyridyl urea **109** bound to PI3K $\gamma$  (**Figure 56**) shows a shift in the peptide chains of the enzyme, in order to accommodate the aryl urea group. This shift exposes the 4-position of the aryl ring to solvent and therefore this position can be used to attach water solubilising groups (WSGs) with the aim of improving compound solubility.

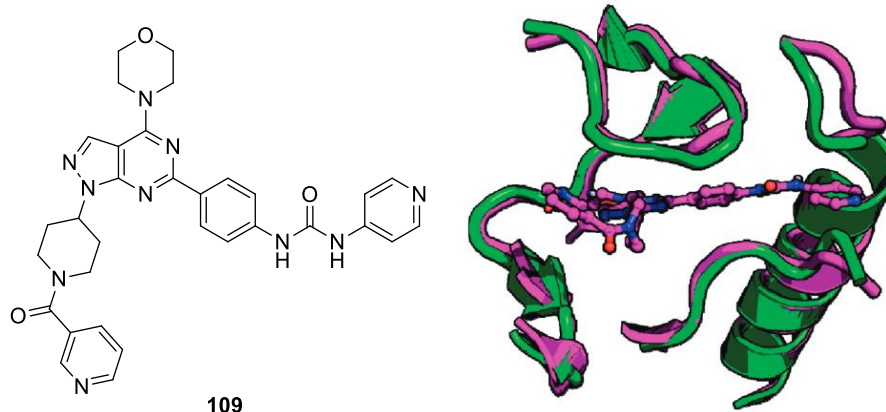
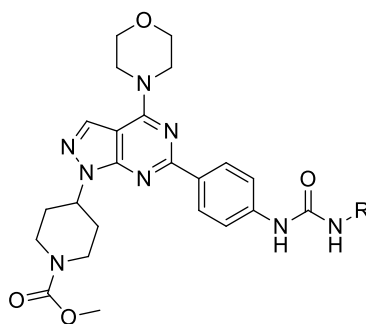


**Figure 56:** X-ray crystal structure to show movement of protein loops (green to purple) in PI3K $\gamma$  to accommodate aryl urea group of **109**. This leaves the 4 position of pyridine ring exposed to solvent.<sup>208</sup> Structure is available in the protein data bank: PDB code 3IBE.

The use of water-solubilising groups in this solvent-exposed position has produced highly potent mTOR compounds with improved physicochemical properties and microsomal stability. Due to the large molecular weight of these compounds, they have been optimised by the authors for intravenous administration.<sup>209</sup> Examples of diaryl urea compounds are shown in **Table 21**.



Entry	Compound No.	R	mTOR pIC <sub>50</sub>	PI3K $\alpha$ pIC <sub>50</sub>	Selectivity	LNCaP pIC <sub>50</sub>	Micro (t <sub>1/2</sub> )
1	<b>110</b>		9.7	7.5	175	7.5	24
2	<b>111</b>		9.5	7.7	60	7.2	9
3	<b>112</b>		9.5	7.8	44	>9.0	>30
4	<b>113</b>		10.1	8.2	75	>9.0	13

NB: micro. Is nude mouse liver microsomes half-life.

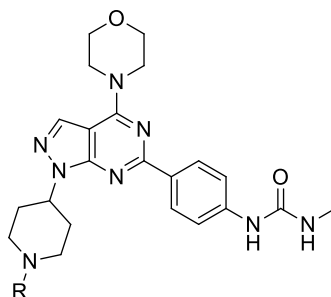
**Table 21:** Aryl urea backpack compounds.<sup>208</sup>

## 2.4.2 Literature Ribose Group Optimisation

Another area which has been explored within the literature is the vector extending from position 1 of the pyrazolopyrimidine ring, often referred to as the ribose region due to the position it occupies in the kinase active site relative to the natural ligand, ATP. Compound **114**, which was identified as a result of a high throughput screen had a piperidine ring in this position and substitution of the piperidine nitrogen has been extensively explored.

Early compound iterations commonly included a benzyl group at this position, most likely due to this group being utilised as a protecting group during the synthesis of these compounds. Despite good mTOR potency, benzyl groups often gave compounds with poor metabolic stability due to dealkylation of the piperidine ring nitrogen and are very lipophilic. For these reasons, the authors explored alternative substituents in this position (**Table 22**)

Methylation (**116**), acylation (**117**) and urea formation (**118**, **119**) were all associated with a reduction in potency. Methyl carbamate **75** offered improved microsomal stability combined with good potency and selectivity.



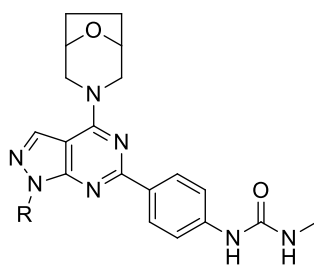
Entry	Compound No.	R	mTOR PIC <sub>50</sub>	PI3K $\alpha$ PIC <sub>50</sub>	Selectivity	LNCaP PIC <sub>50</sub>	Micro (t <sub>1/2</sub> )
1	<b>114</b>		8.9	7.6	16	5.9	>30
2	<b>115</b>		9.3	7.8	27	8.8	3
3	<b>116</b>		7.7	6.8	10	6.1	2
4	<b>117</b>		8.7	6.6	107	6.1	27
5	<b>118</b>		8.7	6.8	75	5.6	NT
6	<b>119</b>		9.0	6.7	190	6.7	>30
7	<b>120</b>		9.3	7	217	7.5	>30

NB: micro. Is nude mouse liver microsomes half-life.

**Table 22:** Exploration of the piperidine ring substituent.<sup>208</sup>

Additional carbamates including isopropyl carbamate and *tert*-butyl carbamate were examined, however these compounds suffered from a reduction in microsomal stability.<sup>105</sup>

Small acyclic alkyl groups were also considered in the 1-position of pyrazolopyrimidine (**Table 23**). These compounds were in general less selective than their piperidine carbamate analogue **120**, however the isopropyl compound **123** and trifluoroethyl derivative **124** both had good selectivity and cellular activity. It is important to note the replacement of morpholine with bridged morpholine in compounds **121-126**. This additional bulk in the hinge region is also shown to improve selectivity for mTOR (*vide infra*)

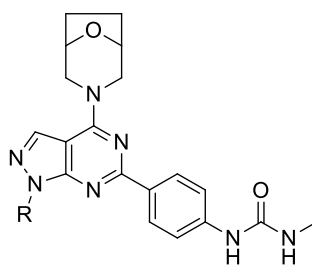


Entry	Compound No.	R	mTOR PIC <sub>50</sub>	PI3K $\alpha$ PIC <sub>50</sub>	Selectivity	LNCaP PIC <sub>50</sub>	Micro (t <sub>1/2</sub> )
1	<b>121</b>		8.9	6.6	184	6.8	>30
2	<b>122</b>		9.1	6.6	364	7.2	>30
3	<b>123</b>		9.9	6.6	1950	8.3	>30
4	<b>124</b>		9.3	5.8	3232	7.4	>30
5	<b>125</b>		8.5	6.4	132	6.2	NT
6	<b>126</b>		7.8	6.0	66	6.4	5

NB: micro. Is nude mouse liver microsomes half-life.

**Table 23:** Exploration of 1-alkyl substituted pyrazolopyrimidines.<sup>105</sup>

Despite good stability at mouse liver microsomes (**Table 23**), compounds **123** and **124** suffered from low stability at human liver microsomes (half-life of 12 minutes and 5 minutes, respectively). The authors therefore turned their attention to cyclic alkyl groups which are more structurally related to piperidines. Based on this, a series of cyclohexyl analogues were prepared (**Table 24**). Cyclohexanone **127** was potent and selective for mTOR, however was only moderately stable in mouse and human liver microsomes. Reduction of the ketone to cyclohexanol compounds **128** and **129** resulted in sub-nanomolar, highly selective compounds with good microsomal stability. Methylation of these compounds to give methyl ethers **130** and **131** resulted in compounds with improved cellular potency, but which had only moderate microsomal stability. Cyclohexyl ketals (**132-134**) had excellent cellular potency and good microsomal stability.



Entry	Compound No.	R	mTOR PIC <sub>50</sub>	PI3K $\alpha$ PIC <sub>50</sub>	Selectivity	LNCaP PIC <sub>50</sub>	Micro.	
							M	H
1	127		9.7	5.9	5913	7.5	20	10
2	128		9.6	6.1	3975	7.7	>30	>30
3	129		9.5	6.6	757	7.7	>30	>30
4	130		9.4	5.9	3079	8.7	>30	15
5	131		9.5	6.2	2136	9.0	17	NT
6	132		9.1	6.2	875	8.7	15	30
7	133		9.7	5.9	5619	8.7	>30	26
8	134		8.9	6.5	305	8.1	>30	>30

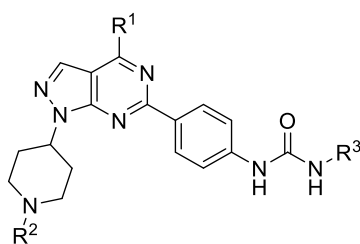
NB: micro. M = nude mouse liver microsomes half-life. H= Human liver microsomes half-life.

**Table 24:** Exploration of 1-cyclohexyl analogues.<sup>105</sup>

Although some investigation has been performed into varying the substituent at position-1 of the pyrazolopyrimidine, this position remains underexplored. The reported SAR focuses mainly on modifying groups such as piperidine and cyclohexyl. This is likely because the installation of the ribose substituent is in the first step of the pyrazolopyrimidine ring synthesis and therefore full bespoke syntheses would be required to vary this position more widely. Nevertheless, this position provides an underexplored opportunity which could be utilised further in an attempt to tune potency, selectivity and physicochemical properties.

### 2.4.3 Literature Hinge Group Optimisation

As intimated previously, the hinge binding morpholine group has been modified within the literature. It was discovered that substitution on the morpholine ring is able to increase selectivity for mTOR over closely related PI3K $\alpha$ .<sup>114</sup> **Table 25** shows some substituted morpholines which have been used as alternative hinge binding groups.



Entry	Compound No.	R <sup>1</sup>	R <sup>2</sup>	R <sup>3</sup>	mTOR pIC <sub>50</sub>	PI3K $\alpha$ pIC <sub>50</sub>	Selectivity
1	120				9.3	7.0	217
2	102				9.4	7.4	108
3	135				9.5	6.3	1531
4	136				9.8	6.2	4141
5	137				9.4	6.2	1410
6	138				9.7	5.7	1803
7	139				9.7	5.3	26665
8	140				9.2	5.4	6913
9	141				9.7	5.4	19414
10	142				9.2	5.3	8886
11	143				7.1	5.4	46
12	144				8.6	6.6	116
13	145				8.7	6.1	360
14	146				8.7	6.3	307
15	147				8.7	6.3	289
16	148				9.2	7.7	32
17	149				9.1	5.4	4985
18	150				8.9	5.3	3666
19	151				9.6	6.3	1846

**Table 25:** Exploration of substituted morpholine hinge binding fragments.<sup>114</sup>

The rationale behind the increase in selectivity noted for substituted morpholine compounds may be attributed to a single amino acid substitution in the hinge region of mTOR. Modelling (**Figure 57**) indicates that in PI3K $\alpha/\gamma$ , Phe961 is likely to be too large to accommodate the additional bulk from a bridged morpholine such as in compound **137**. However, in mTOR the amino acid located at this position is the smaller leucine (Leu961). This point change creates a slightly deeper pocket and therefore the bridged morpholine can be accommodated in the hinge region of mTOR. The same reasoning can be employed to explain the increased selectivity observed for compound **141** over parent morpholine **120**.

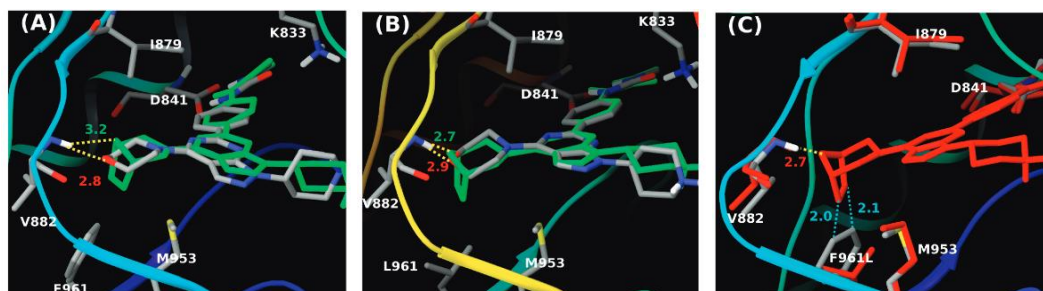


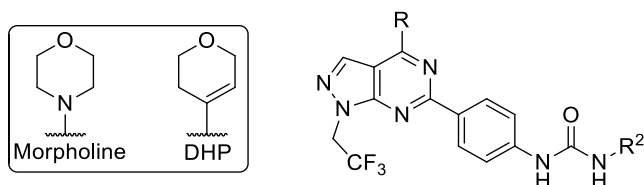
**Figure 57:** Differences in binding of the bridged morpholine in **93** to mTOR and PI3K $\gamma$ . (A) Compounds **102** (colour by element) and **137** (green) docked to PI3K $\gamma$ . Yellow dotted lines indicate hydrogen bonds, with corresponding distance measurements coloured the same as the acceptor oxygen. (B) Compounds **102** (colour by element) and **137** (green) docked to mTOR. (C) Superposition of the complex between **137** and mTOR (red) with PI3K $\gamma$  (coloured by element) with close steric contacts indicated by blue dashed lines. Distances in Angstroms.

Methyl and dimethyl substitution adjacent to the hinge binding nitrogen (compounds **143-145**) is associated with a reduction in potency and selectivity. This is likely due to clashes with the hinge region of the kinase. It is known that the methyl groups in *cis*-2,6-dimethylmorpholine **143** adopt an equatorial conformation, which means that the hinge is too wide for the binding pocket and steric clashes occur with amino acid residues in the hinge region (Tyr867 and Cys885). A similar effect is likely to occur with racemic 2-methyl morpholine which accounts for the reduced potency observed for compounds **144** and **145**.

Methyl substitution was better tolerated at the 3-position of the morpholine ring. It was found that (*R*)- methyl morpholine compounds (**149-151**) were more potent at mTOR whereas the opposite enantiomer (*S*)- methyl morpholine compounds (**146-148**) had a higher activity at PI3K $\alpha$ . This means that the different enantiomers of this hinge can provide compounds with elevated levels of selectivity for mTOR (when (*R*)- isomer is used) or dual mTOR/PI3K compounds (when (*S*)- isomer is used).



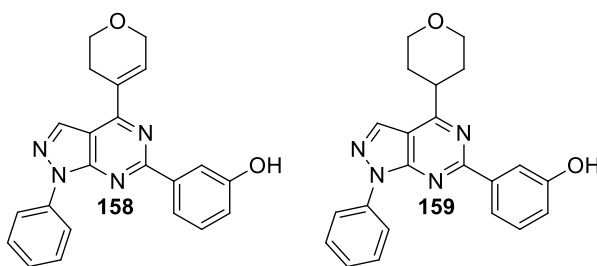
Carbon linked hinge binding fragments have also been investigated in order to provide an alternative to the common morpholine derived fragments. For example, dihydropyran (DHP) has been shown to be an effective replacement for morpholine (**Table 26**).<sup>158</sup>



Entry	Compound No.	R	R <sup>2</sup>	mTOR pIC <sub>50</sub>	PI3K $\alpha$ pIC <sub>50</sub>	Selectivity
1	<b>152</b>	DHP		8.7	6.7	100
2	<b>153</b>	Morpholine		9.0	6.7	194
3	<b>154</b>	DHP		9.0	5.6	2300
4	<b>155</b>	Morpholine		9.2	6.5	525
5	<b>156</b>	DHP		9.0	7.2	66
6	<b>157</b>	Morpholine		9.7	8.0	50

**Table 26:** Morpholine and DHP matched pair compounds.<sup>158</sup>

Hydrogenation of DHP compound **158** to the corresponding tetrahydropyran **159** resulted in a 28-fold decrease in mTOR potency. Notably, the PI3K $\alpha$  potency of tetrahydropyran **159** is also decreased by ~ 16-fold. This suggests a more general intolerance for the saturated hinge binder, rather than a specific incompatibility with mTOR (**Table 27**). This highlights the importance of co-planarity between the core aryl ring and hinge binding fragment. In DHP coplanarity is favoured due to conjugation between the alkene and the pyrazolopyrimidine  $\pi$ -system. In the corresponding THP, there are no orbitals available to overlap with the adjacent  $\pi$ -system and so the sterically favoured orthogonal conformation is adopted. This preference for an orthogonal conformation is reflected in the reduced potency of the THP analogue **159**. **Figure 58** shows the minimum energy conformation of THP **159** overlaid onto a docking study of DHP **158** in an mTOR homology model. This shows how in its minimum energy conformation, a hydrogen bonding interaction to the backbone of Val2240 is not possible. In addition to this, the THP ring has unfavourable steric interactions with the binding pocket.



Entry	Compound No.	R	mTOR PIC <sub>50</sub>	PI3K $\alpha$ PIC <sub>50</sub>	Selectivity
1	158	DHP	7.7	7.2	3.3
2	159	THP	6.3	6.0	2

**Table 27:** comparison between DHP and THP hinge binding fragment.<sup>158</sup>

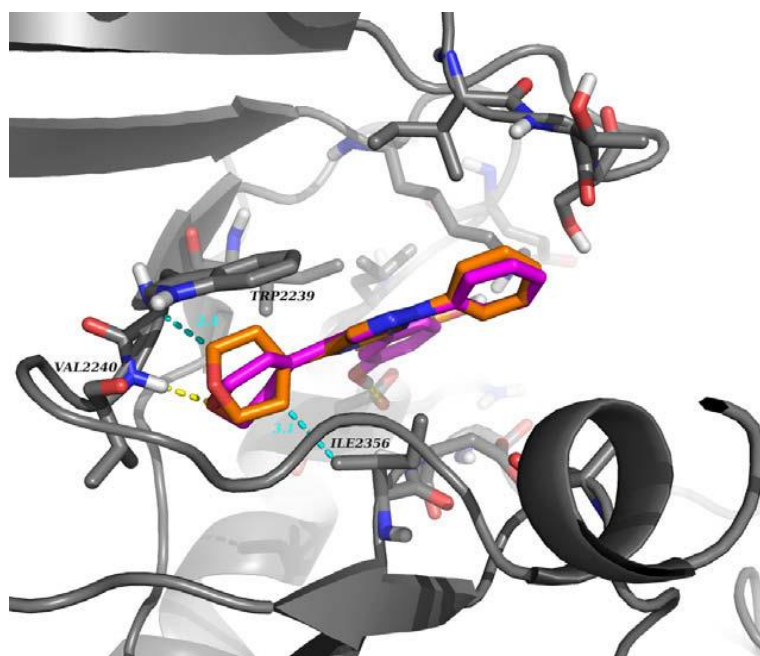


**Figure 58:** Overlay of docked DHP analogue **158** (in magenta) and the minimum energy conformation of THP analogue **159** (in orange) in an mTOR homology model based on the PI3K $\gamma$  crystal structure. The hydrogen bond between the hinge region and the DHP ring is shown in yellow; steric clashes for the THP analogue are shown in cyan.<sup>158</sup>

Building on the hinge binding fragment SAR exploration which has been reported by Wyeth, we therefore considered the suitability of cyclopropylpyran to act as a hinge binding fragment in this class. It was postulated that if cyclopropylpyran could occupy a coplanar conformation

in an analogous manner to DHP it may offer some benefits with respect to selectivity, as observed for substituted morpholine derivatives due to the deeper binding pocket in mTOR (*vide supra*), as well as representing a novel hinge binding motif in this context.

## **2.5 Inhaled Administration of Drugs.**

Before considering compounds for synthesis, it was important to consider the desired route of administration for these compounds, as this will have a large impact on the physicochemical profile which will be pursued.

mTOR signalling is essential for normal cell viability, and therefore inhibition of mTOR can be detrimental to healthy tissues. Common side effects observed with the mTOR inhibitor temsirolimus include: rash, asthenia, stomatitis, nausea, oedema and anorexia. More serious side effects can include: metabolic and hematologic abnormalities, renal failure, pulmonary toxicity, wound-healing complications, cerebral haemorrhage, gastrointestinal perforation and hypersensitivity reactions.<sup>210,211</sup> Temsirolimus is currently approved for use in patients with renal cell carcinoma. In patients with advanced cancer, there is a greater tolerance for side effects, from a regulatory perspective, as these patients will die without treatment and the use of chemotherapies can directly extend their lives. In patients with idiopathic pulmonary fibrosis such side effects may be less acceptable. In a study investigating the tolerability of the two approved IPF therapies, Pirfenidone and Nintedanib, 42% and 40% of patients, respectively discontinued treatment over a 3 year time period.<sup>212</sup> Commonly, patients taking either anti-fibrotic therapy have reported gastrointestinal side effects (vomiting, diarrhoea, dyspepsia) and skin related events (rash and photosensitivity). As these medications only slow lung function decline, and do not stop or reverse the effects of IPF, the benefits are often outweighed by adverse events, particularly in cases where medication may stop being as effective.<sup>213</sup> With this in mind, novel anti-fibrotic therapies with better efficacy and an improved side effect profile would be clearly beneficial to IPF patients.

One strategy to attempt to overcome the severe side effects observed with mTOR inhibition is to develop compounds which are inhaled rather than ingested orally. For a lung disease such as IPF this strategy has several potential benefits over oral administration of drugs. Firstly, inhaled delivery allows administration of the drug directly to the site of action (the lungs). This offers the advantage that significant quantities of the drug are available in the lungs, however systemic drug exposure is potentially kept at a very low level. In addition to this, inhaled medications are often rapidly metabolised into inactive metabolites once they are absorbed from the lungs (sometime called a soft drug approach).<sup>214</sup> With these benefits in mind, the

decision was made within our laboratories to pursue an inhaled strategy for mTOR inhibition to treat IPF.

The favourable physicochemical properties of orally administered drugs are well established, first being outlined in Lipinski's "rule of 5"<sup>215</sup> which states that in general orally active drugs do not violate more than one of the following:

- No more than 5 hydrogen bond donors.
- No more than 10 hydrogen bond acceptors.
- A molecular mass of less than 500 Daltons.
- A logP not greater than 5.

The optimal physicochemical properties of inhaled medications however, are less well defined. This can increase the challenge associated with hit-to-lead development and lead optimisation of medication intended for inhaled delivery. In an attempt to better define these properties, other members of our laboratories have analysed the calculated physicochemical properties of 81 currently marketed respiratory drugs, including 29 drugs that are administered by inhaled or intranasal routes.<sup>216</sup> In this analysis it was found that the properties of inhaled drugs differed from oral drugs. This study concluded that inhaled/ intranasally administered respiratory drugs differ from orally administered drugs by:

- Significantly higher hydrogen bond count and polar surface area.
- Significantly higher molecular weight.
- A trend towards lower lipophilicity.

However, these conclusions were based on a small data set, where a significant proportion of the compounds could be dosed either orally or *via* inhaled administration and therefore formulating design principles based on these observations is not possible. Interestingly the authors note that the range of values including lipophilicity and molecular weight is greater for inhaled compounds. This can potentially be attributed to the fact that a topical compound only has to reach the local site of action and therefore does not have to achieve good bioavailability like an oral compound. The different requirements of inhaled and oral compounds can be exploited in the soft drug approach to ensure that inhaled drugs are poorly absorbed and quickly metabolised once they reach systemic circulation. This is particularly important when a target is known to cause adverse effects when inhibited systemically, considering that a substantial amount of inhaled drug is swallowed by the patient.

Another area of inhaled drug design which must be considered relates to duration of action. Commonly an objective in the design of a respiratory medicine to prolong duration of action, which is most readily achieved by prolonging the retention of the compound within the lungs. Lung retention is often achieved through manipulation of the physicochemical properties of a given compound and studies have shown that increasing lipophilicity/ decreasing solubility and increasing molecular weight can be effective ways to achieve lung retention.<sup>217,218</sup>

Moderate to low solubility, high permeability compounds can effectively be retained in the lungs, however this class of compound can have pharmacokinetics that are difficult to interpret as well as potential macrophage toxicology caused by accumulation of compound within the lung.<sup>219</sup>

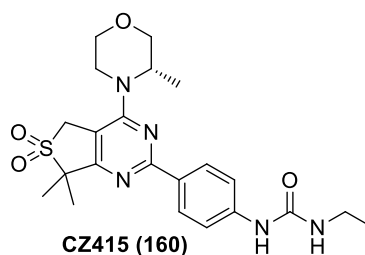
High solubility, low permeability compounds are easy to screen, however their design can be challenging, given that mTOR is an intracellular target and compounds will need to permeate the cell membrane.<sup>220</sup>

Based on all of the above, given the range of physicochemical properties that could potentially yield an effective inhaled mTOR inhibitor, the design hypothesis at the outset of the current study was to attempt to cover a range of physicochemical space when further developing a series of 5,6 bicyclic inhibitors.

## **2.6 CZ415 and Vistusertib – Benchmark Compounds**

When attempting to optimise a novel series of cyclopropylpyran containing bicyclic mTOR inhibitor compounds it is advantageous to consider compounds which are already published in order to benchmark the performance of new compounds against the existing literature.

**CZ415 (160)** is a highly selective bicyclic mTOR inhibitor which was developed by Cellzome, a company which GlaxoSmithKline acquired in 2012. **CZ415 (160)** has been shown to have *in vivo* efficacy against models of arthritis.<sup>221</sup> As we have a full suite of data obtained elsewhere in our laboratories on this published compound, it provides a useful benchmark with which to assess the quality of novel pyrazolopyrimidine containing compounds. The biological and physicochemical data associated with **CZ415** is shown in **Table 28**.



mTOR Kinobead pIC <sub>50</sub>	8.0 (±.7)	ChromLogD/P	4.3/4.3
pAkt pIC <sub>50</sub>	7.8 (±.7)	CAD solubility (µg/mL)	150
Healthy Scar-in-a-Jar pIC <sub>50</sub> (Cell Count)	6.5 (4.5) (±.6)	SLF Solubility (µg/mL)	17
Diseased Scar-in-a-Jar pIC <sub>50</sub>	6.3 (±.7)	FaSSIF Solubility (µg/mL)	18
PI3K $\alpha$ pIC <sub>50</sub>	5.3 (±.7)	Artificial membrane permeability (nm/sec)	200
PI3K $\beta$ pIC <sub>50</sub>	4.8	MDCK Permeability (Pexact) (nm/sec)	363
PI3K $\delta$ pIC <sub>50</sub>	5.0 (±.7)	IVC (Rat/Mouse/Human)	
PI3K $\gamma$ pIC <sub>50</sub>	5.1	Liver microsomes (mL/min/g) (avg.)	0.73/1.27/4.64
DNA-PK pIC <sub>50</sub>	5.5 (±.6)	hERG QUBE	4.6 (±.5)
		Parent aniline Ames test (TA98 and TA100)	Positive (with S9-Mix)

**Table 28:** Data on CZ415 (**160**) collected within our laboratories. N=3 or greater for all assays. Potency ranges are shown for values which fall outside the error of the assay (mTOR, PI3K, DNA-PK, hERG= 0.3 pAkt, SIAJ= 0.5) otherwise potency range is not shown.

**CZ415** has a potency of 10 nM in the primary mTOR kinobead assay and this is maintained in the pAkt cellular assay. Reasonably good potency at the sub-micromolar level is also observed in the phenotypic scar-in-a-jar assay. This level of potency would therefore be the minimum that would be considered in a novel 5,6 bicyclic compound, given that CZ415 is active *in vivo*. Selectivity over closely related lipid kinases is good with >100 fold selectivity observed over all the PI3K isoforms and DNA-PK. Again this is the minimum that we would consider in a novel 5,6 bicyclic compound.

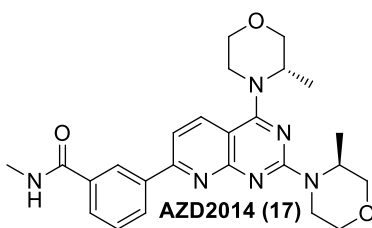
The physicochemical properties of **CZ415** are reasonably well balanced. The permeability of **CZ415** is good and the lipophilicity of the compound is at an acceptable level. The aqueous solubility of **CZ415** is lower than would be optimal for an oral candidate, however the

solubility is reasonable if inhaled routes of administration are considered. As previously mentioned, an inhaled mTOR inhibitor is being targeted and we are attempting to cover a range of physicochemical space with the cyclopropylpyran bicyclic series.

**CZ415** has weak activity at hERG (25  $\mu$ M) which has been associated with potentially fatal cardiac arrhythmia.<sup>222</sup> Given the potency of the compound against mTOR, it is possible there is a safe therapeutic window, however this hERG activity would still ideally be eliminated in any novel template which would represent a successor compound to **CZ415**.

When the parent aniline of **CZ415** was tested in an Ames mutagenicity test, it was found that the compound was mutagenic in the presence of S9-mix. This is a significant barrier to the development of this compound, therefore when developing a novel 5,6 bicyclic compound it was deemed necessary to mitigate any possible genotoxicity risk.

Another literature mTOR inhibitor compound, which has already been discussed in this thesis, is Vistusertib (AZD2014) (**17**). Vistusertib was developed by AstraZeneca and progressed into several PII clinical trials for various forms of cancer, before being terminated in late 2018.<sup>173</sup> Due to the promise of this compound within the mTOR inhibitor space, a suite of in-house data has been obtained to facilitate direct comparison with in-house compounds (**Table 29**).



mTOR Kinobead pIC <sub>50</sub>	8.2 (±.6)	ChromLogD/P	4.6/4.7
pAkt pIC <sub>50</sub>	7.1 (±.5)	CAD solubility (µg/mL)	24
Healthy Scar-in-a-Jar pIC <sub>50</sub> (Cell Count)	6.2 (4.9)	SLF Solubility (µg/mL)	NT
Diseased Scar-in-a-Jar pIC <sub>50</sub>	6.2	FaSSIF Solubility (µg/mL)	116
PI3K $\alpha$ pIC <sub>50</sub>	4.8	Artificial membrane permeability (nm/sec)	475
PI3K $\beta$ pIC <sub>50</sub>	4.5	MDCK Permeability (Pexact) (nm/sec)	NT
PI3K $\delta$ pIC <sub>50</sub>	5.3	IVC (Rat/Mouse/Human) Liver microsomes (mL/min/g) (avg.)	NT
PI3K $\gamma$ pIC <sub>50</sub>	5.1 (±.4)	hERG QUBE	NT
DNA-PK pIC <sub>50</sub>	5.2 (±.4)	Parent aniline Ames test (TA98 and TA100)	NA

**Table 29:** Data on vistusertib (AZD2014) (**17**) generated within our laboratories. N=3 or greater for all assays. Potency ranges are shown for values which fall outside the error of the assay (mTOR, PI3K, DNA-PK= 0.3 pAkt, SIAJ= 0.5) otherwise potency range is not shown.

The primary mTOR potency of **AZD2014** is in the low nanomolar range, however there is a greater than 10-fold reduction in the pAkt cellular assay. The sub-micromolar potency observed in the phenotypic Scar-in-a-jar assays is similar to **CZ415**, and there is a similar level of selectivity over closely related PI3K and DNA-PK kinases. The physicochemical properties are reasonable however CAD solubility is reduced for **AZD2014** compared with **CZ415** whilst artificial membrane permeability is increased. **AZD2014** does not have any potential aniline derived metabolites and therefore does not require an Ames test at this stage.

## 2.7 Project Aims

The aim of this project is to assess the suitability of cyclopropylpyran as a hinge binding fragment in a series of pyrazolopyrimidine based mTOR inhibitor compounds. The



pyrazolopyrimidine template has been established as the most efficient bicyclic system in combination with cyclopropylpyran using computational predictions and biological analysis of a series of cyclopropylpyran containing 5,6 bicyclic systems (*vide supra*).

The remainder of chapter will focus on the development of a series of pyrazolopyrimidine compounds based on this initial hit. The aim is to establish if, through optimization, a compound can be identified which is suitable for progression into PK/PD studies and has the scope to offer a potential alternative to current proprietary compounds which are under development at GSK. For a compound to be considered for further development it would need to fulfil the following criteria:

- Primary mTOR pIC<sub>50</sub> of >8.0.
- Activity is maintained in cellular assay (pAkt) (<10-fold difference in potency).
- pIC<sub>50</sub> of >6.0 in phenotypic “Scar-in-a-jar” assay.
- No less than 100-fold selectivity over any PIKK.
- No toxicology issues (hERG and Ames).
- Improved solubility (compared to initial pyrazolopyrimidine example **73**).
- Permeability maintained at level to ensure intracellular targets can be reached.

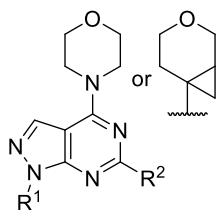
With these criteria in mind for a novel compound, we sought to develop a compound which was able to fulfil these lead criteria.

## **2.8 Literature Matched-Molecular Pair Compounds**

The first stage in the development of novel pyrazolopyrimidine mTOR inhibitors was to assess morpholine containing literature examples, in order to obtain an idea of how the potencies which have been reported within the literature correlate with the platform of biological assays available within our laboratories. Furthermore, cyclopropylpyran matched molecular pairs were proposed for synthesis in order to establish the effect this replacement has on biological activity and physicochemical properties.

As previously mentioned, aside from the hinge, there are two vectors which can be modified to improve potency and physicochemical properties. The *N*-1 substituent, known as the ribose region due to the position it occupies within the kinase active site is commonly a substituted piperidine ring.<sup>108</sup> Compounds containing benzyl, *tert*-butyl carbamate and parent amine have all been proposed for synthesis with two common backpocket substituents.

Another common ribose group is 1,1,1-trifluoroethane which is the best performing substituent from a range of small alkyl groups. Compounds containing this group have also been synthesised with common backpocket substituents. **Table 30** summarises the matched molecular pairs of interest which were proposed for synthesis.



Entry	Compound No.	Hinge	R <sup>1</sup> (Ribose )	R <sup>2</sup> (Backpocket)
1	161	Morpholine		
2	162	CPP		
3	163	Morpholine		
4	164	CPP		
5	165	Morpholine		
6	166	CPP		
7	84	Morpholine		
8	167	CPP		
9	83	Morpholine		
10	168	CPP		
11	169	Morpholine		
12	170	CPP		
13	171	Morpholine		
14	172	CPP		
15	173	Morpholine		
16	174	CPP		

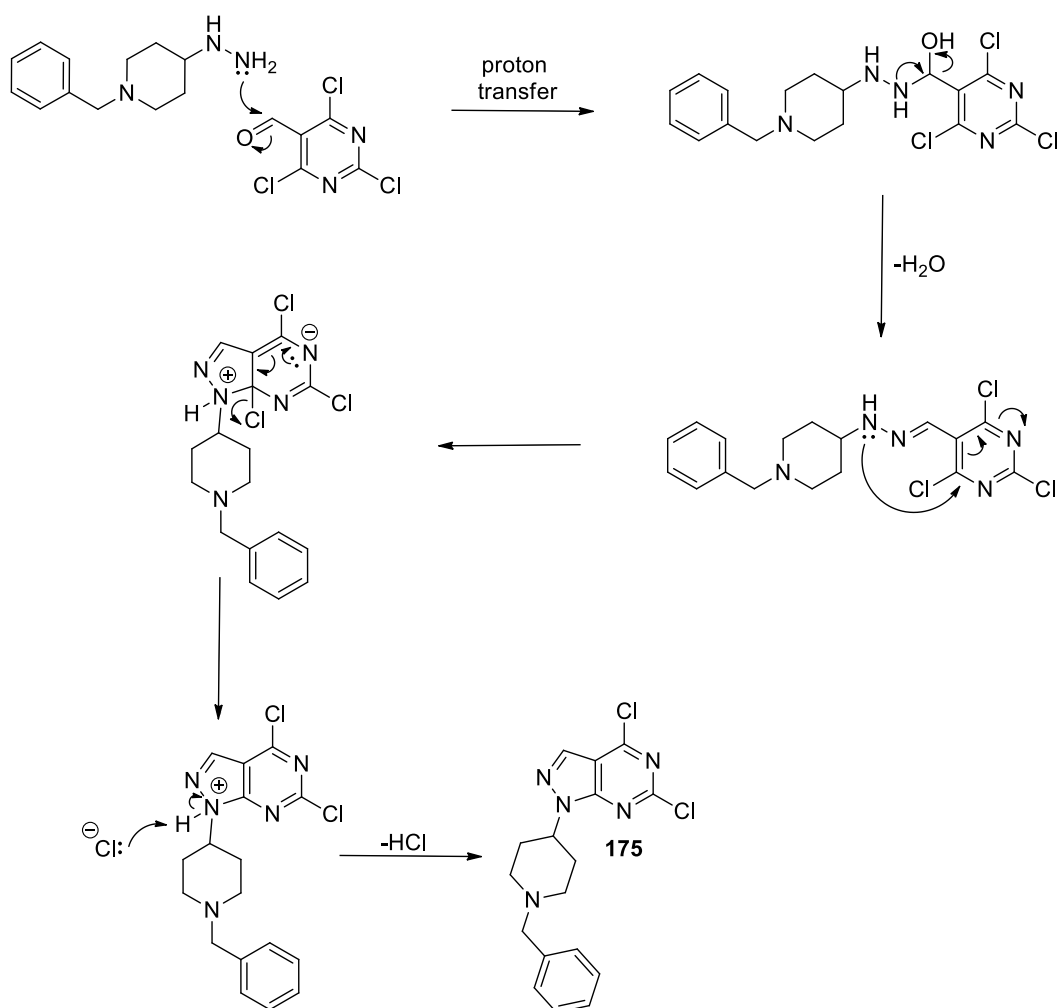
**Table 30:** Summary of proposed pyrazolopyrimidine MMP compounds for synthesis.

### **2.8.1 Synthesis of Literature MMP Compounds**

Compounds which are reported within the literature were synthesised following published procedures.<sup>172</sup> Benzyl piperidine substituted pyrazolopyrimidine core **175** was synthesised *via*

a condensation reaction followed by nucleophilic aromatic substitution between 1-benzyl-4-hydrazinylpiperidine and 2,4,6-trichloropyrimidine-5-carbaldehyde which was previously reported by Wyeth.<sup>172</sup> The proposed mechanism for this reaction is shown in **Scheme 21** and is presumed to be common across all of the pyrazolopyrimidine forming reactions reported in this work.

The benzyl piperidine substituted pyrazolopyrimidine product **175** was very unstable to heat, which has previously been reported.<sup>172</sup> In our hands we found that the product underwent near total degradation to an unidentified mixture of by-products upon concentration of the reaction mixture on a rotary evaporator with the water bath set to 40 °C. To overcome this instability, the reaction mixture was quenched with hydrochloric acid (4 M in dioxane) to form the hydrochloric acid salt of **175**, which was stable to heat. This allowed for the removal of volatiles and the reaction mixture was telescoped and used without further purification.

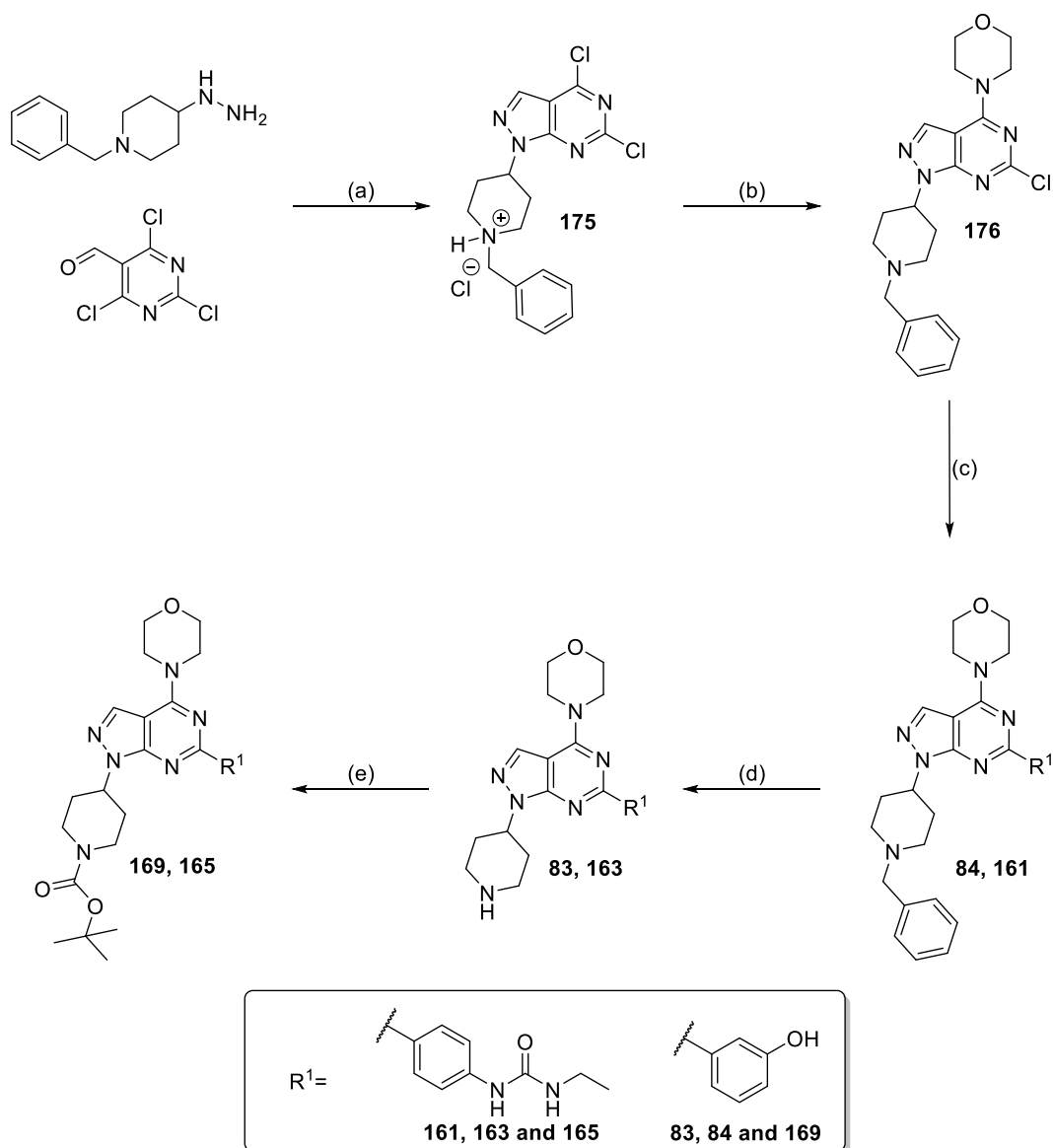


**Scheme 21:** Proposed mechanism for formation of *N*1-substituted pyrazolopyrimidine **175** with alkyl hydrazine and 2,4,6-trichloropyrimidine-5-carbaldehyde.

Dichloride core **175** then underwent nucleophilic aromatic substitution with morpholine at the 4-position of the ring system, which was predicted to be the most susceptible to attack.<sup>223,224</sup> Product **175** is sufficiently electron-rich that a further  $S_NAr$  process will not occur at position 6 without more forcing reaction conditions. At room temperature we are therefore able to obtain the desired mono-substituted product **176** in good yield (71%).

Suzuki-Miyaura cross coupling of **176** with the appropriate pinacol boronate ester furnishes the corresponding 4-ethyl urea (**161**) or 3-phenol (**84**) product. These products were then benzyl deprotected *via* hydrogenolysis using CO-ware apparatus<sup>133</sup> to give piperidine products **163** and **83**. The lower than expected yield in this step may be attributed to purification by MDAP, which was used for convenience on the small reaction scale. The reaction yields remain

unoptimised as an adequate quantity compound was obtained for biological testing. Finally, reaction of piperidines **163** and **83** with Boc anhydride, gave the corresponding *tert*-butyl carbamates **165** and **169** (Scheme 22).



(a) (i) TEA, EtOH, -78-0 °C, 2 h (ii) HCl (4M in dioxane), 96% yield (b) Morpholine, TEA, EtOH, r.t., 1 h, 71% yield (c) aryl boronic acid pinacol ester, Pd(PPh<sub>3</sub>)<sub>4</sub>, Na<sub>2</sub>CO<sub>3</sub>, DME:H<sub>2</sub>O (8:1), 100-150 °C,  $\mu$ Wave, 1.5 h, 33-69% yield (d) COWare apparatus, Pd (5% on carbon), EtOH, Zn, HCl (4M), r.t., 24 h, 33-48% yield (e) Boc<sub>2</sub>O, TEA, DCM, r.t., 2 h, 42-44% yield.

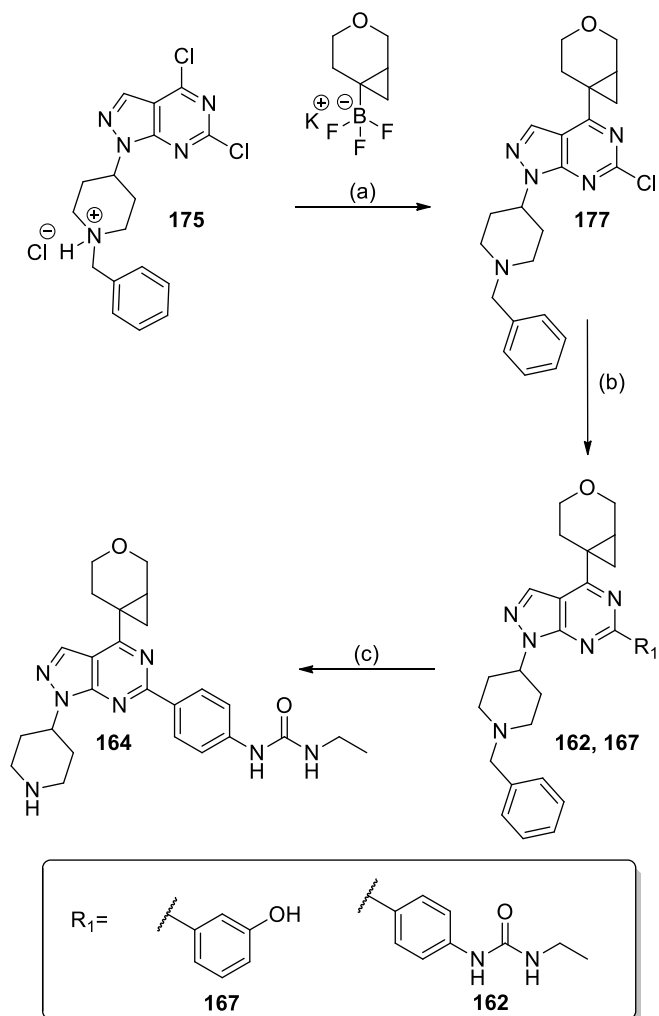
**Scheme 22:** Synthesis of piperidine containing compounds **83**, **84** and **134-137**.

Cyclopropylpyran containing compounds were synthesised from the common dichloro-intermediate **175**. A Suzuki-Miyaura cross coupling reaction was used to install the

cyclopropylpyran hinge binding fragment. This reaction was particularly low yielding (5%), and it was postulated that the reaction product **177** (**Scheme 23**) was unstable on silica columns, and therefore in subsequent attempts of this reaction, the product was telescoped as a crude mixture to the next step. Backpocket groups were introduced into the 6-position of the pyrazolopyrimidine ring *via* Suzuki-Miyaura cross-coupling to give 3-phenol **167** and 4-ethyl urea **162**. A sufficient quantity of compound **162** was obtained to progress further with the synthesis. There were concerns about the use of hydrogenolysis to remove the benzyl protecting group in **162** because of the reported instability of cyclopropyl rings to these conditions.<sup>225</sup> Based on this, an alternative deprotection method using  $\alpha$ -chloroethyl chloroformate was utilised.<sup>226</sup> This reaction provided a reasonable yield (40%) of piperidine **164** after MDAP (**Scheme 23**). The proposed mechanism for this alternative deprotection methodology is shown in **Scheme 24**.

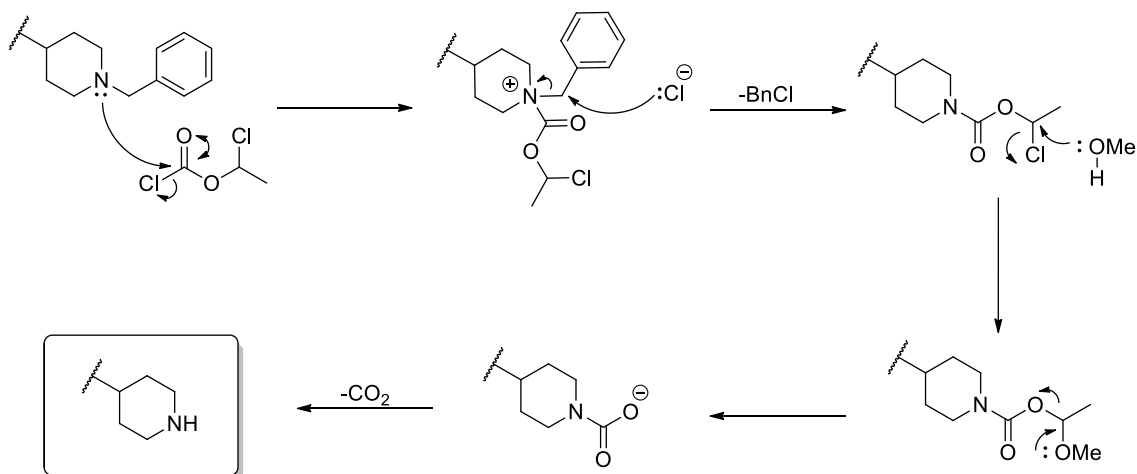
The use of  $\alpha$ -chloroethyl chloroformate in this reaction successfully leads to the desired piperidine product, this has been attributed to the steric bulk provided by the presence of  $\alpha$ -methyl and chloro- groups, which prevent S<sub>N</sub>2 attack of chloride at the  $\alpha$ -carbon. A carbon bearing a chloride is also suitably electron-deficient to prevent an S<sub>N</sub>1 type reaction from occurring by destabilisation of the resulting carbocation.<sup>227</sup> Other chloroformates such as ethyl- and benzyl chloroformate have been observed to fragment to the undesired alkyl chloride and carbon dioxide leading to a reduced yield of the desired deprotected amine (**Scheme 25**).<sup>228</sup>

An insufficient quantity of 3-phenol **167** was obtained to progress this compound further through the synthesis. Similarly, an insufficient quantity of 4-ethyl urea **164** was obtained to form compound **166**. As compound **162** and **164** and **167** had already been furnished, it was felt that this was sufficient for comparison of literature biological data, given the significant challenge of working with the unstable and capricious benzyl piperidine core **175**.

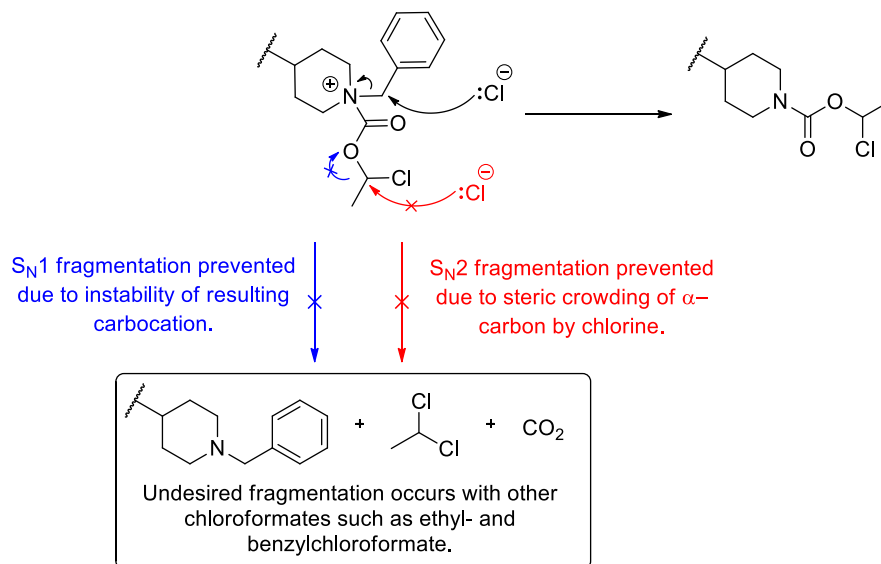


(a) Pd(OAc)<sub>2</sub>, CataCXium® A, Cs<sub>2</sub>CO<sub>3</sub>, toluene/H<sub>2</sub>O (10:1), 100 °C, 16 h, 5% yield (b) aryl boronic acid pinacol ester, Pd(PPh<sub>3</sub>)<sub>4</sub>, Na<sub>2</sub>CO<sub>3</sub>, DME:H<sub>2</sub>O (8:1), 115-120 °C, 2 h, 42-56% yield (c) (i) α-chloroethyl chloroformate, DCM, 0 °C, 2 h, (ii) MeOH, r.t., 68 h, 40% yield.

**Scheme 23:** Synthesis of piperidine-containing compounds **162**, **164** and **167**.



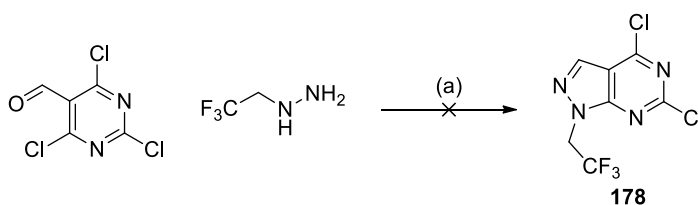
**Scheme 24:** Proposed mechanism for *N*-benzyl deprotection with  $\alpha$ -chloroethyl chloroformate.<sup>227</sup>



**Scheme 25:** Explanation of the importance of  $\alpha$ -chloroethyl chloroformate to the mechanism of the benzyl deprotection of **164**.<sup>227,228</sup>

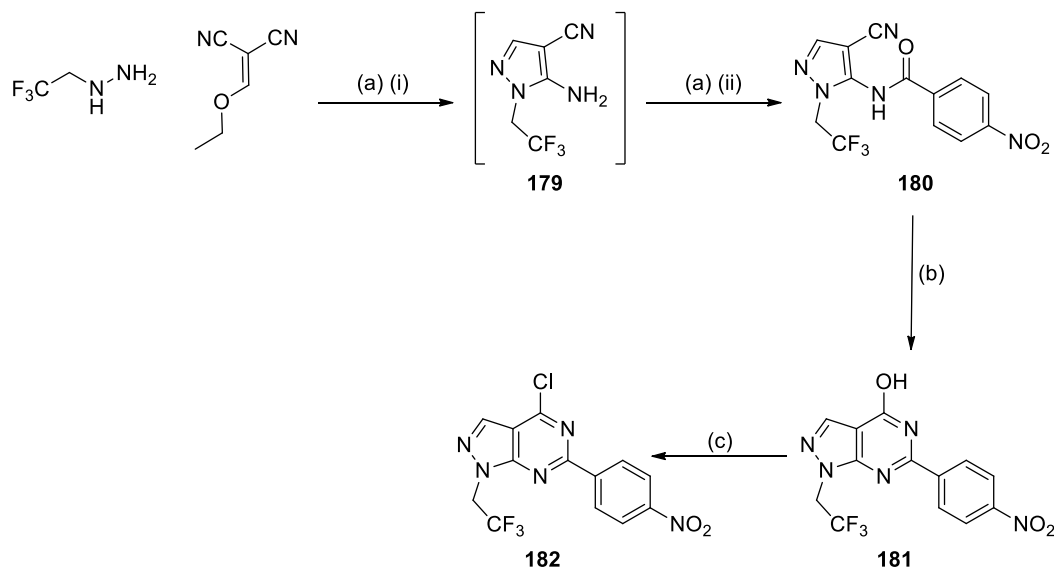
Trifluoroethyl-substituted compound **182** was synthesised following the literature preparation of this compound<sup>158</sup> after an attempt to form dichloro- intermediate **178** using trifluoroethylhydrazine and 2,4,6-trichloropyrimidine-5-carbaldehyde yielded no product with complete degradation of starting materials to a mixture of unidentified by-products (**Scheme 26**).





**Scheme 26:** Failed cyclisation strategy to obtain compound **178**.

Following from this, compound **182** was synthesised by cyclisation of trifluoroethyl hydrazine and 2-(ethoxymethylene)malononitrile to give intermediate **179**. Benzoylation of the intermediate amino group with 4-nitrobenzoyl chloride formed pyrazole **180**. Treatment of **180** with refluxing base and peroxide gave pyrazolopyrimidine **181** in good yield (60%). Chlorination of **181** with POCl<sub>3</sub> provided compound **182** in very good yield (83%) although due to issues with purification this was taken forward to the subsequent step (**Scheme 27**).



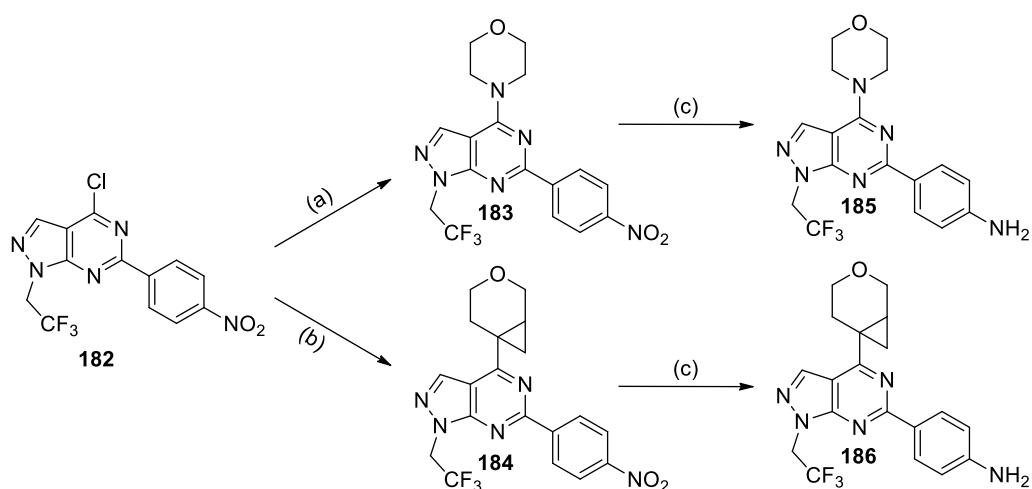
(a) (i) 2,2,2-trifluoroethylhydrazine (70% soln. in H<sub>2</sub>O), EtOH, 95 °C, 0.5 h. (ii) 4-nitrobenzoyl chloride, TEA, DCM/MeOH (2:1) r.t., 1.5 h, 58% yield (b) NaOH (2M), H<sub>2</sub>O<sub>2</sub> (30% soln. in H<sub>2</sub>O), EtOH, 115 °C, 1.5 h, 60% yield (c) POCl<sub>3</sub>, reflux, 1.5 h, 83% yield, used crude.

**Scheme 27:** Synthesis of **182**.

Compound **182** is an appropriate common intermediate to furnish both morpholine and cyclopropylpyran containing compounds. In order to furnish literature morpholine containing compound **183**, heteroaryl chloride **182** underwent a nucleophilic aromatic substitution reaction with morpholine. This reaction was extremely efficient, and a very good yield (85%) was achieved by simply heating the reaction mixture with a hot-air gun for 2 minutes.

Cyclopropylpyran derivative **184** was synthesised *via* Suzuki-Miyaura cross coupling. The yield for this reaction was 69%, which is a very good result for this challenging class of  $sp^2$ - $sp^3$  couplings. It is likely that this superior yield is, in part, down to the lack of competing chloride positions in compound **182**.

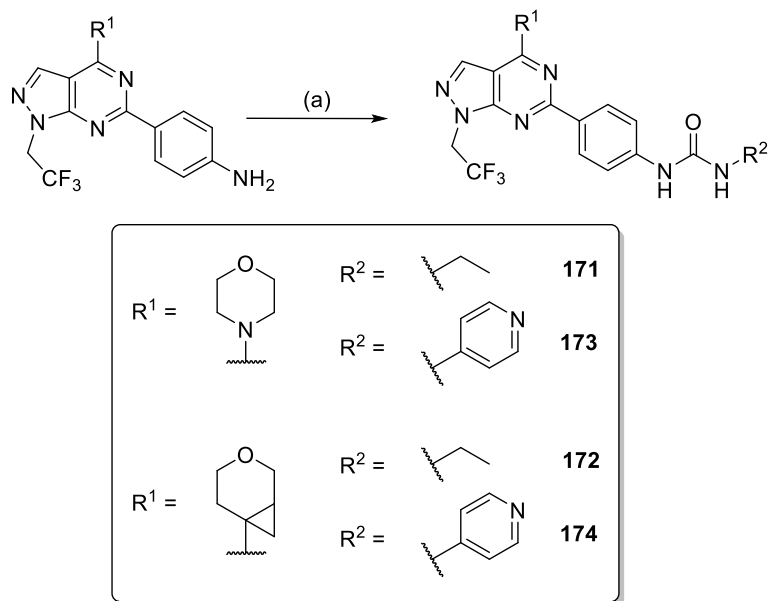
Nitro- containing compounds **183** and **184** were then reduced to the corresponding aniline products **185** and **186** using iron powder under ultrasonic irradiation.<sup>229</sup> These reduction conditions were chosen due to the perceived instability of the cyclopropyl group in **184** under standard hydrogenation conditions (*vide supra*). This method provided both **185** and **186** in excellent yields (94% for both examples) with no further purification required. (**Scheme 28**).



(a) Morpholine, EtOH, TEA, heat gun, 2 min, 85% yield (b) Potassium 3-oxabicyclo[4.1.0]heptan-6-yltrifluoroborate, Pd(OAc)<sub>2</sub>, CataCXium® A, Cs<sub>2</sub>CO<sub>3</sub>, toluene/H<sub>2</sub>O (10:1), 120 °C, 3 h, 69% yield (c) Fe powder, AcOH, EtOH, H<sub>2</sub>O, sonicator, r.t., 1.5-3 h, 94% yield for both examples.

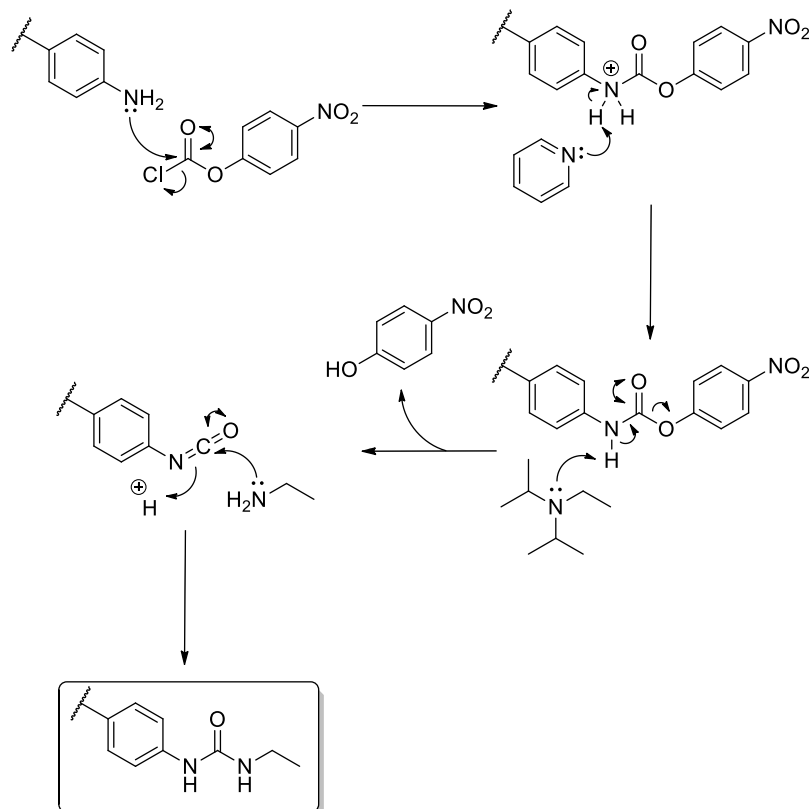
**Scheme 28:** Synthesis of aniline intermediates **185** and **186**.

Anilino- compounds **185** and **186** were converted into 4-ethylurea (**171** and **172**) and 4-(4-pyridyl)urea (**173** and **174**) using *para*-nitrophenyl chloroformate and relevant amine in a 2-step, 1-pot procedure (**Scheme 29**).<sup>230</sup> This reaction is thought to proceed *via* an isocyanate intermediate which is formed *in situ* (**Scheme 30**).



(a) (i) *para*-Nitrophenyl chloroformate, Pyridine, DCM, r.t., 1.5 h (ii) R<sub>2</sub>-NH<sub>2</sub>, DIPEA, r.t., 2.5 h, 24-51% yield.

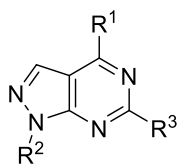
**Scheme 29:** Synthesis of urea compounds **171-174**



**Scheme 30:** Proposed mechanism for urea formation using *para*-nitrophenyl carbamate.

## **2.8.2 Literature Compounds**

As well as the literature compounds which were synthesised, a number of published compounds were purchased from a commercial vendor. The aim was to acquire compounds in order to cover a wide range of reported potencies based on the literature data. This work was carried out in order to establish the validity and potential utility of the published literature SAR (*vide supra*). Prior to the introduction of a chemoproteomic mTOR kinobead assay within our laboratories, a FRAP1 biochemical assay was used to assess compound activity and was found to be unreliable. It has also been noted that other groups have noticed errors with similar assays, for example a publication by AstraZeneca utilised a pAkt cellular assay as the primary assessment of potency.<sup>110</sup> With this uncertainty in mind, a range of literature compounds was therefore tested within the biological assays established in our laboratories (**Table 31**).



Entry	Compound No.	R <sup>1</sup>	R <sup>2</sup>	R <sup>3</sup>	mTOR pIC <sub>50</sub>		PI3Kα pIC <sub>50</sub>	
					GSK	Lit.	GSK	Lit.
1	84				5.4	7.1	6.5*	7.4
2	83				6.0	6.7	6.2*	7.4
4	161				6.9	9.1	6.1*	6.6
5	163				7.7	11.6	5.3*	6.5
6	165				7.3	12.3	5.5 (n=1)	6.1
7	187				6.2	8.1	4.9	5.7
8	99				7.2	8.3	5.0	6.1
9	188				6.6 (±.7)	8.4	5.2	6.0
10	189				7.8*	9.2	5.2*	6.2
11	154				7.0	9.0	5.2	5.6
12	133				8.3	9.7	5.1	5.9

Literature assays: <sup>α</sup>**mTOR** – Biochemical DELFIA assay using purified Flag-tagged truncated human TOR (amino acids 1360-2549).<sup>231</sup> <sup>β</sup>**PI3Kα** – Biochemical plate based fluorescence polarisation (FP) assay.<sup>232</sup> In-house assays: <sup>δ</sup>**mTOR** – Kinobead chemoproteomic binding assay.<sup>175</sup> <sup>γ</sup>**PI3Kα** – Biochemical HTRF assay.<sup>178</sup>

**Table 31:** mTOR and PI3Kα in-house and literature pIC<sub>50</sub> values for published compounds. Potency values marked with \* are N=2. N=3 or greater for all other compounds. Potency ranges are shown for values which fall outside the error of the assays (0.3) otherwise potency range is not shown.

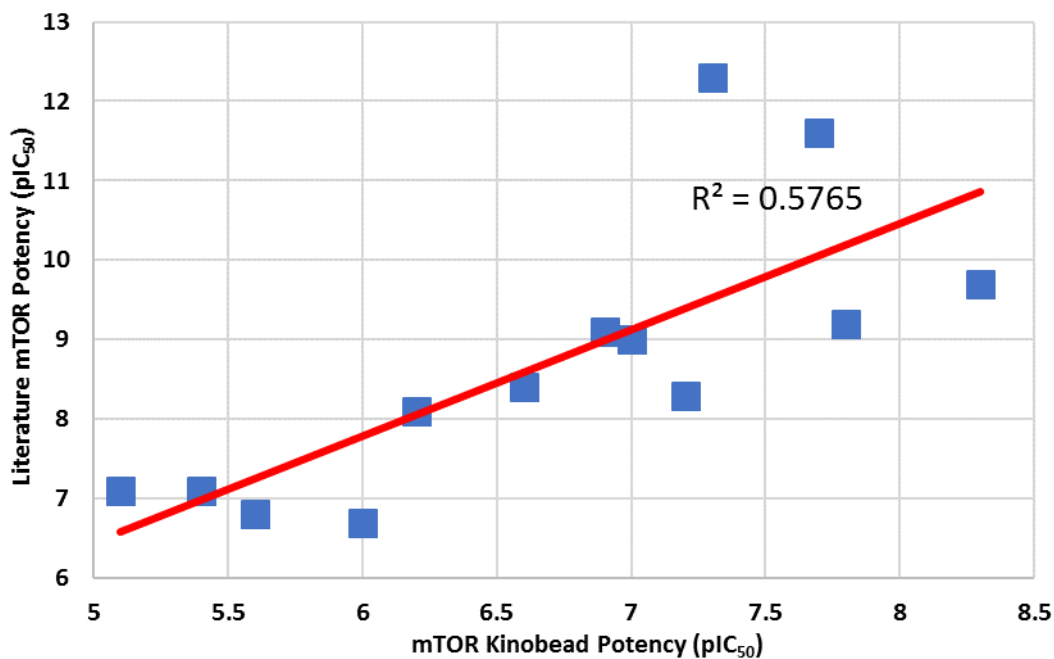


**Figure 59:** Graph comparing literature mTOR potency to in-house mTOR kinobead potency for compounds in **Table 31**.

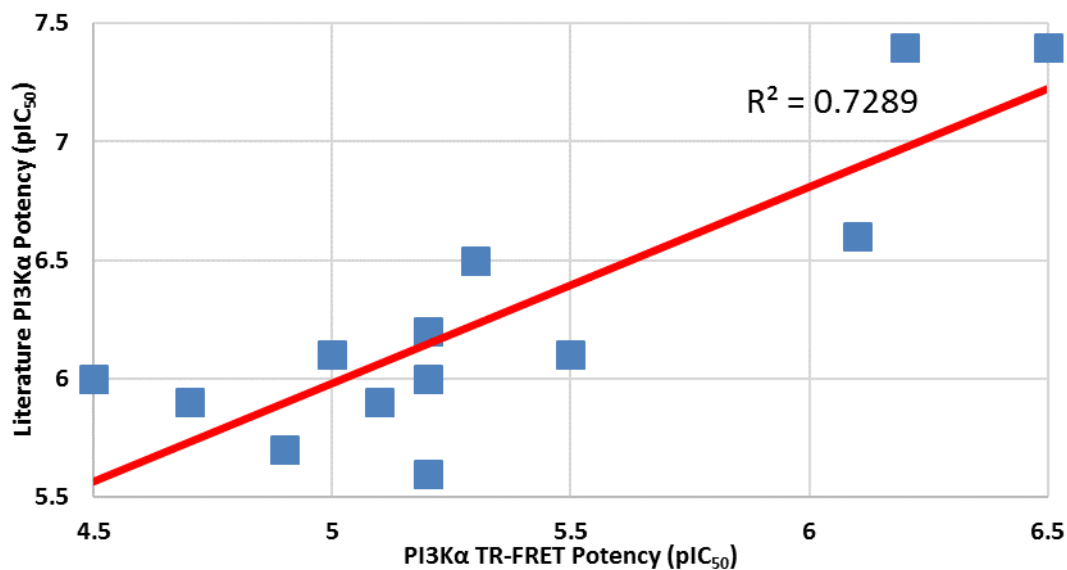


**Figure 60:** Graph comparing literature PI3K $\alpha$  potency to in-house PI3K $\alpha$  TR-FRET potency for compounds in **Table 31**.

For mTOR, the potencies reported in the literature are not a particularly good indication of the potency values obtained in our laboratories. This is likely due to the fact the assays have a very different format. Within the literature, a biochemical (DELFI) style assay is used in which a

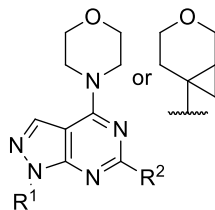
recombinant, truncated version of mTOR is used. In our own studies, a kinobead mTOR assay (*vide supra*) was employed, which uses mTOR from whole cell lysate. This means that the mTOR protein will be associated with other proteins in mTORC1 and mTORC2 complexes and the values obtained from this assay may be a more accurate representation of a biological system. Given there is only a weak correlation ( $R^2=0.58$ ) between the literature potency and measured potency, we were not able to utilise the literature structure-activity relationship (SAR) effectively to optimise for target potency with novel cyclopropylpyran-containing compounds. Nevertheless, synthesis of the compounds was very worthwhile and gave a more realistic assessment of the SAR which could then be used appropriately in future compound design. In addition, the physicochemical data obtained on the analogues provided a strong benchmark for the design process.

### **2.8.3 Cyclopropylpyran Matched Molecular Pair Compounds**

In order to establish the effectiveness of the cyclopropylpyran motif as a hinge binding fragment in the pyrazolopyrimidine series of mTOR inhibitors, several matched pairs were made with the corresponding morpholine systems

**Table 32).**





Entry	Compound No.	Hinge	R <sup>1</sup>	R <sup>2</sup>	pIC <sub>50</sub>		
					mTOR	pAkt	PI3K α,δ
1	161	Morph.			6.9	7.2	6.1 6.1
2	162	CPP			7.2 (±.4)	7.1	5.3 5.6
3	163	Morph.			7.7	6.5 (±1)	5.3 6.0
4	164	CPP			7.1 (±.6)	6.4	NT
5	84	Morph.			5.4	6.7	6.5 6.7
6	167	CPP			5.1	6.1	6.1 6.0
7	171	Morph.			7.5 (±.5)	7.8	6.1 5.9
8	172	CPP			7.2	7.5	5.2 5.2
9	173	Morph.			7.6 (±.7)	7.5	7.6 6.4
10	174	CPP			6.6	7.5	6.1 5.6

**Table 32:** Biological assay data for cyclopropylpyrrolidine/ morpholine matched molecular pair compounds. N=3 or greater for all compounds. Potency ranges are shown for values which fall outside the error of the assay (mTOR= 0.3 pAkt= 0.5) otherwise potency range is not shown. Range is not shown for PI3K isoform assay.

Entry	Compound No.	Hinge	R <sup>1</sup>	R <sup>2</sup>	CAD $\mu\text{g/mL}$	AMP nm/sec	Chrom LogD/ LogP
1	<b>161</b>	Morph.			37	325	5.67/ 6.48
2	<b>162</b>	CPP			20	205	6.92/ 7.58
3	<b>163</b>	Morph.			457	3	1.78/ 3.17
4	<b>164</b>	CPP			491	6.5	2.43/ 3.80
5	<b>84</b>	Morph.			11	345	6.20/ 6.76
6	<b>167</b>	CPP			26	100	7.30/ 7.84
7	<b>171</b>	Morph.			1	-	4.71/ 4.80
8	<b>172</b>	CPP			3	970	5.68/ 5.80
9	<b>173</b>	Morph.			1	120	4.57/ 4.90
10	<b>174</b>	CPP			3	165	5.46/ 5.85

**Table 33:** Physicochemical assay data for cyclopropylpyran/ morpholine matched molecular pair compounds.

Across this small set of matched molecular pairs, the primary potency at mTOR observed for cyclopropylpyran containing compounds is reasonably well maintained from the corresponding morpholine hinged matched molecular pair compound. Cyclopropylpyran compounds exhibit slightly reduced potency in all instances except for **162** vs. **163**. The cyclopropylpyran compounds are less efficient (LipE) owing to their increased lipophilicity, although this increase in lipophilicity does not generally have a negative effect on solubility.

4-Pyridyl urea **174** has the largest reduction in mTOR potency compared to its corresponding morpholine **173** (~10-fold), however it is worth noting the equivalence of cellular pAkt potency for these two compounds.

Although a slight reduction in lipophilic ligand efficiency was observed for the cyclopropylpyran containing compounds, these compounds were still of interest because of

the general increase in selectivity over closely related PI3K lipid kinases that was observed when switching the hinge binding fragment to cyclopropylpyran, as well as the proprietary nature of these compounds.

Taken as a set, these compounds provide good evidence that replacing morpholine for cyclopropylpyran may be tolerated for pyrazolopyrimidine based compounds. This limited set of compounds do indicate that balancing solubility and permeability presents a particular challenge, however as discussed above, we are interested in pursuing a range of physicochemical profiles. We therefore proceeded to optimise both available vectors for mTOR potency and to achieve a balanced solubility and permeability profile.

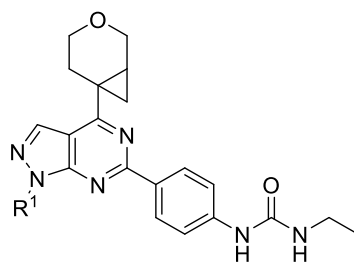
## **2.8 Optimisation of N-1 Substituent**

Optimisation attempts were initially focused on the *N1*-position of pyrazolopyrimidine. This substituent is thought to occupy a solvent-exposed region of the mTOR active site and may therefore tolerate a range of substitution in this position.

The piperidine substituents which are common within the previously published literature were not further investigated. This decision was taken due to the high lipophilicity of substituted compounds (for example in compounds **162** and **167**) and very low permeability of parent piperidine compound **164**, suggesting that finding an acceptable balance of solubility/permeability in this compound class would be challenging.

In an attempt to improve physicochemical properties of cyclopropylpyran compounds such as **162**, the inclusion of water-solubilising cyclohexyl analogues was examined. This has been previously reported within the literature.<sup>105</sup> Cyclohexyl analogues were chosen as they are structurally similar to piperidine-based compounds. However, it was anticipated that the synthesis of these compounds would be more tractable as the instability of intermediates reported (and observed) within the synthesis of substituted piperidine compounds such as **162** were not reported in this case.

Compounds initially proposed for synthesis are summarised in **Table 34**, along with predicted physicochemical properties for these compounds. The ketal functional group in **190** could be deprotected to ketone **191**. This provided a handle for a late-stage modification strategy, enabling chemical diversity to be incorporated into this position. Neutral (**192** and **193**) and basic (**194**) water-solubilising groups were proposed for incorporation into this position.



Entry	Compound No.	R <sup>1</sup>	Predicted Solubility Class	Predicted AMP	cLogD	cLogP
1	<b>190</b>		Low	108	3.35	3.35
2	<b>191</b>		High	128	3.08	3.08
3	<b>192</b>		High	97	2.27	2.27
4	<b>193</b>		High	97	2.27	2.27
5	<b>194</b>		High	216	0.71	3.47

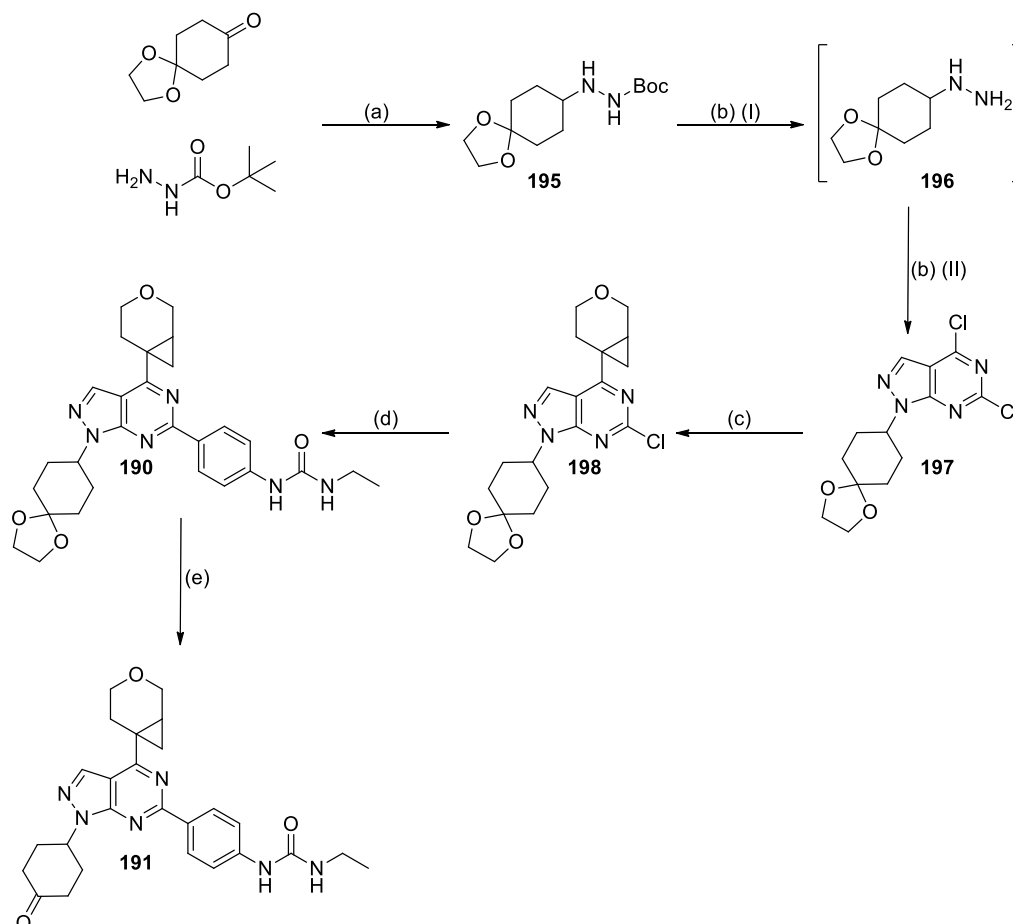
**Table 34:** Predicted physicochemical properties for cyclohexyl compounds **190-194**. NB: Predicted physicochemical data was generated in Helium (Ceiba Solutions). Calculated logP and logD 7.4 values are calculated in Chemaxon.

The physicochemical values predicted for cyclohexyl compounds **190-194** suggest that improvements to solubility can be made, presumably as a consequence of reducing lipophilicity, whilst maintaining permeability in an acceptable space; these compounds were therefore prioritised for synthesis and biological evaluation.

### **2.8.1 Synthesis of Cyclohexyl-N1-Substituted Pyrazolopyrimidine Compounds**

In order to incorporate 1,4-dioxaspiro[4.5]decane at the *N1*-position of pyrazolopyrimidine, 1,4-dioxaspiro[4.5]decan-8-one was combined with *tert*-butylcarbазate in the presence of sodium triacetoxyborohydride (STAB). This reaction was stirred overnight to give Boc-protected hydrazine **195**. Compound **195** was heated in water at reflux for 16 h in order to produce hydrazine intermediate **196** *in situ*. This solution was cooled and 2,4,6-trichloropyrimidine-5-carbaldehyde was added, furnishing the appropriate dichloropyrazolopyrimidine **197**. Suzuki-Miyaura cross coupling to install cyclopropylpyran at the 4-position was somewhat inefficient, leading to formation of significant quantities of bis-coupled product and hydrolysed starting material (hydrolysis of the heteroaryl chloride). These by

products were difficult to remove by purification, and there were concerns about the stability of **198** on silica columns, due to a low recovery from attempted purifications. With this in mind compound, **198** was telescoped to the next stage of the synthesis as a crude reaction mixture. A subsequent Suzuki-Miyaura cross coupling reaction on compound **198** gave compound **190** in reasonable yield (53%). Ketal deprotection of **190** with hydrochloric acid gave ketone **191** in quantitative yield. (Scheme 31).



(a) STAB, DCM, AcOH, r.t., 16 h, 89% yield (b) (i) H<sub>2</sub>O, Reflux, 16 h. (ii) 2,4,6-trichloropyrimidine-5-carbaldehyde, TEA, EtOH/H<sub>2</sub>O (1:1), 0 °C, 0.5 h, 49% yield over 2 steps. (c) Potassium 3-oxabicyclo[4.1.0]heptan-6-yltrifluoroborate, Pd(OAc)<sub>2</sub>, CataCXium® A, Cs<sub>2</sub>CO<sub>3</sub>, toluene/H<sub>2</sub>O (10:1), 100 °C, 16 h, telescoped (d) 1-ethyl-3-(4-(4,4,5,5-tetramethyl-1,3,2-dioxaborolan-2-yl)phenyl)urea, Pd(PPh<sub>3</sub>)<sub>4</sub>, Na<sub>2</sub>CO<sub>3</sub>, DME:H<sub>2</sub>O (8:1), 120 °C, 2 h, 53% yield (e) HCl, THF, r.t. 2 h, quant.

**Scheme 31:** Synthesis of **190** and **191**.

Compound **191** was subsequently further diversified at the ketone position. Reduction with sodium borohydride gave the *trans*-alcohol **192** as the major product (5:1 ratio). Reduction with L-selectride however, gave complete selectivity for the *cis*-alcohol product **193**. This was confirmed by analysis of the coupling constants within the NMR spectra for these compounds

(Figure 61). By considering the dihedral angle between coupled protons in each isomer and using the Karplus relationship,<sup>233,234</sup> we are able to assign the correct stereochemistry to each compound. In both isomers, the proton H<sub>A</sub> is in an axial position, due to the large steric bulk of the pyrazolopyrimidine group. This proton therefore has a larger coupling (~11 Hz) as it has a dihedral angle of ~180° to a vicinal proton, the other vicinally coupled proton has a smaller coupling constant (~4 Hz) as the dihedral angle in this case is ~60°.

The NMR spectrum of **192** shows that the proton H<sub>B</sub> is also in an axial position, as it has similar coupling constants (11.0 Hz and 4.2 Hz), this confirms a *trans*-relationship for the substituents in the cyclohexyl ring. In the NMR spectrum for compound **193** the proton H<sub>B</sub> does not have a clearly defined multiplet, presumably due to the small coupling constants expected for an equatorial proton. Therefore, this indicates a *cis*-relationship for the substituents in the cyclohexyl ring

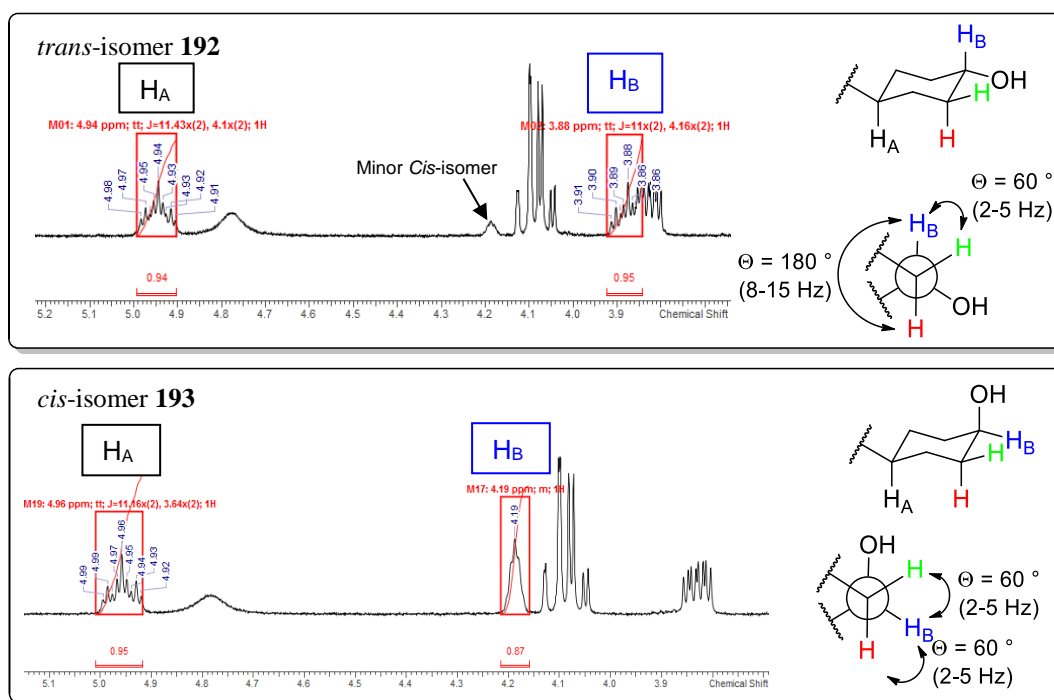
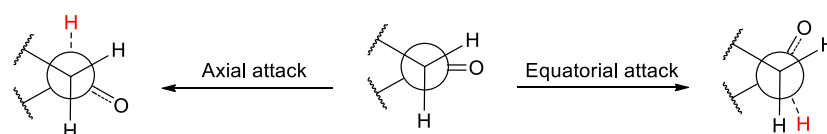


Figure 61: NMR analysis of *trans*-alcohol product **192** and *cis*-alcohol **193** showing the rationale used to assign relative stereochemistry to these two stereoisomers.

The different selectivity observed with these reducing agents can be rationalised using the Felkin-Anh model, which suggests that the transition state for addition to the equatorial face of cyclohexanone involves greater torsional strain than that of addition to the axial face (Figure 62).<sup>235,236</sup>



**Figure 62:** Newmann projections showing the greater eclipsing reactions that result from attack of hydride at equatorial face.

With a small, sterically unhindered nucleophile such as  $\text{NaBH}_4$ , attack at the axial- face is favoured by a predicted  $\sim 1.1 \text{ kcal mol}^{-1}$ . This value would correspond to an 86:14 ratio of *trans*: *cis* product at room temperature, which is similar to what we have observed experimentally. Attack of cyclohexanone with a sterically hindered nucleophile, such as L-selectride, favours equatorial attack by  $\sim 3.7 \text{ kcal mol}^{-1}$ . Computational analysis has suggested this is due to this reaction proceeding *via* a late stage transition state, where the carbonyl carbon has a geometry close to tetrahedral. This is likely to be due to the lower reactivity of sterically demanding hydride reagents. This results in lower overall torsional strain and a very small difference in torsional strain between axial and equatorial attack. In this scenario, selectivity for equatorial attack is dominated by steric effects, leading to the major *cis*- product being almost exclusively formed.<sup>237</sup> (**Figure 63**)

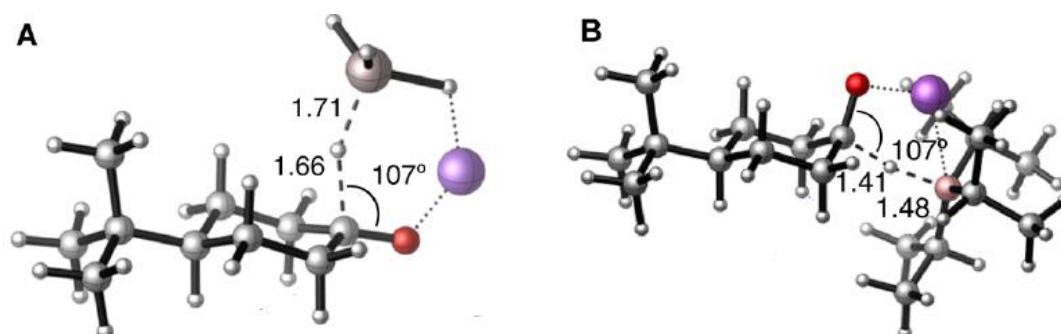
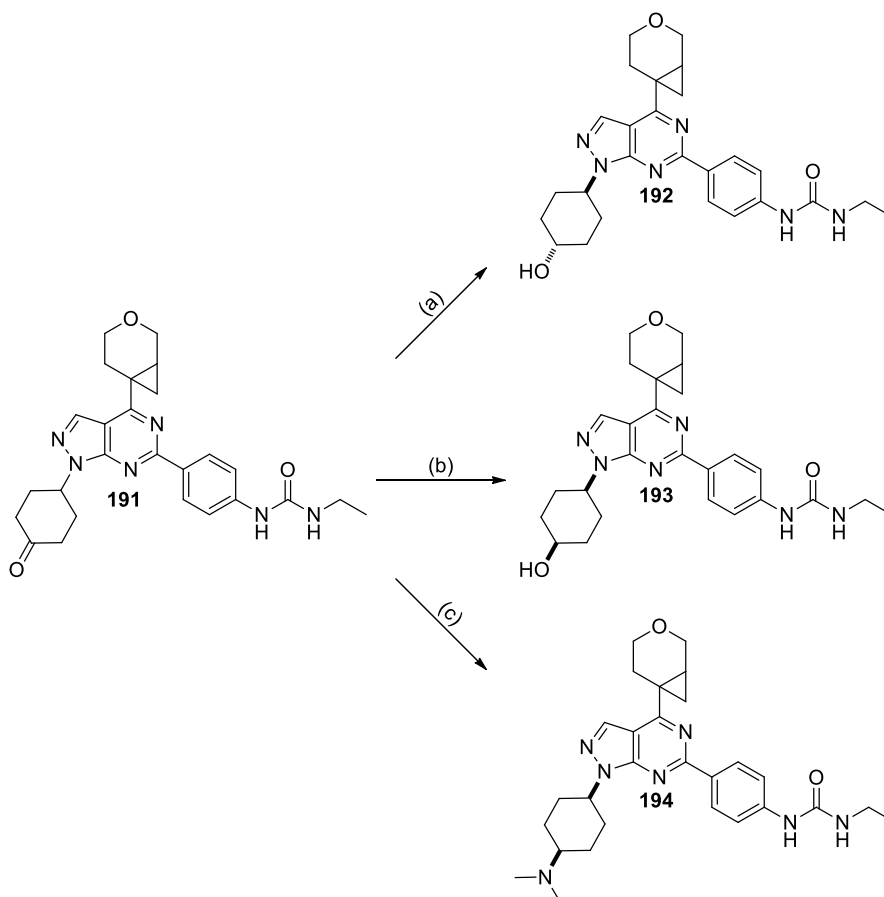


**Figure 63:** Energetically favoured transition states for reduction of *tert*-butyl cyclohexanone with (A) Sterically unhindered nucleophile such as  $\text{LiAlH}_4$  (shown) or  $\text{NaBH}_4$  and (B) sterically hindered nucleophile such as L-selectride (lithium triisopropylhydride was modelled as a surrogate system, as it is less computationally demanding).<sup>237</sup>

Reductive amination of ketone **191** with dimethylamine and sodium triacetoxyborohydride led to tertiary amine **194** (**Scheme 32**). LCMS analysis of the reaction mixture suggested formation of both stereoisomers in a 2.5:1 ratio. Only the major isomer was isolated in sufficient purity, and this was assigned by NMR as the *cis*- isomer **194**. This is presumably favoured due to the increased steric bulk of STAB relative to  $\text{NaBH}_4$ .



(a) NaBH<sub>4</sub>, THF, r.t., 1 h, 45% yield (b) L-Selectride (2M in THF), THF, 50 °C, 1 h, 44% yield (c) dimethylamine (2M in THF), STAB, AcOH, DCE, 50 °C., 3 h, 18% yield.

**Scheme 32:** Synthesis of **192-194**

## 2.8.2 Cyclohexyl-N1-Substituted Compounds

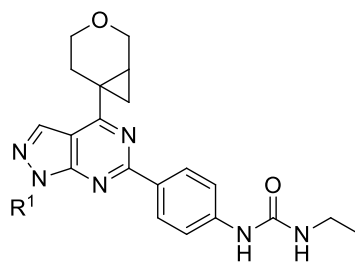
The biological and physicochemical properties of substituted cyclohexyl class of compounds is reported in **Table 35**. Ketal-containing compound **190** displays a moderate increase in potency in comparison to benzyl piperidine **162**. Compound **190** also has a lower molecular weight, meaning this molecule is more efficient than **162** (BEI= 14.5 vs. 12.5). This potency was also maintained within the cellular pAkt assay. The solubility and permeability of **190** is similar to **162**. The increase in mTOR potency and similar physicochemical properties noted for **190** meant that this was a good starting point for derivatization.

Ketone **191** maintains a similar potency to **190** and due to the decrease in molecular weight this compound is more efficient (BEI = 15.4). Ketone **190** has increased solubility and permeability and reduced lipophilicity. This cyclohexanone fragment was not pursued in earlier reports as it only displayed moderate levels of stability towards nude mouse and human



liver microsomes.<sup>105</sup> Microsomal stability is an important parameter for orally administered compounds, as it is desirable for these compounds to remain in the systemic circulation and exert their therapeutic effect for as long as possible. For inhaled compounds, however, the situation is different. Once an inhaled drug compound reaches the systemic circulation, rapid hepatic clearance can help to minimise unwanted side-effects that may be caused by systemic exposure.<sup>238</sup> Therefore as we are targeting an inhaled compound, this cyclohexanone analog remains interesting for further profiling.

The cyclohexyl based compounds **190** and **191** display an increase in selectivity over the corresponding benzyl piperidine **162**. The selectivity of compound **162** for mTOR over PI3K $\delta$  is ~20 fold, whereas with cyclohexyl analogues **190** and **192** this selectivity is ~250 fold and ~125 fold, respectively. The origin of this selectivity increase is not entirely clear as this group is expected to occupy a region which is exposed to solvent.<sup>205</sup> However, literature reports indicate that increases in selectivity when targeting this region are possible.<sup>239</sup> In this case, the authors postulated that this might be attributed to formation of additional hydrogen bonding interactions with the ribose pocket of mTOR, whereas in PI3K isoforms, this interaction is not formed, or not necessary for inhibitory activity. It is plausible that a similar effect is being observed for the cyclohexyl-based compounds in this series.



Entry	Compound No.	R <sup>1</sup>	pIC <sub>50</sub>			CAD (μg/mL)	AMP (nm/sec)	Chrom LogD/LogP
			mTOR	pAkt	PI3K $\alpha,\beta,\delta,\gamma$			
1	<b>162</b>		7.2 (±.4)	7.1	5.3, 5.3, 5.6, 5.3	20	205	6.92/ 7.58
2	<b>190</b>		7.5	7.7	<4.5, <4.5, 5.2, 5.3	33	375	5.67/ 5.93
3	<b>191</b>		7.3	7.4	5.2, 5.0, 5.4, 5.1	52	380	4.81/ 4.96
4	<b>192</b>		7.8	7.6	5.4, 4.8, 5.6, 5.4	21	250	4.24/ 4.31
5	<b>193</b>		7.7	7.6	5.3, 4.8 5.5, 5.6	14	285	4.15/ 4.21
6	<b>194</b>		6.1	6.7	<4.5, 4.8 5.0, 4.9	239	130	3.12/ 6.43

**Table 35:** Biological and physicochemical data for cyclohexyl-N1-substituted compounds **190-194**. Benzyl-piperidine containing compound **162** is included for reference. N=3 for all compounds. Potency ranges are shown for values which fall outside the error of the assay (mTOR= 0.3 pAkt= 0.5) otherwise potency range is not shown. Range is not shown for PI3K selectivity data.

Reduction of **191** to give alcohol stereoisomers **192** and **193** is associated with an increase in potency, however a reduction is seen in both solubility and permeability. The analogous dimethylamine containing compound **194** has a ~40 fold reduction in mTOR potency compared to the corresponding alcohol **193**. Dimethylamine **194** is also ~10 fold less selective than alcohols **192** and **193**. The reason behind this decrease in potency and selectivity was unclear, as this vector is expected to be solvent exposed, although as previously mentioned, this effect may be caused by formation of an additional hydrogen bonding interaction in the case of the more active examples. To understand this phenomenon, we considered the predicted binding of these fragments in the active site of mTOR (**Figure 64**).



## 2.9 Optimisation of Position-6 Substituent (Backpocket Group)

With cyclohexanone **191** identified as an efficient, cellularly potent compound that displayed a moderate increase in solubility and permeability, attention was turned to optimisation of the backpocket vector.

Optimisation was carried out with two different *N*-1 substituents. Ketal **195** was selected due to its favourable properties (*vide supra*) and the opportunity to unmask the cyclohexanone motif. The trifluoroethyl *N*-1 substituent was selected due to the tractable synthesis of this core, which allowed suitable quantities to be synthesised for chiral chromatography. Obtaining single enantiomer intermediates **186a/ 186b** enabled us to synthesise single enantiomer products and also submit material to genotoxicity assays as the single enantiomer (**Figure 65**). Aniline-based backpocket groups were optimised on these two parent compounds in parallel.

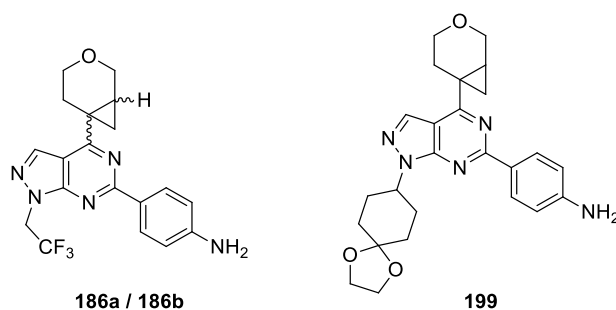


**Figure 65:** Aniline based intermediates **186a/b** and **199** for backpocket optimisation study.

There have been extensive reports of backpocket optimisation within the mTOR literature,<sup>108,114,206,208,209</sup> however, due to our concerns relating to the validity of the literature SAR when compounds were tested in our own hands (*vide supra*) we conducted a new analysis, attempting to optimise for mTOR potency and physicochemical properties. Urea-based backpocket groups are the most highly potent compounds based on earlier reports and molecular modelling has suggested this may be due to the formation of 3 hydrogen bonding interactions from the urea functionality.<sup>108</sup> Additionally, a substituted ethyl moiety, such as hydroxyethyl, is capable of conferring further potency, potentially through the formation of a fourth hydrogen-bonding interaction in the backpocket region and therefore may impart an increase in potency (**Figure 66**). It was also anticipated that inclusion of polar groups at this position would increase the aqueous solubility of the compound. For these reasons, a scan of solubilising groups in the backpocket region was proposed.

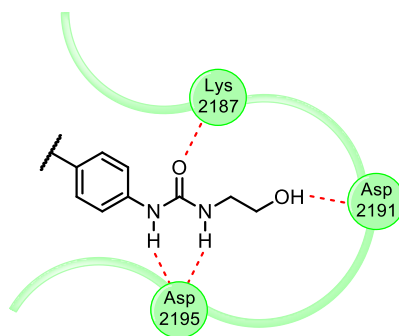
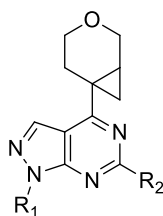


**Figure 66:** Potential hydrogen bonding interactions in back-pocket region.

**Table 36** shows the compounds which were considered for synthesis from intermediates **186** and **199**; this set includes substituted ethyl urea compounds which contain both neutral and basic polar groups. Additionally, thioureas **203** and **209** were proposed for synthesis due to the performance of this group in other compound series examined within our laboratory. Methyl glycinamides **204** and **210** were included as it was perceived that this compound would allow exploration of more highly soluble molecules.

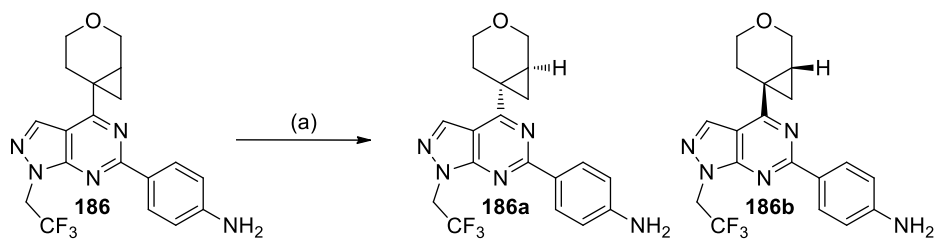


Entry	Compound No.	R <sup>1</sup>	R <sup>2</sup>	Predicted Solubility Class	Predicted AMP	cLogD	cLogP
1	200a/b			Low	188	2.33	2.33
2	201a/b			High	321	1.88	3.02
3	202a/b			High	185	2.28	2.85
4	203a/b			Low	326	3.14	3.14
5	204a/b			High	3.42	1.45	2.53
6	205			High	32	2.03	2.03
7	206			High	26	0.17	1.93
8	207			High	83	1.59	2.73
9	208			High	35	1.99	2.55
10	209			High	66	2.85	2.85
11	210			High	79	2.18	3.26

**Table 36:** Predicted physicochemical properties for proposed compounds **200-210**. NB: Predicted physicochemical data was generated in Helium (Ceiba Solutions). Calculated logP and logD 7.4 values are calculated in Chemaxon.

### **2.9.1 Synthesis of Pyrazolopyrimidine 150 Analogues**

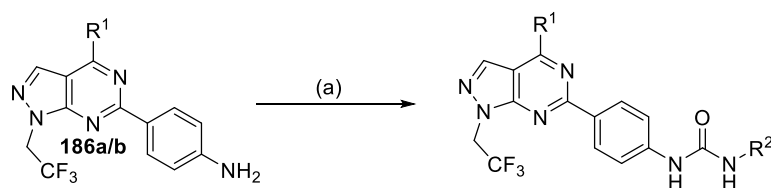
Compound **186** was prepared as a racemic mixture (*vide supra*) and could be separated into a pair of single enantiomers by Chiral HPLC chromatography (**Scheme 33**). This provided enantiopure material required for Ames liability testing, and also facilitated the synthesis of a series of enantiopure final products for biological evaluation.



(a) Chiral HPLC

**Scheme 33:** Chiral purification of **186**. **NB:** Stereochemistry shown was determined by analogy to the crystal structure of tool compound **34a**. Isomer with positive optical rotation was determined to be (1*S*,6*R*) **186a**. Isomer with negative optical rotation was determined to be (1*R*,6*S*) **186b**. It was presumed that stereochemistry was maintained in all derivatives of **186**. Structures are of adequate quality that oxygen is a sufficiently heavy atom to allow for absolute stereochemical determination. For more detail see experimental section.

Intermediate aniline enantiomers **186a** and **186b** were then used to synthesise a series of urea analogues (**196-198**) via the previously mentioned urea formation methodology which utilises *para*-nitrophenyl chloroformate. The products which were synthesised in this manner are summarised in **Table 37**.

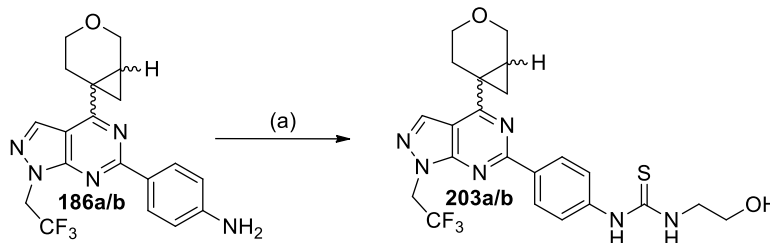


(i) *para*-Nitrophenyl chloroformate, Pyridine, DCM, r.t., 0.5 h (ii) R<sub>2</sub>-NH<sub>2</sub>, DIPEA, r.t., 0.5 h

Entry	Compound No.	R <sup>1</sup>	R <sup>2</sup>	Yield (%)
1	<b>200a</b>			83%
2	<b>201a</b>			97%
3	<b>202a</b>			65%
4	<b>200b</b>			72%
5	<b>201a</b>			85%
6	<b>202b</b>			77%

**Table 37:** Urea analogues synthesised from cyclopropylpyran enantiomers **186a** and **186b**.

Aniline containing compounds **186a** and **186b** were also utilised to synthesise thioureas **203a** and **203b** using 1,1'-thiocarbonyldiimidazole (TCDI). This reaction gave the desired products in very good yield (82-92%). (**Scheme 34**)



(a) (i) TCDI, DCM, pyridine, r.t. 0.5 h (ii) Ethanolamine, r.t. 0.5 h, 82-92% yield

**Scheme 34:** Synthesis of **203a** and **203b**.

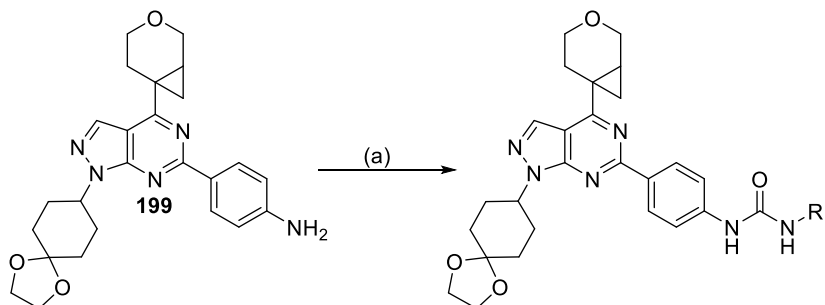
Finally, 4-methylglycinamides **204a** and **204b** were also synthesised from chiral aniline derivatives **186a** and **186b**, respectively. This was achieved *via* a two step synthesis. In the first step, **186** underwent an amide coupling reaction facilitated by HATU with Boc-*N*-methyl glycine. Following this, the intermediate product was immediately deprotected to furnish 4-methylglycinamides **204a** and **204b**. A deprotection procedure<sup>240</sup> using microwave irradiation in the mildly acidic solvent, hexafluoroisopropanol, was used as in our hands, this reaction was convenient and provided a cleaner reaction profile than the more usual TFA/DCM deprotection conditions. (**Scheme 35**).





**Scheme 36:** Synthesis of **199**.

Aniline **199** was derivatized into various urea compounds using *para*-nitrophenyl chloroformate as described above. Compounds synthesised in this fashion are summarised in **Table 38**.

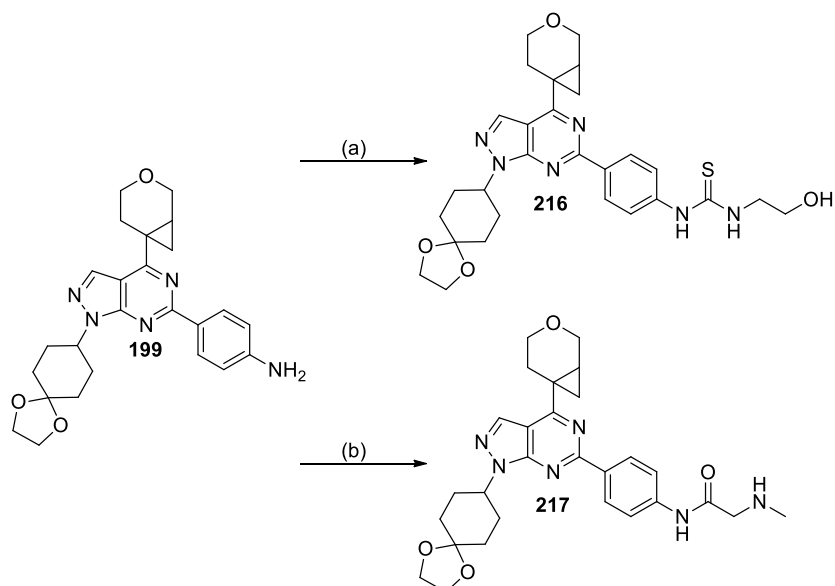


(a) (i) *para*-Nitrophenyl chloroformate, pyridine, DCM, r.t., 1.5 h (ii) R<sup>1</sup>NH<sub>2</sub>, DIPEA, r.t., 1.5 h.

Entry	Compound No.	R <sup>1</sup>	Yield (%)
1	<b>212</b>		70%
2	<b>213</b>		49% (after Boc-deprotection)
3	<b>214</b>		66%
4	<b>215</b>		76%

**Table 38:** Urea analogues synthesised from **199**.

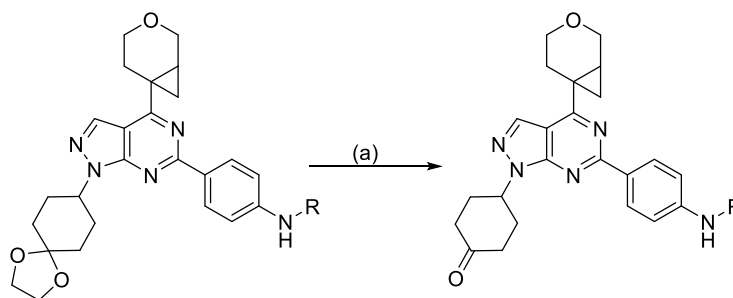
As with trifluoroethyl compound **186**, compound **199** was also converted into thiourea **216** and *N*-methyl glycinamide **217** using the previously described procedures (**Scheme 37**).



(a) (i) TCDI, DCM, pyridine, r.t. 2 h (ii) Ethanolamine, r.t. 0.5 h, 54% yield (b) (i) HATU, DIPEA, Boc-*N*-methyl glycine, 2Me-THF, r.t., 16 h (ii) HFIP, microwave, 150 °C 1.5 h, 13% over 2 steps.

**Scheme 37:** Synthesis of **216** and **217**.

Where there were suitable quantities of material to allow it, ketal compounds were deprotected to give ketone products. **Table 38** highlights the products which were formed *via* this process.

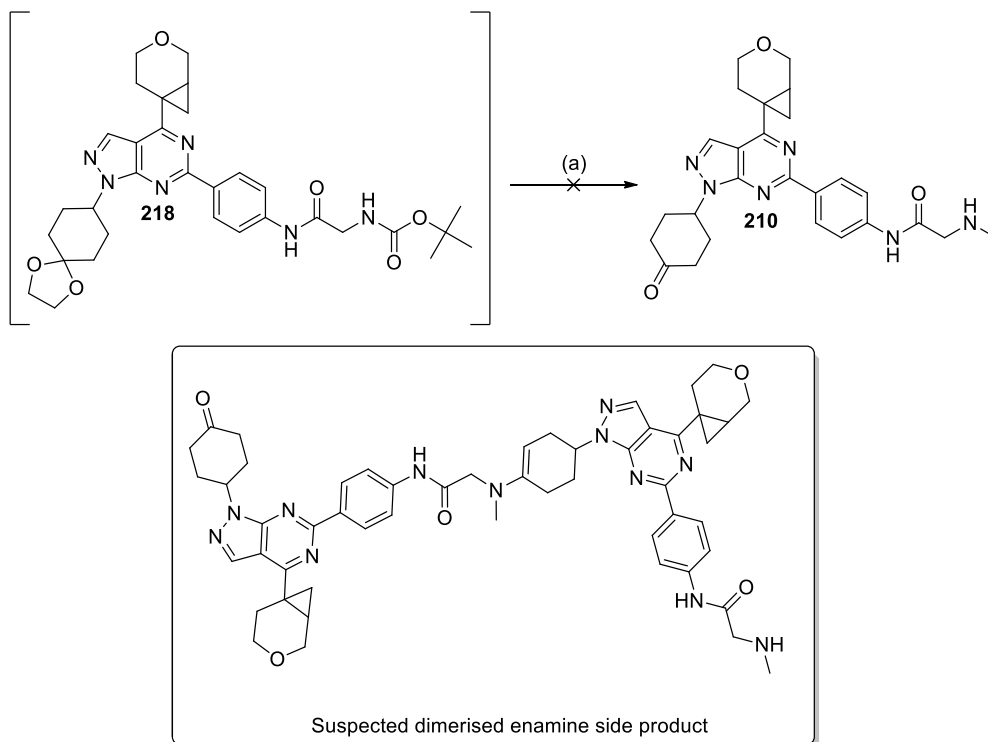


(a) HCl, THF, r.t. 2 h

Entry	Compound No.	R	Yield (%)
1	205		69%
2	207		66%
3	208		93%
4	209		75%

**Table 39:** Synthesis of ketones **205-209**

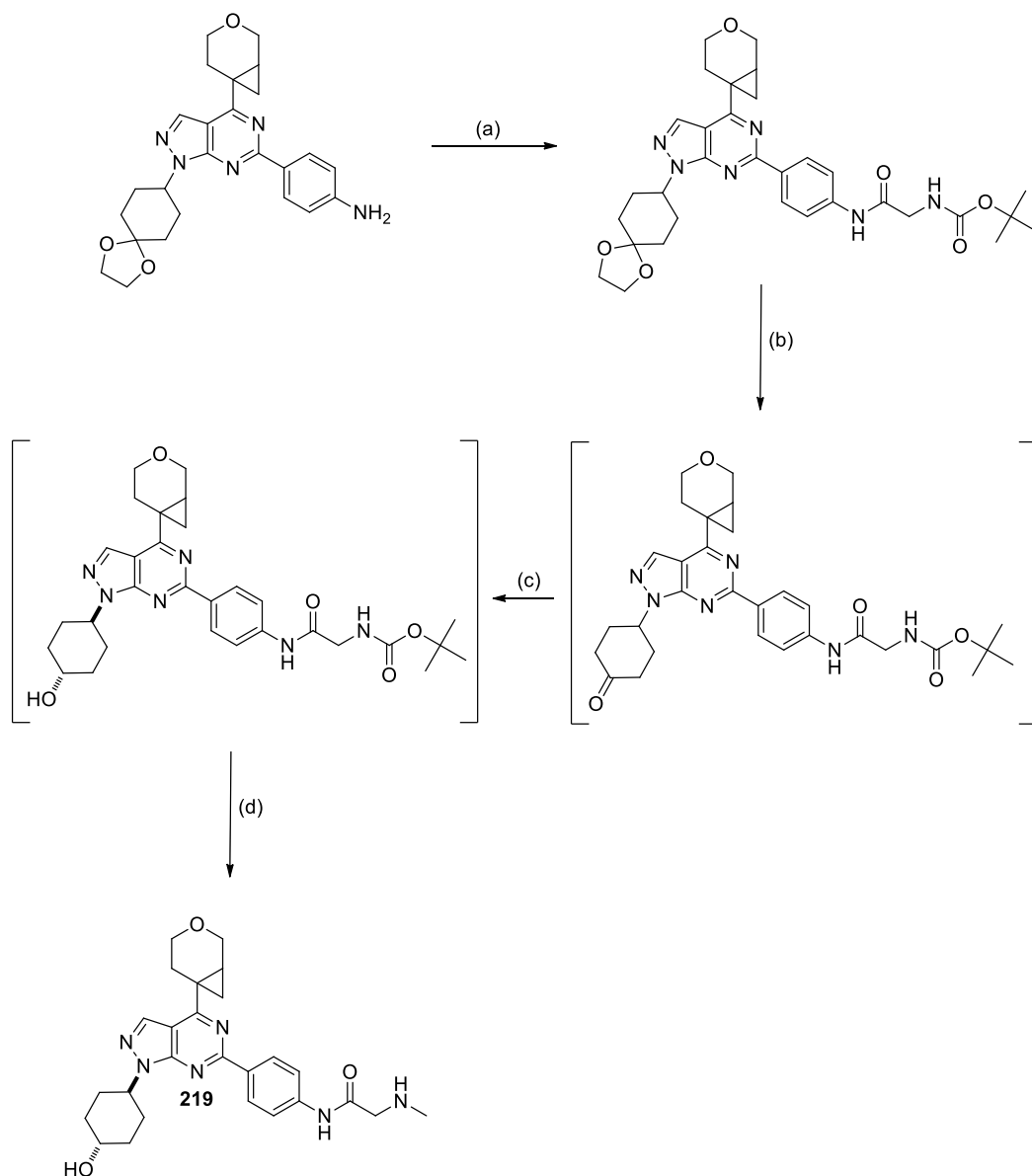
Attempts to ketal deprotect intermediate Boc-*N*-methyl glycinamide **217** resulted in significant quantities of unwanted dimer. It was postulated from LCMS analysis of the reaction mixture to be the structure depicted in **Scheme 38**. As this was likely to be uncontrollable, an alternative strategy was devised to bypass the ketone compound **210** and instead obtain alcohol **219**



(a) HCl, THF, r.t. 2 h

**Scheme 38:** Attempted synthesis of **210**

In order to selectively deprotect the ketal residue whilst leaving the Boc-group intact, a *trans*-acetalization was carried out with acetone.<sup>241</sup> The intermediate ketone was reduced directly to the corresponding alcohol with NaBH<sub>4</sub>. LCMS analysis of the reaction mixture suggested a mixture of stereoisomers (~4:1). This mixture was telescoped to the deprotection step. MDAP purification was able to separate the stereoisomers and give a clean fraction of the major product, which was determined by NMR analysis to be the *trans*-isomer **219**.

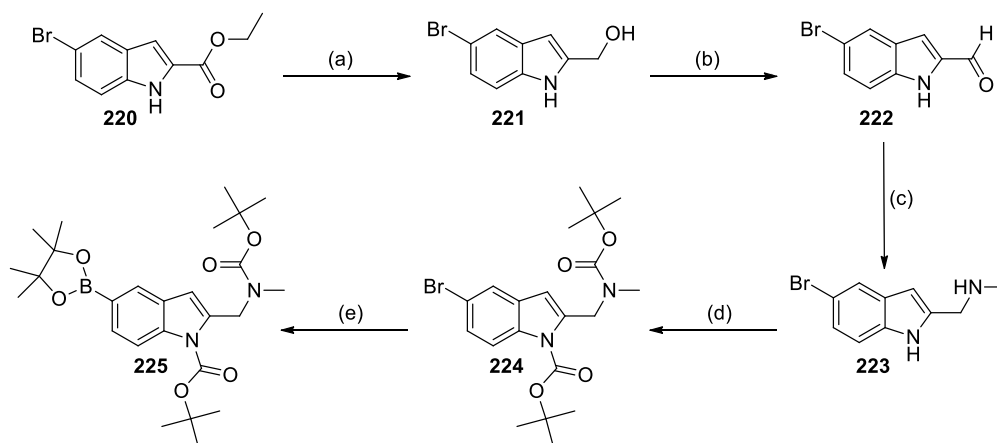


(a) HATU, DIPEA, Boc-*N*-methyl glycine, 2Me-THF, r.t., 24 h (b) Acetone, TsOH, 50 °C, 2.5 h. (c) NaBH<sub>4</sub>, THF, r.t., 1 h. (d) HFIP,  $\mu$ Wave, 150 °C, 2 h, 17% over 4 steps.

**Scheme 39:** Synthesis of **219**.

Finally, an indole backpacket was introduced into intermediate **198**. as this had been successful in other compound series, elsewhere within our laboratory. Indole pinacol boronate **225** was synthesised by an external CRO using the route described in **Scheme 40**. Commercially available ethyl 5-bromo-1*H*-indole-2-carboxylate **220** was reduced to give alcohol **221**. This product was then re-oxidised to give aldehyde **222**, which underwent reductive amination to form secondary amine **223**. The free amine residue as well as the indole

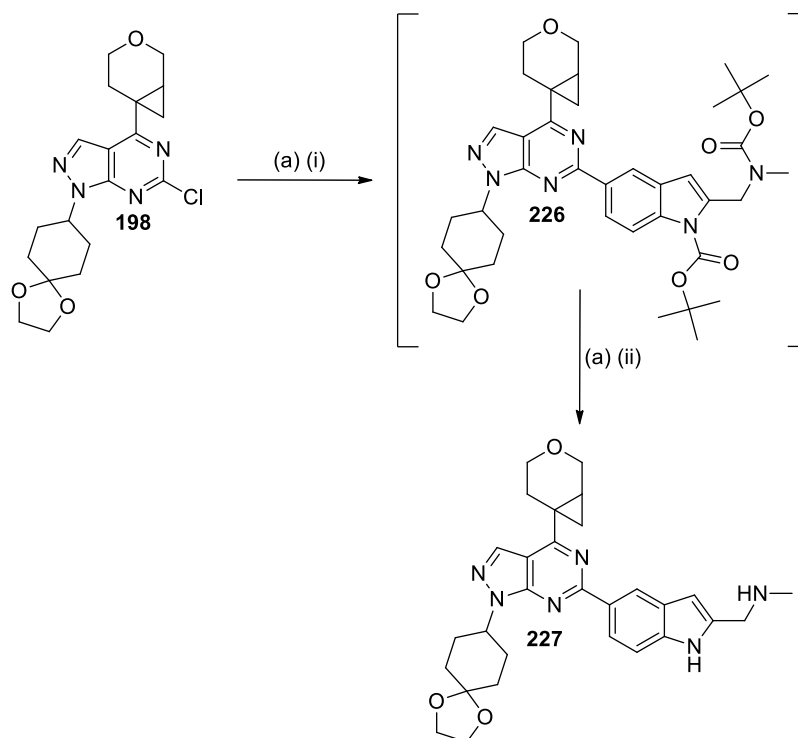
nitrogen in compound **223** were protected to give **220** which was subjected to a Miyaura borylation to give pinacol ester coupling partner **221** (Scheme 40).



(a)  $\text{LiAlH}_4$ , THF, 45 min, 0 °C, 85% yield (b)  $\text{MnO}_2$ , DCM, r.t., 3 h, 55% yield (c)  $\text{MeNH}_2$ ,  $\text{NaBH}_3\text{CN}$ , AcOH, DCE, r.t., 48 h, 47% yield (d)  $\text{Boc}_2\text{O}$ , TEA, DMAP, DCM, r.t., 72 h., 25% yield (e)  $\text{B}_2\text{Pin}_2$ ,  $\text{Pd}(\text{OAc})_2$ , KOAc,  $\text{P}(\text{Ph})_2t\text{-Bu}$ , 1,4-dioxane, 100 °C 4 h, 54% yield.

**Scheme 40:** Synthesis of indole coupling partner **225**, performed by external CRO.

Suzuki-Miyaura cross coupling of chloride **198** and pinacol boronate **225** gave intermediate **226** which was boc-deprotected to give indole containing compound **227** (Scheme 41).



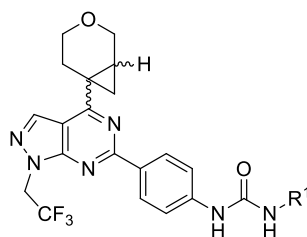
(a) (i) Pinacol boronate **221**, Pd(PPh<sub>3</sub>)<sub>4</sub>, Na<sub>2</sub>CO<sub>3</sub>, DME:H<sub>2</sub>O (8:1), 100 °C, 2 h (ii) HFIP,  $\mu$ Wave, 120 °C 3.5 h, 25% yield over 2 steps.

**Scheme 41:** Synthesis of **227**.

### **2.9.3 Evaluation of Backpocket Optimisation**

**Table 40** displays the associated biological and physicochemical data for the enantiomeric pairs of compounds prepared. Hydroxyethyl urea **196a** has a 4-fold increase in potency over the corresponding ethyl compound **172**. It was postulated that this increase is due to an additional hydrogen bonding interaction as described above. It is also worth noting that ethyl urea **172** is a racemic compound, which likely negatively affects potency compared with single enantiomer **200a**. Modifying the alcohol substituent in **200a** had a negative effect on mTOR potency. It was observed that additional steric bulk in this position reduced mTOR potency, presumably due to a steric clash with the protein. This is exemplified in the decreasing potency trend observed for **200**  $\rightarrow$  **201**  $\rightarrow$  **202**, and this is similar to what was reported within the literature.<sup>108</sup> As expected, the inclusion of both neutral (**200**) and basic (**201** and **202**) polar groups in the backpocket increased solubility over **172**. Permeability is noted to be reduced, but due to the very high permeability of ethyl urea **172** (AMP= 970 nm/sec) permeability is still maintained at an acceptable level. The physicochemical properties of piperazine **202** are well balanced, however, the potency of this compound is significantly reduced.

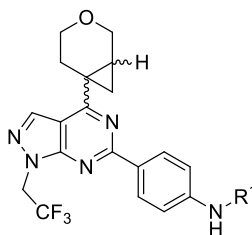




Entry	Compound No.	R <sup>1</sup>	pIC <sub>50</sub>			CAD (μg/mL)	AMP (nm/sec)	LogD/ LogP
			mTOR	pAkt	PI3K $\alpha,\beta,\delta,\gamma$			
1	<b>200a</b>		7.8	7.2	4.9, 4.8 4.7, 4.7	39	215	4.15/ 4.41
2	<b>200b</b>		7.1 (±.4)	6.8	4.9, 4.6, 5.0, 6.2	38	250	4.17/ 4.46
3	<b>201a</b>		6.4	6.3	4.9, 4.9 5.5, 5.2	28	185	3.66/ 5.31
4	<b>201b</b>		5.8	6.0	4.9, 4.8 5.1, 5.4	26	170	3.65/ 5.37
5	<b>202a</b>		5.6	5.8	4.7, 4.6 5.1, <4.5	96	160	3.72/ 4.54
6	<b>202b</b>		<5.3	5.5	4.9, 4.8 5.2, 4.8	99	160	3.59/ 4.48

**Table 40:** Biological and physicochemical data for Compounds **200-202**. N=3 or greater. Potency ranges are shown for values which fall outside the error of the assay (mTOR= 0.3 pAkt= 0.5) otherwise potency range is not shown. Range is not shown for PI3K selectivity data. (a) Stereoisomer 1, assumed (1*S*, 6*R*) by analogy to **34a**. (b) Stereoisomer 2, assumed (1*R*, 6*S*) by analogy to **34a**.

Additionally, a limited number of alternative backpockets were examined (**Table 41**). In the literature, switching from a urea to corresponding thiourea is associated with a decrease in potency (*vide supra*).<sup>108</sup> However, in our hands, a 4-fold increase in potency was observed for thiourea **203a** over corresponding urea **200a**. Thiourea **203a** was 2-fold less soluble than the corresponding urea **200a**, with permeability increasing by ~50%. Glycinamides have been associated with a reduction in potency attributed to the loss of a potential hydrogen bond donor due to absence of nitrogen. In the current study, methyl-glycinamide **204a** was ~3-fold less potent than hydroxyethyl urea **200a** but exhibited a >2-fold increase in solubility.

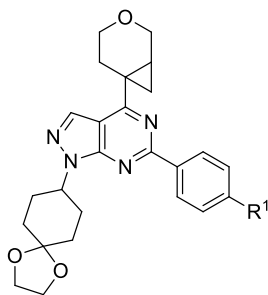


Entry	Compound No.	R <sup>1</sup>	pIC <sub>50</sub>			CAD (μg/mL)	AMP (nm/sec)	LogD/LogP
			mTOR	pAkt	PI3K $\alpha,\beta,\delta,\gamma$			
1	<b>203a</b>		8.4	8.3	<4.5, <4.5, <4.5, <4.5	21	310	4.71/ 4.95
2	<b>203b</b>		7.7	7.7	5.2, <4.5 <4.5, 5.8	21	330	4.72/ 4.96
3	<b>204a</b>		7.3	7.0	4.7, 4.7 5.0, <4.5	49	270	4.25/ 5.32
4	<b>204b</b>		6.0	6.1	5.0, 4.6 5.4, 5.0	49	325	4.17/ 5.42

**Table 41:** Biological and physicochemical data for Compounds **203-204**. N=3 or greater All potency ranges fall within the error of the assay (mTOR= 0.3 pAkt= 0.5) and therefore are not shown. Range is not shown for PI3K selectivity data. NB: compounds labelled (a) Stereoisomer 1, assumed (1*S*, 6*R*) by analogy to **34a**. (b) Stereoisomer 2, assumed (1*R*, 6*S*) by analogy to **34a**.

In parallel, aniline based backpocket groups were investigated with the cyclohexyl ketal substituent in the ribose *N*-1 position (**Table 42**). For these compounds, the hydroxyethyl urea was marginally more potent than the corresponding thiourea **216**, however for hydroxyethyl urea **208** there was a <10-fold drop off within the pAkt cellular assay, whilst thiourea **216** was equipotent in the pAkt assay. This is most likely due to the lower permeability of **212**, meaning that less compound is able to enter the cell. The solubility of thiourea **216** is drastically reduced compared to **212**. Methyl-glycinamide **217** was equipotent with thiourea **216** against the primary mTOR assay. However, there was a ~5-fold decrease in the cellular pAkt assay. As the permeability of this compound is good, this may be due to the nitrogen in this compound being charged at physiological pH, resulting in a cationic compound which cannot cross the cellular phospholipid bilayer.

Amines **213-215** display the same trend as **200-202**, in that the more bulky the backpocket substituent, the less potent the compound, further highlighting that steric bulk in this position is not well tolerated.

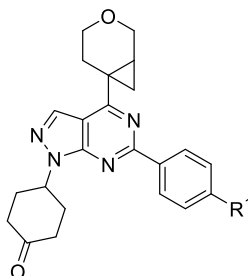


Entry	Compound No.	R <sup>1</sup>	pIC <sub>50</sub>			CAD (μg/mL)	AMP (nm/sec)	LogD/P
			mTOR	pAkt	PI3K $\alpha,\beta,\delta,\gamma$			
1	<b>212</b>		8.2	7.2	5.4, <4.5, 5.8, 5.7	92	88	4.19/4.56
2	<b>213</b>		7.9	6.9	5.2, 4.9, 5.9, 5.2	422	6	3.18/5.11
3	<b>214</b>		6.9 (±.4)	6.3	4.9, 5.0, 6.0, 5.2	414	120	3.65/6.12
4	<b>215</b>		5.9	6.3	<4.5, <4.5, 5.3, <4.5	27	71	3.72/5.45
5	<b>216</b>		8.0	8.0	5.6, <4.5, 5.5, 5.4	1	335	4.84/5.18
6	<b>217</b>		8.0	7.3	4.5, 4.5, 5.2, <4.5	321	320	4.28/5.88

**Table 42:** Biological and physicochemical data for Compounds **212-217**. N=3 or greater. Potency ranges are shown for values which fall outside the error of the assay (mTOR= 0.3 pAkt= 0.5) otherwise potency range is not shown.

Hydroxyethyl urea **205** (Table 43) and the corresponding thiourea **209** had a very similar potency value at mTOR. However, urea **205** compound had a much greater drop-off in the cellular pAkt assay and was 25-fold less potent. The drop in cellular potency is again likely to be due to the low permeability of this compound. Hydroxyethyl thiourea **209** also has a larger drop-off than the corresponding ketal **216**; the logD is lower (4.0 vs. 4.8) and this is also reflected in the permeability value. Compound **207** has a much better aqueous solubility, however the decrease in permeability which results in a large decrease in cellular potency highlights the challenges associated with optimising multiple physicochemical properties simultaneously. There is an interplay between solubility and permeability, and attempting to improve one property often negatively affects the other.<sup>242</sup> This is exemplified in piperazine

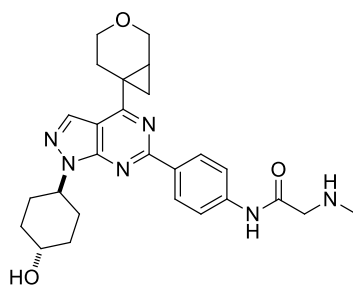
**208** which has very good aqueous solubility but a drastically reduced permeability. The two amine based compounds (**207** and **208**) have poor mTOR potency and their selectivity over PI3K $\delta$  is <10-fold.



Entry	Compound No.	R <sup>1</sup>	pIC <sub>50</sub>			CAD (μg/mL)	AMP (nm/sec)	LogD/P
			mTOR	pAkt	PI3K $\alpha,\beta,\delta,\gamma$			
1	<b>205</b>		8.2	6.8	5.6, 5.0 5.6, 5.5	236	34	3.41/ 3.66
2	<b>207</b>		6.7	6.4*	5.0, 5.0 6.0, 5.2	377	64	3.03/ 4.82
3	<b>208</b>		6.0 (±.4)	6.3	4.8, 4.6 5.2, 4.8	577	13	3.03/ 4.43
4	<b>209</b>		8.3	7.5	5.8, <4.5 5.5, 5.4	21	190	4.00/ 4.30

**Table 43:** Biological and physicochemical data for Compounds **205-209**. Values marked with \* are N=2, all other values are N=3 or greater. Potency ranges are shown for values which fall outside the error of the assay (mTOR= 0.3 pAkt= 0.5) otherwise potency range is not shown.

Due to the chemical instability of *N*-methyl glycineamide **210** (*vide supra*), ketal **218** was deprotected and reduced directly to the corresponding *trans*-alcohol **219**, and the associated biological data is shown in **Table 44**.

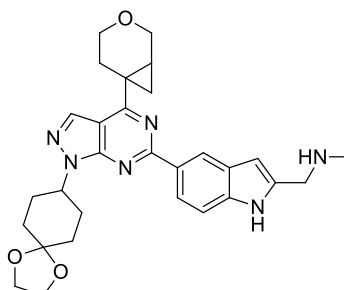


<b>mTOR pIC<sub>50</sub></b>	8.2 (n=2)
<b>pAkt pIC<sub>50</sub></b>	7.1 (n=1)
<b>PI3K<math>\alpha,\beta,\delta,\gamma</math> pIC<sub>50</sub></b>	4.7, 4.9, 5.2, <4.5 (all n=2)
<b>CAD (<math>\mu\text{g/mL}</math>)</b>	168
<b>AMP (nm/sec)</b>	135
<b>ChromLogD/P</b>	2.86/3.97

**Table 44:** Biological and physicochemical data for Compound **219**.

*trans*-Alcohol **219** has similar potency to hydroxyethyl urea **205** and thiourea **209**. It also has a similar reduction in potency within the cellular pAkt assay. The solubility and permeability of these compounds are reasonably balanced and ~1000-fold selectivity is observed over the PI3K isoforms. The observed reduction in cellular potency however precludes this particular compound from further analysis.

Indole compound **227** was synthesised due to the success of this back-pocket motif in other mTOR series within our laboratories, however in the current study, the compound **227** had poor biological activity and therefore was not further considered (**Table 45**).



<b>mTOR PIC<sub>50</sub></b>	6.8
<b>pAkt PIC<sub>50</sub></b>	6.4
<b>PI3K<math>\alpha,\beta,\delta,\gamma</math> pIC<sub>50</sub></b>	4.8, 5.0, 5.0, 4.7
<b>CAD (<math>\mu\text{g/mL}</math>)</b>	301
<b>AMP (nm/sec)</b>	295
<b>ChromLogD/P</b>	4.00/6.97

**Table 45:** Biological and physicochemical data for Compound **227**. All potency ranges fall within the error of the assay (mTOR= 0.3 pAkt= 0.5) and therefore are not shown. Range is not shown for PI3K selectivity data.

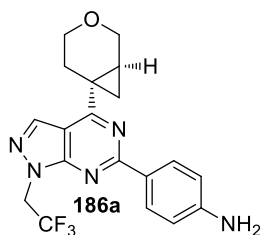
## **2.10 Further Analysis of 203a**

At this stage, **203a** containing a thiourea derived backpocket and fluoroethyl ribose unit was progressed for further profiling to compare it against **CZ415**. This compound showed single digit nanomolar potency in both the mTOR and pAkt assays, and therefore the compound was investigated further, despite the suboptimal aqueous solubility of the compound as this was not anticipated to preclude the development of an inhaled compound.

### **2.10.1 Ames Mutagenicity Test of 203a**

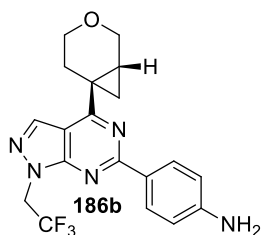
A positive result in the Ames mutagenicity test immediately prevents further development of a compound in question. This is due to the fact that the Ames assay has a high correlation with carcinogenicity in animals.<sup>243</sup> Therefore, a full screening of a compound is required before the compound advances to first time in human (FTIH) studies.<sup>244</sup> A full regulatory GLP Ames screen is resource intensive and requires significant amounts of test compound (~300 mg) in order to test a range of bacterial strains. However, this is impractical early in compound development, and is only routinely performed when a compound is under consideration for candidate selection. Earlier in development a “mini-Ames” assay is utilised. This assay is a miniaturised version of the Ames test, which is run in 6-well plates and usually incorporates two strains of *salmonella*; TA98 (frame shift mutations) and TA100 (base-pair mutations).<sup>245</sup> Within our laboratories this assay requires ~50 mg of material. This assay has been shown to have very high concordance with the GLP Ames screen and, therefore, is an appropriate surrogate for compounds at an earlier stage of development.<sup>246</sup> Generally within the pharmaceutical industry, a clear positive result is defined as at least a two-fold increase in revertant colonies of the bacterial strains used (*i.e.* TA98 or TA100) in just one test article concentration either in the presence or absence of S9 with evidence of a dose-response.<sup>244</sup>

Parent anilines **186a** and **186b** were tested in the mini-Ames assay as it is assumed that these compounds may be formed as metabolites of compounds such as **203a** and **203b** *in vivo*. Morpholine hinged compound **185** was also tested for comparison and to establish what effect, if any, cyclopropylpyran has on this system (**Table 46**, **Table 47** and **Table 48**).



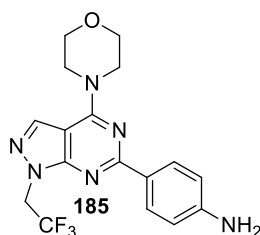
Strain	Dose Per Plate (mg)	Mean revertants per plate	Ratio (Treated to Solvent)
TA100	50	160.0	1.1
	150	137.5	0.9
	500	152.5	1.0
	1500	ppt formed	-
DMSO	Control	151.3	-
TA98	50	31.0	1.0
	100	27.0	0.9
	500	35.0	1.2
	1500	ppt formed	-
DMSO	Control	30.0	-
Result:	<b>Negative</b>		

**Table 46:** Mini-Ames result (in presence of S9-Mix) for Compound **186a**. Ames screening was carried out elsewhere within our laboratories.



Strain	Dose Per Plate (mg)	Mean revertants per plate	Ratio (Treated to Solvent)
TA100	50	151.5	1.0
	150	150.0	1.0
	500	126.0	0.8
	1500	ppt formed	-
DMSO	Control	151.3	-
TA98	50	41.5	1.4
	100	34.0	1.1
	500	35.5	1.2
	1500	ppt formed	-
DMSO	Control	30.0	-
Result:	<b>Negative</b>		

**Table 47:** Mini-Ames result (in presence of S9-Mix) for Compound **186b**. Ames screening was carried out elsewhere within our laboratories.



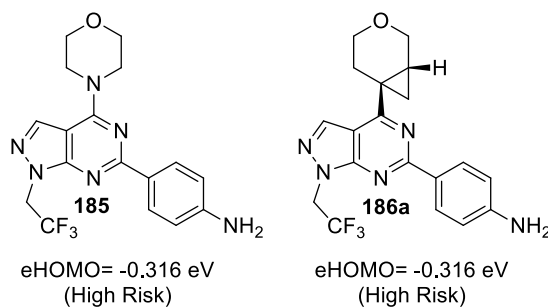
Strain	Dose Per Plate (mg)	Mean revertants per plate	Ratio (Treated to Solvent)
TA100	50	159.5	<b>0.9</b>
	150	149.5	<b>0.9</b>
	500	135.5	<b>0.8</b>
	1500	ppt formed	-
DMSO	Control	172.5	-
TA98	50	94.5	<b>2.2</b>
	100	119.5	<b>2.8</b>
	500	79.0	<b>1.9 (some ppt)</b>
	1500	ppt formed	-
DMSO	Control	42.3	-
Result:	<b>Positive</b>		

**Table 48:** Mini-Ames result (in presence of S9-Mix) for Compound **185**. Ames screening was carried out elsewhere within our laboratories.

The results of this Ames screen show that gratifyingly, whilst the aniline in both enantiomers of the parent aniline **186** do not induce bacterial mutations, the morpholine substituted system **185** significantly increases the mean revertant per plate for TA98, meaning it is positive in the Ames test.

This result indicates a potential toxicological benefit for the novel cyclopropylpyran hinge binding fragment over literature morpholine hinge binding fragments. It is reasoned that the difference is a result of the cyclopropylpyran being less electron donating than morpholine, meaning the extended aromatic system is more electron deficient overall. The correlation between calculated electron density and number of revertant colonies per plate has previously been reported, and strategies to negate Ames liability by decreasing the aryl amine electron density have proved effective.<sup>247</sup> Compounds routinely have the energy of the highest occupied molecular orbital (eHOMO) calculated as a measure of electron density. This is able to give a computational prediction, so the Ames risk of a potential target can be assessed. However, as shown in **Figure 67**, this does not always correctly predict the Ames risk of a compound, therefore synthesis and testing of any important compounds is recommended. With the results obtained, it was possible to continue progression of **186a** to investigate the SAR of aniline based back-pockets and from this thiourea **203a** was identified as a compound of interest for further biological profiling.

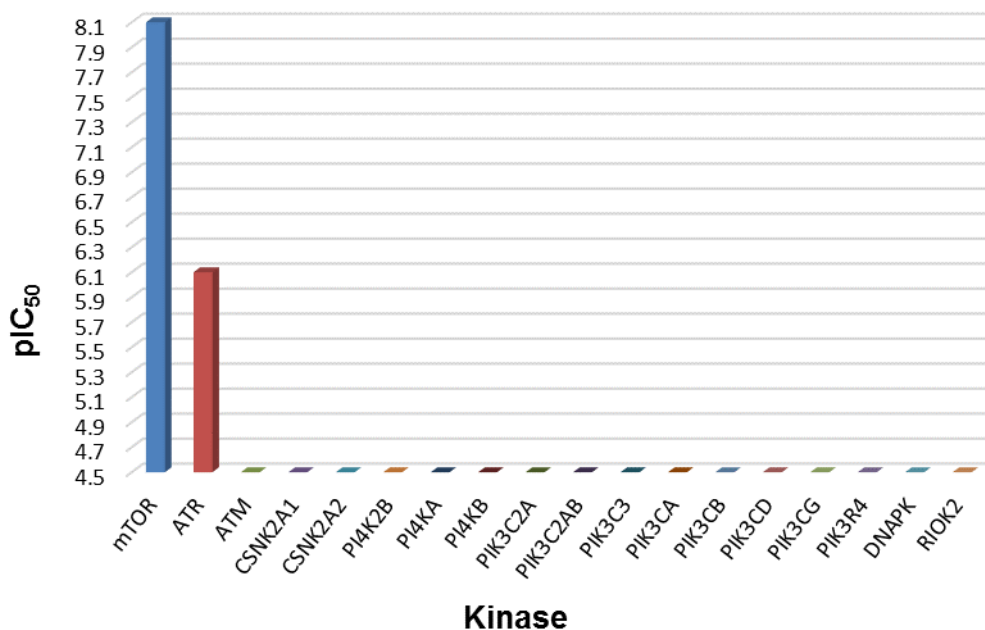




**Figure 67:** Highest occupied molecular orbital energy (eHOMO) calculations (Hartree) calculated in Schrödinger LiveDesign®.

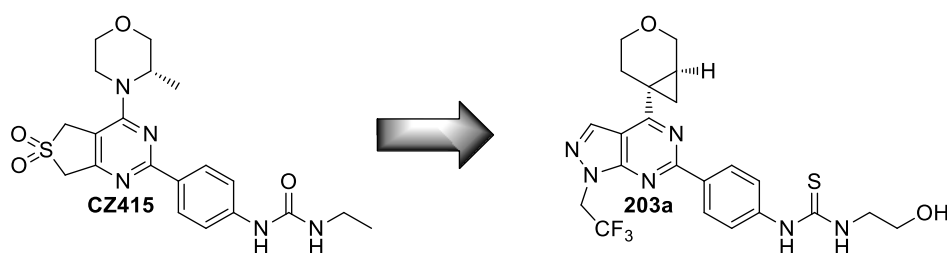
## 2.10.2 Kinobead Lipid Kinase Selectivity Profiling

As discussed above, the lipid kinases and PIKKs have similar structures, therefore it can often be challenging to achieve good levels of selectivity for the desired target over closely related kinases. To investigate promising compounds such as **203a** are tested in a kinobead lipid kinase selectivity panel.<sup>175</sup> This experiment utilised CZK133 Kinobeads and a mixed cell lysate of HeLa, Jurkat and K-562 cells. This gives a good representation of the selectivity for the target of interest (mTOR) and the results of this experiment are shown in **Figure 68**.



**Figure 68:** Results from kinobead lipid kinase selectivity profiling experiment for compound **203a** NB: All results are an average of n=2 experiments.

This experiment shows the high level of selectivity which thiourea **203a** has over closely related kinases. ATR (Ataxia telangiectasia and Rad3 related protein) is a PIKK which is involved in delay of cell cycle progression in response to DNA damage.<sup>248</sup> It has high structural homology with mTOR, so much so that it is sometimes referred to as FRAP related protein-1. Thiourea **203a** has a 100-fold selectivity for mTOR over ATR, meaning it is likely that a therapeutic window could exist where mTOR could be inhibited without inhibiting ATR. In addition to this, **203a** shows high levels of selectivity (>~4000 fold) over all the other lipid kinases/PIKKs included in the selectivity profiling panel.

**2.10.3 Comparison of Compound 203a to CZ415**

	<b>CZ415</b>	<b>203a</b>
mTOR Kinobead pIC <sub>50</sub>	8.0 (±.7)	<b>8.4</b>
pAkt pIC <sub>50</sub>	7.8 (±.7)	<b>8.3</b>
Healthy Scar-in-a-Jar pIC <sub>50</sub> (Cell Count)	6.5 (4.5) (±.6)	<b>6.9 (&lt;4.4) (±.6)</b>
Diseased Scar-in-a-Jar pIC <sub>50</sub>	6.3 (±.7)	<b>7.0</b>
PI3K $\alpha$ pIC <sub>50</sub>	5.3(±.7)	<b>&lt;4.5 (&gt;7900X)</b>
PI3K $\beta$ pIC <sub>50</sub>	4.8	<b>&lt;4.5 (&gt;7900X)</b>
PI3K $\delta$ pIC <sub>50</sub>	5.0 (±.7)	<b>&lt;4.5 (&gt;7900X)</b>
PI3K $\gamma$ pIC <sub>50</sub>	5.1	<b>&lt;4.5 (&gt;7900X)</b>
DNA-PK pIC <sub>50</sub>	5.5 (±.6)	<b>&lt;4.5 (&gt;7900X)</b>
ChromLogD/P	4.3/4.3	<b>4.71/4.95</b>
CAD solubility (µg/mL)	150	<b>19</b>
SLF Solubility (µg/mL)	17	<b>&lt;1</b>
FaSSIF Solubility (µg/mL)	18	<b>NT</b>
Artificial membrane permeability (nm/sec)	200	<b>310</b>
MDCK Permeability (nm/sec)	363	<b>8</b>
IVC (Rat/Mouse/Human) (mL/min/g)	0.73/1.27/4.64	<b>Rat= 2.94, Human= 3.64</b>
hERG QUBE	4.6	<b>&lt;4.3</b>
Parent aniline mini-Ames	Positive (with S9-Mix)	<b>Negative (with S9-Mix)</b>

**Table 49:** Comparison of biological and physicochemical data for **CZ415** and **199a**. N=3 or greater for all assays. Potency ranges are shown for values which fall outside the error of the assay (mTOR, PI3K, DNA-PK, hERG= 0.3 pAkt, SIAJ= 0.5) otherwise potency range is not shown.

In comparing the overall properties of the two compounds (**Table 49**), thiourea **203a** offers a significant advantage over **CZ415** from the perspective of target potency. The primary mTOR potency and the pAkt cellular potency have been increased by ~0.5 log units. In addition to this, the scar-in-a-jar assay results show a similar increase in terms of impact on collagen 1

deposition whilst causing no decrease in cellular count within healthy lung fibroblasts. In fibroblasts derived from Idiopathic Pulmonary Fibrosis patients, compound **203a** is 5-fold more potent in reducing collagen 1 deposition and pro-collagen 1 c-terminal peptide generation.

In addition to the increase of on-target potency, compound **203a** has significantly better general selectivity over closely related PI3K and PIKK kinases. All PI3K isoforms and DNA-PK are below the lower limit of the assay and, therefore, highlight the very high selectivity of compound **203a**. The kinobead lipid kinase selectivity profiling experiment (**Table 49**) shows the wider selectivity of **203a**, with ATR the only kinase to show a response being 100-fold less responsive. **CZ415** on the other hand has low level activity at all 4 PI3K isoforms and DNA-PK.

From a toxicological standpoint compound **203a** is superior to **CZ415**. Although both compounds contain a *N*-aryl degradant which can potentially be formed *in vivo* or would present a major issue in compound development. Hence, there is a strong preference to eliminate Ames-positive degradants or intermediates. The *N*-aryl amine in **CZ415** is Ames positive, meaning it causes mutations in bacterial strains and therefore is likely to be carcinogenic in animals (*vide supra*). This result prevents **CZ415** from being further developed and structural changes to this molecule would be required to mitigate this risk. **203a** also has the potential to be metabolised to form an *N*-aryl amine. However, this has been proven to be Ames negative, meaning that this compound is not mutagenic. This result offers a significant advantage as this compound template can therefore be developed without needed to adopt structural changes to mitigate Ames risk.

hERG is responsible for forming part of the potassium ion (K<sup>+</sup>) channels within the heart and is therefore involved in coordination of heart-beat. hERG can commonly be inhibited by pharmaceuticals in off-target interactions and this inhibition can lead to QT prolongation.<sup>249</sup> Long QT syndrome effects repolarisation of the heart and lead to an irregular heart-beat, potentially leading to a fatal ventricular tachyarrhythmia (Torsades de Pointes). This means hERG is an important anti-target that must be avoided in drug development.<sup>249</sup> Thiourea **203a** was not active at a hERG QUBE assay (a high throughput ion channel screening system developed by Sophion Bioscience<sup>250</sup>) whereas **CZ415** showed low level activity, therefore **203a** represents a safer compound in this aspect.

The clearance of **203a** is moderate in human and liver microsomes. This is potentially useful in the context of identification of compounds for inhaled delivery. The physicochemical

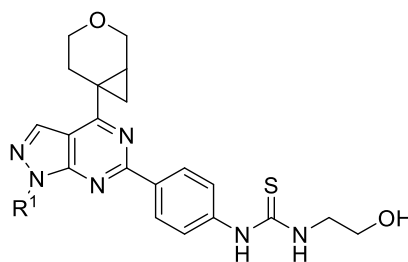
properties of **199a**, however, remain a concern. The CAD solubility of **203a** is much lower than **CZ415** and the SLF solubility is very low. The artificial membrane permeability (AMP) of **199a** is increased, however the MDCK permeability of the compound is much lower. Whilst these results are concerning, it is worth noting that cellular potency data suggests the compound is able to cross the cellular membrane and the compound shows good levels of activity in phenotypic assays. In addition to this, as we are targeting an inhaled route of administration the bioavailability of the compound is not as important as in oral drugs, as delivery of the drug is directly to the site of action. Nevertheless, in an attempt to improve aqueous solubility, a further exploration of the *N1*-position substituent was undertaken.

### **2.11 Attempts to Further Optimise *N1*-Substituent of 203a**

With thiourea **199a** identified as a potent and selective mTOR inhibitor, efforts were then focused on increasing the aqueous solubility by modifying the group in the *N1*-position of the pyrazolopyrimidine ring. In order to do this, we attempted to purchase or synthesise hydrazine starting materials which fulfilled the following criteria:

- The group did not contain any stereocentres (i.e: a linear alkyl group or a symmetrical cyclic system. This was to avoid adding further complexity to the molecule as this would further increase complexity and cost of future development.
- Inclusion of either a polar neutral water solubilising group, or a basic centre in an attempt to increase aqueous solubility.

In order to find groups which met these design criteria, commercially available alkyl hydrazine was considered. This provided a number of suitable groups which had predicted physicochemical properties that suggested improvements in solubility over **203a** (**Table 50**). Tetrahydrothiophene **229** and ethyl ester **232** were predicted to have low solubility, however these compounds are both potential intermediates in the synthesis of compounds **231** and **233** respectively and therefore can be tested to confirm this without significant extra synthetic effort.

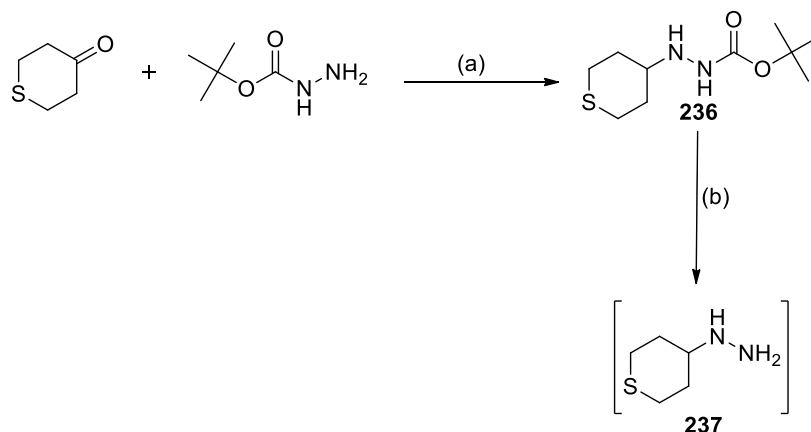


Entry	Compound No.	R <sup>1</sup>	Predicted Solubility Class	Predicted AMP	cLogD	cLogP
1	203		Low	326	3.14	3.14
2	228		High	100	2.11	2.11
3	229		Low	171	3.00	2.00
4	230		High	172	1.79	1.90
5	231		High	31	1.11	1.11
6	232		Low	170	2.15	2.15
7	233		High	25	1.16	1.16
8	234		High	59	1.50	1.50
9	235		High	159	0.70	2.19

**Table 50:** Predicted physicochemical properties for proposed compounds **228-235**. Trifluoroethyl compound **203** is shown for comparison. NB: Predicted physicochemical data was generated in Helium (Ceiba Solutions). Calculated logP and logD 7.4 values are calculated in Chemaxon.

### **2.11.1 Synthesis of Compounds with Varied N1-Substituent**

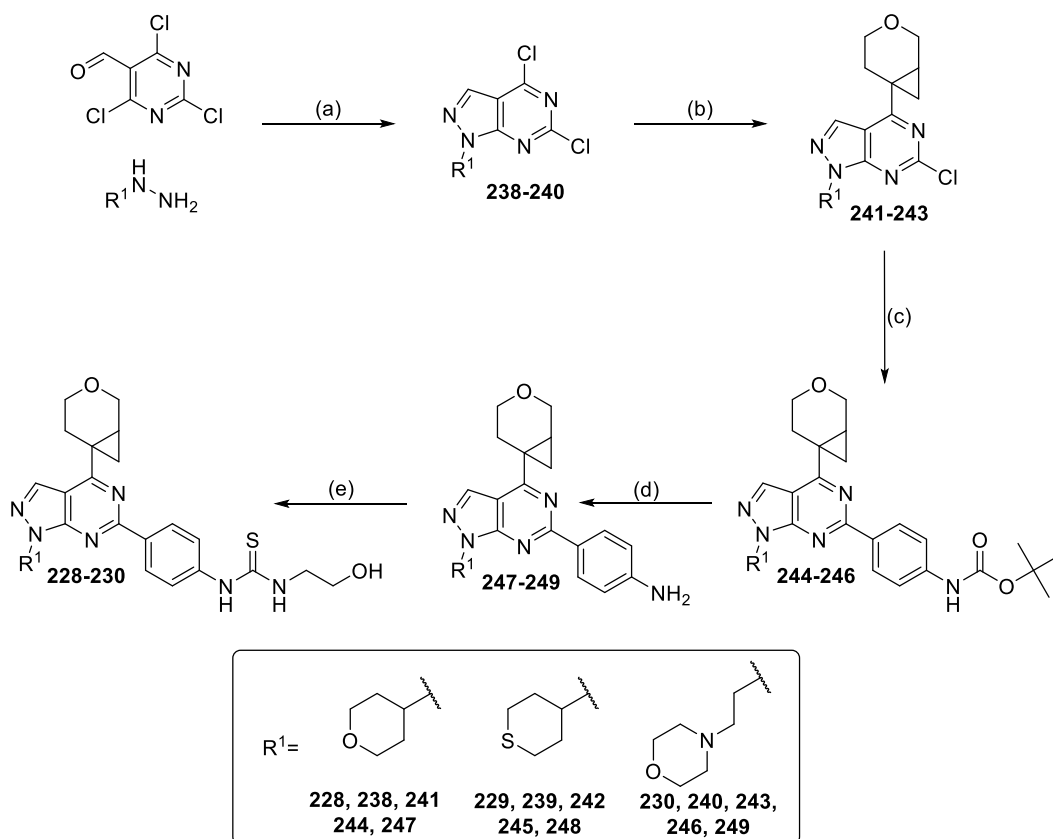
In order to vary the substituent at position *N*-1, individual syntheses were carried out, due to the failure of alkylation or Mitsunobu chemistry in functionalising this position. The group in the *N*-1 position was installed in the first step of the synthesis as an alkyl hydrazine, The alkyl hydrazine starting materials were commercially available with the exception of Tetrahydrothiopyran **236** which was synthesised in an analogous procedure to the cyclohexyl ketal analogue described previously (*vide supra*) **Scheme 42**.



(a) STAB, AcOH, DCM, r.t., 16 h, 96% yield. (b) H<sub>2</sub>O, reflux, 16 h. compound used in next step as an aqueous solution.

**Scheme 42:** Synthesis of **233**

The approach highlighted in **Scheme 43** enabled the synthesis of compounds **228-230**. After synthesis of the substituted pyrazolopyrimidine ring (**238-240**), the cyclopropylpyran hinge binding moiety was introduced by Suzuki-Miyaura cross coupling. Compounds **241-243** were telescoped to the next stage of the synthesis where the Boc-protected *para*-aniline was introduced into position 6 by Suzuki-Miyaura cross coupling. Subsequent deprotection of compounds **244-246** gave free anilines **247-249** which were then converted into the final thiourea derivatives **228-230**.

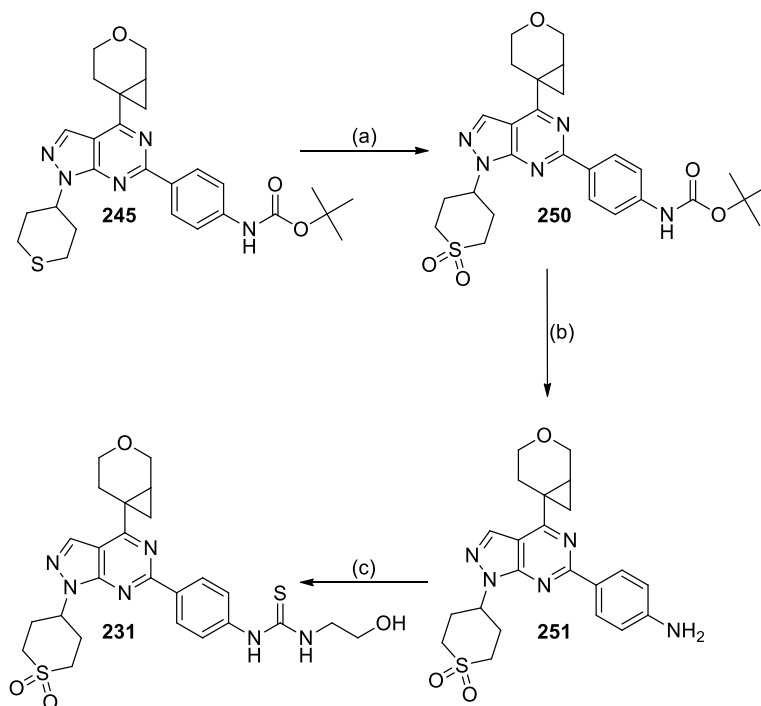


(a) TEA, EtOH, -78-0 °C, 2-4 h, 45-46% (b) Potassium 3-oxabicyclo[4.1.0]heptan-6-yltrifluoroborate, Pd(OAc)<sub>2</sub>, CataCXium® A, Cs<sub>2</sub>CO<sub>3</sub>, toluene/H<sub>2</sub>O (10:1), 110 °C, 2-4 h, telescoped (c) *tert*-butyl (4-(4,4,5,5-tetramethyl-1,3,2-dioxaborolan-2-yl)phenyl)carbamate, Pd(PPh<sub>3</sub>)<sub>4</sub>, Na<sub>2</sub>CO<sub>3</sub>, DME:H<sub>2</sub>O (8:1), 90 °C, 1.5 h, 35% yield (deprotected *in situ* in some instances) (d) HFIP, microwave, 120 °C, 1.5 h, telescoped (e) (i) TCDI, DCM, pyridine, r.t. 1-2 h (ii) Ethanolamine, r.t. 0.5 h, 8-21% yield.

**Scheme 43:** Synthesis of **228-230**.

As previously outlined, further derivatisation of *N*-1 substituents was possible in some instances. Intermediate **245** was oxidised using *m*-CPBA to give cyclic sulfone **250**. From this stage the synthesis was analogous to that described above; Boc-deprotection with HFIP gave aniline **251**, from which the corresponding thiourea **231** was formed (**Scheme 44**).

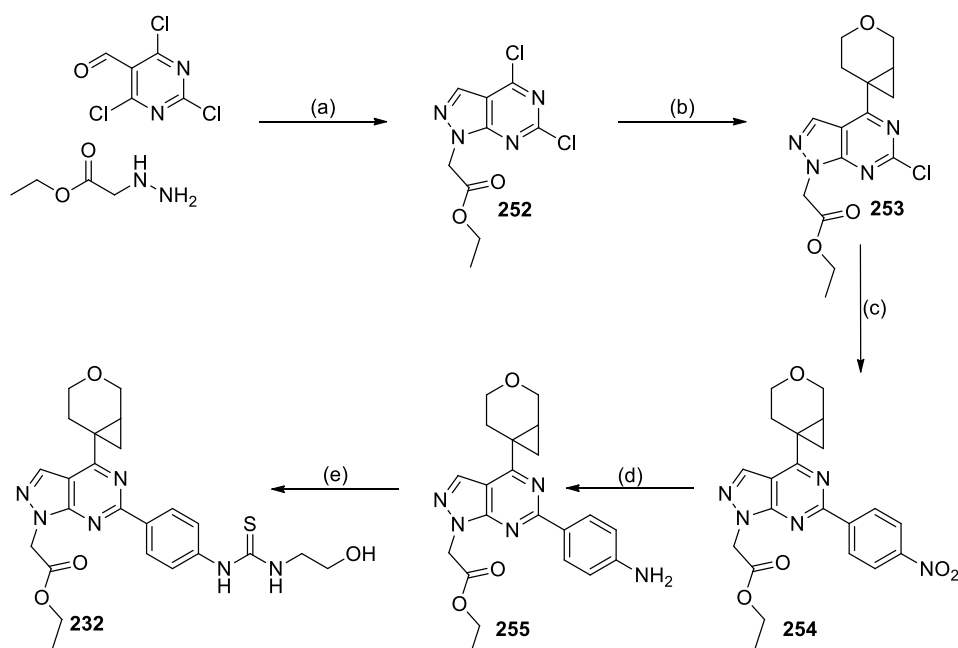




(a) *m*CPBA, DCM, 0 °C, 2.5 h, 75% (b) HFIP,  $\mu$ Wave, 120 °C, 1.5 h, quant. (c) (i) TCDI, DCM, pyridine, r.t. 1 h (ii) Ethanolamine, r.t. 0.5 h, 45%.

**Scheme 44:** Synthesis of **227**.

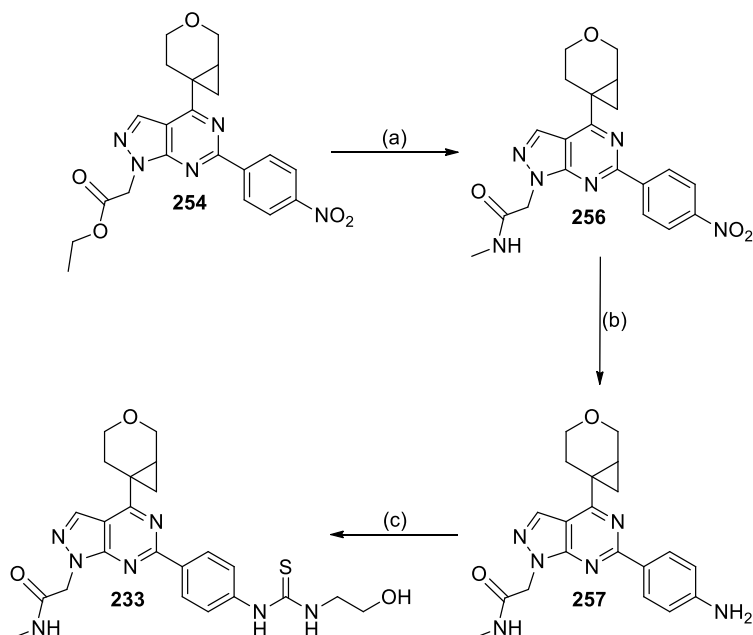
The synthesis of ethyl ester **232** was completed utilising a similar synthesis to compounds **228-230**. (**Scheme 47**). This synthesis differs in that the back-pocket substituent was introduced as a nitro precursor, as this was compatible with further derivatisation of ethyl ester on intermediate compound **254**.



(a) TEA, EtOH,  $-78\text{ }^{\circ}\text{C}$ , 2 h, 51% yield (b) Potassium 3-oxabicyclo[4.1.0]heptan-6-yltrifluoroborate,  $\text{Pd}(\text{OAc})_2$ , CataCXium® A,  $\text{Cs}_2\text{CO}_3$ , toluene/ $\text{H}_2\text{O}$  (10:1),  $110\text{ }^{\circ}\text{C}$  for 1 h followed by  $60\text{ }^{\circ}\text{C}$  for 16 h, 48% yield (c) 4,4,5,5-tetramethyl-2-(4-nitrophenyl)-1,3,2-dioxaborolane,  $\text{Pd}(\text{PPh}_3)_4$ ,  $\text{Na}_2\text{CO}_3$ , DME: $\text{H}_2\text{O}$  (8:1),  $70\text{ }^{\circ}\text{C}$ , 16 h, 74% yield (d) Fe-powder, AcOH, EtOH,  $\text{H}_2\text{O}$ , sonicator, r.t., 4 h, 73% yield (e) (i) TCDI, DCM, pyridine, r.t. 2 h (ii) Ethanolamine, r.t. 0.5 h, 28% yield.

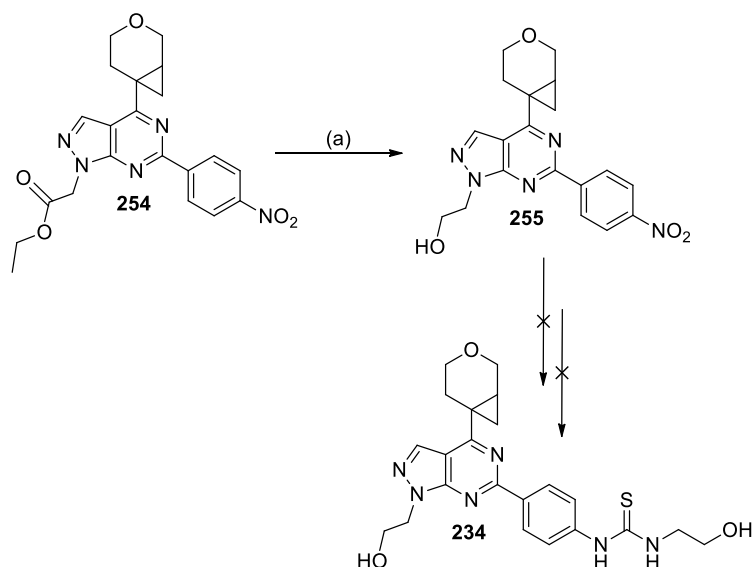
**Scheme 45:** Synthesis of **232**

Similarly, attempts were made to diversify the ethyl ester substituent in compound **254**. Ethyl ester intermediate **254** was successfully converted into the corresponding methyl amide **256** by stirring in methylamine (2M solution in THF). This product could then be reduced to the corresponding aniline **257** before formation of the thiourea compound **233** (Scheme 46). Although reduction of **254** to alcohol **255** was possible, attempts to obtain the desired thiourea product **234** from this intermediate were unsuccessful. This is potentially due to the free alcohol interacting in subsequent reactions and leading to low reaction yields or failed reactions (Scheme 47). Due to this another strategy was pursued to obtain the alcohol **234**.



(a) Methylamine (2M. in THF), r.t., 24 h, quant. (b) Fe-powder, AcOH, EtOH, H<sub>2</sub>O, sonicator, r.t., 1.5 h, 66% yield (c) (i) TCDI, DCM, pyridine, r.t. 2 h (ii) Ethanolanine, r.t. 0.5 h, 34% yield

**Scheme 46:** Synthesis of **233**.

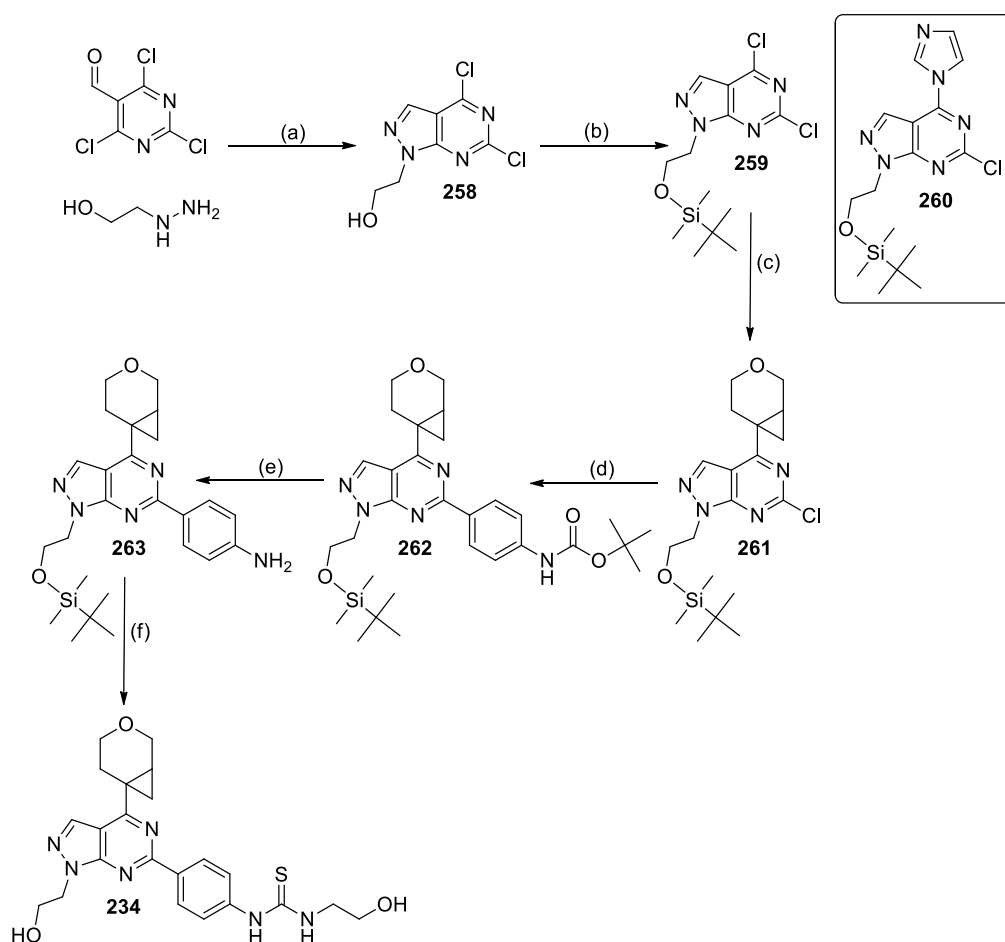


(a) NaBH<sub>4</sub>, THF, r.t., 22 h. 36% yield

**Scheme 47:** Failed synthetic efforts towards **234**.

In order to synthesise alcohol **234** pyrazolopyrimidine **258** was synthesised from 2-hydrazinylethan-1-ol and 2,4,6-trichloropyrimidine-5-carbaldehyde (**Scheme 48**). The primary alcohol in **258** was then protected with a *tert*-butyl dimethylsilyl (TBS) protecting group to give **259**. Temperature control of this reaction was vital as when the reaction was

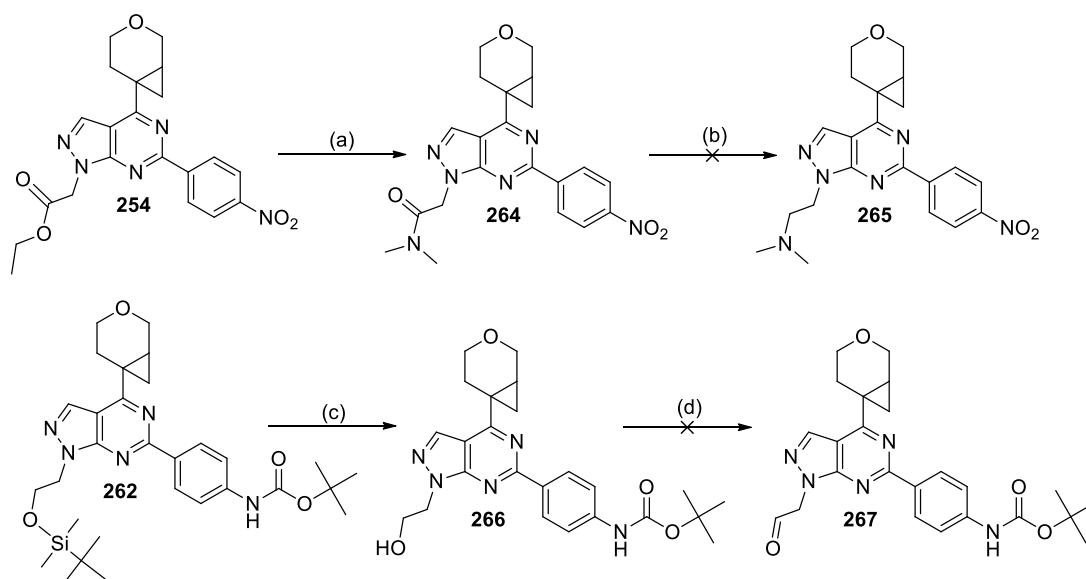
conducted at room temperature an unwanted by-product **260** was exclusively formed. By-product **260** was formed by nucleophilic aromatic substitution at position-4 with imidazole, and this was avoided by cooling reaction to 0 °C. With **259** in hand, two subsequent Suzuki-Miyaura cross-coupling reactions to introduce the cyclopropylpyran hinge binding fragment and the Boc-protected aniline backpacket motif to give compound **262**. Boc-deprotection with HFIP and microwave irradiation successfully unveiled the free aniline **263** whilst leaving the alcohol protected. Thiourea formation was followed by silyl deprotection with tetrabutylammonium fluoride to give final product **234**.



(a) TEA, EtOH, -78-0 °C, 2 h, 68% yield (b) TBDMSCl, imidazole, DMF, 0 °C, 1 h, 99% yield (c) Potassium 3-oxabicyclo[4.1.0]heptan-6-yltrifluoroborate, Pd(OAc)<sub>2</sub>, CataCXium® A, Cs<sub>2</sub>CO<sub>3</sub>, toluene/H<sub>2</sub>O (10:1), 110 °C for 1 h followed by 60 °C for 16 h, 28% yield (d) *tert*-butyl (4-(4,4,5,5-tetramethyl-1,3,2-dioxaborolan-2-yl)phenyl)carbamate, Pd(dppf)Cl<sub>2</sub>.DCM, Na<sub>2</sub>CO<sub>3</sub>, DME:H<sub>2</sub>O (8:1), 90 °C, 1.5 h, 69% yield (e) HFIP,  $\mu$ Wave, 120 °C, 1 h, 92% yield (f) (i) TCDI, DCM, pyridine, r.t., 2 h (ii) Ethanolamine, r.t. 0.5 h. telescoped (iii) TBAF (2M. in THF), 0 °C, 1 h, 68% yield over 3 steps.

**Scheme 48:** Synthesis of **234**.

Several strategies were employed to obtain dimethyl amino compound **235**. Firstly, ethyl ester intermediate **254** was converted into tertiary amide **264**. However, attempts to reduce this amide to the corresponding amine **262**<sup>251</sup> were low yielding and this strategy was abandoned (**Scheme 31**). Another strategy that was examined was to silyl-protect intermediate **262** and oxidise the corresponding free alcohol **266** using Dess-Martin periodinane with the intention of carrying out a reductive amination on the aldehyde product. Oxidation of **266** showed evidence of product present in the reaction mixture by LCMS. Column chromatography of this reaction mixture yielded no desired product. It was presumed that the aldehyde **267** was unstable on silica and therefore this strategy was abandoned.



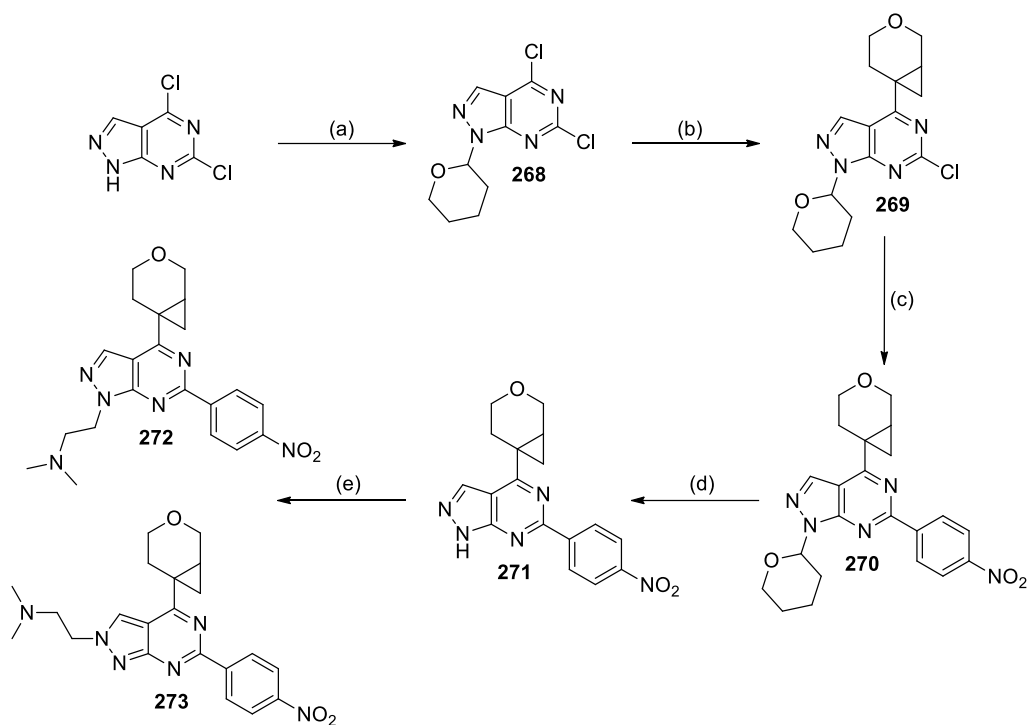
(a) dimethylamine (2M in THF), 60 °C, 36 h, 50% (b) PhSiH<sub>3</sub>, [Ir(COD)Cl]<sub>2</sub>, toluene, 110 °C, 16 h.

(c) TBAF (1M. in THF), 0 °C, 1 h, 99% (d) DMP, r.t., 3.5 h.

**Scheme 49:** Failed synthetic efforts towards **235**

In order to access dimethylamine **235**, a new route was devised (**Scheme 50**). Commercially available 4,6-dichloro-1*H*-pyrazolo[3,4-*d*]pyrimidine was THP protected to give compound **268**. Two subsequent Suzuki-Miyaura cross-coupling reactions were used to introduce the cyclopropylpyran hinge binding fragment to obtain compound **269**, followed by the *para*-nitrobenzene backpocket group to give compound **270**. Deprotection of **270** with hydrochloric acid gave pyrazolopyrimidine **271** in excellent yield. Although previous attempts at alkylating commercially available 4,6-dichloro-1*H*-p231yrazolo[3,4-*d*]pyrimidine had all failed, it was possible to alkylate **271** with sodium hydride and 2-bromo-*N,N*-dimethylethan-1-amine hydrobromide<sup>252</sup> to give 2 isomers of product (**272** and **273**). It was inferred from the <sup>15</sup>N

HMBC NMR spectrum that the major reaction product was the desired regioisomer. (Figure 69).



(a) DHP, *p*-TsOH, THF:DCM (1:1) r.t., 16 h, 36% yield (b) Potassium 3-oxabicyclo[4.1.0]heptan-6-yltrifluoroborate, Pd(OAc)<sub>2</sub>, CataCXium® A, Cs<sub>2</sub>CO<sub>3</sub>, toluene/H<sub>2</sub>O (10:1), 110 °C for 1 h followed by 60 °C for 16 h, 11% yield (c) 4,4,5,5-tetramethyl-2-(4-nitrophenyl)-1,3,2-dioxaborolane, Pd(dppf)Cl<sub>2</sub>, DCM, Na<sub>2</sub>CO<sub>3</sub>, DME:H<sub>2</sub>O (8:1), 90 °C, 1.5 h, 67% yield (d) HCl (2 M in dioxane), r.t., 16 h, 93% yield (e) 2-bromo-*N,N*-dimethylethan-1-amine hydrobromide, NaH, DMF, r.t., 4 h, 48% yield (272), 15% yield (273).

**Scheme 50:** Synthesis of 272 and 273.

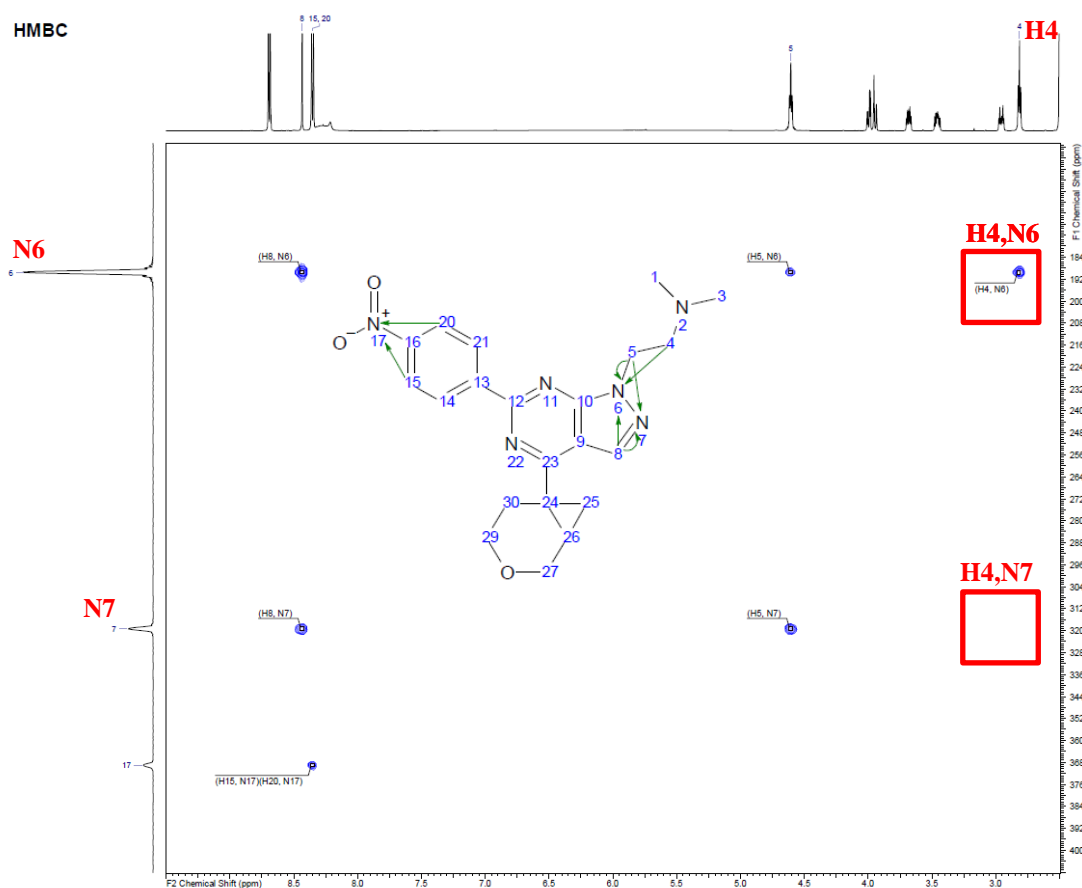
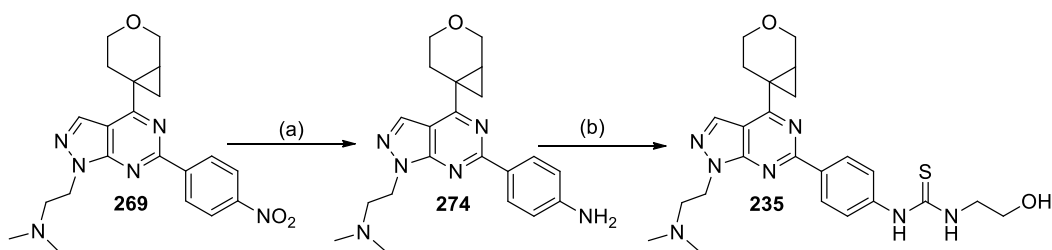


**Figure 69:** Key  $^{15}\text{N}$  HMBC NMR spectrum showing characterising coupling between H4 and N6, Absence of coupling from H4 to N7 suggests the regiochemistry of major compound **272**.

With compound **272** in hand, the nitro- group was reduced to give aniline **274**, from which formation of the thiourea gave final product **235** (**Scheme 51**).



(a) Fe-powder, AcOH, EtOH, H<sub>2</sub>O, sonicator, r.t., 2 h, telescoped (b) (i) TCDI, DCM, pyridine, r.t. 1 h (ii) Ethanolamine, r.t. 0.5 h, 35%

**Scheme 51:** Synthesis of **235**.

### **2.11.2 Biological Profiling of Compound 199a Analogues**

The data on compounds prepared to optimise the *M1* vector of **203a** are summarised in **Table 51**. Tetrahydropyran **228** equipotent with **203a**. It is worth noting that **228** was tested as a racemic mixture whilst **203a** is the most potent single enantiomer, thus the activity of the most potent **228a** enantiomer is potentially slightly higher than 8.4. The cellular pAkt potency for **228** is reduced by 4-fold compared to its potency at mTOR. This compound also does not have significantly better solubility than **203a** and so did not fulfil the requirements of this iteration. For this reason, compound **228** was not progressed further and single enantiomers were not obtained

Tetrahydrothiopyran **229** has an ~8-fold reduced mTOR potency compared with **203a**, however the associated cellular potency (Akt) is similar to that of **203a**. There is no significant difference in solubility, and therefore, this compound was not considered further. Oxidation of the tetrahydrothiopyran to the corresponding cyclic sulfone **231** restores the primary mTOR potency ( $pIC_{50} = 8.4$ ), however the aqueous solubility of this compound is decreased. The low aqueous solubility of this compound was initially surprising considering the decrease in lipophilicity observed for this compound. This can potentially be attributed to intermolecular interactions involving the sulfone functionality, which stabilise crystal packing. This was observed by a group at AstraZeneca, who whilst investigating low solubility on a GPR119 agonist compound found that 59% of methyl-sulfone containing small molecule crystal structures in the CCDC database contain at least one type of interaction involving the sulfone functionality.<sup>253</sup> In addition to low solubility, the cellular potency of **231** decreases by approximately 60-fold compared with the primary mTOR potency. This reduction in cellular potency is most likely caused by the extremely low permeability of this compound.

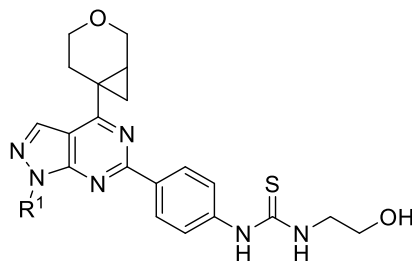
Morpholine **230** has a weaker potency in both mTOR and pAkt and this negates its marginally improved solubility. With cyclic systems failing to give an improved physicochemical profile, attention was turned to small alkyl- based groups.

Ethyl ester **232** has a poor primary mTOR potency and whilst amide **233** had improved potency, this was still considerably lower than **203a**. Amide **229** does have a greater than 2-fold increase in solubility over **203a** however extremely low permeability is likely to be responsible for a more than 100-fold drop-off in potency within the pAkt cellular assay.

Alcohol **234** was equipotent with **203a**, however this compound also has extremely low permeability which likely affects its cellular pAkt potency. The same issue is observed for



dimethylamine **235** which is the most potent compound mTOR inhibitor prepared in the current study ( $pIC_{50} = 8.6$ ). The difficulty encountered in finding a potent group which confers an improved physicochemical profile shows the challenge of further optimising **203a**. In summary, further exploration of the ribose motif did not yield significant improvements over compound **203a**.

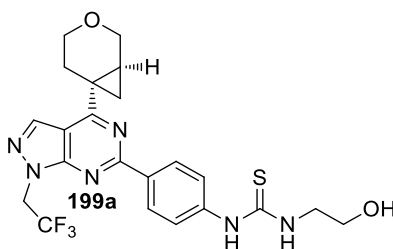


Entry	Compound No.	R <sup>1</sup>	pIC <sub>50</sub>			CAD (µg/mL)	AMP (nm/sec)	LogD/P
			mTOR	pAkt	PI3K $\alpha,\beta,\delta,\gamma$			
1	<b>228</b>		8.4	7.9	5.7, <4.5 5.4, 6.0	21	270	4.30/ 4.41
2	<b>229</b>		7.5	8.0	<4.5, <4.5, 4.8, <4.5	16	-	5.35/ 5.60
3	<b>230</b>		7.5*	6.4*	4.8, <4.5 <4.5, 5.0	27	145	3.68/ 3.69
4	<b>231</b>		8.4	6.6	5.6, <4.5 5.6, 6.0	13	3	3.49/ 3.68
5	<b>232</b>		6.7	6.5	4.5, <4.5 <4.5, 4.8	22	320	4.16/ 4.48
6	<b>233</b>		7.5	5.2	4.8, 4.5 <4.5, 4.9	49	4	2.37/ 2.60
7	<b>234</b>		8.4	6.6	5.7, 4.8 5.0, 5.6	19	3	2.69/ 2.84
8	<b>235</b>		8.6	6.5	5.5 4.7 4.9, 5.6	42	56	2.94/ 3.74

**Table 51:** Biological and physicochemical data for N1-substituted compounds **228-235**. Values marked with \* are N=2, all other values are N=3 or greater. Potency ranges are all within the error of the assay (mTOR= 0.3 pAkt= 0.5) and therefore are not shown. Range is not shown for PI3K selectivity data.

## 2.12 Conclusions and Future Work

The novel cyclopropylpyran hinge binding fragment which was developed in our laboratories has been applied in a 5,6 bicyclic series of mTOR inhibitors where it has been shown to be an effective replacement for morpholine. During this study, and as a result of extensive investigation of literature compounds, it was possible to assert that the literature SAR was not representative of what was observed with the assay platform available in our own laboratories, and therefore this data was not used to guide potency optimisation. The optimisation efforts described above identified thiourea **203a**, a low nanomolar mTOR inhibitor, which has similar activity in a cellular context. When compared with the high quality literature compound **CZ415**, **203a** has higher primary mTOR potency and generally is more selective over closely related lipid kinases. Compound **203a** is superior from a toxicological stand-point, as it has been shown to be Ames negative and has no measurable activity in a hERG assay. The relatively low solubility of **203a** is considered to be manageable, especially given the intended inhaled route of delivery. Based on all of the above, the majority of the aims stated at the beginning of this project have been successfully achieved with **203a** (Table 52)

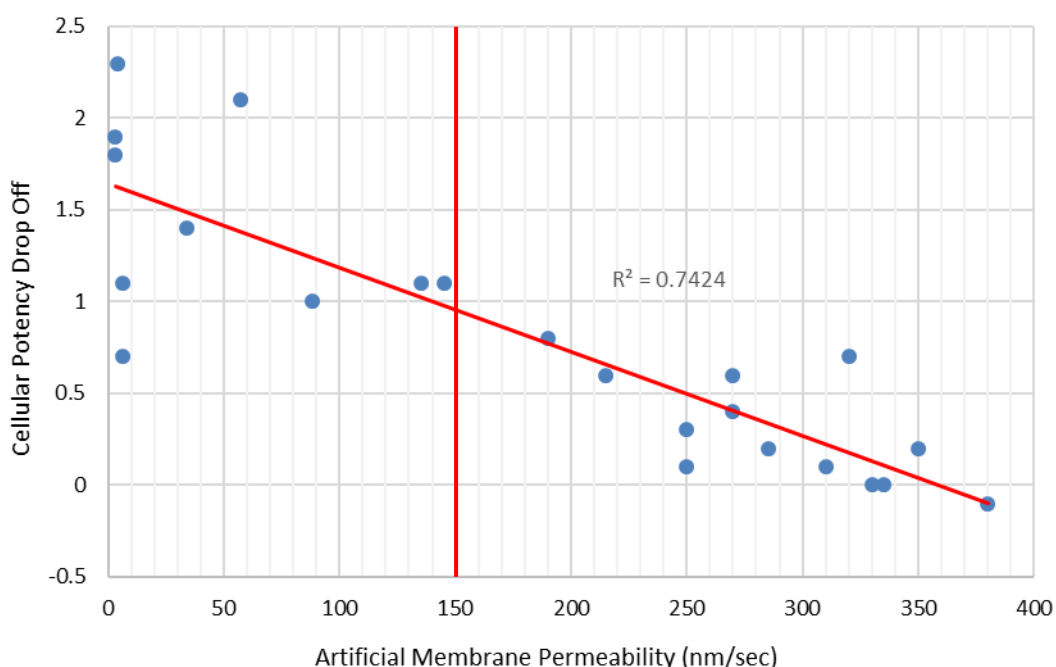


Aim	Result with <b>203a</b>
Primary mTOR pIC <sub>50</sub> of >8.0.	pIC <sub>50</sub> = 8.4
Activity is maintained in cellular assay (pAkt).	pIC <sub>50</sub> = 8.3
pIC <sub>50</sub> of >6.0 in phenotypic “Scar-in-a-jar” assay	pIC <sub>50</sub> = 6.9
No less than 100 fold selectivity over any PIKK	<100-fold potency demonstrated in chemoproteomic competition assay (~100 fold demonstrated over ATR)
No toxicology issues (hERG and Ames).	Parent aniline is Ames Negative in mini-Ames Experiment. <4.3 in hERG QUBE
Improve solubility/ Maintain permeability	Solubility is not sufficiently improved. Compounds that do have acceptable solubility suffer from very low permeability leading to poor cellular potency.

**Table 52:** Summary of performance of **203a** against aims set at start of project.

Having stated this, it is still desirable to synthesise compounds in the pyrazolopyrimidine class with tuned physicochemical properties. The current study has shown that neutral water solubilising groups do not confer sufficient solubility, whilst basic amines result in compounds with very low permeability, which negatively affects cellular potency. Further studies could determine if an acceptable solubility/permeability balance can be achieved within this series of compounds.

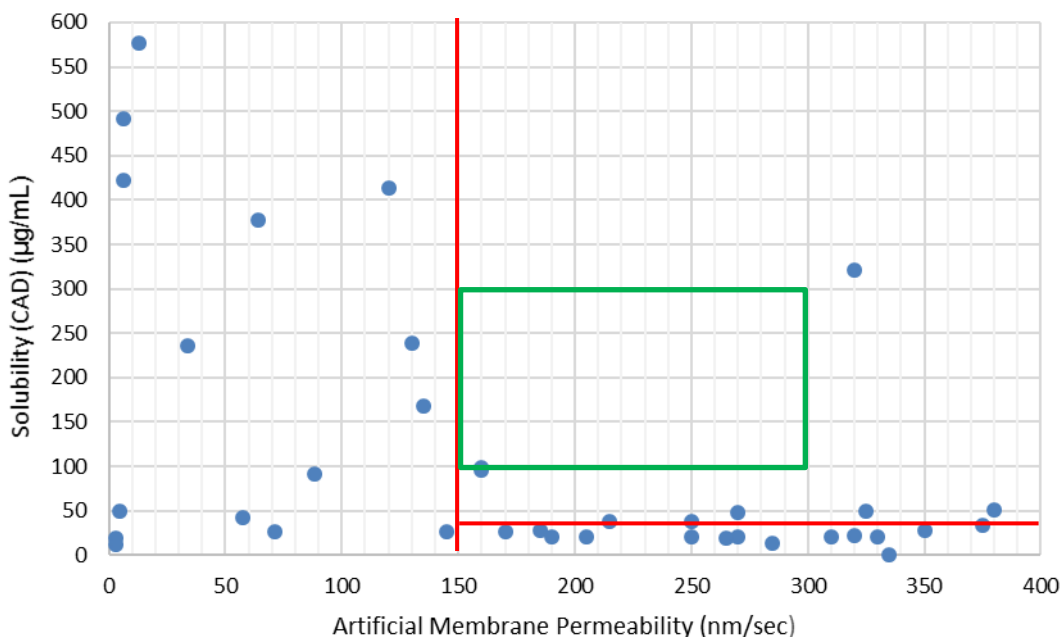
Analysis of the compound in the current study suggest that the observed reduction in cellular potency (pAkt) is inversely correlated to permeability. This is expected as compounds with a low permeability are less able to enter cells and thus interact with intracellular targets. The graph in **Figure 70** suggests that in subsequent studies, a permeability (AMP) of >150 nm/sec should be targeted, as project compounds in this class have a less than 10-fold drop off in cellular potency.



**Figure 70:** Graph showing cellular potency drop off (mTOR pIC<sub>50</sub> – pAkt pIC<sub>50</sub>) vs. Artificial membrane permeability for compounds from the current project. NB: Compounds with primary mTOR potency <7 have been excluded.

By contrast, however, analysis also shows that in this set of project compounds, permeability values of over 150 nm/sec correlates to a solubility of less than 50 µg/mL (**Figure 71**). Although compounds intended for inhaled delivery can have low solubility compared to oral compounds, there are concerns around accumulation of very low solubility compounds in the

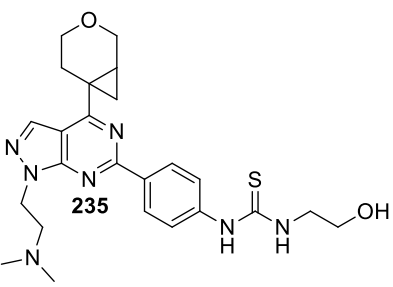
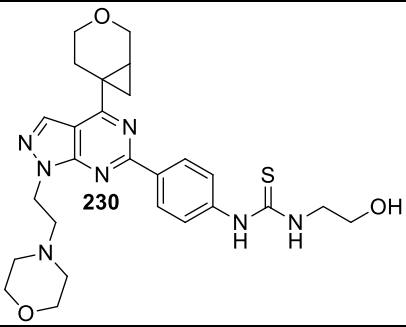
lung and the toxicity related to this.<sup>219</sup> For this reason compounds with a solubility >100  $\mu\text{g/mL}$  should be targeted for future compounds in this series.



**Figure 71:** Graph showing CAD solubility vs. AMP permeability for compounds from the current project. Future iterations should target a physicochemical profile encapsulated by green box.

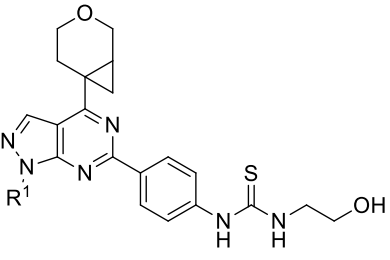
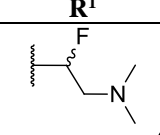
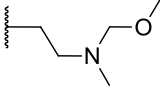
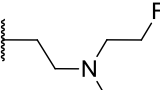
One strategy which could be pursued in future iterations to moderate permeability in compounds with basic amines is to modify the pKa of the amine. By lowering the pKa of the amine, a greater proportion of compound will be uncharged at physiological pH and therefore more easily able to cross the cellular membrane. The matched pair shown in

**Table 53** highlights the potential of this strategy to yield compounds in the desired chemical space. Dimethylamine **235** is the most potent compound currently synthesised at mTOR, however there is a more 100-fold reduction in potency in the cellular pAkt assay. This is likely to be due to the low permeability of this compound which may be caused by ionisation of the amine at physiological pH (predicted pKa = 8.9). The morpholine nitrogen in **230** has a lower predicted pKa and therefore will be significantly less ionised at physiological pH, this translates to this compound having improved permeability, meaning that drop off is only ~10-fold for this compound. The extra steric bulk in morpholine **230** is thought to reduce the primary mTOR activity and therefore further studies would be focused on tuning pKa without lowering biological activity.

		
mTOR pIC <sub>50</sub>	8.6	7.5
pAkt pIC <sub>50</sub>	6.5	6.4
Drop-off (fold)	<b>2.1</b>	<b>1.1</b>
CAD Sol (μg/mL)	45	27
AMP (nm/sec)	56	145
Predicted pKa (Chemaxon)	<b>8.88</b>	<b>6.85</b>

**Table 53:** Comparison of compounds **235** and **230**

**Table 54** shows some proposed future targets, aimed at modifying the amine pKa, these targets plausibly offer the opportunity to achieve cellularly potent compounds in the desired physicochemical space and efforts towards their synthesis would be a logical next step for this project.

	<b>Pka Prediction</b>
	<b>7.1</b>
	<b>6.8</b>
	<b>7.5</b>

**Table 54:** Proposed future synthesis targets for amine pka modification.

In summary, the tactical application of the CPP moiety as a morpholine bioisostere in a pyrazolopyrimidine series has furnished a novel, tractable series of mTOR inhibitors with a promising overall profile as exemplified by compound **203a**. Future studies should focus on tuning the balance of solubility and permeability in order to deliver a high-quality lead compound which could pave the way towards novel treatments in the area of Idiopathic Pulmonary Fibrosis.

# Experimental Section

### **3.1 General Information**

**Solvents and reagents.** Magnetic stirrer bars were stirred vigorously using stirrer hot plates. Solvents and reagents were purchased from commercial suppliers and used as received. Reactions were monitored by thin layer chromatography (TLC) or liquid chromatography-mass spectroscopy (LCMS). Heating was conducted using hotplates with DrySyn adaptors.

**Chromatography.** Thin layer chromatography (TLC) was carried out using polyester-backed precoated silica plates (particle size 0.2 mm). Spots were visualised by ultraviolet (UV) light ( $\lambda_{\text{max}} = 254 \text{ nm}$  or  $365 \text{ nm}$ ) and then stained with potassium permanganate solution followed by gentle heating. Flash column chromatography was carried out using the Teledyne ISCO CombiFlash<sup>®</sup> Rf+ apparatus with RediSep<sup>®</sup> silica cartridges. Fractions were collected by following UV trace ( $\lambda_{\text{max}} = 254 \text{ nm}$  and  $280 \text{ nm}$ ).

**Reverse-Phase Flash Column Chromatography.** Reverse-Phase column chromatography was carried out using Teledyne ISCO CombiFlash<sup>®</sup> Rf+ apparatus and SNAP C-18 silica cartridges of various sizes.

**Formic:** Using a gradient elution with the mobile phases as (A) H<sub>2</sub>O containing 0.1% volume/volume (v/v) formic acid and (B) acetonitrile containing 0.1% (v/v) formic acid. Gradient conditions and flow-rate were variable depending on 2 min LCMS retention time of desired product.

**High pH:** Using a gradient elution with the mobile phases as (A) 10 mM aqueous ammonium bicarbonate solution, adjusted to pH 10 with 0.88 M aqueous ammonia and (B) acetonitrile. Gradient conditions and flow were variable depending on 2 min LCMS retention time of desired product.

**Reverse Phase Preparative- High Performance Liquid Chromatography.** Prep HPLC was carried out on a Grace Revalaris<sup>®</sup> Prep apparatus.

**Formic:** Crude reaction mixtures were loaded into the sample loop of the apparatus in a 1:1 DMSO: MeOH mixture (5 mL max). Using Sunfire prep C18 OBD<sup>™</sup> 5 $\mu$ M 30x100mm column and a gradient elution with the mobile phases as (A) H<sub>2</sub>O containing 0.1% volume/volume (v/v) formic acid and (B) acetonitrile containing 0.1% (v/v) formic acid. Flow-rate was set at 32 mL/min and run-times varied by sample.

**High pH:** Crude reaction mixtures were loaded into the sample loop of the apparatus in a 1:1 DMSO: MeOH mixture (5 mL max). Using Xbridge C18 OBD™ 5 $\mu$ M 30x100mm column and a gradient elution with the mobile phases as (A) H<sub>2</sub>O containing 0.1% volume/volume (v/v) ammonium bicarbonate and (B) acetonitrile containing 0.1% (v/v) ammonium bicarbonate. Flow-rate was set at 32 mL/min and run-times varied by sample.

**Liquid Chromatography Mass Spectrometry.** LCMS analysis was carried out on a Waters Acquity UPLC instrument equipped with a BEH column (50 mm x 2.1 mm, 1.7  $\mu$ m packing diameter) and Waters Micromass ZQ MS using alternate-scan positive and negative electrospray. Analytes were detected as a summed UV wavelength of 210–350 nm. Two liquid phase methods were used:

**Formic:** 40 °C, 1 mL/min flow rate, using a gradient elution with the mobile phases as (A) H<sub>2</sub>O containing 0.1% volume/volume (v/v) formic acid and (B) acetonitrile containing 0.1% (v/v) formic acid. Gradient conditions were initially 1% B, increasing linearly to 97% B over 1.5 min, remaining at 97% B for 0.4 min then increasing to 100% B over 0.1 min.

**High pH:** 40 °C, 1 mL/min flow rate, using a gradient elution with the mobile phases as (A) 10 mM aqueous ammonium bicarbonate solution, adjusted to pH 10 with 0.88 M aqueous ammonia and (B) acetonitrile. Gradient conditions were initially 1% B, increasing linearly to 97% B over 1.5 min, remaining at 97% B for 0.4 min then increasing to 100% B over 0.1 min.

**Nuclear Magnetic Resonance (NMR) Spectroscopy.** Proton (<sup>1</sup>H) and carbon (<sup>13</sup>C) spectra were recorded in deuterated solvents at ambient temperature (unless otherwise stated) using standard pulse methods on any of the following spectrometers and signal frequencies: Bruker AV-400 (<sup>1</sup>H = 400 MHz, <sup>13</sup>C = 101 MHz, <sup>19</sup>F = 376 MHz), Bruker AV-500 (<sup>1</sup>H = 500 MHz, <sup>13</sup>C = 126 MHz), or Bruker AV-600 (<sup>1</sup>H = 600 MHz, <sup>13</sup>C = 150 MHz). Chemical shifts are reported in ppm and are referenced to tetramethylsilane (TMS) or the following solvent peaks: CDCl<sub>3</sub> (<sup>1</sup>H = 7.27 ppm, <sup>13</sup>C = 77.0 ppm), DMSO-*d*<sub>6</sub> (<sup>1</sup>H = 2.50 ppm, <sup>13</sup>C = 39.5 ppm), CD<sub>3</sub>OD (<sup>1</sup>H = 3.31 ppm, <sup>13</sup>C = 49.0 ppm) or CD<sub>3</sub>CN (<sup>1</sup>H = 1.94 ppm, <sup>13</sup>C = 118.7 ppm). Coupling constants are shown to the nearest 0.1 Hz and multiplicities are described as singlet (s), doublet (d), triplet (t), quartet (q), quintet (quin), sextet (sxt), septet (sept), broad (br.) and multiplet (m).



**Infrared (IR) Spectroscopy.** Infrared spectra were recorded using a Perkin Elmer Spectrum 1 or Spectrum 2 machine. Absorption maxima ( $\nu_{\max}$ ) are reported in wavenumbers ( $\text{cm}^{-1}$ ) and are described as strong (s), medium (m), weak (w) and broad (br.).

**High-Resolution Mass Spectrometry (HRMS).** High-resolution mass spectra were recorded on one of two systems:

**System A** – Micromass Q-ToF Ultima hybrid quadrupole time-of-flight mass spectrometer, with analytes separated on an Agilent 1100 Liquid Chromatograph equipped with a Phenomenex Luna C<sub>18</sub> (2) reversed phase column (100 mm x 2.1 mm, 3  $\mu\text{m}$  packing diameter). LC conditions were 0.5 mL/min flow rate, 35 °C, injection volume 2–5  $\mu\text{L}$ , using a gradient elution with (A) H<sub>2</sub>O containing 0.1% (v/v) formic acid and (B) acetonitrile containing 0.1% (v/v) formic acid. Gradient conditions were initially 5% B, increasing linearly to 100% B over 6 min, remaining at 100% B for 2.5 min then decreasing linearly to 5% B over 1 min followed by an equilibration period of 2.5 min prior to the next injection.

**System B** – Waters XEVO G2-XS quadrupole time-of-flight mass spectrometer, with analytes separated on an Acquity UPLC CSH C<sub>18</sub> column (100mm x 2.1mm, 1.7 $\mu\text{m}$  packing diameter). LC conditions were 0.8 mL/min flow rate, 50 °C, injection volume 0.2  $\mu\text{L}$ , using a gradient elution with (A) H<sub>2</sub>O containing 0.1% (v/v) formic acid and (B) acetonitrile containing 0.1% (v/v) formic acid. Gradient conditions were initially 3% B, increasing linearly to 100% B over 8.5 min, remaining at 100% B for 0.5 min then decreasing linearly to 3% B over 0.5 min followed by an equilibration period of 0.5 min prior to the next injection.

Mass to charge ratios (m/z) are reported in Daltons.

**Melting points.** Melting points were recorded on either Stuart SMP10 or Stuart SMP40 melting point apparatus.

**Mass Directed Auto Preparation (MDAP).** Mass-directed automatic purification was carried out using a Waters ZQ MS using alternate scan positive and negative electrospray and a summed UV wavelength of 210–350 nm. Two liquid phase methods were used:

**Formic** – Sunfire C<sub>18</sub> column (100 mm x 19 mm, 5  $\mu\text{m}$  packing diameter, 20 mL/min flow rate) or Sunfire C<sub>18</sub> column (150 mm x 30 mm, 5  $\mu\text{m}$  packing diameter, 40 mL/min flow rate), using a gradient elution at ambient temperature with the mobile phases as (A)

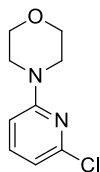
H<sub>2</sub>O containing 0.1% volume/volume (v/v) formic acid and (B) acetonitrile containing 0.1% (v/v) formic acid.

**High pH** – Xbridge C<sub>18</sub> column (100 mm x 19 mm, 5 μm packing diameter, 20 mL/min flow rate) or Xbridge C<sub>18</sub> column (150 mm x 30 mm, 5 μm packing diameter, 40 mL/min flow rate), using a gradient elution at ambient temperature with the mobile phases as (A) 10 mM aqueous ammonium bicarbonate solution, adjusted to pH 10 with 0.88 M aqueous ammonia and (B) acetonitrile.

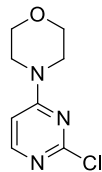
**Hydrophobic frit** cartridges by ISOLUTE® contain a frit which is selectively permeable to organic solutions. These are separated from aqueous phase under gravity. Various cartridge sizes were used.

### **3.2 Tool Compound Synthesis**

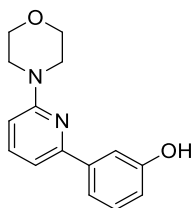
4-(6-Chloropyridin-2-yl)morpholine (43)<sup>254</sup>



A mixture of 2,6-dichloropyridine (1.00 g, 6.76 mmol) and morpholine (1.76 mL, 20.2 mmol) was stirred at 100 °C for 3 h. The reaction was monitored by LCMS and, upon complete consumption of starting material, the reaction was cooled to r.t. and partitioned between ethyl acetate (30 mL) and sat. aq. sodium bicarbonate (30 mL). The aqueous phase was extracted with further ethyl acetate (3 x 10 mL). The combined organic layer was dried (hydrophobic frit) and concentrated *in vacuo*. The resulting residue was purified by flash column chromatography (cyclohexane: ethyl acetate 0-25% (12 column volumes)). The appropriate fractions were concentrated *in vacuo* to give 4-(6-chloropyridin-2-yl) morpholine (1.04 g, 5.24 mmol, 77 % yield) as a colourless cloudy oil. LCMS (formic) rt. 1.00 (100%) MH<sup>+</sup> for desired M= 198.056. <sup>1</sup>H NMR (DMSO-d<sub>6</sub>, 400 MHz) δ = 7.53-7.61 (m, 1H), 6.78 (d, *J* = 8.3 Hz, 1H), 6.70 (d, *J* = 7.6 Hz, 1H), 3.65-3.71 (m, 4H), 3.40-3.47 ppm (m, 4H). <sup>13</sup>C NMR (101 MHz, DMSO-d<sub>6</sub>) δ = 159.5, 148.6, 141.0, 112.4, 105.8, 66.2, 45.3. HRMS (system A) calculated for C<sub>9</sub>H<sub>12</sub>ClN<sub>2</sub>O 199.0633, found 199.0624. FTIR (cm<sup>-1</sup>) 2961, 1593, 1442, 1253, 1115, 955, 775

4-(2-Chloropyrimidin-4-yl)morpholine (44)<sup>131</sup>

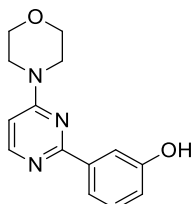
To a mixture of morpholine (0.87 mL, 10.0 mmol) and DIPEA (3.49 mL, 20.0 mmol) in *N,N*-dimethylformamide (13 mL). 2,4-Dichloropyrimidine (1.49 g, 10.0 mmol) was added dropwise and the resulting solution was stirred at r.t. for 1 h. The reaction was monitored by LCMS and upon complete consumption of starting material the reaction was concentrated *in vacuo*. The resulting residue was purified by flash column chromatography (cyclohexane: ethyl acetate 0-50% (12 column volumes)). The appropriate fractions were concentrated *in vacuo* to give 4-(2-chloropyrimidin-4-yl)morpholine (1.40 g, 7.02 mmol, 70 % yield) as a white solid. LCMS (formic) rt. 0.64 (100%) MH<sup>+</sup> for desired M= 199.051. <sup>1</sup>H NMR (CDCl<sub>3</sub>, 400 MHz) δ = 8.07 (d, *J* = 6.1 Hz, 1H), 6.39 (d, *J* = 6.1 Hz, 1H), 3.74-3.82 (m, 4H), 3.62-3.67 (m, 4H). <sup>13</sup>C NMR (101 MHz, CDCl<sub>3</sub>) δ = 162.9, 160.8, 157.5, 101.1, 66.3, 44.2. HRMS (system A) calculated for C<sub>8</sub>H<sub>11</sub>ClN<sub>3</sub>O 200.0585, found 200.0577. FTIR (cm<sup>-1</sup>) 2973, 1579, 1373, 1161, 1112, 859, 822.

3-(6-Morpholinopyridin-2-yl)phenol (31)<sup>255</sup>

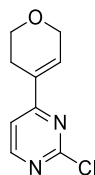
In a 10-20 mL Biotage microwave vial a mixture of 4-(6-chloropyridin-2-yl)morpholine (500 mg, 2.52 mmol), 3-(4,4,5,5-tetramethyl-1,3,2-dioxaborolan-2-yl)phenol (831 mg, 3.78 mmol) Pd(dppf)Cl<sub>2</sub>.CH<sub>2</sub>Cl<sub>2</sub> (206 mg, 0.25 mmol) and potassium carbonate (696 g, 5.03 mmol) was dissolved in 2-propanol (8.3 mL) and water (1.7 mL). The resulting suspension was degassed with a stream of nitrogen for 10 min, sealed and stirred at 100 °C for 16 h. The reaction was monitored by LCMS and, upon complete consumption of starting material, the reaction was cooled to r.t. and filtered through a celite cartridge (10 g). The resulting mixture was concentrated *in vacuo*. The resulting residue was purified by reverse phase flash column chromatography (high-pH, 15-85% (15 column volumes)) to give 3-(6-morpholinopyridin-2-yl)phenol (420 mg, 1.64 mmol, 65% yield) as a white solid. The product was recrystallised from hot toluene to give material of the required quality for X-ray Crystallography. LCMS (high-pH) rt. 0.99 (100%) MH<sup>+</sup> for desired M= 256.121. <sup>1</sup>H NMR (DMSO-d<sub>6</sub>, 600 MHz) δ =

9.44 (br., s, 1H), 7.63 (dd,  $J = 8.3, 7.5$  Hz, 1H), 7.48-7.49 (m, 1H), 7.43-7.46 (m, 1H), 7.22-7.25 (m, 1H), 7.18 (d,  $J = 7.3$  Hz, 1H), 6.79 (ddd,  $J = 8.1, 2.6, 0.7$  Hz, 1H), 6.78 (d,  $J = 8.4$  Hz, 1H), 3.72-3.77 (m, 4H), 3.51-3.56 ppm (m, 4H).  $^{13}\text{C}$  NMR (DMSO- $d_6$ , 151 MHz):  $\delta = 159.2, 158.0, 154.3, 141.0, 138.9, 129.9, 117.6, 116.2, 113.7, 110.0, 106.3, 66.5, 45.6$  ppm. HRMS (system A) calculated for  $\text{C}_{15}\text{H}_{17}\text{N}_2\text{O}_2$  257.1285, found 257.1276 FTIR ( $\text{cm}^{-1}$ ): 3263, 1570, 1438, 1380, 1296, 1215, 1105, 849, 876. M.P: 138-140 °C.

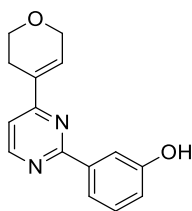
3-(4-Morpholinopyrimidin-2-yl)phenol (35)<sup>255</sup>



In a 10-20 mL Biotage microwave vial a mixture of 4-(2-chloropyrimidin-4-yl)morpholine (800 mg, 4.01 mmol), 3-(4,4,5,5-tetramethyl-1,3,2-dioxaborolan-2-yl)phenol (1.32 g, 6.01 mmol) Pd(II)(dppf) $\text{Cl}_2 \cdot \text{CH}_2\text{Cl}_2$  (327 mg, 0.40 mmol) and potassium carbonate (1.11 g, 8.01 mmol) was dissolved in 2-propanol (12 mL) and water (2.4 mL). The resulting suspension was degassed with a stream of nitrogen for 10 min, sealed and stirred at 100 °C for 16 h. The reaction was monitored by LCMS, and upon complete consumption of starting material, the reaction was cooled to r.t. and filtered through a celite cartridge (10 g). The resulting mixture was concentrated *in vacuo* and dry loaded onto Florisil<sup>®</sup>. The crude reaction mixture was purified by flash column chromatography (cyclohexane: ethyl acetate 0-100% (15 column volumes)). The appropriate fractions were concentrated *in vacuo* to give 3-(4-morpholinopyrimidin-2-yl)phenol (434 mg, 1.69 mmol, 42% yield) as a light orange solid. The product was recrystallised from hot acetonitrile to give material of the required quality for X-ray Crystallography. LCMS (formic) rt. 0.44 (100%)  $\text{MH}^+$  for desired  $\text{M} = 257.116$ .  $^1\text{H}$  NMR (DMSO- $d_6$ , 400 MHz)  $\delta = 9.46$  (s, 1H), 8.33 (d,  $J = 6.0$  Hz, 1H), 7.76-7.81 (m, 2H), 7.22-7.28 (m, 1H), 6.83-6.89 (m, 1H), 6.75 (d,  $J = 6.1$  Hz, 1H), 3.65-3.76 ppm (m, 8H).  $^{13}\text{C}$  NMR (101 MHz, DMSO- $d_6$ )  $\delta = 162.8, 162.1, 157.8, 156.6, 139.9, 129.7, 119.0, 117.7, 114.9, 102.1, 66.3, 44.2$ . HRMS (system A) calculated for  $\text{C}_{14}\text{H}_{16}\text{N}_3\text{O}_2$  258.1237, found 258.1231. FTIR ( $\text{cm}^{-1}$ ) 2957, 1576, 1366, 1186, 1116, 875, 861. M.P:167-169 °C.

2-Chloro-4-(3,6-dihydro-2H-pyran-4-yl)pyrimidine (45)<sup>256</sup>

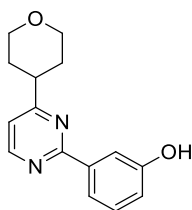
In a 10-20 mL Biotage microwave vial a mixture of 2,4-dichloropyrimidine (1.49 g, 10.0 mmol), 2-(3,6-dihydro-2H-pyran-4-yl)-4,4,5,5-tetramethyl-1,3,2-dioxaborolane (3.15 g, 15.0 mmol), Pd(PPh<sub>3</sub>)<sub>4</sub> (1.15g, 1.00 mmol) and potassium carbonate (4.15g, 30.0 mmol) was dissolved in toluene (12 mL) and *N,N*-dimethylformamide (1.3 mL) and the resulting suspension was degassed with a stream of nitrogen for 10 min, sealed and irradiated in a Biotage initiator+ microwave at 120 °C for a total of 4 h. The reaction was monitored by LCMS and, upon complete consumption of starting material, the reaction was cooled to r.t. and filtered through a celite cartridge (10 g). The resulting mixture was concentrated *in vacuo* and purified by reverse phase flash column chromatography (formic, 15%-55% (15 column volumes)) to give 2-chloro-4-(3,6-dihydro-2H-pyran-4-yl)pyrimidine (740 mg, 3.76 mmol, 38% yield) as an off-white solid. LCMS (formic) rt. 0.79 (99%) MH<sup>+</sup> for desired M= 196.040. <sup>1</sup>H NMR (MeOD, 400 MHz) δ = 8.74 (d, *J* = 5.4 Hz, 1H), 7.69 (d, *J* = 5.4 Hz, 1H), 7.27-7.32 (m, 1H), 4.51-4.56 (m, 2H), 4.04-4.10 (m, 2H), 3.46-3.49 (m, 2H), 2.70-2.76 (m, 2H) <sup>13</sup>C NMR (101 MHz, MeOD) δ = 168.2, 162.3, 161.1, 134.5, 133.3, 115.6, 66.9, 65.3, 26.1 ppm. HRMS (system A) calculated for C<sub>9</sub>H<sub>15</sub>N<sub>2</sub>O<sub>2</sub> 255.1128, found 255.1114. FTIR (cm<sup>-1</sup>) 1703, 1566, 1368, 1340, 1178, 997, 852, 799, 776.

3-(4-(3,6-Dihydro-2H-pyran-4-yl)pyrimidin-2-yl)phenol (36)

In a 10-20 mL Biotage microwave vial a mixture of 2-chloro-4-(3,6-dihydro-2H-pyran-4-yl)pyrimidine (620 mg, 3.15 mmol), 3-(4,4,5,5-tetramethyl-1,3,2-dioxaborolan-2-yl)phenol (1.04 g, 4.73 mmol), Pd(dppf)Cl<sub>2</sub>.CH<sub>2</sub>Cl<sub>2</sub> (257 mg, 0.32 mmol) and potassium carbonate (872 mg, 5.11 mmol) was dissolved in 2-propanol (8.4 mL) and water (6.3 mL). The resulting suspension was degassed with a stream of nitrogen for 10 min, sealed and irradiated at 100 °C in a Biotage initiator+ microwave for 1 h. The reaction was monitored by LCMS and, upon complete consumption of starting material, the reaction was cooled to r.t. and filtered through

a celite cartridge (10 g). The resulting mixture was concentrated *in vacuo* and partitioned between ethyl acetate (20 mL) and water (20 mL). The aqueous phase was extracted with further ethyl acetate (3x 20 mL) and the combined organic layers were dried (hydrophobic frit) and concentrated *in vacuo*. The resulting residue was purified by flash column chromatography (cyclohexane: ethyl acetate 0-100% (15 column volumes)) to give 3-(4-(3,6-dihydro-2*H*-pyran-4-yl)pyrimidin-2-yl)phenol (536 mg, 2.11 mmol, 70% yield) as a white solid. LCMS (formic) rt. 0.90 (99%) MH<sup>+</sup> for desired M= 254.106. <sup>1</sup>H NMR (CDCl<sub>3</sub>, 400 MHz) δ = 8.74 (d, *J* = 5.4 Hz, 1H), 8.07 (d, *J* = 7.5 Hz, 1H), 8.00 (s, 1H), 7.37 (t, *J* = 7.8 Hz, 1H), 7.21 (d, *J* = 5.4 Hz, 1H), 7.06-7.10 (m, 1H), 7.00 (ddd, *J* = 8.0, 2.6, 0.9 Hz, 1H), 4.43-4.48 (m, 2H), 4.00 (t, *J* = 5.4 Hz, 2H), 2.67-2.74 ppm (m, 2H). <sup>13</sup>C NMR (101 MHz, CDCl<sub>3</sub>) δ = 163.6, 163.2, 157.5, 156.0, 139.5, 133.1, 130.4, 129.8, 120.7, 117.8, 114.9, 113.2, 65.8, 64.3, 25.2. HRMS (system B) calculated for C<sub>15</sub>H<sub>15</sub>N<sub>2</sub>O<sub>2</sub> 255.1128, found 255.1114. FTIR (cm<sup>-1</sup>) 3268, 1568, 1430, 1384, 1232, 1130, 780. M.P. 133-135 °C.

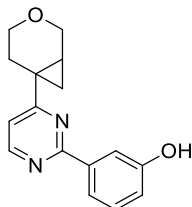
3-(4-(Tetrahydro-2*H*-pyran-4-yl)pyrimidin-2-yl)phenol (37)



To one chamber of a COWare apparatus a mixture of 3-(4-(3,6-dihydro-2*H*-pyran-4-yl)pyrimidin-2-yl)phenol (200 mg, 0.79 mmol) and Palladium (5% on Carbon) (4.20 mg, 0.04 mmol) was added. The resulting mixture was dissolved in acetic acid (4.0 mL) and nitrogen was blown through the apparatus for 5 min. To the second chamber zinc powder (1.03 g, 15.7 mmol) and hydrochloric acid (0.67 mL, 22.2 mmol) were added and the COWare apparatus was sealed. The reaction mixture was stirred at r.t. for 16 h followed by at 50 °C for 4 h. The reaction was monitored by LCMS and, upon complete consumption of starting material, the reaction was cooled to r.t., filtered through a celite cartridge (2.5 g) and concentrated *in vacuo*. The resulting crude mixture was purified by flash column chromatography (cyclohexane: ethyl acetate 0-100% (12 column volumes)) to give 3-(4-(tetrahydro-2*H*-pyran-4-yl)pyrimidin-2-yl)phenol (92 mg, 0.36 mmol, 46% yield) as a pale yellow solid. The product was recrystallised from toluene to give material of the required quality for X-ray crystallography. LCMS (formic) rt. 0.86 (100%) MH<sup>+</sup> for desired M= 256.121. <sup>1</sup>H NMR (DMSO-*d*<sub>6</sub>, 400 MHz) δ = 9.56 (s, 1H), 8.78 (d, *J* = 5.1 Hz, 1H), 7.84-7.89 (m, 2H), 7.29-7.36 (m, 2H), 6.91 (ddd, *J* = 8.1, 2.4, 1.1 Hz, 1H), 3.95-4.03 (m, 2H), 3.38-3.60 (m, 2H), 2.95-3.05 (m, 1H), 1.78-1.90 ppm (m, 4H).

$^{13}\text{C}$  NMR (101 MHz, DMSO- $d_6$ )  $\delta$  = 172.9, 163.4, 158.2, 158.1, 139.2, 130.0, 119.0, 118.2, 117.6, 114.9, 67.3, 42.3, 31.5. HRMS (system A) calculated for  $\text{C}_{15}\text{H}_{17}\text{N}_2\text{O}_2$  257.1285, found 257.1279. FTIR ( $\text{cm}^{-1}$ ) 2961, 2836, 1576, 1383, 1224, 1082, 851. M.P: 159-161 °C.

3-(4-(3-Oxabicyclo[4.1.0]heptan-6-yl)pyrimidin-2-yl)phenol (38)



In a 10-20 mL microwave vial trimethyloxosulfonium chloride (303 mg, 2.36 mmol) and sodium hydride (60 mg, 2.36 mmol) were dissolved in anhydrous DMSO and the reaction was stirred under nitrogen for 20 min, until visible evolution of hydrogen had ceased. A solution of 3-(4-(3,6-dihydro-2H-pyran-4-yl)pyrimidin-2-yl)phenol (300 mg, 1.18 mmol) in anhydrous DMSO (2 mL) was added dropwise and the reaction mixture was stirred at 65 °C for 4 h. The reaction mixture was suspended between ethyl acetate (15 mL) and water (15 mL) and the aqueous layer was extracted with further ethyl acetate (3x 15 mL). The combined organic layer was dried (hydrophobic frit) and concentrated *in vacuo*. The crude reaction mixture was purified by prep HPLC (formic, 32-99% over 40 min) to give 3-(4-(3-oxabicyclo[4.1.0]heptan-6-yl)pyrimidin-2-yl)phenol (56 mg, 0.21 mmol, 18% yield). LCMS (formic) rt. 0.92 (99%)  $\text{MH}^+$  for desired  $\text{M}$ = 268.121.  $^1\text{H}$  NMR (DMSO- $d_6$ , 400 MHz)  $\delta$  = 9.55 (s, 1H), 8.71 (d,  $J$  = 5.4 Hz, 1H), 7.81-7.85 (m, 2H), 7.34 (d,  $J$  = 5.6 Hz, 1H), 7.27-7.32 (m, 1H), 6.90 (ddd,  $J$  = 8.1, 2.4, 1.0 Hz, 1H), 3.94 (dd,  $J$  = 11.5, 4.4 Hz, 1H), 3.88 (dd,  $J$  = 11.2, 1.2 Hz, 1H), 3.61 (dt,  $J$  = 11.5, 5.1 Hz, 1H), 3.38 (ddd,  $J$  = 11.5, 8.8, 5.1 Hz, 1H), 2.70 (dt,  $J$  = 14.2, 4.9 Hz, 1H), 2.00 (ddd,  $J$  = 14.2, 8.7, 5.6 Hz, 1H), 1.84-1.93 (m, 1H), 1.48 (dd,  $J$  = 9.2, 3.8 Hz, 1H), 1.18 (dd,  $J$  = 6.6, 3.9 Hz, 1H).  $^{13}\text{C}$  NMR (DMSO- $d_6$ , 101 MHz)  $\delta$  = 173.1, 162.9, 158.0, 157.6, 139.3, 130.0, 119.0, 118.2, 115.1, 114.9, 65.1, 63.6, 25.0, 23.3, 23.0, 22.5. HRMS (System A) calculated for  $\text{C}_{16}\text{H}_{17}\text{N}_2\text{O}_2$  [ $\text{MH}^+$ ] 269.1285, found 269.1276. FTIR ( $\text{cm}^{-1}$ ) 3268, 1568, 1430, 1384, 1232, 1130, 780. M.P. 133-135 °C.

Chiral Purification of 3-(4-(3-oxabicyclo[4.1.0]heptan-6-yl)pyrimidin-2-yl)phenol (38)

Total sample dissolved in ethanol (3 mL) and heptane (3 mL) and liquid loaded onto the column in 0.5 mL manual injections.

**Column:** Chiralpak IC5 250x20mm (Room Temp)

**Flow Rate:** 20 mL/min (58 bar)

**Detection:** UV Diode Array at 280nm

**Mobile Phase A:** Heptane

**Mobile Phase B:** Ethanol

**Modifier:** Isopropyl amine

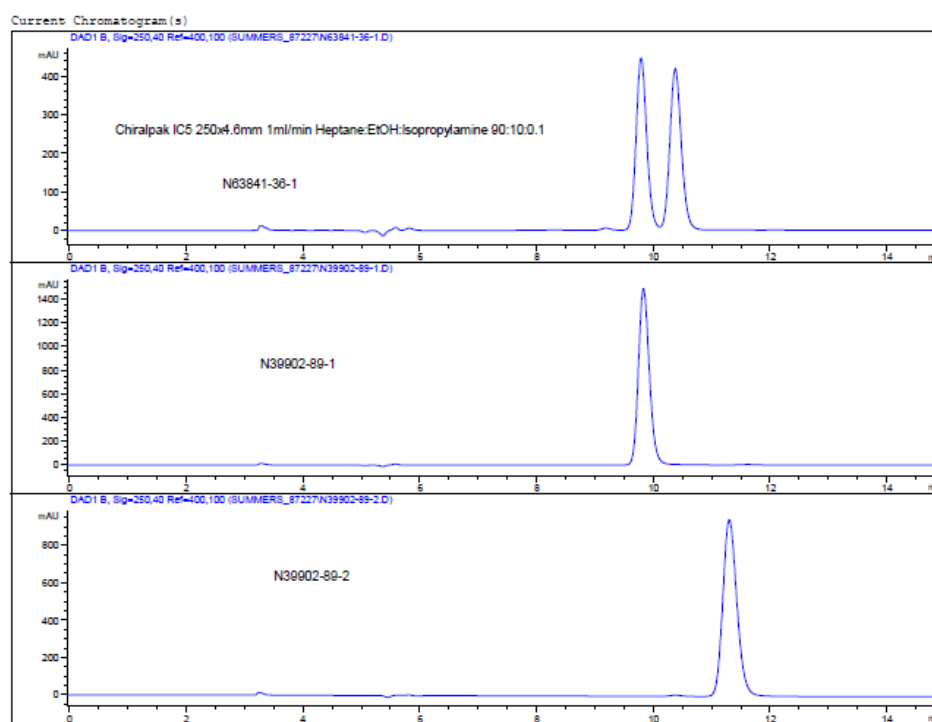
**Isocratic method:** 90:10:0.2 mobile phase A: mobile phase B: modifier

**Runtime:** 20 min.

The combined fractions for isomer 1 (**38a**) and isomer 2 (**38b**) were concentrated by a stream of nitrogen to yield. 1<sup>st</sup> eluting isomer (**38a**) (27 mg, 99.7% chirally pure by chiral HPLC analysis) as a white solid  $\alpha_D^{20} = -100.0$  (0.2 g/100 mL). Confirmed by X-ray crystallography to be **3-(4-((1*R*,6*S*)-3-oxabicyclo[4.1.0]heptan-6-yl)pyrimidin-2-yl)phenol**.

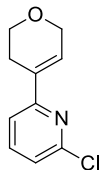
2<sup>nd</sup> eluting isomer (**38b**) (25 mg, 99.5% chirally pure by chiral HPLC analysis) as a white solid  $\alpha_D^{20} = +69.9$  (0.29g/100 mL). Inferred from the X-ray crystal structure of **38a** that **38b** is **3-(4-((1*S*,6*R*)-3-oxabicyclo[4.1.0]heptan-6-yl)pyrimidin-2-yl)phenol**.

the single enantiomer products were recrystallised from toluene to give material of the required quality for X-ray crystallography.

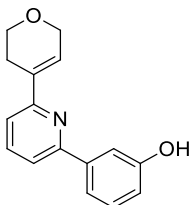


**Figure 72:** Chiral purification of 3-(4-(3-oxabicyclo[4.1.0]heptan-6-yl)pyrimidin-2-yl)phenol (**38**)



2-Chloro-6-(3,6-dihydro-2H-pyran-4-yl)pyridine (46)

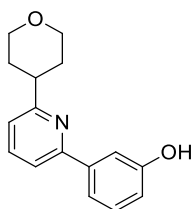
In a 10-20 mL Biotage microwave vial a mixture of 2-bromo-6-chloropyridine (1.92 g, 10.0 mmol), 2-(3,6-dihydro-2H-pyran-4-yl)-4,4,5,5-tetramethyl-1,3,2-dioxaborolane (2.52 g, 12.0 mmol), Pd(dppf)Cl<sub>2</sub>.CH<sub>2</sub>Cl<sub>2</sub> (732 mg, 1.00 mmol) and potassium carbonate (2.76 g, 20.0 mmol) was dissolved in 2-propanol (11 mL) and water (2.2 mL). The resulting suspension was degassed with a stream of nitrogen for 10 min, sealed and stirred at r.t. for 16 h. The reaction was monitored by LCMS and upon complete consumption of starting material the reaction was filtered through a celite cartridge (10 g). The resulting mixture was dried (hydrophobic frit) and concentrated *in vacuo*. The crude reaction mixture was purified by reverse phase flash column chromatography (formic, 30-85% (12 column volumes)) to give 2-chloro-6-(3,6-dihydro-2H-pyran-4-yl)pyridine (1.17 g, 5.98 mmol, 60% yield). LCMS (formic) rt. 0.99 (96%) MH<sup>+</sup> for desired M= 195.045. <sup>1</sup>H NMR (CDCl<sub>3</sub>, 400 MHz) δ = 7.59-7.67 (m, 1H), 7.27-7.30 (m, 2H), 7.20 (d, *J* = 7.8 Hz, 1H), 6.78-6.81 (m, 1H), 4.39 (s, 2H), 3.95 (t, *J* = 5.4 Hz, 2H), 2.59-2.66 (m, 2H). <sup>13</sup>C NMR (101 MHz, CDCl<sub>3</sub>) δ = 157.5, 150.9, 138.9, 132.9, 127.7, 122.3, 116.9, 65.8, 64.3, 25.7 HRMS (system A) calculated for C<sub>10</sub>H<sub>11</sub>ClNO 196.0338, found 196.0324. FTIR (cm<sup>-1</sup>) 1712,1558, 1413, 1360, 1162,1050, 987, 880, 784, 658.

3-(6-(3,6-Dihydro-2H-pyran-4-yl)pyridin-2-yl)phenol (32)

In a 10-20 mL Biotage microwave vial a mixture of 2-chloro-6-(3,6-dihydro-2H-pyran-4-yl)pyridine (500 mg, 2.56 mmol), 3-(4,4,5,5-tetramethyl-1,3,2-dioxaborolan-2-yl)phenol (844 mg, 3.83 mmol), Pd(dppf)Cl<sub>2</sub>.CH<sub>2</sub>Cl<sub>2</sub> (209mg, 0.26 mmol) and potassium carbonate (706 mg, 5.11 mmol) was dissolved in 2-propanol (8.4 mL) and water (1.68 mL). The resulting suspension was degassed with a stream of nitrogen for 10 min, sealed and irradiated at 100 °C in a Biotage initiator+ microwave for 1 h. The reaction was monitored by LCMS and upon complete consumption of starting material the reaction was filtered through a celite cartridge (10 g). The resulting mixture was concentrated *in vacuo* and partitioned between ethyl acetate (20 mL) and water (20 mL). The aqueous phase was extracted with further ethyl acetate (3 x

20 mL). The combined organic layers were dried (hydrophobic frit) and concentrated *in vacuo*. The resulting residue was purified by reverse phase flash column chromatography (high-pH, 30-85% (15 column volumes)) to give 3-(6-(3,6-dihydro-2*H*-pyran-4-yl)pyridin-2-yl)phenol (328 mg, 1.29 mmol, 51% yield) as an amorphous white solid. The product was recrystallised from hot toluene to give material of the required quality for X-ray crystallography. LCMS (formic) rt. 1.01 (100%) MH<sup>+</sup> for desired M= 254.106. <sup>1</sup>H NMR (DMSO-*d*<sub>6</sub>, 400 MHz) δ = 9.52 (br s, 1H), 7.81-7.86 (m, 1H), 7.75 (d, *J* = 7.6 Hz, 1H), 7.57-7.59 (m, 1H), 7.47-7.55 (m, 2H), 7.25-7.31 (m, 1H), 6.86-6.89 (m, 1H), 6.84 (ddd, *J* = 8.1, 2.4, 0.7 Hz, 1H), 4.28-4.35 (m, 2H), 3.87 (t, *J* = 5.5 Hz, 2H), 2.60-2.68 (m, 2H). <sup>13</sup>C NMR (DMSO-*d*<sub>6</sub>, 101 MHz) δ = 158.2, 156.0, 155.3, 140.6, 138.1, 134.2, 130.1, 126.8, 118.8, 117.8, 117.7, 116.5, 113.8, 65.5, 64.2, 40.7, 40.3, 39.8, 40.0, 39.4, 25.8. HRMS (system A) calculated for C<sub>16</sub>H<sub>16</sub>NO<sub>2</sub> 254.1176, found 254.1171. FTIR (cm<sup>-1</sup>) 3251, 1567, 1440, 1213, 1043, 963, 877, 796, 696. M.P. 148-150 °C.

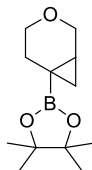
3-(6-(Tetrahydro-2*H*-pyran-4-yl)pyridin-2-yl)phenol (33)



To one chamber of a COware apparatus a mixture of 3-(6-(3,6-dihydro-2*H*-pyran-4-yl)pyridin-2-yl)phenol (300 mg, 1.18 mmol) and Palladium (5% on Carbon) (6.30 mg, 0.06 mmol) was added. The resulting mixture was dissolved in acetic acid (6.0 mL) and nitrogen was blown through the apparatus for 5 min. To the second chamber zinc powder (1.55 g, 23.7 mmol) and hydrochloric acid (1.01 mL, 33.4 mmol) were added and the COware apparatus was sealed. The reaction mixture was stirred at r.t. for 16 h followed by at 50 °C for 4 h. The reaction was monitored by LCMS and, upon complete consumption of starting material, the reaction was cooled to r.t., filtered through a celite cartridge (2.5 g) and concentrated *in vacuo* to give 3-(6-(tetrahydro-2*H*-pyran-4-yl)pyridin-2-yl)phenol (211 mg, 0.83 mmol, 70% yield) as a white solid. The product was recrystallised from toluene to give material of the required quality for X-ray crystallography. LCMS (formic) rt. 0.69 (99%) MH<sup>+</sup> for desired M= 255.126. <sup>1</sup>H NMR (CDCl<sub>3</sub>, 400 MHz) δ = 7.67-7.73 (m, 1H), 7.61 (dd, *J* = 2.4, 1.6 Hz, 1H), 7.52-7.59 (m, 1H), 7.30-7.36 (m, 1H), 7.10-7.14 (m, 1H), 6.89 (ddd, *J* = 8.1, 2.7, 0.9 Hz, 1H), 4.12-4.19 (m, 2H), 3.58-3.66 (m, 2H), 3.05 (tt, *J* = 11.1, 4.0 Hz, 1H), 1.92-2.08 (m, 4H). <sup>13</sup>C NMR (101 MHz, CDCl<sub>3</sub>) δ = 164.0, 156.2, 156.0, 141.2, 137.2, 129.9, 119.4, 119.1, 118.2, 115.9, 113.9,

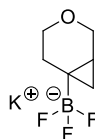
68.2, 43.4, 32.4. HRMS (system A) calculated for C<sub>16</sub>H<sub>18</sub>NO<sub>2</sub>, 256.1332 found 256.1321. FTIR (cm<sup>-1</sup>) 3222, 1584, 1447, 1301, 1220, 1080, 980, 840. M.P. 174-176 °C.

2-(3-Oxabicyclo[4.1.0]heptan-6-yl)-4,4,5,5-tetramethyl-1,3,2-dioxaborolane (50)



To a stirred solution of 2-(3,6-dihydro-2*H*-pyran-4-yl)-4,4,5,5-tetramethyl-1,3,2-dioxaborolane (25.0 g, 119 mmol) in fluorobenzene (240 mL) at -5 °C was added chloriodomethane (315 g, 1.79 mol) in fluorobenzene (240 mL) and diethylzinc (1 M in hexanes) (1.19 L, 1.19 mol). These reagents were added in six equal portions each over a period of 5 mins. Upon completion of the final addition the reaction mixture was warmed to r.t. and stirred for 5 h. The consumption of starting material was monitored by TLC (*n*-hexane: ethyl acetate (5:1) product at rf. 0.4, visualised by PMA stain). The reaction was quenched by addition of 10% aqueous ammonium chloride (500 mL) and the aqueous layer was extracted with diethyl ether (2 x 500 mL). The combined organic layers were dried (Na<sub>2</sub>SO<sub>4</sub>), filtered and concentrated *in vacuo* to afford 2-(3-oxabicyclo[4.1.0]heptan-6-yl)-4,4,5,5-tetramethyl-1,3,2-dioxaborolane (26 g, 92 mmol, 78% yield) as a pale brown solid. TLC (*n*-hexane: ethyl acetate (5:1)) rf. 0.4. <sup>1</sup>H NMR (CDCl<sub>3</sub>, 400 MHz) δ = 4.00 (d, *J* = 11.2 Hz, 1H), 3.84 (dd, *J* = 11.2, 3.4 Hz, 1H), 3.59 (ddd, *J* = 11.2, 6.4, 2.4 Hz, 1H), 3.11-3.19 (m, 1H), 2.03 (ddd, *J* = 14.4, 4.6, 2.7 Hz, 1H), 1.66 (ddd, *J* = 14.4, 11.2, 6.4 Hz, 1H), 1.23 (s, 12H), 1.05-1.11 (m, 1H), 0.95 (dd, *J* = 8.3, 3.2 Hz, 1H), 0.65 ppm (dd, *J* = 5.7, 3.3 Hz, 1H). <sup>13</sup>C NMR (CDCl<sub>3</sub>, 101 MHz) δ = 83.2, 65.5, 64.7, 24.7, 24.7, 17.2, 16.2 ppm (1C not observed). FTIR (cm<sup>-1</sup>) 2927, 1372, 1318, 1140, 1073, 851, 667. Does not ionise.

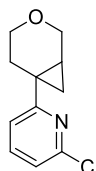
Potassium 3-oxabicyclo[4.1.0]heptan-6-yltrifluoroborate (51)



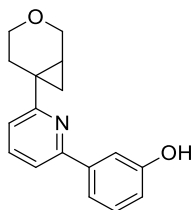
To a stirred solution of 2-(3-oxabicyclo[4.1.0]heptan-6-yl)-4,4,5,5-tetramethyl-1,3,2-dioxaborolane (35.0 g, 156 mmol) in acetonitrile (289 mL) and methanol (289 mL) was added potassium fluoride (36.3 g, 625 mmol) in water (100 mL). The resulting solution was stirred for 10 min. at r.t. and then *L*-(+)-tartaric acid (49.4 g, 312 mmol) was added, followed by THF (175 mL). The resulting solution was stirred at r.t. for 30 min. The resulting reaction mixture was filtered, and the filtrate was concentrated *in vacuo* to afford a crude reaction product. The

crude product was titrated in diethyl ether. The resulting mixture was filtered and dried over high vacuum for 3 h to give 3-oxabicyclo[4.1.0]heptan-6-yltrifluoroborate (32.0 g, 156 mmol, 100 % yield) as an off-white solid.  $^1\text{H}$  NMR (DMSO- $d_6$ , 400 MHz)  $\delta$  = 3.74 (d,  $J$  = 11.0 Hz, 1H), 3.67 (dd,  $J$  = 10.8, 4.2 Hz, 1H), 3.29-3.36 (m, 1H), 2.95-3.03 (m, 1H), 1.71 (dt,  $J$  = 13.8, 4.2 Hz, 1H), 1.31 (ddd,  $J$  = 13.8, 9.8, 5.7 Hz, 1H), 1.08 (s, 1H), 0.46-0.53 (m, 1H), 0.29 (d,  $J$  = 7.6 Hz, 1H), -0.15 - -0.10 ppm (m, 1H)  $^{13}\text{C}$  NMR (DMSO- $d_6$ , 101 MHz):  $\delta$  = 66.9, 64.6, 26.9, 25.4, 14.6, 13.1.

2-(3-Oxabicyclo[4.1.0]heptan-6-yl)-6-chloropyridine (48)



In a 10-20 mL Biotage microwave vial a mixture of 2-(3-oxabicyclo[4.1.0]heptan-6-yl)-4,4,5,5-tetramethyl-1,3,2-dioxaborolane (1.82 g, 8.11 mmol), 2,6-dichloropyridine (1.00 g, 6.76 mmol), caesium hydroxide monohydrate (2.27 g, 13.5 mmol) and Pd(dppf) $\text{Cl}_2 \cdot \text{CH}_2\text{Cl}_2$  (552 mg, 0.68 mmol) was dissolved in tetrahydrofuran (17.5 mL) and water (1.75 mL). The resulting suspension was degassed with a stream of nitrogen for 10 min, sealed and stirred at 100 °C for 3 h. The reaction was monitored by LCMS and, upon complete consumption of starting material, the reaction was cooled to r.t. and filtered through a celite cartridge (2.5 g). The resulting mixture was concentrated *in vacuo* and dissolved in dichloromethane. The crude reaction mixture was purified by flash column chromatography (cyclohexane: ethyl acetate 0-25% (15 column volumes)) to give 2-(3-oxabicyclo[4.1.0]heptan-6-yl)-6-chloropyridine (448 mg, 2.19 mmol, 27% yield) as a yellow oil. LCMS (formic) rt. 1.03 (100%)  $\text{MH}^+$  for desired  $\text{M} = 209.061$ .  $^1\text{H}$  NMR ( $\text{CDCl}_3$ , 400 MHz)  $\delta$  = 7.52-7.59 (m, 1H), 7.14 (dd,  $J$  = 7.8, 0.8 Hz, 1H), 7.10 (dd,  $J$  = 7.8, 0.8 Hz, 1H), 5.32 (s, 1H), 4.04 (dd,  $J$  = 11.6, 4.3 Hz, 1H), 3.96 (dd,  $J$  = 11.4, 1.5 Hz, 1H), 3.65 (dt,  $J$  = 11.6, 5.3 Hz, 1H), 3.47 (ddd,  $J$  = 11.6, 9.1, 5.1 Hz, 1H), 2.47-2.56 (m, 1H), 2.13 (ddd,  $J$  = 14.1, 8.8, 5.7 Hz, 1H), 1.74-1.81 (m, 1H), 1.45 (s, 1H), 1.31-1.37 (m, 1H), 1.23 (s, 2H), 1.11 (dd,  $J$  = 6.3, 4.0 Hz, 1H).  $^{13}\text{C}$  NMR ( $\text{CDCl}_3$ , 101 MHz)  $\delta$  = 166.0, 150.6, 138.7, 120.7, 117.8, 65.7, 63.9, 26.6, 22.5, 21.6, 21.5. HRMS (system B) calculated for  $\text{C}_{11}\text{H}_{13}\text{NOCl}$  210.0680, found 210.0692. FTIR ( $\text{cm}^{-1}$ ) 1584, 1444, 1120, 865, 747.

3-(6-(3-Oxabicyclo[4.1.0]heptan-6-yl)pyridin-2-yl)phenol (34)

In a 10-20 mL Biotage microwave vial a mixture of 4-(3-oxabicyclo[4.1.0]heptan-6-yl)-2-chloropyrimidine (488 mg, 2.33 mmol), 3-(4,4,5,5-tetramethyl-1,3,2-dioxaborolan-2-yl)phenol (768 mg, 3.49 mmol), Pd(dppf)Cl<sub>2</sub>.CH<sub>2</sub>Cl<sub>2</sub> (190 mg, 0.23 mmol) and potassium carbonate (643 mg, 4.65 mmol) was dissolved in 2-propanol (8.2 mL) and water (1.6 mL). The resulting suspension was degassed with a stream of nitrogen for 10 min, sealed and irradiated in a Biotage initiator+ microwave at 100 °C for 1.5 h. The reaction was monitored by LCMS and, upon complete consumption of starting material, the reaction was cooled to r.t. and filtered through a celite cartridge (2.5 g) The resulting mixture was concentrated *in vacuo* and then partitioned between ethyl acetate (20 mL) and water (20 mL), brine (5 mL) was added to aid separation and the aqueous layer was extracted with further ethyl acetate (3 x 20 mL). The combined aqueous layers were dried (hydrophobic frit) and concentrated *in vacuo*. The crude product was purified by reverse-phase flash column chromatography (formic, 20-85% (15 column volumes)) to give 3-(6-(3-oxabicyclo[4.1.0]heptan-6-yl)pyridin-2-yl)phenol (300 mg, 1.12 mmol, 48 % yield) as a white solid. LCMS (formic) rt. 0.94 (100%) MH<sup>+</sup> for desired M= 267.126. <sup>1</sup>H NMR (DMSO-d<sub>6</sub>, 400 MHz) δ = 9.49 (s, 1H), 7.74-7.79 (m, 1H), 7.64 (d, *J* = 7.8 Hz, 1H), 7.51-7.54 (m, 1H), 7.45-7.48 (m, 1H), 7.23-7.30 (m, 2H), 6.82 (ddd, *J* = 8.0, 2.5, 0.9 Hz, 1H), 3.97 (dd, *J* = 11.2, 4.7 Hz, 1H), 3.85 (dd, *J* = 11.4, 1.3 Hz, 1H), 3.57 (dt, *J* = 11.4, 5.3 Hz, 1H), 3.42 (ddd, *J* = 11.6, 8.4, 5.3 Hz, 1H), 2.65 (dt, *J* = 13.9, 5.3 Hz, 1H), 2.04 (ddd, *J* = 13.8, 8.4, 5.3 Hz, 1H), 1.78-1.84 (m, 1H), 1.35 (dd, *J* = 9.0, 3.7 Hz, 1H), 1.04 (dd, *J* = 6.1, 3.8 Hz, 1H). <sup>13</sup>C NMR (101 MHz, CDCl<sub>3</sub>) δ = 164.0, 156.1, 155.3, 141.1, 136.9, 129.8, 119.1, 117.8, 116.9, 115.9, 113.7, 65.9, 64.2, 26.7, 22.7, 21.5, 21.2 HRMS (System A) calculated for C<sub>17</sub>H<sub>18</sub>NO<sub>2</sub> 268.1332, found 268.1325. FTIR (cm<sup>-1</sup>) 3254, 1571, 1439, 1305, 1214, 1175, 1059, 748. M.P. 115-117 °C.

Chiral purification of 3-(6-(3-oxabicyclo[4.1.0]heptan-6-yl)pyridin-2-yl)phenol (34)

Total sample dissolved in ethanol (10 mL) and heptane (10 mL) and liquid loaded onto the column in 0.3 mL manual injections.

**Column:** Chiralpak AD-H (250x4.6 mm, 5 μM, room temp.)

**Flow Rate:** 42.5 mL/min (54 bar)

**Detection:** UV Diode Array at 250 nm

**Mobile Phase A:** Heptane

**Mobile Phase B:** Ethanol

**Modifier:** TFA

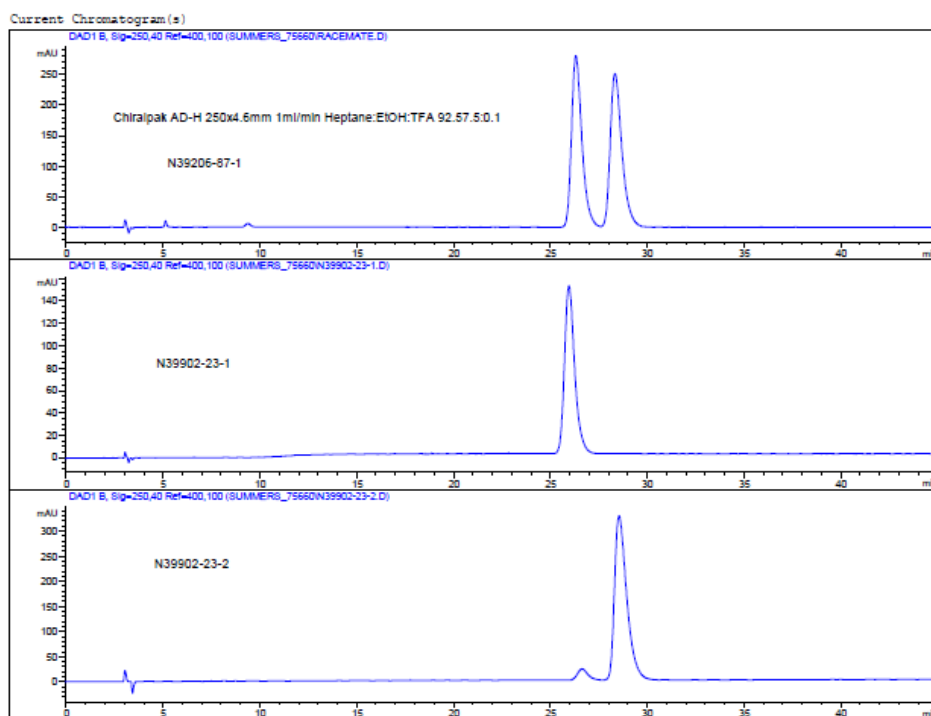
**Isocratic method:** 2000:150:2.5 mobile phase A: mobile phase B: modifier

**Runtime:** 40 min.

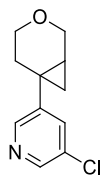
The combined fractions for isomer 1 (**34a**) and isomer 2 (**34b**) were concentrated by a stream of nitrogen to yield. 1<sup>st</sup> eluting isomer (**34a**) (71 mg, >99.9% chirally pure by chiral HPLC analysis) as a white solid ( $\alpha_D^{20}$  (0.5 g/100 mL) = -30.2. Confirmed by X-ray crystallography to be **3-(6-((1*R*,6*S*)-3-oxabicyclo[4.1.0]heptan-6-yl)pyridin-2-yl)phenol**.

2<sup>nd</sup> eluting isomer (**16b**) (83 mg, 94.6% chirally pure by chiral HPLC analysis) as a white solid ( $\alpha_D^{20}$  (1.0 g/100 mL) = +42.2. Inferred from the X-ray crystal structure of **34a** that **34b** is **3-(6-((1*S*,6*R*)-3-oxabicyclo[4.1.0]heptan-6-yl)pyridin-2-yl)phenol**.

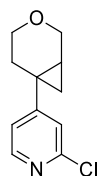
The single enantiomer products were recrystallised from toluene to give material of the required quality for X-ray crystallography.



**Figure 73:** Chiral purification of 3-(6-(3-oxabicyclo[4.1.0]heptan-6-yl)pyridin-2-yl)phenol (**34**)

3-(3-Oxabicyclo[4.1.0]heptan-6-yl)-5-chloropyridine (52)

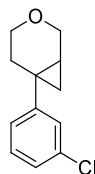
In a 10-20 mL Biotage microwave vial a mixture of potassium 3-oxabicyclo[4.1.0]heptan-6-yltrifluoroborate (600 mg, 2.94 mmol), 3-bromo-5-chloropyridine (736 mg, 3.82 mmol), caesium carbonate (2.87 g, 8.82 mmol), palladium(II) acetate (66mg, 0.29 mmol) and cataCXium® A (211mg, 0.59 mmol) was dissolved in toluene (13.4 mL) and water (1.34 mL). The resulting suspension was degassed with a stream of nitrogen for 10 min, sealed and stirred at 90 °C for 16 h. The reaction was monitored by LCMS and, upon complete consumption of starting material, the reaction was cooled to r.t. and filtered through a celite cartridge (2.5 g). The resulting mixture was concentrated *in vacuo* and dry-loaded onto Florisil®. The crude reaction mixture was purified by flash column chromatography (cyclohexane: ethyl acetate 0% to 50% (15 column volumes)) to give 3-(3-oxabicyclo[4.1.0]heptan-6-yl)-5-chloropyridine (255 mg, 1.22 mmol, 41% yield). LCMS (formic) rt. 0.86 (100%) MH<sup>+</sup> for desired M= 209. <sup>1</sup>H NMR (DMSO-d<sub>6</sub>, 400 MHz) δ = 8.49 (d, *J* = 2.0 Hz, 1H), 8.45 (d, *J* = 2.2 Hz, 1H), 7.77-7.82 (m, 1H), 3.98 (dd, *J* = 11.4, 4.5 Hz, 1H), 3.81 (dd, *J* = 11.4, 1.1 Hz, 1H), 3.50 (dt, *J* = 11.0, 5.4 Hz, 1H), 3.41 (ddd, *J* = 11.7, 8.3, 5.4 Hz, 1H), 2.08 (ddd, *J* = 14.2, 8.8, 6.1 Hz, 1H), 1.99 (dt, *J* = 13.9, 5.1 Hz, 1H), 1.43-1.50 (m, 1H), 1.12 (dd, *J* = 9.2, 4.5 Hz, 1H), 0.94 (dd, *J* = 5.9, 4.6 Hz, 1H). <sup>13</sup>C NMR (CDCl<sub>3</sub>, 101 MHz) δ = 147.0, 146.1, 144.5, 134.8, 132.0, 65.6, 63.8, 30.1, 30.0, 20.0, 18.3, 18.0 HRMS (System B) calculated for C<sub>11</sub>H<sub>12</sub>NOCl 210.0686, found 210.0692. FTIR (cm<sup>-1</sup>) 1573, 1412, 1104, 1078, 884, 707.

4-(3-Oxabicyclo[4.1.0]heptan-6-yl)-2-chloropyridine (53)

In a 10-20 mL Biotage microwave vial a mixture of potassium 3-oxabicyclo[4.1.0]heptan-6-yltrifluoroborate (600 mg, 2.94 mmol), 2-chloro-4-iodopyridine (915 mg, 3.82 mmol), caesium carbonate (2.87 g, 8.82 mmol), palladium(II) acetate (66mg, 0.29 mmol) and cataCXium® A (211mg, 0.59 mmol) was dissolved in toluene (13.4 mL) and water (1.34 mL). The resulting suspension was degassed with a stream of nitrogen for 10 min, sealed and stirred at 90 °C for 16 h. The reaction was monitored by LCMS and, upon complete consumption of

starting material, the reaction was cooled to r.t. and filtered through a celite cartridge (2.5 g). The resulting mixture was concentrated *in vacuo* and dry-loaded onto Florisil<sup>®</sup>. The crude reaction mixture was purified by flash column chromatography (cyclohexane: ethyl acetate 0-100% (15 column volumes to give 4-(3-oxabicyclo[4.1.0]heptan-6-yl)-2-chloropyridine (225 mg, 1.07 mmol, 37% yield) as an amorphous white solid. LCMS (high-pH) rt. 0.95 (96%) MH<sup>+</sup> for desired M= 209.061. <sup>1</sup>H NMR (DMSO-d<sub>6</sub>, 400 MHz) δ = 8.27 (dd, *J* = 5.1, 0.5 Hz, 1H), 7.33 (dd, *J* = 1.7, 0.5 Hz, 1H), 7.25 (dd, *J* = 5.4, 1.7 Hz, 1H), 3.93 (dd, *J* = 11.4, 4.5 Hz, 1H), 3.79 (dd, *J* = 11.4, 1.3 Hz, 1H), 3.50 (dt, *J* = 11.2, 5.1 Hz, 1H), 3.38 (ddd, *J* = 11.5, 8.3, 5.1 Hz, 1H), 2.08-2.15 (m, 1H), 2.02 (ddd, *J* = 13.9, 8.3, 5.6 Hz, 1H), 1.50-1.59 (m, 1H), 1.15 (dd, *J* = 9.2, 4.5 Hz, 1H), 1.04 ppm (dd, *J* = 6.4, 4.6 Hz, 1H). <sup>13</sup>C NMR (DMSO-d<sub>6</sub>, 101 MHz) δ = 165.3, 156.0, 154.9, 126.4, 125.8, 69.8, 68.1, 32.6, 25.6, 25.5 ppm (1C not observed) HRMS (system B) calculated for C<sub>11</sub>H<sub>12</sub>NOCl 210.0686, found 210.0694. FTIR (cm<sup>-1</sup>) 1589, 1387, 1130, 1076, 926, 868.

6-(3-Chlorophenyl)-3-oxabicyclo[4.1.0]heptane (54)

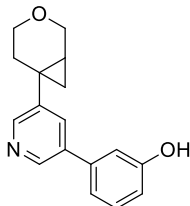


In a 10-20 mL Biotage microwave vial a mixture of potassium 3-oxabicyclo[4.1.0]heptan-6-yltrifluoroborate (600 mg, 2.94 mmol), 1-bromo-3-chlorobenzene (732 mg, 3.82 mmol), caesium carbonate (2.87 g, 8.82 mmol), palladium(II) acetate (66mg, 0.29 mmol) and cataCXium<sup>®</sup> A (211mg, 0.59 mmol) was dissolved in toluene (13.4 mL) and water (1.34 mL). The resulting suspension was degassed with a stream of nitrogen for 10 min, sealed and stirred at 90 °C for 16 h. The reaction was monitored by LCMS and, upon complete consumption of starting material, the reaction was cooled to r.t. and filtered through a celite cartridge (2.5 g). The resulting mixture was concentrated *in vacuo* and dry-loaded onto Florisil<sup>®</sup>. The crude reaction mixture was purified by flash column chromatography (cyclohexane: ethyl acetate 0-30% (12 column volumes)). The appropriate fractions were concentrated *in vacuo* to give 6-(3-chlorophenyl)-3-oxabicyclo[4.1.0]heptane (225 mg, 1.07 mmol, 37% yield) as a colourless oil. LCMS (formic) rt. 1.23 (100%) MH<sup>+</sup> for desired M= 208.065. <sup>1</sup>H NMR (DMSO-d<sub>6</sub>, 400 MHz) δ = 7.29-7.37 (m, 2H), 7.22-7.27 (m, 2H), 3.98 (dd, *J* = 11.5, 4.6 Hz, 1H), 3.77-3.82 (m, 1H), 3.48 (dt, *J* = 11.5, 5.6 Hz, 1H), 3.39 (ddd, *J* = 11.5, 8.3, 5.4 Hz, 1H), 2.05 (ddd, *J* = 13.9, 8.6, 5.6 Hz, 1H), 1.95 (dt, *J* = 13.7, 5.1 Hz, 1H), 1.33-1.42 (m, 1H), 1.02 (dd, *J* = 9.2, 4.5 Hz, 1H), 0.89 ppm (dd, *J* = 5.9, 4.6 Hz, 1H). <sup>13</sup>C NMR (DMSO-d<sub>6</sub>, 101 MHz) δ = 150.4,



133.5, 130.7, 127.1, 126.2, 125.9, 65.4, 63.5, 30.2, 21.9, 19.0, 18.8 ppm. HRMS (System B) calculated for C<sub>12</sub>H<sub>14</sub>OCl 209.0733, found 209.0733. FTIR (cm<sup>-1</sup>) 1596, 1125, 1076, 885, 738.

3-(5-(3-Oxabicyclo[4.1.0]heptan-6-yl)pyridin-3-yl)phenol (40)



In a 2-5 mL Biotage microwave vial a mixture of 3-(3-oxabicyclo[4.1.0]heptan-6-yl)-5-chloropyridine (250 mg, 1.19 mmol), 3-(4,4,5,5-tetramethyl-1,3,2-dioxaborolan-2-yl)phenol (394 mg, 1.79 mmol), Pd(dppf)Cl<sub>2</sub>.CH<sub>2</sub>Cl<sub>2</sub> (97 mg, 0.12 mmol) and potassium carbonate (330 mg, 2.39 mmol) was dissolved in 2-propanol (3.9 mL) and water (0.79 mL). The resulting suspension was degassed with a stream of nitrogen for 10 min, sealed and stirred at 100 °C for 19 h. The reaction was monitored by LCMS and, upon complete consumption of starting material, the reaction was cooled to r.t. and filtered through a celite cartridge (2.5 g). The resulting mixture was concentrated *in vacuo* and dry-loaded onto Florisil<sup>®</sup>. The crude reaction mixture was purified by flash column chromatography (cyclohexane: ethyl acetate 0-100% (15 column volumes)). The appropriate fractions were concentrated *in vacuo* to give 3-(5-(3-oxabicyclo[4.1.0]heptan-6-yl)pyridin-3-yl)phenol (67 mg, 0.25 mmol, 21% yield) as a white solid. LCMS (formic) rt. 0.55 (100%) MH<sup>+</sup> for desired M= 267.126. <sup>1</sup>H NMR (DMSO-d<sub>6</sub>, 600 MHz) δ = 9.58 (s, 1H), 8.63 (d, *J* = 2.2 Hz, 1H), 8.50 (d, *J* = 2.2 Hz, 1H), 7.79-7.82 (m, 1H), 7.27-7.31 (m, 1H), 7.12-7.15 (m, 1H), 7.06-7.09 (m, 1H), 6.81-6.85 (m, 1H), 4.03 (dd, *J* = 11.4, 4.4 Hz, 1H), 3.84 (dd, *J* = 11.4, 1.5 Hz, 1H), 3.51 (dt, *J* = 11.4, 5.5 Hz, 1H), 3.44 (ddd, *J* = 11.7, 8.4, 4.8 Hz, 1H), 2.12 (ddd, *J* = 13.9, 8.4, 5.5 Hz, 1H), 2.04 (dt, *J* = 13.9, 5.1 Hz, 1H), 1.47-1.51 (m, 1H), 1.15 (dd, *J* = 9.2, 4.4 Hz, 1H), 0.95 (dd, *J* = 5.9, 4.8 Hz, 1H). <sup>13</sup>C NMR (DMSO-d<sub>6</sub>, 151 MHz) δ = 158.4, 147.9, 145.4, 143.2, 139.0, 135.8, 132.9, 130.6, 118.2, 115.6, 114.3, 65.4, 63.4, 30.0, 20.1, 18.6, 18.3 HRMS (system B) calculated for C<sub>17</sub>H<sub>18</sub>NO<sub>2</sub> 268.1293, found 268.1331. FTIR (cm<sup>-1</sup>) 2932, 1594, 1460, 1251, 1125, 780. M.P. 176-178 °C.

Chiral purification of 3-(5-(3-Oxabicyclo[4.1.0]heptan-6-yl)pyridin-3-yl)phenol (40)

Total sample dissolved in ethanol (3 mL) and liquid loaded onto the column in 1.5 mL manual injections.

**Column:** Chiralpak IA (30mm x 25cm, 5µm, room temperature)

**Flow Rate:** 30 mL/min

**Detection:** UV Diode Array at 215 nM

**Mobile Phase A:** Heptane

**Mobile Phase B:** Ethanol

**Modifier:** Isopropyl amine.

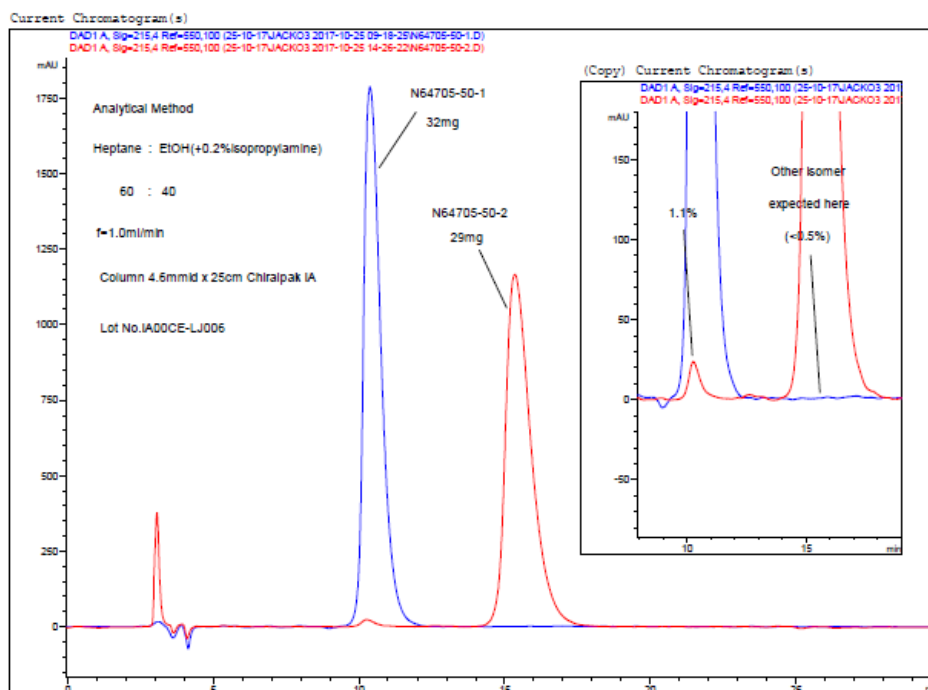
**Isocratic method:** 60:40:0.2 mobile phase A: mobile phase B: modifier

**Runtime:** 30 min.

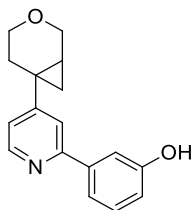
The combined fractions for isomer 1 (**40a**) and isomer 2 (**40a**) were concentrated by a stream of nitrogen to yield. 1<sup>st</sup> eluting isomer (**40a**) (32 mg, 98.9% chirally pure by chiral HPLC analysis) as a white solid ( $\alpha_D^{20}$  (0.5 g/100 mL) = +53.3. Inferred from the X-ray crystal structure of **40b** that **40a** is confirmed by X-ray crystallography to be **3-(5-((1S,6R)-3-oxabicyclo[4.1.0]heptan-6-yl)pyridin-3-yl)phenol**.

2<sup>nd</sup> eluting isomer (**40b**) (29 mg, >99.5% chirally pure by chiral HPLC analysis) as a white solid ( $\alpha_D^{20}$  (1.0 g/100 mL) = -13.3 Confirmed by X-ray crystallography to be **3-(5-((1R,6S)-3-oxabicyclo[4.1.0]heptan-6-yl)pyridin-3-yl)phenol**.

The single enantiomer products were recrystallised from toluene to give material of the required quality for X-ray crystallography.



**Figure 74:** Chiral purification of 3-(5-(3-oxabicyclo[4.1.0]heptan-6-yl)pyridin-3-yl)phenol (**40**)

3-(4-(3-Oxabicyclo[4.1.0]heptan-6-yl)pyridin-2-yl)phenol (41)

In a 2-5 mL Biotage microwave vial a mixture of, 4-(3-oxabicyclo[4.1.0]heptan-6-yl)-2-chloropyridine (200 mg, 0.95 mmol), 3-(4,4,5,5-tetramethyl-1,3,2-dioxaborolan-2-yl)phenol (315 mg, 1.43 mmol), Pd(II)(dppf)Cl<sub>2</sub>.CH<sub>2</sub>Cl<sub>2</sub>(78 mg, 0.10 mmol) and potassium carbonate (264 mg, 1.91 mmol) was dissolved in 2-propanol (3.2 mL) and water (0.64 mL). The resulting suspension was degassed with a stream of nitrogen for 10 min, sealed and stirred at 100 °C for 3 h. The reaction was monitored by LCMS and, upon complete consumption of starting material, the reaction was cooled to r.t. and filtered through a celite cartridge (2.5 g). The resulting mixture was concentrated *in vacuo* and dry-loaded onto Florisil®. The crude reaction mixture was purified by flash column chromatography (cyclohexane: ethyl acetate 0%-100% (15 column volumes)) to give 3-(4-(3-oxabicyclo[4.1.0]heptan-6-yl)pyridin-2-yl)phenol (140 mg, 0.52 mmol, 55% yield) as a white solid. LCMS (formic) rt. 0.56 (100%) MH<sup>+</sup> for desired M= 267.126. <sup>1</sup>H NMR (DMSO-d<sub>6</sub>, 600 MHz) δ = 9.48 (s, 1H), 8.51 (d, *J* = 5.1 Hz, 1H), 7.65 (d, *J* = 1.8 Hz, 1H), 7.51-7.53 (m, 1H), 7.49-7.51 (m, 1H), 7.25-7.29 (m, 1H), 7.19 (dd, *J* = 5.1, 1.8 Hz, 1H), 6.83 (dd, *J* = 8.1, 2.6 Hz, 1H), 3.99 (dd, *J* = 11.4, 4.8 Hz, 1H), 3.83 (dd, *J* = 11.4, 1.1 Hz, 1H), 3.53 (dt, *J* = 11.4, 5.3 Hz, 1H), 3.44 (ddd, *J* = 11.6, 8.3, 5.1 Hz, 1H), 2.18 (dt, *J* = 13.9, 5.3 Hz, 1H), 2.09 (ddd, *J* = 13.9, 8.4, 5.5 Hz, 1H), 1.55-1.59 (m, 1H), 1.17 (dd, *J* = 9.2, 4.8 Hz, 1H), 1.03 ppm (dd, *J* = 6.1, 4.6 Hz, 1H). <sup>13</sup>C NMR (DMSO-d<sub>6</sub>, 151 MHz) δ = 158.1, 157.3, 156.7, 149.8, 140.8, 130.0, 120.4, 117.9, 116.4, 114.0, 65.3, 63.4, 28.4, 21.1, 20.2, 20.2 ppm (1C not observed.) HRMS (system A) calculated for C<sub>17</sub>H<sub>17</sub>NO<sub>2</sub> 268.1332, found 268.1327. FTIR (cm<sup>-1</sup>) 3062, 1604, 1581, 1350, 1220, 1127, 866, 787. M.P. 140-142°C

Chiral purification of 3-(4-(3-oxabicyclo[4.1.0]heptan-6-yl)pyridin-2-yl)phenol (41)

Total sample dissolved in ethanol (7 mL) and liquid loaded onto the column in 0.5 mL manual injections.

**Column:** Chiralpak IF5 (250x30mm, room temp.)

**Flow Rate:** 42.5mL/min (60bar)

**Detection:** UV Diode Array at 280 nM

**Mobile Phase A:** Heptane

**Mobile Phase B:** Ethanol

**Modifier:** Isopropyl amine

**Isocratic method:** 90:10:0.2 mobile phase A: mobile phase B: modifier

**Runtime:** 25 min

The combined fractions for isomer 1 (**41a**) and isomer 2 (**41b**) were concentrated by a stream of nitrogen to yield. 1<sup>st</sup> eluting isomer (**41a**) (57 mg, 99.2% chirally pure by UV) as a white solid ( $\alpha_D^{20}$  (0.22 g/100 mL) = +36.4. Inferred from the X-ray crystal structure of **41b** that **41a** is 3-(4-((1*S*,6*R*)-3-oxabicyclo[4.1.0]heptan-6-yl)pyridin-2-yl)phenol.

2<sup>nd</sup> eluting isomer (**41b**) (60 mg, 95% chirally pure by UV) ( $\alpha_D^{20}$  (0.2 g/100 mL) = -40.0. Confirmed by X-ray crystallography to be 3-(4-((1*R*,6*S*)-3-oxabicyclo[4.1.0]heptan-6-yl)pyridin-2-yl)phenol.

The single enantiomer products were recrystallised from toluene to give material of the required quality for X-ray crystallography.

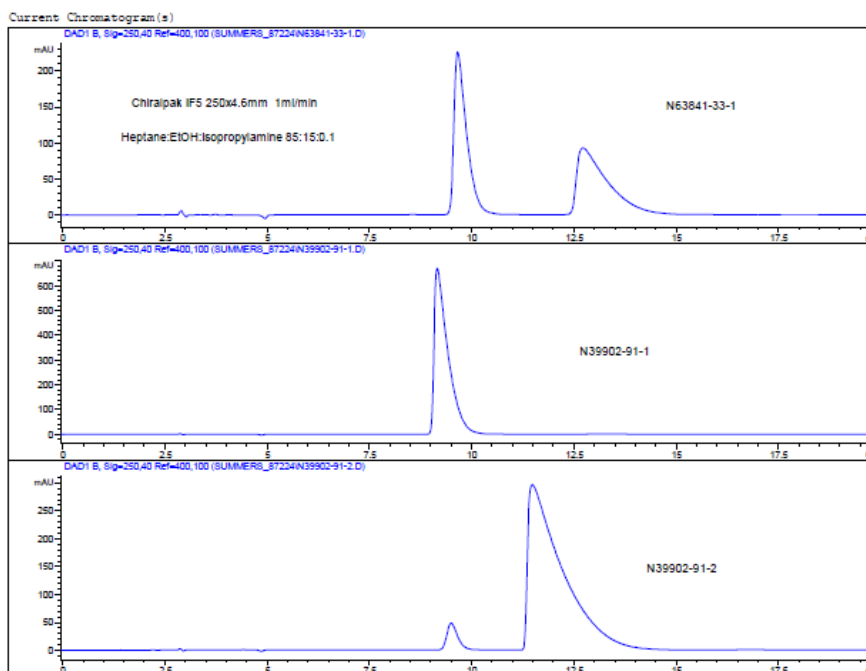
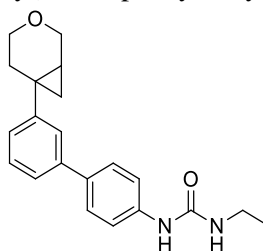


**Figure 75:** Chiral purification of 3-(4-(3-oxabicyclo[4.1.0]heptan-6-yl)pyridin-2-yl)phenol (**41**)

1-(3'-(3-Oxabicyclo[4.1.0]heptan-6-yl)[1,1'biphenyl]-4-yl)-3-ethylurea (**42**)



In a 2-5 mL Biotage microwave vial a mixture of 6-(3-chlorophenyl)-3-oxabicyclo[4.1.0]heptane (250 mg, 1.20 mmol), 1-ethyl-3-(4-(4,4,5,5-tetramethyl-1,3,2-dioxaborolan-2-yl)phenyl)urea (521 mg, 1.80 mmol), Pd(dppf)Cl<sub>2</sub>·CH<sub>2</sub>Cl<sub>2</sub> (98 mg, 0.12 mmol) and potassium carbonate (331 mg, 2.40 mmol) was dissolved in 2-propanol (3.9 mL) and water

(0.79 mL). The resulting suspension was degassed with a stream of nitrogen for 10 min, sealed and stirred at 100 °C for 3 h. The reaction was monitored by LCMS and, upon complete consumption of starting material, the reaction was cooled to r.t. and filtered through a celite cartridge (2.5 g). The resulting mixture was concentrated *in vacuo* and dry-loaded onto Florisil®. The crude reaction mixture was purified by flash column chromatography (cyclohexane: ethyl acetate 0-100% (15 column volumes)) to give 1-(3'-(3-oxabicyclo[4.1.0]heptan-6-yl)[1,1'biphenyl]-4-yl)-3-ethylurea (150 mg, 0.45 mmol, 37% yield) as an off white solid. LCMS (formic) rt. 1.09 (100%) MH<sup>+</sup> for desired M= 336.184. <sup>1</sup>H NMR (DMSO-d<sub>6</sub>, 600 MHz) δ = 8.51 (s, 1H), 7.54 (d, *J* = 8.8 Hz, 2H), 7.48 (d, *J* = 8.8 Hz, 2H), 7.46 (s, 1H), 7.41 (d, *J* = 7.7 Hz, 1H), 7.34 (t, *J* = 7.7 Hz, 1H), 7.20 (d, *J* = 7.7 Hz, 1H), 6.12 (br t, *J* = 5.3 Hz, 1H), 4.02 (dd, *J* = 11.2, 4.6 Hz, 1H), 3.82 (d, *J* = 11.0 Hz, 1H), 3.49 (dt, *J* = 11.4, 5.1 Hz, 1H), 3.42 (ddd, *J* = 11.7, 8.4, 5.5 Hz, 1H), 3.10-3.16 (m, 2H), 2.31 (s, 1H), 2.09 (ddd, *J* = 13.9, 8.1, 5.9 Hz, 1H), 2.02 (dt, *J* = 13.9, 5.9 Hz, 1H), 1.38-1.44 (m, 1H), 1.01-1.13 (m, 4H), 0.87-0.92 ppm (m, 1H). <sup>13</sup>C NMR (DMSO-d<sub>6</sub>, 151 MHz) δ = 155.5, 148.5, 140.6, 133.3, 129.3, 128.7, 127.4, 125.7, 125.0, 124.0, 118.4, 65.6, 63.6, 34.4, 30.7, 22.3, 18.8, 18.6, 15.9 ppm. HRMS (system B) calculated for C<sub>21</sub>H<sub>24</sub>N<sub>2</sub>O<sub>2</sub> 377.1871, found 377.1915. FTIR (cm<sup>-1</sup>) 3322, 2965, 1646, 1546, 1232, 908, 836. M.P. 198-200 °C

Chiral purification of 1-(3'-(3-oxabicyclo[4.1.0]heptan-6-yl)[1,1'biphenyl]-4-yl)-3-ethylurea (42)

Total sample dissolved in ethanol (7.5 mL) and liquid loaded onto the column in 0.5 mL manual injections.

**Column:** Chiralpak ID5 (250x30mm room temp.)

**Flow Rate:** 42.5 mL/min (69bar)

**Detection:** UV Diode Array at 280nm

**Mobile Phase A:** Heptane

**Mobile Phase B:** Ethanol

**Modifier:** Isopropyl amine

**Isocratic method:** 85:15:0.2 mobile phase A: mobile phase B: modifier

**Runtime:** 20 min

The combined fractions for isomer 1 (**42a**) and isomer 2 (**42b**) were concentrated by a stream of nitrogen to yield. 1<sup>st</sup> eluting isomer (**42a**) (59 mg, >99.9% chirally pure by chiral HPLC analysis) as a white solid ( $\alpha_D^{20}$  (0.5 g/100 mL) = -16.0. Inferred from the X-ray crystal structure of **42b** that **42a** is 1-(3'-((1*R*,6*S*)-3-oxabicyclo[4.1.0]heptan-6-yl)-[1,1'-biphenyl]-4-yl)-3-ethylurea.

2<sup>nd</sup> eluting isomer (**42b**) (67 mg, 97.3% chirally pure by chiral HPLC analysis) ( $\alpha_D^{20}$  (0.5 g/100 mL) = +16.0, confirmed by X-ray crystallography to be **1-(3'-((1S,6R)-3-oxabicyclo[4.1.0]heptan-6-yl)-[1,1'-biphenyl]-4-yl)-3-ethylurea**.

The single enantiomer products were recrystallised from toluene to give material of the required quality for X-ray crystallography

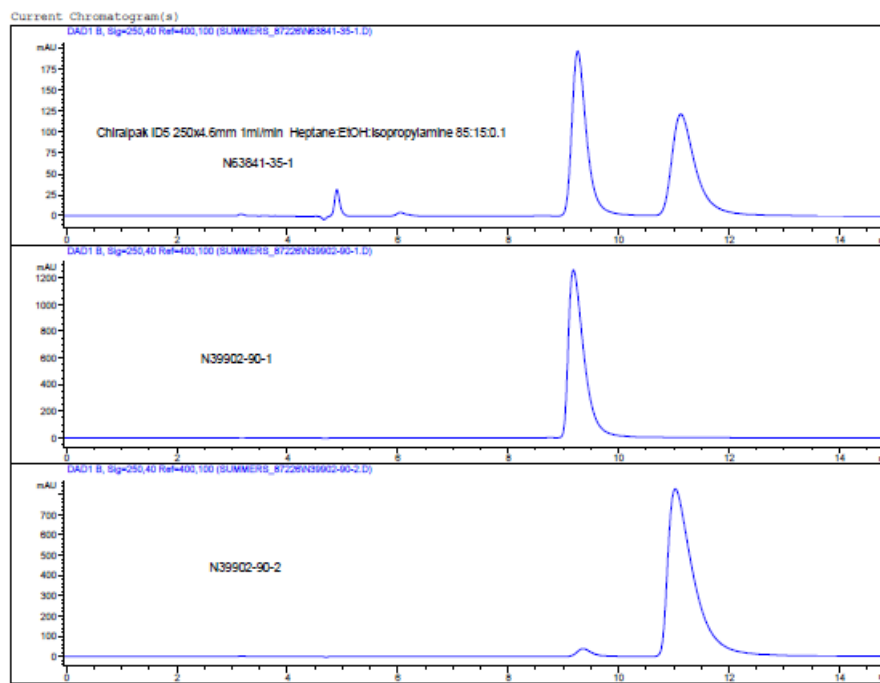
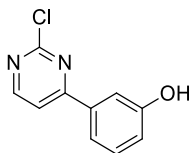


**Figure 76:** Chiral purification of 1-(3'-((3-oxabicyclo[4.1.0]heptan-6-yl)[1,1'-biphenyl]-4-yl)-3-ethylurea (**42**)

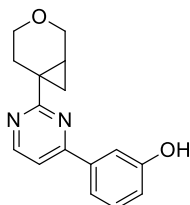
3-(2-Chloropyrimidin-4-yl)phenol (**55**)<sup>257</sup>



In a 10-20 mL Biotage microwave vial a mixture of 3-(4,4,5,5-tetramethyl-1,3,2-dioxaborolan-2-yl)phenol (1.66 g, 7.55 mmol) 2,4-dichloropyrimidine (750 mg, 5.03 mmol), potassium carbonate (1.39 g, 10.1 mmol) and Pd(dppf)Cl<sub>2</sub>.CH<sub>2</sub>Cl<sub>2</sub> (411mg, 0.50 mmol) was dissolved in 2-propanol (16.7 mL) and water (3.3 mL). The resulting suspension was degassed with a stream of nitrogen for 10 min, sealed and stirred at 100 °C for 3 h. The reaction was monitored by LCMS and, upon complete consumption of starting material, the reaction was cooled to r.t. and filtered through a celite cartridge (2.5 g). The resulting mixture was concentrated *in vacuo* and dry-loaded onto Florisil<sup>®</sup>. The crude reaction mixture was purified by flash column chromatography (cyclohexane: ethyl acetate 0-100% (15 column volumes))

to give 3-(2-chloropyrimidin-4-yl)phenol (230 mg, 1.00 mmol, 20% yield). LCMS (formic) rt. 0.85 (90%) MH<sup>+</sup> for desired M= 206.025. <sup>1</sup>H NMR (400 MHz, DMSO-d<sub>6</sub>) δ = 9.77 (br., s, 1H), 8.79 (d, *J* = 5.1 Hz, 1H), 8.06 (d, *J* = 5.1 Hz, 1H), 7.65 - 7.58 (m, 2H), 7.37 (t, *J* = 8.1 Hz, 1H), 7.00 (ddd, *J* = 0.7, 2.2, 8.1 Hz, 1H).

3-(2-(3-Oxabicyclo[4.1.0]heptan-6-yl)pyrimidin-4-yl)phenol (39)



In a 10-20 mL Biotage microwave vial a mixture of potassium 3-oxabicyclo[4.1.0]heptan-6-yltrifluoroborate (224 mg, 1.10 mmol), 3-(2-chloropyrimidin-4-yl)phenol (210 mg, 0.92 mmol), caesium carbonate (596 mg, 1.83 mmol), palladium(II) acetate (33 mg, 0.15 mmol) and cataCXium® A (105 mg, 0.29 mmol) was dissolved in toluene (4.2 mL) and water (0.42 mL). The resulting suspension was degassed with a stream of nitrogen for 10 min, sealed and stirred at 100 °C for 3 h. The reaction was monitored by LCMS and, upon complete consumption of starting material, the reaction was cooled to r.t. and filtered through a celite cartridge (2.5 g). The resulting mixture was concentrated *in vacuo* and dry-loaded onto Florisil®. The crude reaction mixture was purified by flash column chromatography (cyclohexane: ethyl acetate 0-100% (15 column volumes)) to give 3-(2-(3-oxabicyclo[4.1.0]heptan-6-yl)pyrimidin-4-yl)phenol (52 mg, 0.19 mmol, 21% yield) as a white solid. LCMS (formic) rt. 0.94 (100%) MH<sup>+</sup> for desired M= 268.121. <sup>1</sup>H NMR (DMSO-d<sub>6</sub>, 400 MHz) δ = 9.67 (s, 1H), 8.72 (d, *J* = 5.4 Hz, 1H), 7.71 (d, *J* = 5.4 Hz, 1H), 7.62-7.65 (m, 1H), 7.58-7.61 (m, 1H), 7.30-7.37 (m, 1H), 6.94 (ddd, *J* = 8.1, 2.4, 1.0 Hz, 1H), 3.91 (dd, *J* = 11.5, 2.0 Hz, 1H), 3.88 (dd, *J* = 11.5, 3.7 Hz, 1H), 3.65 (ddd, *J* = 11.4, 5.9, 3.9 Hz, 1H), 3.30 (ddd, *J* = 11.2, 10.3, 5.1 Hz, 2H), 3.16 (dt, *J* = 14.4, 4.3 Hz, 1H), 1.94 (ddd, *J* = 14.4, 10.0, 6.0 Hz, 1H), 1.76-1.87 (m, 1H), 1.57 (dd, *J* = 9.0, 3.2 Hz, 1H), 1.09 ppm (dd, *J* = 6.4, 3.4 Hz, 1H). <sup>13</sup>C NMR (DMSO-d<sub>6</sub>, 101 MHz) δ = 172.1, 162.7, 158.4, 158.3, 138.2, 130.4, 118.5, 118.2, 114.0, 113.6, 65.0, 64.0, 25.0, 23.7, 23.5, 22.7 ppm. HRMS. (System B) calculated for C<sub>16</sub>H<sub>16</sub>N<sub>2</sub>O<sub>2</sub> 269.1290, found 269.1292. FTIR (cm<sup>-1</sup>) 3256, 2924, 1569, 1434, 1121, 731. M.P 125-127 °C

Chiral purification of 3-(2-(3-oxabicyclo[4.1.0]heptan-6-yl)pyrimidin-4-yl)phenol (39)

Total sample dissolved in ethanol (2 mL) and liquid loaded onto the column in 1 mL manual injections.

**Column:** Chiralpak AD-H 25x30mm (Room Temp)

**Flow Rate:** 30 mL/min

**Detection:** UV Diode Array at 215nm

**Mobile Phase A:** Heptane

**Mobile Phase B:** Ethanol

**Modifier:** None

**Isocratic method:** 90:10:0.2 mobile phase A: mobile phase B: modifier

**Runtime:** 45 min.

The combined fractions for isomer 1 (**39a**) and isomer 2 (**39b**) were concentrated by a stream of nitrogen to yield; 1<sup>st</sup> eluting isomer (**39a**) (14 mg, 96.5% chirally pure by chiral HPLC analysis)  $\alpha_D^{20} = -60.0$  (0.2 g/100 mL). Inferred from the X-ray crystal structure of **39b** that **39a** is **3-(2-((1*R*,6*S*)-3-oxabicyclo[4.1.0]heptan-6-yl)pyrimidin-4-yl)phenol**.

2<sup>nd</sup> eluting isomer (**39b**) (15 mg, >99.5% chirally pure by chiral HPLC analysis) as a white solid  $\alpha_D^{20} = +34.8$  (0.23 g/100 mL) confirmed by X-ray crystallography to be **3-(2-((1*S*,6*R*)-3-oxabicyclo[4.1.0]heptan-6-yl)pyrimidin-4-yl)phenol**.

Single enantiomer products were recrystallised from toluene to give material of the required quality for X-ray crystallography.

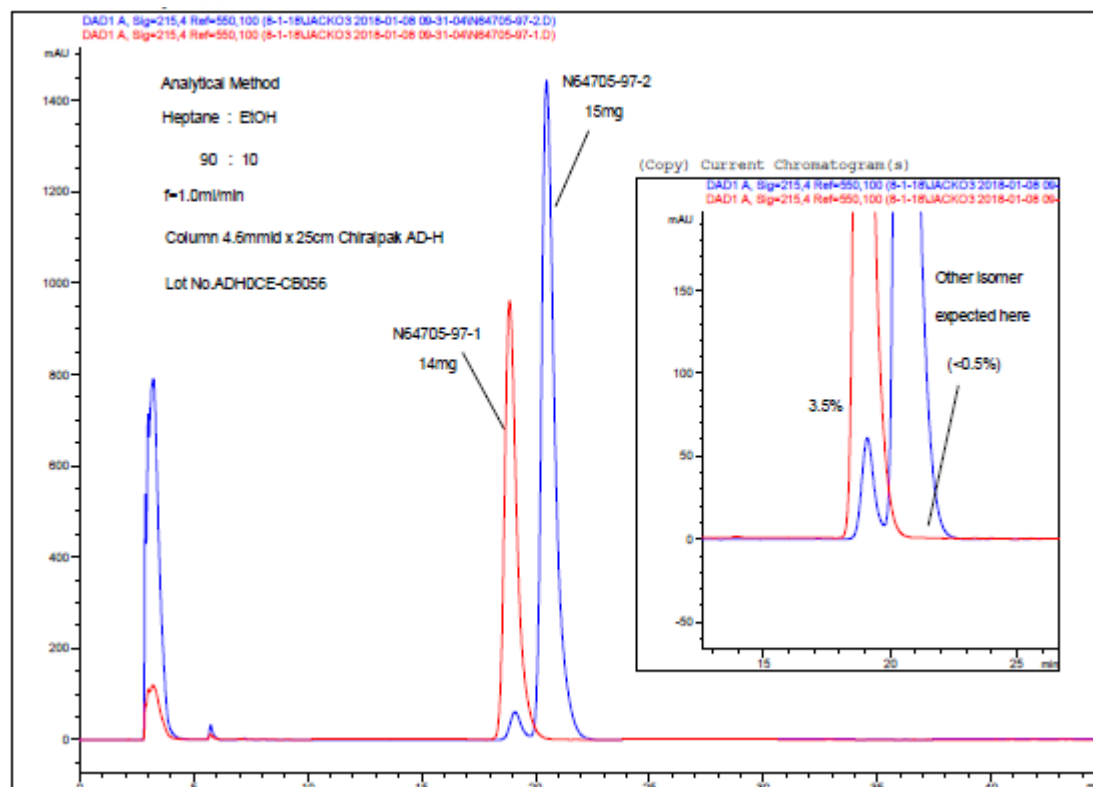


**Figure 77:** Chiral purification of 3-(2-(3-oxabicyclo[4.1.0]heptan-6-yl)pyrimidin-4-yl)phenol (**39**)

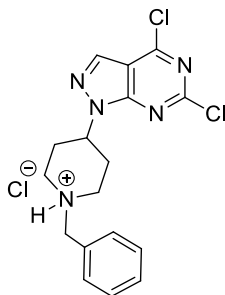


### 3.3 Pyrazolopyrimidine Compounds

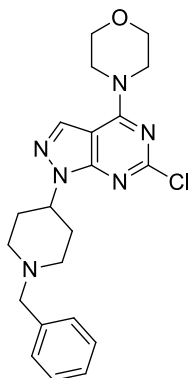
#### 3.3.1 Literature Matched Pair Compounds

1-(1-Benzylpiperidin-4-yl)-4,6-dichloro-1*H*-pyrazolo[3,4-*d*]pyrimidine Hydrochloride

**(175)**<sup>172</sup>

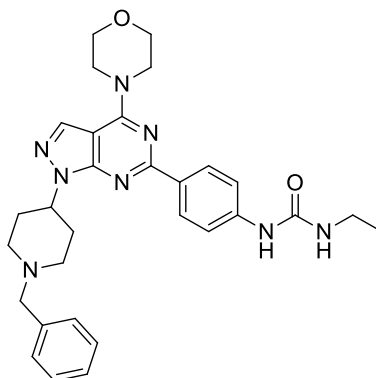


In a 150 mL RBF 2,4,6-trichloropyrimidine-5-carbaldehyde (1.33 g, 6.29 mmol) was dissolved in EtOH (30 mL) and the resulting solution was cooled to -78 °C. 1-benzyl-4-hydrazinylpiperidine dihydrochloride (1.75 g, 6.29 mmol) was added and the reaction was stirred at -78 °C for 0.5 h before warming to 0 °C. The reaction was stirred at 0 °C for a further 1.5 h. The reaction was quenched with sodium bicarbonate (50 mL) and warmed to r.t. The resulting mixture was extracted with DCM (3 x 50 mL). The combined organic layers were dried (hydrophobic frit) and concentrated *in vacuo* using a rotary evaporator with the water bath set to r.t. (product is reported to be unstable when heating to 40 °C). The resulting orange oil was dissolved in MeOH (5 mL) and cooled to 0 °C. HCl (4M in dioxane, 5 mL) was added dropwise. The product was concentrated and triturated with diethyl ether. The product was left under diethyl ether in the freezer for 16 h before being filtered to give 1-(1-benzylpiperidin-4-yl)-4,6-dichloro-1*H*-pyrazolo[3,4-*d*]pyrimidine Hydrochloride (3.22 g, 6.06 mmol, 96 % yield) as a pale orange solid LCMS (formic) rt. 0.63 (92%) MH<sup>+</sup> for desired M= 361.086. <sup>1</sup>H NMR (400 MHz, DMSO-*d*<sub>6</sub>) δ = 8.59 (s, 1H), 7.69 (dd, *J* = 6.4, 2.9 Hz, 2H), 7.28-7.53 (m, 3H), 4.95-5.12 (m, 1H), 4.32 (d, *J* = 5.04 Hz, 2H), 3.45 (br. s., 2H), 3.19-3.34 (m, 2H), 2.53-2.70 (m, 2H), 2.16 (d, *J* = 12.8 Hz, 2H).

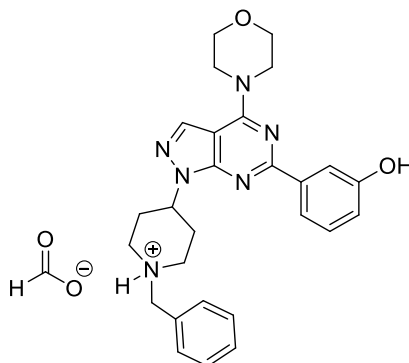
4-(1-(1-Benzylpiperidin-4-yl)-6-chloro-1H-pyrazolo[3,4-d]pyrimidin-4-yl)morpholine(176)<sup>258</sup>

In a 10-20 mL microwave vial 1-(1-benzylpiperidin-4-yl)-4,6-dichloro-1H-pyrazolo[3,4-d]pyrimidine Hydrochloride (1.60 g, 3.01 mmol) was dissolved in EtOH (10.4 mL). Morpholine (0.26 mL, 3.01 mmol) and triethylamine (2.1 mL, 15.1 mmol) were added and the reaction mixture was stirred at r.t. for 1 h. The reaction was monitored by LCMS and upon complete consumption of starting material the reaction was concentrated *in vacuo* and partitioned between ethyl acetate (20 mL) and sodium bicarbonate. The aqueous layer was extracted with further ethyl acetate (3x 10 mL). The combined organic layers were concentrated *in vacuo* to give an orange solid. This crude solid was triturated in cold diethyl ether and filtered under vacuum to give 4-(1-(1-benzylpiperidin-4-yl)-6-chloro-1H-pyrazolo[3,4-d]pyrimidin-4-yl)morpholine (889 mg, 2.13 mmol, 71% yield) as a pale orange amorphous solid. LCMS (formic) rt. 0.63 (97%) MH<sup>+</sup> for desired M= 412.178. <sup>1</sup>H NMR (DMSO-d<sub>6</sub>, 400 MHz) δ = 8.33 (s, 1H), 7.34 (d, *J* = 4.4 Hz, 4H), 7.21-7.29 (m, 1H), 4.48-4.66 (m, 1H), 3.81-3.97 (m, 4H), 3.74 (br t, *J* = 4.6 Hz, 4H), 3.31 (s, 1H), 2.93 (br d, *J* = 9.3 Hz, 2H), 2.04-2.24 (m, 4H), 1.76-1.92 ppm (m, 2H). <sup>13</sup>C NMR (101 MHz, DMSO-d<sub>6</sub>) δ = 157.2, 156.7, 154.5, 139.0, 133.8, 129.1, 128.6, 127.3, 99.3, 66.2, 62.4, 54.5, 52.5, 31.4 (1C not observed). HRMS calculated for C<sub>21</sub>H<sub>26</sub>ClN<sub>6</sub>O 413.1858, found 413.1853. FTIR (cm<sup>-1</sup>) 1570, 1445, 1308, 1117, 992, 945, 777, 732.

1-(4-(1-(1-Benzylpiperidin-4-yl)-4-morpholino-1H-pyrazolo[3,4-d]pyrimidin-6-yl)phenyl)-3-ethylurea (161)<sup>258</sup>

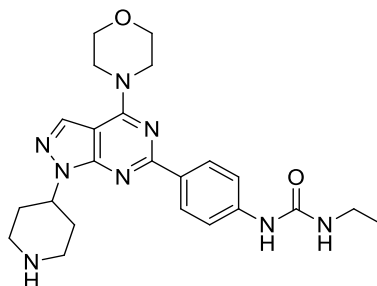


In a 10-20 mL microwave vial a mixture of 4-(1-(1-benzylpiperidin-4-yl)-6-chloro-1H-pyrazolo[3,4-d]pyrimidin-4-yl)morpholine (200 mg, 0.48 mmol), 1-ethyl-3-(4-(4,4,5,5-tetramethyl-1,3,2-dioxaborolan-2-yl)phenyl)urea (232 mg, 0.80 mmol), Pd(PPh<sub>3</sub>)<sub>4</sub> (56 mg, 0.05 mmol) and sodium carbonate (103 mg, 0.97 mmol) was dissolved in DME (8 mL) and water (1 mL). The resulting suspension was degassed with a stream of nitrogen for 10 min, sealed and irradiated in a Biotage initiator+ microwave at 150 °C for 1 h. The reaction was monitored by LCMS and, upon complete consumption of starting material, the reaction was cooled to r.t. and filtered through a celite cartridge (10 g). The resulting mixture was concentrated *in vacuo* the reaction mixture was purified by Mass Directed Auto Purification (MDAP) (formic, Method 2) to give 1-(4-(1-(1-benzylpiperidin-4-yl)-4-morpholino-1H-pyrazolo[3,4-d]pyrimidin-6-yl)phenyl)-3-ethylurea (86 mg, 0.16 mmol, 33% yield) as a golden amorphous solid. LCMS (formic) rt. 0.69 (100%) MH<sup>+</sup> for desired M= 540.296. <sup>1</sup>H NMR (400 MHz, DMSO-d<sub>6</sub>) δ = 8.69 (s, 1H), 8.31 (d, *J* = 8.8 Hz, 2H), 8.26 (s, 1H), 8.14 (s, 1H), 7.51 (d, *J* = 8.8 Hz, 2H), 7.34-7.40 (m, 4H), 7.30 (dd, *J* = 2.9, 5.9 Hz, 1H), 6.17 (t, *J* = 5.6 Hz, 1H), 4.82 (br. s., 1H), 3.99 (d, *J* = 4.7 Hz, 4H), 3.79 (t, *J* = 4.7 Hz, 4H), 3.64 (s, 2H), 3.09-3.18 (m, 2H), 3.02 (d, *J*=11.0 Hz, 2H), 2.12-2.38 (m, 4H), 1.85-2.00 (m, 2H), 1.08 (t, *J* = 7.2 Hz, 3H). <sup>13</sup>C NMR (DMSO-d<sub>6</sub>, 101 MHz) δ = 163.4, 159.9, 157.1, 155.4, 155.1, 143.3, 129.5, 129.3, 128.7, 127.6, 117.3, 99.0, 66.4, 62.1, 52.4, 34.4, 31.3, 15.9 (4C not observed). HRMS calculated for C<sub>30</sub>H<sub>25</sub>N<sub>8</sub>O<sub>2</sub> 541.2961, found 541.3036. FTIR (cm<sup>-1</sup>) 3306, 1541, 1389, 1224, 940.

3-(1-(1-Benzylpiperidin-4-yl)-4-morpholino-1H-pyrazolo[3,4-d]pyrimidin-6-yl)phenolFormic acid salt (84)

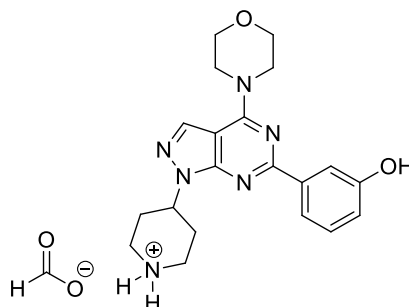
In a 10-20 mL microwave vial a mixture of 4-(1-(1-benzylpiperidin-4-yl)-6-chloro-1H-pyrazolo[3,4-d]pyrimidin-4-yl)morpholine (200 mg, 0.48 mmol), 3-(4,4,5,5-tetramethyl-1,3,2-dioxaborolan-2-yl)phenol (176 mg, 0.80 mmol), Pd(PPh<sub>3</sub>)<sub>4</sub> (56 mg, 0.05 mmol) and sodium carbonate was dissolved in DME (8 mL) and water (1 mL). The resulting suspension was degassed with a stream of nitrogen for 10 min, sealed and irradiated in a Biotage initiator+ microwave at 100 °C for 1.5 h. The reaction was monitored by LCMS and, upon complete consumption of starting material, the reaction was cooled to r.t. and filtered through a celite cartridge (10 g). The resulting mixture was concentrated *in vacuo* and dissolved in MeOH. The crude reaction mixture was purified by reverse phase column chromatography (formic, 5-55%, (12 column volumes)) to give 3-(1-(1-benzylpiperidin-4-yl)-4-morpholino-1H-pyrazolo[3,4-d]pyrimidin-6-yl)phenol Formic acid salt (172 mg, 0.33 mmol, 69% yield) as an amorphous yellow solid. LCMS rt. 0.69 (97%) MH<sup>+</sup> for desired M= 470.243. <sup>1</sup>H NMR (400 MHz, DMSO-d<sub>6</sub>) δ = 8.30 (s, 1H), 8.16 (s, 1H), 7.73-7.95 (m, 2H), 7.15-7.41 (m, 6H), 6.55-6.92 (m, 1H), 4.61-4.94 (m, 1H), 3.92-4.15 (m, 4H), 3.72-3.86 (m, 4H), 3.00 (d, *J* = 8.8 Hz, 2H), 2.08-2.35 (m, 4H), 1.80-2.03 (m, 2H). <sup>13</sup>C NMR (101 MHz, DMSO-d<sub>6</sub>) δ = 159.9, 157.8, 157.1, 154.9, 139.8, 138.7, 133.2, 129.6, 129.3, 128.7, 127.4, 119.5, 117.8, 115.4, 99.4, 66.4, 62.3, 54.1, 52.6, 31.4. HRMS (system B) calculated for C<sub>27</sub>H<sub>31</sub>N<sub>2</sub>O<sub>6</sub> 471.2508, found 471.2508. FTIR (cm<sup>-1</sup>) 1557, 1439, 1236, 1114, 784, 735, 696.

1-Ethyl-3-(4-(4-morpholino-1-(piperidin-4-yl)-1H-pyrazolo[3,4-d]pyrimidin-6-yl)phenyl)urea (163)<sup>258</sup>



In one chamber of a COware apparatus 1-(4-(1-(1-benzylpiperidin-4-yl)-4-morpholino-1H-pyrazolo[3,4-d]pyrimidin-6-yl)phenyl)-3-ethylurea (75 mg, 0.14 mmol) and Pd/C (5%) (1.5 mg, 0.01 mmol) were dissolved in EtOH (3 mL). To the other chamber zinc powder (181 mg, 2.27 mmol) and HCl (4M) (0.12 mL, 3.38 mmol) were added and the CO-ware apparatus was sealed. The reaction was stirred at r.t. for 24 h. The reaction mixture was filtered through celite (2.5g) and concentrated *in vacuo*. The resulting residue was dissolved in MeOH and passed through an SCX column eluting with ammonia in MeOH (4M) to give 1-ethyl-3-(4-(4-morpholino-1-(piperidin-4-yl)-1H-pyrazolo[3,4-d]pyrimidin-6-yl)phenyl)urea (30 mg, 0.067 mmol, 48% yield) as an amorphous white solid. LCMS (formic) rt. 0.57 (95%) MH<sup>+</sup> for desired M=450.249. <sup>1</sup>H NMR (400 MHz, MeOD)  $\delta$  = 8.26-8.51 (m, 2H), 8.13 (s, 1H), 7.15-7.70 (m, 2H), 4.98 (s, 1H), 4.01-4.19 (m, 4H), 3.76-3.92 (m, 4H), 3.17-3.30 (m, 4H), 2.87 (dt,  $J$  = 12.6, 2.2 Hz, 2H), 2.26 (dd,  $J$  = 12.2, 3.9 Hz, 2H), 2.01 (d,  $J$  = 10.27 Hz, 2H), 1.19 (t,  $J$  = 7.21 Hz, 3H). <sup>13</sup>C NMR (101 MHz, MeOD)  $\delta$  = 160.5, 157.1, 156.6, 154.9, 142.0, 132.3, 132.0, 128.9, 117.6, 98.9, 66.3, 54.1, 45.4, 44.9, 34.3, 31.7, 14.2 (4C not observed).

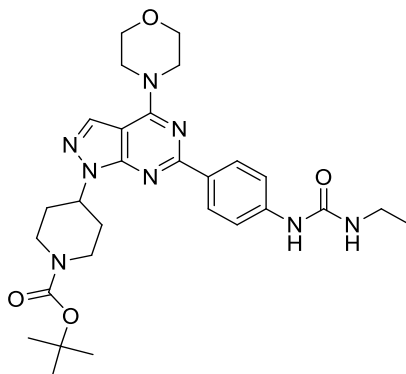
3-(4-Morpholino-1-(piperidin-4-yl)-1H-pyrazolo[3,4-d]pyrimidin-6-yl)phenol Formic acid salt (83)



In one chamber of a CO-ware apparatus 3-(1-(1-benzylpiperidin-4-yl)-4-morpholino-1H-pyrazolo[3,4-d]pyrimidin-6-yl)phenol Formic acid salt (100 mg, 0.21 mmol) and Pd/C (5%) (2.3 mg, 0.02 mmol) were dissolved in EtOH (4 mL). To the other chamber zinc powder (278

mg, 4.25 mmol) and HCl (4M) (0.18 mL, 5.95 mmol) were added and the CO-ware apparatus was sealed. The reaction was stirred at r.t. for 24 h. The reaction mixture was filtered through celite (2.5g) and concentrated *in vacuo* and the resulting residue was purified by Mass Directed Auto Purification (MDAP) (formic, method B) to give 3-(4-morpholino-1-(piperidin-4-yl)-1*H*-pyrazolo[3,4-*d*]pyrimidin-6-yl)phenol Formic acid salt (30 mg, 0.07 mmol, 33% yield) as an amorphous white solid. LCMS (formic) 0.56 (100%) MH<sup>+</sup> for desired M= 380.156. <sup>1</sup>H NMR (400 MHz, DMSO-*d*<sub>6</sub>) δ = 8.36 (s, 1H), 8.31 (s, 1H), 7.84-7.95 (m, 2H), 7.27 (t, *J* = 8.0 Hz, 1H), 6.80-6.95 (m, 1H), 4.97 (ddd, *J* = 11.4, 7.5, 4.2 Hz, 1H), 4.01 (t, *J* = 4.5 Hz, 4H), 3.70-3.85 (m, 4H), 3.29 (d, *J* = 12.5 Hz, 2H), 2.83-3.06 (m, 2H), 2.26 (dq, *J* = 12.3, 3.8 Hz, 2H), 1.98 (d, *J* = 10.5 Hz, 2H). <sup>13</sup>C NMR (101 MHz, DMSO-*d*<sub>6</sub>) δ = 157.9, 145.9, 133.4, 129.6, 129.6, 119.5, 117.9, 115.5, 99.4, 94.2, 87.9, 66.4, 55.4, 53.3, 44.2, 30.5. HRMS (system B) calculated for C<sub>20</sub>H<sub>25</sub>N<sub>6</sub>O<sub>2</sub> 381.2039, found 381.2034. FTIR (cm<sup>-1</sup>) 1561, 1443, 1391. 1002, 894, 785.

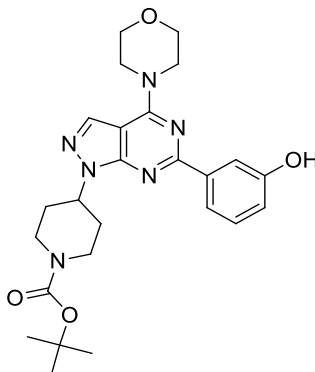
*tert*-Butyl-4-(6-(3-ethylureido)phenyl)-4-morpholino-1*H*-pyrazolo[3,4-*d*]pyrimidin-1-yl)piperidine-1-carboxylate (**165**)<sup>258</sup>



In a 0.5-2 mL microwave vial 1-ethyl-3-(4-(4-morpholino-1-(piperidin-4-yl)-1*H*-pyrazolo[3,4-*d*]pyrimidin-6-yl)phenyl)urea (10 mg, 0.02 mmol) was dissolved in DCM (0.5 mL) before triethylamine (10 μL, 0.07 mmol) and Boc-anhydride (6 μL, 0.03 mmol) were added. The reaction was sealed and stirred at r.t. for 2 h. The reaction mixture was concentrated by blown nitrogen and dissolved in MeOH. The crude reaction mixture was purified by Mass Directed Auto Purification (MDAP) (formic, method D) to give *tert*-butyl 4-(6-(3-ethylureido)phenyl)-4-morpholino-1*H*-pyrazolo[3,4-*d*]pyrimidin-1-yl)piperidine-1-carboxylate (5 mg, 9.3 μmol, 42% yield) as an amorphous white solid. LCMS (formic) rt. 1.20 (100%) MH<sup>+</sup> for desired M= 550.302. <sup>1</sup>H NMR (MeOD, 400 MHz) δ = 8.37 (d, *J* = 8.8 Hz, 2H), 8.13 (s, 1H), 7.47 (d, *J* = 8.8 Hz, 2H), 5.06 (tt, *J* = 11.5, 4.2 Hz, 1H), 4.23-4.33 (m, 2H), 4.02-4.10 (m, 4H), 3.83-3.92 (m, 4H), 3.27 (q, *J* = 7.6 Hz, 2H), 2.97-3.17 (m, 2H), 2.21 (qd, *J* = 12.3, 4.3 Hz, 2H), 1.94-2.06 (m, 2H), 1.53 (s, 9H), 1.19 ppm (t, *J* = 7.2 Hz, 3H).

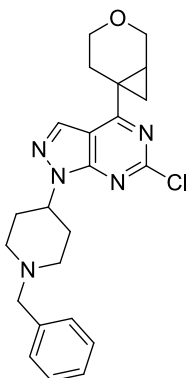
$^{13}\text{C}$  NMR (101 MHz, MeOD)  $\delta$  = 160.6, 157.1, 156.6, 155.1, 155.0, 142.0, 132.5, 131.9, 128.9, 117.5, 99.0, 79.9, 66.3, 54.0, 45.4, 34.3, 30.8, 27.3, 14.3 (1C not observed). HRMS (system B) calculated for  $\text{C}_{28}\text{H}_{39}\text{N}_8\text{O}_4$  551.3094, found 551.3088.

*tert*-Butyl-4-(6-(3-hydroxyphenyl)-4-morpholino-1*H*-pyrazolo[3,4-*d*]pyrimidin-1-yl)piperidine-1-carboxylate (169)



In a 0.5-2 mL microwave vial 3-(4-morpholino-1-(piperidin-4-yl)-1*H*-pyrazolo[3,4-*d*]pyrimidin-6-yl)phenol (17 mg, 0.04 mmol) was dissolved in DCM (0.5 mL) before triethylamine (18  $\mu\text{L}$ , 0.13 mmol) and Boc-anhydride (12  $\mu\text{L}$ , 0.05 mmol) were added. The reaction was sealed and stirred at r.t. for 2 h. The reaction mixture was concentrated by blown nitrogen and dissolved in MeOH. The crude reaction mixture was purified by Mass Directed Auto Purification (MDAP) (formic, method D) to give *tert*-butyl-4-(6-(3-hydroxyphenyl)-4-morpholino-1*H*-pyrazolo[3,4-*d*]pyrimidin-1-yl)piperidine-1-carboxylate (9 mg, 0.02 mmol, 44% yield). LCMS (formic) rt. 1.24 (99%)  $\text{MH}^+$  for desired  $\text{M} = 480.249$ .  $^1\text{H}$  NMR (MeOD, 400 MHz)  $\delta$  = 10.33 (br., s, 1H), 9.11 (s, 1H), 8.66-8.72 (m, 2H), 8.08 (t,  $J = 7.9$  Hz, 1H), 7.69 (ddd,  $J = 8.0, 2.5, 1.0$  Hz, 1H), 5.80 (tt,  $J = 11.3, 4.2$  Hz, 1H), 4.87-5.00 (m, 2H), 4.78-4.84 (m, 4H), 4.56-4.66 (m, 4H), 3.85 (br s, 2H), 2.70-2.90 (m, 4H), 2.26 (s, 9H).  $^{13}\text{C}$  NMR (MeOD, 101 MHz)  $\delta$  = 160.8, 158.6, 157.9, 155.7, 155.2, 140.6, 134.1, 130.4, 120.3, 118.6, 116.2, 100.2, 80.1, 67.2, 54.6, 32.2, 29.4 (2C not observed). HRMS (system B) calculated for  $\text{C}_{24}\text{H}_{37}\text{N}_2\text{O}_8$  481.2550, found 481.2563. FTIR ( $\text{cm}^{-1}$ ) 1672, 1561, 1429, 1367, 1236, 1154, 1006, 892, 779.

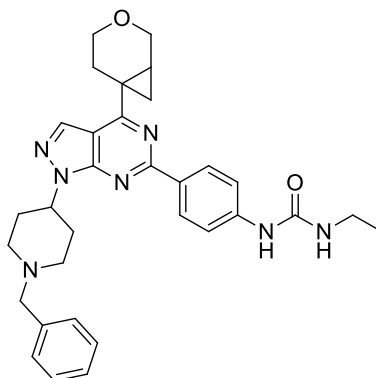
1-(1-Benzylpiperidin-4-yl)-4-(3-oxabicyclo[4.1.0]heptan-6-yl)-6-chloro-1H-pyrazolo[3,4-d]pyrimidine (177)



In a 10-20 mL microwave vial a mixture of potassium 3-oxabicyclo[4.1.0]heptan-6-yltrifluoroborate (691 mg, 3.39 mmol), 1-(1-benzylpiperidin-4-yl)-4,6-dichloro-1H-pyrazolo[3,4-d]pyrimidine hydrochloride (1.50g, 2.82 mmol), caesium carbonate (2.29 g, 7.05 mmol), palladium (II) acetate (51 mg, 0.23 mmol) and cataCXium® A (162 mg, 0.45 mmol) was dissolved in toluene (12 mL) and water (1.2 mL). The resulting suspension was degassed with a stream of nitrogen for 10 min, sealed and stirred at 100 °C for 16 h. The reaction was monitored by LCMS and, upon complete consumption of starting material, the reaction was cooled to r.t. and filtered through a celite cartridge (10 g). The resulting mixture was concentrated *in vacuo*. The resulting mixture was concentrated *in vacuo* and dry-loaded onto Florisil®. The crude reaction mixture was purified by flash column chromatography (cyclohexane: ethyl acetate 0%-100% (15 column volumes)) to give 1-(1-benzylpiperidin-4-yl)-4-(3-oxabicyclo[4.1.0]heptan-6-yl)-6-chloro-1H-pyrazolo[3,4-d]pyrimidine (65 mg, 0.15 mmol, 5% yield) as an amorphous white solid. LCMS (formic) rt. 0.69 (90%) MH<sup>+</sup> for desired M= 423.183. <sup>1</sup>H NMR (400 MHz, CDCl<sub>3</sub>) δ 8.13 (s, 1H), 7.31-7.41 (m, 4H), 7.23-7.30 (m, 1H), 4.82 (tt, *J* = 11.5, 4.8 Hz, 1H), 3.95-4.10 (m, 2H), 3.78 (ddd, *J* = 11.6, 6.0, 3.7 Hz, 1H), 3.61 (s, 2H), 3.41-3.54 (m, 1H), 3.06 (d, *J* = 11.5 Hz, 2H), 2.88 (td, *J* = 13.9, 4.3 Hz, 1H), 2.13-2.49 (m, 6H), 1.88-2.04 (m, 2H), 1.65 (dd, *J* = 9.3, 4.2 Hz, 1H), 1.42 (dd, *J* = 6.7, 4.2 Hz, 1H). Product was telescoped to next step ~90% pure. Full analysis was not taken.

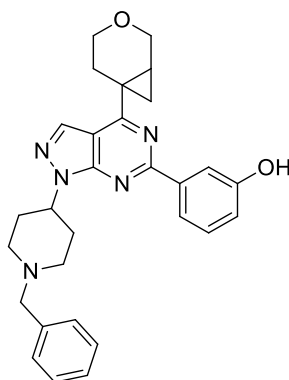


1-(4-(1-(1-Benzylpiperidin-4-yl)-4-(3-oxabicyclo[4.1.0]heptan-6-yl)-1H-pyrazolo[3,4-d]pyrimidin-6-yl)phenyl)-3-ethylurea (162)



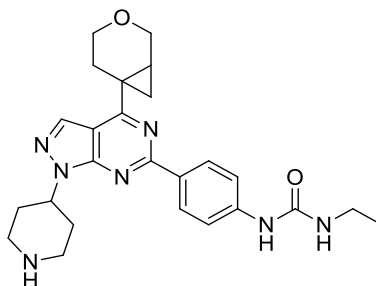
In a 2-5 mL microwave vial a mixture of 1-ethyl-3-(4-(4,4,5,5-tetramethyl-1,3,2-dioxaborolan-2-yl)phenyl)urea (110 mg, 0.38 mmol), 1-(1-benzylpiperidin-4-yl)-4-(3-oxabicyclo[4.1.0]heptan-6-yl)-6-chloro-1H-pyrazolo[3,4-d]pyrimidine (150 mg, 0.23 mmol), sodium carbonate (49 mg, 0.46 mmol) and Pd(PPh<sub>3</sub>)<sub>4</sub> (27 mg, 0.02 mmol) was dissolved in DME (2 mL) and water (0.25 mL). The resulting suspension was degassed with a stream of nitrogen for 10 min, sealed and stirred at 120 °C for 2 h. The reaction was monitored by LCMS and, upon complete consumption of starting material, the reaction was cooled to r.t. and filtered through a celite cartridge (2.5g). The resulting mixture was concentrated *in vacuo* and purified by Mass Directed Auto Purification (MDAP) (High pH, Method 4) to give 1-(4-(1-(1-benzylpiperidin-4-yl)-4-(3-oxabicyclo[4.1.0]heptan-6-yl)-1H-pyrazolo[3,4-d]pyrimidin-6-yl)phenyl)-3-ethylurea (70 mg, 0.13 mmol, 56% yield) as an amorphous white solid. LCMS (formic) r.t. 0.76 (97%) MH<sup>+</sup> for desired M=551.301. <sup>1</sup>H NMR (MeOD, 400 MHz) δ = 8.47 (d, *J* = 8.8 Hz, 2H), 8.21 (s, 1H), 7.51 (d, *J* = 8.8 Hz, 2H), 7.39-7.43 (m, 2H), 7.34-7.39 (m, 2H), 7.27-7.32 (m, 1H), 4.93 (tt, *J* = 11.5, 4.2 Hz, 1H), 4.09 (dd, *J* = 11.5, 3.9 Hz, 1H), 4.05 (dd, *J* = 11.5, 1.7 Hz, 1H), 3.78 (ddd, *J* = 11.7, 5.9, 4.2 Hz, 1H), 3.65 (s, 2H), 3.54 (ddd, *J* = 11.7, 9.5, 5.1 Hz, 1H), 3.28 (d, *J* = 7.3 Hz, 2H), 3.11 (br d, *J* = 11.5 Hz, 2H), 3.03 (dt, *J* = 14.0, 4.6 Hz, 1H), 2.30-2.51 (m, 5H), 2.23-2.30 (m, 1H), 1.91-2.08 (m, 2H), 1.69 (dd, *J* = 9.2, 4.0 Hz, 1H), 1.35 (dd, *J* = 6.7, 4.3 Hz, 1H), 1.20 ppm (t, *J* = 7.2 Hz, 3H). <sup>13</sup>C NMR (101 MHz, MeOD) δ = 159.9, 156.5, 153.7, 142.3, 137.3, 132.1, 132.1, 131.5, 129.3, 129.1, 127.9, 127.0, 117.7, 109.5, 65.1, 63.7, 62.5, 54.5, 52.3, 34.3, 30.6, 26.4, 24.3, 22.7, 22.3, 14.2. HRMS (system B) calculated for C<sub>32</sub>H<sub>38</sub>N<sub>7</sub>O<sub>2</sub> 552.3087, found 552.3090. FTIR (cm<sup>-1</sup>) 1656, 1552, 1384, 1307, 1227, 1169, 971, 804, 736, 698

3-(1-(1-Benzylpiperidin-4-yl)-4-(3-oxabicyclo[4.1.0]heptan-6-yl)-1H-pyrazolo[3,4-d]pyrimidin-6-yl)phenol (167)

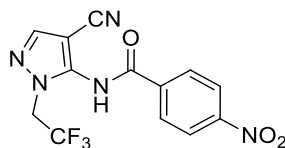


In a 2-5 mL microwave vial a mixture of 1-ethyl-3-(4-(4,4,5,5-tetramethyl-1,3,2-dioxaborolan-2-yl)phenyl)urea (110 mg, 0.38 mmol), 1-(1-benzylpiperidin-4-yl)-4-(3-oxabicyclo[4.1.0]heptan-6-yl)-6-chloro-1H-pyrazolo[3,4-d]pyrimidine (150 mg, 0.23 mmol) sodium carbonate (49 mg, 0.46 mmol) and Pd(PPh<sub>3</sub>)<sub>4</sub> (27 mg, 0.02 mmol) was dissolved in DME (2 mL) and water (0.25 mL). The resulting suspension was degassed with a stream of nitrogen for 10 min, sealed and stirred at 115 °C for 2 h. The reaction was monitored by LCMS and, upon complete consumption of starting material, the reaction was cooled to r.t. and filtered through a celite cartridge (2.5g). The resulting mixture was concentrated *in vacuo* and purified by Mass Directed Auto Purification (MDAP) (High pH, Method 4). The appropriate fractions were concentrated *in vacuo* to give 3-(1-(1-benzylpiperidin-4-yl)-4-(3-oxabicyclo[4.1.0]heptan-6-yl)-1H-pyrazolo[3,4-d]pyrimidin-6-yl)phenol (46 mg, 0.1 mmol, 42% yield) as an amorphous off-white solid. LCMS (formic) rt. 0.74 (97%) MH<sup>+</sup> for desired M=481.248. <sup>1</sup>H NMR (DMSO-d<sub>6</sub>, 400 MHz) δ = 8.38 (s, 1H), 7.92-7.99 (m, 2H), 7.31-7.40 (m, 5H), 7.24-7.30 (m, 1H), 6.92 (ddd, *J* = 8.1, 2.3, 1.1 Hz, 1H), 4.75-4.97 (m, 1H), 3.99 (dd, *J* = 11.5, 3.9 Hz, 1H), 3.94 (dd, *J* = 11.5, 1.5 Hz, 1H), 3.69 (ddd, *J* = 11.5, 5.9, 4.4 Hz, 1H), 3.58 (s, 2H), 3.44 (ddd, *J* = 11.5, 9.3, 5.1 Hz, 1H), 2.93-3.06 (m, 3H), 2.18-2.32 (m, 6H), 1.90-2.00 (m, 2H), 1.66 (dd, *J* = 9.2, 4.0 Hz, 1H), 1.33 (dd, *J* = 6.6, 4.2 Hz, 1H) <sup>13</sup>C NMR (101 MHz, DMSO-d<sub>6</sub>) δ = 169.8, 159.5, 158.0, 153.6, 139.3, 138.9, 133.0, 130.0, 129.2, 128.7, 127.4, 119.6, 118.3, 115.4, 110.0, 65.1, 63.7, 62.4, 54.5, 52.5, 31.6, 26.2, 24.7, 23.9, 23.1.

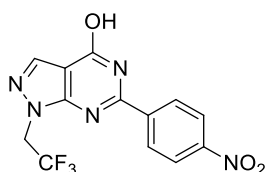
1-(4-(4-(3-Oxabicyclo[4.1.0]heptan-6-yl)-1-(piperidin-4-yl)-1H-pyrazolo[3,4-d]pyrimidin-6-yl)phenyl)-3-ethylurea (164)



In a 2-5 mL microwave vial 1-(4-(1-(1-benzylpiperidin-4-yl)-4-(3-oxabicyclo[4.1.0]heptan-6-yl)-1H-pyrazolo[3,4-d]pyrimidin-6-yl)phenyl)-3-ethylurea (60 mg, 0.11 mmol) was dissolved in DCM (1 mL). The resulting solution was cooled to 0 °C and chloroethyl chloroformate (18 µL, 0.16 mmol) was added. The resulting yellow solution was stirred at 0 °C for 2 h. The reaction mixture was concentrated *in vacuo* and then stirred in MeOH at r.t. for 68 h. The resulting mixture was concentrated *in vacuo* and purified by Mass Directed Auto Purification (MDAP) (formic, Method 2) to give 1-(4-(4-(3-oxabicyclo[4.1.0]heptan-6-yl)-1-(piperidin-4-yl)-1H-pyrazolo[3,4-d]pyrimidin-6-yl)phenyl)-3-ethylurea (20 mg, 0.04 mmol, 40% yield) as an amorphous white solid. LCMS (formic) rt. 0.62 (99%) MH<sup>+</sup> for desired M= 461.254. <sup>1</sup>H NMR (DMSO-d<sub>6</sub>, 400 MHz) δ = 9.05 (s, 1H), 8.40 (d, *J* = 8.8 Hz, 2H), 8.35 (s, 1H), 7.57 (d, *J* = 8.8 Hz, 2H), 6.52 (t, *J* = 5.4 Hz, 1H), 5.03-5.11 (m, 1H), 3.99 (dd, *J* = 11.5, 4.2 Hz, 1H), 3.94 (dd, *J* = 11.2, 1.5 Hz, 1H), 3.68 (ddd, *J* = 11.5, 5.9, 4.6 Hz, 1H), 3.44 (ddd, *J* = 11.6, 9.2, 5.1 Hz, 1H), 3.31 (br d, *J* = 10.5 Hz, 2H), 3.18 (s, 1H), 3.09-3.17 (m, 2H), 2.92-3.06 (m, 3H), 2.20-2.34 (m, 4H), 2.03 (br d, *J* = 12.0 Hz, 2H), 1.65 (dd, *J* = 9.2, 4.0 Hz, 1H), 1.31 (dd, *J* = 6.6, 4.2 Hz, 1H), 1.07 ppm (t, *J* = 7.1 Hz, 3H). <sup>13</sup>C NMR (101 MHz, DMSO-d<sub>6</sub>) δ = 169.5, 155.4, 153.7, 144.0, 133.2, 130.1, 129.6, 117.5, 114.3, 109.5, 65.2, 63.8, 53.1, 44.0, 34.4, 30.4, 26.3, 24.7, 23.8, 23.0, 15.9. HRMS (system B) calculated for C<sub>25</sub>H<sub>32</sub>N<sub>7</sub>O<sub>2</sub> 462.2617, found 462.2620. FTIR (cm<sup>-1</sup>) 1680, 1534, 1383, 1309, 1223, 1170.

*N*-(4-Cyano-1-(2,2,2-trifluoroethyl)-1*H*-pyrazol-5-yl)-4-nitrobenzamide (**180**)<sup>158</sup>

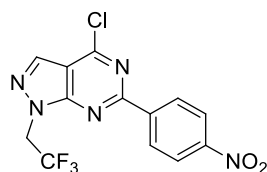
In a 100 mL RBF (2,2,2-trifluoroethyl)hydrazine (70% solution in water) (1.93 mL, 15.3 mmol) was dissolved in EtOH (10 mL). The reaction was flushed with nitrogen and cooled to 0 °C. 2-(ethoxymethylene)malononitrile (1.87 g, 15.3 mmol) was added in one portion and the reaction was heated to 95 °C for 0.5 h. LCMS analysis indicated complete conversion to desired intermediate. The reaction mixture was cooled and concentrated *in vacuo* to give a red solid. The resultant residue was dissolved in DCM (20 mL) and acetonitrile (10 mL) and cooled to 0 °C. 4-nitrobenzoyl chloride (4.27 g, 23.0 mmol) and triethylamine (8.55 mL, 61.4 mmol) was added and the reaction was stirred at r.t. for 1.5 h. The reaction mixture was diluted with ethyl acetate (200 mL) and washed with sat. aq. sodium bicarbonate (250 mL). The combined organic layers were dried (hydrophobic frit) and concentrated *in vacuo* to give a dark red gum. The crude residue was purified by flash column chromatography (cyclohexane: ethyl acetate 0-100% (15 column volumes)) to give *N*-(4-cyano-1-(2,2,2-trifluoroethyl)-1*H*-pyrazol-5-yl)-4-nitrobenzamide (3.03 g, 8.93 mmol, 58% yield) as an amorphous orange solid. LCMS (formic) rt. 0.97 (94%) MH- for desired M=339.058. <sup>1</sup>H NMR (400 MHz, DMSO-*d*<sub>6</sub>) δ = 8.41-8.48 (m, 2H), 8.18-8.28 (m, 3H), 5.27 (q, *J* = 9.0 Hz, 2H) <sup>13</sup>C NMR (101 MHz, DMSO-*d*<sub>6</sub>) δ = 164.8, 150.4, 143.3, 143.0, 138.2, 130.2, 124.3, 123.5 (q, *J*<sub>CF</sub> = 279.5 Hz, 1C), 112.9, 89.8, 49.5 (q, *J*<sub>CF</sub> = 36.0 Hz, 1C). HRMS calculated for C<sub>13</sub>H<sub>8</sub>F<sub>3</sub>N<sub>5</sub>O<sub>3</sub> 340.0679, found 340.0656. FTIR (cm<sup>-1</sup>) 3247, 2249, 1698, 1527.2, 1262, 1173, 1085.

6-(4-Nitrophenyl)-1-(2,2,2-trifluoroethyl)-1*H*-pyrazolo[3,4-*d*]pyrimidin-4-ol (**181**)<sup>158</sup>

In a 150 mL RBF *N*-(4-cyano-1-(2,2,2-trifluoroethyl)-1*H*-pyrazol-5-yl)-4-nitrobenzamide (1.63g, 4.80 mmol) was dissolved in EtOH (12 mL) and sodium hydroxide (2.0 M) (26.1 mL, 52.2 mmol). The reaction mixture was cooled to 0 °C and hydrogen peroxide (30% aqueous) (5.44 mL, 53.2 mmol) was added. The reaction was heated to 95 °C and stirred for 1 h. LCMS analysis indicated complete conversion to desired intermediate. The reaction was heated to

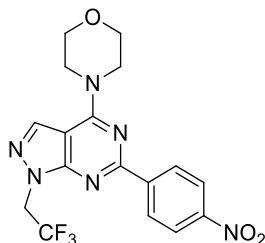
115 °C and stirred for 1.5 h. The reaction mixture was concentrated *in vacuo* to remove EtOH and the resulting aqueous solution was acidified to pH 1 with HCl (2M), at this point a yellow precipitate formed. The precipitate was collected by filtration under reduced pressure and dried in a drying piston for 16 h to give 6-(4-nitrophenyl)-1-(2,2,2-trifluoroethyl)-1*H*-pyrazolo[3,4-*d*]pyrimidin-4-ol (1.16 g, 2.87 mmol, 60% yield) as an amorphous yellow solid. LCMS (formic) rt. 0.97 (93%) MH<sup>+</sup> for desired M= 339.058. <sup>1</sup>H NMR (DMSO-*d*<sub>6</sub>, 400 MHz): δ = 12.86 (br., s, 1H), 8.44 (d, *J* = 9.0 Hz, 2H), 8.39 (d, *J* = 9.3 Hz, 1H), 8.29 (s, 1H), 5.35 ppm (q, *J* = 9.1 Hz, 2H). <sup>13</sup>C NMR (101 MHz, DMSO-*d*<sub>6</sub>) δ = 158.3, 154.9, 153.9, 149.9, 138.1, 136.7, 131.2, 130.3, 124.0 (q, <sup>1</sup>*J*<sub>CF</sub> = 280.2 Hz, 1C), 105.4, 47.8 (q, <sup>2</sup>*J*<sub>CF</sub> = 34.5 Hz, 1C). HRMS calculated for C<sub>13</sub>H<sub>9</sub>N<sub>5</sub>O<sub>3</sub>F<sub>3</sub> 340.0657, found 340.0656. FTIR (cm<sup>-1</sup>) 3119, 1698, 1523, 1347, 1151, 854, 708.

4-Chloro-6-(4-nitrophenyl)-1-(2,2,2-trifluoroethyl)-1*H*-pyrazolo[3,4-*d*]pyrimidine (182)<sup>158</sup>



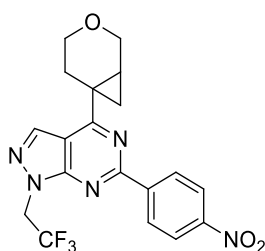
In a 50 mL RBF 6-(4-nitrophenyl)-1-(2,2,2-trifluoroethyl)-1*H*-pyrazolo[3,4-*d*]pyrimidin-4-ol (1 g, 2.65 mmol) was dissolved in POCl<sub>3</sub> (10 mL). The reaction mixture was heated at reflux for 1.5 h. After this time the initial yellow solution transformed to an orange solution. The reaction was diluted with DCM and concentrated *in vacuo*. The resulting tan solid was crushed and washed with water. This aqueous suspension was filtered under reduced pressure and the product was dried in a drying piston for 1 h to give 4-chloro-6-(4-nitrophenyl)-1-(2,2,2-trifluoroethyl)-1*H*-pyrazolo[3,4-*d*]pyrimidine (930 mg, 2.21 mmol, 83% yield) as an amorphous tan solid. LCMS (formic) 1.37 (85%) MH<sup>+</sup> for desired M=357.024. H NMR (400 MHz, DMSO-*d*<sub>6</sub>) δ 8.62-8.76 (m, 3H), 8.36-8.46 (m, 2H), 5.59 (q, *J* = 8.8 Hz, 2H) Product was telescoped to next step <90% pure. Full analysis was not taken due to impurities.

4-(6-(4-Nitrophenyl)-1-(2,2,2-trifluoroethyl)-1*H*-pyrazolo[3,4-*d*]pyrimidin-4-yl)morpholine  
**(183)**



In a 10-20 mL microwave vial 4-chloro-6-(4-nitrophenyl)-1-(2,2,2-trifluoroethyl)-1*H*-pyrazolo[3,4-*d*]pyrimidine (250 mg, 0.59 mmol) was dissolved in EtOH (4 mL). Morpholine (57  $\mu$ L, 0.65 mmol) and triethylamine (0.41 mL, 2.97 mmol) was added and the reaction was heated with the aid of a hot-air gun until all solid had dissolved (ca. 2 min). The reaction mixture was cooled to r.t. at which point a precipitate formed. The precipitate was filtered *in vacuo* and washed with MeOH. The resulting brown solid was dried in a vacuum oven for 16 h to give 4-(6-(4-nitrophenyl)-1-(2,2,2-trifluoroethyl)-1*H*-pyrazolo[3,4-*d*]pyrimidin-4-yl)morpholine (205 mg, 0.50 mmol, 85% yield) as an amorphous tan solid. LCMS (formic) rt. 1.30 (97%)  $MH^+$  for desired  $M = 408.341$ .  $^1H$  NMR (400 MHz, DMSO- $d_6$ )  $\delta = 8.63$ -8.79 (m, 2H), 8.52 (s, 1H), 8.29-8.39 (m, 2H), 5.37 (q,  $J = 9.1$  Hz, 2H), 4.06 (br., s., 4H), 3.82 (m., 4H).  $^{13}C$  NMR (101 MHz, DMSO- $d_6$ )  $\delta = 157.2$ , 149.2, 144.0, 135.8, 129.8, 124.1, 121.9, 120.6, 112.0, 99.4, 66.3 ppm (2C not observed). HRMS calculated for  $C_{17}H_{15}F_3N_6O_3$  395.1418, found 395.1408. FTIR ( $cm^{-1}$ ) 1563, 1341, 1265, 1157, 1119, 941, 713.

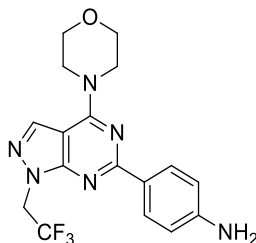
4-(3-Oxabicyclo[4.1.0]heptan-6-yl)-6-(4-nitrophenyl)-1-(2,2,2-trifluoroethyl)-1*H*-pyrazolo[3,4-*d*]pyrimidine **(184)**



In a 2-5 mL microwave vial a mixture of potassium 3-oxabicyclo[4.1.0]heptan-6-yltrifluoroborate (548 mg, 2.68 mmol), 4-chloro-6-(4-nitrophenyl)-1-(2,2,2-trifluoroethyl)-1*H*-pyrazolo[3,4-*d*]pyrimidine (500 mg, 1.12 mmol), caesium carbonate (1.82 g, 5.59 mmol), palladium(II) acetate (40 mg, 0.18 mmol) and cataCXium® A (128 mg, 0.36 mmol) was dissolved in toluene (3.6 mL) and water (0.36 mL). The resulting suspension was degassed

with a stream of nitrogen for 10 min, sealed and stirred at 120 °C for 3 h. The reaction was monitored by LCMS and, upon complete consumption of starting material, the reaction was cooled to r.t. and filtered through a celite cartridge (10 g). The resulting mixture was concentrated *in vacuo*. The resulting mixture was concentrated *in vacuo* and dry-loaded onto Florisil®. The reaction was purified by Flash Column chromatography (cyclohexane: ethyl acetate 0-100% (15 column volumes)) to give 4-(3-oxabicyclo[4.1.0]heptan-6-yl)-6-(4-nitrophenyl)-1-(2,2,2-trifluoroethyl)-1*H*-pyrazolo[3,4*d*]pyrimidine (324 mg, 0.77 mmol, 69% yield) as an amorphous tan solid. LCMS (formic) rt. 1.41 (96%) MH<sup>+</sup> for desired = 419.121. <sup>1</sup>H NMR (DMSO-*d*<sub>6</sub>, 400 MHz) δ = 8.75 (d, *J* = 9.0 Hz, 2H), 8.62 (s, 1H), 8.38 (d, *J* = 9.0 Hz, 2H), 5.51 (q, *J* = 9.0 Hz, 2H), 4.01 (dd, *J* = 11.2, 3.9 Hz, 1H), 3.96 (dd, *J* = 11.5, 1.5 Hz, 1H), 3.70 (ddd, *J* = 10.3, 5.9, 4.6 Hz, 1H), 3.48 (ddd, *J* = 11.2, 9.0, 5.4 Hz, 1H), 2.97 (dt, *J* = 14.2, 4.7 Hz, 1H), 2.25-2.37 (m, 2H), 1.73 (dd, *J* = 9.2, 4.0 Hz, 2H), 1.42 ppm (dd, *J* = 6.7, 4.3 Hz, 1H). <sup>13</sup>C NMR (101 MHz, DMSO-*d*<sub>6</sub>) δ = 171.31, 158.37, 155.34, 149.45, 143.33, 135.65, 129.99, 129.95, 124.30, 124.14 (q, <sup>1</sup>*J*<sub>CF</sub> = 280.2 Hz, 1C), 110.45, 65.08, 63.66, 47.51 (q, <sup>2</sup>*J*<sub>CF</sub> = 34.5 Hz, 1C), 26.09, 24.99, 24.77, 24.02. HRMS calculated for C<sub>19</sub>H<sub>16</sub>F<sub>3</sub>N<sub>5</sub>O<sub>3</sub> 420.1283, found 420.1281 FTIR (cm<sup>-1</sup>) 1557, 1346, 1264, 927, 854.

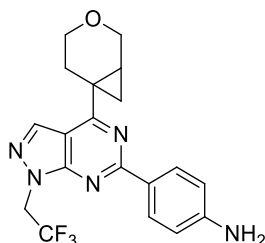
4-(4-Morpholino-1-(2,2,2-trifluoroethyl)-1*H*-pyrazolo[3,4-*d*]pyrimidin-6-yl)aniline (185)



In a 10-20 mL microwave vial 4-(6-(4-nitrophenyl)-1-(2,2,2-trifluoroethyl)-1*H*-pyrazolo[3,4-*d*]pyrimidin-4-yl)morpholine (130mg, 0.32 mmol) was dissolved in acetic acid (2 mL), EtOH (2 mL) and water (1 mL). Iron powder (89 mg, 1.59 mmol) was added and the resulting suspension was sonicated for 3 h. The reaction mixture was filtered to remove iron and partitioned between ethyl acetate (5 mL) and potassium hydroxide (2M) (5 mL). The organic layer was washed with brine (5 mL) and water (5 mL). The organic layer was then dried (hydrophobic frit) and concentrated *in vacuo* to give 4-(4-morpholino-1-(2,2,2-trifluoroethyl)-1*H*-pyrazolo[3,4-*d*]pyrimidin-6-yl)aniline (113 mg, 0.30 mmol, 94% yield) as an amorphous yellow solid. LCMS (formic) rt. 0.98 (100%) MH<sup>+</sup> for desired M=378.142. <sup>1</sup>H NMR (400 MHz, DMSO-*d*<sub>6</sub>) δ = 8.35 (s, 1H), 8.18 (d, *J* = 8.6 Hz, 2H), 6.39-6.83 (m, 2H), 5.60 (s, 2H), 5.24 (q, *J* = 9.1 Hz, 2H), 3.98 (t, *J* = 4.5 Hz, 4H), 3.79 (t, *J*=4.9 Hz, 4H). <sup>13</sup>C NMR (101 MHz,

DMSO- $d_6$ )  $\delta$  = 161.6, 157.3, 157.1, 151.9, 135.4, 130.3, 125.1, 124.3 (q,  $^1J_{CF}$  = 281.0 Hz, 1C), 113.4, 98.3, 66.4, 47.0 (q,  $^2J_{CF}$  = 33.8 Hz, 1C), 45.4. HRMS calculated for  $C_{17}H_{17}F_3N_6O$  379.1481, found 379.1493. FTIR ( $cm^{-1}$ ) 1569, 1394, 1267, 1158, 1007, 789.

4-(4-(3-Oxabicyclo[4.1.0]heptan-6-yl)-6-(4-nitrophenyl)-1-(2,2,2-trifluoroethyl)-1H-pyrazolo[3,4-d]pyrimidine (186)



In a 10-20 mL microwave vial 4-(3-oxabicyclo[4.1.0]heptan-6-yl)-6-(4-nitrophenyl)-1-(2,2,2-trifluoroethyl)-1H-pyrazolo[3,4-d]pyrimidine (200 mg, 0.48 mmol) was dissolved in EtOH (3.5 mL), acetic acid (3.5 mL) and water (1.8 mL). Iron powder (133mg, 2.39 mmol) was added and the reaction was placed in a sonicator for 1.5 h. The reaction mixture was filtered to remove iron and partitioned between ethyl acetate (10 mL) and sodium hydroxide (2 M) (10 mL). The aqueous layer was extracted with ethyl acetate (3x 5 mL). The combined organic layers were dried (hydrophobic frit) and concentrated *in vacuo* to give 4-(4-(3-oxabicyclo[4.1.0]heptan-6-yl)-1-(2,2,2-trifluoroethyl)-1H-pyrazolo[3,4-d]pyrimidin-6-yl)aniline (175 mg, 0.45 mmol, 94% yield) as an amorphous yellow solid.

Chiral Purification of 4-(3-oxabicyclo[4.1.0]heptan-6-yl)-6-(4-nitrophenyl)-1-(2,2,2-trifluoroethyl)-1H-pyrazolo[3,4-d]pyrimidine (186)

Total sample dissolved in ethanol (24 mL) and liquid loaded onto the column in 4 mL manual injections.

**Column:** 30mm x 25cm Chiralcel OJ-H (5 $\mu$ m)

**Flow Rate:** 30 mL/min

**Detection:** UV Diode Array at 215 nM

**Mobile Phase A:** Heptane

**Mobile Phase B:** Ethanol

**Modifier:** Isopropyl amine.

**Isocratic method:** 50:50:0.2 mobile phase A: mobile phase B: modifier

**Runtime:** 30 min.

The combined fractions for isomer 1 (**186a**) and isomer 2 (**186a**) were concentrated *in vacuo* to yield. 1st eluting isomer (**186a**) (58 mg, >99.5% chirally pure by chiral HPLC analysis) as



a white solid ( $\alpha_D^{20}$  (0.24 g/100 mL) = +33.3 implied from crystal structure of **(38a)** that positive rotation is 1*S*, 6*R*.

2<sup>nd</sup> eluting isomer (**186b**) (63 mg, >99.5% chirally pure by chiral HPLC analysis) as a white solid ( $\alpha_D^{20}$  (0.24 g/100 mL) = -33.3 implied from crystal structure of **(40b)** that negative rotation is 1*R*, 6*S*.

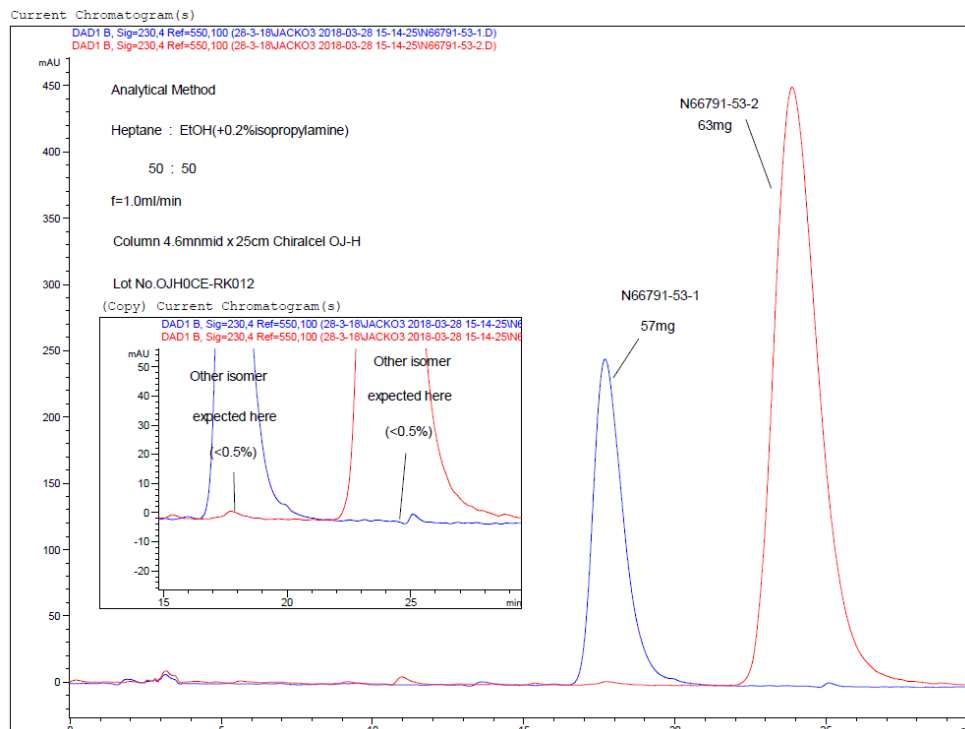
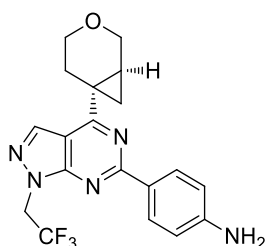


**Figure 78:** Chiral purification of compound **186**

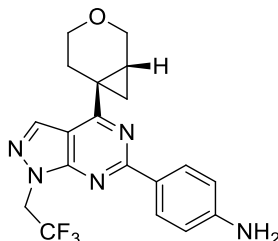
4-(4-((1*S*,6*R*)-3-Oxabicyclo[4.1.0]heptan-6-yl)-1-(2,2,2-trifluoroethyl)-1*H*-pyrazolo[3,4-*d*]pyrimidin-6-yl)aniline (**186a**)



LCMS (formic) rt. 1.13 (100%)  $MH^+$  for desired  $M = 389.146$ .  $^1H$  NMR (DMSO- $d_6$ , 600 MHz)  $\delta = 8.41$  (s, 1H), 8.25 (d,  $J = 8.4$  Hz, 2H), 6.66 (d,  $J = 8.4$  Hz, 2H), 5.74 (s, 2H), 5.35 (q,  $J = 9.0$  Hz, 2H), 3.99 (dd,  $J = 11.4, 4.4$  Hz, 1H), 3.94 (dd,  $J = 11.4, 1.1$  Hz, 1H), 3.65-3.70 (m, 1H), 3.44 (ddd,  $J = 11.6, 9.4, 5.1$  Hz, 1H), 2.94 (dt,  $J = 13.9, 4.8$  Hz, 1H), 2.27 (ddd,  $J = 14.4, 9.1, 5.9$  Hz, 1H), 2.20-2.23 (m, 1H), 1.63 (dd,  $J = 9.2, 4.0$  Hz, 1H), 1.31 (dd,  $J = 6.8, 4.2$  Hz, 1H).  $^{13}C$  NMR (151 MHz, DMSO- $d_6$ )  $\delta = 169.90, 161.34, 155.90, 152.41, 135.22, 130.53$ ,

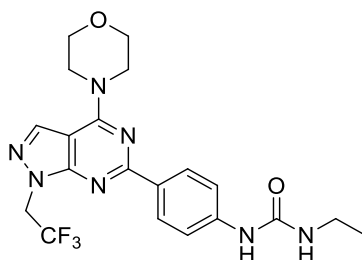
124.44, 124.23 (q,  $^1J_{CF} = 280.3$  Hz, 1C), 113.7, 108.6, 65.1, 63.7, 47.1 (q,  $^2J_{CF} = 34.8$  Hz, 1C), 26.2, 24.7, 23.9, 23.0. HRMS calculated for  $C_{19}H_{18}F_3N_5O$  390.1542, found 390.1537. FTIR ( $cm^{-1}$ ) 3429, 3351, 3241, 1567, 1384, 1267, 1141, 923.  $\alpha_D^{20}$  (0.24 g/100 mL) = +33.3.

4-(4-((1R,6S)-3-Oxabicyclo[4.1.0]heptan-6-yl)-1-(2,2,2-trifluoroethyl)-1H-pyrazolo[3,4-d]pyrimidin-6-yl)aniline (186b)



LCMS (formic) rt. 1.12 (100%) MH+ for desired M= 389.146.  $^1H$  NMR (DMSO- $d_6$ , 600 MHz)  $\delta$  = 8.41 (s, 1H), 8.25 (d,  $J = 8.4$  Hz, 2H), 6.66 (d,  $J = 8.4$  Hz, 2H), 5.74 (s, 2H), 5.35 (q,  $J = 9.0$  Hz, 2H), 3.99 (dd,  $J = 11.4, 4.0$  Hz, 1H), 3.94 (d,  $J = 11.0$  Hz, 1H), 3.64-3.71 (m, 1H), 3.44 (ddd,  $J = 12.1, 9.2, 5.1$  Hz, 1H), 2.94 (dt,  $J = 13.9, 4.6$  Hz, 1H), 2.27 (ddd,  $J = 14.7, 9.5, 5.9$  Hz, 1H), 2.19-2.23 (m, 1H), 1.63 (dd,  $J = 9.0, 3.9$  Hz, 1H), 1.31 ppm (dd,  $J = 6.2, 4.4$  Hz, 1H).  $^{13}C$  NMR (151 MHz, DMSO- $d_6$ )  $\delta$  = 169.9, 161.3, 155.9, 152.4, 135.2, 130.5, 124.4, 124.2 (q,  $^1J = 280.3$  Hz, 1C), 113.7, 108.6, 65.1, 63.7, 47.1 (q,  $^2J = 33.9$  Hz, 1C), 26.1, 24.7, 23.9, 23.0. HRMS calculated for  $C_{19}H_{18}F_3N_5O$  390.1542, found 390.1542. FTIR ( $cm^{-1}$ ) 3424, 3361, 3241, 1568, 1384, 1266, 1140, 924.  $\alpha_D^{20}$  (0.24 g/100 mL) = -33.3.

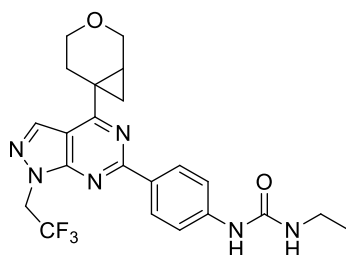
1-ethyl-3-(4-(4-Morpholino-1-(2,2,2-trifluoroethyl)-1H-pyrazolo[3,4-d]pyrimidin-6-yl)phenyl)urea (171)



In a 2-5 mL microwave vial 4-(4-morpholino-1-(2,2,2-trifluoroethyl)-1H-pyrazolo[3,4-d]pyrimidin-6-yl)aniline (50 mg, 0.13 mmol) and 4-nitrophenyl chloroformate (32mg, 0.16 mmol) were dissolved in DCM (2 mL). Pyridine (21  $\mu$ L, 0.26 mmol) was added and the reaction was stirred at r.t. for 1.5 h. Ethanamine (2M in THF) (0.2 mL, 0.40 mmol) and DIPEA (35  $\mu$ L, 0.2 mmol) were added and the reaction was stirred for a further 1 h. The reaction was partitioned between DCM (5 mL) and water (5 mL) and the resulting mixture was separated

using a hydrophobic frit. The organic layer was concentrated *in vacuo* and purified by Mass Directed Auto Purification (formic, method C) to give 1-ethyl-3-(4-(4-morpholino-1-(2,2,2-trifluoroethyl)-1*H*-pyrazolo[3,4-*d*]pyrimidin-6-yl)phenyl)urea (15 mg, 0.03 mmol, 24% yield) LCMS (formic) rt. 1.05 (99%)  $MH^+$  for desired  $M=449.179$ .  $^1H$  NMR (400 MHz, DMSO- $d_6$ )  $\delta$  = 8.76 (s, 1H), 8.42 (s, 1H), 8.34 (d,  $J=8.80$  Hz, 2H), 7.52 (d,  $J = 8.8$  Hz, 2H), 6.24 (t,  $J = 5.5$  Hz, 1H), 5.29 (q,  $J = 9.1$  Hz, 2H), 4.02 (br. s., 4H), 3.80 (t,  $J = 4.8$  Hz, 4H), 3.08-3.19 (m, 2H), 1.07 (t,  $J = 7.2$  Hz, 3H)  $^{13}C$  NMR (101 MHz, DMSO- $d_6$ )  $\delta$  = 161.0, 157.1, 155.4, 143.6, 135.5, 130.4, 129.5, 117.3, 112.0, 98.7, 66.4, 34.4, 15.9 (3C not observed). HRMS calculated for  $C_{20}H_{22}F_3N_7O_2$  450.1865 found 450.1866 FTIR ( $cm^{-1}$ ) 1643, 1556, 1464, 1392, 1232, 1004, 939, 792.

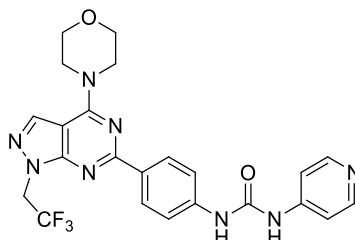
1-(4-(4-(3-Oxabicyclo[4.1.0]heptan-6-yl)-1-(2,2,2-trifluoroethyl)-1*H*-pyrazolo[3,4-*d*]pyrimidin-6-yl)phenyl)-3-ethylurea (172)



In a 2-5 mL microwave vial 4-(4-(3-oxabicyclo[4.1.0]heptan-6-yl)-1-(2,2,2-trifluoroethyl)-1*H*-pyrazolo[3,4-*d*]pyrimidin-6-yl)aniline (50 mg, 0.13 mmol) and 4-nitrophenyl chloroformate (32mg, 0.16 mmol) were dissolved in DCM (2 mL). Pyridine (21  $\mu$ L, 0.26 mmol) was added and the reaction was stirred at r.t. for 1.5 h. Ethanamine (2M in THF) (0.2 mL, 0.40 mmol) and DIPEA (35  $\mu$ L, 0.2 mmol) were added and the reaction was stirred for a further 1 h. The reaction was partitioned between DCM (5 mL) and water (5 mL) and the resulting mixture was separated using a hydrophobic frit. The organic layer was concentrated *in vacuo* and purified by Mass Directed Auto Purification (formic, method C) to give 1-(4-(4-(3-oxabicyclo[4.1.0]heptan-6-yl)-1-(2,2,2-trifluoroethyl)-1*H*-pyrazolo[3,4-*d*]pyrimidin-6-yl)phenyl)-3-ethylurea (30 mg, 0.07 mmol, 51% yield) as an amorphous white solid. LCMS (formic) rt. 1.15 (98%)  $MH^+$  for desired  $M=460.183$ .  $^1H$  NMR (400 MHz, DMSO- $d_6$ )  $\delta$  = 8.78 (s, 1H), 8.49 (s, 1H), 8.41 (d,  $J = 8.8$  Hz, 2H), 7.57 (d,  $J = 8.8$  Hz, 2H), 6.22 (t,  $J = 5.5$  Hz, 1H), 5.41 (q,  $J = 9.3$  Hz, 1H), 4.00 (dd,  $J = 11.2, 3.9$  Hz, 1H), 3.95 (dd,  $J = 11.7, 1.0$  Hz, 1H), 3.69 (ddd,  $J = 11.5, 5.9, 4.6$  Hz, 1H), 3.46 (ddd,  $J = 11.5, 9.0, 4.9$  Hz, 1H), 3.19 - 3.11 (m, 2H), 2.96 (td,  $J = 13.9, 4.7$  Hz, 1H), 2.34 - 2.23 (m, 2H), 1.67 (dd,  $J = 9.2, 4.0$  Hz, 1H), 1.35 (dd,  $J = 6.6, 4.2$  Hz, 1H), 1.08 (t,  $J = 7.2$  Hz, 3H)  $^{13}C$  NMR (101 MHz, DMSO- $d_6$ )  $\delta$  = 170.4,

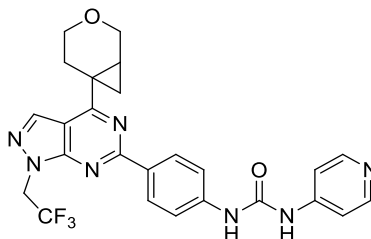
160.5, 155.7, 155.3, 144.0, 135.4, 129.9, 129.6, 124.2 (q,  $^1J_{CF} = 280.2$  Hz, 1C), 117.6, 109.3, 65.1, 63.7, 47.3 (q,  $^2J_{CF} = 37.4$  Hz, 1C), 34.5, 26.2, 24.8, 24.2, 23.4, 15.9. HRMS calculated for  $C_{22}H_{23}F_3N_6O_2$  461.1913, found 461.1911. FTIR ( $cm^{-1}$ ) 3335, 1646, 1551, 1164, 657.

1-(4-(4-Morpholino-1-(2,2,2-trifluoroethyl)-1H-pyrazolo[3,4-d]pyrimidin-6-yl)phenyl)-3-(pyridin-4-yl)urea (173)



In a 2-5 mL microwave vial 4-(4-morpholino-1-(2,2,2-trifluoroethyl)-1H-pyrazolo[3,4-d]pyrimidin-6-yl)aniline (50 mg, 0.13 mmol) and 4-nitrophenyl chloroformate (32mg, 0.16 mmol) were dissolved in DCM (2 mL). Pyridine (21  $\mu$ L, 0.26 mmol) was added and the reaction was stirred at r.t. for 1.5 h. Pyridin-4-amine (36 mg, 0.39 mmol) and DIPEA (35  $\mu$ L, 0.2 mmol) were added and the reaction was stirred for a further 1 h. The reaction was partitioned between DCM (5 mL) and water (5 mL) and the resulting mixture was separated using a hydrophobic frit. The organic layer was concentrated *in vacuo* and purified by Mass Directed Auto Purification (formic, method C) to give 1-(4-(4-morpholino-1-(2,2,2-trifluoroethyl)-1H-pyrazolo[3,4-d]pyrimidin-6-yl)phenyl)-3-(pyridin-4-yl)urea (22 mg, 0.04 mmol, 33% yield) as an amorphous off white solid. LCMS (formic) rt. 0.73 (100%)  $MH^+$  for desired  $M = 498.174$ .  $^1H$  NMR (400 MHz,  $DMSO-d_6$ )  $\delta = 9.20$  (d,  $J = 3.7$  Hz, 2H), 8.40-8.45 (m, 3H), 8.38 (d,  $J = 6.1$  Hz, 2H), 7.61 (d,  $J = 9.1$  Hz, 2H), 7.42-7.49 (m, 2H), 5.31 (q,  $J = 9.1$  Hz, 2H), 4.03 (br. s., 4H), 3.81 (t,  $J = 4.9$  Hz, 4H)  $^{13}C$  NMR (101 MHz,  $DMSO-d_6$ )  $\delta = 160.7$ , 157.2, 157.1, 152.5, 150.6, 146.9, 142.1, 137.0, 135.6, 131.9, 129.6, 118.3, 112.8, 98.8, 66.4, (2C not observed) HMRS calculated for  $C_{23}H_{21}F_3N_8O_2$  499.1818, found 499.1819. FTIR ( $cm^{-1}$ ) 1728, 1597, 1563, 1391, 1167, 1113, 1005, 938, 788, 514.

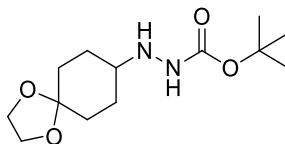
1-(4-(4-(3-Oxabicyclo[4.1.0]heptan-6-yl)-1-(2,2,2-trifluoroethyl)-1H-pyrazolo[3,4-d]pyrimidin-6-yl)phenyl)-3-(pyridin-4-yl)urea (174)



In a 2-5 mL microwave vial 4-(4-(3-oxabicyclo[4.1.0]heptan-6-yl)-1-(2,2,2-trifluoroethyl)-1H-pyrazolo[3,4-d]pyrimidin-6-yl)aniline (50 mg, 0.13 mmol) and 4-nitrophenyl chloroformate (32mg, 0.16 mmol) were dissolved in DCM (2 mL). Pyridine (21  $\mu$ L, 0.26 mmol) was added and the reaction was stirred at r.t. for 1.5 h. Pyridin-4-amine (36 mg, 0.39 mmol) and DIPEA (35  $\mu$ L, 0.2 mmol) were added and the reaction was stirred for a further 1 h. The reaction was partitioned between DCM (5 mL) and water (5 mL) and the resulting mixture was separated using a hydrophobic frit. The organic layer was concentrated *in vacuo* and purified by Mass Directed Auto Purification (formic, method C) to give 1-(4-(4-(3-oxabicyclo[4.1.0]heptan-6-yl)-1-(2,2,2-trifluoroethyl)-1H-pyrazolo[3,4-d]pyrimidin-6-yl)phenyl)-3-(pyridin-4-yl)urea (29 mg, 0.06 mmol, 44% yield) as an amorphous white solid. LCMS (formic) rt. 0.81 (100%)  $MH^+$  for desired  $M = 509.179$ .  $^1H$  NMR (400 MHz, DMSO- $d_6$ )  $\delta = 9.20$  (d,  $J = 11.0$  Hz, 1H), 8.51 (s, 1H), 8.49 (d,  $J = 8.8$  Hz, 2H), 8.39 (d,  $J = 5.2$  Hz, 2H), 7.65 (d,  $J = 9.0$  Hz, 2H), 7.47 (dd,  $J = 5.2, 1.5$  Hz, 2H), 5.43 (q,  $J = 9.0$  Hz, 2H), 4.01 (dd,  $J = 11.2, 4.2$  Hz, 1H), 3.95 (dd,  $J = 11.2, 1.2$  Hz, 1H), 3.69 (ddd,  $J = 11.7, 5.9, 4.4$  Hz, 1H), 3.46 (ddd,  $J = 11.5, 9.3, 4.9$  Hz, 1H), 2.97 (td,  $J = 14.1, 4.9$  Hz, 1H), 2.35 - 2.24 (m, 2H), 1.69 (dd,  $J = 9.2, 4.0$  Hz, 1H), 1.37 (dd,  $J = 6.6, 4.2$  Hz, 1H).  $^{13}C$  NMR (101 MHz, DMSO- $d_6$ )  $\delta = 170.6, 160.3, 155.7, 152.4, 150.7, 146.7, 142.4, 135.4, 131.3, 129.8, 124.2$  (q,  $^1J_{CF} = 281.0$  Hz, 1C), 118.5, 112.9, 109.5, 65.1, 63.7, 47.3 (q,  $^2J_{CF} = 34.5$  Hz, 1C), 26.2, 24.8, 24.3, 23.5. HRMS calculated for  $C_{25}H_{22}F_3N_7O_2$  510.1865, found 510.1866. FTIR ( $cm^{-1}$ ) 1706, 1575, 1529, 1387, 1302, 1250, 1198, 805, 745, 659.

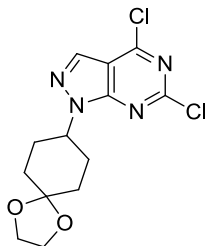
### 3.3.2 Cyclohexyl-N1-Substituted compounds

*tert*-Butyl 2-(1,4-dioxaspiro[4.5]decan-8-yl)hydrazine-1-carboxylate (195)<sup>259</sup>



In a 250 mL RBF *tert*-butyl hydrazine carboxylate (2.54 g, 19.2 mmol) and 1,4-dioxaspiro[4.5]decan-8-one (3.0g, 19.2 mmol) were dissolved in DCM (64 mL) and acetic acid (4 mL). The reaction mixture was cooled to 0 °C and STAB (6.11g, 28.8 mmol) were added. The reaction mixture was stirred at r.t. for 16 h. The reaction was quenched with potassium bisulfate (10% aq., 50 mL) and diluted with water (50 mL). The organic layer was further washed with NaOH (1M), dried (hydrophobic frit) and concentrated *in vacuo*. The resulting colourless oil was triturated in petroleum ether to give *tert*-butyl 2-(1,4-dioxaspiro[4.5]decan-8-yl)hydrazine-1-carboxylate (4.65 g, 17.1 mmol, 89% yield). <sup>1</sup>H NMR (400 MHz, DMSO-*d*<sub>6</sub>) δ = 7.92-8.23 (m, 1H), 4.21 (br., s., 1H), 3.83 (s, 4H), 2.70-2.90 (m, 1H), 1.56-1.78 (m, 4H), 1.26-1.49 (m, 13H).

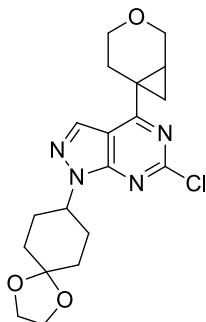
4,6-Dichloro-1-(1,4-dioxaspiro[4.5]decan-8-yl)-1*H*-pyrazolo[3,4-*d*]pyrimidine (197)<sup>259</sup>



In a 100 mL RBF *tert*-butyl 2-(1,4-dioxaspiro[4.5]decan-8-yl)hydrazine-1-carboxylate (1.45 g, 5.49 mmol) was suspended in water (12 mL) and the reaction was stirred at reflux for 14 h. After this time the white suspension had turned to a pale-yellow solution. The reaction mixture was cooled to 0 °C, triethylamine (1.1 mL, 8.04 mmol) and EtOH (12 mL) were added. 2,4,6-trichloropyrimidine-5-carbaldehyde (1.0 g, 4.73 mmol) was added in a portion wise manner. The reaction was stirred at 0 °C for 0.5 h. The reaction mixture was concentrated *in vacuo* and partitioned between water and DCM. The combined organic layers were dried (hydrophobic frit) and concentrated *in vacuo*. The resulting residue was triturated in diethyl ether to give 4,6-dichloro-1-(1,4-dioxaspiro[4.5]decan-8-yl)-1*H*-pyrazolo[3,4-*d*]pyrimidine (760 mg, 2.31 mmol, 49% yield) as an amorphous off-white solid. LCMS (formic) rt. 1.17 (99%) MH<sup>+</sup> for desired M= 328.049. <sup>1</sup>H NMR (400 MHz, DMSO-*d*<sub>6</sub>) δ = 8.55 (s, 1H), 4.85 (tt, *J* = 11.4, 4.0 Hz, 1H), 3.81-4.05 (m, 4H), 2.21 (dq, *J* = 11.7, 4.3 Hz, 2H), 1.95 (dd, *J* = 11.9, 2.6 Hz, 2H),

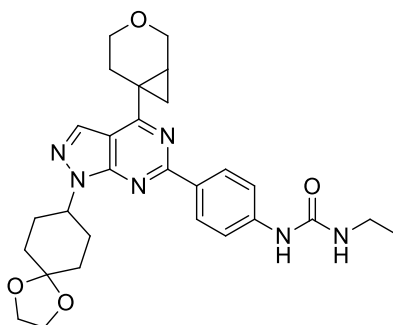
1.69-1.88 (m, 4H).  $^{13}\text{C}$  NMR (DMSO- $d_6$ , 101 MHz)  $\delta$  = 155.3, 154.8, 153.7, 133.2, 113.2, 107.4, 64.3, 64.2, 55.6, 33.2, 29.3 ppm. HRMS (system B) calculated for  $\text{C}_{13}\text{H}_{14}\text{Cl}_2\text{N}_4\text{O}_2$  329.0559, found 329.0573. FTIR ( $\text{cm}^{-1}$ ) 1584, 1211, 1108, 963, 774.

4-(3-Oxabicyclo[4.1.0]heptan-6-yl)-6-chloro-1-(1,4-dioxaspiro[4.5]decan-8-yl)-1H-pyrazolo[3,4-d]pyrimidine (198)



In a 100 RBF a mixture of potassium 3-oxabicyclo[4.1.0]heptan-6-yltrifluoroborate (2.2 g, 10.3 mmol), 4,6-dichloro-1-(1,4-dioxaspiro[4.5]decan-8-yl)-1H-pyrazolo[3,4-d]pyrimidine (2.82 g, 8.57 mmol), caesium carbonate (8.37 g, 25.7 mmol), palladium (II) acetate (308 mg, 1.37 mmol) and cataCXium® A (983 mg, 2.74 mmol) was dissolved in toluene (39 mL) and water (3.9 mL). The resulting suspension was degassed with a stream of nitrogen for 10 min, sealed and stirred at 100 °C for 16 h. The reaction was monitored by LCMS and, upon complete consumption of starting material, the reaction was cooled to r.t. and filtered through a celite cartridge (10 g). The resulting mixture was concentrated *in vacuo*. Due to a potential instability of this compound on silica, the reaction mixture was telescoped to the next step as a crude reaction mixture.

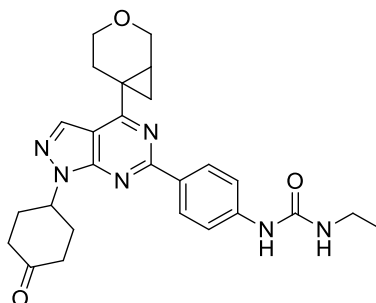
1-(4-(4-(3-Oxabicyclo[4.1.0]heptan-6-yl)-1-(1,4-dioxaspiro[4.5]decan-8-yl)-1H-pyrazolo[3,4-d]pyrimidin-6-yl)phenyl)-3-ethylurea (190)



In a 2-5 mL microwave vial a mixture of 1-ethyl-3-(4-(4,4,5,5-tetramethyl-1,3,2-dioxaborolan-2-yl)phenyl)urea (490 mg, 1.69 mmol), 4-(3-oxabicyclo[4.1.0]heptan-6-yl)-6-

chloro-1-(1,4-dioxaspiro[4.5]decan-8-yl)-1*H*-pyrazolo[3,4-*d*]pyrimidine (800 mg, 1.02 mmol (50% wt.)) sodium carbonate (217 mg, 2.05 mmol) and Pd(PPh<sub>3</sub>)<sub>4</sub> (118 mg, 0.10 mmol) was dissolved in DME (9 mL) and water (1.1 mL). The resulting suspension was degassed with a stream of nitrogen for 10 min, sealed and stirred at 120 °C for 2 h. The reaction was monitored by LCMS and, upon complete consumption of starting material, the reaction was cooled to r.t. and filtered through a celite cartridge (2.5g). The resulting mixture was concentrated *in vacuo* and purified by Mass Directed Auto Purification (MDAP) (high-pH, Method 3) to give 1-(4-(4-(3-oxabicyclo[4.1.0]heptan-6-yl)-1-(1,4-dioxaspiro[4.5]decan-8-yl)-1*H*-pyrazolo[3,4-*d*]pyrimidin-6-yl)phenyl)-3-ethylurea (280 mg, 0.54 mmol, 53% yield). LCMS (formic) rt. 1.16 (100%) MH<sup>+</sup> for desired M= 518.618. <sup>1</sup>H NMR (CDCl<sub>3</sub>, 400 MHz) δ = 8.54 (d, *J* = 8.8 Hz, 2H), 8.08 (s, 1H), 7.48 (d, *J* = 8.6 Hz, 2H), 6.75 (s, 1H), 4.91-5.07 (m, 2H), 4.10 (dd, *J* = 11.5, 1.2 Hz, 1H), 4.05 (dd, *J* = 8.1, 3.9 Hz, 1H), 4.02-4.04 (m, 4H), 3.82 (ddd, *J* = 11.6, 6.1, 3.7 Hz, 1H), 3.51 (ddd, *J* = 11.6, 9.8, 5.0 Hz, 1H), 3.32-3.40 (m, 2H), 3.04 (dt, *J* = 13.8, 4.3 Hz, 1H), 2.42-2.56 (m, 2H), 2.37 (ddd, *J* = 14.0, 9.8, 6.0 Hz, 1H), 2.22-2.29 (m, 1H), 1.95-2.10 (m, 4H), 1.87 (td, *J* = 13.0, 3.7 Hz, 2H), 1.70 (dd, *J* = 9.0, 4.2 Hz, 2H), 1.37 (dd, *J* = 6.6, 4.4 Hz, 1H), 1.21 (t, *J* = 7.2 Hz, 3H) <sup>13</sup>C NMR (101 MHz, DMSO-*d*<sub>6</sub>) δ = 169.7, 159.5, 155.3, 153.7, 143.7, 132.9, 130.3, 129.6, 117.5, 109.5, 107.6, 65.1, 64.3, 64.3, 63.8, 54.2, 34.4, 33.5, 29.4, 26.3, 24.7, 23.7, 23.0, 15.9. HRMS (system B) calculated for C<sub>28</sub>H<sub>34</sub>N<sub>6</sub>O<sub>4</sub> 519.2720, found 519.2720. FTIR (cm<sup>-1</sup>) 1553, 1385, 1238, 1033, 924.52, 694.

1-(4-(4-(3-Oxabicyclo[4.1.0]heptan-6-yl)-1-(4-oxocyclohexyl)-1*H*-pyrazolo[3,4-*d*]pyrimidin-6-yl)phenyl)-3-ethylurea (191)

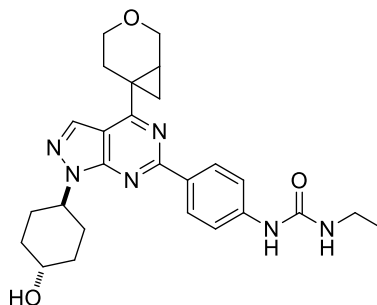


In a scintillation vial 1-(4-(4-(3-oxabicyclo[4.1.0]heptan-6-yl)-1-(1,4-dioxaspiro[4.5]decan-8-yl)-1*H*-pyrazolo[3,4-*d*]pyrimidin-6-yl)phenyl)-3-ethylurea (260 mg, 0.43 mmol) was dissolved in THF (2.1 mL). HCl (0.35 mL, 4.26 mmol) was added and the reaction was stirred for 2 h. The reaction mixture was concentrated *in vacuo* and partitioned between DCM (10 mL) and water. (10 mL). The combined organic layers were dried (hydrophobic frit) and concentrated *in vacuo* to give 1-(4-(4-(3-oxabicyclo[4.1.0]heptan-6-yl)-1-(4-oxocyclohexyl)-1*H*-pyrazolo[3,4-*d*]pyrimidin-6-yl)phenyl)-3-ethylurea (239 mg, 0.43 mmol, 100 % yield) as



a white amorphous solid. LCMS (high-pH) rt. 1.07 (100%)  $MH^+$  for desired  $M= 474.565$ .  $^1H$  NMR ( $CDCl_3$ , 400 MHz)  $\delta = 8.53$  (d,  $J = 8.6$  Hz, 2H), 8.10 (s, 1H), 7.50 (d,  $J = 8.8$  Hz, 2H), 6.93 (s, 1H), 5.35-5.45 (m, 1H), 5.32 (s, 1H), 5.06 (br s, 1H), 4.10 (dd,  $J = 11.5, 1.5$  Hz, 1H), 4.06 (dd,  $J = 11.7, 3.7$  Hz, 1H), 3.82 (ddd,  $J = 11.6, 5.9, 3.8$  Hz, 1H), 3.51 (ddd,  $J = 11.5, 9.8, 5.1$  Hz, 1H), 3.31-3.40 (m, 2H), 3.04 (dt,  $J = 13.9, 4.4$  Hz, 1H), 2.58-2.75 (m, 6H), 2.32-2.44 (m, 3H), 2.23-2.31 (m, 1H), 1.60-1.78 (m, 3H), 1.39 (dd,  $J = 6.7, 4.3$  Hz, 1H), 1.21 ppm (t,  $J = 7.2$  Hz, 3H)  $^{13}C$  NMR (101 MHz,  $CDCl_3$ )  $\delta = 209.5, 169.6, 159.8, 155.3, 154.0, 141.4, 132.7, 132.4, 129.8, 119.4, 109.9, 65.5, 64.2, 53.2, 39.3, 35.3, 30.9, 26.5, 24.7, 23.8, 22.8, 15.1$ . HRMS calculated for  $C_{26}H_{30}N_6O_3$  475.2444, found 475. 2462. FTIR ( $cm^{-1}$ ) 1535, 1385, 1306, 1170, 853, 804.

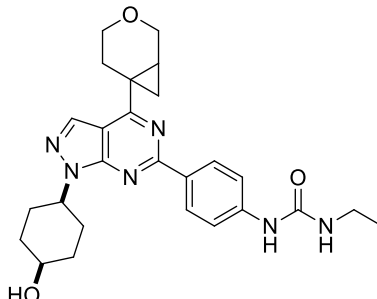
1-(4-(4-(3-Oxabicyclo[4.1.0]heptan-6-yl)-1-((1*r*,4*r*)-4-hydroxycyclohexyl)-1*H*-pyrazolo[3,4-*d*]pyrimidin-6-yl)phenyl)-3-ethylurea (192)



In a scintillation vial 1-(4-(4-(3-oxabicyclo[4.1.0]heptan-6-yl)-1-(4-oxocyclohexyl)-1*H*-pyrazolo[3,4-*d*]pyrimidin-6-yl)phenyl)-3-ethylurea (50 mg, 0.09 mmol) was dissolved in THF (1.7 mL). Sodium borohydride (17mg, 0.49 mmol) was added and the reaction was stirred at r.t. for 1 h. The reaction was partitioned between ethyl acetate (10 mL) and sat. aq. sodium bicarbonate (10 mL). The aqueous layer was extracted with further ethyl acetate (3x 5 mL). The combined organic layers were dried (hydrophobic frit) and concentrated *in vacuo*. The resulting residue was purified by Mass Directed Auto Purification (MDAP) (high-pH, Method 3) to give 1-(4-(4-(3-oxabicyclo[4.1.0]heptan-6-yl)-1-((1*r*,4*r*)-4-hydroxycyclohexyl)-1*H*-pyrazolo[3,4-*d*]pyrimidin-6-yl)phenyl)-3-ethylurea (19 mg, 0.04 mmol, 45% yield) as an amorphous white solid. LCMS (high-pH) rt. 0.98 (100%)  $MH^+$  for desired  $M= 476.254$ .  $^1H$  NMR ( $DMSO-d_6$ , 400 MHz)  $\delta = 8.75$  (s, 1H), 8.38 (d,  $J = 8.1$  Hz, 2H), 8.30 (s, 1H), 7.56 (d,  $J = 8.8$  Hz, 2H), 6.20 (t,  $J = 5.5$  Hz, 1H), 4.83 (tt,  $J = 11.7, 3.9$  Hz, 1H), 4.69 (d,  $J = 4.2$  Hz, 1H), 3.98 (dd,  $J = 11.5, 3.9$  Hz, 1H), 3.94 (dd,  $J = 11.5, 1.5$  Hz, 1H), 3.68 (ddd,  $J = 11.7, 5.6, 4.2$  Hz, 1H), 3.54-3.63 (m, 1H), 3.44 (ddd,  $J = 11.5, 9.5, 5.1$  Hz, 1H), 3.10-3.20 (m, 2H), 2.95 (dt,  $J = 13.9, 4.4$  Hz, 1H), 2.18-2.31 (m, 2H), 1.90-2.11 (m, 5H), 1.64 (dd,  $J = 9.0, 3.9$  Hz, 1H), 1.48 (br s, 2H), 1.30 (dd,  $J = 6.6, 4.2$  Hz, 1H), 1.08 ppm (t,  $J = 7.2$  Hz, 3H).  $^{13}C$  NMR

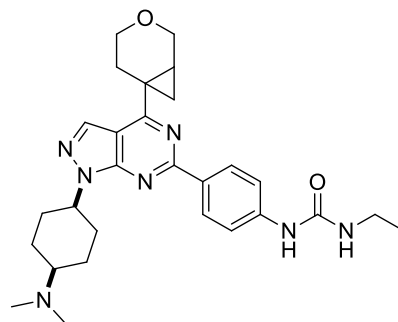
(DMSO- $d_6$ , 101 MHz)  $\delta$  = 169.7, 159.5, 155.3, 153.6, 143.7, 130.3, 129.6, 117.5, 109.5, 68.5, 65.2, 63.8, 55.2, 34.6, 34.4, 30.3, 26.3, 24.7, 23.7, 22.9, 15.9 ppm. HRMS calculated for  $C_{26}H_{32}N_6O_3$  477.2614, found 477.2617. FTIR ( $cm^{-1}$ ) 3329, 1537, 1386, 1230, 1057.

1-(4-(4-(3-Oxabicyclo[4.1.0]heptan-6-yl)-1-((1s,4s)-4-hydroxycyclohexyl)-1H-pyrazolo[3,4-*d*]pyrimidin-6-yl)phenyl)-3-ethylurea (193)



In a scintillation vial 1-(4-(4-(3-oxabicyclo[4.1.0]heptan-6-yl)-1-(4-oxocyclohexyl)-1H-pyrazolo[3,4-*d*]pyrimidin-6-yl)phenyl)-3-ethylurea (40 mg, 0.072 mmol) was dissolved in THF (1.4 mL). *L*-selectride (2 M in THF) (0.18 mL, 0.35 mmol) was added and the reaction was stirred at 50 °C for 1 h. The reaction was partitioned between ethyl acetate (10 mL) and sat. aq. sodium bicarbonate (10 mL). The aqueous layer was extracted with further ethyl acetate (3x 5 mL). The combined organic layers were dried (hydrophobic frit) and concentrated *in vacuo*. The resulting residue was purified by Mass Directed Auto Purification (MDAP) (high-pH, Method 3) to give 1-(4-(4-(3-oxabicyclo[4.1.0]heptan-6-yl)-1-((1s,4s)-4-hydroxycyclohexyl)-1H-pyrazolo[3,4-*d*]pyrimidin-6-yl)phenyl)-3-ethylurea (15 mg, 0.031 mmol, 44% yield) as a white solid. LCMS (high-pH) rt. 0.98 (100%)  $MH^+$  for desired  $M=476.254$ .  $^1H$  NMR (DMSO- $d_6$ , 400 MHz)  $\delta$  = 8.75 (s, 1H), 8.38 (d,  $J$  = 8.1 Hz, 2H), 8.31 (s, 1H), 7.52-7.57 (m, 2H), 6.21 (t,  $J$  = 5.5 Hz, 1H), 4.87 (tt,  $J$  = 11.3, 3.7 Hz, 1H), 4.49 (d,  $J$  = 2.7 Hz, 1H), 3.99 (dd,  $J$  = 11.2, 3.9 Hz, 1H), 3.94 (dd,  $J$  = 11.0, 1.5 Hz, 2H), 3.69 (ddd,  $J$  = 11.5, 5.9, 4.4 Hz, 1H), 3.44 (ddd,  $J$  = 11.5, 9.5, 4.9 Hz, 1H), 3.10-3.18 (m, 2H), 2.96 (dt,  $J$  = 14.1, 4.7 Hz, 1H), 2.36-2.45 (m, 2H), 2.19-2.31 (m, 2H), 1.80-2.05 (m, 3H), 1.62-1.76 (m, 5H), 1.30 (dd,  $J$  = 6.6, 4.2 Hz, 1H), 1.08 ppm (t,  $J$  = 7.2 Hz, 3H).  $^{13}C$  NMR (DMSO- $d_6$ , 101 MHz)  $\delta$  = 169.6, 159.4, 155.3, 153.5, 143.6, 130.4, 129.5, 117.5, 109.4, 65.2, 63.8, 63.4, 55.3, 34.4, 32.0, 26.4, 26.3, 24.7, 23.7, 22.9, 15.9 ppm. HRMS calculated for  $C_{26}H_{32}N_6O_3$  477.2614, found 477.2614. FTIR ( $cm^{-1}$ ) 3332, 1535, 1360, 1243, 1080.

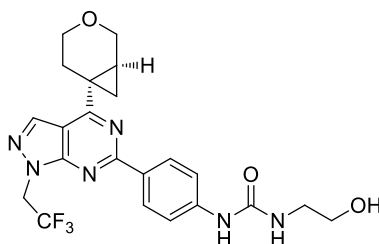
1-(4-(4-(3-Oxabicyclo[4.1.0]heptan-6-yl)-1-((1s,4s)-4-(dimethylamino)cyclohexyl)-1H-pyrazolo[3,4-d]pyrimidin-6-yl)phenyl)-3-ethylurea (194)



In a scintillation vial 1-(4-(4-(3-oxabicyclo[4.1.0]heptan-6-yl)-1-(4-oxocyclohexyl)-1H-pyrazolo[3,4-d]pyrimidin-6-yl)phenyl)-3-ethylurea (50 mg, 0.09 mmol) was dissolved in DCE (1.8 mL) and acetic acid (16  $\mu$ L, 0.27 mmol). STAB (57 mg, 0.27 mmol) and dimethylamine (2M in THF) (0.14 mL, 0.27 mmol) were added and the reaction was stirred at 50  $^{\circ}$ C for 3 h. The reaction mixture was partitioned between DCM (10 mL) and sat. aq. sodium bicarbonate (10 mL). The aqueous layer was extracted with further DCM (3x 5 mL). The combined organic layers were dried (hydrophobic frit) and concentrated *in vacuo*. The resulting residue was purified by Mass Directed Auto Purification (MDAP) (high-pH, Method 3) to give 1-(4-(4-(3-oxabicyclo[4.1.0]heptan-6-yl)-1-((1s,4s)-4-(dimethylamino)cyclohexyl)-1H-pyrazolo[3,4-d]pyrimidin-6-yl)phenyl)-3-ethylurea (8mg, 18% yield) as an amorphous white solid. LCMS (high-pH) rt. 1.20 (98%)  $MH^{+}$  for desired  $M = 503.301$ .  $^1H$  NMR ( $CDCl_3$ , 400 MHz)  $\delta = 8.53$  (d,  $J = 8.8$  Hz, 2H), 8.08 (s, 1H), 7.48 (d,  $J = 8.8$  Hz, 2H), 6.89 (s, 1H), 5.00-5.12 (m, 2H), 4.10 (dd,  $J = 11.2, 1.7$  Hz, 1H), 4.05 (dd,  $J = 11.5, 3.7$  Hz, 1H), 3.81 (ddd,  $J = 11.5, 6.0, 3.8$  Hz, 1H), 3.50 (ddd,  $J = 11.5, 9.9, 5.0$  Hz, 1H), 3.35 (qd,  $J = 7.3, 5.6$  Hz, 2H), 3.04 (dt,  $J = 13.9, 4.4$  Hz, 1H), 2.45-2.57 (m, 2H), 2.35-2.41 (m, 1H), 2.33 (s, 5H), 2.21-2.30 (m, 2H), 2.14-2.35 (m, 1H), 2.07-2.18 (m, 2H), 1.78-1.93 (m, 2H), 1.62-1.77 (m, 3H), 1.36 (dd,  $J = 6.6, 4.2$  Hz, 1H), 1.20 ppm (t,  $J = 7.2$  Hz, 3H)  $^{13}C$  NMR ( $CDCl_3$ , 101 MHz)  $\delta = 169.3, 159.5, 155.4, 153.7, 141.1, 133.1, 131.7, 129.8, 119.6, 109.7, 65.5, 64.3, 60.5, 54.3, 42.9, 35.3, 27.2, 27.0, 26.6, 24.7, 23.6, 22.6, 15.4$  ppm. HRMS calculated for  $C_{28}H_{37}N_7O_2$  504.3086, found 504.3086. FTIR ( $cm^{-1}$ ) 3349, 2932, 1555, 1387, 1236, 1172.

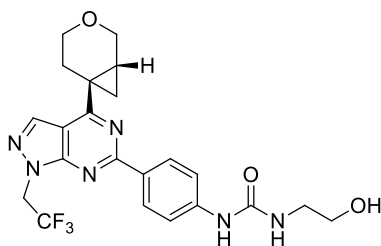
### 3.3.3 Backpacket Optimisation Compounds

4-(4-((1S,6R)-3-Oxabicyclo[4.1.0]heptan-6-yl)-1-(2,2,2-trifluoroethyl)-1H-pyrazolo[3,4-d]pyrimidin-6-yl)aniline (200a)



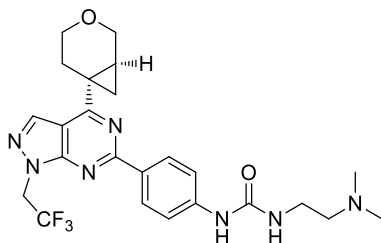
In a 2-5 mL microwave vial 4-(4-((1S,6R)-3-oxabicyclo[4.1.0]heptan-6-yl)-1-(2,2,2-trifluoroethyl)-1H-pyrazolo[3,4-d]pyrimidin-6-yl)aniline (20 mg, 0.05 mmol) and 4-nitrophenyl chloroformate (12 mg, 0.06 mmol) was dissolved in DCM (1 mL). Pyridine (21  $\mu$ L, 0.26 mmol) was added and the reaction was stirred at r.t. for 1.5 h. Ethanolamine (16  $\mu$ L, 0.26 mmol) and DIPEA (13  $\mu$ L, 0.08 mmol) were added and the reaction was stirred for a further 1 h. The reaction was partitioned between DCM (5 mL) and water (5 mL) and the resulting mixture was separated using a hydrophobic frit. The organic layer was concentrated *in vacuo* and purified by prep HPLC (formic, 30-85%, 20 min) to give 4-(4-((1S,6R)-3-oxabicyclo[4.1.0]heptan-6-yl)-1-(2,2,2-trifluoroethyl)-1H-pyrazolo[3,4-d]pyrimidin-6-yl)aniline (20 mg, 0.043 mmol, 83% yield) as an amorphous white solid LCMS (formic) rt. 0.97 (100%)  $MH^+$  for desired  $M=476.178$ .  $^1H$  NMR (400 MHz, DMSO- $d_6$ )  $\delta$  = 8.95 (s, 1H), 8.49 (s, 1H), 8.42 (d,  $J$  = 8.8 Hz, 2H), 7.56 (d,  $J$  = 8.8 Hz, 2H), 6.34 (t,  $J$  = 5.5 Hz, 1H), 5.45 - 5.43 (m, 1H), 5.41 (q,  $J$  = 9.0 Hz, 2H), 4.75 (br s, 1H), 4.00 (dd,  $J$  = 11.5, 4.2 Hz, 1H), 3.95 (dd,  $J$  = 11.5, 1.7 Hz, 1H), 3.69 (ddd,  $J$  = 11.5, 5.7, 4.3 Hz, 2H), 3.50 - 3.44 (m, 3H), 3.19 (q,  $J$  = 5.6 Hz, 2H), 2.96 (td,  $J$  = 14.2, 4.6 Hz, 1H), 2.34 - 2.24 (m, 3H), 1.67 (dd,  $J$  = 9.3, 4.2 Hz, 1H), 1.35 (dd,  $J$  = 6.6, 4.2 Hz, 1H). HRMS calculated for  $C_{22}H_{23}F_3N_6O_3$  477.1862, found 477.1865. FTIR ( $cm^{-1}$ ) 3295, 2954, 1660, 1539, 1386, 1239, 1152, 1064, 805

4-(4-((1*R*,6*S*)-3-Oxabicyclo[4.1.0]heptan-6-yl)-1-(2,2,2-trifluoroethyl)-1*H*-pyrazolo[3,4-*d*]pyrimidin-6-yl)aniline (200b)



In a 2-5 mL microwave vial 4-(4-((1*R*,6*S*)-3-oxabicyclo[4.1.0]heptan-6-yl)-1-(2,2,2-trifluoroethyl)-1*H*-pyrazolo[3,4-*d*]pyrimidin-6-yl)aniline (20 mg, 0.05 mmol) and 4-nitrophenyl chloroformate (12mg, 0.06 mmol) was dissolved in DCM (1 mL). Pyridine (21  $\mu$ L, 0.26 mmol) was added and the reaction was stirred at r.t. for 1.5 h. Ethanolamine (16  $\mu$ L, 0.26 mmol) and DIPEA (13  $\mu$ L, 0.08 mmol) were added and the reaction was stirred for a further 1 h. The reaction was partitioned between DCM (5 mL) and water (5 mL) and the resulting mixture was separated using a hydrophobic frit. The organic layer was concentrated *in vacuo* and purified by prep HPLC (formic, 30-85%, 20 min) to give 4-(4-((1*R*,6*S*)-3-oxabicyclo[4.1.0]heptan-6-yl)-1-(2,2,2-trifluoroethyl)-1*H*-pyrazolo[3,4-*d*]pyrimidin-6-yl)aniline (18 mg, 0.036 mmol, 72% yield) as a white solid. LCMS (formic) rt. 1.01 (100%)  $MH^+$  for desired  $M=476.460$ .  $^1H$  NMR (400 MHz, DMSO- $d_6$ )  $\delta$  = 8.95 (s, 1H), 8.49 (s, 1H), 8.42 (d,  $J$  = 8.8 Hz, 2H), 7.56 (d,  $J$  = 8.8 Hz, 2H), 6.34 (t,  $J$  = 5.5 Hz, 1H), 5.45 - 5.43 (m, 1H), 5.41 (q,  $J$  = 9.0 Hz, 2H), 4.75 (br s, 1H), 4.00 (dd,  $J$  = 11.5, 4.2 Hz, 1H), 3.95 (dd,  $J$  = 11.5, 1.7 Hz, 1H), 3.69 (ddd,  $J$  = 11.5, 5.7, 4.3 Hz, 2H), 3.50 - 3.44 (m, 3H), 3.19 (q,  $J$  = 5.6 Hz, 2H), 2.96 (td,  $J$  = 14.2, 4.6 Hz, 1H), 2.34 - 2.24 (m, 3H), 1.67 (dd,  $J$  = 9.3, 4.2 Hz, 1H), 1.35 (dd,  $J$  = 6.6, 4.2 Hz, 1H). HRMS calculated for  $C_{22}H_{23}F_3N_6O_3$  477.1862, found 477.1865. FTIR ( $cm^{-1}$ ) 3306, 2959, 1659, 1539, 1386, 1239, 1152, 1064.

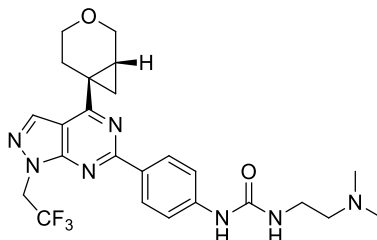
1-(4-(4-((1*S*,6*R*)-3-Oxabicyclo[4.1.0]heptan-6-yl)-1-(2,2,2-trifluoroethyl)-1*H*-pyrazolo[3,4-*d*]pyrimidin-6-yl)phenyl)-3-(2-(dimethylamino)ethyl)urea (201a)



In a 2-5 mL microwave vial 4-(4-((1*S*,6*R*)-3-oxabicyclo[4.1.0]heptan-6-yl)-1-(2,2,2-trifluoroethyl)-1*H*-pyrazolo[3,4-*d*]pyrimidin-6-yl)aniline (20 mg, 0.05 mmol) and 4-nitrophenyl chloroformate (12mg, 0.06 mmol) was dissolved in DCM (1 mL). Pyridine (21

$\mu\text{L}$ , 0.26 mmol) was added and the reaction was stirred at r.t. for 1.5 h. *NI,NI*-dimethylethane-1,2-diamine (28  $\mu\text{L}$ , 0.26 mmol) and DIPEA (13  $\mu\text{L}$ , 0.08 mmol) were added and the reaction was stirred for a further 1 h. The reaction was partitioned between DCM (5 mL) and water (5 mL) and the resulting mixture was separated using a hydrophobic frit. The organic layer was concentrated *in vacuo* and purified by prep HPLC (formic, 30-85%, 20 min) to give 1-(4-(4-((1*S*,6*R*)-3-oxabicyclo[4.1.0]heptan-6-yl)-1-(2,2,2-trifluoroethyl)-1*H*-pyrazolo[3,4-*d*]pyrimidin-6-yl)phenyl)-3-(2-(dimethylamino)ethyl)urea (25 mg, 0.050 mmol, 97% yield) as an amorphous white solid. LCMS (formic) rt. 0.73 (100%)  $\text{MH}^+$  for desired  $\text{M} = 503.226$ .  $^1\text{H}$  NMR ( $\text{CDCl}_3$ , 400 MHz)  $\delta = 8.52$  (d,  $J = 7.9$  Hz, 2H), 8.19 (s, 1H), 7.51 (d,  $J = 8.1$  Hz, 2H), 5.43 (br s, 1H), 5.11 (q,  $J = 8.3$  Hz, 2H), 4.11 (dd,  $J = 11.2, 1.5$  Hz, 1H), 4.06 (dd,  $J = 11.5, 3.9$  Hz, 1H), 3.83 (ddd,  $J = 11.6, 6.1, 3.9$  Hz, 1H), 3.52 (ddd,  $J = 11.7, 9.8, 5.1$  Hz, 1H), 3.37 (q,  $J = 5.4$  Hz, 2H), 3.04 (dt,  $J = 13.9, 4.4$  Hz, 1H), 2.51-2.60 (m, 2H), 2.39 (ddd,  $J = 13.9, 9.8, 6.1$  Hz, 1H), 2.35 (s, 6H), 2.26-2.33 (m, 1H), 1.72 (dd,  $J = 9.3, 4.2$  Hz, 1H), 1.42 ppm (dd,  $J = 6.7, 4.3$  Hz, 1H).  $^{13}\text{C}$  NMR (101 MHz,  $\text{CDCl}_3$ )  $\delta = 170.0, 161.0, 155.9, 142.5, 134.5, 131.6, 129.8, 123.2$  (q,  $^1J_{\text{CF}} = 278.0$  Hz, 1C), 118.6, 109.5, 65.5, 64.2, 47.5 (q,  $^2J_{\text{CF}} = 36.0$  Hz, 1C), 45.2, 26.5, 24.7, 24.1, 23.0. HRMS calculated for  $\text{C}_{24}\text{H}_{28}\text{F}_3\text{N}_7\text{O}_2$  504.2335, found 504.2342. FTIR ( $\text{cm}^{-1}$ ) 3343, 2943, 1670, 1539, 1385, 1266, 1151, 1045, 807.

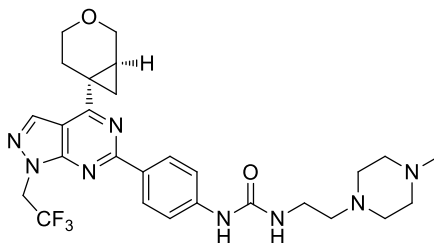
4-(4-((1*R*,6*S*)-3-Oxabicyclo[4.1.0]heptan-6-yl)-1-(2,2,2-trifluoroethyl)-1*H*-pyrazolo[3,4-*d*]pyrimidin-6-yl)phenyl)-3-(2-(dimethylamino)ethyl)urea (**201b**)



In a 2-5 mL microwave vial 4-(4-((1*R*,6*S*)-3-oxabicyclo[4.1.0]heptan-6-yl)-1-(2,2,2-trifluoroethyl)-1*H*-pyrazolo[3,4-*d*]pyrimidin-6-yl)aniline (20 mg, 0.05 mmol) and 4-nitrophenyl chloroformate (12mg, 0.06 mmol) was dissolved in DCM (1 mL). Pyridine (21  $\mu\text{L}$ , 0.26 mmol) was added and the reaction was stirred at r.t. for 1.5 h. *NI,NI*-dimethylethane-1,2-diamine (28  $\mu\text{L}$ , 0.26 mmol) and DIPEA (13  $\mu\text{L}$ , 0.08 mmol) were added and the reaction was stirred for a further 1 h. The reaction was partitioned between DCM (5 mL) and water (5 mL) and the resulting mixture was separated using a hydrophobic frit. The organic layer was concentrated *in vacuo* and purified by prep HPLC (formic, 30-85%, 20 min) to give 1-(4-(4-((1*R*,6*S*)-3-oxabicyclo[4.1.0]heptan-6-yl)-1-(2,2,2-trifluoroethyl)-1*H*-pyrazolo[3,4-*d*]pyrimidin-6-yl)phenyl)-3-(2-(dimethylamino)ethyl)urea (22 mg, 0.044 mmol,

85% yield) as an amorphous white solid. LCMS (formic) rt. 0.70 (100%)  $MH^+$  for desired  $M=503.226$ .  $^1H$  NMR ( $CDCl_3$ , 400 MHz)  $\delta = 8.51$  (d,  $J = 8.8$  Hz, 2H), 8.18 (s, 1H), 7.52 (d,  $J = 8.8$  Hz, 2H), 5.61 (br s, 1H), 5.11 (q,  $J = 8.3$  Hz, 2H), 4.10 (dd,  $J = 11.7, 1.5$  Hz, 1H), 4.06 (dd,  $J = 11.7, 3.4$  Hz, 1H), 3.82 (ddd,  $J = 11.6, 6.1, 3.9$  Hz, 1H), 3.52 (ddd,  $J = 11.6, 9.8, 5.0$  Hz, 1H), 3.37 (q,  $J = 5.1$  Hz, 2H), 3.00-3.07 (m, 1H), 2.51-2.60 (m, 2H), 2.39 (ddd,  $J = 13.9, 10.0, 5.9$  Hz, 1H), 2.35 (s, 6H), 2.26-2.32 (m, 1H), 1.71 (dd,  $J = 9.3, 4.2$  Hz, 1H), 1.42 ppm (dd,  $J = 6.7, 4.3$  Hz, 1H).  $^{13}C$  NMR (101 MHz,  $CDCl_3$ )  $\delta = 169.9, 161.1, 155.9, 142.5, 134.5, 131.5, 129.8, 123.2$  (q,  $^1J_{CF} = 281.0$  Hz, 1C), 118.7, 112.0, 109.5, 65.5, 64.2, 47.5 (q,  $^2J_{CF} = 35.2$  Hz, 1C), 45.2, 26.5, 24.7, 24.1, 23.0. HRMS calculated for  $C_{24}H_{28}F_3N_7O_2$  504.2335, found 504.2342. FTIR ( $cm^{-1}$ ) 3332, 2943, 1670, 1539, 1385, 1266, 1151, 1044, 806.

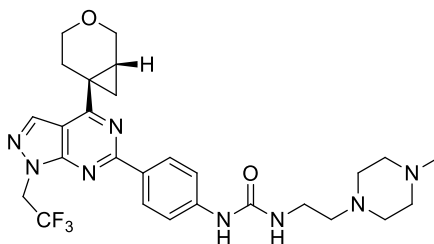
1-(4-(4-((1*S*,6*R*)-3-oxabicyclo[4.1.0]heptan-6-yl)-1-(2,2,2-trifluoroethyl)-1*H*-pyrazolo[3,4-*d*]pyrimidin-6-yl)phenyl)-3-(2-(4-methylpiperazin-1-yl)ethyl)urea (202a)



In a 2-5 mL microwave vial 4-(4-((1*S*,6*R*)-3-oxabicyclo[4.1.0]heptan-6-yl)-1-(2,2,2-trifluoroethyl)-1*H*-pyrazolo[3,4-*d*]pyrimidin-6-yl)aniline (20 mg, 0.05 mmol) and 4-nitrophenyl chloroformate (12mg, 0.06 mmol) was dissolved in DCM (1 mL). Pyridine (21  $\mu$ L, 0.26 mmol) was added and the reaction was stirred at r.t. for 1.5 h. 2-(4-methylpiperazin-1-yl)ethan-1-amine (37mg, 0.26 mmol) and DIPEA (13  $\mu$ L, 0.08 mmol) were added and the reaction was stirred for a further 1 h. The reaction was partitioned between DCM (5 mL) and water (5 mL) and the resulting mixture was separated using a hydrophobic frit. The organic layer was concentrated *in vacuo* and purified by prep HPLC (formic, 30-85%, 20 min) to give 2-(4-methylpiperazin-1-yl)ethan-1-amine to give 1-(4-(4-((1*S*,6*R*)-3-oxabicyclo[4.1.0]heptan-6-yl)-1-(2,2,2-trifluoroethyl)-1*H*-pyrazolo[3,4-*d*]pyrimidin-6-yl)phenyl)-3-(2-(4-methylpiperazin-1-yl)ethyl)urea (37 mg, 0.33 mmol, 65% yield) as an amorphous off-white solid. LCMS (high-pH) rt. 1.06 (100%)  $MH^+$  for desired  $M=558.268$ .  $^1H$  NMR ( $DMSO-d_6$ , 400 MHz)  $\delta = 9.00$  (s, 1H), 8.49 (s, 1H), 8.41 (d,  $J = 9.0$  Hz, 2H), 7.57 (d,  $J = 8.8$  Hz, 2H), 6.71-7.02 (m, 1H), 6.18 (t,  $J = 5.4$  Hz, 1H), 5.41 (q,  $J = 9.1$  Hz, 2H), 4.00 (dd,  $J = 11.7, 4.2$  Hz, 1H), 3.95 (dd,  $J = 11.2, 1.5$  Hz, 1H), 3.69 (ddd,  $J = 11.5, 5.9, 4.4$  Hz, 1H), 3.46 (ddd,  $J = 11.5, 9.3, 5.1$  Hz, 1H), 3.20-3.26 (m, 2H), 2.96 (dt,  $J = 14.1, 4.7$  Hz, 1H), 2.24-2.44 (m, 11H), 2.17 (s, 3H), 1.67 (dd,  $J = 9.3, 3.9$  Hz, 1H), 1.35 (dd,  $J = 6.6, 4.2$  Hz, 1H).  $^{13}C$  NMR (101 MHz,

CDCl<sub>3</sub>)  $\delta$  = 170.0, 160.9, 155.9, 141.8, 134.5, 132.2, 129.9, 123.2 (q,  $^1J_{CF}$  = 264.1 Hz, 1C), 119.4, 112.0, 109.6, 65.5, 64.2, 57.6, 55.1, 53.0, 47.6 (q,  $^2J_{CF}$  = 36.0 Hz, 1C), 46.1, 26.5, 24.8, 24.2, 23.1. HRMS calculated for C<sub>27</sub>H<sub>33</sub>F<sub>3</sub>N<sub>8</sub>O<sub>2</sub> 559.2757, found 559.2756 FTIR (cm<sup>-1</sup>) 3338, 2937, 1652, 1538, 1385, 1385, 1262, 1149, 1012 806.

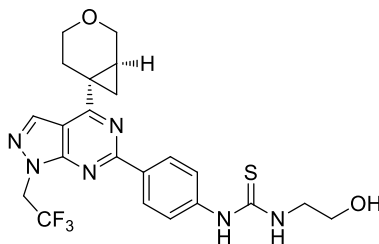
1-(4-(4-((1*R*,6*S*)-3-Oxabicyclo[4.1.0]heptan-6-yl)-1-(2,2,2-trifluoroethyl)-1*H*-pyrazolo[3,4-*d*]pyrimidin-6-yl)phenyl)-3-(2-(4-methylpiperazin-1-yl)ethyl)urea (202b)



In a 2-5 mL microwave vial 4-(4-((1*R*,6*S*)-3-oxabicyclo[4.1.0]heptan-6-yl)-1-(2,2,2-trifluoroethyl)-1*H*-pyrazolo[3,4-*d*]pyrimidin-6-yl)aniline (20 mg, 0.05 mmol) and 4-nitrophenyl chloroformate (12mg, 0.06 mmol) was dissolved in DCM (1 mL). Pyridine (21  $\mu$ L, 0.26 mmol) was added and the reaction was stirred at r.t. for 1.5 h. 2-(4-methylpiperazin-1-yl)ethan-1-amine (37mg, 0.26 mmol) and DIPEA (13  $\mu$ L, 0.08 mmol) were added and the reaction was stirred for a further 1 h. The reaction was partitioned between DCM (5 mL) and water (5 mL) and the resulting mixture was separated using a hydrophobic frit. The organic layer was concentrated *in vacuo* and purified by prep HPLC (formic, 30-85%, 20 min) to give 2-(4-methylpiperazin-1-yl)ethan-1-amine to give 1-(4-(4-((1*R*,6*S*)-3-oxabicyclo[4.1.0]heptan-6-yl)-1-(2,2,2-trifluoroethyl)-1*H*-pyrazolo[3,4-*d*]pyrimidin-6-yl)phenyl)-3-(2-(4-methylpiperazin-1-yl)ethyl)urea (37 mg, 0.26 mmol, 77% yield) as an amorphous off-white solid. LCMS (high-pH) rt. 1.06 (100%) MH<sup>+</sup> for desired M= 558.268. <sup>1</sup>H NMR (CDCl<sub>3</sub>, 400 MHz)  $\delta$  = 8.53 (d,  $J$  = 8.8 Hz, 2H), 8.20 (s, 1H), 7.52 (d,  $J$  = 8.8 Hz, 2H), 5.36-5.46 (m, 1H), 5.12 (q,  $J$  = 8.3 Hz, 2H), 4.12 (dd,  $J$  = 11.5, 1.5 Hz, 1H), 4.07 (dd,  $J$  = 11.2, 3.4 Hz, 1H), 3.83 (ddd,  $J$  = 11.6, 6.0, 3.9 Hz, 1H), 3.46-3.59 (m, 1H), 3.41 (q,  $J$  = 5.3 Hz, 2H), 3.04 (dt,  $J$  = 13.9, 4.4 Hz, 1H), 2.45-2.63 (m, 9H), 2.40 (ddd,  $J$  = 13.9, 9.8, 6.1 Hz, 1H), 2.32 (s, 3H), 2.27-2.31 (m, 1H), 1.72 (dd,  $J$  = 9.3, 4.2 Hz, 1H), 1.43 ppm (dd,  $J$  = 6.7, 4.3 Hz, 1H). <sup>13</sup>C NMR (101 MHz, CDCl<sub>3</sub>)  $\delta$  = 170.0, 160.9, 155.9, 141.8, 134.5, 132.2, 129.9, 123.2 (q,  $^1J_{CF}$  = 264.1 Hz, 1C), 119.4, 112.0, 109.6, 65.5, 64.2, 57.6, 55.1, 53.0, 47.6 (q,  $^2J_{CF}$  = 36.0 Hz, 1C), 46.1, 26.5, 24.8, 24.2, 23.1. HRMS calculated for C<sub>27</sub>H<sub>33</sub>F<sub>3</sub>N<sub>8</sub>O<sub>2</sub> 559.2757, found 559.2754. FTIR (cm<sup>-1</sup>) 3338, 2936, 1651, 1537, 1385, 1262, 1149, 1013, 806.

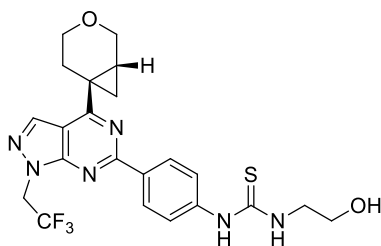


1-(4-(4-((1*S*,6*R*)-3-Oxabicyclo[4.1.0]heptan-6-yl)-1-(2,2,2-trifluoroethyl)-1*H*-pyrazolo[3,4-*d*]pyrimidin-6-yl)phenyl)-3-(2-hydroxyethyl)thiourea (203a)



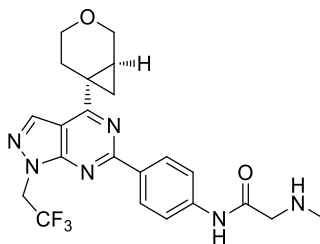
In a 2-5 mL microwave vial 4-(4-((1*S*,6*R*)-3-oxabicyclo[4.1.0]heptan-6-yl)-1-(2,2,2-trifluoroethyl)-1*H*-pyrazolo[3,4-*d*]pyrimidin-6-yl)aniline (25 mg, 0.064 mmol) was dissolved in DCM (1 mL). 1,1'-Thiocarbonyldiimidazole (17 mg, 0.096 mmol) and pyridine (10  $\mu$ L, 0.13 mmol) were added and the reaction was stirred at r.t. for 2 h. LCMS analysis showed complete conversion to desired intermediate. Ethanolamine (19  $\mu$ L, 0.32 mmol) was added and the reaction was stirred at r.t. for 0.5 h. The reaction mixture was concentrated *in vacuo* and the resulting residue was purified by preparative HPLC (formic, 30-85%, 15 min) to give 1-(4-(4-((1*S*,6*R*)-3-oxabicyclo[4.1.0]heptan-6-yl)-1-(2,2,2-trifluoroethyl)-1*H*-pyrazolo[3,4-*d*]pyrimidin-6-yl)phenyl)-3-(2-hydroxyethyl)thiourea (29 mg, 0.059 mmol, 92% yield) as an amorphous white solid. LCMS (formic) rt. 1.04 (100%)  $MH^+$  for desired  $M=492.156$ .  $^1H$  NMR (DMSO- $d_6$ , 400 MHz)  $\delta$  = 9.95 (br s, 1H), 8.51 (s, 1H), 8.47 (d,  $J$  = 8.8 Hz, 2H), 8.00 (br., s, 1H), 7.72 (d,  $J$  = 8.6 Hz, 2H), 5.43 (q,  $J$  = 9.0 Hz, 2H), 4.84 (br s, 1H), 4.00 (dd,  $J$  = 11.5, 4.2 Hz, 1H), 3.94 (d,  $J$  = 11.0 Hz, 1H), 3.64-3.72 (m, 1H), 3.59 (br s, 4H), 3.46 (ddd,  $J$  = 11.4, 9.2, 5.3 Hz, 1H), 2.97 (dt,  $J$  = 13.9, 4.9 Hz, 1H), 2.25-2.35 (m, 2H), 1.68 (dd,  $J$  = 9.2, 4.0 Hz, 1H), 1.37 ppm (dd,  $J$  = 6.5, 4.3 Hz, 1H).  $^{13}C$  NMR (101 MHz, DMSO- $d_6$ )  $\delta$  = 180.8, 170.6, 160.2, 155.7, 142.9, 135.4, 132.4, 129.3, 124.2 (q,  $^1J_{CF}$  = 280.2 Hz, 1C), 122.2, 109.5, 65.1, 63.7, 59.6, 47.3 (q,  $^2J_{CF}$  = 33.8 Hz, 1C), 47.0, 26.1, 24.9, 24.4, 23.6. HRMS calculated for  $C_{22}H_{23}F_3N_6O_2S$  493.1634, found 493.1635. FTIR ( $cm^{-1}$ ) 3167, 2942, 1539, 1385, 1263, 1152, 1046, 927, 807.

1-(4-(4-((1*R*,6*S*)-3-Oxabicyclo[4.1.0]heptan-6-yl)-1-(2,2,2-trifluoroethyl)-1*H*-pyrazolo[3,4-*d*]pyrimidin-6-yl)phenyl)-3-(2-hydroxyethyl)thiourea (203b)



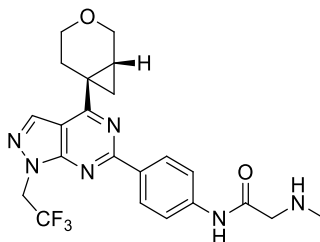
In a 2-5 mL microwave vial 4-(4-((1*R*,6*S*)-3-oxabicyclo[4.1.0]heptan-6-yl)-1-(2,2,2-trifluoroethyl)-1*H*-pyrazolo[3,4-*d*]pyrimidin-6-yl)aniline (25 mg, 0.064 mmol) was dissolved in DCM (1 mL). 1,1'-Thiocarbonyldiimidazole (17 mg, 0.096 mmol) and pyridine (10  $\mu$ L, 0.13 mmol) were added and the reaction was stirred at r.t. for 2 h. LCMS analysis showed complete conversion to desired intermediate. Ethanolamine (19  $\mu$ L, 0.32 mmol) was added and the reaction was stirred at r.t. for 0.5 h. The reaction mixture was concentrated *in vacuo* and the resulting residue was purified by preparative HPLC (formic, 30-85%, 15 min) to give 1-(4-(4-((1*R*,6*S*)-3-oxabicyclo[4.1.0]heptan-6-yl)-1-(2,2,2-trifluoroethyl)-1*H*-pyrazolo[3,4-*d*]pyrimidin-6-yl)phenyl)-3-(2-hydroxyethyl)thiourea (26 mg, 0.053 mmol, 82% yield) as an amorphous white solid. LCMS (formic) rt.1.04 (100%)  $MH^+$  for desired  $M=492.156$ .  $^1H$  NMR (DMSO- $d_6$ , 400 MHz)  $\delta$  = 9.96 (br., s, 1H), 8.52 (s, 1H), 8.47 (d,  $J$  = 8.8 Hz, 2H), 8.01 (br s, 1H), 7.72 (d,  $J$  = 8.1 Hz, 2H), 5.43 (q,  $J$  = 9.0 Hz, 2H), 4.84 (br., s, 1H), 4.00 (dd,  $J$  = 11.5, 4.2 Hz, 1H), 3.95 (dd,  $J$  = 11.2, 1.2 Hz, 1H), 3.69 (ddd,  $J$  = 11.7, 5.9, 4.9 Hz, 1H), 3.59 (br s, 4H), 3.46 (ddd,  $J$  = 11.7, 8.8, 5.4 Hz, 1H), 3.08-3.27 (m, 1H), 2.98 (dt,  $J$  = 13.9, 4.8 Hz, 1H), 2.24-2.35 (m, 2H), 1.69 (dd,  $J$  = 9.3, 4.2 Hz, 1H), 1.37 ppm (dd,  $J$  = 6.6, 4.2 Hz, 1H).  $^{13}C$  NMR (101 MHz, DMSO- $d_6$ )  $\delta$  = 180.7, 170.6, 160.2, 155.7, 142.9, 135.4, 132.4, 129.3, 124.2 (q,  $^1J_{CF}$  = 280.2 Hz, 1C), 109.5, 65.1, 63.7, 59.6, 47.3 (q,  $^2J_{CF}$  = 34.5 Hz, 1C), 47.0, 26.1, 24.9, 24.4, 23.5. HRMS calculated for  $C_{22}H_{23}F_3N_6O_2S$  493.1634, found 493.1633. FTIR ( $cm^{-1}$ ) 3167, 2948, 1522, 1384, 1263, 1045, 926, 807.

*N*-(4-(4-((1*S*,6*R*)-3-Oxabicyclo[4.1.0]heptan-6-yl)-1-(2,2,2-trifluoroethyl)-1*H*-pyrazolo[3,4-*d*]pyrimidin-6-yl)phenyl)-2-(methylamino)acetamide (204a)



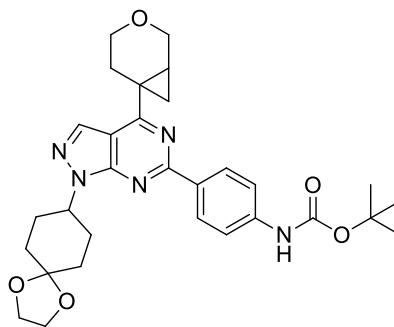
In a 2-5 mL microwave vial 4-(4-((1*S*,6*R*)-3-oxabicyclo[4.1.0]heptan-6-yl)-1-(2,2,2-trifluoroethyl)-1*H*-pyrazolo[3,4-*d*]pyrimidin-6-yl)aniline (27 mg, 0.07 mmol), Boc-*N*-methylglycine (22 mg, 0.12 mmol), HATU (53 mg, 0.14 mmol) and DIPEA (30  $\mu$ L) were dissolved in 2-MeTHF (1 mL) and the reaction mixture was stirred at r.t. for 16 h. The reaction mixture was partitioned between DCM (5 mL) and water (5 mL) and the aqueous layer was extracted with DCM (3x 5 mL). The combined organic layers were dried (hydrophobic frit) and concentrated *in vacuo*. The resulting crude mixture was dissolved in hexafluoroisopropanol (2.5 mL) and heated in microwave at 150  $^{\circ}$ C for 2 h. The resulting reaction mixture was concentrated *in vacuo* and purified by preparative HPLC (High-pH, 55-95%, 15 mins) to give *N*-(4-(4-((1*S*,6*R*)-3-oxabicyclo[4.1.0]heptan-6-yl)-1-(2,2,2-trifluoroethyl)-1*H*-pyrazolo[3,4-*d*]pyrimidin-6-yl)phenyl)-2-(methylamino)acetamide (18 mg, 0.039 mmol, 57% yield) as an amorphous white solid. LCMS (formic) rt. 0.73 (96%)  $MH^{+}$  for desired  $M = 460.183$ .  $^1H$  NMR ( $CDCl_3$ , 400 MHz)  $\delta = 9.44$  (s, 1H), 8.53-8.61 (m, 2H), 8.20 (s, 1H), 7.73-7.79 (m, 2H), 5.13 (q,  $J = 8.3$  Hz, 2H), 4.12 (dd,  $J = 11.0, 1.5$  Hz, 1H), 4.07 (dd,  $J = 11.2, 3.7$  Hz, 1H), 3.83 (ddd,  $J = 11.6, 6.0, 3.7$  Hz, 1H), 3.53 (ddd,  $J = 11.7, 9.7, 5.0$  Hz, 1H), 3.41 (s, 2H), 3.05 (dt,  $J = 13.9, 4.4$  Hz, 1H), 2.56 (s, 3H), 2.40 (ddd,  $J = 13.9, 9.8, 5.9$  Hz, 1H), 2.26-2.35 (m, 1H), 1.73 (dd,  $J = 9.3, 4.2$  Hz, 1H), 1.44 (dd,  $J = 6.7, 4.3$  Hz, 1H).  $^{13}C$  NMR (101 MHz,  $CDCl_3$ )  $\delta = 170.1, 169.9, 160.8, 155.8, 140.2, 134.5, 133.1, 129.8, 123.2$  (q,  $^1J_{CF} = 279.5$  Hz, 1C), 119.0, 110.0, 65.5, 64.2, 55.2, 47.6 (q,  $^2J_{CF} = 35.5$  Hz, 1C), 36.9, 26.46, 24.8, 24.2, 23.1. HRMS calculated for  $C_{22}H_{23}F_3N_6O_2$  461.1913, found 461.1913. FTIR ( $cm^{-1}$ ) 3290, 2855, 1682, 1572, 1525, 1386, 1150, 1043, 806.

*N*-(4-(4-((1*R*,6*S*)-3-Oxabicyclo[4.1.0]heptan-6-yl)-1-(2,2,2-trifluoroethyl)-1*H*-pyrazolo[3,4-*d*]pyrimidin-6-yl)phenyl)-2-(methylamino)acetamide (204b)



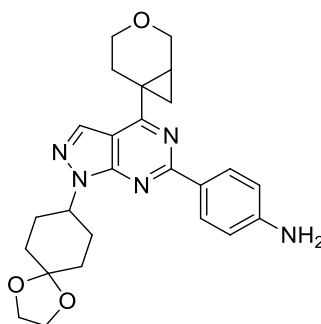
In a 2-5 mL microwave vial 4-(4-((1*R*,6*S*)-3-oxabicyclo[4.1.0]heptan-6-yl)-1-(2,2,2-trifluoroethyl)-1*H*-pyrazolo[3,4-*d*]pyrimidin-6-yl)aniline (27 mg, 0.07 mmol), Boc-*N*-methylglycine (22 mg, 0.12 mmol), HATU (53 mg, 0.14 mmol) and DIPEA (30  $\mu$ L) were dissolved in 2Me-THF (1 mL) and the reaction mixture was stirred at r.t. for 16 h. The reaction mixture was partitioned between DCM (5 mL) and water (5 mL) and the aqueous layer was extracted with DCM (3x 5 mL). The combined organic layers were dried (hydrophobic frit) and concentrated *in vacuo*. The resulting crude mixture was dissolved in hexafluoroisopropanol (2.5 mL) and heated in microwave at 150  $^{\circ}$ C for 2 h. The resulting reaction mixture was concentrated *in vacuo* and purified by preparative HPLC (High-pH, 55-95%, 15 mins) to give *N*-(4-(4-((1*R*,6*S*)-3-oxabicyclo[4.1.0]heptan-6-yl)-1-(2,2,2-trifluoroethyl)-1*H*-pyrazolo[3,4-*d*]pyrimidin-6-yl)phenyl)-2-(methylamino)acetamide (16 mg, 0.04 mmol, 50% yield) as an amorphous white solid. LCMS (formic) rt. 0.73 (97%)  $\text{MH}^+$  for desired  $\text{M} = 460.183$ .  $^1\text{H}$  NMR ( $\text{CDCl}_3$ , 400 MHz)  $\delta = 9.44$  (s, 1H), 8.57 (d,  $J = 8.8$  Hz, 2H), 8.20 (s, 1H), 7.76 (d,  $J = 8.8$  Hz, 2H), 5.13 (q,  $J = 8.5$  Hz, 2H), 4.12 (dd,  $J = 11.5, 1.5$  Hz, 1H), 4.08 (dd,  $J = 11.5, 3.7$  Hz, 1H), 3.84 (ddd,  $J = 11.6, 6.0, 3.7$  Hz, 1H), 3.53 (ddd,  $J = 11.6, 9.7, 5.1$  Hz, 1H), 3.42 (s, 2H), 3.05 (dt,  $J = 13.8, 4.5$  Hz, 1H), 2.64 (s, 1H), 2.57 (s, 3H), 2.41 (ddd,  $J = 13.9, 9.7, 6.0$  Hz, 1H), 2.28-2.34 (m, 1H), 1.73 (dd,  $J = 9.3, 4.2$  Hz, 1H), 1.44 ppm (dd,  $J = 6.6, 4.2$  Hz, 1H).  $^{13}\text{C}$  NMR (101 MHz,  $\text{CDCl}_3$ )  $\delta = 170.1, 169.9, 160.8, 155.8, 140.2, 134.5, 133.1, 129.8, 123.2$  (q,  $^1J_{\text{CF}} = 281.7$  Hz, 1C), 119.0, 109.7, 65.5, 64.2, 55.2, 47.6 (q,  $^2J_{\text{CF}} = 36.0$  Hz, 1C), 36.9, 26.5, 24.8, 24.2, 23.1. HRMS calculated for  $\text{C}_{22}\text{H}_{23}\text{F}_3\text{N}_6\text{O}_2$  461.1913, found 461.1914. FTIR ( $\text{cm}^{-1}$ ) 3290, 2852, 1681, 1572, 1385, 1151, 1043, 805.

*tert*-butyl-(4-(4-(3-Oxabicyclo[4.1.0]heptan-6-yl)-1-(1,4-dioxaspiro[4.5]decan-8-yl)-1*H*-pyrazolo[3,4-*d*]pyrimidin-6-yl)phenyl)carbamate (211)



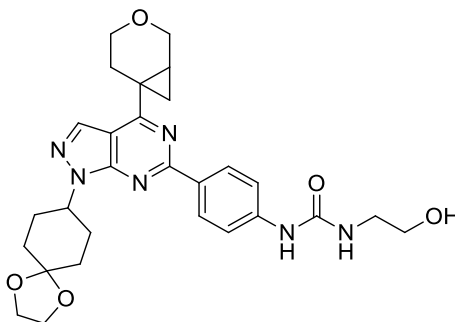
In a 2-5 mL microwave vial a mixture of 4-(3-oxabicyclo[4.1.0]heptan-6-yl)-6-chloro-1-(1,4-dioxaspiro[4.5]decan-8-yl)-1*H*-pyrazolo[3,4-*d*]pyrimidine (1.28 g, 1.87 mmol), *tert*-butyl (4-(4,4,5,5-tetramethyl-1,3,2-dioxaborolan-2-yl)phenyl)carbamate (983 mg, 3.08 mmol), sodium carbonate (396 mg, 3.73 mmol) and Pd(PPh<sub>3</sub>)<sub>4</sub> (216 mg, 0.19 mmol) was dissolved in DME (16.6 mL) and water (2.1 mL). The resulting suspension was degassed with a stream of nitrogen for 10 min, sealed and stirred at 100 °C for 1.5 h. The reaction was monitored by LCMS and, upon complete consumption of starting material, the reaction was cooled to r.t. and filtered through a celite cartridge (10 g). The reaction mixture was purified by flash column chromatography (cyclohexane: ethyl acetate 0-60% (12 column volumes)) to give *tert*-butyl (4-(4-(3-oxabicyclo[4.1.0]heptan-6-yl)-1-(1,4-dioxaspiro[4.5]decan-8-yl)-1*H*-pyrazolo[3,4-*d*]pyrimidin-6-yl)phenyl)carbamate (672 mg, 1.23 mmol, 66% yield) as an amorphous yellow solid. LCMS (formic) rt. 1.48 (97%) MH<sup>+</sup> for desired M= 547.279. <sup>1</sup>H NMR (DMSO-*d*<sub>6</sub>, 400 MHz) δ = 9.59 (s, 1H), 8.42 (d, *J* = 8.8 Hz, 2H), 8.32 (s, 1H), 7.62 (d, *J* = 8.8 Hz, 2H), 4.93-5.04 (m, 1H), 3.88-4.00 (m, 6H), 3.68 (ddd, *J* = 11.6, 5.8, 4.4 Hz, 1H), 3.44 (ddd, *J* = 12.0, 9.0, 5.1 Hz, 1H), 2.95 (dt, *J* = 13.9, 4.6 Hz, 1H), 2.16-2.35 (m, 4H), 1.74-1.98 (m, 6H), 1.65 (dd, *J* = 9.3, 3.9 Hz, 1H), 1.51 (s, 9H), 1.30 ppm (dd, *J* = 6.6, 4.2 Hz, 1H). <sup>13</sup>C NMR (DMSO-*d*<sub>6</sub>, 101 MHz) δ = 169.2, 158.8, 153.1, 152.6, 142.0, 132.4, 131.0, 128.9, 117.6, 109.1, 107.1, 79.3, 64.6, 63.8, 63.7, 63.2, 53.7, 33.0, 28.9, 28.1, 25.8, 24.2, 23.2, 22.5 ppm. HRMS calculated for C<sub>30</sub>H<sub>37</sub>N<sub>5</sub>O<sub>5</sub> 548.2873, found 548.2872. FTIR (cm<sup>-1</sup>) 3267, 2937, 1728, 1561, 1384, 1309, 1150, 1034, 808.

4-(4-(3-Oxabicyclo[4.1.0]heptan-6-yl)-1-(1,4-dioxaspiro[4.5]decan-8-yl)-1H-pyrazolo[3,4-d]pyrimidin-6-yl)aniline (199)



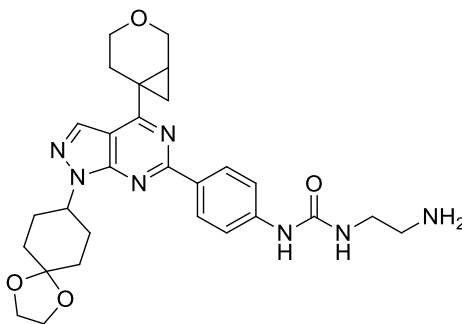
In a 2-5 mL microwave vial *tert*-butyl 4-(4-(3-oxabicyclo[4.1.0]heptan-6-yl)-1-(1,4-dioxaspiro[4.5]decan-8-yl)-1H-pyrazolo[3,4-d]pyrimidin-6-yl)phenyl)carbamate (610 mg, 1.08 mmol) was dissolved in hexafluoroisopropanol (3 mL) and the reaction was irradiated to 150 °C in a Biotage initiator+ microwave for 1 h. The reaction was concentrated *in vacuo* and triturated with diethyl ether to give 4-(4-(3-oxabicyclo[4.1.0]heptan-6-yl)-1-(1,4-dioxaspiro[4.5]decan-8-yl)-1H-pyrazolo[3,4-d]pyrimidin-6-yl)aniline (487 mg, 1.08 mmol, 100% yield) as an amorphous tan solid. LCMS (formic) rt. 1.15 (92%) MH<sup>+</sup> for desired M=447.227. <sup>1</sup>H NMR (DMSO-d<sub>6</sub>, 600 MHz) δ = 8.24 (s, 1H), 8.23 (d, *J* = 8.4 Hz, 2H), 6.66 (d, *J* = 8.8 Hz, 2H), 5.66 (s, 2H), 4.94 (tt, *J* = 11.4, 4.0 Hz, 1H), 3.89-3.99 (m, 6H), 3.67 (ddd, *J* = 11.5, 5.8, 4.4 Hz, 1H), 3.43 (ddd, *J* = 11.5, 9.4, 5.1 Hz, 1H), 2.94 (dt, *J* = 14.1, 4.5 Hz, 1H), 2.52-2.55 (m, 1H), 2.21-2.30 (m, 3H), 2.16-2.20 (m, 1H), 1.78-1.94 (m, 7H), 1.61 (dd, *J* = 9.2, 4.0 Hz, 1H), 1.27 (dd, *J* = 6.8, 4.2 Hz, 1H). <sup>13</sup>C NMR (DMSO-d<sub>6</sub>, 151 MHz) δ = 169.2, 160.3, 153.8, 152.0, 132.7, 130.3, 125.0, 113.7, 108.8, 107.6, 65.2, 64.3, 64.3, 63.8, 54.0, 33.5, 29.4, 26.3, 24.6, 23.4, 22.7. HRMS calculated for C<sub>25</sub>H<sub>29</sub>N<sub>5</sub>O<sub>3</sub> 448.2349 found 448.2350. FTIR (cm<sup>-1</sup>) 3357, 2952, 1548, 1383, 1303, 1111, 807.

1-(4-(4-(3-Oxabicyclo[4.1.0]heptan-6-yl)-1-(1,4-dioxaspiro[4.5]decan-8-yl)-1H-pyrazolo[3,4-d]pyrimidin-6-yl)phenyl)-3-(2-hydroxyethyl)urea (212)



In a 2-5 mL microwave vial 4-(4-(3-oxabicyclo[4.1.0]heptan-6-yl)-1-(1,4-dioxaspiro[4.5]decan-8-yl)-1H-pyrazolo[3,4-d]pyrimidin-6-yl)aniline (60 mg, 0.13 mmol) and 4-nitrophenyl chloroformate (33 mg, 0.16 mmol) were dissolved in DCM (2 mL). Pyridine (21  $\mu$ L, 0.26 mmol) was added and the reaction was stirred at r.t. for 1.5 h. Ethanolamine (40  $\mu$ L, 0.67 mmol) and DIPEA (35  $\mu$ L, 0.2 mmol) were added and the reaction was stirred for a further 1 h. The reaction was partitioned between DCM (5 mL) and water (5 mL) and the resulting mixture was separated using a hydrophobic frit. The organic layer was concentrated *in vacuo* and purified by prep HPLC (formic, 30-85%, 20 min) to give 1-(4-(4-(3-oxabicyclo[4.1.0]heptan-6-yl)-1-(1,4-dioxaspiro[4.5]decan-8-yl)-1H-pyrazolo[3,4-d]pyrimidin-6-yl)phenyl)-3-(2-hydroxyethyl)urea (50 mg, 0.094 mmol, 70% yield) as an amorphous white solid. LCMS (formic) rt. 1.00 (99%)  $MH^+$  for desired  $M=534.259$   $^1H$  NMR (DMSO- $d_6$ , 400 MHz)  $\delta$  = 8.88 (s, 1H), 8.37-8.43 (m, 2H), 8.32 (s, 1H), 7.52-7.58 (m, 2H), 6.29 (t,  $J$  = 5.5 Hz, 1H), 4.98 (tt,  $J$  = 11.5, 3.9 Hz, 1H), 4.74 (br s, 1H), 3.89-4.00 (m, 6H), 3.68 (ddd,  $J$  = 11.5, 5.7, 4.3 Hz, 1H), 3.34-3.51 (m, 3H), 3.19 (q,  $J$  = 5.6 Hz, 2H), 2.95 (dt,  $J$  = 14.0, 4.7 Hz, 1H), 2.52-2.69 (m, 1H), 2.19-2.34 (m, 4H), 1.77-1.96 (m, 6H), 1.65 (dd,  $J$  = 9.3, 3.9 Hz, 1H), 1.30 (dd,  $J$  = 6.7, 4.0 Hz, 1H).  $^{13}C$  NMR (DMSO- $d_6$ , 151 MHz)  $\delta$  = 169.7, 159.4, 155.5, 153.7, 143.6, 132.9, 130.4, 129.6, 117.5, 109.5, 107.6, 65.2, 64.3, 64.3, 63.8, 60.8, 54.2, 42.3, 33.5, 29.4, 26.3, 24.7, 23.7, 23.0. HRMS calculated for  $C_{28}H_{34}N_6O_5$  535.2669, found 535.2665. FTIR ( $cm^{-1}$ ) 3335, 2931, 2858, 1664, 1536, 1385, 1236, 1100, 803.

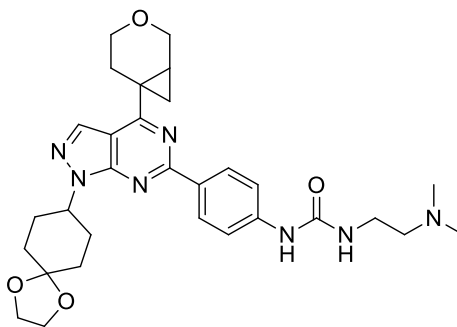
1-(4-(4-(3-Oxabicyclo[4.1.0]heptan-6-yl)-1-(1,4-dioxaspiro[4.5]decan-8-yl)-1H-pyrazolo[3,4-d]pyrimidin-6-yl)phenyl)-3-(2-aminoethyl)urea (213)



In a 2-5 mL microwave vial 4-(4-(3-oxabicyclo[4.1.0]heptan-6-yl)-1-(1,4-dioxaspiro[4.5]decan-8-yl)-1H-pyrazolo[3,4-d]pyrimidin-6-yl)aniline (50 mg, 0.11 mmol) and 4-nitrophenyl chloroformate (27 mg, 0.13 mmol) were dissolved in DCM (2 mL). Pyridine (21  $\mu$ L, 0.26 mmol) was added and the reaction was stirred at r.t. for 1.5 h. *tert*-butyl (2-aminoethyl)carbamate (88  $\mu$ L, 0.56 mmol) and DIPEA (29  $\mu$ L, 0.17 mmol) were added and the reaction was stirred for a further 1 h. The reaction was partitioned between DCM (5 mL) and water (5 mL) and the resulting mixture was separated using a hydrophobic frit. The organic layer was concentrated *in vacuo*. The resulting crude product was dissolved in hexafluoroisopropanol and heated in a microwave at 120  $^{\circ}$ C for 2 h. by preparative HPLC (High-pH, 30-85%, 30 min) to give 1-(4-(4-(3-oxabicyclo[4.1.0]heptan-6-yl)-1-(1,4-dioxaspiro[4.5]decan-8-yl)-1H-pyrazolo[3,4-d]pyrimidin-6-yl)phenyl)-3-(2-aminoethyl)urea (29 mg, 0.054 mmol, 49% yield). LCMS (high-pH) rt. 1.09 MH<sup>+</sup> for desired M = 533.275. <sup>1</sup>H NMR (DMSO-d<sub>6</sub>, 400 MHz)  $\delta$  = 8.89 (br., s, 1H), 8.40 (d, *J* = 8.8 Hz, 2H), 8.32 (s, 1H), 7.55 (d, *J* = 8.8 Hz, 2H), 6.33 (t, *J* = 5.6 Hz, 1H), 4.99 (tt, *J* = 11.3, 4.2 Hz, 1H), 3.90-4.05 (m, 6H), 3.68 (ddd, *J* = 11.4, 5.7, 4.4 Hz, 1H), 3.44 (ddd, *J* = 11.7, 9.3, 5.1 Hz, 1H), 3.11 (q, *J* = 6.1 Hz, 2H), 2.96 (dt, *J* = 13.9, 4.8 Hz, 1H), 2.64 (t, *J* = 6.2 Hz, 1H), 2.55 (s, 2H), 2.19-2.31 (m, 4H), 1.77-1.97 (m, 6H), 1.65 (dd, *J* = 9.3, 3.9 Hz, 1H), 1.30 ppm (dd, *J* = 6.6, 4.2 Hz, 1H). <sup>13</sup>C NMR (DMSO-d<sub>6</sub>, 101 MHz)  $\delta$  = 164.5, 154.8, 151.7, 149.0, 136.8, 127.8, 127.2, 124.9, 114.1, 105.0, 103.0, 60.7, 59.7, 59.6, 59.5, 49.7, 36.7, 36.2, 28.9, 24.4, 21.8, 19.9, 18.9, 17.9 ppm. HRMS calculated for C<sub>28</sub>H<sub>35</sub>N<sub>7</sub>O<sub>4</sub> 534.2829, found 534.2823. FTIR (cm<sup>-1</sup>) 3350, 2948, 1536, 1307, 1169, 1100, 806.

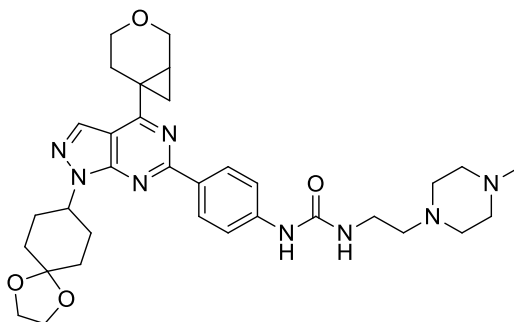


1-(4-(4-(3-Oxabicyclo[4.1.0]heptan-6-yl)-1-(1,4-dioxaspiro[4.5]decan-8-yl)-1H-pyrazolo[3,4-d]pyrimidin-6-yl)phenyl)-3-(2-(dimethylamino)ethyl)urea (214)



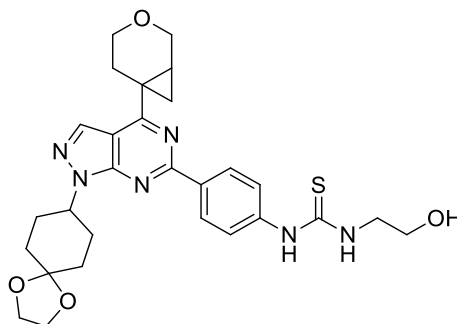
In a 2-5 mL microwave vial 4-(4-(3-oxabicyclo[4.1.0]heptan-6-yl)-1-(1,4-dioxaspiro[4.5]decan-8-yl)-1H-pyrazolo[3,4-d]pyrimidin-6-yl)aniline (60 mg, 0.13 mmol) and 4-nitrophenyl chloroformate (33 mg, 0.16 mmol) were dissolved in DCM (2 mL). Pyridine (21  $\mu$ L, 0.26 mmol) was added and the reaction was stirred at r.t. for 1.5 h. *N,N*-dimethylethane-1,2-diamine (72  $\mu$ L, 0.67 mmol) and DIPEA (35  $\mu$ L, 0.2 mmol) were added and the reaction was stirred for a further 1 h. The reaction was partitioned between DCM (5 mL) and water (5 mL) and the resulting mixture was separated using a hydrophobic frit. The organic layer was concentrated *in vacuo* and purified by prep HPLC (High-pH, 30-85%, 20 min) to give 1-(4-(4-(3-oxabicyclo[4.1.0]heptan-6-yl)-1-(1,4-dioxaspiro[4.5]decan-8-yl)-1H-pyrazolo[3,4-d]pyrimidin-6-yl)phenyl)-3-(2-(dimethylamino)ethyl)urea (50 mg, 0.089 mmol, 66% yield) as an amorphous white solid. LCMS (formic) rt. 0.73 (100%)  $MH^+$  for desired  $M=534.259$ .  $^1H$  NMR (DMSO- $d_6$ , 400 MHz)  $\delta$  = 8.96 (s, 1H), 8.37-8.42 (m, 2H), 8.32 (s, 1H), 7.52-7.57 (m, 2H), 6.19 (t,  $J$  = 5.3 Hz, 1H), 4.99 (tt,  $J$  = 11.4, 4.0 Hz, 1H), 3.89-4.01 (m, 6H), 3.68 (ddd,  $J$  = 11.4, 5.7, 4.4 Hz, 1H), 3.34-3.51 (m, 1H), 3.17-3.26 (m, 2H), 2.96 (dt,  $J$  = 13.9, 4.6 Hz, 1H), 2.35 (t,  $J$  = 6.2 Hz, 2H), 2.21-2.31 (m, 4H), 2.19 (s, 6H), 1.77-1.97 (m, 6H), 1.65 (dd,  $J$  = 9.2, 4.0 Hz, 1H), 1.30 (dd,  $J$  = 6.7, 4.0 Hz, 1H).  $^{13}C$  NMR (DMSO- $d_6$ , 101 MHz)  $\delta$  = 169.7, 159.5, 155.3, 153.7, 143.7, 132.9, 130.3, 129.6, 117.4, 109.5, 107.6, 65.2, 64.3, 64.3, 63.8, 58.9, 54.2, 45.5, 37.4, 33.5, 29.4, 26.3, 24.7, 23.7, 23.0 ppm. HRMS calculated for  $C_{30}H_{39}N_7O_4$  562.3142, found 562.3140. FTIR ( $cm^{-1}$ ) 3346, 2937, 2874, 1536, 1308, 1101, 1035, 852.

1-(4-(4-(3-Oxabicyclo[4.1.0]heptan-6-yl)-1-(1,4-dioxaspiro[4.5]decan-8-yl)-1H-pyrazolo[3,4-d]pyrimidin-6-yl)phenyl)-3-(2-(4-methylpiperazin-1-yl)ethyl)urea (215)



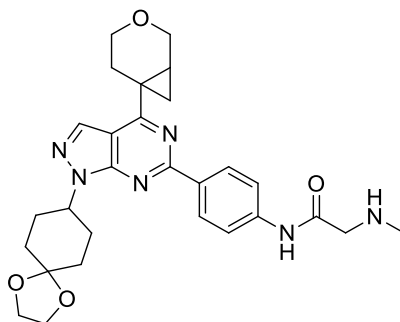
In a 2-5 mL microwave vial 4-(4-(3-oxabicyclo[4.1.0]heptan-6-yl)-1-(1,4-dioxaspiro[4.5]decan-8-yl)-1H-pyrazolo[3,4-d]pyrimidin-6-yl)aniline (60 mg, 0.13 mmol) and 4-nitrophenyl chloroformate (33 mg, 0.16 mmol) were dissolved in DCM (2 mL). Pyridine (21  $\mu$ L, 0.26 mmol) was added and the reaction was stirred at r.t. for 1.5 h. 2-(4-methylpiperazin-1-yl)ethan-1-amine (96 mg, 0.67 mmol) and DIPEA (35  $\mu$ L, 0.2 mmol) were added and the reaction was stirred for a further 1 h. The reaction was partitioned between DCM (5 mL) and water (5 mL) and the resulting mixture was separated using a hydrophobic frit. The organic layer was concentrated *in vacuo* and purified by prep HPLC (High-pH, 30-85%, 20 min) to give 1-(4-(4-(3-oxabicyclo[4.1.0]heptan-6-yl)-1-(1,4-dioxaspiro[4.5]decan-8-yl)-1H-pyrazolo[3,4-d]pyrimidin-6-yl)phenyl)-3-(2-(4-methylpiperazin-1-yl)ethyl)urea. (63 mg, 0.10 mmol, 76% yield) LCMS (formic) rt. 0.68 (100%)  $MH^+$  for desired  $M=616.349$ .  $^1H$  NMR (DMSO- $d_6$ , 400 MHz)  $\delta$  = 8.97 (s, 1H), 8.37-8.43 (m, 2H), 8.31 (s, 1H), 7.52-7.59 (m, 2H), 6.17 (t,  $J$  = 5.3 Hz, 1H), 4.98 (tt,  $J$  = 11.4, 3.9 Hz, 1H), 3.90-4.00 (m, 5H), 3.58-3.77 (m, 1H), 3.34-3.51 (m, 1H), 3.23 (q,  $J$  = 6.1 Hz, 2H), 2.95 (dt,  $J$  = 13.9, 4.6 Hz, 1H), 2.54-2.82 (m, 1H), 2.31-2.48 (m, 9H), 2.19-2.31 (m, 5H), 2.17 (s, 3H), 1.76-1.97 (m, 6H), 1.65 (dd,  $J$  = 9.2, 3.8 Hz, 1H), 1.30 (dd,  $J$  = 6.5, 4.0 Hz, 1H).  $^{13}C$  NMR (DMSO- $d_6$ , 101 MHz)  $\delta$  = 169.7, 159.5, 155.3, 153.7, 143.7, 132.9, 130.3, 129.6, 117.4, 109.5, 107.6, 65.2, 64.3, 64.3, 63.8, 57.8, 55.2, 54.2, 53.1, 46.3, 36.8, 33.5, 29.4, 26.3, 24.7, 23.7, 23.0 ppm. HRMS calculated for  $C_{33}H_{44}N_8O_4$  617.3520, found 617.3562. FTIR ( $cm^{-1}$ ) 3325, 2942, 1675, 1534, 1386, 1169, 1102, 852.

1-(4-(4-(3-Oxabicyclo[4.1.0]heptan-6-yl)-1-(1,4-dioxaspiro[4.5]decan-8-yl)-1*H*-pyrazolo[3,4-*d*]pyrimidin-6-yl)phenyl)-3-(2-hydroxyethyl)thiourea (216)



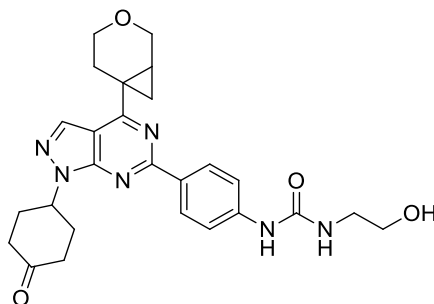
In a 2-5 mL microwave vial 4-(4-(3-oxabicyclo[4.1.0]heptan-6-yl)-1-(1,4-dioxaspiro[4.5]decan-8-yl)-1*H*-pyrazolo[3,4-*d*]pyrimidin-6-yl)aniline (60 mg, 0.13 mmol) was dissolved in DCM (2 mL). 1,1'-Thiocarbonyldiimidazole (36 mg, 0.20 mmol) and pyridine (22  $\mu$ L, 0.27 mmol) were added and the reaction was stirred at r.t. for 2 h. LCMS analysis showed complete conversion to desired intermediate. Ethanolamine (40  $\mu$ L, 0.67 mmol) was added and the reaction was stirred at r.t. for 0.5 h. The reaction mixture was concentrated *in vacuo* and the resulting residue was purified by prep HPLC (formic, 30-85%, 15 min) to give 1-(4-(4-(3-oxabicyclo[4.1.0]heptan-6-yl)-1-(1,4-dioxaspiro[4.5]decan-8-yl)-1*H*-pyrazolo[3,4-*d*]pyrimidin-6-yl)phenyl)-3-(2-hydroxyethyl)thiourea (40 mg, 0.073 mmol, 54% yield) as an amorphous white solid. LCMS (formic) rt. 1.09 (100%)  $MH^+$  for desired  $M=550.236$ .  $^1H$  NMR (DMSO- $d_6$ , 400 MHz)  $\delta$  = 9.88 (br s, 1H), 8.42-8.52 (m, 2H), 8.35 (s, 1H), 7.91 (br s, 1H), 7.67-7.72 (m, 2H), 5.00 (tt,  $J$  = 11.4, 4.0 Hz, 1H), 4.83 (br s, 1H), 3.88-4.02 (m, 6H), 3.68 (ddd,  $J$  = 11.6, 5.7, 4.4 Hz, 1H), 3.55-3.62 (m, 4H), 3.33-3.51 (m, 1H), 2.97 (dt,  $J$  = 14.0, 4.6 Hz, 1H), 2.21-2.34 (m, 4H), 1.90-1.98 (m, 2H), 1.77-1.90 (m, 4H), 1.67 (dd,  $J$  = 9.0, 3.9 Hz, 1H), 1.32 (dd,  $J$  = 6.7, 4.0 Hz, 1H).  $^{13}C$  NMR (DMSO- $d_6$ , 151 MHz)  $\delta$  = 180.7, 169.9, 159.1, 153.6, 142.4, 133.0, 132.9, 129.2, 122.1, 109.7, 107.6, 65.2, 64.3, 64.3, 63.8, 59.6, 54.3, 47.0, 33.5, 29.4, 26.2, 24.7, 23.9, 23.2 ppm. HRMS calculated for  $C_{28}H_{34}N_6O_4S$  551.2440, found 551.2436. FTIR ( $cm^{-1}$ ) 3340, 3172, 2937, 1536, 1387, 1306, 1105, 1035.

*N*-(4-(4-(3-Oxabicyclo[4.1.0]heptan-6-yl)-1-(1,4-dioxaspiro[4.5]decan-8-yl)-1*H*-pyrazolo[3,4-*d*]pyrimidin-6-yl)phenyl)-2-(methylamino)acetamide (217)



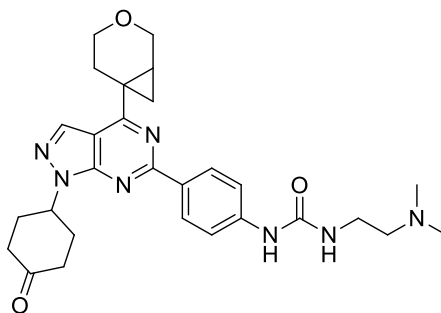
In a 2-5 mL microwave vial 4-(4-(3-oxabicyclo[4.1.0]heptan-6-yl)-1-(1,4-dioxaspiro[4.5]decan-8-yl)-1*H*-pyrazolo[3,4-*d*]pyrimidin-6-yl)aniline (50 mg, 0.11 mmol), Boc-*N*-methylglycine (36 mg, 0.19 mmol), HATU (85 mg, 0.22 mmol) and DIPEA (49  $\mu$ L, 0.28 mmol) were dissolved in 2-MeTHF (1.1 mL) and the reaction mixture was stirred at r.t. for 24 h. The reaction mixture was partitioned between ethyl acetate (5 mL) and water (5 mL) and the aqueous layer was extracted with ethyl acetate (3x 5 mL). The combined organic layers were dried (hydrophobic frit) and concentrated *in vacuo*. The resulting crude mixture was dissolved in hexafluoroisopropanol (2.5 mL) and heated in microwave at 100 °C for 3.5 h. The resulting reaction mixture was concentrated *in vacuo* and purified by prep HPLC (High-pH, 30-85%, 20 min) to give *N*-(4-(4-(3-oxabicyclo[4.1.0]heptan-6-yl)-1-(1,4-dioxaspiro[4.5]decan-8-yl)-1*H*-pyrazolo[3,4-*d*]pyrimidin-6-yl)phenyl)-2-(methylamino)acetamide (7.2 mg, 0.014 mmol, 13% yield) LCMS (formic) rt. 0.76 (98%)  $MH^+$  for desired  $M = 518.264$ .  $^1H$  NMR ( $CDCl_3$ , 400 MHz)  $\delta = 9.44$  (s, 1H), 8.58 (d,  $J = 8.8$  Hz, 2H), 8.09 (s, 1H), 7.76 (d,  $J = 8.8$  Hz, 2H), 5.02 (tt,  $J = 11.5, 4.0$  Hz, 1H), 4.12 (dd,  $J = 11.2, 1.0$  Hz, 1H), 4.07 (dd,  $J = 8.6, 3.7$  Hz, 1H), 4.02-4.06 (m, 4H), 3.83 (ddd,  $J = 11.5, 6.1, 3.4$  Hz, 1H), 3.52 (ddd,  $J = 11.5, 10.0, 4.9$  Hz, 1H), 3.44 (s, 2H), 3.06 (dt,  $J = 14.0, 4.4$  Hz, 1H), 2.58 (s, 3H), 2.43-2.57 (m, 2H), 2.38 (ddd,  $J = 14.1, 10.0, 6.0$  Hz, 1H), 2.28-2.30 (m, 1H), 2.24-2.31 (m, 1H), 1.95-2.13 (m, 5H), 1.89 (td,  $J = 13.4, 4.2$  Hz, 2H), 1.72 (dd,  $J = 9.5, 4.2$  Hz, 3H), 1.39 ppm (dd,  $J = 6.7, 4.3$  Hz, 1H)  $^{13}C$  NMR ( $CDCl_3$ , 101 MHz)  $\delta = 169.5, 159.5, 153.8, 139.8, 133.9, 132.0, 129.6, 119.0, 109.8, 107.8, 65.5, 64.5, 64.4, 64.3, 55.1, 54.6, 49.0, 36.8, 33.7, 29.2, 26.6, 24.7, 23.7, 22.6$  ppm. HRMS calculated for  $C_{28}H_{34}N_6O_4$  519.2720, found 519.2718. FTIR ( $cm^{-1}$ ) 2945, 1675, 1540, 1311, 1171, 804.

1-(4-(4-(3-Oxabicyclo[4.1.0]heptan-6-yl)-1-(4-oxocyclohexyl)-1H-pyrazolo[3,4-d]pyrimidin-6-yl)phenyl)-3-(2-hydroxyethyl)urea (205)



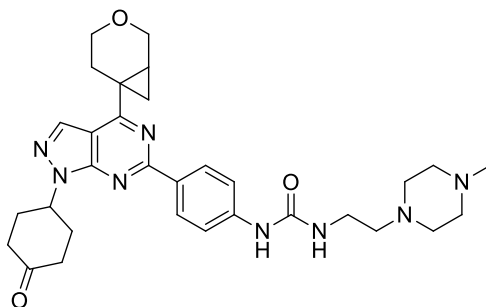
In a 0.5-2 mL microwave vial 1-(4-(4-(3-oxabicyclo[4.1.0]heptan-6-yl)-1-(1,4-dioxaspiro[4.5]decan-8-yl)-1H-pyrazolo[3,4-d]pyrimidin-6-yl)phenyl)-3-(2-hydroxyethyl)urea (33 mg, 0.062 mmol) was dissolved in THF (0.3 mL) and water (0.3 mL). HCl (50  $\mu$ L, 0.61 mmol) was added and the reaction was stirred at r.t. for 2 h. The reaction mixture was concentrated *in vacuo* and partitioned between DCM (10 mL) and sodium hydroxide (1 M) (10 mL). The combined organic layers were dried (hydrophobic frit) and concentrated *in vacuo* to give 1-(4-(4-(3-oxabicyclo[4.1.0]heptan-6-yl)-1-(4-oxocyclohexyl)-1H-pyrazolo[3,4-d]pyrimidin-6-yl)phenyl)-3-(2-hydroxyethyl)urea (21 mg, 0.043 mmol, 69% yield) as an amorphous white solid. LCMS (formic) 0.99 (95%)  $MH^+$  for desired  $M=490.233$ .  $^1H$  NMR (DMSO- $d_6$ , 400 MHz)  $\delta$  = 8.89 (s, 1H), 8.42 (d,  $J$  = 8.8 Hz, 2H), 8.36 (s, 1H), 7.56 (d,  $J$  = 9.0 Hz, 2H), 6.23-6.40 (m, 1H), 5.43 (tt,  $J$  = 10.0, 3.9 Hz, 1H), 3.99 (dd,  $J$  = 11.5, 3.9 Hz, 1H), 3.94 (dd,  $J$  = 11.2, 1.2 Hz, 1H), 3.69 (ddd,  $J$  = 11.5, 5.7, 4.5 Hz, 1H), 3.41-3.50 (m, 4H), 3.18 (s, 3H), 2.96 (dt,  $J$  = 13.9, 4.6 Hz, 1H), 2.69-2.83 (m, 2H), 2.38-2.47 (m, 4H), 2.20-2.36 (m, 4H), 1.66 (dd,  $J$  = 9.3, 3.9 Hz, 1H), 1.32 ppm (dd,  $J$  = 6.6, 4.2 Hz, 1H).  $^{13}C$  NMR (DMSO- $d_6$ , 101 MHz)  $\delta$  = 209.5, 169.8, 159.6, 155.5, 153.9, 143.7, 133.2, 130.3, 129.6, 117.5, 109.6, 65.2, 63.8, 60.8, 53.1, 42.3, 39.2, 31.0, 26.3, 24.7, 23.8, 23.0 ppm. FTIR ( $cm^{-1}$ ) 3246, 2957, 1658, 1558, 1356, 1250, 1100, 1034, 805.

(4-(3-Oxabicyclo[4.1.0]heptan-6-yl)-1-(4-oxocyclohexyl)-1H-pyrazolo[3,4-d]pyrimidin-6-yl)phenyl)-3-(2-(dimethylamino)ethyl)urea (207)



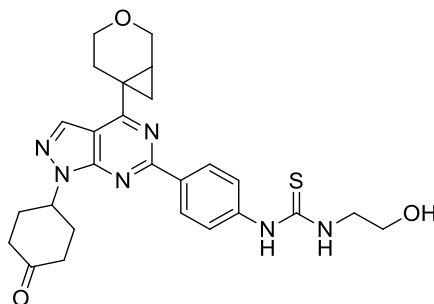
In a 0.5-2 mL microwave vial 1-(4-(4-(3-oxabicyclo[4.1.0]heptan-6-yl)-1-(1,4-dioxaspiro[4.5]decan-8-yl)-1H-pyrazolo[3,4-d]pyrimidin-6-yl)phenyl)-3-(2-(dimethylamino)ethyl)urea (23 mg, 0.041 mmol) was dissolved in THF (0.2 mL) and water (0.2 mL). HCl (33  $\mu$ L, 0.41 mmol) was added and the reaction was stirred at r.t. for 2 h. The reaction mixture was concentrated *in vacuo* and partitioned between DCM (10 mL) and sodium hydroxide (1 M) (10 mL). The combined organic layers were dried (hydrophobic frit) and concentrated *in vacuo* to give (4-(3-oxabicyclo[4.1.0]heptan-6-yl)-1-(4-oxocyclohexyl)-1H-pyrazolo[3,4-d]pyrimidin-6-yl)phenyl)-3-(2-(dimethylamino)ethyl)urea (14 mg, 0.027 mmol, 66% yield). LCMS (formic) rt. 0.67 (96%)  $MH^+$  for desired  $M = 517.280$ .  $^1H$  NMR (400 MHz,  $CDCl_3$ )  $\delta = 8.54 - 8.45$  (m, 2H), 8.09 (s, 1H), 7.59 - 7.52 (m, 2H), 6.34 - 6.14 (m, 1H), 5.46 - 5.36 (m, 1H), 4.11 (dd,  $J = 1.2, 11.7$  Hz, 1H), 4.06 (dd,  $J = 3.9, 11.5$  Hz, 1H), 3.83 (ddd,  $J = 3.7, 6.0, 11.6$  Hz, 1H), 3.56 - 3.47 (m, 2H), 3.43 - 3.22 (m, 2H), 3.05 (td,  $J = 4.3, 13.9$  Hz, 1H), 2.88 - 2.77 (m, 2H), 2.75 - 2.61 (m, 6H), 2.56 (s, 6H), 2.47 - 2.33 (m, 3H), 2.32 - 2.25 (m, 1H), 1.71 (dd,  $J = 4.2, 9.3$  Hz, 1H), 1.39 (dd,  $J = 4.2, 6.1$  Hz, 1H).  $^{13}C$  NMR (DMSO- $d_6$ , 151 MHz)  $\delta = 209.5, 169.9, 159.6, 155.5, 153.9, 143.6, 133.2, 130.5, 129.6, 117.6, 109.6, 65.2, 63.8, 53.2, 40.6, 39.2, 31.0, 26.3, 24.7, 23.8, 23.0$  ppm (1C not observed). HRMS calculated for  $C_{28}H_{35}N_7O_3$  518.2880, found 518.2881. FTIR ( $cm^{-1}$ ) 3322, 2915, 1693, 1536, 1227, 1170, 1023, 805.

1-(4-(4-(3-Oxabicyclo[4.1.0]heptan-6-yl)-1-(4-oxocyclohexyl)-1H-pyrazolo[3,4-d]pyrimidin-6-yl)phenyl)-3-(2-(4-methylpiperazin-1-yl)ethyl)urea (208)



In a 0.5-2 mL microwave vial 1-(4-(4-(3-oxabicyclo[4.1.0]heptan-6-yl)-1-(1,4-dioxaspiro[4.5]decan-8-yl)-1H-pyrazolo[3,4-d]pyrimidin-6-yl)phenyl)-3-(2-(4-methylpiperazin-1-yl)ethyl)urea (37 mg, 0.06 mmol) was dissolved in THF (0.3 mL) and water (0.3 mL). HCl (50  $\mu$ L, 0.61 mmol) was added and the reaction was stirred at r.t. for 2 h. The reaction mixture was concentrated *in vacuo* and partitioned between DCM (10 mL) and sodium hydroxide (1 M) (10 mL). The combined organic layers were dried (hydrophobic frit) and concentrated *in vacuo* to give 1-(4-(4-(3-oxabicyclo[4.1.0]heptan-6-yl)-1-(4-oxocyclohexyl)-1H-pyrazolo[3,4-d]pyrimidin-6-yl)phenyl)-3-(2-(4-methylpiperazin-1-yl)ethyl)urea (32 mg, 0.056 mmol, 93% yield) as an amorphous white solid. LCMS (formic) rt. 0.63 (100%)  $MH^+$  for desired  $M = 572.714$ .  $^1H$  NMR (DMSO- $d_6$ , 400 MHz)  $\delta = 8.97$  (s, 1H), 8.38-8.44 (m, 2H), 8.36 (s, 1H), 7.57 (d,  $J = 8.8$  Hz, 2H), 6.16 (t,  $J = 5.3$  Hz, 1H), 5.42 (tt,  $J = 10.3, 4.2$  Hz, 1H), 3.99 (dd,  $J = 11.2, 3.9$  Hz, 1H), 3.94 (dd,  $J = 11.2, 1.2$  Hz, 1H), 3.69 (ddd,  $J = 11.5, 5.6, 4.4$  Hz, 1H), 3.44 (ddd,  $J = 11.5, 9.3, 5.1$  Hz, 1H), 3.17-3.26 (m, 2H), 2.96 (dt,  $J = 13.9, 4.8$  Hz, 1H), 2.71-2.82 (m, 2H), 2.21-2.48 (m, 18H), 2.18 (s, 3H), 1.66 (dd,  $J = 9.2, 4.0$  Hz, 1H), 1.32 ppm (dd,  $J = 6.6, 4.2$  Hz, 1H).  $^{13}C$  NMR (101 MHz, DMSO- $d_6$ )  $\delta = 209.47, 169.83, 159.61, 155.30, 153.85, 143.73, 133.16, 130.30, 129.61, 117.46, 109.56, 65.16, 63.76, 57.76, 55.17, 53.14, 53.06, 46.22, 39.24, 36.81, 30.98, 26.26, 24.74, 23.81, 23.03$ . HRMS calculated for  $C_{31}H_{40}N_8O_3$  573.3302, Found 573.3300. FTIR ( $cm^{-1}$ ) 3440, 3350, 2942, 1701, 1562, 1388, 1309, 1167, 805.

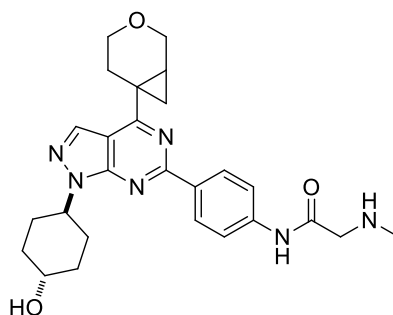
1-(4-(4-(3-Oxabicyclo[4.1.0]heptan-6-yl)-1-(4-oxocyclohexyl)-1H-pyrazolo[3,4-d]pyrimidin-6-yl)phenyl)-3-(2-hydroxyethyl)thiourea (209)



In a 0.5-2 mL microwave vial 1-(4-(4-(3-oxabicyclo[4.1.0]heptan-6-yl)-1-(4-dioxaspiro[4.5]decan-8-yl)-1H-pyrazolo[3,4-d]pyrimidin-6-yl)phenyl)-3-(2-(4-methylpiperazin-1-yl)ethyl)urea (37 mg, 0.06 mmol) was dissolved in THF (0.2 mL) and water (0.2 mL). HCl (39  $\mu$ L, 0.47 mmol) was added and the reaction was stirred at r.t. for 2 h. The reaction mixture was concentrated *in vacuo* and partitioned between DCM (10 mL) and sodium hydroxide (1 M) (10 mL). The combined organic layers were dried (hydrophobic frit) and concentrated *in vacuo* to give 1-(4-(4-(3-oxabicyclo[4.1.0]heptan-6-yl)-1-(4-oxocyclohexyl)-1H-pyrazolo[3,4-d]pyrimidin-6-yl)phenyl)-3-(2-hydroxyethyl)thiourea (18 mg, 0.036 mmol, 75% yield) as an amorphous white solid. LCMS (formic) rt. 0.99 (98%)  $MH^+$  for desired M= 506.210.  $^1H$  NMR (DMSO- $d_6$ , 400 MHz)  $\delta$  = 9.88 (br s, 1H), 8.48 (d,  $J$  = 8.8 Hz, 2H), 8.39 (s, 1H), 7.91 (br s, 1H), 7.71 (d,  $J$  = 8.8 Hz, 2H), 5.44 (tt,  $J$  = 10.3, 3.9 Hz, 1H), 4.83 (br s, 1H), 4.00 (dd,  $J$  = 11.5, 3.9 Hz, 1H), 3.95 (dd,  $J$  = 11.2, 1.5 Hz, 1H), 3.69 (ddd,  $J$  = 11.6, 5.7, 4.4 Hz, 1H), 3.55-3.62 (m, 4H), 3.45 (ddd,  $J$  = 11.7, 9.3, 5.1 Hz, 1H), 2.98 (dt,  $J$  = 14.0, 4.7 Hz, 1H), 2.70-2.82 (m, 2H), 2.39-2.48 (m, 4H), 2.19-2.36 (m, 4H), 1.68 (dd,  $J$  = 9.3, 3.9 Hz, 1H), 1.34 (dd,  $J$  = 6.6, 4.2 Hz, 1H).  $^{13}C$  NMR (DMSO- $d_6$ , 101 MHz)  $\delta$  = 209.4, 180.8, 170.0, 159.3, 153.8, 142.5, 133.2, 129.2, 122.2, 109.8, 65.2, 63.8, 59.6, 53.3, 47.0, 39.2, 30.9, 26.2, 24.8, 24.0, 23.2 ppm. (1C not observed). HRMS calculated for  $C_{26}H_{30}N_6O_3S$  507.2178 found 507.2180. FTIR ( $cm^{-1}$ ) 3293, 3167, 2652, 1716, 1540, 1384, 1127, 1040, 807.



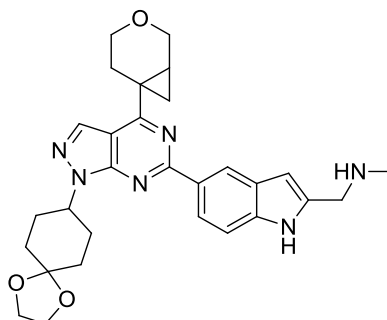
*N*-(4-(4-(3-Oxabicyclo[4.1.0]heptan-6-yl)-1-(4-hydroxycyclohexyl)-1*H*-pyrazolo[3,4-*d*]pyrimidin-6-yl)phenyl)-2-(methylamino)acetamide (219)



In a 2-5 mL microwave vial a mixture of 4-(4-(3-oxabicyclo[4.1.0]heptan-6-yl)-1-(1,4-dioxaspiro[4.5]decan-8-yl)-1*H*-pyrazolo[3,4-*d*]pyrimidin-6-yl)aniline (150 mg, 0.34 mmol), *N*-(*tert*-butoxycarbonyl)-*N*-methylglycine (108 mg, 0.57 mmol), HATU (255 mg, 0.67 mmol) and DIPEA (0.15 mL, 0.84 mmol) was dissolved in 2-MeTHF (2 mL) and the reaction was sealed and stirred at r.t. for 24 h. The reaction was quenched with water (5 mL) and partitioned between water (5 mL) and ethyl acetate (5 mL) and extracted with further ethyl acetate (3x 5 mL). The combined organic layer was dried (hydrophobic frit) and concentrated *in vacuo*. The crude reaction mixture was dissolved in acetone (9 mL) and tosic acid (85 mg, 0.44 mmol) was added. The reaction was stirred at 50 °C for 2.5 h. The reaction mixture was partitioned between DCM (10 mL) and sat. aq. sodium bicarbonate (10 mL) and extracted with further DCM (2 x 10 mL). The combined organic layer was dried (hydrophobic frit) and concentrated *in vacuo*. The crude reaction mixture was dissolved in tetrahydrofuran (1.2 mL) and sodium borohydride (11 mg, 0.29 mmol) was added. The reaction was stirred for at r.t. for 1 h. The reaction was then partitioned between ethyl acetate (10 mL) and sat. aq. sodium bicarbonate (10 mL). The aqueous layer was extracted with further ethyl acetate (2x 10 mL). The combined organic layer was dried (hydrophobic frit) and concentrated *in vacuo*. The crude reaction mixture was dissolved in hexafluoroisopropanol (2 mL) and irradiated in a Biotage initiator+ microwave at 120 °C for 2 h. The reaction mixture was concentrated *in vacuo* and purified by Mass Directed Auto Purification (MDAP) (formic, method 2, extended run) to give *N*-(4-(4-(3-oxabicyclo[4.1.0]heptan-6-yl)-1-(4-hydroxycyclohexyl)-1*H*-pyrazolo[3,4-*d*]pyrimidin-6-yl)phenyl)-2-(methylamino)acetamide (5 mg, 10.2 μmol, 17% yield). LCMS (formic) rt. 0.61 (97%) MH<sup>+</sup> for desired M= 476.254. <sup>1</sup>H NMR (400 MHz, DMSO-*d*<sub>6</sub>) δ = 8.47 (d, *J* = 8.8 Hz, 2H), 8.33 (s, 1H), 7.82 (d, *J* = 8.8 Hz, 2H), 4.85 (tt, *J* = 3.8, 11.5 Hz, 1H), 3.99 (dd, *J* = 3.9, 11.5 Hz, 1H), 3.94 (dd, *J* = 1.2, 11.2 Hz, 1H), 3.71 - 3.65 (m, 1H), 3.59 (tt, *J* = 4.2, 10.8 Hz, 1H), 3.44 (ddd, *J* = 5.1, 9.8, 11.7 Hz, 1H), 3.35 (s, 2H), 2.96 (td, *J* = 4.6, 13.9 Hz, 1H), 2.37 (s, 3H), 2.32 - 2.21 (m, 2H), 2.13 - 1.91 (m, 6H), 1.66 (dd, *J* = 3.8, 9.2 Hz, 1H), 1.54 - 1.42

(m, 2H), 1.31 (dd,  $J = 4.2, 6.6$  Hz, 1H).  $^{13}\text{C}$  NMR (101 MHz, DMSO- $d_6$ )  $\delta = 170.4, 169.8, 159.1, 153.6, 141.5, 132.9, 132.7, 129.5, 119.3, 109.7, 68.5, 65.1, 63.8, 55.3, 54.8, 36.1, 34.62, 30.4, 26.3, 24.7, 23.8, 23.1$ . HRMS calculated for  $\text{C}_{26}\text{H}_{32}\text{N}_6\text{O}_3$  477.2614, found 477.2624. FTIR ( $\text{cm}^{-1}$ ) 3323, 2945, 1675, 1592, 1540, 1309, 1170, 804.

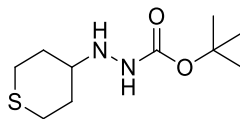
1-(5-(4-(3-Oxabicyclo[4.1.0]heptan-6-yl)-1-(1,4-dioxaspiro[4.5]decan-8-yl)-1H-pyrazolo[3,4-d]pyrimidin-6-yl)-1H-indol-2-yl)-N-methylmethanamine (227)



In a 2-5 mL microwave vial 4-(3-oxabicyclo[4.1.0]heptan-6-yl)-6-chloro-1-(1,4-dioxaspiro[4.5]decan-8-yl)-1H-pyrazolo[3,4-d]pyrimidine (150 mg, 0.32 mmol), *tert*-butyl 2-(((*tert*-butoxycarbonyl)(methyl)amino)methyl)-5-(4,4,5,5-tetramethyl-1,3,2-dioxaborolan-2-yl)-1H-indole-1-carboxylate (253 mg, 0.52 mmol), sodium carbonate (67 mg, 0.63 mmol) and  $\text{Pd}(\text{PPh}_3)_4$  (36 mg, 0.031 mmol) were dissolved in DME (2.8 mL) and water (0.35 mL). The reaction was stirred at 100 °C for 2h. The resulting crude reaction mixture was filtered through celite (10g column) and concentrated *in vacuo*. The resulting crude reaction mixture was dissolved in hexafluoroisopropanol (3 mL) and irradiated in a Biotage initiator+ microwave at 120 °C for 3.5 h. The reaction mixture was concentrated *in vacuo* and purified by prep HPLC (High-pH, 30-95%, 30 min) to give 1-(5-(4-(3-oxabicyclo[4.1.0]heptan-6-yl)-1-(1,4-dioxaspiro[4.5]decan-8-yl)-1H-pyrazolo[3,4-d]pyrimidin-6-yl)-1H-indol-2-yl)-N-methylmethanamine (44 mg, 0.085 mmol, 25 % yield). LCMS (formic, DMSO) rt. 0.80 (99%)  $\text{MH}^+$  for desired  $\text{M} = 514.630$ .  $^1\text{H}$  NMR (DMSO- $d_6$ , 400 MHz)  $\delta = 11.15$  (br s, 1H), 8.70 (d,  $J = 1.2$  Hz, 1H), 8.27-8.32 (m, 2H), 7.42 (d,  $J = 8.6$  Hz, 1H), 6.42 (s, 1H), 4.97-5.06 (m, 1H), 3.89-4.03 (m, 6H), 3.80 (s, 2H), 3.70 (ddd,  $J = 11.4, 5.8, 4.5$  Hz, 1H), 3.34-3.53 (m, 1H), 2.99 (dt,  $J = 13.9, 4.6$  Hz, 1H), 2.33 (s, 3H), 2.21-2.31 (m, 4H), 1.90-2.04 (m, 2H), 1.79-1.90 (m, 4H), 1.68 (dd,  $J = 9.3, 3.9$  Hz, 1H), 1.31 (dd,  $J = 6.6, 4.2$  Hz, 1H).  $^{13}\text{C}$  NMR (DMSO- $d_6$ , 101 MHz)  $\delta = 169.4, 161.1, 153.9, 140.7, 138.4, 132.8, 128.8, 128.6, 121.8, 121.0, 111.2, 109.3, 107.6, 100.8, 65.2, 64.3, 64.3, 63.8, 54.1, 48.8, 36.1, 33.5, 29.4, 26.3, 24.7, 23.6, 22.9$ . HRMS calculated for  $\text{C}_{29}\text{H}_{34}\text{N}_6\text{O}_3$  515.2770, found 515.2770. FTIR ( $\text{cm}^{-1}$ ) 3293, 2942, 1557, 1382, 1098, 1034, 802.

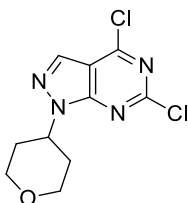
### 3.3.4 N1-Substituent Optimisation Compounds

*tert*-Butyl 2-(tetrahydro-2*H*-thiopyran-4-yl)hydrazine-1-carboxylate (236)<sup>260</sup>



In a 100 mL RBF *tert*-butyl hydrazinecarboxylate (1.42 g, 10.8 mmol) and tetrahydro-4*H*-thiopyran-4-one (1.25 g, 10.8 mmol) were dissolved in DCM (35 mL) and acetic acid (2.25 mL). The reaction was cooled and STAB (3.42 g, 16.1 mmol) was added in a single portion. The resulting reaction was stirred at r.t. for 16 h. The reaction was quenched with 10% aqueous sodium bisulfate (25 mL) and water (10 mL). The aqueous layer was extracted with DCM (3x 20 mL). The combined organic layers were washed with sodium hydroxide (20 mL), dried (hydrophobic frit) and concentrated *in vacuo* to give *tert*-butyl 2-(tetrahydro-2*H*-thiopyran-4-yl)hydrazine-1-carboxylate (2.39 g, 10.3 mmol, 96% yield) as an amorphous white solid. <sup>1</sup>H NMR (DMSO-*d*<sub>6</sub>, 400 MHz)  $\delta$  = 7.99-8.33 (br s, 1H), 4.26 (br s, 1H), 2.60-2.80 (m, 4H), 2.44-2.49 (m, 2H), 1.89-2.00 (m, 2H), 1.39 ppm (s, 9H).

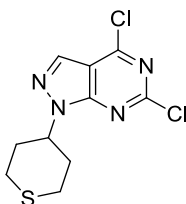
4,6-Dichloro-1-(tetrahydro-2*H*-pyran-4-yl)-1*H*-pyrazolo[3,4-*d*]pyrimidine (238)<sup>261</sup>



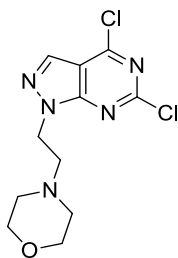
2,4,6-trichloropyrimidine-5-carbaldehyde (300 mg, 1.42 mmol) was dissolved in EtOH (10 mL). The reaction was cooled to -78 °C. (tetrahydro-2*H*-pyran-4-yl)hydrazine hydrochloride (217 mg, 1.42 mmol) and triethylamine (1.0 mL, 7.10 mmol) were added and the reaction was stirred at -78 °C for 0.5 h before warming to 0 °C and stirring for a further 1.5 h. The reaction mixture was diluted with DCM (20 mL) and washed with sat. aq. sodium bicarbonate (20 mL). The combined organic layers were dried (hydrophobic frit) and concentrated *in vacuo*. The reaction mixture was purified by flash column chromatography (cyclohexane: ethyl acetate 0-50% (12 column volumes)) to give 4,6-dichloro-1-(tetrahydro-2*H*-pyran-4-yl)-1*H*-pyrazolo[3,4-*d*]pyrimidine (176 mg, 0.64 mmol, 45% yield) as an amorphous white solid. LCMS (formic) rt. 1.02 (100%) MH<sup>+</sup> for desired M = 272.023. <sup>1</sup>H NMR (CDCl<sub>3</sub>, 400 MHz)  $\delta$  = 8.18 (s, 1H), 5.03 (tt, *J* = 11.7, 4.2 Hz, 1H), 4.18 (dd, *J* = 11.4, 4.3 Hz, 2H), 3.65 (td, *J* = 12.1, 2.2 Hz, 2H), 2.36-2.50 (m, 2H), 1.93-2.02 ppm (m, 2H). <sup>13</sup>C NMR (CDCl<sub>3</sub>, 101 MHz)  $\delta$  = 156.3, 155.4, 153.5, 132.4, 112.9, 77.3, 77.2, 77.0, 76.7, 66.9, 54.4, 32.0 ppm. HRMS

calculated for  $C_{10}H_{10}Cl_2N_4O$  273.0310, found 273.0310. FTIR ( $cm^{-1}$ ) 2874, 1590, 1374, 1128, 956, 831.

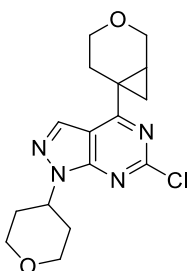
4,6-Dichloro-1-(tetrahydro-2H-thiopyran-4-yl)-1H-pyrazolo[3,4-d]pyrimidine (239)<sup>262</sup>



In a 500 mL RBF *tert*-butyl 2-(tetrahydro-2H-thiopyran-4-yl)hydrazine-1-carboxylate (2.39 g, 10.3 mmol) was suspended in water (58 mL). The reaction was stirred at reflux for 14 h. In this time the white suspension formed a colourless solution. The reaction mixture was cooled to 0 °C. EtOH (58 mL) and triethylamine (2.4 mL, 17.5 mmol) were added followed by portion wise addition of 2,4,6-trichloropyrimidine-5-carbaldehyde (2.16g, 10.3 mmol) . The resulting yellow suspension was stirred at 0 °C for 1 h. The reaction was concentrated *in vacuo* to remove EtOH. The resulting aqueous suspension was extracted with DCM (3x 25 mL). The combined organic layers were dried (hydrophobic frit) and concentrated *in vacuo*. The crude reaction mixture was purified by flash column chromatography (cyclohexane: ethyl acetate 0-65% (15 column volumes)) to give 4,6-dichloro-1-(tetrahydro-2H-thiopyran-4-yl)-1H-pyrazolo[3,4-d]pyrimidine (1.36 g, 4.70 mmol, 46% yield) as a fluffy white solid. LCMS (formic, 10 min run) rt. 5.46 (97%)  $MH^+$  for desired  $M = 289.178$ .  $^1H$  NMR (DMSO- $d_6$ , 400 MHz)  $\delta = 8.55$  (s, 1H), 4.81 (tt,  $J = 10.8, 4.9$  Hz, 1H), 2.87-3.04 (m, 2H), 2.72-2.80 (m, 2H), 2.14-2.28 ppm (m, 4H).  $^{13}C$  NMR (DMSO- $d_6$ , 101 MHz)  $\delta = 155.3, 154.9, 153.4, 133.3, 113.1, 56.3, 33.7, 27.5$  ppm. HRMS calculated for  $C_{10}H_{10}Cl_2N_4S$  289.0081, found 289.0082. FTIR ( $cm^{-1}$ ) 1585, 1375, 1129, 944, 837.

4-(2-(4,6-Dichloro-1*H*-pyrazolo[3,4-*d*]pyrimidin-1-yl)ethyl)morpholine (240)<sup>263</sup>

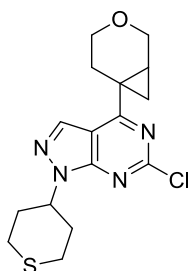
2,4,6-trichloropyrimidine-5-carbaldehyde (544 mg, 2.57 mmol) was dissolved in EtOH (10 mL). The reaction was cooled to -78 °C. 4-(2-hydrazinylethyl)morpholine (374 mg, 2.57 mmol) and triethylamine (0.35 mL, 2.57 mmol) were added and the reaction was stirred at -78 °C for 2 h before warming to 0 °C and stirring for a further 2 h. The reaction mixture was diluted with DCM (20 mL) and washed with sat. aq. sodium bicarbonate (20 mL). The combined organic layers were dried (hydrophobic frit) and concentrated *in vacuo*. The crude reaction mixture was purified by flash column chromatography (cyclohexane: ethyl acetate 25-100% (15 column volumes)) to give 4-(2-(4,6-dichloro-1*H*-pyrazolo[3,4-*d*]pyrimidin-1-yl)ethyl)morpholine (358 mg, 1.19 mmol, 46 % yield) as an amorphous white solid. LCMS (formic) rt. 0.38 (100%) MH<sup>+</sup> for desired M=301.050. <sup>1</sup>H NMR (DMSO-*d*<sub>6</sub>, 400 MHz) δ = 8.56 (s, 1H), 4.56 (t, *J* = 6.2 Hz, 2H), 3.41-3.47 (m, 4H), 2.81 (br t, *J* = 5.7 Hz, 2H), 2.39-2.49 ppm (m, 4H) <sup>13</sup>C NMR (DMSO-*d*<sub>6</sub>, 101 MHz) δ = 155.4, 154.9, 154.7, 133.5, 112.9, 66.4, 56.9, 53.3, 45.1 ppm. HRMS calculated for C<sub>11</sub>H<sub>13</sub>Cl<sub>2</sub>N<sub>5</sub>O 302.0575, found 302.0579. FTIR (cm<sup>-1</sup>) 2954, 1587, 1378, 1205, 1116, 853.

4-(3-Oxabicyclo[4.1.0]heptan-6-yl)-6-chloro-1-(tetrahydro-2*H*-pyran-4-yl)-1*H*-pyrazolo[3,4-*d*]pyrimidine (241)

In a 10-20 mL microwave vial a mixture of potassium 3-oxabicyclo[4.1.0]heptan-6-yltrifluoroborate (486 g, 2.38 mmol), 4,6-dichloro-1-(tetrahydro-2*H*-pyran-4-yl)-1*H*-pyrazolo[3,4-*d*]pyrimidine (500 mg, 1.83 mmol), caesium carbonate (1.78 g, 5.49 mmol), palladium (II) acetate (66 mg, 0.29 mmol) and cataCXium<sup>®</sup> A (210 mg, 0.59 mmol) was dissolved in toluene (8.3 mL) and water (0.83 mL). The resulting suspension was degassed

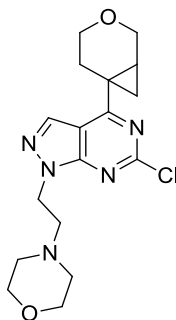
with a stream of nitrogen for 10 min, sealed and stirred at 110 °C for 2 h. The reaction was monitored by LCMS and, upon complete consumption of starting material, the reaction was cooled to r.t. and filtered through a celite cartridge (10 g). The resulting mixture was concentrated *in vacuo* to give 4-(3-oxabicyclo[4.1.0]heptan-6-yl)-6-chloro-1-(tetrahydro-2H-pyran-4-yl)-1H-pyrazolo[3,4-d]pyrimidine as a sticky white solid. LCMS (formic) rt. 1.06 (85%) MH<sup>+</sup> for desired M= 334.120. Due to a potential instability of this compound on silica, the reaction mixture was telescoped to the next step as a crude reaction mixture.

4-(3-Oxabicyclo[4.1.0]heptan-6-yl)-6-chloro-1-(tetrahydro-2H-thiopyran-4-yl)-1H-pyrazolo[3,4-d]pyrimidine (241)



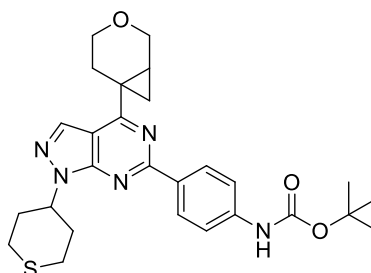
In a 100 mL RBF a mixture of potassium 3-oxabicyclo[4.1.0]heptan-6-yltrifluoroborate (1.02 g, 4.98 mmol), 4,6-dichloro-1-(tetrahydro-2H-thiopyran-4-yl)-1H-pyrazolo[3,4-d]pyrimidine (1.2 g, 4.15 mmol), caesium carbonate (4.06 g, 12.45 mmol), palladium(II) acetate (149 mg, 0.66 mmol) and cataCXium<sup>®</sup> A (476 mg, 1.33 mmol) was dissolved in toluene (18.8 mL) and water (1.9 mL). The resulting suspension was degassed with a stream of nitrogen for 10 min and then a reflux condenser was fitted, and the reaction was stirred at 110 °C for 4 h. The reaction was monitored by LCMS and, upon complete consumption of starting material, the reaction was cooled to r.t. and filtered through a celite cartridge (10 g). The resulting mixture was concentrated *in vacuo* to give 4-(3-oxabicyclo[4.1.0]heptan-6-yl)-6-chloro-1-(tetrahydro-2H-thiopyran-4-yl)-1H-pyrazolo[3,4-d]pyrimidine as an amorphous brown solid. LCMS (formic) rt. 1.25 (87%) MH<sup>+</sup> for desired M= 350.097. Due to a potential instability of this compound on silica, the reaction mixture was telescoped to the next step as a crude reaction mixture.

4-(2-(4-(3-Oxabicyclo[4.1.0]heptan-6-yl)-6-chloro-1H-pyrazolo[3,4-d]pyrimidin-1-yl)ethyl)morpholine (243)



In a 10-20 mL microwave vial a mixture of potassium 3-oxabicyclo[4.1.0]heptan-6-yltrifluoroborate (344 g, 1.67 mmol), 4-(2-(4,6-dichloro-1H-pyrazolo[3,4-d]pyrimidin-1-yl)ethyl)morpholine (340 mg, 1.13 mmol), caesium carbonate (1.10 g, 3.38 mmol), palladium (II) acetate (40 mg, 0.18 mmol) and cataCXium® A (129 mg, 0.36 mmol) was dissolved in toluene (5.1 mL) and water (0.51 mL). The resulting suspension was degassed with a stream of nitrogen for 10 min, sealed and stirred at 110 °C for 2 h. The reaction was monitored by LCMS and, upon complete consumption of starting material, the reaction was cooled to r.t. and filtered through a celite cartridge (10 g). The resulting mixture was concentrated *in vacuo* to give 4-(2-(4-(3-oxabicyclo[4.1.0]heptan-6-yl)-6-chloro-1H-pyrazolo[3,4-d]pyrimidin-1-yl)ethyl)morpholine as an orange oil. LCMS (formic) rt. 0.54 (47%) MH<sup>+</sup> for desired M=363.146. Due to a potential instability of this compound on silica, the reaction mixture was telescoped to the next step as a crude reaction mixture.

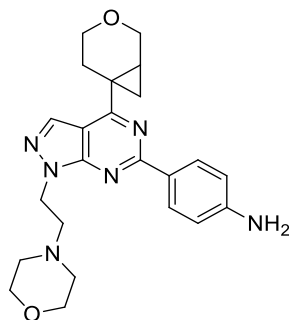
tert-Butyl (4-(4-(3-oxabicyclo[4.1.0]heptan-6-yl)-1-(tetrahydro-2H-thiopyran-4-yl)-1H-pyrazolo[3,4-d]pyrimidin-6-yl)phenyl)carbamate (244)



In a 10-20 mL microwave vial a mixture of 4-(3-oxabicyclo[4.1.0]heptan-6-yl)-6-chloro-1-(tetrahydro-2H-thiopyran-4-yl)-1H-pyrazolo[3,4-d]pyrimidine (700 mg, 1.76 mmol), *tert*-butyl (4-(4,4,5,5-tetramethyl-1,3,2-dioxaborolan-2-yl)phenyl)carbamate (914 mg, 2.83 mmol), sodium carbonate (368 mg, 3.47 mmol) and Pd(PPh<sub>3</sub>)<sub>4</sub> (201 mg, 0.17 mmol) The

resulting suspension was degassed with a stream of nitrogen for 10 min, sealed and stirred at 90 °C for 1.5 h. The reaction mixture was concentrated *in vacuo* and purified by preparative HPLC (formic, 15-85%, 15 min) to give 4-(4-(3-oxabicyclo[4.1.0]heptan-6-yl)-1-(tetrahydro-2H-pyran-4-yl)-1H-pyrazolo[3,4-*d*]pyrimidin-6-yl)aniline (113 mg, 0.28 mmol, 48 % yield). LCMS (formic) rt. 1.02 (96%) MH<sup>+</sup> for desired M= 391.201. <sup>1</sup>H NMR (CDCl<sub>3</sub>, 400 MHz) δ = 8.42 (d, *J* = 8.8 Hz, 2H), 8.07 (s, 1H), 6.79 (d, *J* = 8.6 Hz, 2H), 5.12 (tt, *J* = 11.6, 4.2 Hz, 1H), 4.20 (br dd, *J* = 11.4, 3.5 Hz, 2H), 4.11 (dd, *J* = 11.5, 1.2 Hz, 1H), 4.06 (dd, *J* = 11.5, 3.9 Hz, 1H), 3.83 (ddd, *J* = 11.6, 6.1, 3.7 Hz, 1H), 3.70 (td, *J* = 12.0, 2.2 Hz, 2H), 3.51 (ddd, *J* = 11.5, 10.0, 4.9 Hz, 1H), 3.05 (dt, *J* = 13.9, 4.4 Hz, 1H), 2.43-2.55 (m, 2H), 2.37 (ddd, *J* = 13.9, 9.9, 6.0 Hz, 1H), 2.26 (dddd, *J* = 9.1, 6.7, 3.8, 1.2 Hz, 1H), 1.95-2.07 (m, 2H), 1.70 (dd, *J* = 9.3, 4.2 Hz, 1H), 1.36 ppm (dd, *J* = 6.6, 4.2 Hz, 1H)

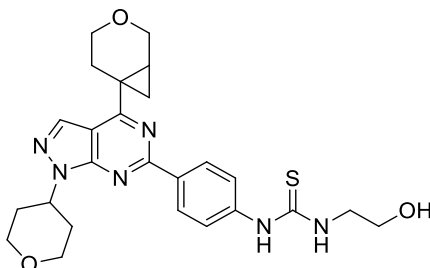
4-(4-(3-Oxabicyclo[4.1.0]heptan-6-yl)-1-(2-morpholinoethyl)-1H-pyrazolo[3,4-*d*]pyrimidin-6-yl)aniline (249)



In a 2-5 mL microwave vial a mixture using 4-(2-(4-(3-oxabicyclo[4.1.0]heptan-6-yl)-6-chloro-1H-pyrazolo[3,4-*d*]pyrimidin-1-yl)ethyl)morpholine (90% wt.) (180 mg, 0.45 mmol), *tert*-butyl (4-(4,4,5,5-tetramethyl-1,3,2-dioxaborolan-2-yl)phenyl)carbamate (235 mg, 1.65 mmol), sodium carbonate (94 mg, 0.89 mmol) and Pd(PPh<sub>3</sub>)<sub>4</sub> (52 mg, 0.045 mmol) was dissolved in DME (4 mL) and water (0.4 mL). The resulting suspension was degassed with a stream of nitrogen for 10 min, sealed and stirred at 90 °C for 1.5 h. The reaction was monitored by LCMS and, upon complete consumption of starting material, the reaction was cooled to r.t. and filtered through a celite cartridge (2.5 g). The resulting crude residue was dissolved in hexafluoroisopropanol (5 mL) and irradiated to 120 °C in a Biotage initiator + microwave for 1 h. The reaction mixture was concentrated *in vacuo* to give 4-(4-(3-oxabicyclo[4.1.0]heptan-6-yl)-1-(2-morpholinoethyl)-1H-pyrazolo[3,4-*d*]pyrimidin-6-yl)aniline (73 mg, 0.14 mmol, 28% yield) as an amorphous white solid. LCMS (formic) rt. 0.54 (80%) MH<sup>+</sup> for desired M= 420.227. Crude product was telescoped to the next step of the synthesis.

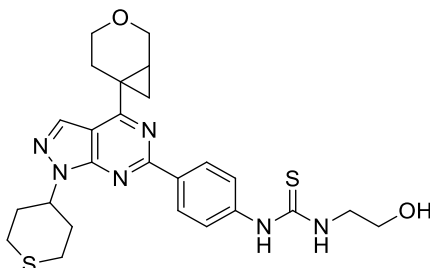


1-(4-(4-(3-Oxabicyclo[4.1.0]heptan-6-yl)-1-(tetrahydro-2H-pyran-4-yl)-1H-pyrazolo[3,4-d]pyrimidin-6-yl)phenyl)-3-(2-hydroxyethyl)thiourea (228)



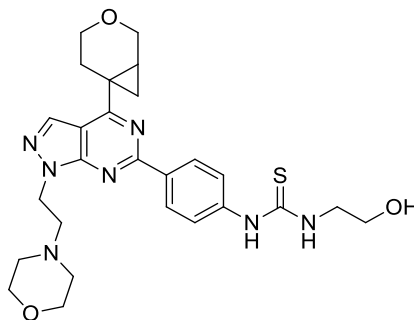
In a 2-5 mL microwave vial 4-(4-(3-oxabicyclo[4.1.0]heptan-6-yl)-1-(tetrahydro-2H-pyran-4-yl)-1H-pyrazolo[3,4-d]pyrimidin-6-yl)aniline (100 mg, 0.26 mmol) was dissolved in DCM (2 mL). 1,1'-Thiocarbonyldiimidazole (68 mg, 0.38 mmol) and pyridine (41  $\mu$ L, 0.51 mmol) were added and the reaction was stirred at r.t. for 2 h. LCMS analysis showed complete conversion to desired intermediate. Ethanolamine (40  $\mu$ L, 0.67 mmol) was added and the reaction was stirred at r.t. for 0.5 h. The reaction mixture was concentrated *in vacuo* and the resulting residue was triturated in DCM to give 1-(4-(4-(3-oxabicyclo[4.1.0]heptan-6-yl)-1-(tetrahydro-2H-pyran-4-yl)-1H-pyrazolo[3,4-d]pyrimidin-6-yl)phenyl)-3-(2-hydroxyethyl)thiourea (10 mg, 0.020 mmol, 8% yield) as an off-white solid. LCMS (formic) rt. 1.02 (100%)  $MH^+$  for desired  $M=494.210$ .  $^1H$  NMR (DMSO- $d_6$ , 400 MHz)  $\delta$  = 9.93 (br s, 1H), 8.46 (d,  $J$  = 8.8 Hz, 2H), 8.37 (s, 1H), 7.96 (br s, 1H), 7.71 (d,  $J$  = 8.8 Hz, 2H), 5.13 (tt,  $J$  = 11.5, 4.2 Hz, 1H), 4.84 (br s, 1H), 4.04 (br dd,  $J$  = 11.4, 3.5 Hz, 2H), 3.99 (dd,  $J$  = 11.5, 4.2 Hz, 1H), 3.94 (dd,  $J$  = 11.2, 1.2 Hz, 1H), 3.69 (ddd,  $J$  = 11.5, 5.6, 4.4 Hz, 1H), 3.63 (dd,  $J$  = 11.7, 1.2 Hz, 2H), 3.59 (br s, 4H), 3.45 (ddd,  $J$  = 11.6, 9.2, 5.1 Hz, 1H), 2.97 (dt,  $J$  = 14.1, 4.7 Hz, 1H), 2.18-2.34 (m, 4H), 1.94 (br d,  $J$  = 11.0 Hz, 2H), 1.67 (dd,  $J$  = 9.2, 4.0 Hz, 1H), 1.33 ppm (dd,  $J$  = 6.6, 4.2 Hz, 1H)  $^{13}C$  NMR (DMSO- $d_6$ , 101 MHz)  $\delta$  = 180.8, 170.0, 159.2, 153.6, 142.5, 133.1, 129.1, 109.8, 66.6, 65.1, 63.8, 59.6, 59.6, 53.3, 47.0, 38.7, 32.4, 26.2, 24.8, 23.9, 23.2 (1C not observed). HRMS calculated for  $C_{25}H_{30}N_6O_3S$  495.2178, found 495.2180. FTIR ( $cm^{-1}$ ) 3246, 2951, 1648, 1548, 1384, 1129, 971, 804.

1-(4-(4-(3-Oxabicyclo[4.1.0]heptan-6-yl)-1-(tetrahydro-2H-thiopyran-4-yl)-1H-pyrazolo[3,4-d]pyrimidin-6-yl)phenyl)-3-(2-hydroxyethyl)thiourea (229)



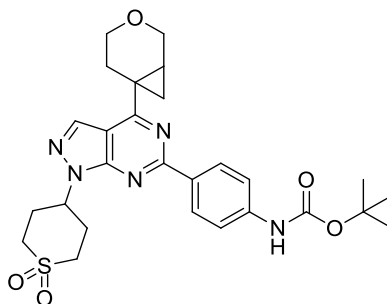
In a 2-5 mL microwave vial *tert*-butyl 4-(4-(4-(3-oxabicyclo[4.1.0]heptan-6-yl)-1-(tetrahydro-2H-thiopyran-4-yl)-1H-pyrazolo[3,4-d]pyrimidin-6-yl)phenyl)carbamate (100 mg, 0.20 mmol) was dissolved in hexafluoroisopropanol (2.5 mL) and heated to 120 °C in a microwave for 1.5 h. The reaction mixture was concentrated *in vacuo*. The resulting crude reaction mixture was dissolved in DCM (4 mL). 1,1'-Thiocarbonyldiimidazole (78 mg, 0.44 mmol) and pyridine (47  $\mu$ L, 0.59 mmol) were added and the reaction was stirred at r.t. for 1 h. LCMS analysis showed complete conversion to desired intermediate. Ethanolamine (40  $\mu$ L, 0.67 mmol) was added and the reaction was stirred at r.t. for 0.5 h. The reaction mixture was concentrated *in vacuo* and the resulting residue was purified by preparative HPLC (High-pH, 30-85%, 15 min) to give 1-(4-(4-(3-oxabicyclo[4.1.0]heptan-6-yl)-1-(tetrahydro-2H-thiopyran-4-yl)-1H-pyrazolo[3,4-d]pyrimidin-6-yl)phenyl)-3-(2-hydroxyethyl)thiourea (16 mg, 0.031 mmol, 16% yield) as an amorphous fluffy white solid. LCMS (high-pH) rt. 1.13 (100%)  $MH^+$  for desired  $M=510.187$ .  $^1H$  NMR (DMSO- $d_6$ , 400 MHz)  $\delta$  = 9.90 (br s, 1H), 9.81-10.04 (m, 1H), 8.46 (d,  $J$  = 8.8 Hz, 2H), 8.37 (s, 1H), 7.89-8.00 (m, 1H), 7.70 (d,  $J$  = 8.8 Hz, 2H), 4.95 (tt,  $J$  = 10.5, 4.4 Hz, 1H), 4.83 (br s, 1H), 3.99 (dd,  $J$  = 11.2, 3.9 Hz, 1H), 3.94 (d,  $J$  = 10.0 Hz, 1H), 3.69 (ddd,  $J$  = 10.9, 5.4, 4.4 Hz, 1H), 3.59 (s, 4H), 3.45 (ddd,  $J$  = 11.7, 9.3, 5.1 Hz, 1H), 2.93-3.03 (m, 3H), 2.80 (br d,  $J$  = 13.7 Hz, 2H), 2.21-2.36 (m, 6H), 1.67 (dd,  $J$  = 9.3, 3.9 Hz, 1H), 1.33 (dd,  $J$  = 6.5, 4.0 Hz, 1H)  $^{13}C$  NMR (DMSO- $d_6$ , 101 MHz)  $\delta$  = 180.7, 170.0, 159.2, 153.4, 133.2, 133.1, 129.1, 129.1, 122.1, 109.7, 65.1, 63.7, 55.2, 47.0, 33.8, 27.9, 26.2, 24.8, 24.0, 23.2, 21.0. HRMS calculated for  $C_{25}H_{30}N_6O_2S_2$  511.1950, found 511.1948. FTIR ( $cm^{-1}$ ) 3301, 2929, 1537, 1386, 1300, 1061, 946, 802.

1-(4-(4-(3-Oxabicyclo[4.1.0]heptan-6-yl)-1-(2-morpholinoethyl)-1*H*-pyrazolo[3,4-*d*]pyrimidin-6-yl)phenyl)-3-(2-hydroxyethyl)thiourea (230)



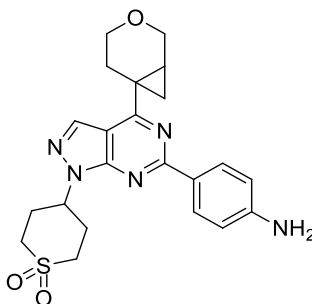
In a 2-5 mL microwave vial 4-(4-(3-oxabicyclo[4.1.0]heptan-6-yl)-1-(2-morpholinoethyl)-1*H*-pyrazolo[3,4-*d*]pyrimidin-6-yl)aniline (80% wt.) (73 mg, 0.14 mmol) was dissolved in DCM (2.5 mL). 1,1'-Thiocarbonyldiimidazole (37 mg, 0.21 mmol) and pyridine (22  $\mu$ L, 0.28 mmol) were added and the reaction was stirred at r.t. for 1 h. LCMS analysis showed complete conversion to desired intermediate. Ethanolamine (42  $\mu$ L, 0.69 mmol) was added and the reaction was stirred at r.t. for 0.5 h. The reaction mixture was concentrated *in vacuo* and the resulting residue was purified by preparative HPLC (High-pH, 30-85%, 25 min) to give 1-(4-(4-(3-oxabicyclo[4.1.0]heptan-6-yl)-1-(2-morpholinoethyl)-1*H*-pyrazolo[3,4-*d*]pyrimidin-6-yl)phenyl)-3-(2-hydroxyethyl)thiourea (15 mg, 0.028 mmol, 21 % yield) as an off-white solid. LCMS (formic, DMSO) 0.56 (97%)  $MH^+$  for desired  $M= 523.237$ .  $^1H$  NMR (DMSO- $d_6$ , 400 MHz):  $\delta = 9.87$  (br s, 1H), 8.43 (d,  $J = 8.6$  Hz, 2H), 8.36 (s, 1H), 7.93 (br s, 1H), 7.69 (d,  $J = 8.6$  Hz, 2H), 4.83 (br s, 1H), 4.61 (t,  $J = 6.2$  Hz, 2H), 4.00 (dd,  $J = 11.2, 3.9$  Hz, 1H), 3.94 (d,  $J = 10.8$  Hz, 1H), 3.65-3.72 (m, 1H), 3.53-3.63 (m, 4H), 3.46 (ddd,  $J = 11.2, 9.0, 5.1$  Hz, 1H), 3.39-3.45 (m, 4H), 2.98 (dt,  $J = 13.9, 4.6$  Hz, 1H), 2.78-2.87 (m, 2H), 2.46-2.49 (m, 4H), 2.21-2.34 (m, 2H), 1.66 (dd,  $J = 9.3, 3.9$  Hz, 1H), 1.34 (dd,  $J = 6.5, 4.0$  Hz, 1H).  $^{13}C$  NMR (DMSO- $d_6$ , 101 MHz):  $\delta = 180.7, 169.9, 159.2, 154.6, 133.3, 129.0, 122.1, 109.4, 66.6, 65.2, 63.7, 59.6, 57.4, 53.5, 47.0, 44.0, 26.2, 24.7, 24.1, 23.3$  ppm. HRMS calculated for  $C_{26}H_{33}N_7O_3S$  524.2444, found 524.2445. FTIR ( $cm^{-1}$ ) 3168, 2656, 1519, 1384, 1118, 1044, 802.

*tert*-Butyl (4-(4-(3-oxabicyclo[4.1.0]heptan-6-yl)-1-(1,1-dioxidotetrahydro-2*H*-thiopyran-4-yl)-1*H*-pyrazolo[3,4-*d*]pyrimidin-6-yl)phenyl)carbamate (250)



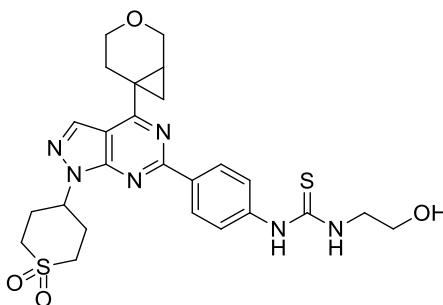
In a 2-5 mL microwave vial *tert*-butyl (4-(4-(3-oxabicyclo[4.1.0]heptan-6-yl)-1-(tetrahydro-2*H*-thiopyran-4-yl)-1*H*-pyrazolo[3,4-*d*]pyrimidin-6-yl)phenyl)carbamate (100 mg, 0.20 mmol) was dissolved in DCM (2 mL) and cooled to 0 °C. *meta*-Chloroperbenzoic acid (119 mg, 0.69 mmol) was added and the reaction was stirred at 0 °C for 2.5 h. The reaction mixture was diluted in DCM (10 mL). The organic layer was washed with sodium sulfite (10% solution) (10 mL) and sat. aq. sodium bicarbonate (10 mL). The combined organic layers were dried (hydrophobic frit) and concentrated *in vacuo*. The resulting crude residue was purified by flash column chromatography (cyclohexane: ethyl acetate 0-100% (20 column volumes)) to give *tert*-butyl (4-(4-(3-oxabicyclo[4.1.0]heptan-6-yl)-1-(1,1-dioxidotetrahydro-2*H*-thiopyran-4-yl)-1*H*-pyrazolo[3,4-*d*]pyrimidin-6-yl)phenyl)carbamate (80 mg, 0.15 mmol, 75% yield) as a pale yellow oil. LCMS (formic) rt. 1.30 (100%) MH<sup>+</sup> for desired M= 539.220. <sup>1</sup>H NMR (DMSO-*d*<sub>6</sub>, 600 MHz) δ = 9.61 (s, 1H), 8.44 (d, *J* = 8.8 Hz, 2H), 8.40 (s, 1H), 7.63 (d, *J* = 8.8 Hz, 2H), 5.35 (tt, *J* = 10.6, 3.7 Hz, 1H), 3.99 (dd, *J* = 11.4, 4.4 Hz, 1H), 3.95 (dd, *J* = 11.4, 1.1 Hz, 1H), 3.69 (ddd, *J* = 11.7, 5.9, 4.8 Hz, 1H), 3.58 (td, *J* = 13.2, 2.9 Hz, 2H), 3.45 (ddd, *J* = 11.6, 9.4, 5.1 Hz, 1H), 3.24-3.29 (m, 2H), 2.95 (dt, *J* = 14.0, 4.7 Hz, 1H), 2.63-2.73 (m, 2H), 2.52-2.53 (m, 1H), 2.22-2.35 (m, 4H), 1.66 (dd, *J* = 9.2, 4.0 Hz, 1H), 1.51 (s, 9H), 1.33 ppm (dd, *J* = 6.6, 4.0 Hz, 1H). <sup>13</sup>C NMR (DMSO-*d*<sub>6</sub>, 151 MHz) δ = 170.1, 159.5, 153.8, 153.1, 142.7, 133.6, 131.3, 129.5, 118.1, 109.7, 79.9, 65.1, 63.7, 49.4, 40.6, 29.7, 28.6, 26.2, 24.8, 23.9, 23.2 ppm. HRMS calculated for C<sub>27</sub>H<sub>33</sub>N<sub>5</sub>O<sub>5</sub>S 540.2281 found 540.2280. FTIR (cm<sup>-1</sup>) 3345, 2929, 1532, 1388, 1285, 1147, 1043, 805.

4-(6-(4-Aminophenyl)-4-(3-oxabicyclo[4.1.0]heptan-6-yl)-1H-pyrazolo[3,4-d]pyrimidin-1-yl)tetrahydro-2H-thiopyran 1,1-dioxide (251)



In a 2-5 mL microwave vial *tert*-butyl (4-(4-(3-oxabicyclo[4.1.0]heptan-6-yl)-1-(1,1-dioxidotetrahydro-2H-thiopyran-4-yl)-1H-pyrazolo[3,4-d]pyrimidin-6-yl)phenyl)carbamate (74 mg, 0.12 mmol) was dissolved in hexafluoroisopropanol (3 mL) and the reaction was irradiated to 120 °C in a Biotage initiator+ microwave for 1.5 h. The resulting mixture was concentrated *in vacuo* to give 4-(6-(4-aminophenyl)-4-(3-oxabicyclo[4.1.0]heptan-6-yl)-1H-pyrazolo[3,4-d]pyrimidin-1-yl)tetrahydro-2H-thiopyran 1,1-dioxide (54 mg, 0.12 mmol, quant. yield) as an amorphous pale yellow solid. LCMS (formic) rt. 0.92 (98%) MH<sup>+</sup> for desired M= 439.16. <sup>1</sup>H NMR (DMSO-d<sub>6</sub>, 400 MHz) δ = 8.31 (s, 1H), 8.25 (d, *J* = 8.6 Hz, 2H), 6.66 (d, *J* = 8.6 Hz, 2H), 5.69 (s, 2H), 5.30 (tt, *J* = 10.5, 3.4 Hz, 1H), 3.98 (dd, *J* = 11.2, 3.7 Hz, 1H), 3.93 (d, *J* = 11.0 Hz, 1H), 3.64-3.72 (m, 1H), 3.52-3.62 (m, 2H), 3.43 (ddd, *J* = 11.4, 9.4, 5.1 Hz, 1H), 3.27 (br s, 1H), 2.94 (dt, *J* = 13.9, 4.6 Hz, 1H), 2.59-2.76 (m, 2H), 2.16-2.36 (m, 4H), 1.62 (dd, *J* = 9.2, 3.8 Hz, 1H), 1.28 (dd, *J* = 6.4, 4.2 Hz, 1H).

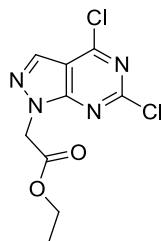
1-(4-(4-(3-Oxabicyclo[4.1.0]heptan-6-yl)-1-(1,1-dioxidotetrahydro-2H-thiopyran-4-yl)-1H-pyrazolo[3,4-d]pyrimidin-6-yl)phenyl)-3-(2-hydroxyethyl)thiourea (231)



In a 2-5 mL microwave vial 4-(6-(4-aminophenyl)-4-(3-oxabicyclo[4.1.0]heptan-6-yl)-1H-pyrazolo[3,4-d]pyrimidin-1-yl)tetrahydro-2H-thiopyran 1,1-dioxide (49 mg, 0.109 mmol) was dissolved in DCM (2 mL). 1,1'-Thiocarbonyldiimidazole (29 mg, 0.16 mmol) and pyridine (18 μL, 0.22 mmol) were added and the reaction was stirred at r.t. for 1 h. LCMS analysis showed complete conversion to desired intermediate. Ethanolamine (33 μL, 0.55 mmol) was added and the reaction was stirred at r.t. for 0.5 h. The reaction mixture was concentrated *in*

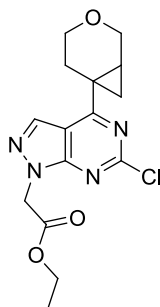
*vacuo* and the resulting residue was purified by preparative HPLC (formic, 30-85% over 15 min) to give 1-(4-(4-(3-oxabicyclo[4.1.0]heptan-6-yl)-1-(1,1-dioxidotetrahydro-2*H*-thiopyran-4-yl)-1*H*-pyrazolo[3,4-*d*]pyrimidin-6-yl)phenyl)-3-(2-hydroxyethyl)thiourea (26 mg, 0.049 mmol, 45% yield) as an amorphous off-white solid. LCMS (formic) rt. 0.89 (98%) MH<sup>+</sup> for desired M= 542.177. <sup>1</sup>H NMR (DMSO-*d*<sub>6</sub>, 400 MHz) δ = 9.88 (br., s, 1H), 8.47 (d, *J* = 8.8 Hz, 2H), 8.42 (s, 1H), 7.92 (br., s, 1H), 7.70 (d, *J* = 8.8 Hz, 2H), 5.36 (tt, *J* = 11.0, 3.7 Hz, 1H), 4.83 (br s, 1H), 3.99 (dd, *J* = 11.2, 3.9 Hz, 1H), 3.94 (dd, *J* = 11.2, 1.5 Hz, 1H), 3.69 (ddd, *J* = 10.9, 5.6, 4.6 Hz, 1H), 3.53-3.62 (m, 6H), 3.45 (ddd, *J* = 11.2, 9.0, 5.4 Hz, 1H), 3.22-3.29 (m, 2H), 3.18 (d, *J* = 4.4 Hz, 1H), 2.97 (dt, *J* = 14.1, 4.7 Hz, 1H), 2.63-2.76 (m, 2H), 2.22-2.39 (m, 4H), 1.67 (dd, *J* = 9.2, 4.0 Hz, 1H), 1.34 (dd, *J* = 6.7, 4.3 Hz, 1H). <sup>13</sup>C NMR (DMSO-*d*<sub>6</sub>, 101 MHz) δ = 170.2, 159.3, 153.7, 142.9, 142.6, 129.2, 109.8, 65.1, 63.7, 59.6, 51.9, 49.4, 47.0, 29.6, 26.2, 24.8, 24.0, 23.3 (3C Not observed). HRMS calculated for C<sub>25</sub>H<sub>30</sub>N<sub>6</sub>O<sub>4</sub>S<sub>2</sub> 543.1848, found 543.1846. FTIR (cm<sup>-1</sup>) 3345, 2941, 1533, 1385, 1298, 1130, 845.

Ethyl 2-(4,6-dichloro-1*H*-pyrazolo[3,4-*d*]pyrimidin-1-yl)acetate (252)<sup>264</sup>



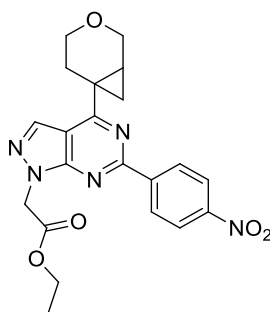
2,4,6-trichloropyrimidine-5-carbaldehyde (5.0 g, 23.7 mmol) was dissolved in EtOH (150 mL). The reaction was cooled to -78 °C. ethyl amino glycinate hydrochloride (3.66 g, 23.7 mmol) and triethylamine (3.3 mL, 23.7 mmol) were added and the reaction was stirred at -78 °C for 0.5 h before warming to 0 °C and stirring for a further 1.5 h. The reaction mixture was diluted with DCM (200 mL) and washed with sat. aq. sodium bicarbonate (200 mL). The combined organic layers were dried (hydrophobic frit) and concentrated *in vacuo*. The reaction mixture was purified by flash column chromatography (cyclohexane: ethyl acetate 0-75% (18 column volumes)) to give ethyl 2-(4,6-dichloro-1*H*-pyrazolo[3,4-*d*]pyrimidin-1-yl)acetate (3.33 g, 3.67 mmol, 51% yield) as an amorphous white solid. LCMS (formic) rt. 1.01 (96%) MH<sup>+</sup> for desired M=275.089. <sup>1</sup>H NMR (DMSO-*d*<sub>6</sub>, 400 MHz) δ = 8.63 (s, 1H), 5.41 (s, 2H), 4.19 (q, *J* = 7.1 Hz, 2H), 1.22 (t, *J* = 7.1 Hz, 3H). <sup>13</sup>C NMR (DMSO-*d*<sub>6</sub>, 101 MHz) δ = 167.5, 156.0, 155.3, 155.0, 134.2, 113.2, 62.1, 49.3, 14.4. HRMS calculated for C<sub>9</sub>H<sub>8</sub>Cl<sub>2</sub>N<sub>4</sub>O<sub>2</sub> 275.0103, found 275.0103. FTIR (cm<sup>-1</sup>) 1739, 1586, 1216, 1131, 812.

Ethyl 2-(4-(3-oxabicyclo[4.1.0]heptan-6-yl)-6-chloro-1*H*-pyrazolo[3,4-*d*]pyrimidin-1-yl)acetate (253)



In a 150 mL RBF a mixture of potassium 3-oxabicyclo[4.1.0]heptan-6-yltrifluoroborate (2.20 g, 10.8 mmol), ethyl 2-(4,6-dichloro-1*H*-pyrazolo[3,4-*d*]pyrimidin-1-yl)acetate (3.0 g, 10.8 mmol), caesium carbonate (10.55 g, 32.4 mmol), palladium (II) acetate (388 mg, 1.72 mmol) and cataCXium® A (1.24 g, 3.45 mmol) was dissolved in toluene (49 mL) and water (4.9 mL). The resulting suspension was degassed with a stream of nitrogen for 10 min, fitted with a reflux condenser and stirred at 110 °C for 1 h then at 60 °C for 16 h. The reaction was monitored by LCMS and, upon complete consumption of starting material, the reaction was cooled to r.t. and filtered through a celite cartridge (10 g). The reaction mixture was purified by reverse phase flash column chromatography (formic, 30-895% (15 column volumes) to give ethyl 2-(4-(3-oxabicyclo[4.1.0]heptan-6-yl)-6-chloro-1*H*-pyrazolo[3,4-*d*]pyrimidin-1-yl)acetate (1.75 g, 5.20 mmol, 48% yield) as an amorphous pale yellow solid. LCMS (formic) rt. 1.06 (100%) MH<sup>+</sup> for desired M= 336.099. <sup>1</sup>H NMR (DMSO-*d*<sub>6</sub>, 400 MHz) δ = 8.55 (s, 1H), 5.33 (s, 2H), 4.17 (q, *J* = 7.1 Hz, 2H), 3.96 (dd, *J* = 11.5, 4.2 Hz, 1H), 3.90 (dd, *J* = 11.5, 1.5 Hz, 1H), 3.65 (ddd, *J* = 11.6, 5.8, 4.4 Hz, 1H), 3.42 (ddd, *J* = 11.6, 9.2, 5.1 Hz, 1H), 2.80 (dt, *J* = 14.2, 4.8 Hz, 1H), 2.53-2.67 (m, 1H), 2.25 (ddd, *J* = 14.3, 8.9, 5.9 Hz, 1H), 2.12-2.19 (m, 1H), 1.63 (dd, *J* = 9.3, 4.2 Hz, 1H), 1.40 (dd, *J* = 6.8, 4.2 Hz, 1H), 1.21 (t, *J* = 7.2 Hz, 3H). <sup>13</sup>C NMR (DMSO-*d*<sub>6</sub>, 101 MHz) δ = 173.5, 167.8, 156.9, 155.0, 134.8, 110.8, 64.9, 63.5, 61.9, 48.7, 26.0, 25.1, 24.9, 24.4, 14.4. HRMS calculated for C<sub>15</sub>H<sub>17</sub>ClN<sub>4</sub>O<sub>3</sub> 337.1067, found 337.1066. FTIR (cm<sup>-1</sup>) 1733, 1556, 1262, 1144, 1028, 800.

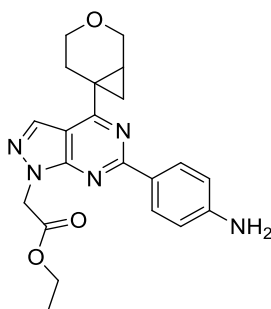
2-(4-(3-Oxabicyclo[4.1.0]heptan-6-yl)-6-(4-nitrophenyl)-1*H*-pyrazolo[3,4-*d*]pyrimidin-1-yl)acetate (254)



In a 50 mL RBF ethyl 2-(4-(3-oxabicyclo[4.1.0]heptan-6-yl)-6-chloro-1*H*-pyrazolo[3,4-*d*]pyrimidin-1-yl)acetate (1.0 g, 2.64 mmol), 4,4,5,5-tetramethyl-2-(4-nitrophenyl)-1,3,2-dioxaborolane (990 mg, 3.96 mmol), sodium carbonate (560 mg, 5.29 mmol) and Pd(II)(dppf)Cl<sub>2</sub>.CH<sub>2</sub>Cl<sub>2</sub> (216 mg, 0.26 mmol) were dissolved in DME (23 mL) and water (3 mL). The reaction was stirred at 70 °C for 16 h. The reaction mixture was cooled to r.t. and filtered through celite (10 g) and concentrated *in vacuo*. The resulting residue was partitioned between dichloromethane (20 mL) and sat. aq. sodium bicarbonate (20 mL). The aqueous layer was extracted with further dichloromethane (3 x 20 mL). The combined organic layers were dried (hydrophobic frit) and concentrated *in vacuo*. The resulting residue was purified by flash column chromatography (cyclohexane: ethyl acetate 0-75% (15 column volumes)) to give ethyl 2-(4-(3-oxabicyclo[4.1.0]heptan-6-yl)-6-(4-nitrophenyl)-1*H*-pyrazolo[3,4-*d*]pyrimidin-1-yl)acetate (825 mg, 1.95 mmol, 74% yield) as an amorphous pale yellow solid. LCMS (high-pH) rt. 1.34 (100%) MH<sup>+</sup> for desired M=423.154. <sup>1</sup>H NMR (CDCl<sub>3</sub>, 400 MHz) δ = 8.74 (d, *J* = 9.0 Hz, 2H), 8.34 (d, *J* = 9.0 Hz, 2H), 8.26 (s, 1H), 5.35 (s, 2H), 4.30 (q, *J* = 7.3 Hz, 2H), 4.14 (dd, *J* = 11.5, 1.5 Hz, 1H), 4.09 (dd, *J* = 11.2, 3.4 Hz, 1H), 3.85 (ddd, *J* = 11.6, 6.0, 3.9 Hz, 1H), 3.55 (ddd, *J* = 11.6, 9.7, 5.1 Hz, 1H), 3.07 (dt, *J* = 13.9, 4.7 Hz, 1H), 2.43 (ddd, *J* = 13.9, 9.7, 6.0 Hz, 1H), 2.29-2.37 (m, 1H), 1.76 (dd, *J* = 9.2, 4.3 Hz, 1H), 1.49 (dd, *J* = 6.6, 4.4 Hz, 2H), 1.33 (t, *J* = 7.2 Hz, 3H). <sup>13</sup>C NMR (CDCl<sub>3</sub>, 101 MHz) δ = 170.5, 167.5, 158.5, 154.9, 149.3, 143.6, 133.7, 129.5, 123.6, 110.5, 77.3, 77.2, 77.0, 76.7, 65.5, 64.1, 62.1, 48.1, 26.4, 24.8, 24.5, 23.5, 14.1. HRMS calculated for C<sub>21</sub>H<sub>21</sub>N<sub>5</sub>O<sub>5</sub> 424.1621, found 424.1624. FTIR (cm<sup>-1</sup>) 1643, 1556, 1392, 1153, 1004, 792.

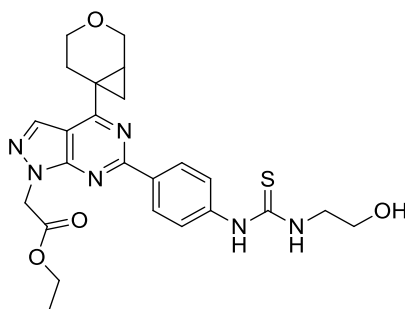


Ethyl 2-(6-(4-aminophenyl)-4-(3-oxabicyclo[4.1.0]heptan-6-yl)-1H-pyrazolo[3,4-d]pyrimidin-1-yl)acetate (255)



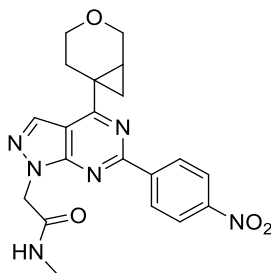
In a 10-20 mL microwave vial ethyl 2-(4-(3-oxabicyclo[4.1.0]heptan-6-yl)-6-(4-nitrophenyl)-1H-pyrazolo[3,4-d]pyrimidin-1-yl)acetate (347 mg, 0.82 mmol) and iron powder (230 mg, 4.10 mmol) were dissolved in EtOH (6 mL), acetic acid (6 mL) and water (3 mL) and the resulting suspension was sonicated for 4 h. The reaction mixture was filtered through celite (10 g) and partitioned between DCM (20 mL) and water (20 mL). The aqueous layer was extracted with further DCM (3x 20 mL) and the combined organic layers were concentrated *in vacuo* to give ethyl 2-(6-(4-aminophenyl)-4-(3-oxabicyclo[4.1.0]heptan-6-yl)-1H-pyrazolo[3,4-d]pyrimidin-1-yl)acetate (234 mg, 0.60 mmol, 73% yield) as a pale orange solid. LMCS (formic) rt. 1.06 (92%) MH<sup>+</sup> for desired M= 393.447. <sup>1</sup>H NMR (DMSO-d<sub>6</sub>, 400 MHz) δ = 8.32 (s, 1H), 8.18-8.23 (m, 2H), 6.61-6.70 (m, 2H), 5.69 (br., s, 2H), 5.32 (s, 2H), 4.18 (q, J = 7.1 Hz, 2H), 4.00 (dd, J = 11.2, 4.2 Hz, 1H), 3.94 (dd, J = 11.2, 1.2 Hz, 1H), 3.68 (ddd, J = 11.7, 5.6, 4.6 Hz, 1H), 3.45 (ddd, J = 11.6, 9.2, 5.1 Hz, 1H), 2.95 (dt, J = 13.9, 4.6 Hz, 1H), 2.27 (ddd, J = 14.7, 9.3, 5.9 Hz, 1H), 2.18-2.24 (m, 1H), 1.62 (dd, J = 9.0, 3.9 Hz, 1H), 1.31 (dd, J = 6.6, 3.9 Hz, 1H), 1.22 (t, J = 7.1 Hz, 3H). <sup>13</sup>C NMR (101 MHz, DMSO-d<sub>6</sub>) δ= 169.5, 168.3, 160.9, 155.2, 152.2, 134.0, 130.4, 124.7, 113.7, 108.6, 65.2, 63.7, 61.7, 48.2, 26.2, 24.7, 23.8, 23.0, 14.5. HRMS calculated for C<sub>21</sub>H<sub>24</sub>N<sub>5</sub>O<sub>3</sub> 394.1879, found 394.1881. FTIR (cm<sup>-1</sup>) 3343, 1739, 1571, 1387, 1199, 806.

Ethyl 2-(4-(3-oxabicyclo[4.1.0]heptan-6-yl)-6-(4-(3-(2-hydroxyethyl)thioureido)phenyl)-1H-pyrazolo[3,4-d]pyrimidin-1-yl)acetate (232)



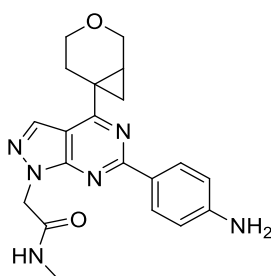
In a 2-5 mL microwave vial ethyl 2-(6-(4-aminophenyl)-4-(3-oxabicyclo[4.1.0]heptan-6-yl)-1H-pyrazolo[3,4-d]pyrimidin-1-yl)acetate (180 mg, 0.42 mmol) was dissolved in DCM (10 mL). 1,1'-Thiocarbonyldiimidazole (113 mg, 0.63 mmol) and pyridine (68  $\mu$ L, 0.84 mmol) were added and the reaction was stirred at r.t. for 2 h. LCMS analysis showed complete conversion to desired intermediate. Ethanolamine (127  $\mu$ L, 2.10 mmol) was added and the reaction was stirred at r.t. for 0.5 h. The reaction mixture was concentrated *in vacuo* and the resulting residue was purified by preparative HPLC (formic, 30-85% 15 min) to give ethyl 2-(4-(3-oxabicyclo[4.1.0]heptan-6-yl)-6-(4-(3-(2-hydroxyethyl)thioureido)phenyl)-1H-pyrazolo[3,4-d]pyrimidin-1-yl)acetate (58 mg, 0.12 mmol, 28% yield). LCMS (formic) rt. 0.97 (97%)  $MH^+$  for desired  $M=496.189$ .  $^1H$  NMR (DMSO- $d_6$ , 400 MHz)  $\delta$  = 9.94 (br s, 1H), 8.40-8.48 (m, 3H), 7.98 (br s, 1H), 7.70 (d,  $J$  = 8.6 Hz, 2H), 5.39 (s, 2H), 4.75-4.96 (m, 1H), 4.19 (q,  $J$  = 7.1 Hz, 2H), 4.01 (dd,  $J$  = 11.2, 4.2 Hz, 1H), 3.95 (dd,  $J$  = 11.2, 1.0 Hz, 1H), 3.65-3.72 (m, 1H), 3.55-3.61 (m, 4H), 3.47 (ddd,  $J$  = 11.5, 9.2, 5.3 Hz, 1H), 2.99 (dt,  $J$  = 14.1, 4.8 Hz, 1H), 2.21-2.38 (m, 2H), 1.68 (dd,  $J$  = 9.3, 3.9 Hz, 1H), 1.37 (dd,  $J$  = 6.6, 4.2 Hz, 1H), 1.22 (t,  $J$  = 7.1 Hz, 3H).  $^{13}C$  NMR (DMSO- $d_6$ , 101 MHz)  $\delta$  = 180.7, 170.2, 168.2, 159.8, 155.0, 142.7, 134.2, 132.6, 129.2, 122.1, 109.5, 65.2, 63.7, 61.8, 59.6, 48.4, 47.0, 26.2, 24.8, 24.3, 23.5, 14.5 HRMS calculated for  $C_{24}H_{29}N_6O_4S$  497.1971, found 497.1964. FTIR ( $cm^{-1}$ ) 3343, 1739, 1607, 1571, 1387, 1199, 1013, 806.

2-(4-(3-Oxabicyclo[4.1.0]heptan-6-yl)-6-(4-nitrophenyl)-1*H*-pyrazolo[3,4-*d*]pyrimidin-1-yl)-*N*-methylacetamide (256)



ethyl 2-(4-(3-oxabicyclo[4.1.0]heptan-6-yl)-6-(4-nitrophenyl)-1*H*-pyrazolo[3,4-*d*]pyrimidin-1-yl)acetate (100 mg, 0.24 mmol) was dissolved in methylamine (2M in THF) (2 mL, 4.0 mmol) and the reaction was stirred at r.t. for 24 h. The reaction mixture was concentrated *in vacuo* to give 2-(4-(3-oxabicyclo[4.1.0]heptan-6-yl)-6-(4-nitrophenyl)-1*H*-pyrazolo[3,4-*d*]pyrimidin-1-yl)-*N*-methylacetamide (106 mg, 0.24 mmol, quant. yield) LCMS (formic) rt. 1.04 (93%)  $MH^+$  for desired  $M = 408.155$ .  $^1H$  NMR (DMSO- $d_6$ , 400 MHz)  $\delta = 8.72$  (d,  $J = 9.0$  Hz, 2H), 8.51 (s, 1H), 8.39 (d,  $J = 9.0$  Hz, 2H), 8.11 (br q,  $J = 4.7$  Hz, 1H), 5.17 (s, 2H), 4.02 (dd,  $J = 11.5, 4.2$  Hz, 1H), 3.97 (dd,  $J = 11.5, 1.5$  Hz, 1H), 3.71 (ddd,  $J = 11.5, 5.7, 4.6$  Hz, 1H), 3.48 (ddd,  $J = 11.6, 9.1, 5.3$  Hz, 1H), 2.98 (dt,  $J = 14.1, 4.8$  Hz, 1H), 2.64 (d,  $J = 4.6$  Hz, 3H), 2.25-2.40 (m, 2H), 1.72 (dd,  $J = 9.3, 4.2$  Hz, 1H), 1.41 (dd,  $J = 6.8, 4.2$  Hz, 1H).  $^{13}C$  NMR (DMSO- $d_6$ , 101 MHz)  $\delta = 170.6, 166.9, 157.8, 154.8, 149.3, 143.7, 134.1, 129.8, 124.3, 110.5, 65.1, 63.7, 49.7, 26.2, 26.1, 24.9, 24.5, 23.7$ . HRMS calculated for  $C_{20}H_{20}N_6O_4$ , 408.1546, found  $[M+2H]^{2+}/2$  205.0859. FTIR ( $cm^{-1}$ ) 3290, 1663, 1553, 1347, 1128, 1027, 807.

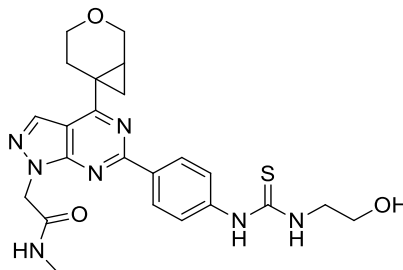
2-(6-(4-Aminophenyl)-4-(3-oxabicyclo[4.1.0]heptan-6-yl)-1*H*-pyrazolo[3,4-*d*]pyrimidin-1-yl)-*N*-methylacetamide (257)



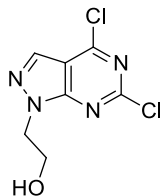
In a 2-5 mL microwave vial 2-(4-(3-oxabicyclo[4.1.0]heptan-6-yl)-6-(4-nitrophenyl)-1*H*-pyrazolo[3,4-*d*]pyrimidin-1-yl)-*N*-methylacetamide (100 mg, 0.25 mmol) and iron powder (68 mg, 1.22 mmol) were dissolved in EtOH (2 mL), acetic acid (2 mL) and water (1 mL) and the resulting suspension was sonicated for 1.5 h. The reaction mixture was filtered through a celite cartridge (2.5 g) and concentrated *in vacuo* to give 2-(6-(4-aminophenyl)-4-(3-

oxabicyclo[4.1.0]heptan-6-yl)-1*H*-pyrazolo[3,4-*d*]pyrimidin-1-yl)-*N*-methylacetamide (69 mg, 0.16 mmol, 66% yield) as an amorphous pale yellow solid LCMS (formic) rt. 0.75 (86%)  $MH^+$  for desired  $M = 378.180$ . Crude product was telescoped to the next step of the synthesis.

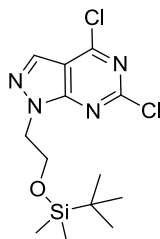
2-(4-(3-Oxabicyclo[4.1.0]heptan-6-yl)-6-(4-(3-(2-hydroxyethyl)thioureido)phenyl)-1*H*-pyrazolo[3,4-*d*]pyrimidin-1-yl)-*N*-methylacetamide (233)



In a 2-5 mL microwave vial ethyl 2-(6-(4-aminophenyl)-4-(3-oxabicyclo[4.1.0]heptan-6-yl)-1*H*-pyrazolo[3,4-*d*]pyrimidin-1-yl)-*N*-methylacetamide (60 mg, 0.14 mmol) was dissolved in DCM (2 mL). 1,1'-Thiocarbonyldiimidazole (36 mg, 0.20 mmol) and pyridine (22  $\mu$ L, 0.27 mmol) were added and the reaction was stirred at r.t. for 2 h. LCMS analysis showed complete conversion to desired intermediate. Ethanamine (41  $\mu$ L, 0.67 mmol) was added and the reaction was stirred at r.t. for 0.5 h. The reaction mixture was concentrated *in vacuo* and the resulting residue was purified by preparative HPLC (High-pH, 15-55%, 30 min) to give 2-(4-(3-oxabicyclo[4.1.0]heptan-6-yl)-6-(4-(3-(2-hydroxyethyl)thioureido)phenyl)-1*H*-pyrazolo[3,4-*d*]pyrimidin-1-yl)-*N*-methylacetamide (22 mg, 0.046 mmol, 34% yield) as an amorphous white solid. LCMS (formic) rt. 0.76 (100%)  $MH^+$  for desired  $M = 481.190$ .  $^1H$  NMR (DMSO- $d_6$ , 400 MHz)  $\delta = 9.96$  (br., s, 1H), 8.43 (d,  $J = 8.8$  Hz, 2H), 8.39 (s, 1H), 7.93-8.16 (m, 2H), 7.70 (d,  $J = 8.8$  Hz, 2H), 5.11 (s, 2H), 4.83 (br., s, 1H), 4.01 (dd,  $J = 11.5, 3.9$  Hz, 1H), 3.95 (dd,  $J = 11.2, 1.2$  Hz, 1H), 3.69 (ddd,  $J = 11.5, 5.9, 4.6$  Hz, 1H), 3.58 (s, 4H), 3.47 (ddd,  $J = 11.7, 9.3, 5.4$  Hz, 2H), 2.98 (dt,  $J = 14.1, 4.7$  Hz, 1H), 2.64 (d,  $J = 4.4$  Hz, 4H), 1.67 (dd,  $J = 9.3, 3.9$  Hz, 1H), 1.35 (dd,  $J = 6.6, 4.2$  Hz, 1H)  $^{13}C$  NMR (DMSO- $d_6$ , 101 MHz)  $\delta = 180.7, 169.9, 167.1, 159.6, 155.1, 142.6, 133.9, 132.7, 129.1, 122.0, 109.6, 65.2, 63.7, 59.7, 49.5, 47.0, 26.3, 26.1, 24.7, 24.1, 23.3$ . HRMS calculated for  $C_{23}H_{27}N_7O_3S$  482.1974, found 482.1975. FTIR ( $cm^{-1}$ ) 3275, 1667, 1537, 1387, 1172, 1023, 806.

2-(4,6-Dichloro-1*H*-pyrazolo[3,4-*d*]pyrimidin-1-yl)ethan-1-ol (258)<sup>262</sup>

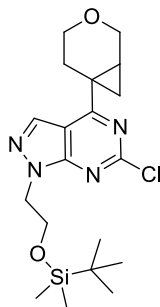
2,4,6-trichloropyrimidine-5-carbaldehyde (1.5 g, 7.09 mmol) was dissolved in EtOH (50 mL). The reaction was cooled to -78 °C. 2-hydrazinyethan-1-ol (0.491 ml, 7.80 mmol) and triethylamine (1.1 mL, 7.80 mmol) were added and the reaction was stirred at -78 °C for 0.5 h before warming to 0 °C and stirring for a further 1.5 h. The reaction mixture was diluted with DCM (100 mL) and washed with sat. aq. sodium bicarbonate (100 mL). The combined organic layers were dried (hydrophobic frit) and concentrated *in vacuo*. The reaction mixture was purified by flash column chromatography (cyclohexane: ethyl acetate 0-100% (15 column volumes)) to give 2-(4,6-dichloro-1*H*-pyrazolo[3,4-*d*]pyrimidin-1-yl)ethan-1-ol (1.12 g, 4.81 mmol, 68% yield). LCMS (formic) rt. 0.69 (98%) MH<sup>+</sup> for desired M= 231.992. <sup>1</sup>H NMR (DMSO-*d*<sub>6</sub>, 400 MHz) δ = 8.56 (s, 1H), 4.85 (br s, 1H), 4.46 (t, *J* = 5.5 Hz, 2H), 3.85 ppm (t, *J* = 5.5 Hz, 2H). <sup>13</sup>C NMR (DMSO-*d*<sub>6</sub>, 101 MHz) δ = 155.4, 154.9, 154.8, 133.4, 113.1, 59.5, 50.8 ppm HRMS calculated for C<sub>7</sub>H<sub>6</sub>Cl<sub>2</sub>N<sub>4</sub>O 232.9997, found 233.0008. FTIR (cm<sup>-1</sup>) 3401, 1538, 1540, 1310, 1135, 815.

1-(2-((*tert*-Butyldimethylsilyl)oxy)ethyl)-4,6-dichloro-1*H*-pyrazolo[3,4-*d*]pyrimidine (259)

In a 100 mL RBF 2-(4,6-dichloro-1*H*-pyrazolo[3,4-*d*]pyrimidin-1-yl)ethan-1-ol (950 mg, 4.08 mmol) was dissolved in *N,N*-Dimethylformamide (20 mL) and the reaction was cooled to 0 °C *tert*-butyldimethylsilyl chloride (922 mg, 6.11 mmol) and imidazole (305 mg, 4.48 mmol) were added and the reaction was stirred at 0 °C for 1 h. Note: leaving this reaction overnight or warming to room temperature resulting in nucleophilic displacement of the 4-chloride with imidazole. After 1 h the reaction was quenched with 5% aqueous lithium chloride (20 mL) and extracted with ethyl acetate (20 mL). The organic layer was washed with 5% aqueous lithium chloride (3 x 20 mL). The combined organic layer was dried (hydrophobic frit) and concentrated *in vacuo* to give 1-(2-((*tert*-butyldimethylsilyl)oxy)ethyl)-4,6-dichloro-1*H*-pyrazolo[3,4-*d*]pyrimidine (1.47 g, 4.02 mmol, 99% yield) as an amorphous white solid.

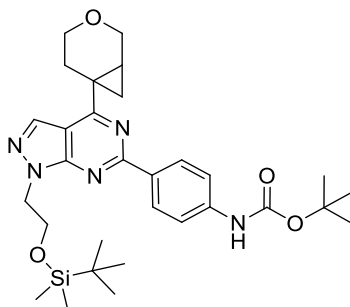
LCMS (formic) rt. 1.54 (95%)  $MH^+$  for desired  $M=346.078$ .  $^1H$  NMR ( $CDCl_3$ , 400 MHz)  $\delta$  = 8.17 (s, 1H), 4.59 (t,  $J$  = 5.5 Hz, 2H), 4.07 (t,  $J$  = 5.5 Hz, 2H), 0.75 (s, 8H), -0.09 ppm (s, 6H).  $^{13}C$  NMR (101 MHz,  $CDCl_3$ )  $\delta$  = 156.5, 155.3, 155.0, 132.6, 112.6, 61.1, 50.2, 25.5, 17.9, -5.7. HRMS calculated for  $C_{13}H_{21}Cl_2N_4OSi$  347.0864, found 347.0857. FTIR ( $cm^{-1}$ ) 2938, 1587, 1379, 1230, 1097, 773.

4-(3-Oxabicyclo[4.1.0]heptan-6-yl)-1-(2-((*tert*-butyldimethylsilyl)oxy)ethyl)-6-chloro-1*H*-pyrazolo[3,4-*d*]pyrimidine (261)



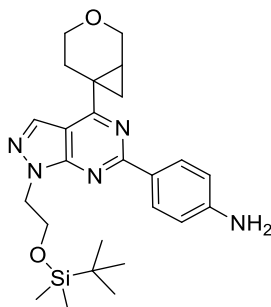
In a 100 mL RBF a mixture of potassium 3-oxabicyclo[4.1.0]heptan-6-yltrifluoroborate (984 mg, 4.83 mmol), 1-(2-((*tert*-butyldimethylsilyl)oxy)ethyl)-4,6-dichloro-1*H*-pyrazolo[3,4-*d*]pyrimidine (1.47 g, 4.02 mmol), caesium carbonate (2.62 g, 8.04 mmol), palladium(II) acetate (388 mg, 1.72 mmol) and cataCXium® A (461 mg, 1.29 mmol) was dissolved in toluene (18 mL) and water (1.8 mL). The resulting suspension was degassed with a stream of nitrogen for 10 min, fitted with a reflux condenser and stirred at 110 °C for 1 h then at 60 °C for 16 h. The reaction was monitored by LCMS and, upon complete consumption of starting material, the reaction was cooled to r.t. and filtered through a celite cartridge (10 g) and concentrated *in vacuo* to give 4-(3-oxabicyclo[4.1.0]heptan-6-yl)-1-(2-((*tert*-butyldimethylsilyl)oxy)ethyl)-6-chloro-1*H*-pyrazolo[3,4-*d*]pyrimidine (462 mg, 1.13 mmol, 28% yield) as a pale yellow oil. LCMS (formic) rt. 1.53 (86%)  $MH^+$  for desired  $M= 408.175$ . Due to a potential instability of this compound on silica, the reaction mixture was telescoped to the next step as a crude reaction mixture.

*tert*-Butyl (4-(4-(3-oxabicyclo[4.1.0]heptan-6-yl)-1-(2-((*tert*-butyldimethylsilyl)oxy)ethyl)-1*H*-pyrazolo[3,4-*d*]pyrimidin-6-yl)phenyl)carbamate (262)



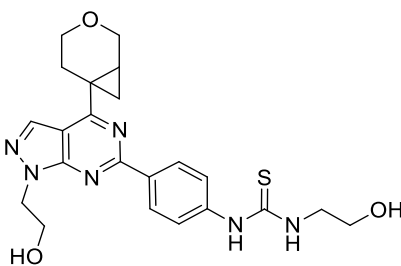
In a 10-20 mL microwave vial a mixture of 4-(3-oxabicyclo[4.1.0]heptan-6-yl)-1-(2-((*tert*-butyldimethylsilyl)oxy)ethyl)-6-chloro-1*H*-pyrazolo[3,4-*d*]pyrimidine (462 mg, 0.97 mmol), *tert*-butyl (4-(4,4,5,5-tetramethyl-1,3,2-dioxaborolan-2-yl)phenyl)carbamate (465 mg, 1.46 mmol), sodium carbonate (206 mg, 1.94 mmol) and Pd(dppf)Cl<sub>2</sub>.CH<sub>2</sub>Cl<sub>2</sub> (87 mg, 0.10 mmol) was dissolved in DME (15.4 mL) and water (1.9 mL). The resulting suspension was degassed with a stream of nitrogen for 10 min, sealed and stirred at 90 °C for 1.5 h. The reaction was monitored by LCMS and, upon complete consumption of starting material, the reaction was cooled to r.t. and filtered through a celite cartridge (10 g) and concentrated *in vacuo*. The reaction mixture was purified by flash column chromatography (cyclohexane: ethyl acetate 0-100% (15 column volumes)) to give *tert*-butyl (4-(4-(3-oxabicyclo[4.1.0]heptan-6-yl)-1-(2-((*tert*-butyldimethylsilyl)oxy)ethyl)-1*H*-pyrazolo[3,4-*d*]pyrimidin-6-yl)phenyl)carbamate (394 mg, 0.67 mmol, 69% yield) as an amorphous white solid. LCMS (formic) rt. 1.71 (95%) MH<sup>+</sup> for desired M=565.308. <sup>1</sup>H NMR (CDCl<sub>3</sub>, 400 MHz) δ = 8.53 (d, *J* = 8.8 Hz, 2H), 8.08 (s, 1H), 7.49 (d, *J* = 8.8 Hz, 2H), 6.60-6.69 (m, 1H), 6.65 (s, 1H), 4.65 (t, *J* = 6.1 Hz, 2H), 4.03-4.16 (m, 4H), 3.82 (ddd, *J* = 11.7, 6.1, 3.7 Hz, 1H), 3.52 (ddd, *J* = 11.5, 10.0, 5.4 Hz, 1H), 3.02 (dt, *J* = 13.9, 4.4 Hz, 1H), 2.38 (ddd, *J* = 14.2, 10.0, 6.1 Hz, 1H), 2.21-2.29 (m, 1H), 1.68 (dd, *J* = 9.3, 4.2 Hz, 1H), 1.56 (s, 9H), 1.37 (dd, *J* = 6.8, 4.2 Hz, 1H), 0.77 (s, 9H), -0.07 (s, 6H). <sup>13</sup>C NMR (DMSO-*d*<sub>6</sub>, 101 MHz) δ = 169.6, 159.5, 155.1, 153.1, 142.5, 133.2, 131.6, 129.3, 118.1, 109.5, 79.8, 65.2, 63.7, 61.5, 49.3, 28.6, 26.3, 25.9, 24.6, 23.7, 22.7, 18.1, -5.2. HRMS calculated for C<sub>30</sub>H<sub>43</sub>N<sub>5</sub>O<sub>4</sub>Si 566.3163, found 566.3165. FTIR (cm<sup>-1</sup>) 1729, 1529, 1388, 1153, 804.

4-(4-(3-Oxabicyclo[4.1.0]heptan-6-yl)-1-(2-((*tert*-butyldimethylsilyl)oxy)ethyl)-1*H*-pyrazolo[3,4-*d*]pyrimidin-6-yl)aniline (263)



In a 2-5 mL microwave vial *tert*-butyl 4-(4-(3-oxabicyclo[4.1.0]heptan-6-yl)-1-(2-((*tert*-butyldimethylsilyl)oxy)ethyl)-1*H*-pyrazolo[3,4-*d*]pyrimidin-6-yl)phenyl)carbamate (100 mg, 0.17 mmol) was dissolved in hexafluoroisopropanol (5 mL). The reaction mixture was irradiated to 120 °C in a Biotage initiator+ microwave for 1 h. The reaction mixture was concentrated *in vacuo* to give 4-(4-(3-oxabicyclo[4.1.0]heptan-6-yl)-1-(2-((*tert*-butyldimethylsilyl)oxy)ethyl)-1*H*-pyrazolo[3,4-*d*]pyrimidin-6-yl)aniline (76 mg, 0.16 mmol, 92% yield) as a yellow oil. LCMS (formic) rt. 1.46 (96%) MH<sup>+</sup> for desired M= 465.256. <sup>1</sup>H NMR (CDCl<sub>3</sub>, 400 MHz) δ = 8.42 (d, *J* = 8.8 Hz, 2H), 8.05 (s, 1H), 6.76 (d, *J* = 8.8 Hz, 2H), 4.62 (t, *J* = 6.2 Hz, 2H), 4.08-4.10 (m, 1H), 0.00 (dd, *J* = 11.2, 3.7 Hz, 1H), 3.93 (s, 2H), 3.81 (ddd, *J* = 11.6, 6.1, 3.7 Hz, 1H), 3.49-3.54 (m, 1H), 2.96-3.08 (m, 1H), 2.37 (ddd, *J* = 14.1, 9.9, 5.9 Hz, 1H), 2.24 (ddd, *J* = 3.7, 2.4, 1.5 Hz, 1H), 1.66 (dd, *J* = 9.2, 4.0 Hz, 1H), 1.34 (dd, *J* = 6.6, 4.2 Hz, 1H), 1.22 (t, *J* = 7.0 Hz, 2H), 0.75-0.81 (m, 10H), -0.05-0.04 (m, 1H), -0.06 ppm (s, 6H)

1-(4-(4-(3-Oxabicyclo[4.1.0]heptan-6-yl)-1-(2-hydroxyethyl)-1*H*-pyrazolo[3,4-*d*]pyrimidin-6-yl)phenyl)-3-(2-hydroxyethyl)thiourea (234)

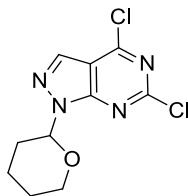


In a 2-5 mL microwave vial 4-(4-(3-oxabicyclo[4.1.0]heptan-6-yl)-1-(2-((*tert*-butyldimethylsilyl)oxy)ethyl)-1*H*-pyrazolo[3,4-*d*]pyrimidin-6-yl)aniline (85% wt.) (64 mg, 0.12 mmol) was dissolved in DCM (2 mL). 1,1'-Thiocarbonyldiimidazole (31 mg, 0.18 mmol) and pyridine (19 μL, 0.23 mmol) were added and the reaction was stirred at r.t. for 2 h. LCMS



analysis showed complete conversion to desired intermediate. Ethanolamine (35  $\mu\text{L}$ , 0.58 mmol) was added and the reaction was stirred at r.t. for 0.5 h. The reaction mixture was concentrated *in vacuo* and the resulting residue was dissolved in tetrahydrofuran (2 mL). the reaction was cooled to 0  $^{\circ}\text{C}$  and tetrabutylammonium fluoride (1M in THF) (0.12 mL, 0.12 mmol) was added. The reaction was stirred at 0  $^{\circ}\text{C}$  for 1 h. The reaction was quenched with water (5 mL) and extracted with DCM (3x 5 mL). The combined organic layers were dried (hydrophobic frit) and concentrated *in vacuo*. The reaction mixture was purified by preparative HPLC (formic, 15-55%, 30 min) to give 1-(4-(4-(3-oxabicyclo[4.1.0]heptan-6-yl)-1-(2-hydroxyethyl)-1*H*-pyrazolo[3,4-*d*]pyrimidin-6-yl)phenyl)-3-(2-hydroxyethyl)thiourea (36 mg, 0.08 mmol, 68% yield). LCMS (formic) rt. 0.79 (100%)  $\text{MH}^+$  for desired  $\text{M} = 454.179$ .  $^1\text{H}$  NMR (DMSO- $d_6$ , 400 MHz)  $\delta = 9.87$  (br., s, 1H), 8.40-8.49 (m, 2H), 8.37 (s, 1H), 7.91 (br., s, 1H), 7.65-7.74 (m,  $J = 8.8$  Hz, 2H), 4.85 (t,  $J = 5.6$  Hz, 2H), 4.53 (t,  $J = 5.9$  Hz, 2H), 3.86-4.03 (m, 5H), 3.69 (dt,  $J = 10.8, 5.5$  Hz, 1H), 3.59-3.61 (m, 1H), 3.35-3.56 (m, 2H), 2.97 (dt,  $J = 14.0, 4.7$  Hz, 1H), 2.20-2.35 (m, 2H), 1.66 (dd,  $J = 9.3, 3.9$  Hz, 1H), 1.34 (dd,  $J = 6.6, 4.2$  Hz, 1H).  $^{13}\text{C}$  NMR (DMSO- $d_6$ , 101 MHz)  $\delta = 180.7, 169.8, 159.6, 159.3, 154.7, 133.1, 129.1, 126.0, 122.1, 109.6, 65.2, 63.7, 59.7, 49.6, 47.0, 26.3, 24.7, 23.9, 23.1$  (1C not observed). HRMS calculated for  $\text{C}_{22}\text{H}_{26}\text{N}_6\text{O}_3\text{S}$  455.1865, found 455.1864. FTIR ( $\text{cm}^{-1}$ ) 3280, 2931, 1536, 1386, 1298, 1039, 805.

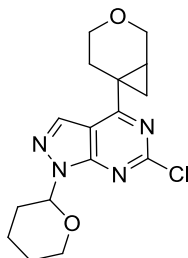
4,6-Dichloro-1-(tetrahydro-2*H*-pyran-2-yl)-1*H*-pyrazolo[3,4-*d*]pyrimidine (268)<sup>265</sup>



In a 150 mL RBF 4,6-dichloro-1*H*-pyrazolo[3,4-*d*]pyrimidine (2.0 g, 10.58 mmol) and tosic acid (201 mg, 1.06 mmol) was dissolved in THF (32 mL) and DCM (32 mL). 3,4-dihydro-2*H*-pyran (1.50 mL, 15.87 mmol) was added and the reaction was stirred for r.t. for 16 h. The reaction mixture was concentrated between sat. aq. sodium bicarbonate (100 mL) and ethyl acetate (100 mL). The organic layer was dried (hydrophobic frit) and concentrated *in vacuo*. The resulting oil was triturated in cyclohexane and the resulting white solid was washed with cyclohexane to give 4,6-dichloro-1-(tetrahydro-2*H*-pyran-2-yl)-1*H*-pyrazolo[3,4-*d*]pyrimidine (1.17 g, 3.86 mmol, 36% yield) as a pale yellow solid. LCMS (formic) rt. 1.11 (76%)  $\text{MH}^+$  for desired  $\text{M} = 272.023$ .  $^1\text{H}$  NMR (DMSO- $d_6$ , 400 MHz)  $\delta = 8.60$  (s, 1H), 5.95 (dd,  $J = 10.0, 2.7$  Hz, 1H), 3.90-4.02 (m, 1H), 3.60-3.80 (m, 1H), 2.29-2.48 (m, 1H), 2.04 (dtd,

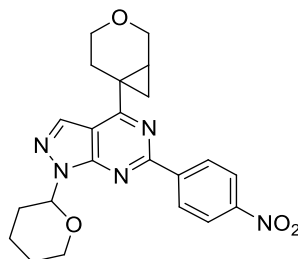
$J = 13.2, 3.9, 1.8$  Hz, 1H), 1.94 (dq,  $J = 13.0, 3.3$  Hz, 2H), 1.79 (dt,  $J = 12.8, 3.6$  Hz, 1H), 1.50-1.68 ppm (m, 3H).

4-(3-Oxabicyclo[4.1.0]heptan-6-yl)-6-chloro-1-(tetrahydro-2H-pyran-2-yl)-1H-pyrazolo[3,4-d]pyrimidine (269)

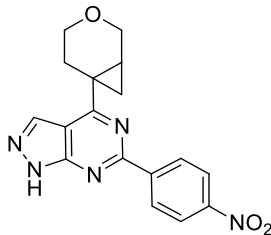


In a 100 mL RBF a mixture of potassium 3-oxabicyclo[4.1.0]heptan-6-yltrifluoroborate (1.00 mg, 4.93 mmol), 4,6-dichloro-1-(tetrahydro-2H-pyran-2-yl)-1H-pyrazolo[3,4-d]pyrimidine (1.15 g, 3.78 mmol), caesium carbonate (3.70 g, 11.4 mmol), palladium (II) acetate (136 mg, 0.61 mmol) and cataCXium® A (435 mg, 1.21 mmol) was dissolved in toluene (18 mL) and water (1.8 mL). The resulting suspension was degassed with a stream of nitrogen for 10 min, fitted with a reflux condenser and stirred at 110 °C for 1 h then at 60 °C for 16 h. The reaction was monitored by LCMS and, upon complete consumption of starting material, the reaction was cooled to r.t. and filtered through a celite cartridge (10 g) and concentrated *in vacuo*. The reaction mixture was purified by preparative HPLC (water: acetonitrile 30% to 85% over 30 mins, 0.1% formic acid modifier) to give 4-(3-oxabicyclo[4.1.0]heptan-6-yl)-6-chloro-1-(tetrahydro-2H-pyran-2-yl)-1H-pyrazolo[3,4-d]pyrimidine (143 mg, 0.43 mmol, 11% yield) as an amorphous white solid. LCMS (formic) rt. 1.15 (100%) MH<sup>+</sup> for desired M=335.120. <sup>1</sup>H NMR (400 MHz, DMSO-d<sub>6</sub>)  $\delta = 8.52$  (s, 1H), 5.91 (dd,  $J = 2.4, 10.3$  Hz, 1H), 3.98 - 3.92 (m, 2H), 3.90 (dd,  $J = 1.5, 11.7$  Hz, 1H), 3.76 - 3.68 (m, 1H), 3.50 (ddd,  $J = 4.2, 5.9, 11.5$  Hz, 1H), 3.44 - 3.36 (m, 1H), 2.76 (td,  $J = 4.7, 14.1$  Hz, 1H), 2.48 - 2.34 (m, 1H), 2.27 - 2.19 (m, 1H), 2.17 - 2.09 (m, 1H), 2.07 - 1.95 (m, 1H), 1.93 - 1.85 (m, 1H), 1.85 - 1.75 (m, 2H), 1.64 - 1.52 (m, 3H), 1.37 (dd,  $J = 4.3, 7.0$  Hz, 1H). <sup>13</sup>C NMR (DMSO-d<sub>6</sub>, 101 MHz):  $\delta = 173.3, 156.9, 154.7, 154.7, 134.6, 111.2, 111.1, 82.3, 67.6, 64.9, 63.6, 36.3, 34.4, 34.4, 29.1, 26.9, 26.8, 26.1, 25.1, 24.9, 24.8, 24.1, 24.0, 22.5$  ppm Note: Product is a mixture of diastereomers, this is the reason for the extra peaks in the <sup>13</sup>C NMR. HRMS calculated for C<sub>16</sub>H<sub>19</sub>ClN<sub>4</sub>O<sub>2</sub> 335.1275 found 335.1270. FTIR (cm<sup>-1</sup>) 1557, 1223, 1153, 803.

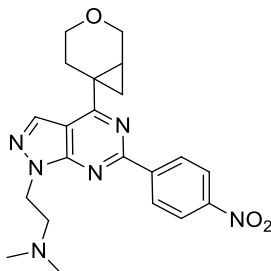
4-(3-Oxabicyclo[4.1.0]heptan-6-yl)-6-(4-nitrophenyl)-1-(tetrahydro-2H-pyran-2-yl)-1H-pyrazolo[3,4-d]pyrimidine (270)



In a 2-5 mL microwave vial a mixture 4-(3-oxabicyclo[4.1.0]heptan-6-yl)-6-chloro-1-(tetrahydro-2H-pyran-2-yl)-1H-pyrazolo[3,4-d]pyrimidine (140 mg, 0.42 mmol), 4,5,5-tetramethyl-2-(4-nitrophenyl)-1,3,2-dioxaborolane (156 mg, 0.63 mmol), potassium carbonate (116 mg, 0.84 mmol) and Pd(dppf)Cl<sub>2</sub>.CH<sub>2</sub>Cl<sub>2</sub> (34 mg, 0.042 mmol) was dissolved in DME (3.7 mL) and water (0.46 mL). The resulting suspension was degassed with a stream of nitrogen for 10 min, sealed and stirred at 90 °C for 1.5 h. The reaction was monitored by LCMS and, upon complete consumption of starting material, the reaction was cooled to r.t. and filtered through a celite cartridge (10 g) and concentrated *in vacuo*. The reaction mixture was purified by flash column chromatography (cyclohexane: ethyl acetate 0-50% (15 column volumes)) to give 4-(3-oxabicyclo[4.1.0]heptan-6-yl)-6-(4-nitrophenyl)-1-(tetrahydro-2H-pyran-2-yl)-1H-pyrazolo[3,4-d]pyrimidine (118 mg, 0.28 mmol, 67% yield) as an amorphous pale yellow solid. LCMS (formic) rt. 1.41 (92%) MH<sup>+</sup> for desired M= 491.253. <sup>1</sup>H NMR (DMSO-d<sub>6</sub>, 400 MHz) δ = 8.75 (d, *J* = 9.0 Hz, 2H), 8.53 (s, 1H), 8.40 (d, *J* = 9.0 Hz, 2H), 6.16 (dd, *J* = 10.0, 2.4 Hz, 1H), 3.94-4.03 (m, 3H), 3.74-3.82 (m, 1H), 3.66-3.73 (m, 1H), 3.43-3.60 (m, 1H), 2.96 (dt, *J* = 13.9, 4.8 Hz, 1H), 2.52-2.57 (m, 2H), 2.26-2.38 (m, 2H), 2.03-2.14 (m, 1H), 1.90-2.00 (m, 1H), 1.77-1.89 (m, 1H), 1.68-1.76 (m, 1H), 1.55-1.66 (m, 2H), 1.40 (dd, *J* = 6.8, 4.2 Hz, 1H). <sup>13</sup>C NMR (DMSO-d<sub>6</sub>, 101 MHz) δ = 170.8, 157.9, 154.3, 149.4, 143.6, 134.3, 129.9, 124.3, 112.0, 110.8, 82.3, 67.7, 65.1, 63.7, 29.3, 26.2, 25.2, 24.9, 24.4 ppm Note: Product is a mixture of diastereomers, this is the reason for the extra peaks in the <sup>13</sup>C NMR HRMS calculated for C<sub>22</sub>H<sub>23</sub>N<sub>5</sub>O<sub>4</sub> 422.1828 found 422.1828 FTIR (cm<sup>-1</sup>) 1552, 1341, 1038, 807.

4-(3-Oxabicyclo[4.1.0]heptan-6-yl)-6-(4-nitrophenyl)-1H-pyrazolo[3,4-d]pyrimidine (271)

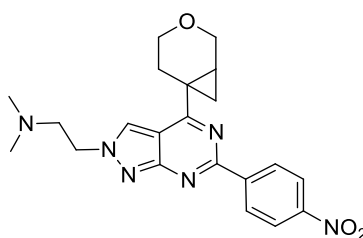
In a 2-5 mL microwave vial 4-(3-oxabicyclo[4.1.0]heptan-6-yl)-6-(4-nitrophenyl)-1-(tetrahydro-2H-pyran-2-yl)-1H-pyrazolo[3,4-d]pyrimidine (110 mg, 0.26 mmol) was dissolved in HCl (2 M in 1,4 dioxane) (2 mL, 4.0 mmol) and the reaction was stirred at r.t. for 16 h. The reaction mixture was concentrated *in vacuo* to give 4-(3-oxabicyclo[4.1.0]heptan-6-yl)-6-(4-nitrophenyl)-1H-pyrazolo[3,4-d]pyrimidine (98 mg, 0.24 mmol, 93% yield) as an amorphous pale yellow solid. LCMS rt. 1.11 (82%) MH<sup>+</sup> for desired M=337.117. <sup>1</sup>H NMR (DMSO-d<sub>6</sub>, 400 MHz)  $\delta$  = 8.69 (d, *J* = 9.0 Hz, 2H), 8.45 (s, 1H), 8.38 (d, *J* = 9.0 Hz, 2H), 4.01 (dd, *J* = 11.2, 3.9 Hz, 1H), 3.96 (dd, *J* = 11.5, 1.5 Hz, 1H), 3.70 (ddd, *J* = 11.4, 5.7, 4.4 Hz, 1H), 3.57 (s, 1H), 3.43-3.50 (m, 1H), 2.98 (dt, *J* = 14.1, 4.7 Hz, 1H), 2.25-2.36 (m, 2H), 1.69 (dd, *J* = 9.3, 4.2 Hz, 2H), 1.38 ppm (dd, *J* = 6.6, 4.2 Hz, 1H). <sup>13</sup>C NMR (DMSO-d<sub>6</sub>, 101 MHz)  $\delta$  = 170.3, 157.7, 149.2, 144.0, 129.7, 124.3, 109.8, 65.1, 63.7, 26.2, 24.8, 24.2, 23.4 ppm (1C not observed). HRMS calculated for C<sub>17</sub>H<sub>15</sub>N<sub>5</sub>O<sub>3</sub> 338.1253, found 338.1245 FTIR (cm<sup>-1</sup>) 1557, 1343, 1298, 1040, 808.

2-(4-(3-Oxabicyclo[4.1.0]heptan-6-yl)-6-(4-nitrophenyl)-1H-pyrazolo[3,4-d]pyrimidin-1-yl)-N,N-dimethylethan-1-amine (272)

In a 2-5 mL microwave vial 4-(3-oxabicyclo[4.1.0]heptan-6-yl)-6-(4-nitrophenyl)-1H-pyrazolo[3,4-d]pyrimidine (65 mg, 0.19 mmol) was dissolved in *N,N*-dimethylformamide (2 mL). Sodium hydride (60%) (16 mg, 0.41 mmol) was added and the reaction was stirred at r.t. for 1 h. 2-bromo-*N,N*-dimethylethan-1-amine hydrobromide (49 mg, 0.21 mmol) was dissolved in *N,N*-dimethylformamide (2 mL) and this solution was added dropwise to the reaction mixture. The reaction was stirred at r.t. for 4 h. The reaction mixture was partitioned between diethyl ether (10 mL) and sat. aq. sodium bicarbonate (10 mL). The aqueous layer was extracted with diethyl ether (2x 5 mL) and the combined organic layers were dried

(hydrophobic frit) and concentrated *in vacuo*. The reaction mixture was purified by preparative HPLC (formic, 15-55% 30 min) to give 2-(4-(3-oxabicyclo[4.1.0]heptan-6-yl)-6-(4-nitrophenyl)-1*H*-pyrazolo[3,4-*d*]pyrimidin-1-yl)-*N,N*-dimethylethan-1-amine (38 mg, 0.09 mmol, 48% yield) as a waxy white solid. LCMS (formic) rt. 0.75 (100%) MH<sup>+</sup> for desired M=408.462. <sup>1</sup>H NMR (DMSO-*d*<sub>6</sub>, 600 MHz) δ = 8.70 (d, *J* = 8.8 Hz, 2H), 8.44 (s, 1H), 8.36 (d, *J* = 8.8 Hz, 3H), 4.61 (t, *J* = 6.4 Hz, 2H), 4.00 (dd, *J* = 11.7, 4.0 Hz, 1H), 3.95 (d, *J* = 11.0 Hz, 1H), 3.67-3.71 (m, 1H), 3.47 (ddd, *J* = 11.7, 9.2, 5.1 Hz, 1H), 2.96 (dt, *J* = 13.9, 4.8 Hz, 1H), 2.82 (t, *J* = 6.4 Hz, 2H), 2.26-2.33 (m, 2H), 2.20 (s, 6H), 1.69 (dd, *J* = 9.5, 4.0 Hz, 1H), 1.38 ppm (dd, *J* = 6.6, 4.0 Hz, 1H). <sup>13</sup>C NMR (DMSO-*d*<sub>6</sub>, 151 MHz) δ = 170.5, 157.4, 154.1, 149.2, 143.8, 133.4, 129.7, 124.3, 110.3, 65.1, 63.7, 58.1, 45.4, 44.9, 26.2, 24.8, 24.4, 23.7 ppm HRMS calculated for C<sub>21</sub>H<sub>24</sub>N<sub>6</sub>O<sub>3</sub> 409.1988, found 409.1985, FTIR (cm<sup>-1</sup>) 1559, 1513, 1345, 1129, 852. Confirmed as the desired regioisomer by <sup>15</sup>N HMBC NMR.

2-(4-(3-Oxabicyclo[4.1.0]heptan-6-yl)-6-(4-nitrophenyl)-2*H*-pyrazolo[3,4-*d*]pyrimidin-2-yl)-*N,N*-dimethylethan-1-amine (273)

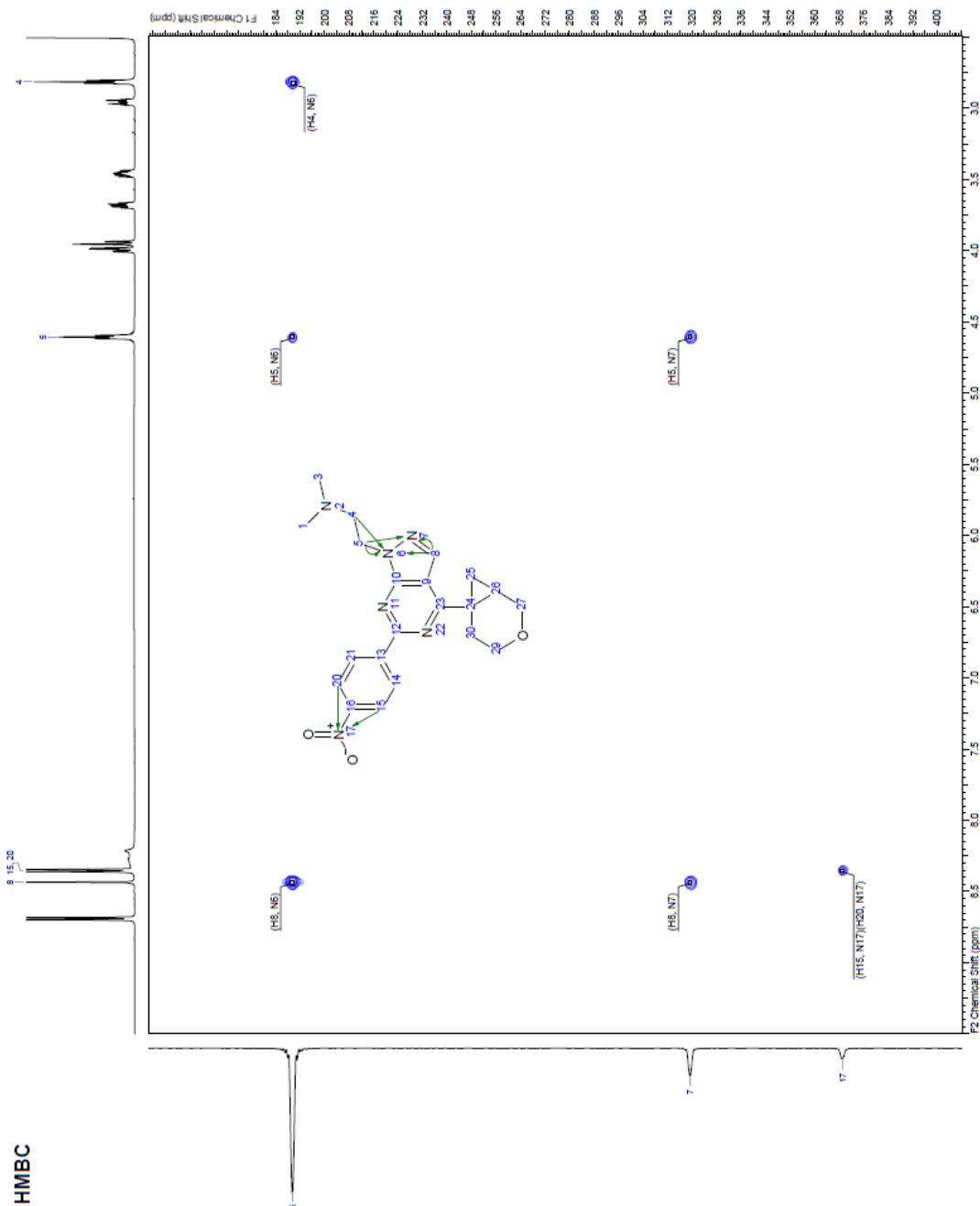


The minor isomer: 2-(4-(3-oxabicyclo[4.1.0]heptan-6-yl)-6-(4-nitrophenyl)-2*H*-pyrazolo[3,4-*d*]pyrimidin-2-yl)-*N,N*-dimethylethan-1-amine formic acid salt (12 mg, 0.029 mmol, 15% yield) LCMS (formic) rt. 0.71 (100%) MH<sup>+</sup> for desired M=408.462. <sup>1</sup>H NMR (DMSO-*d*<sub>6</sub>, 400 MHz) δ = 8.93 (s, 1H), 8.71 (d, *J* = 9.0 Hz, 2H), 8.37 (d, *J* = 8.8 Hz, 2H), 8.20 (s, 1H), 4.58 (t, *J* = 6.4 Hz, 2H), 3.93-4.00 (m, 2H), 3.68-3.76 (m, 1H), 3.46 (ddd, *J* = 11.2, 9.6, 5.1 Hz, 1H), 2.96 (dt, *J* = 13.9, 4.5 Hz, 1H), 2.87 (t, *J* = 6.4 Hz, 2H), 2.17-2.31 (m, 8H), 1.69 (dd, *J* = 9.2, 4.0 Hz, 1H), 1.36 (dd, *J* = 6.6, 4.2 Hz, 1H). HRMS calculated for C<sub>21</sub>H<sub>24</sub>N<sub>6</sub>O<sub>3</sub> 409.1988, found 409.1985 FTIR (cm<sup>-1</sup>) 1571, 1527, 1400, 1165, 852.

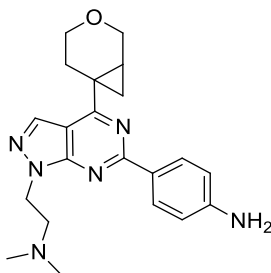
<sup>15</sup>N HMBC NMR for 2-(4-(3-oxabicyclo[4.1.0]heptan-6-yl)-6-(4-nitrophenyl)-1H-pyrazolo[3,4-d]pyrimidin-1-yl)-N,N-dimethylethan-1-amine (272)

Spectrum: PT18595 Sample:  
 N68376-71-1 Solvent: DMSO  
 DMSO Experiment:  
 15N-HMBC SubmitterID:  
 dms74676 AnalystID:  
 sar0155 Submitter:  
 Summers, Declan M Analyst:  
 Richards, Stephen A

Acquisition Time (sec) 01:31.1 (0.0029)  
 Comment N68376-71-1 Solvent: DMSO  
 N68376-71-1 Solvent: DMSO  
 Submitted: dms74676  
 Analyst: sar0155 Submitter:  
 Richards, Stephen A  
 Date: 2018-12-21 08:  
 27  
 MW 394.43626  
 MW Name N68376-71-1  
 Frequency (MHz) 125.761  
 Nucleus 15N  
 P1 (µs) 12.00  
 Pulse Program zgpg30  
 CPD (µs) 1024.94  
 Carrier Channel 15N  
 Pulse Count 2048  
 Acquisition Date 2018-12-21  
 Solvent DMSO-d6  
 HMBC  
 Sweep Width (Hz) 24078.33  
 F2 (ppm) 400.138  
 F1 (ppm) 24078.33  
 Spectrum: PT18595 Sample:  
 N68376-71-1 Solvent: DMSO  
 DMSO Experiment:  
 15N-HMBC SubmitterID:  
 dms74676 AnalystID:  
 sar0155 Submitter:  
 Summers, Declan M Analyst:  
 Richards, Stephen A

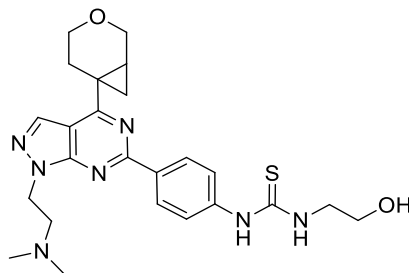


4-(4-(3-Oxabicyclo[4.1.0]heptan-6-yl)-1-(2-(dimethylamino)ethyl)-1H-pyrazolo[3,4-d]pyrimidin-6-yl)aniline (273)



In a 2-5 mL microwave vial 2-(4-(3-oxabicyclo[4.1.0]heptan-6-yl)-6-(4-nitrophenyl)-1H-pyrazolo[3,4-d]pyrimidin-1-yl)-N,N-dimethylethan-1-amine (38 mg, 0.093 mmol) was dissolved in a mixture of acetic acid (0.75 mL), ethanol (0.75 mL) and water (0.35 mL). iron powder (26 mg, 0.46 mmol) was added and the reaction was sonicated for 2 h. The reaction mixture was filtered through celite (2.5 g) and concentrated *in vacuo*. The resulting residue was partitioned between DCM (10 mL) and sodium hydroxide (1M) (10 mL). The aqueous layer was extracted with DCM (2x 10 mL) and the combined organic layers were dried (hydrophobic frit) and concentrated *in vacuo* to give 4-(4-(3-oxabicyclo[4.1.0]heptan-6-yl)-1-(2-(dimethylamino)ethyl)-1H-pyrazolo[3,4-d]pyrimidin-6-yl)aniline as an amorphous orange solid. LCMS (formic) rt. 0.53 (88%) MH<sup>+</sup> for desired M=378.217. The reaction was telescoped to the next step as a crude mixture without further purification.

1-(4-(4-(3-oxabicyclo[4.1.0]heptan-6-yl)-1-(2-(dimethylamino)ethyl)-1H-pyrazolo[3,4-d]pyrimidin-6-yl)phenyl)-3-(2-hydroxyethyl)thiourea (235)



In a 2-5 mL microwave vial 4-(4-(3-oxabicyclo[4.1.0]heptan-6-yl)-1-(2-(dimethylamino)ethyl)-1H-pyrazolo[3,4-d]pyrimidin-6-yl)aniline (31 mg, 0.082 mmol) was dissolved in DCM (0.5 mL). 1,1'-Thiocarbonyldiimidazole (22 mg, 0.12 mmol) and pyridine (13 µL, 0.16 mmol) were added and the reaction was stirred at r.t. for 1 h. LCMS analysis showed complete conversion to desired intermediate. Ethanolamine (25 µL, 0.41 mmol) was added and the reaction was stirred at r.t. for 0.5 h. The reaction mixture was concentrated *in vacuo*. The reaction mixture was purified by mass directed auto purification Mass Directed Auto Purification (MDAP) (High pH, Method C) to give 1-(4-(4-(3-oxabicyclo[4.1.0]heptan-

6-yl)-1-(2-(dimethylamino)ethyl)-1*H*-pyrazolo[3,4-*d*]pyrimidin-6-yl)phenyl)-3-(2-hydroxyethyl)thiourea (14 mg, 0.029 mmol, 35% yield) as a white solid. LCMS (formic) rt. 0.95 (100%) MH<sup>+</sup> for desired M= 481.22 <sup>1</sup>H NMR (DMSO-*d*<sub>6</sub>, 400 MHz) δ = 9.89 (br s, 1H), 8.44 (d, *J* = 8.0 Hz, 2H), 8.36 (s, 1H), 7.94 (br s, 1H), 7.69 (d, *J* = 8.8 Hz, 2H), 4.83 (br s, 1H), 4.57 (t, *J* = 6.4 Hz, 2H), 4.00 (dd, *J* = 11.2, 3.9 Hz, 1H), 3.94 (dd, *J* = 11.0, 1.2 Hz, 1H), 3.68(ddd, *J* = 11.5, 5.4, 4.2 Hz, 1H), 3.46 (ddd, *J* = 11.6, 9.2, 5.1 Hz, 1H), 3.30 (s, 3H), 2.98 (dt, *J* = 13.9, 4.8 Hz, 1H), 2.79 (t, *J* = 6.2 Hz, 2H), 2.47 (br s, 1H), 2.22-2.36 (m, 2H), 2.18 (s, 7H), 1.67 (dd, *J* = 9.3, 3.9 Hz, 1H), 1.34 ppm (dd, *J* = 6.6, 4.2 Hz, 1H). <sup>13</sup>C NMR (DMSO-*d*<sub>6</sub>, 101 MHz) δ = 180.7, 169.9, 159.3, 154.4, 142.5, 133.2, 129.1, 109.5, 65.2, 63.7, 59.6, 58.3, 47.0, 45.5, 44.8, 26.2, 24.7, 24.0, 23.2 ppm HRMS calculated for C<sub>24</sub>H<sub>31</sub>N<sub>7</sub>O<sub>2</sub>S 482.2338, found 482.2335 FTIR (cm<sup>-1</sup>) 3154, 2937, 1557, 1302, 1184, 1017, 805.



## Appendix

### X-Ray Crystal Structure Data

Single-crystal data were recorded at 123(2) K on Oxford Diffraction Gemini and Xcalibur diffractometers with Mo- $K\alpha$  ( $\lambda = 0.71073$  Å) or Cu- $K\alpha$  ( $\lambda = 1.5418$  Å) radiation. The structures were refined to convergence on  $F^2$  and against all independent reflections by full-matrix least-squares using SHELXL programs. The structures of compounds **31**, **32**, **35** and **41** were modelled as disordered. In each case the disordered atoms were modelled over two sites and suitable restraints were applied to bond distances and to displacement parameters. Selected crystallographic and refinement parameters are given in **Table 55** and full data in CIF format are available from the Cambridge Crystallographic Data Centre, deposition numbers CCDC 1864311, CCDC 1864312, CCDC 1864313, CCDC 1864314, CCDC 1864315, CCDC 1864316, CCDC 1864317, CCDC 1864318, CCDC 1864319.

Structure	31	32	33
<b>Mol. Formula</b>	C <sub>15</sub> H <sub>16</sub> N <sub>2</sub> O <sub>2</sub>	C <sub>16</sub> H <sub>15</sub> NO <sub>2</sub>	C <sub>16</sub> H <sub>17</sub> NO <sub>2</sub>
<b>Temperature (K)</b>	123(2)	123(2)	123(2)
<b>Wavelength (Å)</b>	0.71073	1.54184	0.71073
<b>Crystal system</b>	Monoclinic	Monoclinic	Orthorhombic
<b>Space group</b>	<i>P</i> 2 <sub>1</sub> / <i>c</i>	<i>P</i> 2 <sub>1</sub> / <i>c</i>	<i>P</i> 2 <sub>1</sub> 2 <sub>1</sub> 2 <sub>1</sub>
<b><i>a</i> (Å)</b>	10.4866(8)	10.5011(10)	6.9822(4)
<b><i>b</i> (Å)</b>	7.3258(5)	7.2937(7)	9.2048(5)
<b><i>c</i> (Å)</b>	16.9403(13)	16.9261(17)	20.9748(10)
<b><math>\beta</math> (°)</b>	98.012(7)	97.472(9)	90
<b>Volume (Å<sup>3</sup>)</b>	1288.70(17)	1288.1(2)	1348.05(12)
<b>Z</b>	4	4	4
<b>2Theta max (°)</b>	59.86	146.0	57.97
<b>Reflections collected</b>	9869	9684	13126
<b>Independent reflections</b>	3368	2541	3418
	[R(int)=0.0322]	[R(int)=0.0274]	[R(int)=0.0484]
<b>Observed reflections</b>	2624	2146	2639
<b>No. of parameters</b>	192	186	176
<b>Goodness-of-fit</b>	1.030	1.067	1.037
<b>Final R [I&gt;2<math>\sigma</math>(I)]</b>	0.0466	0.0453	0.0483
<b>wR2 (all data)</b>	0.1201	0.1320	0.0955
<b>Largest difference peak (eÅ<sup>-3</sup>)</b>	0.274	0.249	0.164
<b>Deepest hole (eÅ<sup>-3</sup>)</b>	-0.256	-0.177	-0.191
<b>Flack parameter</b>			0.1(8)

Structure	34	38	39
<b>Mol. Formula</b>	C <sub>17</sub> H <sub>17</sub> NO <sub>2</sub>	C <sub>16</sub> H <sub>16</sub> N <sub>2</sub> O <sub>2</sub>	C <sub>16</sub> H <sub>16</sub> N <sub>2</sub> O <sub>2</sub>
<b>Temperature (K)</b>	123(2)	123(2)	123(2)
<b>Wavelength (Å)</b>	1.54184	1.54184	1.54184
<b>Crystal system</b>	Monoclinic	Orthorhombic	Orthorhombic
<b>Space group</b>	<i>P</i> 2 <sub>1</sub>	<i>P</i> 2 <sub>1</sub> 2 <sub>1</sub> 2 <sub>1</sub>	<i>P</i> 2 <sub>1</sub> 2 <sub>1</sub> 2 <sub>1</sub>
<b><i>a</i> (Å)</b>	10.1735(2)	15.6642(4)	9.3226(5)
<b><i>b</i> (Å)</b>	7.7700(2)	17.9458(5)	13.2407(7)
<b><i>c</i> (Å)</b>	17.2706(3)	19.1274(5)	20.8949(13)
<b><math>\beta</math> (°)</b>	92.8080(10)	90	90
<b>Volume (Å<sup>3</sup>)</b>	1363.57(5)	5376.8(2)	2579.2(3)
<b>Z</b>	4	16	8
<b>2Theta max (°)</b>	146.3	146.3	146.3
<b>Reflections collected</b>	11491	20680	9155
<b>Independent reflections</b>	5060	10509	5061
	[R(int)=0.0215]	[R(int)=0.0304]	[R(int)=0.0399]
<b>Observed reflections</b>	4827	9703	4064
<b>No. of parameters</b>	378	761	370
<b>Goodness-of-fit</b>	1.043	1.026	1.030
<b>Final R [I&gt;2<math>\sigma</math>(I)]</b>	0.0341	0.0420	0.0552
<b>wR2 (all data)</b>	0.0905	0.1131	0.1355
<b>Largest difference peak (eÅ<sup>-3</sup>)</b>	0.191	0.176	0.260
<b>Deepest hole (eÅ<sup>-3</sup>)</b>	-0.225	-0.193	-0.196
<b>Flack parameter</b>	0.0(2)	0.01(8)	0.1(5)
Structure	40	41	42
<b>Mol. Formula</b>	C <sub>17</sub> H <sub>17</sub> NO <sub>2</sub>	C <sub>17</sub> H <sub>17</sub> NO <sub>2</sub>	C <sub>21</sub> H <sub>24</sub> N <sub>2</sub> O <sub>2</sub>
<b>Temperature (K)</b>	123(2)	123(2)	123(2)
<b>Wavelength (Å)</b>	1.54184	1.54184	1.54184
<b>Crystal system</b>	Monoclinic	Monoclinic	Orthorhombic
<b>Space group</b>	<i>P</i> 2 <sub>1</sub>	<i>P</i> 2 <sub>1</sub>	<i>P</i> 2 <sub>1</sub> 2 <sub>1</sub> 2 <sub>1</sub>
<b><i>a</i> (Å)</b>	9.5011(2)	10.1442(5)	8.3093(3)
<b><i>b</i> (Å)</b>	12.8508(3)	12.3116(9)	11.7953(4)
<b><i>c</i> (Å)</b>	11.0499(2)	10.9694(6)	18.3070(5)
<b><math>\beta</math> (°)</b>	94.675(2)	91.540(5)	90
<b>Volume (Å<sup>3</sup>)</b>	1344.67(5)	1369.49(14)	1794.28(10)
<b>Z</b>	4	4	4
<b>2Theta max (°)</b>	146.4	146.4	146.1
<b>Reflections collected</b>	10435	12171	6473
<b>Independent reflections</b>	5277	4972	3513
	[R(int)=0.0299]	[R(int)=0.0493]	[R(int)=0.0257]
<b>Observed reflections</b>	4830	4073	3267
<b>No. of parameters</b>	369	378	236
<b>Goodness-of-fit</b>	1.050	1.044	1.030
<b>Final R [I&gt;2<math>\sigma</math>(I)]</b>	0.0424	0.0692	0.0390
<b>wR2 (all data)</b>	0.1133	0.2022	0.1006
<b>Largest difference peak (eÅ<sup>-3</sup>)</b>	0.251	0.441	0.134
<b>Deepest hole (eÅ<sup>-3</sup>)</b>	-0.221	-0.215	-0.211
<b>Flack parameter</b>	-0.11(15)	-0.1(6)	-0.1(3)

Table 55: X-ray crystal structure data for compounds 31-34 and 39-42.

## **PI3K $\delta$ Protein Co-Crystal Structure Data**

The protein was expressed and purified as described previously.<sup>266</sup> Crystals were grown by co-crystallisation of PI3K delta with an inhibitor previously seen to give reproducible high quality crystals using a modified version of the protocol described previously.<sup>266</sup> A 50 mM compound stock solution in DMSO was prepared from which 3.5  $\mu$ L was mixed with 28  $\mu$ L of 5% w/v n-dodecyl- $\beta$ -D-maltoside (DDM) prior to addition to 280  $\mu$ L of protein solution at 5 mg/ml (in 20 mM Tris/HCl pH 7.2, 50 mM ammonium sulphate, 5 mM dithiothreitol, 1% ethylene glycol, 1% betaine, 0.02% CHAPS). The mixture was incubated at room temperature for 60 min and then spun at 4 °C for 15 min. A crystal seeding solution was made by transferring an existing PI3K delta crystal into 5  $\mu$ L of Morpheus screen (Molecular Dimensions Ltd) condition G2 (0.1 M buffer system 1 pH 6.5, 0.1 M carboxylic acids, 30% ethylene glycol/PEG 8000). The crystal was crushed and added to 1mL of Morpheus screen condition G2 and vortexed vigorously. The seed stock was typically thawed and then diluted by a factor of 20 to 40 with Morpheus screen condition G2 and then vortexed before use in the crystallisation protocol. The crystallisation was carried out by sitting drop vapour diffusion using plates prepared with a Mosquito liquid handling robot with crystallisation drops consisting of 200 nL protein, 200 nL well solution and 100 nL seeding solution, using Morpheus screen condition G2 for the wells. Crystals were transferred for soaking to drops containing Morpheus screen condition G2 with 10% glycerol and 5% compound solution (200mM compound stock solution in DMSO) added. The crystals were soaked for 18 hours prior to flash freezing direct from the soaking drop in liquid nitrogen ready for data collection.

X-ray diffraction data were collected at 100 K using Pilatus-6M detectors at the Diamond Light Source and the European Synchrotron Radiation Facility. The data were processed and scaled utilising XDS,<sup>267</sup> AIMLESS<sup>268</sup> and the CCP4 suite of programs.<sup>269</sup> Data collection statistics are given in the table below. The structure was determined using the coordinates of an isomorphous unliganded protein model (unpublished). Coot<sup>270</sup> was used for model building and refinement was carried out with autoBUSTER.<sup>271</sup> The ligand geometry was checked using MOGUL.<sup>272</sup> The final model statistics are given below.

Coordinates have been deposited with the Protein Data Bank with accession codes  
Compound **31**: 6hi1, Compound **34**: 6hi9 , Compound **33**: 6hi2.

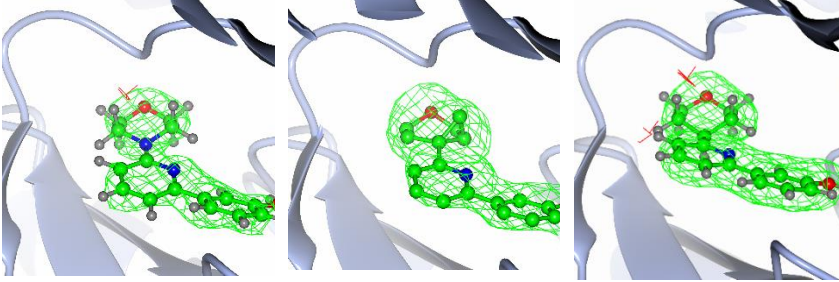
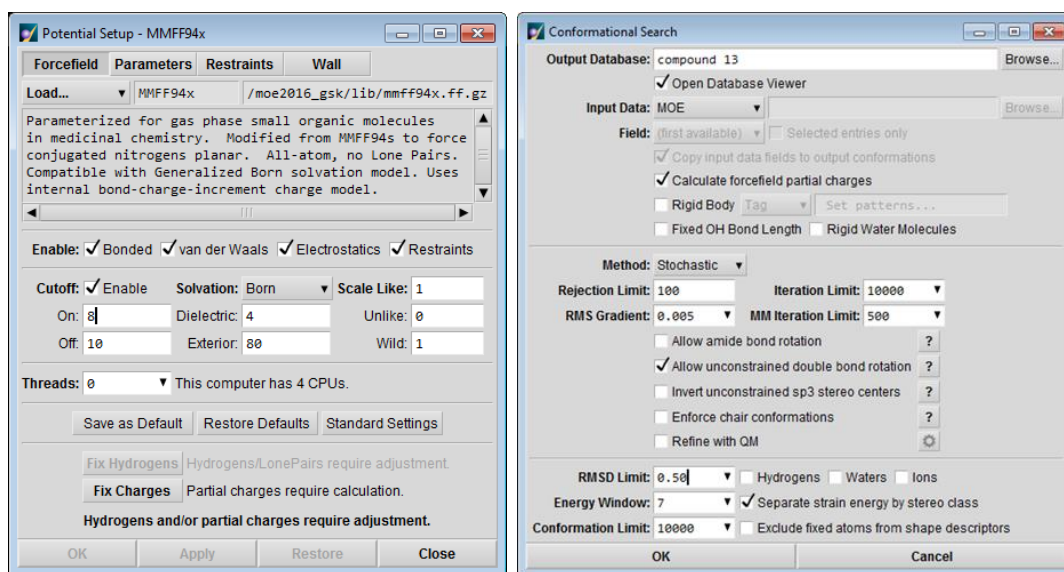
	Compound 31	Compound 34	Compound 33
<b>Resolution</b>	2.07Å	1.9Å	2.08Å
<b>X-ray source</b>	DLS, I04	ESRF, ID23eh1	ESRF, ID23eh1
<b>Space Group</b>	C2	C2	C2
<b>Cell Dimensions</b>			
<b>a,b,c (Å)</b>	141.57, 64.36, 116.30	141.74, 64.49, 116.4	141.91, 64.32, 116.14
<b><math>\alpha, \beta, \gamma</math> (°)</b>	90, 103.24, 90	90, 103.17, 90	90, 102.69, 90
<b>Processing</b>	XDS/Aimless	XDS/Aimless	XDS/Aimless
<b>Resolution (Å)</b>	54.02-2.07(2.12-2.07)	49.7-1.9(1.97-1.9)	49.49-2.08(2.15-2.08)
<b>R<sub>merge</sub><sup>b</sup></b>	0.061(0.662)	0.034 (0.784)	0.056(0.758)
<b>CC(1/2)</b>	0.997(0.575)	0.999(0.583)	0.999(0.555)
<b>Mean I/<math>\sigma</math>I</b>	12.1(2.0)	14.6(1.6)	13.1(1.7)
<b>Completeness (%)</b>	99.4(100.0)	99.3(98.4)	98.5(96.3)
<b>Redundancy</b>	3.3(3.4)	3.4(3.4)	3.5(3.5)
<b>No. Reflections</b>	207396(15416)	273454(26030)	208930(20413)
<b>No. Unique Reflections</b>	61934(4553)	80061(7699)	60535(5780)
<b>Refinement</b>			
<b>Programme used</b>	BUSTER 2.11.5	BUSTER 2.11.7	BUSTER 2.11.7
<b>Resolution (Å)</b>	30-2.07	38-1.90	50-2.08
<b>R<sub>work</sub>/R<sub>free</sub></b>	0.211/0.254	0.175/0.196	0.175/0.212
<b>No. Reflections</b>	61898	80056	60539
<b>Completeness in range</b>	97.31	99.1	98.2
<b>No. atoms</b>			
<b>Protein</b>	6944	6917	6923
<b>Ligand</b>	19 (non-hydrogen)	20	19
<b>Water</b>	494	615	504
<b>B-factors</b>			
<b>Protein</b>	42.84	50.19	55.96
<b>Ligand</b>	37.55	49.95	39.86
<b>Water</b>	50.97	56.70	57.42
<b>R.M.S deviations</b>			
<b>Bond lengths (Å)</b>	0.010	0.010	0.010
<b>Bond angles (°)</b>	1.04	0.94	0.99
<b>Fo-Fc omit map using final refined coordinates, contoured at 3<math>\sigma</math>s.</b>			

Table 56: Parameters for PI3K $\delta$  Co-crystal structures of Compounds 31, 34 and 35.

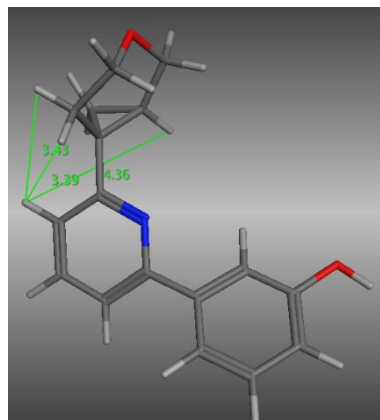
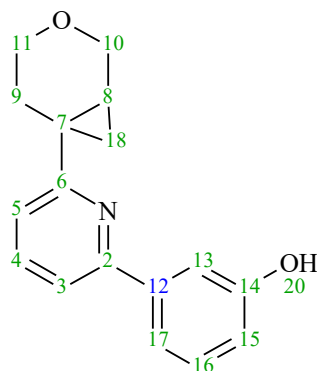
## ROESY NMR Experimental and Spectra

### Molecular Mechanical Modelling Details

Molecular mechanical modelling was carried out in 2016.08 release of Chemical Computing Group's Molecular Operating Environment (MOE) software. Forcefield (MMFF94x) Parameterized for gas phase small organic molecules in organic chemistry. Modified from MMFF94s to force conjugated nitrogens planar. All-atoms, no lone pairs. Compatible with generalised Bonn solvation model. Uses internal bond-charge-increment charge model. Searches were run to completion and all low energy conformers retained.



**Figure 79:** Setup parameters for molecular mechanical modelling performed in MOE.

**3-(6-(3-oxabicyclo[4.1.0]heptan-6-yl)pyridin-2-yl)phenol (34)**

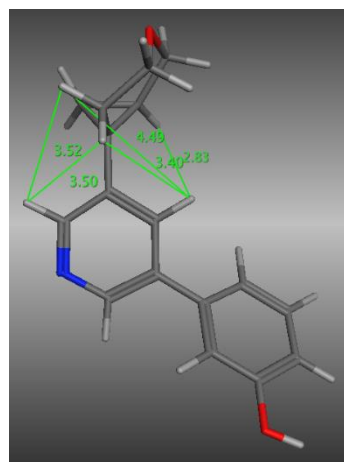
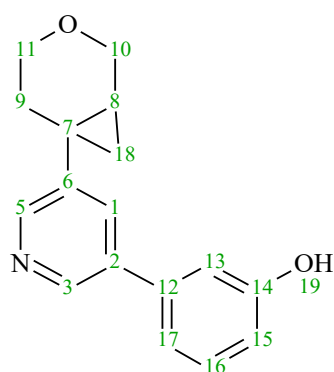
	mol	mseq	E	dE	9'-5CH	9''-5CH	5CH-8CH
<b>1</b>		1	52.9349	0.0000	3.3913	3.4344	4.3609
2		1	52.9473	0.0124	3.4444	3.4001	4.3541
3		1	52.9511	0.0162	3.4471	3.4030	4.3511
4		1	52.9511	0.0162	3.4452	3.4020	4.3525
5		1	52.9918	0.0569	3.4515	3.4094	4.3480
6		1	53.0306	0.0957	4.4582	3.3275	2.9274
7		1	53.0787	0.1438	4.4615	3.3346	2.9206
8		1	53.1151	0.1802	4.4645	3.3385	2.9159
9		1	53.9253	0.9904	4.2535	3.0134	2.8402

**Table 57:** Low energy conformers generated in MOE for Compound **34**. Model of Conformer 1 is displayed.

<u>NOE</u>	<u>Magnitude</u>	<u>NOE Distance</u>	<u>Comment</u>
18'-18''	100.0	1.75	Geminal ROE internal yardstick
9CH'-5CH	16.0	2.37	Closer approach than any of the molecular mechanics models
9CH''-5CH	4.6	2.92	Closer approach than any of the molecular mechanics models
8CH-5CH	4.9	2.89	
9''-18''	9.6	2.59	Indicates 9'' is syn to the cyclopropyl

**Table 58:** Key ROE (NOE) restraints for Compound **34**.

**3-(5-(3-oxabicyclo[4.1.0]heptan-6-yl)pyridin-3-yl)phenol (40)**

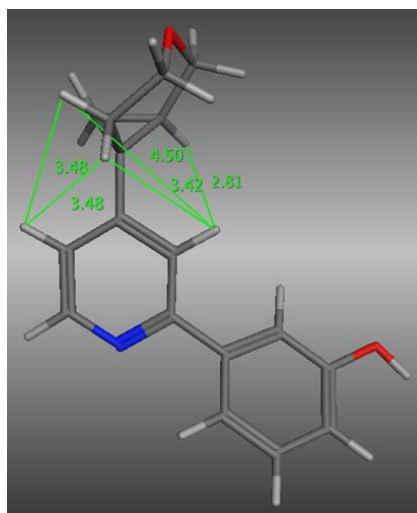
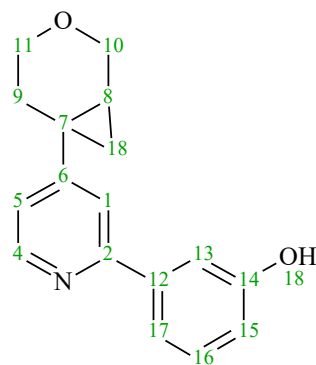


	mol	mseq	E	dE	9'-5CH	9"-5CH	9'-1CH	9"-1CH	5CH-8CH	1CH-8CH
1		1	57.5443	0.0000	3.5196	3.5021	3.4025	4.4924	4.3186	2.8346
2		1	57.5541	0.0099	3.4984	3.4881	3.4166	4.5019	4.3291	2.8224
3		1	57.5542	0.0099	3.5006	3.4906	3.4148	4.5017	4.3286	2.8247
4		1	57.5665	0.0222	3.5080	3.4992	3.4214	4.5046	4.3227	2.8172
5		1	57.5910	0.0467	3.5175	3.5037	3.4152	4.4988	4.3179	2.8221
6		1	57.6256	0.0813	4.5323	3.4414	3.4644	3.4621	2.8518	4.3079
7		1	57.6306	0.0863	4.5325	3.4397	3.4680	3.4650	2.8536	4.3055
8		1	57.6441	0.0998	4.5393	3.4515	3.4676	3.4638	2.8428	4.3043
9		1	57.6697	0.1254	4.5379	3.4489	3.4713	3.4663	2.8454	4.3030

**Table 59:** Low energy conformers generated in MOE for Compound 40. Model of Conformer 1 is displayed.

			<b>Comment</b>
<b>NOE</b>	<b>Magnitude</b>	<b>Distance</b>	<b>r<sup>1/6</sup> average NOE Distances</b>
18'-18''	100.0	1.75	Geminal ROE internal yardstick
9CH'-5CH	3.1	3.12	
9CH''-5CH	4.7	2.91	
9'-1CH	3.4	3.07	
9''-1CH	4.8	2.90	
8CH-1CH	7.0	2.72	
8CH-5CH	2.8	3.18	
9'-18''	6.7	2.74	9' is syn to cyclopropyl

**Table 60:** Key ROE (NOE) restraints for Compound 40.

**3-(4-(3-oxabicyclo[4.1.0]heptan-6-yl)pyridin-2-yl)phenol) (41)**

	mol	mseq	E	dE	9'-5CH	9''-5CH	9'-1CH	9''-1CH	5CH-8CH	1CH-8CH
1		1	52.4317	0.0000	3.4821	3.4801	3.4192	4.5019	4.3333	2.8143
2		1	52.4317	0.0000	3.4798	3.4807	4.5035	3.4208	4.3330	2.8122
3		1	52.4345	0.0028	3.5006	3.5064	3.3981	4.4873	4.3185	2.8301
4		1	52.4712	0.0395	3.4984	3.4973	3.4197	4.5013	4.3215	2.8125
5		1	52.4715	0.0398	3.5047	3.5070	3.4116	4.4952	4.3152	2.8172
6		1	52.4716	0.0399	3.4419	4.5298	3.4581	3.4531	2.8393	4.3097
7		1	52.4929	0.0612	3.4512	4.5348	3.4662	3.4581	2.8304	4.3041
8		1	52.5105	0.0788	3.4464	4.5311	3.4713	3.4627	2.8336	4.3010
9		1	52.5827	0.1510	4.5302	3.4428	3.4516	3.4574	2.8379	4.3110

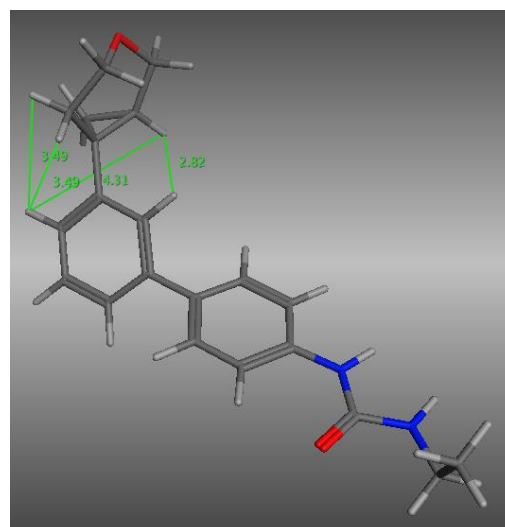
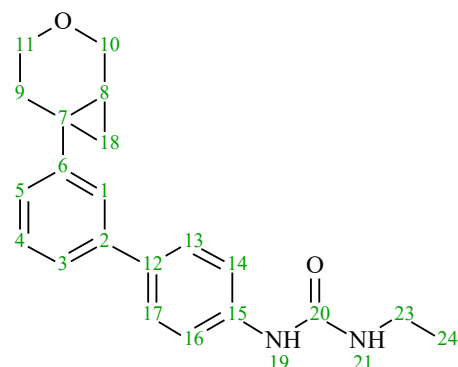
**Table 61:** Low energy conformers generated in MOE for Compound **41**. Model of Conformer 1 is displayed.

			<b>Comment</b>
<b>NOE</b>	<b>Magnitude</b>	<b>Distance</b>	<b>r<sup>1/6</sup> average NOE Distances</b>
18'-18''	100.0	1.75	Geminal ROE internal yardstick
9CH'-5CH	5.9	2.80	
9CH''-5CH	3.1	3.12	
9'-1CH	10.0	2.57	
9''-1CH	5.4	2.85	
8CH-5CH	6.7	2.74	
8CH-1CH	10.4	2.55	
9''-18''	6.7	2.74	9'' is <i>syn</i> to the cyclopropyl

**Table 62:** Key ROE (NOE) restraints for Compound **41**.



**1-(3'-(3-oxabicyclo[4.1.0]heptan-6-yl)[1,1'biphenyl]-4-yl)-3-ethylurea**  
**(42)**



	mol	mseq	E	dE	9'-5CH	9''-5CH	9'-1CH	9''-1CH	5CH-8CH	1CH-8CH
1		1	42.0857	0.0000	3.4922	3.4906	3.3901	4.4759	4.3058	2.8189
2		1	42.0858	0.0000	3.4900	3.4914	4.4750	3.3901	4.3062	2.8175
3		1	42.0891	0.0034	3.4931	3.4926	3.3876	4.4751	4.3038	2.8216
4		1	42.0891	0.0034	3.4921	3.4932	4.4752	3.3879	4.3035	2.8203
5		1	42.0896	0.0039	3.4958	3.4942	3.3983	4.4800	4.3023	2.8104
6		1	42.0897	0.0039	3.4940	3.4949	4.4798	3.3976	4.3022	2.8101
7		1	42.0927	0.0069	3.5023	3.5017	4.4745	3.3899	4.2969	2.8166
8		1	42.0928	0.0070	3.5017	3.5028	3.3897	4.4747	4.2971	2.8163
9		1	42.1174	0.0317	4.5169	3.4343	3.4382	3.4474	2.8195	4.3035
10		1	42.1175	0.0317	4.5157	3.4334	3.4388	3.4481	2.8214	4.3026
11		1	42.1349	0.0492	3.4362	4.5178	3.4588	3.4452	2.8188	4.2969
12		1	42.1349	0.0492	3.4357	4.5169	3.4588	3.4456	2.8199	4.2954
13		1	42.1431	0.0574	3.4367	4.5182	3.4581	3.4454	2.8182	4.2958
14		1	42.1432	0.0575	3.4335	4.5155	3.4604	3.4479	2.8208	4.2941
15		1	43.0110	0.9253	4.3126	3.0967	3.0670	3.8664	2.7551	4.3611
16		1	43.0110	0.9253	4.3136	3.0980	3.0657	3.8643	2.7549	4.3610
17		1	47.2168	5.1311	3.8907	3.2725	4.4543	3.7191	4.3859	2.7067

**Table 63:** Low energy conformers generated in MOE for Compound **42**. Model of Conformer 1 is displayed.

NOE	Magnitude	Distance	Comment
18 <sup>l</sup> -18 <sup>''</sup>	100.0	1.75	Geminal ROE Internal yardstick
9CH <sup>l</sup> -5CH	2.3	3.28	
9CH <sup>''</sup> -5CH	3.4	3.07	
9CH <sup>l</sup> -1CH	4.1	2.98	
9CH <sup>''</sup> -1CH	5.3	2.85	
8CH-5CH	5.0	2.88	
8CH-1CH	7.7	2.68	
9 <sup>''</sup> -18 <sup>''</sup>	6.7	2.74	9 <sup>''</sup> is syn to the cyclopropyl

**Table 64:** Key ROE (NOE) restraints for Compound **42**.

**Cyclopropylpyran Stereochemical Assignment**

The stereochemical assignment of cyclopropylpyran **186** in Chapter I was determined by analogy to small molecule X-ray crystal structures of tool compounds synthesised in chapter I. It was assumed that compounds with the same rotational sign were the same enantiomer. Data which was considered to assign **186a** and **186b** is shown in **Table 65**.

Compound No.	Structure	Isomer	Enantiomer	Sign	$\alpha_D$	X-ray Structure	Most Active?
34		1	<i>1R,6S</i>	-	30.2	Yes	No
		2	<i>1S,6R</i>	+	42.2	No	Yes
38		1	<i>1R,6S</i>	-	100.0	Yes	No
		2	<i>1S,6R</i>	+	69.9	No	Yes
39		1	<i>1R,6S</i>	-	60.0	No	Yes
		2	<i>1S,6R</i>	+	34.8	Yes	No
40		1	<i>1S,6R</i>	+	15.4	Yes	Equal
		2	<i>1R,6S</i>	-	30.8	No	Equal
41		1	<i>1S,6R</i>	+	36.4	No	No
		2	<i>1R,6S</i>	-	40.0	Yes	Yes
42		1	<i>1R,6S</i>	-	16.0	No	Equal
		2	<i>1S,6R</i>	+	16.0	Yes	Equal

**Table 65:** Cyclopropylpyran Stereochemical Assignment.

## Assay Experimental Procedures

### PI3K-Isoform HTRF Assay

Inhibition of PI3K enzymatic activity was determined using an HTRF assay kit based on the method described by Gray *et al.*<sup>178</sup> Reactions were performed in assay buffer containing 50 mM HEPES, pH 7.0, 150 mM NaCl, 10 mM MgCl<sub>2</sub>, 2.3 mM sodium cholate, 10 μM CHAPS, and 1 mM DTT. Enzymes were preincubated with compound, serially diluted 4-fold in 100% DMSO, for 15 min prior to reaction initiation upon addition of substrate solution containing ATP at  $K_M$  for the specific isoform tested ( $\alpha$  at 250 μM,  $\beta$  at 400 μM,  $\delta$  at 80 μM, and  $\gamma$  at 15 μM), PIP<sub>2</sub> at either 5 μM (PI3K $\delta$ ) or 8 μM (PI3K $\alpha$ ,  $\beta$ , and  $\gamma$ ) and 10 nM biotin-PIP<sub>3</sub>. Assays were quenched after 60 min by addition of a quench/detection solution prepared in 50 mM HEPES, pH 7.0, 150 mM NaCl, 2.3 mM sodium cholate, 10 μM CHAPS, 30 mM EDTA, 40 mM potassium fluoride, and 1 mM DTT containing 16.5 nM GRP-1 PH domain, 8.3 nM streptavidin-APC, and 2 nM europium-anti-GST and were left for a further 60 min in the dark to equilibrate prior to reading using a Perkin Elmer EnVision plate reader. Ratio data were normalized to high (DMSO) and low (no enzyme or enzyme in the presence of 8.3 μM wortmannin) controls prior to fitting using a logistical four-parameter equation (equation 1, **Figure 80**) to determine IC<sub>50</sub>, where  $y$  is the response; Bottom is the lowest plateau of the curve; Top is the highest plateau of the curve;  $x$  is the molar concentration of inhibitor; and  $S$  is the Hill Slope.

$$y = \text{Bottom} + \frac{\text{Top} - \text{Bottom}}{1 + \left(\frac{x}{IC_{50}}\right)^S}$$

**Figure 80:** Equation 1

Taking the negative natural log ( $-\log_{10}$ ) of this figure affords the pIC<sub>50</sub>. IC<sub>50</sub> can be converted to  $K_i$ , and therefore p $K_i$ , using the Cheng-Prusoff Equation (Equation 2, **Figure 81**).<sup>8</sup>

$$K_i = \frac{IC_{50}}{1 + \left(\frac{[S]}{K_M}\right)}$$

**Figure 81:** Equation 2

Therefore, for assays carried out at  $K_M$ (ATP), the  $K_i$  is approximately 2-fold more potent than the measured value, which corresponds to roughly 0.3 log unit increase in pIC<sub>50</sub>.

### **Phospho-Akt Cellular Assay**

Level of Akt (Ser373) phosphorylation was measured with an electrochemiluminescent compound, MSD SULFO-TAG label. Procedure is as previously described.<sup>273</sup> Briefly, Frozen human lung fibroblasts (HLF) were cultured in Fibroblast Basal Medium with Fibroblast Basal Medium supplement pack containing FBS, hFGF-B, Insulin, GA-1000 at 37 °C for 5 days. Following this, cells were plated onto 384 well black U-clear Greiner flat bottom plates. Cells were incubated with either vehicle or increasing concentrations of test compound for 1 h. After this time 10 µL Platelet-Derived Growth Factor BB (PDGF-BB) and 10 µL cell signalling lysis buffer was added and plates were shaken for 30 min to ensure lysis. 30 µL of lysate was added to 384 well GAR plate containing 10µl Rabbit pAkt antibody, diluted 1:1500 with block buffer. MSD GAR plates are MULTI-ARRAY plates coated with goat anti-rabbit antibody and are used in applications that require the immobilization of polyclonal capture antibodies (e.g. antibodies from crude sera). The detection system uses SULFO-TAG labels that emit light upon electrochemical stimulation initiated at the electrode surfaces of the plates. The GAR plates were sealed and shaken in a cold room overnight. GAR plates were washed with tris buffered saline (TBS) wash buffer, 10 µL mouse total AKT detection antibody diluted 1:1500 with block buffer was added and plates were shaken for an 1 h. GAR plates were washed with TBS wash buffer 10 µL of the anti-MOUSE MSD detection antibody diluted 1:500 with block buffer added and plates were shaken for an 1 h. GAR plates were washed with TBS wash buffer. 30 µL 2x MSD read buffer was added to wells and plates were read immediately on MSD Sector Imager 6000

### **mTOR Kinobead Proteomic Binding Assay**

Levels of compound binding to mTOR is measured in a Kinobead chemoproteomic binding assay, similar to those previously described within the literature.<sup>175</sup> As a general overview, This chemoproteomic assay is a competition binding assay based on affinity enrichment of endogenous mTOR (from HuT-78 total lysate) on a binding matrix in the presence of free test compound. After the incubation of HuT-78 lysate with the binding matrix and test compounds, unbound proteins are removed by washing the matrix and the remaining captured proteins are eluted from the matrix completely. Eluted proteins are spotted on a nitrocellulose membrane followed by a two-step incubation with a rabbit anti-mTOR antibody and an anti-rabbit antibody coupled to an infrared dye (800 nm wavelength). The membrane is then scanned on a Licor Odyssey scanner and signal intensities are quantified. Reduced binding of mTOR to the matrix in the presence of an inhibitor will lead to a lower/absent signal.

### **“Scar-in-a-Jar” Phenotypic Assay**

Collagen biosynthesis in 96 well format was measured by a high-content imaging based molecular crowding assay modified from a previously described method.<sup>177</sup> Briefly, confluent lung fibroblasts were cultured in Dulbecco’s modified Eagle’s medium (DMEM) containing 0.4% foetal bovine serum (FCS) and ascorbic acid (100µM), in the presence of mixed Ficoll 70 and Ficoll 400 as molecular crowding agents. These were stimulated with TGFβ1 (1 ng/ml) and incubated with either vehicle (0.1% DMSO) or increasing concentrations of test compound for 48 hours. Lung fibroblasts were fixed and stained with antibody specific for human collagen 1, fluorescent secondary antibody (Alex Fluor488) and nuclei counterstained with 4',6-diamidino-2-phenylindole (DAPI) for per cell normalisation. Fluorescent signal quantified on the INCELL 6000 high content system.

### **Charged Aerosol Detection (CAD) solubility**

Kinetic solubility measurement using HPLC-CAD technique. The kinetic aqueous solubility at pH7.4 is determined by measuring the concentration of solute in solution after precipitation from DMSO stock solution. The DMSO stock solution is diluted 20-fold with PBS pH7.4 and the solubility of the compound is measured after 1-hour equilibration at room temperature. In this procedure quantification is done using a Charged Aerosol Detector (CAD). The actual DMSO concentration of the stock solution is also determined using this technique. Calibration parameters generated for CAD response of two calibrants (Primidone and Ketoconazole) are used to calculate the solubility of solutes taking into account the density of the compound and ion-pairing effects.<sup>179</sup>

### **ChromLogD**

Chromatographic hydrophobicity index (Chi-LogD7.4) was determined by fast-gradient HPLC, according to literature procedures,<sup>274,275</sup> using a Waters Aquity UPLC System, Phenomenex Gemini NX 50 × 2 mm, 3 µM HPLC column, 0–100% pH 7.40 ammonium acetate buffer/acetonitrile gradient. Retention time was compared to standards of known pH to derive the Chromatographic Hydrophobicity Index (CHI).  $\text{ChromLogD} = 0.0857\text{CHI} - 2$ .

### **Artificial Membrane Permeability**

Permeability across a lipid membrane was measured using the published protocol.<sup>276</sup>

**References**

- (1) Huang, M.; Shen, A.; Ding, J.; Geng, M. *Trends Pharmacol. Sci.* **2014**, *35*, 41..
- (2) Ma, W. W.; Adjei, A. A. *CA Cancer J. Clin.* **2009**, *59*, 111.
- (3) Sun, C.; Bernards, R. *Trends Biochem. Sci.* **2014**, *39*, 465.
- (4) Clark, J. D.; Flanagan, M. E.; Telliez, J.-B. *J. Med. Chem.* **2014**, *57*, 5023.
- (5) Barnes, P. J. *Nat. Rev. Drug Discov.* **2013**, *12*, 543.
- (6) Muth, F.; Günther, M.; Bauer, S. M.; Döring, E.; Fischer, S.; Maier, J.; Drückes, P.; Köppler, J.; Trappe, J.; Rothbauer, U.; Koch, P.; Laufer, S. A. *J. Med. Chem.* **2015**, *58*, 443.
- (7) Kikuchi, R.; Nakamura, K.; MacLauchlan, S.; Ngo, D. T.-M.; Shimizu, I.; Fuster, J. J.; Katanasaka, Y.; Yoshida, S.; Qiu, Y.; Yamaguchi, T. P.; Matsushita, T.; Murohara, T.; Gokce, N.; Bates, D. O.; Hamburg, N. M.; Walsh, K. *Nat. Med.* **2014**, *20*, 1464.
- (8) Raghu, G.; Weycker, D.; Edelsberg, J.; Bradford, W. Z.; Oster, G. *Am. J. Respir. Crit. Care Med.* **2006**, *174*, 810.
- (9) Selman, M.; Pardo, A. *Am. J. Respir. Crit. Care Med.* **2014**, *189*, 1161.
- (10) Maher, T. M.; Wells, A. U.; Laurent, G. J. *Eur. Respir. J.* **2007**, *30*, 835.
- (11) IPF Clinical Research Network. *N. Engl. J. Med.* **2012**, *366*, 1968.
- (12) Maher, T. M. *Expert Opin. Med. Diagn.* **2008**, *2*, 1317.
- (13) Leslie, K. O.; Wick, M. R. *Practical pulmonary pathology : a diagnostic approach*; Elsevier/Saunders: Philadelphia, PA, **2011**.
- (14) European Respiratory Science Research Committee. *Am. J. Respir. Crit. Care Med.* **2002**, *165*, 277.
- (15) Hutchinson, J.; Fogarty, A.; Hubbard, R.; McKeever, T. *Eur. Respir. J.* **2015**, *46*, 795.
- (16) Miller, K. D.; Siegel, R. L.; Lin, C. C.; Mariotto, A. B.; Kramer, J. L.; Rowland, J. H.; Stein, K. D.; Alteri, R.; Jemal, A. *CA Cancer J. Clin.* **2016**, *66*, 271.
- (17) Raghu, G.; Collard, H. R.; Egan, J. J.; Martinez, F. J.; Behr, J.; Brown, K. K.; Colby, T. V.; Cordier, J. F.; Flaherty, K. R.; Lasky, J. A.; Lynch, D. A.; Ryu, J. H.; Swigris, J. J.; Wells, A. U.; Ancochea, J.; Bouros, D.; Carvalho, C.; Costabel, U.; Ebina, M.; Hansell, D. M.; Johkoh, T.; Kim, D. S.; King, T. E., Jr.; Kondoh, Y.; Myers, J.; Muller, N. L.; Nicholson, A. G.; Richeldi, L.; Selman, M.; Dudden, R. F.; Griss, B. S.; Protzko, S. L.; Schunemann, H. J. *Am. J. Respir. Crit. Care Med.* **2011**, *183*, 788.
- (18) Jankowich, M. D.; Rounds, S. I. S. *Chest* **2012**, *141*, 222.
- (19) Lawrence, J.; Nho, R. *Int. J. Mol. Sci.* **2018**, *19*.

- (20) Thannickal, V. J.; Lee, D. Y.; White, E. S.; Cui, Z.; Larios, J. M.; Chacon, R.; Horowitz, J. C.; Day, R. M.; Thomas, P. E. *J. Biol. Chem.* **2003**, *278*, 12384.
- (21) Zhang, H. Y.; Phan, S. H. *Am. J. Respir. Cell Mol. Biol.* **1999**, *21*, 658.
- (22) Tamura, M.; Gu, J.; Danen, E. H.; Takino, T.; Miyamoto, S.; Yamada, K. M. *J. Biol. Chem.* **1999**, *274*, 20693.
- (23) Nho, R. S.; Hergert, P.; Kahm, J.; Jessurun, J.; Henke, C. *Am. J. Pathol.* **2011**, *179*, 2420.
- (24) Xia, H.; Diebold, D.; Nho, R.; Perlman, D.; Kleidon, J.; Kahm, J.; Avdulov, S.; Peterson, M.; Nerva, J.; Bitterman, P.; Henke, C. *J. Exp. Med.* **2008**, *205*, 1659.
- (25) George, T. J.; Arnaoutakis, G. J.; Shah, A. S. *Arch. Surg.* **2011**, *146*, 1204.
- (26) Kaneko, M.; Inoue, H.; Nakazawa, R.; Azuma, N.; Suzuki, M.; Yamauchi, S.; Margolin, S. B.; Tsubota, K.; Saito, I. *Clin. Exp. Immunol.* **1998**, *113*, 72.
- (27) Oku, H.; Shimizu, T.; Kawabata, T.; Nagira, M.; Hikita, I.; Ueyama, A.; Matsushima, S.; Torii, M.; Arimura, A. *Eur. J. Pharmacol.* **2008**, *590*, 400.
- (28) Nathan, S. D.; Albera, C.; Bradford, W. Z.; Costabel, U.; Glaspole, I.; Glassberg, M. K.; Kardatzke, D. R.; Daigl, M.; Kirchgaessler, K.-U.; Lancaster, L. H.; Lederer, D. J.; Pereira, C. A.; Swigris, J. J.; Valeyre, D.; Noble, P. W. *The Lancet Respir. Med.* **2017**, *5*, 33.
- (29) Mora, A. L.; Rojas, M.; Pardo, A.; Selman, M. *Nature Rev. Drug Discov.* **2017**, *16*, 755.
- (30) NICE. *Pirfenidone for treating idiopathic pulmonary fibrosis, Technology appraisal guidance (TA504)*. **2018**. <https://www.nice.org.uk/guidance/ta504> accessed 27.3.2019
- (31) Hoffmann-La Roche. *Package leaflet: Information for the user Esbriet 267 mg hard capsules*. **2018**. <https://www.medicines.org.uk/emc/files/pil.3705.pdf> accessed 27.3.2019
- (32) Wollin, L.; Wex, E.; Pautsch, A.; Schnapp, G.; Hostettler, K. E.; Stowasser, S.; Kolb, M. *Eur. Respir. J.* **2015**, *45*, 1434.
- (33) Richeldi, L.; du Bois, R. M.; Raghu, G.; Azuma, A.; Brown, K. K.; Costabel, U.; Cottin, V.; Flaherty, K. R.; Hansell, D. M.; Inoue, Y.; Kim, D. S.; Kolb, M.; Nicholson, A. G.; Noble, P. W.; Selman, M.; Taniguchi, H.; Brun, M.; Le Maulf, F.; Girard, M.; Stowasser, S.; Schlenker-Herceg, R.; Disse, B.; Collard, H. R. *N. Engl. J. Med.* **2014**, *370*, 2071.

- (34) NICE. *Nintedanib for treating idiopathic pulmonary fibrosis, Technology appraisal guidance (TA379)* **2016**. <https://www.nice.org.uk/guidance/ta379> accessed 27.3.2019.
- (35) Waldmann, T. A. *Nat. Med.* **2003**, 9, 269.
- (36) Werner, R. G. *J. Biotechnol.* **2004**, 113, 171.
- (37) Levêque, D.; Wisniewski, S.; Jehl, F. *Pharmacokinetics of therapeutic monoclonal antibodies used in oncology*, **2005**; Vol. 25.
- (38) Rodgers, J. A. C. a. K. In *Encyclopaedia Britannica* 2009.
- (39) Manning, G.; Whyte, D. B.; Martinez, R.; Hunter, T.; Sudarsanam, S. *Science* **2002**, 298, 1912.
- (40) Image of Phosphorylation Cascade:  
[http://bio1151b.nicerweb.com/Locked/media/ch11/phosphorylation\\_cascade.html](http://bio1151b.nicerweb.com/Locked/media/ch11/phosphorylation_cascade.html) accessed 27.3.2019.
- (41) Ferguson, F. M.; Gray, N. S. *Nat. Rev. Drug Discovery* **2018**, 17, 353.
- (42) Cowan-Jacob, S. W.; Mobitz, H.; Fabbro, D. *Curr. Opin. Cell Biol.* **2009**, 21, 280.
- (43) Fabbro, D. *Mol. Pharmacol.* **2015**, 87, 766.
- (44) Fu, J. J., Q.; Zhang, C. *Nature Education* **2010**, 9.
- (45) Fabbro, D.; Cowan-Jacob, S. W.; Mobitz, H.; Martiny-Baron, G. *Methods Mol. Biol.* **2012**, 795, 1.
- (46) Hanks, S. K.; Hunter, T. *FASEB J.* **1995**, 9, 576.
- (47) Nolen, B.; Taylor, S.; Ghosh, G. *Mol. Cell* **2004**, 15, 661.
- (48) Liu, Q.; Sabnis, Y.; Zhao, Z.; Zhang, T.; Buhrlage, Sara J.; Jones, Lyn H.; Gray, Nathanael S. *Chem. Biol.* **2013**, 20, 146.
- (49) S Kim, E.; Dhillon, S. *Ibrutinib: A Review of Its Use in Patients with Mantle Cell Lymphoma or Chronic Lymphocytic Leukaemia*, **2015**; Vol. 75.
- (50) Hossam, M.; Lasheen, D. S.; Abouzeid, K. A. M. *Arch. Pharm.* **2016**, 349, 573.
- (51) Dalton, S. E.; Dittus, L.; Thomas, D. A.; Convery, M. A.; Nunes, J.; Bush, J. T.; Evans, J. P.; Werner, T.; Bantscheff, M.; Murphy, J. A.; Campos, S. *J. Am. Chem. Soc.* **2018**, 140, 932.
- (52) Wood, E. R.; Truesdale, A. T.; McDonald, O. B.; Yuan, D.; Hassell, A.; Dickerson, S. H.; Ellis, B.; Pennisi, C.; Horne, E.; Lackey, K.; Alligood, K. J.; Rusnak, D. W.; Gilmer, T. M.; Shewchuk, L. *Cancer Res.* **2004**, 64, 6652.
- (53) Cowan-Jacob, S. W.; Jahnke, W.; Knapp, S. *Future Med. Chem.* **2014**, 6, 541.
- (54) Iqbal, N.; Iqbal, N. *Chemother. Res. Pract.* **2014**, 2014, 357027.
- (55) Keating, G. M.; Santoro, A. *Drugs* **2009**, 69, 223.



- (56) Pargellis, C.; Tong, L.; Churchill, L.; Cirillo, P. F.; Gilmore, T.; Graham, A. G.; Grob, P. M.; Hickey, E. R.; Moss, N.; Pav, S.; Regan, J. *Nat. Struct. Biol.* **2002**, *9*, 268.
- (57) Kufareva, I.; Abagyan, R. *J. Med. Chem.* **2008**, *51*, 7921.
- (58) Roskoski, R. *Pharmacol. Res.* **2016**, *103*, 26.
- (59) Adjei, A. A.; LoRusso, P.; Ribas, A.; Sosman, J. A.; Pavlick, A.; Dy, G. K.; Zhou, X.; Gangolli, E.; Kneissl, M.; Faucette, S.; Neuwirth, R.; Bózon, V. *Invest. New Drugs* **2017**, *35*, 47.
- (60) Adrián, F. J.; Ding, Q.; Sim, T.; Velentza, A.; Sloan, C.; Liu, Y.; Zhang, G.; Hur, W.; Ding, S.; Manley, P.; Mestan, J.; Fabbro, D.; Gray, N. S. *Nat. Chem. Biol.* **2006**, *2*, 95.
- (61) Hunter, T. *Cell* **1995**, *83*, 1.
- (62) Smith, G. C. M.; Jackson, S. P. In *Handbook of Cell Signaling (Second Edition)*; Bradshaw, R. A., Dennis, E. A., Eds.; Academic Press: San Diego, **2010**, p 575.
- (63) Chen, D.; Lin, X.; Zhang, C.; Liu, Z.; Chen, Z.; Li, Z.; Wang, J.; Li, B.; Hu, Y.; Dong, B.; Shen, L.; Ji, J.; Gao, J.; Zhang, X. *Cell Death Dis.* **2018**, *9*, 123.
- (64) Bendell, J. C.; Varghese, A. M.; Hyman, D. M.; Bauer, T. M.; Pant, S.; Callies, S.; Lin, J.; Martinez, R.; Wickremsinhe, E.; Fink, A.; Wacheck, V.; Moore, K. N. *Clin. Cancer. Res.* **2018**, *24*, 3253.
- (65) Dienstmann, R.; Rodon, J.; Serra, V.; Tabernero, J. *Mol. Cancer Ther.* **2014**, *13*, 1021.
- (66) Schmelzle, T.; Hall, M. N. *Cell* **2000**, *103*, 253.
- (67) Raught, B.; Gingras, A. C.; Sonenberg, N. *Proc. Natl. Acad. Sci. U. S. A.* **2001**, *98*, 7037.
- (68) Engelman, J. A.; Luo, J.; Cantley, L. C. *Nat. Rev. Genet.* **2006**, *7*, 606.
- (69) Janku, F. *Cancer Treat. Rev.* **2017**, *59*, 93.
- (70) Malemud, C. J. *Future Med. Chem.* **2015**, *7*, 1137.
- (71) Nho, R. S.; Peterson, M.; Hergert, P.; Henke, C. A. *PLoS One* **2013**, *8*, 61017.
- (72) Sarbassov, D. D.; Guertin, D. A.; Ali, S. M.; Sabatini, D. M. *Science* **2005**, *307*, 1098.
- (73) Citrin, D. E.; Shankavaram, U.; Horton, J. A.; Shield, W., 3rd; Zhao, S.; Asano, H.; White, A.; Sowers, A.; Thetford, A.; Chung, E. J. *J. Natl. Cancer Inst.* **2013**, *105*, 1474.
- (74) Chung, E. J.; Sowers, A.; Thetford, A.; McKay-Corkum, G.; Chung, S. I.; Mitchell, J. B.; Citrin, D. E. *Int. J. Radiat. Oncol. Biol. Phys.* **2016**, *96*, 857.

- (75) Citrin, D. E.; Mitchell, J. B. *Semin. Radiat. Oncol.* **2017**, *27*, 316.
- (76) Wander, S. A.; Hennessy, B. T.; Slingerland, J. M. *J. Clin. Invest.* **2011**, *121*, 1231.
- (77) Kuo, C. J.; Chung, J.; Fiorentino, D. F.; Flanagan, W. M.; Blenis, J.; Crabtree, G. R. *Nature* **1992**, *358*, 70.
- (78) Laplante, M.; Sabatini, D. M. *Cell* **2012**, *149*, 274.
- (79) Saxton, R. A.; Sabatini, D. M. *Cell* **2017**, *168*, 960.
- (80) Nojima, H.; Tokunaga, C.; Eguchi, S.; Oshiro, N.; Hidayat, S.; Yoshino, K.; Hara, K.; Tanaka, N.; Avruch, J.; Yonezawa, K. *J. Biol. Chem.* **2003**, *278*, 15461.
- (81) Schalm, S. S.; Fingar, D. C.; Sabatini, D. M.; Blenis, J. *Curr. Biol.* **2003**, *13*, 797.
- (82) Sancak, Y.; Thoreen, C. C.; Peterson, T. R.; Lindquist, R. A.; Kang, S. A.; Spooner, E.; Carr, S. A.; Sabatini, D. M. *Mol. Cell* **2007**, *25*, 903.
- (83) Holmes, B.; Artinian, N.; Anderson, L.; Martin, J.; Masri, J.; Cloninger, C.; Bernath, A.; Bashir, T.; Benavides-Serrato, A.; Gera, J. *Cell. Signal.* **2012**, *24*, 309.
- (84) Pearce, L. R.; Sommer, E. M.; Sakamoto, K.; Wullschleger, S.; Alessi, Dario R. *Biochem. J.* **2011**, *436*, 169.
- (85) Lu, M.; Wang, J.; Ives, H. E.; Pearce, D. *J. Biol. Chem.* **2011**, *286*, 30647.
- (86) Peterson, T. R.; Laplante, M.; Thoreen, C. C.; Sancak, Y.; Kang, S. A.; Kuehl, W. M.; Gray, N. S.; Sabatini, D. M. *Cell* **2009**, *137*, 873.
- (87) Kaizuka, T.; Hara, T.; Oshiro, N.; Kikkawa, U.; Yonezawa, K.; Takehana, K.; Iemura, S.-i.; Natsume, T.; Mizushima, N. *J. Biol. Chem.* **2010**, *285*, 20109.
- (88) Yang, H.; Rudge, D. G.; Koos, J. D.; Vaidialingam, B.; Yang, H. J.; Pavletich, N. P. *Nature* **2013**, *497*, 217.
- (89) Syed, F.; Sherris, D.; Paus, R.; Varmeh, S.; Singh, S.; Pandolfi, P. P.; Bayat, A. *Am. J. Pathol.* **2012**, *181*, 1642.
- (90) Palm, W.; Park, Y.; Wright, K.; Pavlova, N. N.; Tuveson, D. A.; Thompson, C. B. *Cell* **2015**, *162*, 259.
- (91) Richeldi, L.; Collard, H. R.; Jones, M. G. *The Lancet* **2017**, *389*, 1941.
- (92) Lamouille, S.; Derynck, R. *Cells Tissues Organs* **2011**, *193*, 8.
- (93) Nho, R. S.; Hergert, P. *PLoS One* **2014**, *9*, e94616.
- (94) Coppé, J.-P.; Desprez, P.-Y.; Krtolica, A.; Campisi, J. *Annu. Rev. Pathol.* **2010**, *5*, 99.
- (95) Kuwano, K.; Araya, J.; Hara, H.; Minagawa, S.; Takasaka, N.; Ito, S.; Kobayashi, K.; Nakayama, K. *Respir. Investig.* **2016**, *54*, 397.
- (96) Park, J. S.; Park, H. J.; Park, Y. S.; Lee, S. M.; Yim, J. J.; Yoo, C. G.; Han, S. K.; Kim, Y. W. *BMC Pulm. Med.* **2014**, *14*, 168.

- (97) Mercer, P. F.; Woodcock, H. V.; Eley, J. D.; Plate, M.; Sulikowski, M. G.; Durrenberger, P. F.; Franklin, L.; Nanthakumar, C. B.; Man, Y.; Genovese, F.; McAnulty, R. J.; Yang, S.; Maher, T. M.; Nicholson, A. G.; Blanchard, A. D.; Marshall, R. P.; Lukey, P. T.; Chambers, R. C. *Thorax* **2016**, *71*, 701.
- (98) Seto, B. *Clin. Transl. Med.* **2012**, *1*, 29.
- (99) Abraham, R. T.; Wiederrecht, G. J. *Annu. Rev. Immunol.* **1996**, *14*, 483.
- (100) Lawrence, J. C.; Lin, T. A.; McMahon, L. P.; Choi, K. M. *Curr. Top. Microbiol. Immunol.* **2004**, *279*, 199.
- (101) Sehgal, S. N. *Transplant. Proc.* **2003**, *35*, 7s.
- (102) Kwitkowski, V. E.; Prowell, T. M.; Ibrahim, A.; Farrell, A. T.; Justice, R.; Mitchell, S. S.; Sridhara, R.; Pazdur, R. *Oncologist* **2010**, *15*, 428.
- (103) Carew, J. S.; Kelly, K. R.; Nawrocki, S. T. *Target. Oncol.* **2011**, *6*, 17.
- (104) Manning, B. D. *J. Cell Biol.* **2004**, *167*, 399.
- (105) Curran, K. J.; Verheijen, J. C.; Kaplan, J.; Richard, D. J.; Toral-Barza, L.; Hollander, I.; Lucas, J.; Ayril-Kaloustian, S.; Yu, K.; Zask, A. *Bioorg. Med. Chem. Lett.* **2010**, *20*, 1440.
- (106) Malagu, K.; Duggan, H.; Menear, K.; Hummersone, M.; Gomez, S.; Bailey, C.; Edwards, P.; Drzewiecki, J.; Leroux, F.; Quesada, M. J.; Hermann, G.; Maine, S.; Molyneaux, C. A.; Le Gall, A.; Pullen, J.; Hickson, I.; Smith, L.; Maguire, S.; Martin, N.; Smith, G.; Pass, M. *Bioorg. Med. Chem. Lett.* **2009**, *19*, 5950.
- (107) Chresta, C. M.; Davies, B. R.; Hickson, I.; Harding, T.; Cosulich, S.; Critchlow, S. E.; Vincent, J. P.; Ellston, R.; Jones, D.; Sini, P.; James, D.; Howard, Z.; Dudley, P.; Hughes, G.; Smith, L.; Maguire, S.; Hummersone, M.; Malagu, K.; Menear, K.; Jenkins, R.; Jacobsen, M.; Smith, G. C.; Guichard, S.; Pass, M. *Cancer Res.* **2010**, *70*, 288.
- (108) Verheijen, J. C.; Richard, D. J.; Curran, K.; Kaplan, J.; Lefever, M.; Nowak, P.; Malwitz, D. J.; Brooijmans, N.; Toral-Barza, L.; Zhang, W.-G.; Lucas, J.; Hollander, I.; Ayril-Kaloustian, S.; Mansour, T. S.; Yu, K.; Zask, A. *J. Med. Chem.* **2009**, *52*, 8010.
- (109) Gupta, M.; Hendrickson, A. E.; Yun, S. S.; Han, J. J.; Schneider, P. A.; Koh, B. D.; Stenson, M. J.; Wellik, L. E.; Shing, J. C.; Peterson, K. L.; Flatten, K. S.; Hess, A. D.; Smith, B. D.; Karp, J. E.; Barr, S.; Witzig, T. E.; Kaufmann, S. H. *Blood* **2012**, *119*, 476.

- (110) Pike, K. G.; Malagu, K.; Hummersone, M. G.; Menear, K. A.; Duggan, H. M.; Gomez, S.; Martin, N. M.; Ruston, L.; Pass, S. L.; Pass, M. *Bioorg. Med. Chem. Lett.* **2013**, *23*, 1212.
- (111) Liu, K. K. C.; Bailey, S.; Dinh, D. M.; Lam, H.; Li, C.; Wells, P. A.; Yin, M.-J.; Zou, A. *Bioorg. Med. Chem. Lett.* **2012**, *22*, 5114.
- (112) Zhu, W.; Sun, C.; Xu, S.; Wu, C.; Wu, J.; Xu, M.; Zhao, H.; Chen, L.; Zeng, W.; Zheng, P. *Biorg. Med. Chem.* **2014**, *22*, 6746.
- (113) Cohen, F.; Bergeron, P.; Blackwood, E.; Bowman, K. K.; Chen, H.; Dipasquale, A. G.; Epler, J. A.; Koehler, M. F.; Lau, K.; Lewis, C.; Liu, L.; Ly, C. Q.; Malek, S.; Nonomiya, J.; Ortwine, D. F.; Pei, Z.; Robarge, K. D.; Sideris, S.; Trinh, L.; Truong, T.; Wu, J.; Zhao, X.; Lyssikatos, J. P. *J. Med. Chem.* **2011**, *54*, 3426.
- (114) Zask, A.; Kaplan, J.; Verheijen, J. C.; Richard, D. J.; Curran, K.; Brooijmans, N.; Bennett, E. M.; Toral-Barza, L.; Hollander, I.; Ayrál-Kaloustian, S.; Yu, K. *J. Med. Chem.* **2009**, *52*, 7942.
- (115) Hobbs, H. *Synthesis of cyclopropylpyran containing compounds* Unpublished Work **2015**
- (116) Lovering, F.; Bikker, J.; Humblet, C. *J. Med. Chem.* **2009**, *52*, 6752.
- (117) Lovering, F. *MedChemComm* **2013**, *4*, 515.
- (118) Micheli, F.; Cavanni, P.; Andreotti, D.; Arban, R.; Benedetti, R.; Bertani, B.; Bettati, M.; Bettelini, L.; Bonanomi, G.; Braggio, S.; Carletti, R.; Checchia, A.; Corsi, M.; Fazzolari, E.; Fontana, S.; Marchioro, C.; Merlo-Pich, E.; Negri, M.; Oliosi, B.; Ratti, E.; Read, K. D.; Roscic, M.; Sartori, I.; Spada, S.; Tedesco, G.; Tarsi, L.; Terreni, S.; Visentini, F.; Zocchi, A.; Zonzini, L.; Di Fabio, R. *J. Med. Chem.* **2010**, *53*, 4989.
- (119) Sharma, H.; Santra, S.; Dutta, A. *Future Med. Chem.* **2015**, *7*, 2385.
- (120) Elitzin, V. I.; Harvey, K. A.; Kim, H.; Salmons, M.; Sharp, M. J.; Tabet, E. A.; Toczko, M. A. *Organic Process Research & Development* **2010**, *14*, 912.
- (121) Pal, S. *Dihedral angle scanning studies*. Unpublished Work **2015**.
- (122) Bochevarov, A. D.; Harder, E.; Hughes, T. F.; Greenwood, J. R.; Braden, D. A.; Philipp, D. M.; Rinaldo, D.; Halls, M. D.; Zhang, J.; Friesner, R. A. *Int. J. Quantum Chem.* **2013**, *113*, 2110.
- (123) Chemical Computing Group ULC: 1010 Sherbooke St. West, Suite #910, Montreal, QC, Canada, H3A 2R7, 2017.
- (124) Collins, C. J. *Chem. Rev.* **1969**, *69*, 543.
- (125) Dorko, E. A.; Hencher, J. L.; Bauer, S. H. *Tetrahedron* **1968**, *24*, 2425.

- (126) Walsh, A. D. *Nature* **1947**, *159*, 712.
- (127) de Meijere, A. *Angew. Chemie. Int. Ed.* **1979**, *18*, 809.
- (128) Hobbs, H.; Moody, H.; Inglis, G.; Peace, S. *Synthesis of 2-pyridyl CPP containing biologically active molecules*. Unpublished Work **2018**.
- (129) N. Deqiang, P. C. R., J. Singh, A. F. Kluge, H. Mazdiyasi, Z. Zhu, L. Qiao, K. Kuntz 2011.
- (130) J. Clayden, S. W., N. Greeves and P. Wothers. *Organic Chemistry*; 1st ed.; Oxford University Press.
- (131) Sengmany, S.; Lebre, J.; Le Gall, E.; Léonel, E. *Tetrahedron* **2015**, *71*, 4859.
- (132) Reizman, B. J.; Jensen, K. F. *Org. Process. Rev. Dev.* **2012**, *16*, 1770.
- (133) Modvig, A.; Andersen, T. L.; Taaning, R. H.; Lindhardt, A. T.; Skrydstrup, T. J. *Org. Chem.* **2014**, *79*, 5861.
- (134) Corey, E. J.; Chaykovsky, M. *J. Am. Chem. Soc.* **1965**, *87*, 1353.
- (135) Simmons, H. E.; Smith, R. D. *J. Am. Chem. Soc.* **1958**, *80*, 5323.
- (136) Simmons, H. E.; Smith, R. D. *J. Am. Chem. Soc.* **1959**, *81*, 4256.
- (137) Lennox, A. J. J.; Lloyd-Jones, G. C. *Angew. Chem. Int. Ed.* **2012**, *51*, 9385.
- (138) Harris, M. R.; Li, Q.; Lian, Y.; Xiao, J.; Londregan, A. T. *Org. Lett.* **2017**, *19*, 2450.
- (139) Davies, H. *CPP Suzuki-Miyaura cross coupling optimisation*. Unpublished work. **2016**.
- (140) Molander, G. A.; Sandrock, D. L. *Curr. Opin. Drug. Discov. Devel.* **2009**, *12*, 811.
- (141) Miyaura, N.; Yamada, K.; Suzuki, A. *Tetrahedron Lett.* **1979**, *20*, 3437.
- (142) Miyaura, N.; Yanagi, T.; Suzuki, A. *Synth. Commun.* **1981**, *11*, 513.
- (143) Brown, D. G.; Boström, J. *J. Med. Chem.* **2016**, *59*, 4443.
- (144) Suzuki, A. *Angew. Chem. Int. Ed. Engl.* **2011**, *50*, 6722.
- (145) Amatore, C.; Jutand, A.; Le Duc, G. *Chem. Eur. J.* **2011**, *17*, 2492.
- (146) Amatore, C.; Jutand, A.; Le Duc, G. *Chem. Eur. J.* **2012**, *18*, 6616.
- (147) Amatore, C.; Le Duc, G.; Jutand, A. *Chem. Eur. J.* **2013**, *19*, 10082.
- (148) Carrow, B. P.; Hartwig, J. F. *J. Am. Chem. Soc.* **2011**, *133*, 2116.
- (149) Thomas, A. A.; Denmark, S. E. *Science* **2016**, *352*, 329.
- (150) Butters, M.; Harvey, J. N.; Jover, J.; Lennox, A. J. J.; Lloyd-Jones, G. C.; Murray, P. M. *Angew. Chem. Int. Ed.* **2010**, *49*, 5156.
- (151) Amatore, C.; Jutand, A.; Le Duc, G. *Angew. Chem. Int. Ed.* **2012**, *51*, 1379.
- (152) Ma, N. L.; Siu, F. M.; Tsang, C. W. *Chem. Phys. Lett.* **2000**, *322*, 65.
- (153) Uenishi, J.; Beau, J. M.; Armstrong, R. W.; Kishi, Y. *J. Am. Chem. Soc.* **1987**, *109*, 4756.

- (154) Stambuli, J. P.; Bühl, M.; Hartwig, J. F. *J. Am. Chem. Soc.* **2002**, *124*, 9346.
- (155) Köllhofer, A.; Pullmann, T.; Plenio, H. *Angew. Chem. Int. Ed.* **2003**, *42*, 1056.
- (156) Zapf, A.; Ehrentraut, A.; Beller, M. *Angew. Chem. Int. Ed.* **2000**, *39*, 4153.
- (157) Macrae, C. F.; Edgington, P. R.; McCabe, P.; Pidcock, E.; Shields, G. P.; Taylor, R.; Towler, M.; van de Streek, J. *J. Appl. Crystallogr.* **2006**, *39*, 453.
- (158) Kaplan, J.; Verheijen, J. C.; Brooijmans, N.; Toral-Barza, L.; Hollander, I.; Yu, K.; Zask, A. *Bioorg. Med. Chem. Lett.* **2010**, *20*, 640.
- (159) Pogany, P. *Natural bond orbital analysis of CPP containing compounds*. Unpublished Work. 2018.
- (160) Weinhold, F.; Landis, C. R.; Glendening, E. D. *Int. Rev. Phys. Chem.* **2016**, *35*, 399.
- (161) <http://www.chem.wisc.edu/areas/reich/nmr/08-tech-02-noe.htm>. Accessed: 27.3.2019
- (162) Claridge, L. H. a. T. *Introduction to Organic Spectroscopy* Oxford Science Publications: Oxford, 1997.
- (163) [https://www.ucl.ac.uk/nmr/NMR\\_lecture\\_notes/l\\_6b\\_NOE\\_web.pdf](https://www.ucl.ac.uk/nmr/NMR_lecture_notes/l_6b_NOE_web.pdf) Accessed: 27.3.2019
- (164) Molecular Operating Environment (MOE), C. C. G. U., 1010 Sherbooke St. West, Suite #910, Montreal, QC, Canada, H3A 2R7, **2019**.
- (165) Bolleddula, J.; Dement, K.; Driscoll, J.; Worboys, P.; J Brassil, P.; Bourdet, D. *Drug Metab. Rev.*, **2014**, *46*. 379-419.
- (166) Borman, S. T. U. *Chemical & Engineering News Archive* **1992**, *70*, 5.
- (167) Arnott, J. A.; Planey, S. L. *Expert Opin. Drug. Discov.* **2012**, *7*, 863.
- (168) Chen, Z.; Venkatesan, A. M.; Dehnhardt, C. M.; Ayral-Kaloustian, S.; Brooijmans, N.; Mallon, R.; Feldberg, L.; Hollander, I.; Lucas, J.; Yu, K.; Kong, F.; Mansour, T. *S. J. Med. Chem.* **2010**, *53*, 3169.
- (169) Sutherlin, D. P.; Sampath, D.; Berry, M.; Castanedo, G.; Chang, Z.; Chuckowree, I.; Dotson, J.; Folkes, A.; Friedman, L.; Goldsmith, R.; Heffron, T.; Lee, L.; Lesnick, J.; Lewis, C.; Mathieu, S.; Nonomiya, J.; Olivero, A.; Pang, J.; Prior, W. W.; Salphati, L.; Sideris, S.; Tian, Q.; Tsui, V.; Wan, N. C.; Wang, S.; Wiesmann, C.; Wong, S.; Zhu, B.-Y. *J. Med. Chem.* **2010**, *53*, 1086.
- (170) Verheijen, J. C.; Yu, K.; Toral-Barza, L.; Hollander, I.; Zask, A. *Bioorg. Med. Chem. Lett.* **2010**, *20*, 375.
- (171) Dehnhardt, C. M.; Venkatesan, A. M.; Delos Santos, E.; Chen, Z.; Santos, O.; Ayral-Kaloustian, S.; Brooijmans, N.; Mallon, R.; Hollander, I.; Feldberg, L.; Lucas, J.;

- Chaudhary, I.; Yu, K.; Gibbons, J.; Abraham, R.; Mansour, T. S. *J. Med. Chem.* **2010**, *53*, 798.
- (172) Gilbert, A. M.; Nowak, P.; Brooijmans, N.; Bursavich, M. G.; Dehnhardt, C.; Santos, E. D.; Feldberg, L. R.; Hollander, I.; Kim, S.; Lombardi, S.; Park, K.; Venkatesan, A. M.; Mallon, R. *Bioorg. Med. Chem. Lett.* **2010**, *20*, 636.
- (173) Taylor, P.; Questex: FierceBiotech, **2018**  
<https://www.fiercebiotech.com/biotech/az-drops-mid-stage-cancer-drug-vistusertib> Accessed: 27.3.2019
- (174) Naing, A.; Aghajanian, C.; Raymond, E.; Kurzrock, R.; Blanco, M.; Oelmann, E.; Grinsted, L.; Burke, W.; Kaye, S.; Banerji, U. *Mol. Cancer Ther.* **2011**, *10*, A168.
- (175) Médard, G.; Pachl, F.; Ruprecht, B.; Klaeger, S.; Heinzlmeir, S.; Helm, D.; Qiao, H.; Ku, X.; Wilhelm, M.; Kuehne, T.; Wu, Z.; Dittmann, A.; Hopf, C.; Kramer, K.; Kuster, B. *J. Proteome Res.* **2015**, *14*, 1574.
- (176) Phillipou, A. *Phospho Akt Assay*. Unpublished work, **2015**
- (177) Chen, C. Z. C.; Peng, Y. X.; Wang, Z. B.; Fish, P. V.; Kaar, J. L.; Koepsel, R. R.; Russell, A. J.; Lareu, R. R.; Raghunath, M. *Br. J. Pharmacol.* **2009**, *158*, 1196.
- (178) Gray, A.; Olsson, H.; Batty, I. H.; Priganica, L.; Peter Downes, C. *Anal. Biochem.* **2003**, *313*, 234.
- (179) Robinson, M. W.; Hill, A. P.; Readshaw, S. A.; Hollerton, J. C.; Upton, R. J.; Lynn, S. M.; Besley, S. C.; Boughtflower, B. *J. Anal. Chem.* **2017**, *89*, 1772.
- (180) Margareth R. C. Marques, R. L., and May Almukainzi *Dissolution Technologies* **2011**, *18*, 15.
- (181) Irvine, J. D.; Takahashi, L.; Lockhart, K.; Cheong, J.; Tolan, J. W.; Selick, H. E.; Grove, J. R. *J. Pharm. Sci.* **1999**, *88*, 28.
- (182) Lombardo, F.; Obach, R. S.; Shalaeva, M. Y.; Gao, F. *J. Med. Chem.* **2004**, *47*, 1242.
- (183) Yamazaki, K.; Kanaoka, M. *J. Pharm. Sci.* **2004**, *93*, 1480.
- (184) Shamovsky, I.; Connolly, S.; David, L.; Ivanova, S.; Nordén, B.; Springthorpe, B.; Urbahns, K. *J. Med. Chem.* **2008**, *51*, 1162.
- (185) Silverman, R. B. *The Organic Chemistry of Drug Design and Drug Action*; Second Edition ed.; Elsevier Academic Press: Waltham, 2004.
- (186) Valkó, K.; Bevan, C.; Reynolds, D. *Anal. Chem.* **1997**, *69*, 2022.
- (187) Lombardo, F.; Shalaeva, M. Y.; Tupper, K. A.; Gao, F.; Abraham, M. H. *J. Med. Chem.* **2000**, *43*, 2922.
- (188) Scherrer, R. A.; Howard, S. M. *J. Med. Chem.* **1977**, *20*, 53.



- (189) Young, R. J.; Green, D. V.; Luscombe, C. N.; Hill, A. P. *Drug Discov. Today* **2011**, *16*, 822.
- (190) Brian Houston, J. *Biochem. Pharmacol.* **1994**, *47*, 1469.
- (191) Obach, R. S. *Drug Metab. Disposition* **1999**, *27*, 1350.
- (192) McCarren, P.; Springer, C.; Whitehead, L. *J. Cheminform.* **2011**, *3*, 51.
- (193) Bus, J. S.; Popp, J. A. *Food Chem. Toxicol.* **1987**, *25*, 619.
- (194) Beland, F. A.; Kadlubar, F. F. In *Chemical Carcinogenesis and Mutagenesis I*; Cooper, C. S., Grover, P. L., Eds.; Springer Berlin Heidelberg: Berlin, Heidelberg, **1990**, p 267.
- (195) Ames, B. N. *Genetics* **1974**, *78*, 91.
- (196) Hengstler, J. G.; Oesch, F. In *Encyclopedia of Genetics*; Brenner, S., Miller, J. H., Eds.; Academic Press: New York, **2001**, p 51.
- (197) Nicolle, S. *Synthesis of 5,6 bicyclic CPP compounds*. Unpublished Work, **2017**.
- (198) Keserü, G. M.; Makara, G. M. *Nat. Rev. Drug Discov.* **2009**, *8*, 203.
- (199) Freeman-Cook, K. D.; Hoffman, R. L.; Johnson, T. W. *Future Med. Chem.* **2013**, *5*, 113.
- (200) Johnson, T. W.; Dress, K. R.; Edwards, M. *Bioorg. Med. Chem. Lett.* **2009**, *19*, (201) Peters, J. U.; Schnider, P.; Mattei, P.; Kansy, M. *ChemMedChem* **2009**, *4*, 680.
- (202) Kramer, C.; Heinisch, T.; Fligge, T.; Beck, B.; Clark, T. *ChemMedChem* **2009**, *4*, 1529.
- (203) Waring, M. J. *Bioorg. Med. Chem. Lett.* **2009**, *19*, 2844.
- (204) Abad-Zapatero, C.; Metz, J. T. *Drug Discov. Today* **2005**, *10*, 464.
- (205) Ma, X.; Hu, Y. *Expert Opin. Drug Discov.* **2013**, *8*, 991.
- (206) Nowak, P.; Cole, D. C.; Brooijmans, N.; Bursavich, M. G.; Curran, K. J.; Ellingboe, J. W.; Gibbons, J. J.; Hollander, I.; Hu, Y.; Kaplan, J.; Malwitz, D. J.; Toral-Barza, L.; Verheijen, J. C.; Zask, A.; Zhang, W. G.; Yu, K. *J. Med. Chem.* **2009**, *52*, 7081.
- (207) Hopkins, A. L.; Groom, C. R.; Alex, A. *Drug Discovery Today* **2004**, *9*, 430.
- (208) Zask, A.; Verheijen, J. C.; Curran, K.; Kaplan, J.; Richard, D. J.; Nowak, P.; Malwitz, D. J.; Brooijmans, N.; Bard, J.; Svenson, K.; Lucas, J.; Toral-Barza, L.; Zhang, W.-G.; Hollander, I.; Gibbons, J. J.; Abraham, R. T.; Ayrál-Kaloustian, S.; Mansour, T. S.; Yu, K. *J. Med. Chem.* **2009**, *52*, 5013.
- (209) Richard, D. J.; Verheijen, J. C.; Curran, K.; Kaplan, J.; Toral-Barza, L.; Hollander, I.; Lucas, J.; Yu, K.; Zask, A. *Bioorg. Med. Chem. Lett.* **2009**, *19*, 6830.
- (210) Pallet, N.; Legendre, C. *Expert Opin. Drug Saf.* **2013**, *12*, 177.



- (211) Bellmunt, J.; Szczylik, C.; Feingold, J.; Strahs, A.; Berkenblit, A. *Ann. Oncol.* **2008**, *19*, 1387.
- (212) Achaiah, A.; Dexter, L.; Cowan, E.; Babu, K. S.; Titmus, V.; Hooper, R. *Eur. Respir. J.* **2017**, *50*.
- (213) Torrisi, S. E.; Pavone, M.; Vancheri, A.; Vancheri, C. *European Respiratory Review* **2017**, *26*.
- (214) Bodor, N.; Buchwald, P. In *Pure Appl. Chem.* **2008**; Vol. 80, p 1669.
- (215) Lipinski, C. A.; Lombardo, F.; Dominy, B. W.; Feeney, P. J. *Adv. Drug Del. Rev.* **1997**, *23*, 3.
- (216) Ritchie, T. J.; Luscombe, C. N.; Macdonald, S. J. F. *J. Chem. Inf. Model.* **2009**, *49*, 1025.
- (217) Macdonald, S. J. F.; Cameron, R.; Demaine, D. A.; Fenton, R. J.; Foster, G.; Gower, D.; Hamblin, J. N.; Hamilton, S.; Hart, G. J.; Hill, A. P.; Inglis, G. G. A.; Jin, B.; Jones, H. T.; McConnell, D. B.; McKimm-Breschkin, J.; Mills, G.; Nguyen, V.; Owens, I. J.; Parry, N.; Shanahan, S. E.; Smith, D.; Watson, K. G.; Wu, W.-Y.; Tucker, S. P. *J. Med. Chem.* **2005**, *48*, 2964.
- (218) Patton, J. S. *Adv. Drug Del. Rev.* **1996**, *19*, 3.
- (219) Forbes, B.; O'Lone, R.; Allen, P. P.; Cahn, A.; Clarke, C.; Collinge, M.; Dailey, L. A.; Donnelly, L. E.; Dybowski, J.; Hassall, D.; Hildebrand, D.; Jones, R.; Kilgour, J.; Klapwijk, J.; Maier, C. C.; McGovern, T.; Nikula, K.; Parry, J. D.; Reed, M. D.; Robinson, I.; Tomlinson, L.; Wolfreys, A. *Adv. Drug Del. Rev.* **2014**, *71*, 15.
- (220) GSK. Unpublished Work. **2015**.
- (221) Cansfield, A. D.; Ladduwahetty, T.; Sunose, M.; Ellard, K.; Lynch, R.; Newton, A. L.; Lewis, A.; Bennett, G.; Zinn, N.; Thomson, D. W.; Rüger, A. J.; Feutrill, J. T.; Rausch, O.; Watt, A. P.; Bergamini, G. *ACS Med. Chem. Lett.* **2016**, *7*, 768.
- (222) Raschi, E.; Ceccarini, L.; De Ponti, F.; Recanatini, M. *Expert Opin. Drug Metab. Toxicol.* **2009**, *5*, 1005.
- (223) Garcia, Y.; Schoenebeck, F.; Legault, C. Y.; Merlic, C. A.; Houk, K. N. *J. Am. Chem. Soc.* **2009**, *131*, 6632.
- (224) Handy, S. T.; Zhang, Y. *Chem. Commun.* **2006**, 299.
- (225) Newham, J. *Chem. Rev.* **1963**, *63*, 123.
- (226) Yang, B. V.; O'Rourke, D.; Li, J. *Synlett* **1993**, *1993*, 195.
- (227) Olofson, R. A.; Martz, J. T.; Senet, J. P.; Piteau, M.; Malfroot, T. *J. Org. Chem.* **1984**, *49*, 2081.

- (228) Olofson, R. A.; Schnur, R. C.; Bunes, L.; Pepe, J. P. *Tetrahedron Lett.* **1977**, *18*, 1567.
- (229) Gamble, A. B.; Garner, J.; Gordon, C. P.; O'Conner, S. M. J.; Keller, P. A. *Synth. Commun.* **2007**, *37*, 2777.
- (230) Liu, Q.; Luedtke, N. W.; Tor, Y. *Tetrahedron Lett.* **2001**, *42*, 1445.
- (231) Toral-Barza, L.; Zhang, W.-G.; Lamison, C.; LaRocque, J.; Gibbons, J.; Yu, K. *Biochem. Biophys. Res. Commun.* **2005**, *332*, 304.
- (232) Zask, A.; Kaplan, J.; Toral-Barza, L.; Hollander, I.; Young, M.; Tischler, M.; Gaydos, C.; Cinque, M.; Lucas, J.; Yu, K. *J. Med. Chem.* **2008**, *51*, 1319.
- (233) Karplus, M.; Anderson, D. H. *J. Chem. Phys.* **1959**, *30*, 6.
- (234) Karplus, M. *J. Am. Chem. Soc.* **1963**, *85*, 2870.
- (235) Chérest, M.; Felkin, H.; Prudent, N. *Tetrahedron Lett.* **1968**, *9*, 2199.
- (236) Chérest, M.; Felkin, H. *Tetrahedron Lett.* **1971**, *12*, 383.
- (237) Neufeldt, S. R.; Jiménez-Osés, G.; Comins, D. L.; Houk, K. N. *J. Org. Chem.* **2014**, *79*, 11609.
- (238) Winkler, J.; Hochhaus, G.; Derendorf, H. *Proc. Am. Thorac. Soc.* **2004**, *1*, 356.
- (239) D'Angelo, N. D.; Kim, T.-S.; Andrews, K.; Booker, S. K.; Caenepeel, S.; Chen, K.; D'Amico, D.; Freeman, D.; Jiang, J.; Liu, L.; McCarter, J. D.; San Miguel, T.; Mullady, E. L.; Schrag, M.; Subramanian, R.; Tang, J.; Wahl, R. C.; Wang, L.; Whittington, D. A.; Wu, T.; Xi, N.; Xu, Y.; Yakowec, P.; Yang, K.; Zalameda, L. P.; Zhang, N.; Hughes, P.; Norman, M. H. *J. Med. Chem.* **2011**, *54*, 1789.
- (240) Choy, J.; Jaime-Figueroa, S.; Jiang, L.; Wagner, P. *Synth. Commun.* **2008**, *38*, 3840.
- (241) Colvin, E. W.; Raphael, R. A.; Roberts, J. S. *Journal of the Chemical Society D: Chemical Communications* **1971**, 858.
- (242) Dahan, A.; Miller, J. M. *The AAPS journal* **2012**, *14*, 244.
- (243) Guideline, I. H. T. In *International Conference on Harmonization of Technical Requirements for Registration of Pharmaceuticals for Human Use. ICH Expert Working Group* **2011**, p 1.
- (244) Escobar, P. A.; Kemper, R. A.; Tarca, J.; Nicolette, J.; Kenyon, M.; Glowienke, S.; Sawant, S. G.; Christensen, J.; Johnson, T. E.; McKnight, C.; Ward, G.; Galloway, S. M.; Custer, L.; Gocke, E.; O'Donovan, M. R.; Braun, K.; Snyder, R. D.; Mahadevan, B. *Mutat. Res-Rev Mutat.* **2013**, *752*, 99.
- (245) Brooks, T. *Mutagenesis* **1995**, *10*, 447.
- (246) Diehl, M. S.; Willaby, S. L.; Snyder, R. D. *Environ. Mol. Mutag.* **2000**, *36*, 72.

- (247) Palmer, C.; Parish, M.; Kephart, S.; Bouzida, D.; Cui, J.; Deal, J.; Dong, L.; Gu, D.; Linton, A.; McAlpine, I.; Yamazaki, S.; Smith, E.; John-Baptiste, A.; Bagrodia, S.; Kania, R.; Guo, C. *Bioorg. Med. Chem. Lett.* **2012**, *22*, 7605.
- (248) Sancar, A.; Lindsey-Boltz, L. A.; Unsal-Kacmaz, K.; Linn, S. *Annu. Rev. Biochem* **2004**, *73*, 39.
- (249) Sanguinetti, M. C.; Tristani-Firouzi, M. *Nature* **2006**, *440*, 463.
- (250) Danker, T.; Möller, C. *Front. Pharmacol.* **2014**, *5*, 203.
- (251) Andrews, K. G.; Summers, D. M.; Donnelly, L. J.; Denton, R. M. *Chem. Commun.* **2016**, *52*, 1855.
- (252) Díaz, J. L.; Corbera, J.; Cuberes, R.; Contijoch, M.; Enrech, R.; Yeste, S.; Montero, A.; Dordal, A.; Monroy, X.; Almansa, C. *MedChemComm* **2017**, *8*, 1235.
- (253) Scott, J. S.; Birch, A. M.; Brocklehurst, K. J.; Broo, A.; Brown, H. S.; Butlin, R. J.; Clarke, D. S.; Davidsson, Ö.; Ertan, A.; Goldberg, K.; Groombridge, S. D.; Hudson, J. A.; Laber, D.; Leach, A. G.; MacFaul, P. A.; McKerrecher, D.; Pickup, A.; Schofield, P.; Svensson, P. H.; Sörme, P.; Teague, J. *J. Med. Chem.* **2012**, *55*, 5361.
- (254) Gerber, R.; Frech, C. M. *Chemistry Eur. J.* **2011**, *17*, 11893.
- (255) Shuttleworth, S. J.; Mcdonald, E.; Large, J.M. **2007**. *WO/2007/042810*.  
<https://patentscope.wipo.int/search/en/detail.jsf?docId=WO2007042810>  
 Accessed: 27.3.2019
- (256) Amans, D; Atkinson, S. J.; Harrison, L; Hirst, D.; Law, R.; Lindon, M.; Preston, A.; Seal, J.; Wellaway, C. **2016**. *WO/2014/14007*  
<https://patentscope.wipo.int/search/en/detail.jsf?docId=IN211707531> Accessed:  
 27.3.2019
- (257) William, A. D.; Lee, A. C. H.; Goh, K. C.; Blanchard, S.; Poulsen, A.; Teo, E. L.; Nagaraj, H.; Lee, C. P.; Wang, H.; Williams, M.; Sun, E. T.; Hu, C.; Jayaraman, R.; Pasha, M. K.; Ethirajulu, K.; Wood, J. M.; Dymock, B. W. *J. Med. Chem.* **2012**, *55*, 169.
- (258) Zask, A. N.; Wojciech, P; Verheijen, J.; Curran, K. J.; Kaplan, J.; Malwitz, D.; Bursavich, M. G.; Cole, D. C.; Ayrál-Kaloustian, S.; Yu, K.; Richard, D. J.; Lefever, M. **2009**. *U2008228964*.  
<https://patentscope.wipo.int/search/en/detail.jsf?docId=AU181446662> Accessed:  
 27.3.2019
- (259) Zask, A. K., Aaron, J.; Verheijen, J. C.; Curran, K. J.; Richard, D. J.; Ayrál-Kaloustian, S. **2009** *US 20090098086*.

- <https://patentscope.wipo.int/search/en/detail.jsf?docId=US43028351> Accessed: 27.3.2019
- (260) Ranatunge, R. R.; Augustyniak, M.; Bandarage, U. K.; Earl, R. A.; Ellis, J. L.; Garvey, D. S.; Janero, D. R.; Letts, L. G.; Martino, A. M.; Murty, M. G.; Richardson, S. K.; Schroeder, J. D.; Shumway, M. J.; Tam, S. W.; Trocha, A. M.; Young, D. V. *J. Med. Chem.* **2004**, *47*, 2180.
- (261) Liang, C. **2010** *WO/2010/056320*.  
<https://patentscope.wipo.int/search/en/detail.jsf?docId=WO2010056320>  
 Accessed: 27.3.2019
- (262) Feng, J.; Nancy-Ellen, H. ; Hermann, J. C. ; Kim, K.; Liu, J.-J.; Scott, N. R.; Lin, Y; Zak, M.; Guiling, Z. **2013**. *WO2013182546*.  
<https://patentscope.wipo.int/search/en/detail.jsf?docId=WO2013182546>  
 Accessed: 27.3.2019
- (263) Chao, Q. H., Michael J.; Holladay, M. W.; Rowbottom, M. **2013**. *US20130303533*.  
<https://patentscope.wipo.int/search/en/detail.jsf?docId=US95593838> Accessed: 27.3.2019
- (264) Buchstaller, H.-P.; Ulrich, E.; Klein, M; Christina, E.; Bomke, J. *US20120208808*.  
<https://patentscope.wipo.int/search/en/detail.jsf?docId=US74070764> Accessed: 27.3.2019
- (265) Su, Q.; Ioannidis, S.; Chuaqui, C.; Almeida, L.; Alimzhanov, M.; Bebernitz, G.; Bell, K.; Block, M.; Howard, T.; Huang, S.; Huszar, D.; Read, J. A.; Rivard Costa, C.; Shi, J.; Su, M.; Ye, M.; Zinda, M. *J. Med. Chem.* **2014**, *57*, 144.
- (266) Down, K.; Amour, A.; Baldwin, I. R.; Cooper, A. W. J.; Deakin, A. M.; Felton, L. M.; Guntrip, S. B.; Hardy, C.; Harrison, Z. A.; Jones, K. L.; Jones, P.; Keeling, S. E.; Le, J.; Livia, S.; Lucas, F.; Lunniss, C. J.; Parr, N. J.; Robinson, E.; Rowland, P.; Smith, S.; Thomas, D. A.; Vitulli, G.; Washio, Y.; Hamblin, J. N. *J. Med. Chem.* **2015**, *58*, 7381.
- (267) Kabsch, W. *Acta Crystallographica Section D* **2010**, *66*, 125.
- (268) Evans, P. R.; Murshudov, G. N. *Acta Crystallographica Section D* **2013**, *69*, 1204.
- (269) Winn, M. D.; Ballard, C. C.; Cowtan, K. D.; Dodson, E. J.; Emsley, P.; Evans, P. R.; Keegan, R. M.; Krissinel, E. B.; Leslie, A. G. W.; McCoy, A.; McNicholas, S. J.; Murshudov, G. N.; Pannu, N. S.; Potterton, E. A.; Powell, H. R.; Read, R. J.; Vagin, A.; Wilson, K. S. *Acta Crystallographica Section D* **2011**, *67*, 235.
- (270) Emsley, P.; Lohkamp, B.; Scott, W. G.; Cowtan, K. *Acta Crystallographica Section D* **2010**, *66*, 486.

- (271) G. Bricogne, E. B., M. Brandl, C. Flensburg, P. Keller, W. Paciorek, P. Roversi, A. Sharff, O.S. Smart, C. Vonnrhein & T.O. Womack; Global Phasing Ltd: Cambridge, 2014.
- (272) Bruno, I. J.; Cole, J. C.; Kessler, M.; Luo, J.; Motherwell, W. D. S.; Purkis, L. H.; Smith, B. R.; Taylor, R.; Cooper, R. I.; Harris, S. E.; Orpen, A. G. *J. Chem. Inf. Comput. Sci.* **2004**, *44*, 2133.
- (273) <https://www.mesoscale.com/en/products/phospho-ser473-total-akt-whole-cell-lysate-kit-k15100d/> Accessed: 27.3.2019
- (274) Klara, V.; Shenaz, N.; Chris, B.; Abraham, M. H.; Reynolds D. P. *J. Pharm. Sci.* **2003**, *92*, 2236.
- (275) Camurri, G.; Zaramella, A. *Anal. Chem.* **2001**, *73*, 3716.
- (276) Ballell, L.; Bates, R. H.; Young, R. J.; Alvarez-Gomez, D.; Alvarez-Ruiz, E.; Barroso, V.; Blanco, D.; Crespo, B.; Escribano, J.; Gonzalez, R.; Lozano, S.; Huss, S.; Santos-Villarejo, A.; Martin-Plaza, J. J.; Mendoza, A.; Rebollo-Lopez, M. J.; Remuinan-Blanco, M.; Lavandera, J. L.; Perez-Herran, E.; Gamo-Benito, F. J.; Garcia-Bustos, J. F.; Barros, D.; Castro, J. P.; Cammack, N. *ChemMedChem* **2013**, *8*, 313.